The Dissertation Committee for Jennifer Elaine Tanner certifies that this is the approved version of the following dissertation:

DESIGN PROVISIONS FOR AUTOCLAVED AERATED CONCRETE (AAC) STRUCTURAL SYSTEMS

Committee:

Richard E. Klingner, Supervisor

Ned H. Burns

Linda J. Hayes

Michael E. Kreger

Sharon L. Wood

DESIGN PROVISIONS FOR AUTOCLAVED AERATED CONCRETE (AAC) STRUCTURAL SYSTEMS

by

Jennifer Elaine Tanner, M.S., B.S.E.

Dissertation

Presented to the Faculty of the Graduate School of
The University of Texas at Austin
in Partial Fulfillment
of the Requirements
for the Degree of

Doctor of Philosophy

The University of Texas at Austin
May 2003

Dedication

To my family

Acknowledgements

Financial and technical support was provided by the Autoclaved Aerated Concrete Products Association. This group of individuals provided an example of how cooperation with industry, academia and technical societies should function. In particular, I thank Ron Barnett, Felipe Babbit, and Keith Itzler.

I wish to express my gratitude and appreciation to Dr. Richard Klingner for his guidance and support in this research. Working under his supervision has been a unique learning experience into a methodology of research and understanding structural engineering. Jorge Varela has also been an integral part of this research throughout the entire journey. I am very grateful for the dedication of both of these individuals.

I am grateful for the contributions of Matthew Brightman, Jaime Argudo and Ulises Cancino in various aspects of this work. Learning as a group has been an important part of the experience; I appreciate all of these team members. The work of undergraduate students was fundamental to the progress of the research. I especially appreciate the insights of Geoff Mitchell and Ross Sassen.

I am grateful for the support and comments of the dissertation committee who have also helped to guide this research.

The support staff at the Ferguson Structural Engineering Laboratory has been helpful in many ways. I thank the lab technicians, Blake Stasney, Wayne Fontenot, Mike Bell, Dennis Fillip and Ray Madonna for their knowledge and time spent assisting with our project. I thank the office staff of Regina Forward, Hortensia Peoples, Dee Smith, and Mary Jo Moore for making many details run smoothly.

I appreciate the support and camaraderie of the graduate students working in the laboratory, who have provided support throughout the process. The

friendships I have formed here are a special part of my life. In particular I thank Brian, Yajai, Regan, Anna, Nat, Jorge, Gabriella, Taichiro and Greg.

Finally, I thank my family and many friends who have supported me during the process, especially Martin.

DESIGN PROVISIONS FOR AAC STRUCTURAL SYSTEMS

Publication No._____

Jennifer Elaine Tanner, Ph.D.

The University of Texas at Austin, 2003

Supervisor: Richard E. Klingner

The objective of this research program was to develop reliable design provisions for AAC structural systems. Typical AAC construction uses AAC shear walls combined with AAC floor or roof diaphragms. AAC shear walls are the predominant structural application of AAC. Because the behavior of AAC shear walls under combinations of reversed cyclic in-plane loading and gravity load is potentially complex, design provisions for AAC shear walls are of fundamental importance.

A comprehensive testing program was developed. The first phase of that testing program was intended to determine the behavior of AAC shear walls subjected to reversed cyclic lateral loads. Walls were made of a variety of AAC units, including masonry-type units and reinforced panels, laid either horizontally

or vertically. The aspect ratio of the specimens (ratio of height to base length) varied from 0.6 to 3, and each specimen was designed to fail in either shear or flexure. Based on test results, procedures and corresponding design equations were developed to predict the behavior of AAC shear walls as governed by flexure, shear, and other limit states.

The second phase of the testing program involved the design, construction and testing, under reversed cyclic lateral loads, of a full-scale, two-story AAC assemblage specimen. Results from this second phase were used to validate the previously developed design provisions for shear walls, to evaluate proposed procedures for the design of AAC floor systems and connections, and to evaluate the overall behavior of AAC structures.

The mechanical properties of a material are fundamental to the design process for that material. Mechanical properties of AAC were determined at the Ferguson Structural Engineering Laboratory and validated with the results of material tests performed at other laboratories. Based on the results of those tests, design-related equations for material properties were developed for use in design provisions.

The combination of these three facets has resulted in comprehensive and reliable design provisions for typical AAC structural systems, verified through extensive testing.

Table of Contents

LIST OF TABLES

LIST OF FIGURES

CHAPTER 1
Introduction

1.1 GENERAL

The growing use of Autoclaved Aerated Concrete (AAC) in the United States requires that appropriate design provisions be developed for this material. At present, such design provisions are not addressed by structural design codes in the United States.

AAC shear walls are the predominant structural application of AAC. Because the behavior of AAC shear walls under combinations of reversed cyclic in-plane loading and gravity load is potentially complex, design provisions for AAC shear walls are of fundamental importance. This was the motivation for an extensive experimental and analytical investigation in the United States.

The research forms part of a research program supported by the Autoclaved Aerated Concrete Products Association (AACPA), and carried out at the Phil M. Ferguson Structural Engineering Laboratory of The University of Texas at Austin.

1.2 SCOPE OF STUDY

The goal of this research was to produce draft design provisions for AAC in the United States, and a comprehensive technical justification for those provisions. Results of the study at The University of Texas at Austin, together with studies completed at other institutions, formed the basis for design equations for different AAC elements. Values of the force-reduction factor R and corresponding displacement-amplification factor C_d for the seismic design of

AAC shear wall structures in the United States were also proposed as part of this study.

The study at The University of Texas at Austin consisted of two phases. Phase I consisted of a series of fourteen AAC shear wall specimens with aspect ratios ranging from 0.64 (shear-dominated walls) to 3.17 (flexure-dominated walls). The specimens were designed and tested using a variety of AAC panel and block orientations, reinforcement layouts, and axial loads. Results from those tests were used to develop design provisions for AAC shear walls and pier elements. Results of this phase also provided experimental information necessary to develop analytical models, and to define appropriate values of drift ratio and displacement ductility capacities for AAC shear walls used in the procedure to select the factors R and C_d for the seismic design of AAC shear wall structures.

Phase II of the study involved testing a full-scale, two-story AAC assemblage specimen, consisting of two flanged AAC shear walls connected by AAC diaphragms at each level, under reversed cyclic loads. Results from tests on this assemblage specimen were used to validate the design equations developed during Phase I, to verify the integrity of different connection details proposed for use in AAC construction, and to validate overall design approaches proposed as a result of Phase I testing.

1.3 OBJECTIVES OF STUDY

The objectives of the study carried out at The University of Texas at Austin were to:

- determine fundamental material properties of AAC manufactured in the United States, including a synthesis of data from other sources;

- verify basic procedures to predict the behavior of AAC shear wall specimens, including flexural cracking, web-shear cracking, flexure-shear cracking, sliding shear, crushing of the diagonal strut, and flexural behavior;
- determine the differences in behavior of AAC shear walls with the same overall geometry, but with different arrangements and amounts of reinforcement;
- determine the differences in behavior of AAC shear walls with the same overall geometry, reinforcement, and axial load, but with different layouts of panel and block elements;
- evaluate the behavior of different flexure-dominated AAC shear walls to verify proposed design of ductile AAC shear wall structures in seismic zones;
- test an assemblage specimen to verify proposed approaches for the design of AAC shear walls for flexure-dominated behavior, to verify proposed design equations for AAC shear walls, and to verify the proposed analytical models and the observed behavior of the flexure-dominated specimens;
- ascertain the performance of proposed details for AAC floor diaphragms and connections between diaphragms and AAC shear walls;
- define appropriate values of drift ratio and displacement ductility capacities for AAC shear walls;
- develop analytical models that represent the flexural and shear behavior of AAC shear walls under lateral loads;
- predict the performance of AAC shear wall structures subjected to earthquake ground motions;
- develop a procedure to propose values of the force-reduction factor (R) and displacement-amplification factor (C_d) for the seismic design of AAC shear wall structures in the United States; and

- synthesize data on tests on reinforced AAC panels from other sources to produce design provisions for those elements.

1.4 ORGANIZATION OF STUDY

The completed work is described in several resources. The development of test setup and results of pilot specimens are presented in Brightman (2000). Portions of this chapter were authored by Varela and are also contained in Varela (2003). Development of general design provisions is presented in this dissertation. Development of the force-reduction factor (R) and the displacement amplification factor (C_d) are presented by Varela (2003). Proposed design provisions for reinforced AAC panels and a synthesis of data from the University of Alabama at Birmingham are presented by Argudo (2003). A study of low-strength AAC shear wall specimens is to be presented by Cancino (2003). Table 1.1 shows how responsibility for each study element was shared by different Graduate Research Assistants.

Table 1.1 Study elements done for each Graduate Research Assistant

Study Element	**GRA**
development of test setup and results of tests on pilot specimens	Brightman, Tanner, and Varela
development of general design provisions	Tanner and Argudo
development of R and C_d factors	Varela
synthesis of material testing data	Argudo and Tanner
study of low-strength AAC shear walls	Cancino and Varela

1.5 SCOPE OF DISSERTATION

This dissertation focuses on proposing design provisions for AAC structural systems. The proposed provisions are divided into provisions for factory-reinforced AAC panels and field-reinforced AAC masonry. Provisions

for the former are presented and proposed to the American Concrete Institute (ACI) Committee 523A; and provisions for the latter are presented and proposed to the Masonry Standards Joint Committee (MSJC), AAC Masonry Subcommittee.

The proposed design provisions for AAC shear walls are based on results of a comprehensive study to evaluate the in-plane behavior of AAC shear walls, the fundamental lateral force-resisting element of AAC buildings. The first phase of the testing program evaluated a suite of 14 shear wall specimens with aspect ratio (ratio of height to base length) between 0.6 and 3. Walls were made of a variety of types of AAC units, including masonry-type units and reinforced panels, laid either horizontally or vertically. Because the behavior of flexure-dominated AAC shear walls is inherently easier to predict than that of shear-dominated walls, and because the prediction of shear capacity is important in the capacity design of AAC shear walls, initial tests emphasized shear-dominated specimens.

The second phase of testing involved the design, construction and testing of a full-scale, two-story AAC assemblage specimen. Results from the assemblage specimen were used to validate the behavior that had been predicted based on the AAC shear walls studied in Phase I. Design provisions for structural integrity for AAC construction are proposed based on the results of the Two-story Assemblage Specimen.

Mechanical properties of AAC were determined at the Ferguson Structural Engineering Laboratory and were verified with test results at other laboratories. Design equations to determine material properties are an integral part of Phase 1.

1.6 OBJECTIVES OF DISSERTATION

The objectives of this dissertation were to:

- determine fundamental material properties of AAC manufactured in the United States, including a synthesis of data from other sources;
- verify basic procedures to predict the behavior of AAC shear wall specimens, including flexural cracking, web-shear cracking, flexure-shear cracking, sliding shear, crushing of the diagonal strut, and flexural behavior;
- determine the differences in behavior of AAC shear walls with the same overall geometry, but with different arrangements and amounts of reinforcement;
- determine the differences in behavior of AAC shear walls with the same overall geometry, reinforcement, and axial load, but with different layouts of panel and block elements;
- determine the effect of factory-installed and field-installed reinforcement;
- evaluate the behavior of different flexure-dominated AAC shear walls to verify proposed design of ductile AAC shear wall structures in seismic zones;
- test an assemblage specimen to verify proposed approach for the design of AAC shear walls for flexure-dominated behavior, to verify proposed design equations for AAC shear walls, and to verify the proposed analytical models and the observed behavior of the flexure-dominated specimens; and
- determine the load-carrying mechanisms of an AAC floor diaphragm and verify the current connection details for

conventional pre-cast concrete and masonry are acceptable in AAC construction.

1.7 ORGANIZATION OF DISSERTATION

This dissertation contains a description of the experimental program, including construction techniques. Chapter 2 provides background information for Autoclave Aerated Concrete and the construction process. Material tests performed at The University of Texas at Austin are presented in Chapter 3, along with verification from material tests at other laboratories. The testing programs for AAC shear walls and the Two-story Assemblage Specimen are presented in Chapter 4. Results from the shear wall specimens are presented in Chapters 5 and 6. The development of models to predict the behavior of AAC shear walls is included in Chapter 7 along with additional models specific to the behavior of vertical panels. Chapter 8 presents the results of the AAC Two-story Assemblage Specimen. The technical justification for proposed design provisions for the ACI and MSJC frameworks is presented in Chapter 9. Chapter 10 contains the summary and conclusions.

CHAPTER 2
Background

2.1 DESCRIPTION OF AUTOCLAVED AERATED CONCRETE

Autoclaved Aerated Concrete (AAC) is a lightweight cellular material composed of portland cement, quicklime, water, and finely ground sand (using a ball mill). Some or all of the sand can be replaced by fly ash (Chusid 1999). In the most common method of production, the dry materials are mixed with water to form a slurry. Aluminum power is added to the slurry as it is poured into one-third to one-half of the height of the forms (Figure 2.1). As the aluminum powder reacts with the alkaline cement, hydrogen gas forms which causes the slurry to increase in volume by two to three times. As the quicklime reacts with the water, sufficient heat is created to produce an accelerated initial set in the portland cement within three to four hours. At this time the mass is self-supporting; the molds are stripped and cut into the desired shapes using wires steel wires subject to tension (Figure 2.2). The cut shapes are then cured in an autoclave, producing a final material with about one-fifth to one-third the density of structural concrete. The material can be easily cut and shaped with hand tools (RILEM 1993). The cellular structure of AAC is shown in Figure 2.3.

Figure 2.1: AAC slurry in molds during the rising process

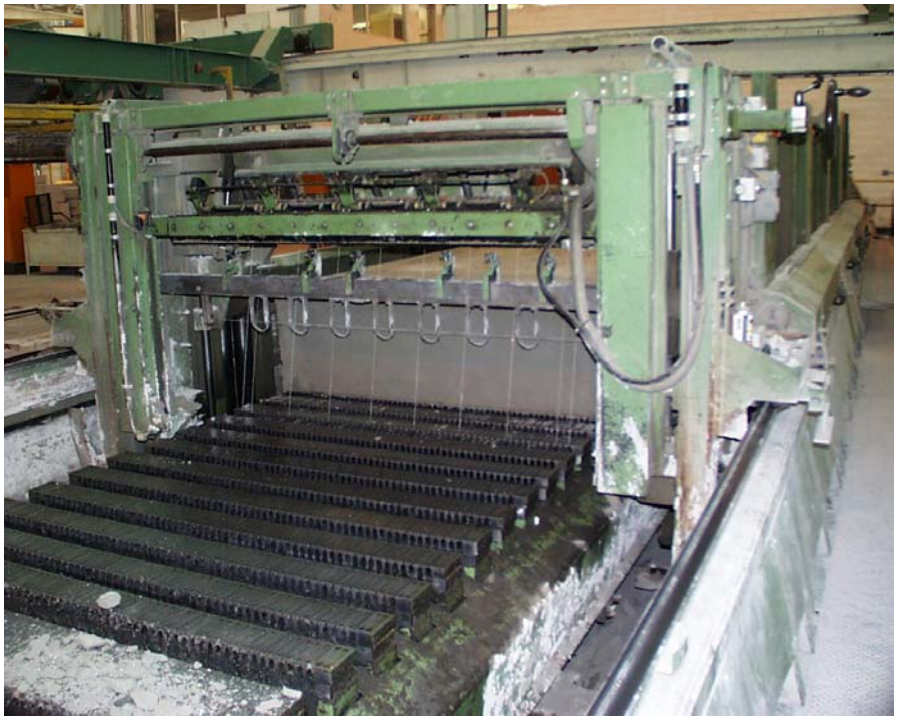

Figure 2.2: Cutting AAC mass after the forms are stripped

Figure 2.3 Cellular structure of AAC

2.2 CURRENT USE OF AAC

AAC is a versatile material with typical products shown in Figure 2.4. Tradition elements include masonry-type units (blocks), floor panels, roof panels, wall panels, lintels, beams. Non-traditional elements include special shapes such as arches. These elements can be used in a variety of applications including residential, commercial and industrial construction. Reinforced wall panels can be used as cladding systems as well as loadbearing and non-loadbearing exterior and interior wall systems. Reinforced floor and roof panels can be efficiently used to provide the horizontal diaphragm system while supporting the necessary gravity loads.

The standard units in AAC structural systems are AAC shear walls and floor diaphragms. Shear walls may be constructed of modular blocks or panels oriented horizontally or vertically. Modular blocks are 8 in. (200 mm) in height and are 24 in. (610 mm) long. Wall panels are 24 inches (610 mm) in height and may have lengths up to 240 inches (6.10 m). The thickness of blocks and panels

is variable, with a common thickness of 8 in. (200 mm) to 10 in. (250 mm). Floor panels have a width of 24 in. (610 mm) and are produced in lengths up to 240 in. (6.10 m). The height of floor and roof panels is variable, with a common thickness of 8 in. (200 mm) to 10 in. (250 mm).

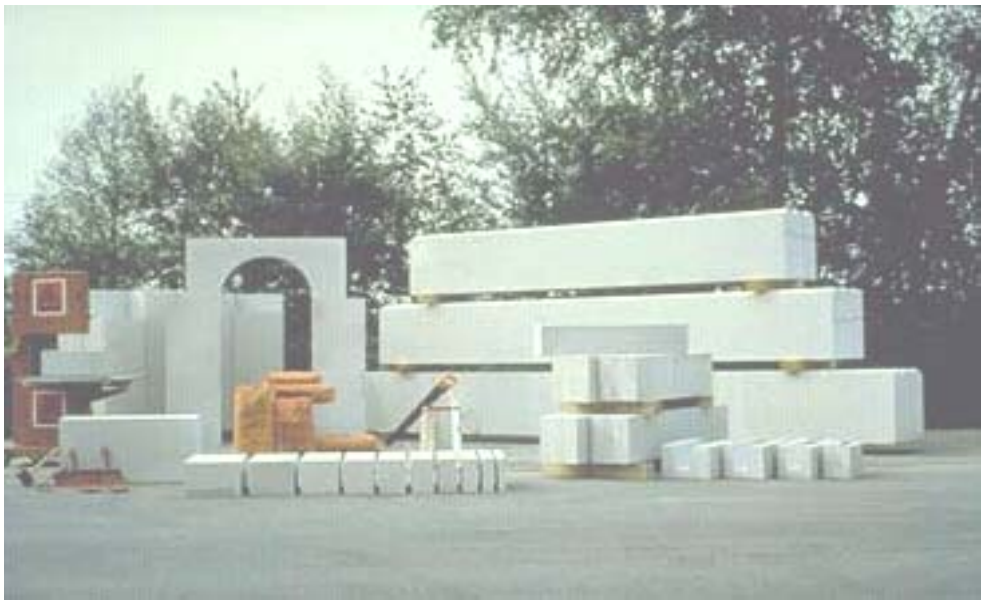

Figure 2.4 Examples of AAC elements

Welded wire reinforcement in AAC panels consists of longitudinal wires, parallel to the axis of the panel and transverse, or cross-wires. Typical details for welded wire mesh are shown in Figure 2.5. Longitudinal wire are generally 0.3 in. (7 mm) in diameter and cross-wires are generally 0.2 in. (5 mm) in diameter. Typical spacing for longitudinal wires in a heavily reinforced mesh is 3 in. (76 mm), while typical spacing for longitudinal wires in a lightly reinforced mesh is 10 in. (250 mm). Typical spacing for cross-wires is 20 in. (0.51 m) in either mesh.

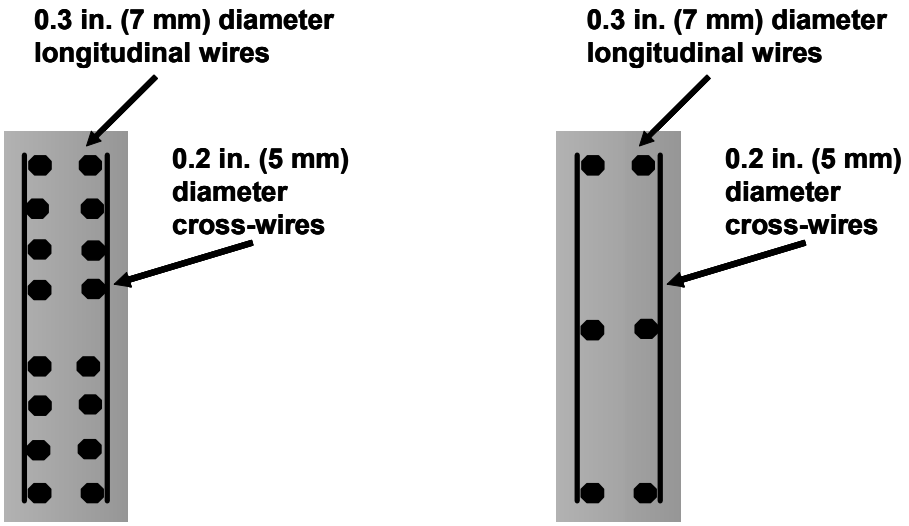

Figure 2.5: Typical details of heavy and light welded wire mesh in reinforced AAC panels

Individual AAC units are bonded together by thin-bed mortar. Joints are approximately 1/32 in. to 1/8 in. (1 mm to 3 mm) thick. Thin-bed mortar is a mix of portland cement, fine silica sand, polymers such as latex or vinylester, and admixtures such as water-retention admixtures. The compressive strength of the thin-bed mortar is greater than that of the AAC itself. A series of 2 in. (50 mm) by 2 in. (50 mm) thin-bed mortar cubes were tested FSEL after curing in a laboratory environment for approximately 1 year. The average compressive strength of 12 cubes was 2100 psi (14.5 MPa), which is greater than the maximum compressive strength of the AAC.

2.3 DESIGN PROVISIONS FOR AAC STRUCTURAL SYSTEMS

Currently design provisions do not exist in the United States for AAC structural systems. The structure of the design provisions is intended to form part

of the current design provisions used for both masonry (Masonry Standards Joint Committee) and concrete (American Concrete Institute 318-02).

Design provisions for field-reinforced structures are subject to review by the AAC Masonry Subcommittee of the Masonry Standards Joint Committee (MSJC). These structures consist of unreinforced AAC modular blocks with reinforcement placed in grouted cores or keys during the construction process.

Design provisions for factory-reinforced AAC panels are under discussion by American Concrete Institute (ACI) Subcommittee 523A. These proposed code provisions will be placed in a separate document that uses the same structure as the ACI318-02.

2.4 TYPICAL THERMAL AND ACOUSTICAL CHARACTERISTICS OF AAC

One advantage of AAC is the excellent thermal and acoustical properties that result from the porosity of AAC. The fire rating of a solid 8 in. (200 mm) panel or modular block is 6 hours or greater. The thermal efficiency of a material may be measured through an R-value. The R-value for a solid 8 in. (200 mm) Class 4 AAC wall is 8[1]; this is four to six times the R-value for a hollow 8 in. CMU and two to three times the R-value for an 8 in. (200 mm) CMU structure with 2 in. (50 mm) air cavity and exterior wythe of clay masonry (Drysdale, et. all 1994). Because of its internal porosity, AAC has very low sound transmission, making it potentially useful acoustically. The sound transmission coefficient of AAC is higher than other building materials of the same weight[1].

[1] Ytong Product Information, *Residential Buildings*, Haines City, FL.

2.5 CONSTRUCTION PROCESS FOR AAC SYSTEMS

Although the general construction process for AAC walls is independent of whether horizontal panels, vertical panels or blocks are used, additional measures can be taken to improve the performance of walls constructed of vertical panels. The construction practices for shear walls are presented in Sections 2.5.1 and 2.5.2. Construction techniques for AAC floor diaphragms and grouting procedures are presented in Sections 2.5.3 and 2.5.4.

2.5.1 Construction Guidelines for Horizontal Panels and Modular Blocks

First, the top of the concrete base or foundation is roughened by light bush-hammering, cleaned with compressed air, pre-wetted, and leveled by placing shims on top, level to within a tolerance of ±1/32 inch (0.8 mm). Next, an ASTM C270, Type S mortar by proportion is placed on top of a post-tensioned concrete foundation between the shims (Figure 2.6).

Figure 2.6 Placing Type S mortar by proportion on concrete foundation

Before placing each panel or modular block, the bed joint was cleaned with compressed air, sanded to remove surface roughness and pre-wetted prior to applying thin-bed mortar. Subsequent panels were not leveled with shims. Due to the tight tolerances and uniform layer of the thin-bed mortar, the remaining panels were not out of plumb. The process of placing panels is shown in Figure 2.4 and Figure 2.6.

In modular block construction each unit is placed using shims and longitudinally aligned through a guide string connected to two guide poles located

at each end of the wall, such as the structural tubes shown in Figure 2.8. The plumb was verified every three courses; any error in plumb was correct by adjusting the block placement.

Figure 2.7 Placing a layer of thin-bed mortar on AAC panel in Shear Wall Specimen 1

Figure 2.8 Placing second course of AAC panels in Shear Wall Specimen 1

2.5.2 Construction Guidelines for Vertical Panels

The concrete foundation surface is roughened and pre-wetted before applying the Type S leveling bed mortar as described in Section 2.5.1. Two shims were used to level each panel as shown in Figure 2.9. During the construction process for the first specimen with panels oriented vertically (Shear Wall Specimen 2), thin-bed mortar was initially applied to one vertical face of the panel. Based on an observed lack of coverage, mortar was reapplied to both vertical joints. The panels were also clamped together to apply pressure to the face of the joint. Two clamps were used at the midheight of the panel and a single clamp was used at the top of the panel (Figure 2.10 and Figure 2.11). Mortar coverage was ensured when excess mortar became visible at the exterior section of the head joint after clamping. The panels were fixed from moving out-of-plane by clamping the first panel to the lateral support system and nailing a 3/4 in. (18 mm) board to the top of adjacent panels (Figure 2.11).

Figure 2.9: Preparing the foundation surface to place a vertical panel

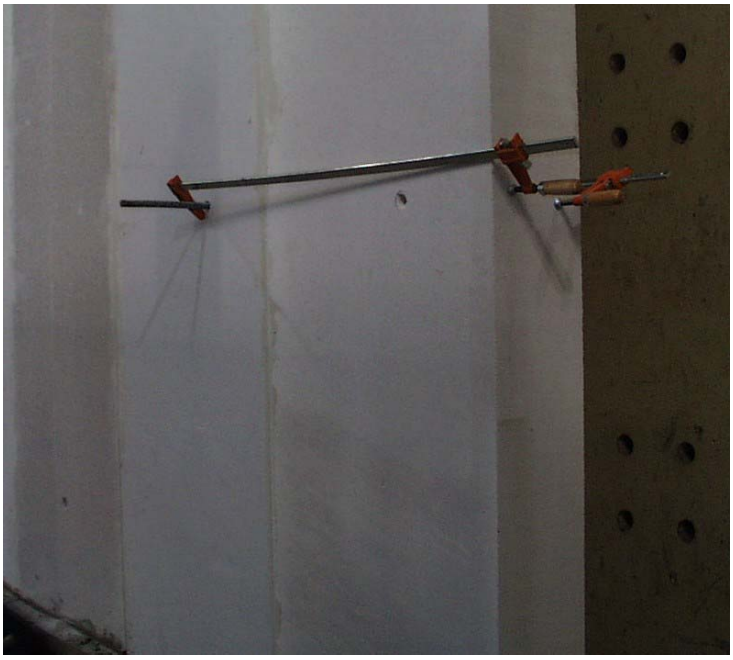

Figure 2.10: Clamping technique used at midheight of Shear Wall Specimen 2

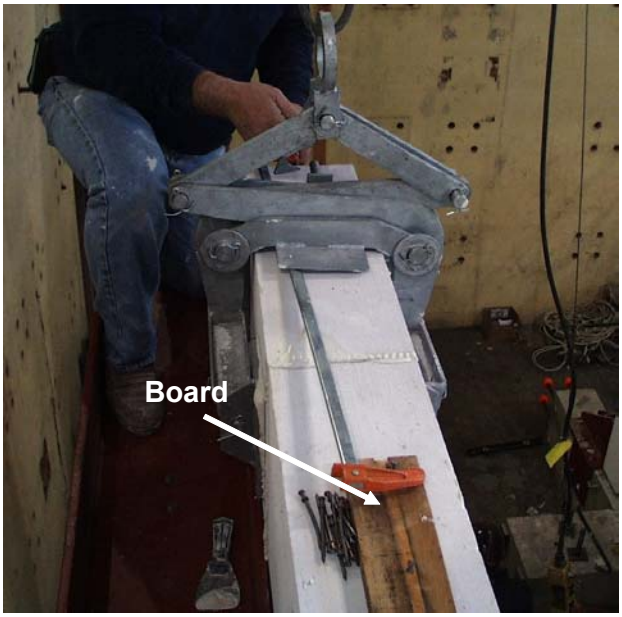

Figure 2.11: Clamping technique used at top of Shear Wall Specimen 2

2.5.3 Construction Guidelines for Floor Slab Panels

AAC floor slab panels rest directly on the gravity load bearing system. The AAC vertical surface of the floor panel is cleaned with compressed air, sanded to remove surface roughness, and pre-wetted prior to applying thin-bed mortar. Thin-bed mortar is applied to the area of the panel below the grouted key as shown in Figure 2.12. The floor panels that comprise the slab are placed on the gravity load bearing system and the required reinforcement is placed in the bond beam and grouted keys. The grouting process is described in the following section.

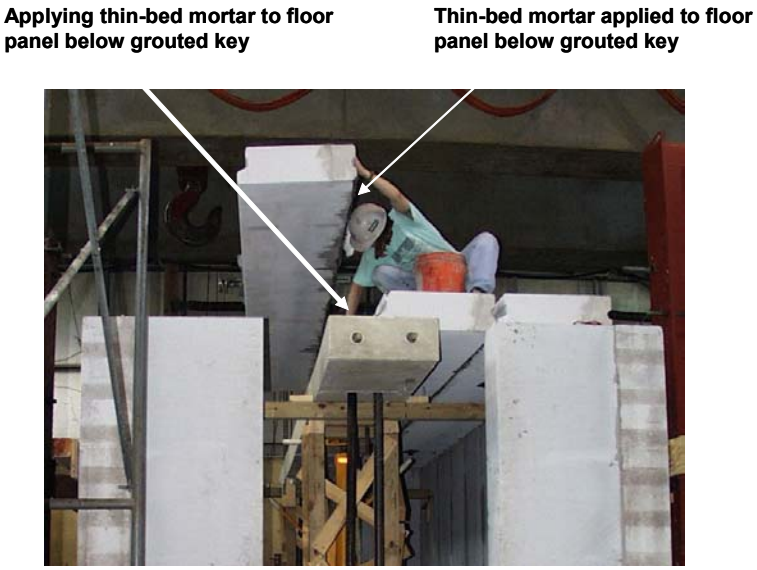

Figure 2.12: Placement of AAC floor panel in slab of Two-story Assemblage Specimen

2.5.4 Construction Guidelines for Grouted Reinforcement

Reinforcement is placed in grouted cores or keys to connect elements within a structure. The internal reinforcement is secured with rebar chairs prior to grouting. The AAC surface is cleaned with compressed air and pre-wetted. ASTM 476 coarse grout proportioned by volume with an approximate slump between 10 in. (250 mm) and 12 in. (300 mm) is placed in the core or key. The grout is vibrated throughout the depth of the grouted cell, bond beam or grouted key. A connection including reinforcement in a grouted cell, bond beam, and grouted key is shown in Figure 2.13.

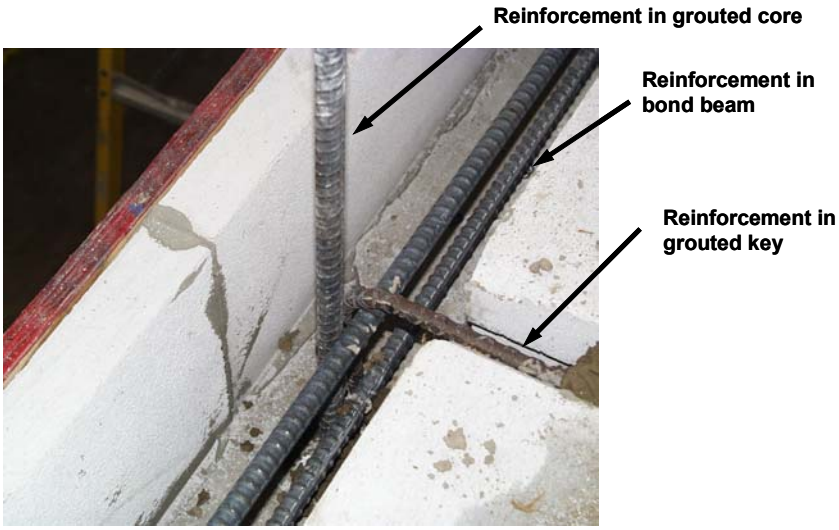

Figure 2.13: Bond beam and grouted key in the Two-Story Assemblage Specimen

2.6 LITERATURE REVIEW

The literature review presented in the following two sections focused on previous research carried out on the material properties of AAC, behavior of AAC walls, and information on the behavior of shear wall structures.

2.6.1 Previous Research on AAC Mechanical Properties

Additional research on material properties was performed for individual AAC manufactures. The data were made available through the manufacturers and is referenced throughout the text in the form of footnotes. Material testing was performed for Ytong at the University of Alabama at Birmingham[2] and at the

[2] Internal report by Fouad H. Fouad, *Material Properties and Structural Behavior of Plain and Reinforced AAC Components*, University of Alabama at Birmingham, February 28, 2002.

University of Texas at Arlington[3,4]. The material testing at the University of Alabama at Birmingham included tests to determine the following: compressive strength; modulus of rupture; modulus of elasticity; direct shear; bond strength; and freeze-thaw resistance. ASTM 519 tests were performed at the University of Texas at Arlington to determine the diagonal tensile strength of regular and tongue and groove AAC masonry. Tests were performed for the Aerated Concrete Corporation of America (ACCOA) by Construction Technology Laboratories (CTL)[5] to determine the following material properties: compressive strength; modulus of rupture; diagonal tensile strength; modulus of elasticity; and water penetration and leakage of AAC.

2.6.2 Previous Research on AAC Panels and Walls

The out-of-plane flexural behavior of non-load bearing AAC walls constructed with blocks in running bond was studied, to investigate the flexural strength of the walls parallel or perpendicular to the bed joints (Al-Shaleh and Attiogbe 1997). That study concluded that the out-of-plane flexural strength of the AAC walls was the same parallel or perpendicular to the bed joints. Additional tests to determine the out-of-plane flexural strength of AAC masonry

---

[3] Internal report by John H. Matthys, *Structural Properties of Masonry Assemblages Constructed of Regular Ytong Masonry Units,* University of Texas at Arlington, May 1996.

[4] Internal report by John H. Matthys, *Structural Properties of Masonry Assemblages Constructed of Tongue and Groove Ytong Masonry Units,* University of Texas at Arlington, July 1997.

[5] Internal report by Construction Technology Laboratories, Inc. *Material Tests of ACCOA Autoclaved Aerated Concrete (AAC) Masonry Blocks and Assemblies*. CTL Project No. 183035, Construction Technology Laboratories, Inc., Stokie, IL, August 11, 1999.

walls were performed at the University of Texas at Arlington[3] and at the University of Alabama at Birmingham[1].

Prior research on AAC walls has focused primarily on the behavior of walls constructed using AAC masonry-type units. For example, one research project (de Vekey *et al*. 1986) studied the performance of AAC wallettes and walls under lateral loads to study the effect of thickness, moisture content, and specimen size on the flexural strength. That study concluded that the flexural strength of the specimens decreased as the thickness of the specimen increased, the flexural strength decreased as the moisture content increased, and the flexural strength increased as the size of the unit decreased when the load was applied perpendicular to the bed joints, and it was about the same when the load was applied parallel to the bed joints. A suite of 12 shear-wall specimens subject to in-plane lateral loads with varying axial load were tested by Hebel International in Germany[6]. All of the specimens measured 8.2 ft (2.5 m) by 8.2 ft (2.5 m) giving an aspect ratio of 1.0. The test results indicated distributed web-shear cracking was a failure mode in all shear wall specimens when lateral restraint against sliding was provided. Background on determining the behavior of AAC shear walls is described by Brightman (2000).

Full scale testing on Ytong AAC infill walls was performed by the Building Research Institute NISI in Sofia, Bulgaria[7]. A series of nine confined

---

[6] Personal communication, Violandi Vratsanou, Hebel AG, Germany, November 2000.

[7] Internal report by Building Research Institute NISI. *Carrying out Experimental Investigations to Determine the Behavior and the Bearing Capacity of Autoclaved Concrete Walls with Confining Reinforced Concrete Elements under Reversible Horizontal Load*. Building Research Institute NISI –Sofia Bulgaria, September 1997.

AAC masonry shear walls was tested, 6 of which contained openings. The study concludes that confined AAC masonry is a viable alternative for one- to three-story lateral load-resisting systems.

Based on the literature review, insufficient research exists on AAC structures to develop design provisions for AAC shear-walls. In areas of low seismic risk, AAC structures are designed by applying traditional theories on masonry design and reinforced concrete design. The insufficient research on AAC structures clearly indicated the need for more experimental data on AAC shear walls subjected to reversed cyclic lateral loads.

CHAPTER 3
Mechanical Properties of AAC

3.1 MECHANICAL PROPERTIES OF AAC

The mechanical properties of a material are required to predict the performance of a structural element made from that material. Mechanical properties required for the design of an AAC shear wall are discussed in this chapter.

3.2 AVAILABLE RESOURCES

Tests were performed at The University of Texas at Austin to determine the compressive strength, splitting tensile strength, modulus of elasticity and the shear strength of AAC joints. The AAC material used in construction of the shear wall specimens and assemblage specimen was supplied by three manufacturers. These manufactures were Contec Mexicana, Hebel / Matrix (now Babb International, Inc.) and Ytong. A total of eight shipments were sent to UT Austin: two from Contec; two from Ytong; two from Hebel / Matrix and two from Babb. Tests to determine the compressive strength, splitting tensile strength and modulus of elasticity were performed on modular blocks from each AAC shipment, except the first Hebel shipment, which consisted only of panels.

Extensive material testing was performed at the University of Alabama at Birmingham[8]. A synthesis of this material testing related to the splitting tensile

[8] Internal report by Fouad H. Fouad, *Material Properties and Structural Behavior of Plain and Reinforced AAC Components*, The University of Alabama at Birmingham, February 28, 2002.

strength, modulus of elasticity, and direct shear is presented in this chapter. A complete synthesis of the tests performed at the University of Alabama at Birmingham is presented in Argudo (2003).

3.3 COMPRESSIVE STRENGTH OF AAC CORES AND GROUT CORES

The compressive strength for each AAC material shipment at UT Austin was tested using cores with nominal dimensions of 4 in. (100 mm) by 8 in. (200 mm). Compression tests were also performed cores of ASTM C476 coarse grout cast in AAC molds. In referring to those tests, the name of the specimen group refers to the AAC manufacturer and the number after the name denotes the shipment in which the material arrived.

3.3.1 Specimen Preparation and Testing Procedure for Compression Tests on AAC Cores and Grout Cores

The nominal dimensions of each core were 4 in. (100 mm) by 8 in. (200 mm). The AAC cores were removed from modular blocks with a Hilti core drill with a water-cooled diamond coring bit. When a 4 in. (100 mm) core bit is used with an 8 in. (200 mm) panel or modular block, the result is a core with a diameter of 3.75 in. (95 mm) and a length of 7.75 in. (197 mm), for an aspect ratio of 2 to 1. AAC cores were not capped, because their loaded surfaces were quite planar, and capping is not required for ASTM C1386 compression specimens.

The ASTM476 coarse grout cores were cast in the void in the AAC block left from the AAC coring process. This simulates the loss of water in grout due to absorption by the AAC. Prior to pouring the grout, the 4 in. (100 mm) diameter voids in each modular block were pre-wetted. The coarse grout was placed in three layers, each of which was rodded 25 times to compact the coarse

grout. After curing for 28 days in field conditions representative of a non air-conditioned laboratory environment where the assemblage specimen was tested, the specimens were removed from the molds by soaking the AAC form block and chipping the surrounding AAC with a chisel. With the exception of a few initial tests, sulfur caps were placed on the top and bottom faces of the grout cores. In each grout specimen, the name refers to the manufacturer of the block in which the specimen was cast. The number after the "b" refers to the batch in which the coarse grout was mixed, and the number after the "s" refers to the specimen number. Specimens cast in Babb blocks were all cast in the same batch. Grout cast in Contec blocks was mixed in two different batches.

As shown in Figure 3.1, specimens were tested in a 120-kip (533-kN) Tinius Olsen testing machine with an upper hemispherical head. Loads were measured with a 50-kip (222-kN) load cell, and data were acquired in real time using a HP 7500 scanner.

Figure 3.1: Test setup for compression tests of AAC cores

3.3.2 Compression Test Results for AAC Cores

Results of tests for compressive strength and density for the compression tests performed at UT Austin are presented in Table 3.1, which shows dry density, density at the time of testing, moisture content and the measured compressive strength. With the exception of Hebel-2, the moisture contents are within or quite close to the range of 5% to 15% specified by ASTM C1386.

Table 3.1: Summary of results for compressive strength and density of AAC cores tested at C1386 moisture requirements

Material	Dry Density ρ_{dry} (pcf)	Measured Density at test (pcf)	Moisture Content (%)	Measured Compressive Strength f_{AAC} (psi)
Contec-1	39.9	NA	NA	781
Contec-2	35.9	37.6	4.7	1040
Babb-1	40.2	44.1	9.7	1140
Hebel-2	39.5	40.0	1.3	1330
Ytong-2	34.3	39.1	14.0	650
Babb-2	33.5	35.6	6.3	496

3.3.3 Compression Test Results for Grout Cores

Results of tests for compressive strength and density of ASTM C476 coarse grout cores are presented in Table 3.2. The first data points from the first two specimens tested, Hebel-b1-s1 and Hebel-b1-s2, are not valid because these specimens failed prematurely due to local stresses at uneven surfaces on the loading faces. This problem was solved in the remaining specimens by using sulfur caps.

In several cases the grout strength exceeded the load cell capacity. Since the objective of the test was to determine the modulus of elasticity rather than the compressive strength, the test was discontinued as the load approached the capacity of the load cell. These data points are indicated with asterisks in Table 3.2. The tested compressive strengths range from 2740 psi to above 4500 psi.

Table 3.2: Summary of results for compressive strength of grout cores

Grout specimen	Measured compressive strength f_{AAC} (psi)	Grout specimen	Measured compressive strength f_{AAC} (psi)	Grout specimen	Measured compressive strength f_{AAC} (psi)
Babb-b1-s1	3675	Contec-b1-s1	3290	Hebel-b1-s1	1694
Babb-b1-s2	4550 *	Contec-b1-s2	2740	Hebel-b1-s2	2210
Babb-b1-s3	3870	Contec-b2-s1	3905 *	Hebel-b2-s1	4290 *
Babb-b1-s4	4060	Contec-b2-s2	4270 *	Hebel-b2-s2	4530 *

* Test ended early due to load cell at maximum reading

3.4 Relationship between tested strength of AAC Cores and AAC Cubes

An independent study of the relationship between AAC cores and AAC cubes was performed to justify that the results of compression tests on 4 in. (100 mm) by 8 in. (200 mm) cores are equivalent to a C1386 test performed on 4 in. (100 mm) cubes. This study consisted of testing 6 cubes and 6 cores; three of each specimen type were extracted from a single wall panel. The results of these tests indicate that the test results from 4 in. (100 mm) cubes and 4 in. (100 mm) by 8 in. (200 mm) cylinders are identical.

3.4.1 Specimen Preparation for AAC Cores and AAC Cubes

Cores were removed from AAC elements using a Hilti core drill with a water-cooled diamond coring bit as described in Section 3.3.1. Cubes were removed from AAC wall panels using a dry circular saw to extract roughly cubical blocks of AAC, which were then cut into 4 in. (100 mm) cubes using a water-cooled circular saw.

The modular blocks and floor panels have a nominal thickness of 8 in. (200 mm). In the case of the wall panels, the length of the core was reduced from 10 in. (250 mm) to 8 in. (200 mm) using a water-cooled circular saw. The cut surface was then milled using a dry sander with a fixed disk. All cores were oriented so that they would be tested perpendicular to the direction of rise. The direction of rise was indicated on the cubes. The surfaces of two opposite faces of the cubes were milled using a dry sander.

The cube specimens were air-dried for 7 to 9 days and tested. An initial specimen (Cube Specimen WP1-4) was tested in compression and subsequently oven-dried to determine its moisture content at time of test. Because that moisture content slightly exceeded the maximum value specified in ASTM C1386, the remaining WP1 and WP2 cube specimens were then carefully oven-dried at 120-140 °F (49-50 °C) for 24 to 36 hours. The core specimens from WP1 and WP 2 were air-dried for 14 to 17 days, and the WP2 core specimens were oven-dried at 120-140 °F (49-50 °C) for an additional 24 to 36 hours (RILEM 1993).

3.4.2 Test Method for Compression Tests on AAC Cubes and Cores

Each specimen was tested in a universal testing machine, using a steel plate and load cell at the base of the specimen and a hemispherical head at the top. The test setups for the cubes and the cores are shown in Figure 3.2 and Figure 3.1 respectively. Data were acquired in real time using a HP 7500 scanner.

Figure 3.2 Test setup for compression tests of AAC cubes

The upper contact surface of Cube Specimen WP1-1 was concave downward. After placing the swivel head on the specimen, daylight was visible at the corners of the loaded surface. The upper loaded surface of Cube Specimen WP1-3 was slightly concave downward, and talcum powder was applied to the top and bottom of that interface to eliminate the gap in the same way capping the specimen would eliminate the gap between the test specimen and the loading surfaces. Although the capping procedure was not performed in accordance with ASTM C1386, this test result is not believed to be affected, because the results fall between the lowest and highest results from tests performed in accordance with ASTM C1386.

The remaining cube specimens were tested with their most-plane surfaces in contact with the loading heads. In some cases the loading surface was milled; in other cases, it was not. Neoprene pads would have eliminated the distinction between milled and non-milled, but were not used because they are not addressed by ASTM C1386. The cores were loaded on a cut and milled face at one end, and on a molded or wire-cut surface at the other end.

3.4.3 Compression Test Results for AAC Cubes and Cores

In this section the results of the compression tests are presented. The goal is to compare the results of 4 in. (100 mm) AAC cubes and 4 in. (100 mm) by 8 in. (200 mm) AAC cores to validate the testing of cores rather than cubes. Compressive strengths of the cubes ranged from 346 psi (2.4 MPa) to 503 psi (3.5 MPa). The lowest strength corresponded to Cube Specimen WP1-1, because a local failure occurred at the center of its concave-down loading surface. For that reason, that test is not included in the average. The results of the remaining compression tests on the cubes are presented in Table 3.3. Excluding the results for Cube Specimen WP1-1, the average compressive strength of AAC material taken from Panels WP1 and WP2 was 441 psi (9.0 MPa) and 465 psi (9.7 MPa), with COVs of 9% and 10% respectively. The average compressive strength of the wall-panel cubes was 457 psi (3.1 MPa), with a COV of 9%. The moisture contents were conditioned to nearly 15% with the exception of Cube WP1-4 and Cube WP2-1, whose moisture contents were approximately 20%. Despite these relatively high moisture contents, their compressive strengths were within 1% and 12% of the average of the other specimens. Therefore, their compressive-strength data were included in this evaluation.

Table 3.3: Results from cubes taken from wall panels

Specimen	Surface	f_{AAC} psi (MPa)	Moisture Content (%)	Average psi (MPa)	COV (%)	Average psi (MPa)	COV (%)
WP1-1	Milled (Domed)	346 (2.4)	15.7	441 (3.0)	9.0	457 (3.1)	9.0
WP1-3	Non-milled	413 (2.8)	14.8				
WP1-4	Milled	469 (3.2)	20.1				
WP2-1	Milled	400 (2.8)	19.0	465 (3.2)	9.7		
WP2-2	Non-milled	477 (3.3)	15.6				
WP2-3	Non-milled	503 (3.5)	14.7				
WP2-4	Milled	480 (3.3)	15.0				

The compressive strengths of the cores taken from wall panels ranged from 401 psi (2.8 MPa) to 479 psi (3.3 MPa), and are shown in Table 3.4. The average compressive strengths of cores taken from Panels WP1 and WP2 were 462 psi (3.2 MPa) and 410 psi (2.8 MPa) respectively, with corresponding COVs of 3% and 2%. The average compressive strength of cores taken from Panels WP1 and WP2 was 436 psi (3.0 MPa), with a COV of 7%. The moisture contents of the cores at time of test complied with ASTM C1386.

Table 3.4 Results from cores taken from wall panels

Specimen	f_{AAC} psi (MPa)	Moisture Content (%)	Average psi (MPa)	COV (%)	Average psi (MPa)	COV (%)
WP1-1	448 (3.1)	9.9	462 (3.2)	3.4	436 (3.0)	7.0
WP1-2	460 (3.2)	11.8				
WP1-3	479 (3.3)	11.7				
WP2-1	417 (2.9)	14.0	410 (2.8)	2.0		
WP2-2	413 (2.8)	14.9				
WP2-3	401 (2.8)	14.8				

The difference in compressive strengths for both groups is 21 psi, corresponding to less than 5%. In conclusion, 4 in. (100 mm) AAC cubes and 4

in. (100 mm) diameter AAC cores have essentially the same tested compressive strength.

3.5 STRESS-STRAIN BEHAVIOR OF AAC CORES AND GROUT CORES

Tests were performed to measure the strains up to failure of the AAC or ASTM C476 coarse grout core. Strains were measured with a standard extensometer for testing concrete cylinders consisting of a set of rings attached to the core (Figure 3.3). The lower ring remains fixed and the upper ring pivots around a vertical pin. The vertical displacement reading is measured and converted into a strain by dividing the average displacement by the gage length (distance between pins inside rings). The center ring is optional and measures transverse displacement. The transverse displacement is converted into a strain by dividing the average displacement by the diameter of the specimen. The standard extensometer to measure transverse strain in concrete cylinders was used in all tests except Contec Shipment 1 and Babb Shipment 2. The transverse strain data from the other specimens was sufficient to define the relationship between vertical strain and transverse strain.

Figure 3.3: Standard extensometer for measuring compressive stress versus strain

3.5.1 Stress-Strain Results for AAC Cores

Stress-strain curves for each specimen are presented in Figure 3.4 through Figure 3.9. The unloading branch of the stress-strain curve for theses specimens was reliably determined in Tests performed from Contec Shipment 1. In the remaining specimens the unloading branch was not obtained. This is a function of the speed of loading, the stiffness of the test machine and the speed of data acquisition system. In the remaining groups of specimens, except for Babb Shipment 2 strains of up to 0.0025 were reached and strains of 0.003 or nearly 0.003 were achieved. Data from Babb Shipment 2 indicate strains above 0.0025 for initial tests only. One reason for low strains in the remaining specimens may be slip between the specimen and the standard extensometer for testing concrete cylinders. This is possible since these tests were performed independently from the others. It is also possible that the low compressive strength affected the

results. This stress-strain behavior is different than the remaining 31 specimens. In addition the anomalous material strength may have affected the strain results.

The strains reached over a gradient are larger than the strains reached in a uniaxial compression test. Ferguson reports that maximum useful strains of 0.0025 are achieved in uniaxial compression tests while strains of 0.003 to 0.0045 occur in a beam where a strain gradient exists (1998). The same behavior is expected in AAC and a maximum useful strain of 0.003 is proposed for the design provisions.

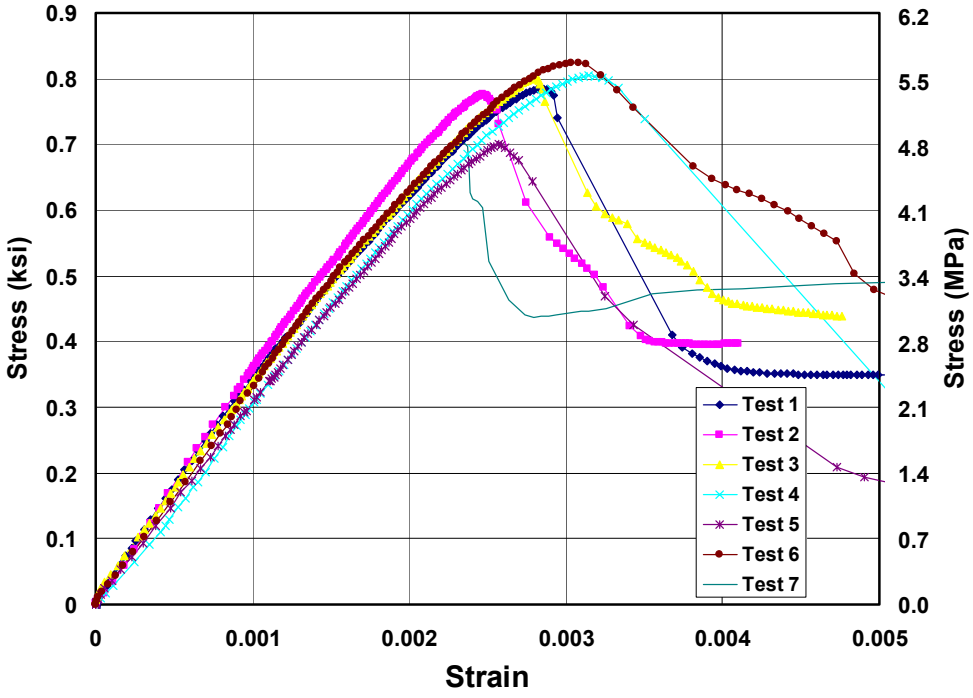

Figure 3.4: Compressive stress versus strain for Contec Shipment 1

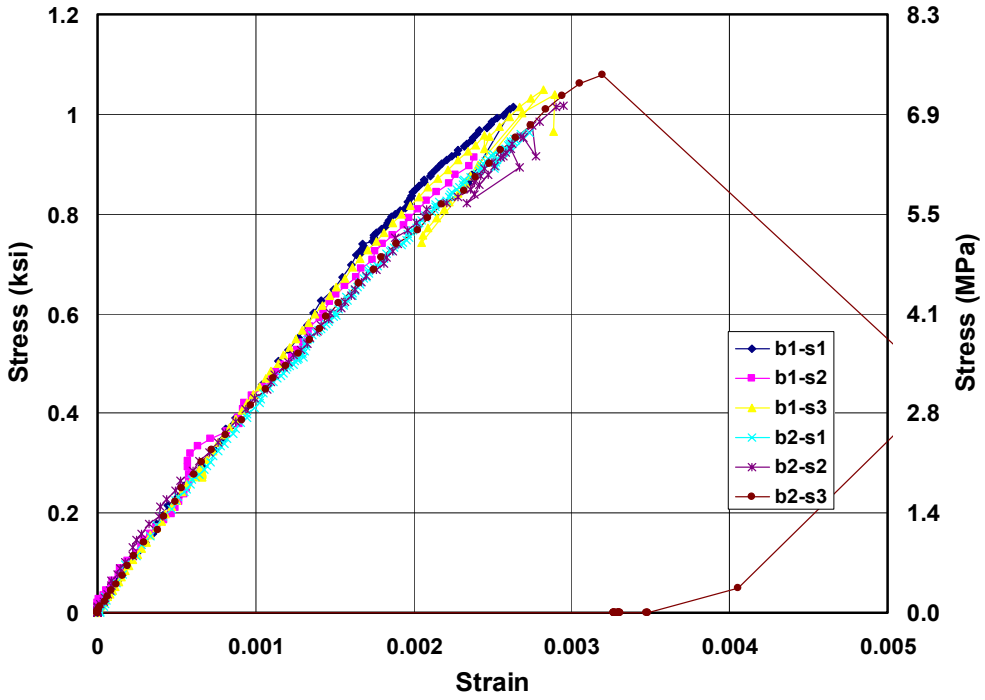

Figure 3.5: Compressive stress versus strain for Contec Shipment 2

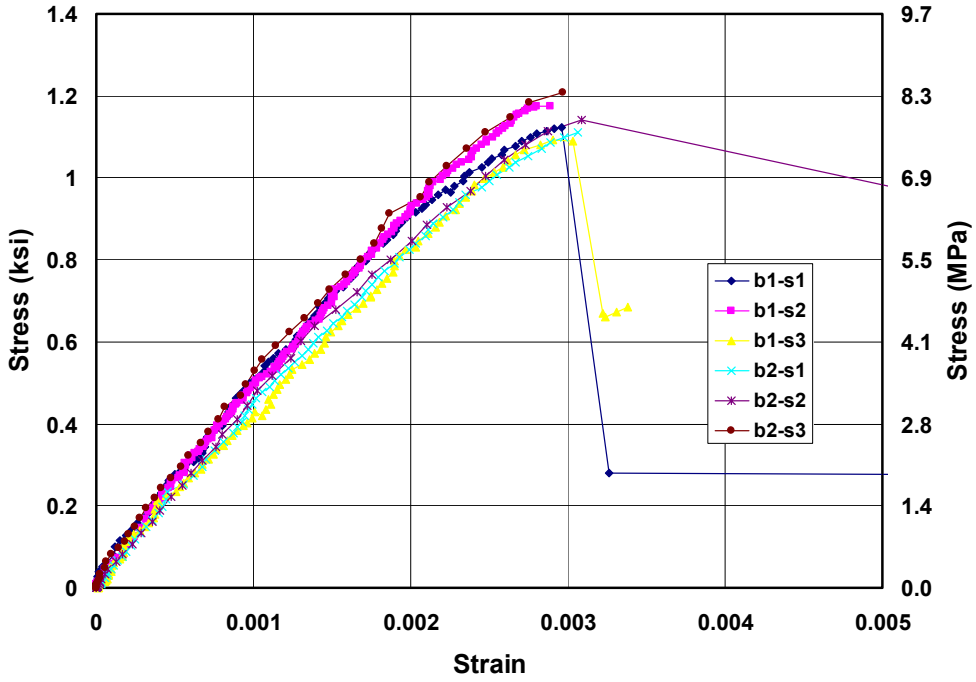

Figure 3.6: Compressive stress versus strain for Babb Shipment 1

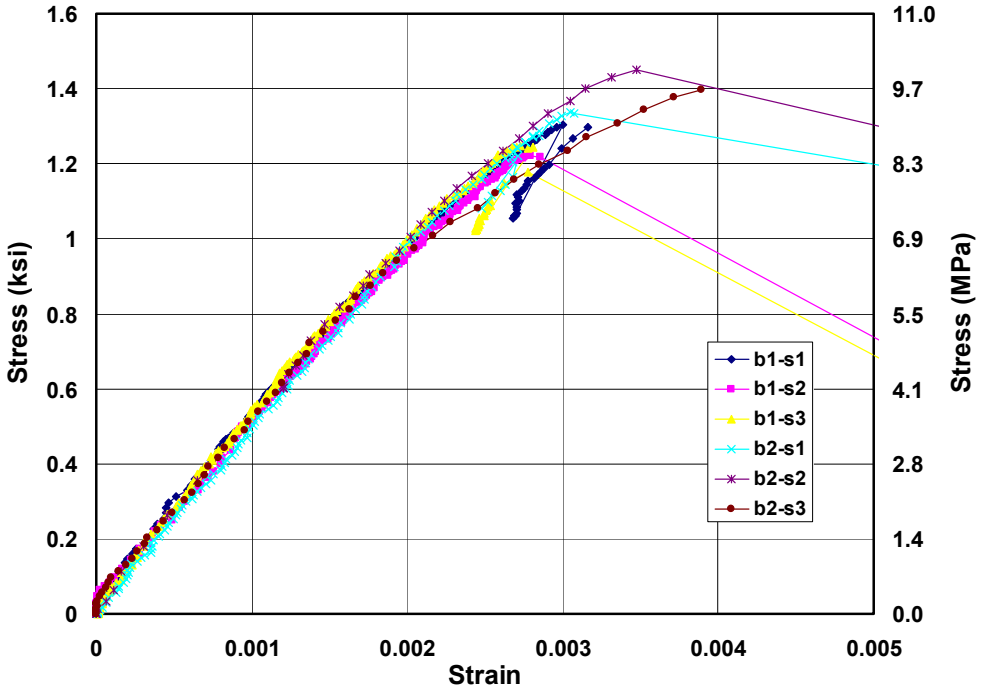

Figure 3.7: Compressive stress versus strain for Hebel Shipment 2

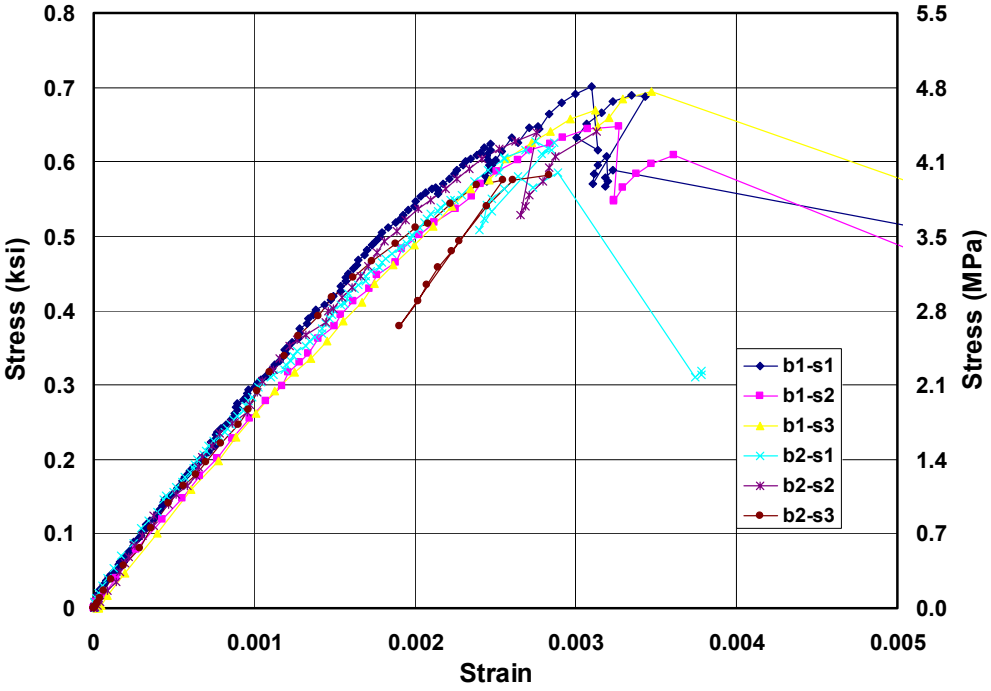

Figure 3.8: Compressive stress versus strain for Ytong Shipment 2

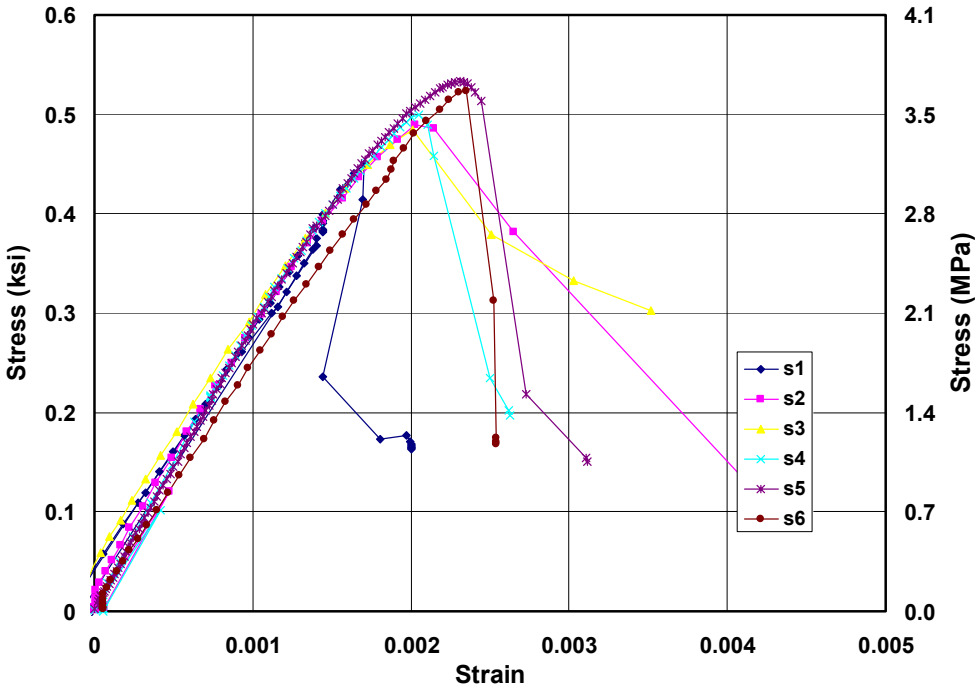

Figure 3.9: Compressive stress versus strain for Babb Shipment 2

3.5.2 Stress-strain Results for Grout Cores

The stress-strain curves for the ASTM C476 coarse grout cores are presented in Figure 3.10 to Figure 3.12. Because this coarse grout is similar to concrete, stress-strain behavior was also expected to be similar to that of concrete. The maximum strain was not determined in five specimens because they were not tested to failure. Out of the remaining four, the maximum strains range from 0.001 to 0.0038, Babb-b1-s1 does not reach the expected value of about 0.0025 for concrete subject to uniaxial compression (Ferguson 1998). This difference may have been due to slipping of the specimen inside the standard extensometer for testing concrete cylinders. Since the coring process leaves the grout surface smooth, slip may have occurred if the horizontal pins were not tight. The

modulus of elasticity calculated using the extensometer agrees with the known results for the modulus of elasticity of concrete as discussed in Section 3.6.2.

The displacement of the crosshead of the loading machine was also measured and was significantly larger than the deformation measured by the standard extensometer. An example of the stress-strain curves using both of these measurements for one set of grout specimens is presented in Figure 3.13. The displacement of the loading crosshead was measured with respect to the floor using a linear potentiometer mounted to a deformed reinforcing bar approximately 4 ft. (1.2 m) long and attached to a fixed base. Any flexural or axial deformation of the bar would cause the measured displacements to be smaller than the actual displacements resulting in an apparent modulus of elasticity larger than the true value. Although the base of the test machine is fixed, a very small movement could introduce error into the results from reading displacements between the loading crosshead and the floor. It would have been better to read the displacement between the base of the test machine and the loading crosshead to verify these results.

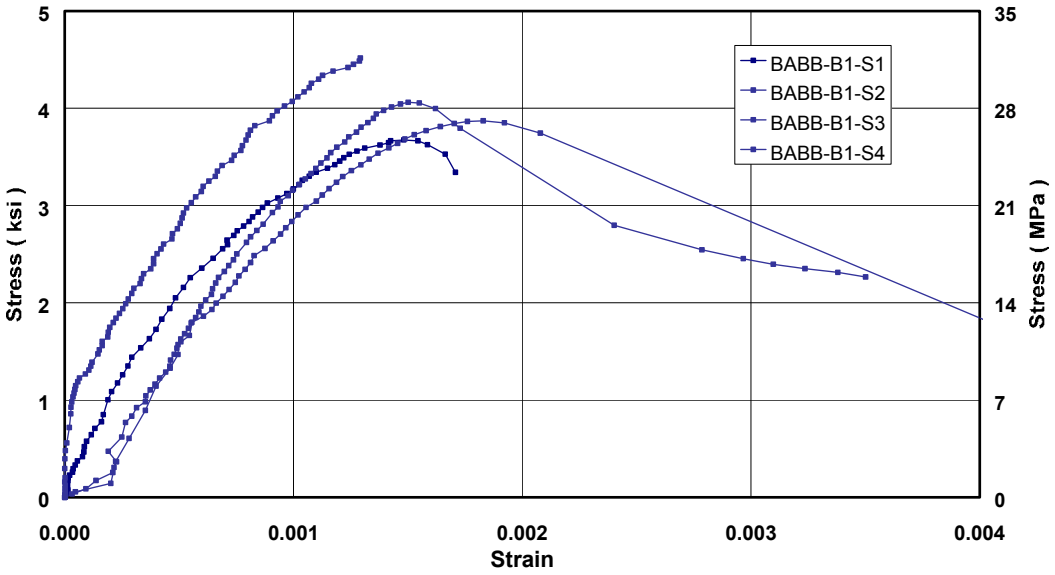

Figure 3.10: Compressive stress versus strain for grout cores cast in Babb Shipment 1

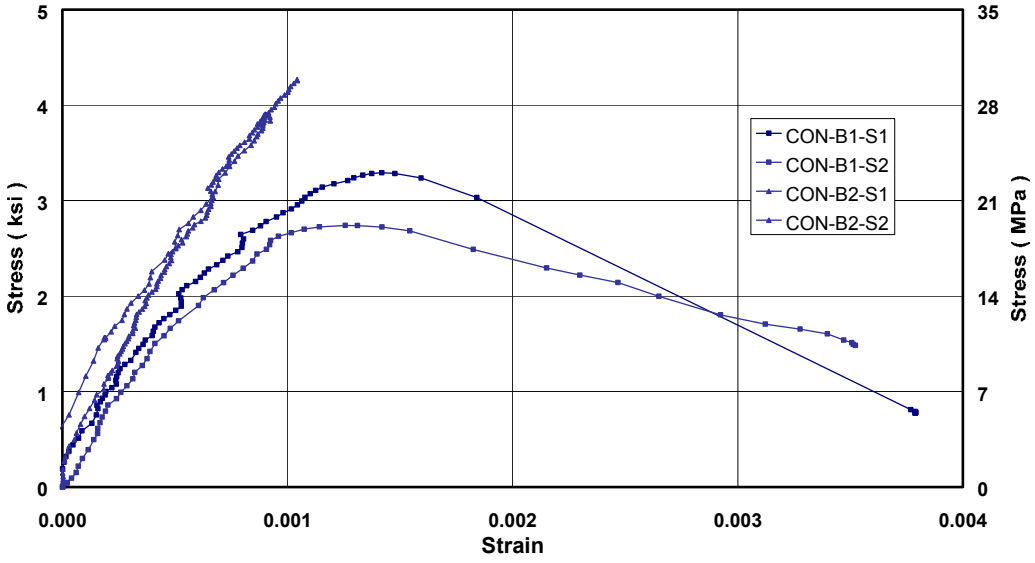

Figure 3.11: Compressive stress versus strain for grout cores cast in Contec Shipment 2

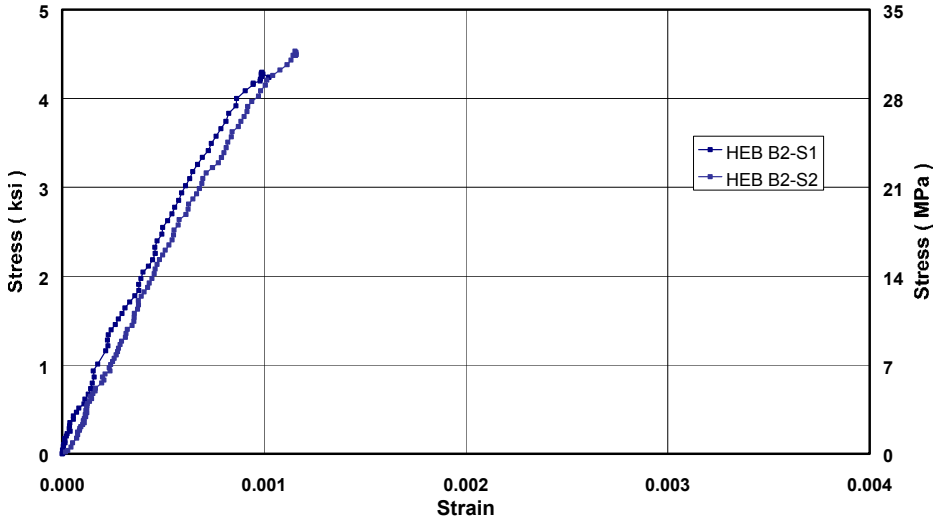

Figure 3.12: Compressive stress versus strain for grout cores cast in Hebel Shipment 2

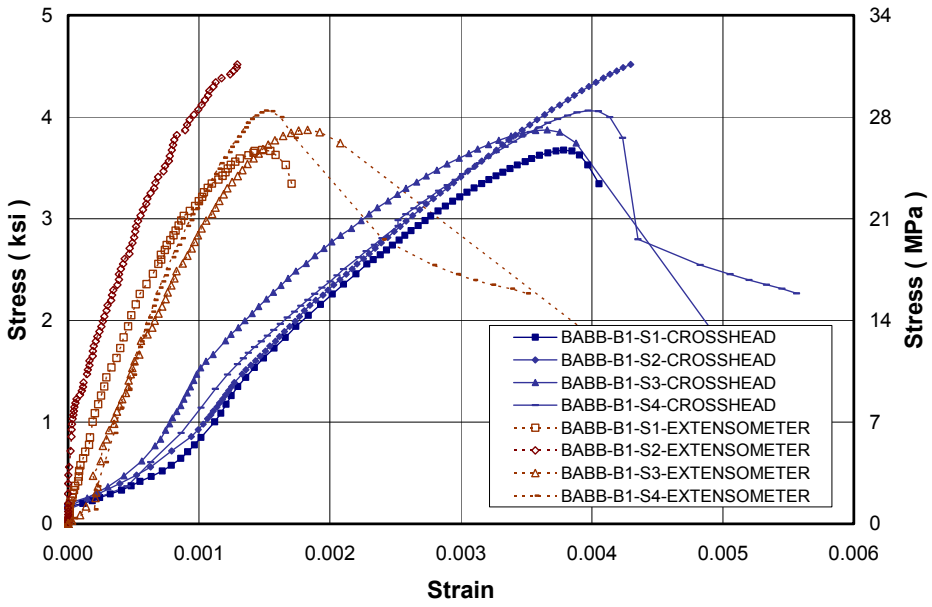

Figure 3.13: Compressive stress versus strain from standard extensometer and test machine loading crosshead movement for grout cores cast in Babb AAC

3.6 MODULUS OF ELASTICITY

The stress-strain relationship of AAC in compression tests performed at UT Austin was used to determine the modulus of elasticity for AAC cores and ASTM C476 coarse grout cores. The specimen preparation and testing procedure is described in Sections 3.3.1 and 3.5.

Additional data for the modulus of elasticity are provided for Ytong material by the University of Alabama at Birmingham and for Aerated Concrete Corporation of America (ACCOA) by Construction Technology Laboratories

(CTL)[9]. Tests at UAB were performed on 4-in. (100 mm) by 4-in. (100 mm) by 12-in. (300 mm) prisms to determine the modulus of elasticity for AAC from three different manufacturers. Compression tests were performed at UT Austin on four 4-in. (100 mm) by 8-in. (200 mm) cores to determine the compressive strength and modulus of elasticity. Strains are reported up to a stress of $0.4f_{AAC}$. This group of tests represents a single material class.

3.6.1 Test Results for Modulus of Elasticity of the AAC Cores

UT Austin tests were performed on 4-in. (100 mm) x 8-in. (200 mm) cores with the load applied perpendicular to the direction of rise. The UT Austin specimens were cured in a laboratory environment and weighed within 3 days of testing. The moisture content varied from 1.3% to 16.6%. This variability could have resulted from coring the specimens at different times.

UAB tests were also performed on prisms with load applied perpendicular to the direction of rise, conditioned to moisture contents between 8% and 15%. The results of modulus of elasticity tests for load perpendicular to the direction of rise for tests at UAB, UT Austin and the previously cited results of tests performed at CTL are presented in Table 3.5.

---

[9] Internal report by Construction Technology Laboratories, Inc. *Material Tests of ACCOA Autoclaved Aerated Concrete (AAC) Masonry Blocks and Assemblies*. CTL Project No. 183035, Construction Technology Laboratories, Inc., Stokie, IL August 11, 1999.

Table 3.5: Modulus of elasticity for load perpendicular to the direction of rise for tests at UAB, UT Austin and CTL

Data Source	Manuf.	Dry Density, pcf	MC (%)	Meas. density (pcf)	Meas. E, ksi	COV (%) for E	Meas. f_{AAC} psi	COV (%) for f_{AAC}
UAB	Hebel	24	8.2	26.0	186	39.5	290	15
	Ytong	35	12	39.2	310	4.9	600	5.3
	Contec	32	13.6	36.4	294	4.9	570	11.5
UT Austin	Contec 1	42.3	5	46.5	323	7.9	781	5.6
	Contec 2	35.9	4.7	37.6	424	2.7	1040	4.7
	Babb 1	39.9	10.4	44.1	462	7.1	1140	3.8
	Hebel 2	39.5	1.3	40.0	511	9.3	1330	6.6
	Ytong 2	34.3	14.1	39.1	269	3.4	650	6.8
	Babb 2	35	16.6	40.8	271	11.7	496	6
CTL	ACCOA	NA	NA	NA	460	13.6	913	5.6

Figure 3.14 shows the modulus of elasticity versus compressive strength for the test results for the averages of 46 specimens. A linear regression for the data from UAB and UT Austin gives Equation (3.1), with a correlation coefficient (R^2) of 0.97. It is proposed to determine the modulus of elasticity as a nonlinear function of the compressive strength, as shown in Equation (3.2) and Figure 3.14. A summary of data from UAB indicates that the modulus of elasticity tested parallel to the direction of rise is 25 ksi (170 MPa) to 50 ksi (340 MPa) lower than the case of loading perpendicular to the direction of rise (Argudo 2003).

$$E = 0.3 f_{AAC} + 105 \qquad \text{Equation (3.1)}$$

$$E = 6500\, f_{AAC}^{0.6}$$

f_{AAC} and E in psi Equation (3.2)

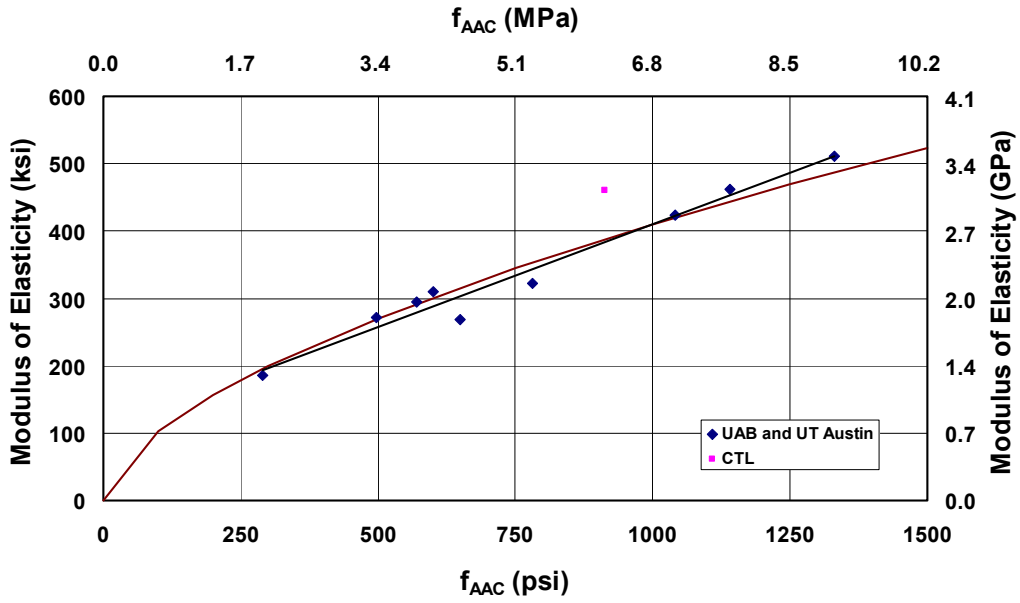

Figure 3.14: Modulus of elasticity versus compressive strength for loading parallel to the direction of rise at UAB and UT Austin

3.6.2 Test Results for Modulus of Elasticity of Grout Cores

Results for the modulus of elasticity of ASTM C476 coarse grout cores, presented in Table 3.6, range from 3275 ksi (24 GPa) to 4790 ksi (33 GPa), with an average of 4150 ksi (28.6 GPa) and a COV of 14.6%. The tested values of modulus of elasticity within each batch are close to the average for that batch, suggesting that the water-cement ratio could have varied between batches of coarse grout.

The modulus of elasticity for each specimen based on the displacement between the loading crosshead and the base of the test machine, is also presented. Since the modulus of elasticity based on the extensometer readings and on the loading cross-head of the test machine vary significantly, both results were

compared to the modulus of elasticity of concrete defined in the ACI 318-02 (Equation (3.3)). The modulus of elasticity for coarse grout is expected to be similar to that of concrete because of the presence of pea gravel in the coarse grout. The better agreement between the modulus of elasticity based on the extensometer readings and Equation (3.3), confirms the suspicions regarding error in the tests measuring only the displacement of the loading crosshead.

$$E_{grout} = 57{,}000\sqrt{f_{grout}} \qquad \text{Equation (3.3)}$$

E_{grout} in psi

f_{grout} in psi

Table 3.6: Modulus of elasticity for grout cores based on extensometer readings

Specimen	E based on ring displacement ksi (GPa)	Average E per batch ksi (GPa)	Average f_{grout} per batch psi (MPa)	E based on Equation (3.3)
Babb-b1-s1	4475 (30.8)	-	-	-
Babb-b1-s2	3945 (27.2)	-	-	-
Babb-b1-s3	3275 (22.6)	-	-	-
Babb-b1-s4	3410 (23.5)	3775 (26.0)	4040 (27.8)	3623 (25.0)
Contec-b1-s1	3470 (23.9)	-	-	-
Contec-b1-s2	4025 (27.7)	3749 (25.8)	3020 (20.8)	3132 (21.6)
Contec-b2-s1	4795 (33.0)	-	-	-
Contec-b2-s2	4590 (31.6)	4693 (32.3)	4085 (28.1)*	3643 (25.1)
Hebel-b2-s1	4740 (32.6)	-	-	-
Hebel-b2-s2	4790 (33.0)	4765 (32.8)	4500 (31.0)*	3824 (26.3)

3.7 TENSILE STRENGTH

3.7.1 Splitting Tensile Strength

Data for splitting tensile strength of material in each AAC shipment were obtained at UT Austin using tests performed in accordance with ASTM C1006. Each point in Figure 3.15 Figure 3.16 represent the average for a group of specimens. A total of 49 specimens are included in the results of Figure 3.16. The specimens were oriented so that splitting tensile stresses acted parallel to the direction of rise. Data on field density of each shipment were also obtained. In most cases, densities were determined within one day of when splitting tensile strengths were performed. In the Ytong 1 and Contec 1 specimens the difference in time was as great as 4 months. This is not believed to be significant, however, because those times were more than a year after the production date of the material. Although the densities are not required by ASTM C1006, it is recommended to measure the densities of units subject to ASTM C1006 tests to confirm that the moisture content falls within the range of 5%-15% as required by ASTM C1386.

Eight data points are available, each representing a series of 4 to 8 specimens. The collected data are presented in Table 3.7, and a graph of the relationship between tensile strength and field density shows a good R-squared value of 0.84 (Figure 3.15). Equation (3.4) is used to determine the splitting tensile strength as a function of the densities measured under field conditions at UT Austin. With the exception of Hebel Shipment 2 and Contec Shipment 2 Test a, the moisture contents in Table 3.7 are between 4.1 and 16.6. Because those moisture contents generally fall in the 5% to 15% range permitted by ASTM C1386, the corresponding densities are referred to here as “1386 densities.”

There are two data points for Contec Shipment 2. The splitting tensile strength, field density and dry density for the first data point (Contec 2a) were presented in a preliminary report. After those data were submitted, it was found that the field and dry densities corresponded to a calculated moisture content less than zero. This value is physically impossible, so the tests were repeated (Contec 2b). Later, a calculation error was found in the field density originally reported for Contec 2a. That value is still regarded as suspicious, however, because the corresponding moisture content is 45%. For this reason, values for Contec 2b only (and not Contec 2a) are shown in Figure 3.16.

Finally, Babb Shipment 2 is not included in the linear regression of Figure 3.15 because the splitting tensile strength appeared to be anomalous. Further investigation revealed a low compressive strength for that material. The relationship between splitting tensile strength and compressive strength is presented in Figure 3.16. The linear regression of Equation (3.5) has a correlation coefficient (R^2) value of 0.93, which is better than the correlation coefficient (R^2) of 0.84 from the density relationship (Figure 3.15). Expressing the splitting tensile strength as a function of the compressive strength describes the test results including the apparently anomalous data for Babb Shipment 2 and provides an improved correlation coefficient. A similar case existed for the average of the results of a group of tests performed on a shipment of material tested at the University of Alabama at Birmingham (Ytong G3). The tested modulus of rupture, shear strength, tensile bond strength and compressive strength were characteristically lower for Ytong G3 than other AAC material of the same density. The low tested values for the modulus of rupture and shear strength are

included if they are expressed as a function of the compressive strength (Argudo 2003).

Equation (3.6) relates the splitting tensile strength and the square root of the compressive strength; the correlation is as good as for the linear regression. In addition, this expression passes through the origin of the graph, indicating that as the compressive strength of the material approaches zero so does the splitting tensile strength. This expression is also consistent in form with the ACI 318-02 expression for tensile strength.

Table 3.7: Results of C1006 splitting tensile strength tests performed at UT Austin

Shipment	Average f_t psi (MPa)	COV (%)	Measured Density pcf (kg/m^3)	Dry Density pcf (kg/m^3)	Moisture Content (%)	Average f_{AAC} psi (MPa)
Contec 1	71.2 (0.49)	10.5	42.3 (677)	39.9 (638)	6.0	781 (5.4)
Ytong 1	55.3 (0.38)	14.2	32.8 (525)	31.5 (504)	4.1	517 (3.6)
Ytong 2	62.7 (0.43)	4	38.7 (620)	34.0 (544)	13.8	650 (4.5)
Hebel 2	88.4 (0.61)	5.2	48.9 (782)	39.5 (632)	23.8	1330 (9.2)
Contec 2b	74.6 (0.51)	1.8	37.9 (606)	35.9 (574)	5.6	1040 (7.2)
Babb 1	84.7 (0.58)	10.1	45.2 (723)	39.9 (638)	13.3	1140 (7.9)
Babb 2a	52.5 (0.36)	12.7	42.6 (653)	34.5 (560)	23.5	495 (3.4)
Babb 2b	45.0 (0.31)	14.9	40.8 (681)	35.0 (552)	16.6	495 (3.4)
Contec 2a	54.0 (0.37)	6.8	52.2 (835)	35.9 (574)	45.4	1040 (7.2)

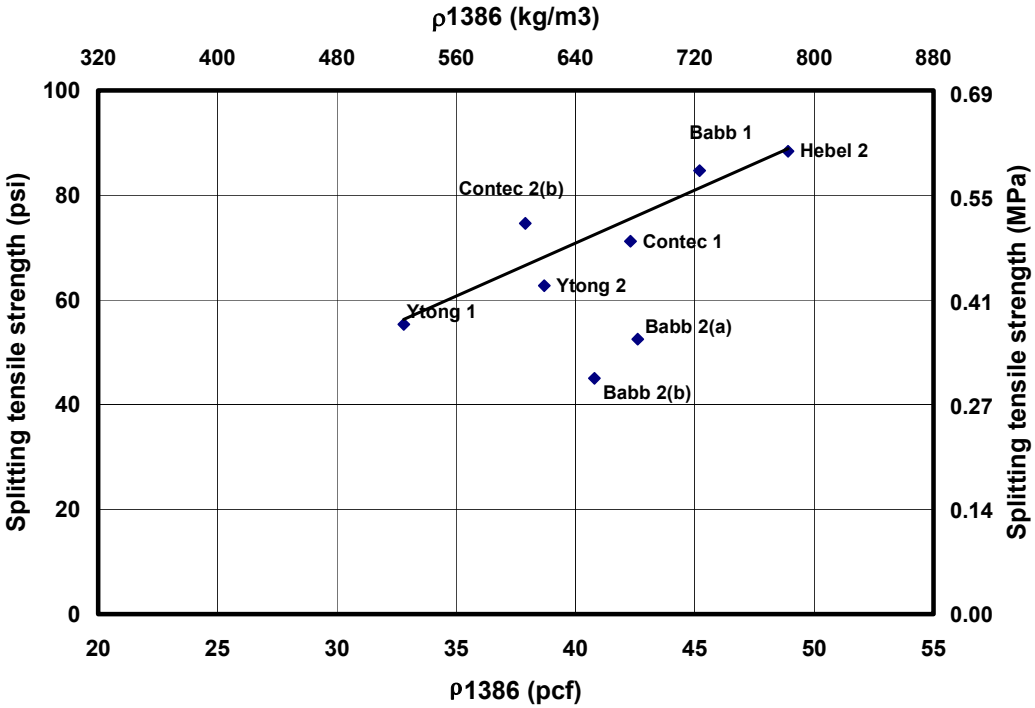

Figure 3.15: Splitting tensile strength versus density

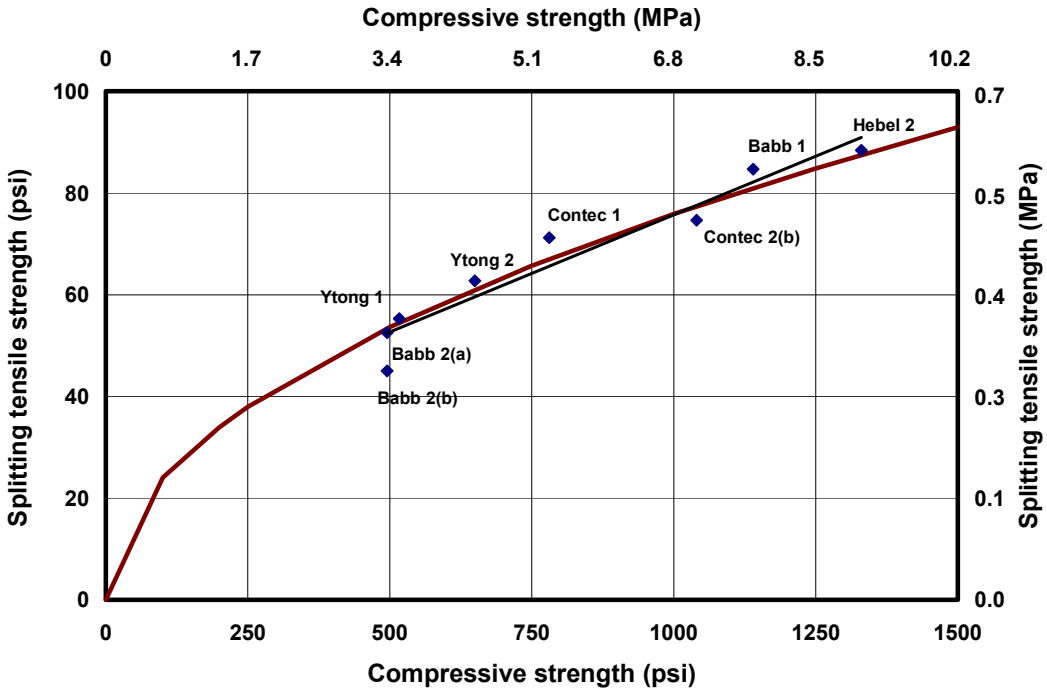

Figure 3.16: Splitting tensile strength versus compressive strength

$$f_t = 2\rho_{1386} - 10.3$$

ρ_{1386} in pcf, f_t in psi Equation (3.4)

$$f_t = 0.05 f_{AAC} + 30$$

f_t and f_{AAC} in psi Equation (3.5)

$$f_t = 2.4\sqrt{f_{AAC}}$$

f_t and f_{AAC} in psi Equation (3.6)

The results of the relationship between the splitting tensile strength and the compressive strength are further verified by the Dutch standard NEN 3838 which defines the design tensile strength f_t' as a function of the specified compressive strength , f_{AAC}' (Argudo 2003).

3.7.2 Relationship between Modulus of Rupture and Splitting Tensile Strength

At UT Austin, using splitting tensile data from UT Austin and modulus of rupture data from UAB, a relationship between splitting tensile strength and modulus of rupture was determined. The average of three data points for each class of AAC is reported in Table 3.8. The dry densities reported by UAB were converted to the corresponding densities at a moisture content of 10%, a value that represents the average the range of moisture contents (8% to 12%) of the specimens in the UAB tests (Snow 1999).

Although UT Austin did not record moisture contents for their splitting tensile tests, those moisture contents were subsequently estimated based on similar specimens stored under similar conditions in the laboratory. Those specimens had moisture contents averaging about 10%.

Table 3.8 shows values of modulus of rupture reported by UAB for different classes and corresponding oven-dry densities of AAC. Using a moisture content of 10% as explained above, the corresponding density for those specimens is calculated. Using Equation (3.4), the splitting tensile strength of those specimens at that same density is also calculated. The average ratio between the

reported modulus of rupture and the calculated splitting tensile strength is 2.26, with a COV of 19.1%. For design purposes, a ratio of 2.0 is proposed (Equation (3.7)). A detailed comparison of Equation (3.8) with the tests performed in the final UAB report is presented in Argudo (2003).

$$f_r = 2f_t \qquad \text{Equation (3.7)}$$

$$f_r = 2.26f_t \qquad \text{Equation (3.8)}$$

Table 3.8: Ratios between measured modulus of rupture at C1386 density and splitting tensile strength estimated using oven-dry density for different classes of AAC

Oven-dry density pcf (kg/m^3)	Calculated density at 10% MC pcf (kg/m^3)	Calculated f_t at 10% MC psi (MPa)	Measured f_r at ~10% MC psi (MPa)	f_r / f_t
32.0 (2.0)	35.2 (2.2)	60.2 (0.41)	123.0 (0.85)	2.04
38.0 (2.4)	41.8 (2.6)	73.4 (0.51)	202.0 (1.39)	2.75
42.0 (2.6)	46.2 (2.9)	82.2 (0.57)	162.0 (1.12)	1.97

3.8 DIRECT SHEAR

Design of the assemblage specimen required verification of the direct-shear capacity between elements. For that purpose, direct-shear tests were conducted on AAC modular units to determine the direct-shear capacity of different types of joints.

3.8.1 Specimen Construction for Direct-shear Tests

Specimens were developed to determine the direct-shear capacity between ASTM C476 coarse grout and AAC, and between thin-bed mortar and AAC, or

between a combination of grout and thin-bed mortar. Additional specimens were developed to determine the coefficient of friction between AAC and AAC.

3.8.1.1 Specimen construction for direct-shear tests to determine the capacity of AAC joints

Examples of each specimen are presented in Figure 3.17 through Figure 3.22. The unit dimensions indicated in Figure 3.17 and Figure 3.18 are listed in Table 3.9.

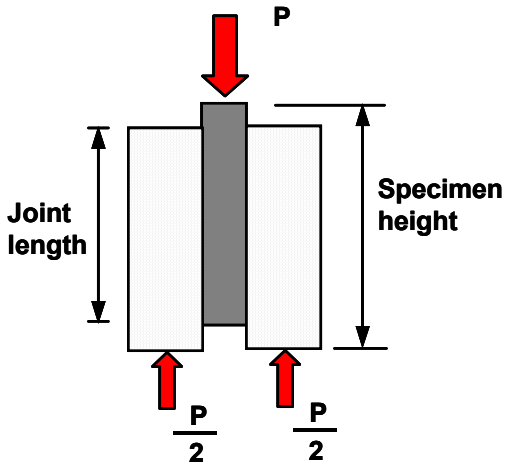

Figure 3.17: Elevation of direct-shear specimens (grout only)

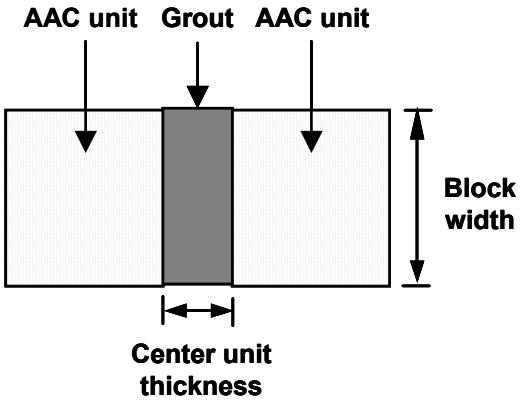

Figure 3.18: Plan view of direct-shear specimens (grout only)

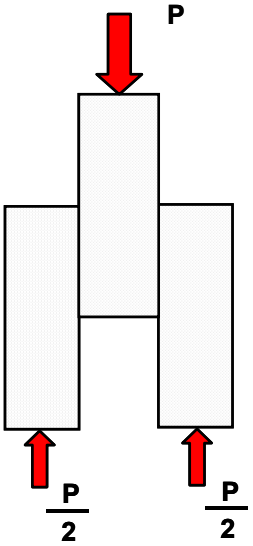

Figure 3.19: Elevation of direct-shear specimens (thin-bed mortar only)

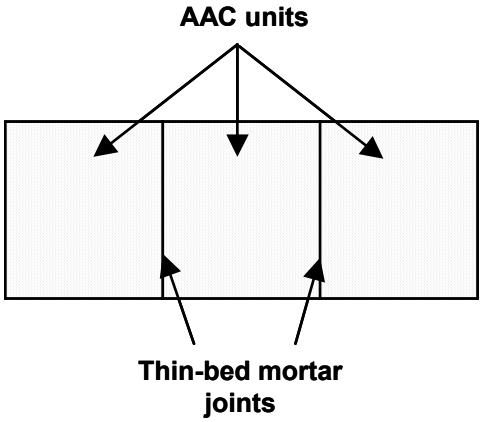

Figure 3.20: Plan view of direct-shear specimens (thin-bed mortar only)

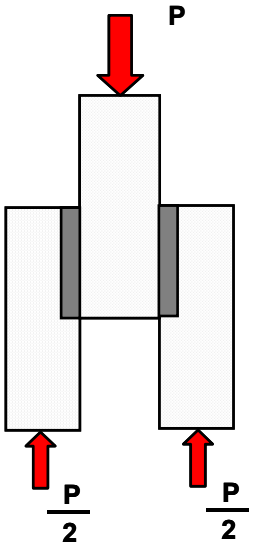

Figure 3.21: Elevation of direct-shear specimens (thin-bed mortar and grout)

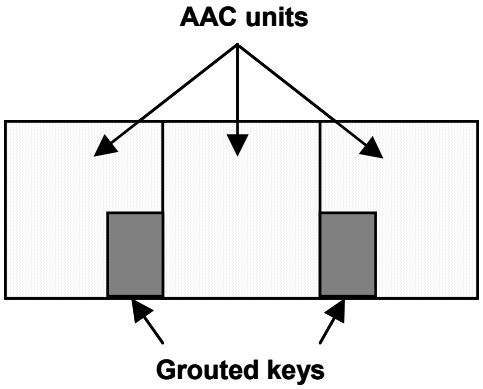

Figure 3.22: Plan view of direct-shear specimens (thin-bed mortar and grout)

Table 3.9: Dimensions of direct-shear specimens

Specimen Type	Block width in. (mm)	Joint length in. (mm)	Center unit thickness in. (mm)	Specimen height in. (mm)
Grout only	7.75 (197)	22 (381)	4 (102)	27-28 (686-711)
Thin-bed mortar only	7.75 (197)	15 (559)	7.75 (197)	33 (838)
Grout and thin-bed mortar	7.75 (197)	12 (305)	7.75 (197)	36 (914)

Notation for each specimen type is as follows: DS-GR-1, direct-shear specimen with grout only; DS-TB-1, direct-shear specimen with thin-bed mortar only; and DS-TB-GR-1, direct-shear specimen with grout and thin-bed mortar. The number following the notation corresponds to the specimen number.

In each case, the joint length was limited so that the expected capacity of the specimens as governed by direct shear, would be less than the capacity as limited by crushing of the AAC.

The construction procedure was intended to represent field conditions.

- The grout-only specimens were constructed by placing AAC along the entire length of the joint, to reproduce the loss of water associated with placing grout adjacent to AAC. Where the grout did not touch the AAC, an AAC block was placed next to the grout, and a paper towel was used as a permeable bond breaker. The AAC units created the formwork for the grout, and were pre-wetted before the grout was placed.

- The thin-bed mortar specimens were constructed on their sides. This allowed the weight of the block to apply pressure on the thin-bed mortar joint, and represents field conditions for either panels or blocks. Each block surface was cleaned with a wet brush. Two batches of AAC were used in the construction of the 5 direct-shear specimens with thin-bed mortar only. Mortar was applied to one unit, and the next unit was placed; the second unit was subjected to small lateral movements until excess mortar was observed at the joint interface, indicating sufficient mortar coverage.

- The combined specimens were constructed in two steps. First, thin-bed mortar was applied to the units, and they were clamped together to cure. Two days later, the grout was cast in a 2 in. (51 mm) by 4 in. (100 mm) cutout. Again, the AAC served as the formwork, and was pre-wetted before casting the grout.

3.8.1.2 Construction of direct-shear tests to determine the coefficient of friction between AAC and AAC

Additional direct-shear tests were performed using unmortared AAC units clamped together to determine the coefficient of friction between AAC and AAC. The clamping force was applied with threaded rods (Figure 3.23) running through the centerline of a 3-in. (76-mm) core in each AAC modular block. Three specimens were constructed, and each was subjected to three levels of applied clamping force: 5 kips (22 kN); 10 kips (44 kN); and 15 kips (67 kN). No damage was observed from the clamping force or the observed sliding. The notation for each coefficient of friction test begins with DS-COF. The first number identified the specimen number and the second number identifies the value of clamping force in kips.

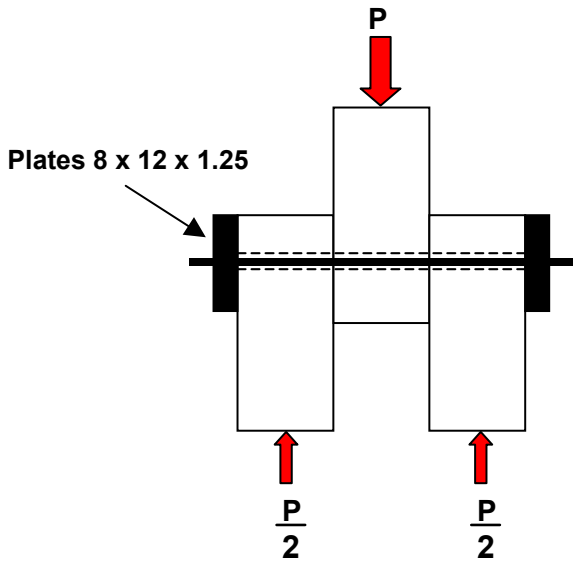

Figure 3.23: Direct-shear specimen to determine coefficient of friction for AAC

3.8.2 Test setup for Direct-shear Tests

Each specimen was tested in a Satec 600-kip (2760 kN) universal testing machine with a hemispherical loading head. Load was applied and monitored using the load cell from the universal machine. The vertical displacement of the center unit was measured using a linear potentiometer placed on the lower table of the testing machine. The specimen was also marked with a horizontal line perpendicular to the interface between individual AAC units, making relative displacements across that interface directly visible. Data were recorded in real time using a Hewlett-Packard 7500 scanner and the FSEL data-acquisition software. The test setup for the combined thin-bed mortar and grout specimens is shown in Figure 3.24.

Figure 3.24: Typical setup for direct-shear tests

3.8.3 Results of Direct-shear Tests with Grout-only Specimens

The peak load and maximum stress for each specimen are presented in Table 3.10. The average shear stress for each joint is the total load divided by the observed failure area (Equation (3.9)). The shear strength is based on the maximum load resisted by each specimen. The mean shear strength is 58 psi (0.4 MPa), with a COV of 22%. The proposed design shear strength of this joint is 36 psi (0.25 MPa) which corresponds to the 5% lower fractile, 36.7 psi (0.25 MPa), of this test data. A very small lower fractile was selected due to the brittle nature of this failure mechanism, the small number of test specimens, and the variability among those three data points. The ratios of tested values to the proposed design values range from 1.4 to 2.0.

Table 3.10: Summary of results from direct-shear tests (grout only)

Specimen	Test age, days	Maximum load, kips (kN)	Maximum stress, psi (MPa)
DS-GR-1	16	16.9 (75)	49.6 (0.34)
DS-GR-2	16	24.8 (110)	72.7 (0.5)
DS-GR-3	16	17.5 (78)	51.3 (0.35)
		Average	58 (0.4)
		COV (%)	22

$$\tau_{ave} = \frac{P}{A} \qquad \text{Equation (3.9)}$$

Each failure can be classified as a shear-bond failure, a material failure or a combination of the two. A shear-bond failure is characterized by a smooth surface along the grout side of the failure. A material failure has AAC along the grout side of the joint failure. In the case of the direct-shear specimens at UT Austin, the failure is combined. This can be observed by the presence of smooth

surfaces and AAC material along the grout failure surface (Figure 3.25). For all failure surfaces, at least 30% of the surface area was covered by AAC, indicating that failure was influenced by the strength of the AAC material itself. Pre-wetting of the AAC units may have increased the shear-bond capacity of the interface, and forced the failure to occur in the AAC material.

Figure 3.25: Failure surface of Direct-shear Specimen DS-GR-1

Force-displacement graphs for the grout-only specimens are presented in Figure 3.26. In each case, a peak load was reached; and the load dropped at the same time as a crack formed in one joint. The load then increased to another peak. The second increase in load is due to a redistribution of the load at the cracked joint. This redistribution is attributed to an initial joint bond failure and then a subsequent material failure. The abrupt increases in displacement without any increase in load and increases in load without any corresponding increase in

displacement for Specimens DS-GR-2 and DS-GR3 are due to sticking of the piston in the linear potentiometer used in those two specimens.

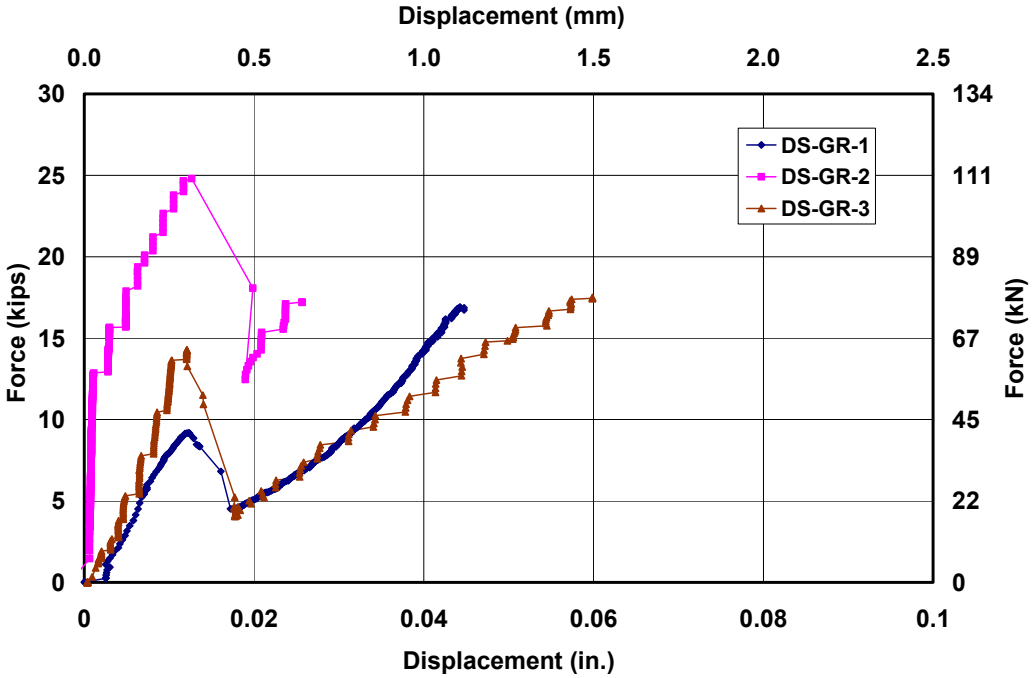

Figure 3.26: Force-displacement graph for direct-shear specimens (grout only)

3.8.4 Results of Direct-shear Tests with Thin-bed Mortar Specimens

The peak load and maximum stress for each specimen are presented in Table 3.11. The average shear stress for each joint is the total load divided by the area of the joint (Equation (3.9)). The shear strength is based on the maximum load resisted by each specimen. The mean shear strength is 72 psi (0.5 MPa), with a COV of 40%.

Table 3.11: Summary of results from direct-shear tests (thin-bed mortar only)

Specimen	Test age, days	Maximum load, kips (kN)	Maximum stress, psi (MPa)
DS-TB-1	20	26.2 (117)	112.8 (0.78)
DS-TB-2	20	7.9 (35)	34.0 (0.23)
DS-TB-3	20	18.6 (83)	79.8 (0.55)
DS-TB-4	21	17.5 (78)	75.1 (0.52)
DS-TB-5	21	13.5 (60)	58.1 (0.4)
		Average	72 psi (0.5)
		COV (%)	40

Due to the large variation in the test results for the direct-shear strength, it was suspected that the thin-bed mortar may be sensitive to the mixing process. Additional specimens were tested with two batches of thin-bed mortar mixed by different individuals; the construction was performed by one individual, to eliminate the possibility of differences in construction technique. Three specimens were tested with the first set of thin-bed mortar; these specimens are designated with a "1" after the "TB" in the name. The three specimens constructed with the second batch of thin-bed mortar were designated with a "2" after the "TB". The ratio of water to cementious material by weight for the TB1 specimens was 0.31 and the water-cement for the TB2 specimens was 0.34. The test results for these specimens are presented in Table 3.12. The measured stresses for Control Group 1 ranged from 27 psi (0.2 MPa) to 82 psi (0.6 MPa) while the range of measured stresses for Control Group 2 ranged from 29 psi (0.2 MPa) to 97 psi (0.7 MPa). This high variation is not sensitive to the construction practices in mixing thin-bed mortar. The final average of all the specimens is 63.9 psi (0.44 MPa) with a corresponding COV of 44%. The proposed design value for the shear strength of a joint is 18 psi (0.12 MPa), corresponding to a 5% lower fractile of the test results. Again, a very small lower fractile was selected due to the brittle nature of this failure mechanism, the small number of data points

available, and the variability among those three data points. The ratios of tested values to the proposed design values range from 1.5 to 5.4.

Table 3.12: Summary of results from additional direct-shear tests (thin-bed mortar only)

Specimen	Test age, days	Maximum load, kips (kN)	Maximum stress, psi (MPa)
DS-TB1-1	13	10.9 (49)	46.3 (0.3)
DS-TB1-2	13	19.3 (86)	81.9 (0.6)
DS-TB1-3	13	6.3 (28)	26.7 (0.2)
DS-TB2-1	14	6.9 (31)	29.1 (0.2)
DS-TB2-2	14	22.9 (102)	97.2 (0.7)
DS-TB2-3	14	14.5 (65)	61.4 (0.4)

The failure modes for these specimens ranged from a bond failure at the joint to a combined joint and material failure. In some specimens, flexural cracks were observed on the outer side of the legs resulting from the eccentricity of reactions and tensile stresses due to Poisson effects. The eccentric reaction might produce local moments at the joint surfaces, decreasing the tested shear strength. Eliminating the specimens with these flexural cracks did not significantly change the average shear stress or reduce the COV, however. Furthermore, eliminating the results of joints with a material failure did not significantly change the average shear stress or the COV.

Force-displacement graphs for the direct-shear specimens (thin-bed mortar only) are presented in Figure 3.27. As with the grout-only tests, the load reduced abruptly when a crack formed in one joint. In three cases, the load increased beyond the initial peak.

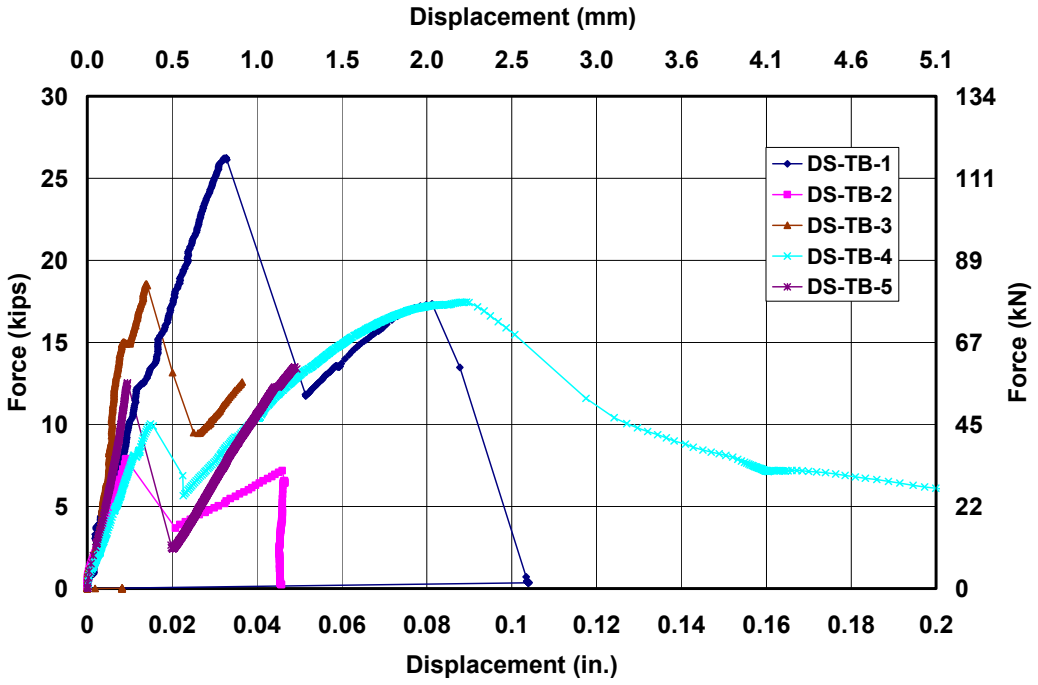

Figure 3.27: Force-displacement graph for direct-shear specimens (thin-bed mortar only)

3.8.5 Results of Direct-shear Tests with Grout and Thin-bed Mortar Specimens

Direct-shear specimens with ASTM C476 coarse grout and thin-bed mortar may fail by propagation of a crack directly through the joint between AAC units, or around the perimeter of the grouted key (Figure 3.28). In tests performed at UT Austin, some failures occurred around the perimeter of the grouted cell rather than straight through the joint. The area used in Equation (3.9) was the entire length of the failure path for each specimen (Figure 3.28), multiplied by the vertical length of the joint between units. In this way, the failure path was

considered in calculating the shear strength. The mean shear strength is 44 psi (0.3 MPa) with a COV of 11%. The 5% lower fractile for this test data is 36 psi (0.24 MPa).

Table 3.13: Summary of results from direct-shear tests

Specimen	Test age, days	Maximum load, kips (kN)	Maximum stress, psi (MPa)
DS-TB-GR-1	21	8.4 (38)	39.9 (0.28)
DS-TB-GR-2	21	10.4 (46)	49.5 (0.34)
DS-TB-GR-3	14	8.0 (36)	42.9 (0.3)
		Average	44 (0.3)
		COV (%)	11

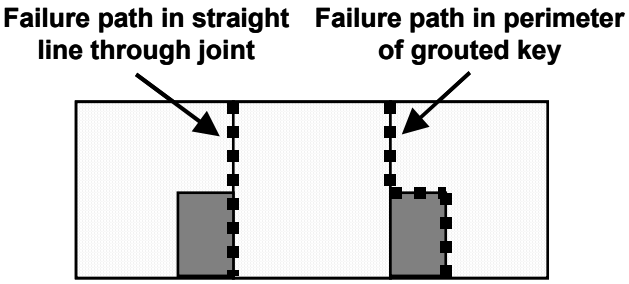

Figure 3.28: Potential failure paths in direct-shear specimens (thin-bed mortar and grout)

Specimens with grout and thin-bed mortar had a capacity lower than that of the mortar-only or the grout-only specimens. One possible explanation could be shrinkage cracks, which could decrease the shear capacity of the joint, and which were observed at the grout-AAC interface prior to testing. Shrinkage cracks were not observed in the grout-only specimens, even though curing conditions were the same for both types of specimens.

Force-displacement graphs for direct-shear specimens (combined grout and thin-bed mortar) are presented in Figure 3.29. In these tests, the load dropped at the formation of a crack in the grout or at crushing of a corner of the lower AAC unit. Since the cutouts in the AAC units extended along the entire length of the unit, a smaller portion of the unit resisted compression below the joint. After each drop in load, a subsequent increase was observed.

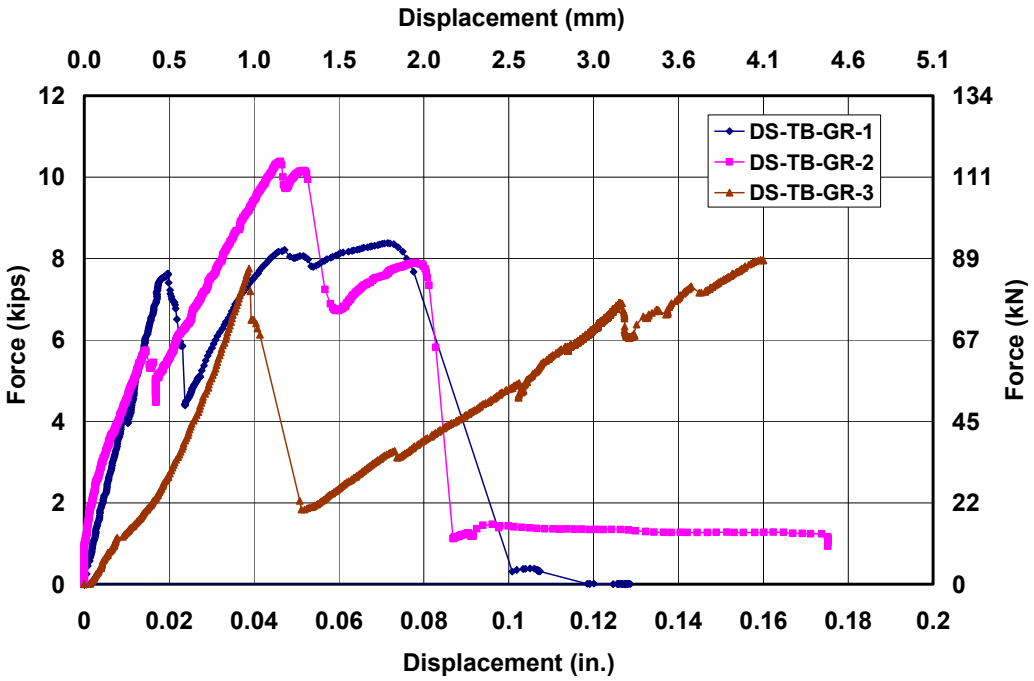

Figure 3.29: Force-displacement graph for direct-shear specimens (thin-bed mortar and grout)

3.8.6 Results of Direct-shear Specimens with Clamping force

The test results are presented in Table 3.14. The coefficient of friction is determined by Equation (3.10), where P is the clamping force. The average coefficient of friction is 0.85, with a COV of 8%. A 10% lower fractile is 0.76,

and the proposed design value for coefficient of friction between AAC and AAC is 0.75.

Table 3.14: Results for coefficient of friction between AAC and AAC

Specimen	Maximum Vertical Load kips (kN)	Measured Clamping Force kips (kN)	Coefficient of Friction
DS-COF-1–5	7.7 (34)	4.8 (21)	0.80
DS-COF-2–5	9.3 (41)	5.3 (24)	0.87
DS-COF-3–5	8.8 (39)	4.8 (21)	0.93
DS-COF-1–10	13.7 (61)	9.2 (41)	0.75
DS-COF-2–10	20.3 (90)	10.6 (47)	0.96
DS-COF-3–10	17.1 (76)	10.3 (46)	0.83
DS-COF-1–15	24.4 (109)	14.1 (63)	0.86
DS-COF-2–15	27.9 (124)	16.1 (72)	0.87
DS-COF-3–15	21.5 (96)	14.0 (62)	0.77
		Average	0.85
		COV (%)	8

$$\mu = \frac{P}{2N} \qquad \text{Equation (3.10)}$$

3.9 STRESS-STRAIN BEHAVIOR OF REINFORCEMENT

Stress-strain tests were performed on three of the #5 (16 mm diameter) reinforcing bars used in the shear wall specimens. The stress-strain curves are presented in Figure 3.30. The average yield strength is 77 ksi (530 GPa), which is almost identical to the reported mill tests of 75 ksi (520 GPa). Measured strains of 0.05 were obtained for all three specimens. The ultimate strength of the reinforcement is 110 ksi (758 GPa).

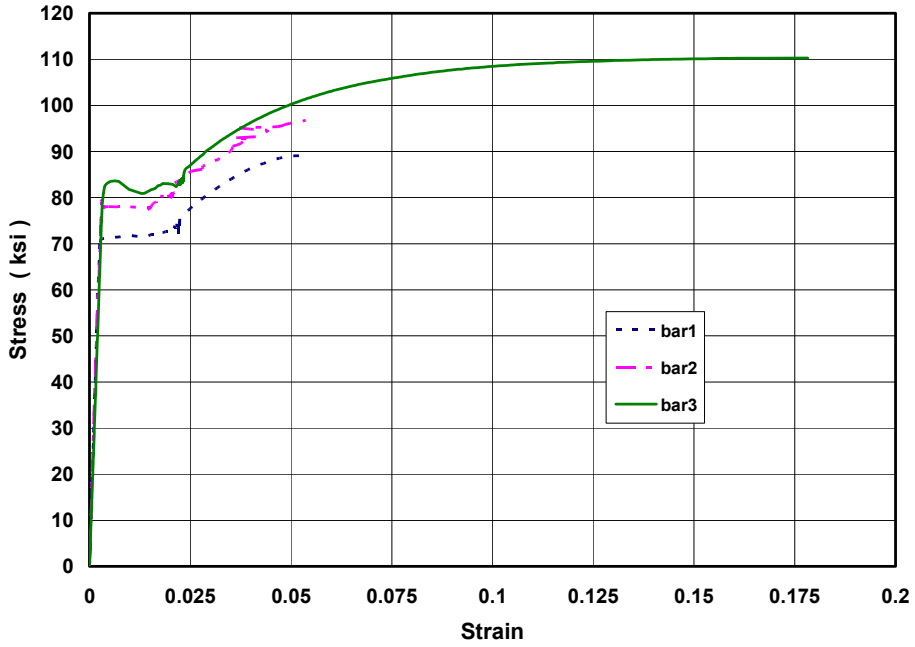

Figure 3.30: Stress-strain relationship for reinforcement in AAC shear walls

Stress-strain tests were performed on four of the #4 (13 mm diameter) reinforcing bars used in the Two-story Assemblage Specimen. The stress-strain curves are presented in Figure 3.31. The yield strength is 75 ksi (520 GPa) in two bars and 65 ksi (450 GPa) in another two bars. These tests indicate that although the bars were ordered from the same heat they probably came from separate heats.

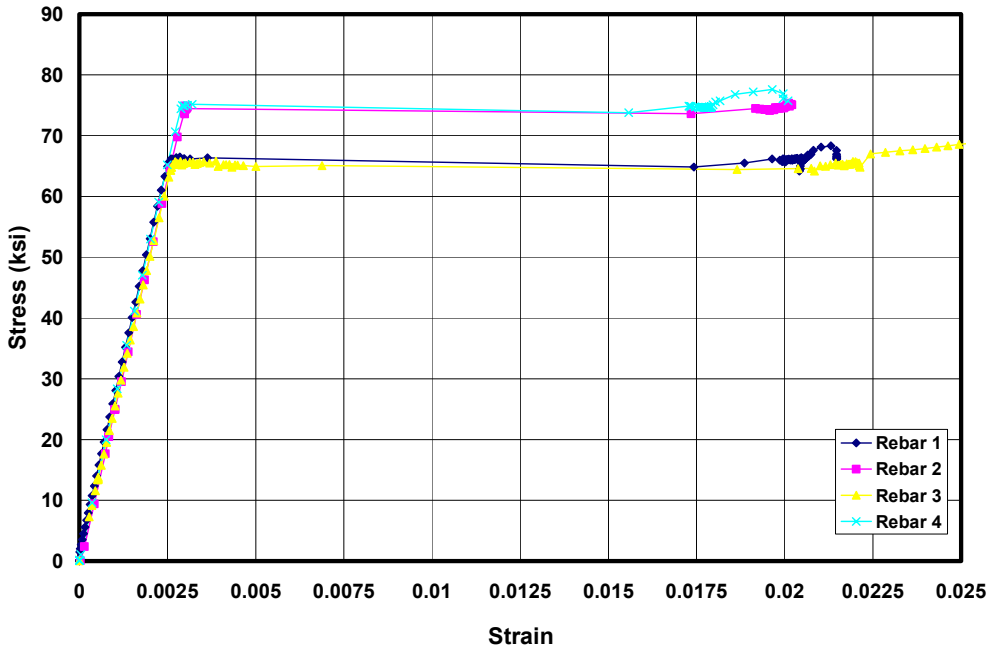

Figure 3.31: Stress-strain relationship for reinforcement in AAC shear walls

CHAPTER 4
Testing Program

The testing program for AAC shear walls consists of two phases. Phase I consists of a suite of 14 AAC shear wall specimens subject to lateral cyclic loads. The development of the testing program is described in Brightman (2000). Both shear-dominated and flexure dominated shear wall specimens were tested. The wall geometry, reinforcement and axial load were designed to force a particular mode of behavior. A full description of this testing program is found in Appendix B and was written by Varela (2003).

Phase II of the experimental program consisted of testing a two-story, full-scale assemblage specimen with AAC shear walls and untopped AAC floor diaphragms. The specimen was subject to reversed cyclic loads applied at each floor level. In this chapter, the objectives, test setup, loading equipment, loading history and instrumentation of that assemblage are presented.

4.1 OBJECTIVES OF TESTING PROGRAM (PHASE II)

The objectives of the assemblage were to verify that a system of squat walls designed to fail in a flexure-dominated mode would indeed fail in flexure; to verify proposed design provisions for AAC shear walls; to verify that lateral load could be transferred through AAC floor diaphragms; to verify proposed design procedures for such diaphragms; and to verify the proposed analytical models for the flexure-dominated specimens.

4.2 DESCRIPTION OF SPECIMEN

The Two-Story AAC Assemblage Specimen consisted of two flanged walls connected by floor slabs, and is shown in isometric view in Figure 4.1. The walls were constructed with vertical AAC panels, and the floor slabs were constructed with untopped AAC floor panels. The following sections describe the details of the Two-Story AAC Assemblage Specimen and justify the decisions made in construction. Additional plan views and elevations of the specimen are presented in Appendix A.

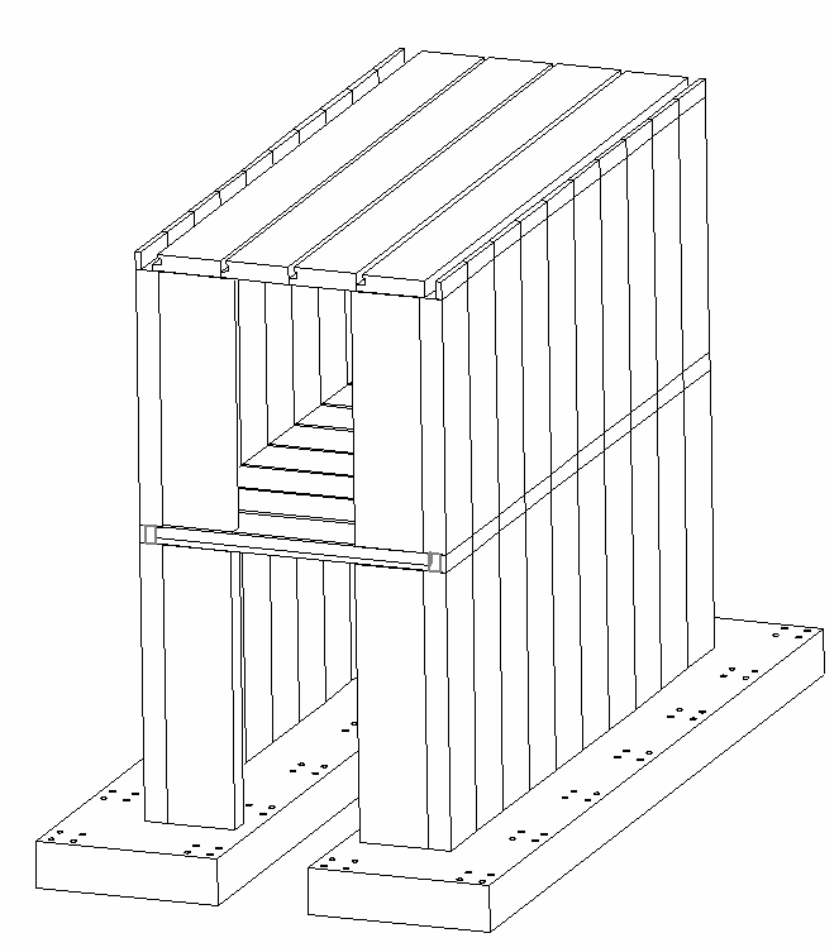

Figure 4.1: Isometric View of Two-story AAC Assemblage Specimen

4.2.1 Wall Configuration

The plan dimensions of the assemblage were 20 ft (6.1 m) long by 9.33 ft (2.8 m) wide (Figure 4.2). These dimensions were governed by laboratory space restrictions. Another potential configuration would have been using 12 ft. (3.7 m) walls and a distance of 17.33 ft. (5.1 m) between the wall ends. The wall length of 20 ft. (6.1 m) was selected in order to meet the design goal of forcing flexural behavior in a squat wall. The maximum width was determined by laboratory space restrictions. Flanged walls were selected because this is a very common layout in actual construction. Flanges are usually present in the form of returns at wall corners, or even as extended elements. Flanged walls were also selected because it was thought that flanges would increase the crushing resistance and stability of the unconfined compression toes of the AAC shear walls. In a real building, the in-plane behavior of walls is affected by some tributary width of the perpendicular walls. In addition, the flanges add stability to the compression toe and provide out-of-plane support for the entire system. The flanges represent the contributing portions of the walls perpendicular to the direction of loading. The flange length was selected as 30 in. (0.76 m) to allow access to the interior of the specimen.

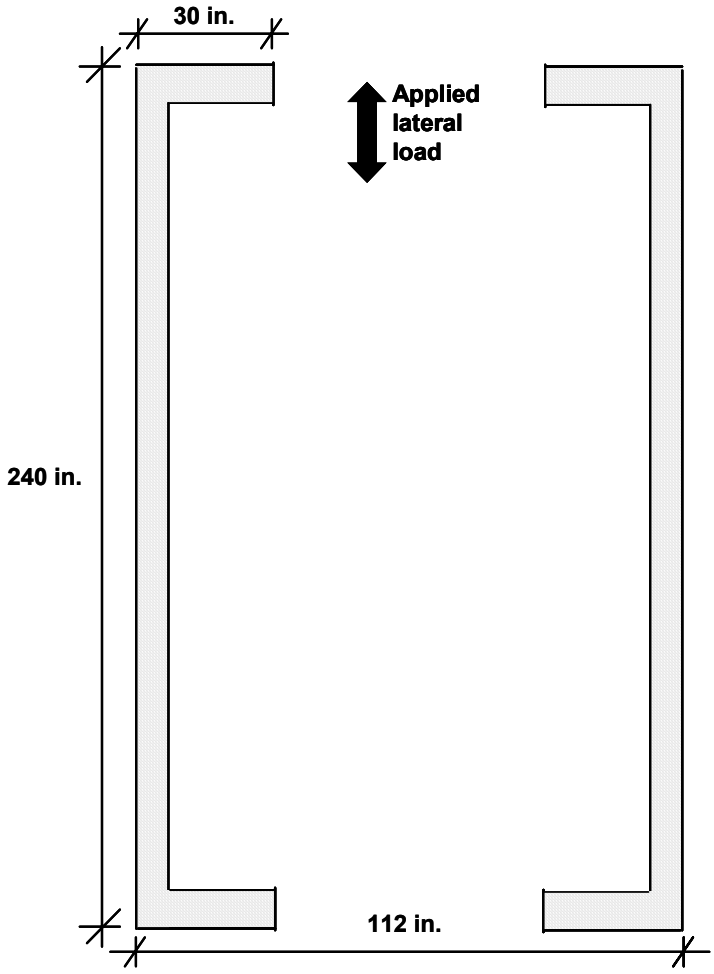

Figure 4.2: Plan layout of shear walls in the AAC assemblage

The walls were connected by an untopped AAC diaphragm at each floor level. Diaphragm details are presented in Sections 4.2.3 and 4.2.4.

4.2.2 AAC Layout and Web-to-flange Connection at Corners

Potential options for AAC units were horizontal panels, modular blocks and vertical panels. Vertical panels were selected for the assemblage because these are potentially the most vulnerable configuration, based on the observed behavior of single-story, lineal AAC shear walls (Chapter 9).

The purpose of the web-to-flange connections at the corners was to transfer shear between the flange and web. This connection is necessary if the flanges are to provide out-of-plane stability and it also permits the flange and web to work together to slightly increase the nominal flexural capacity. Since vertical panels are manufactured with cores placed at head joints only, vertical reinforcement was placed in the vertical joints between the outside two panes at each end of each web, and consisted of a total of 4 #4 bars. The selection of vertical reinforcement is discussed in Section 4.2.8. To transfer shear from between the web and flange, two 8 mm Heli-fix® spiral anchors were used at intervals of 2 ft (0.6 m). A picture and a cross-sectional view of one of the 16 in. (0.41 m) long ties used in the assemblage specimen are shown in Figure 4.4 and Figure 4.5. The final wall layout, including web-to-flange connections, is presented in Figure 4.3.

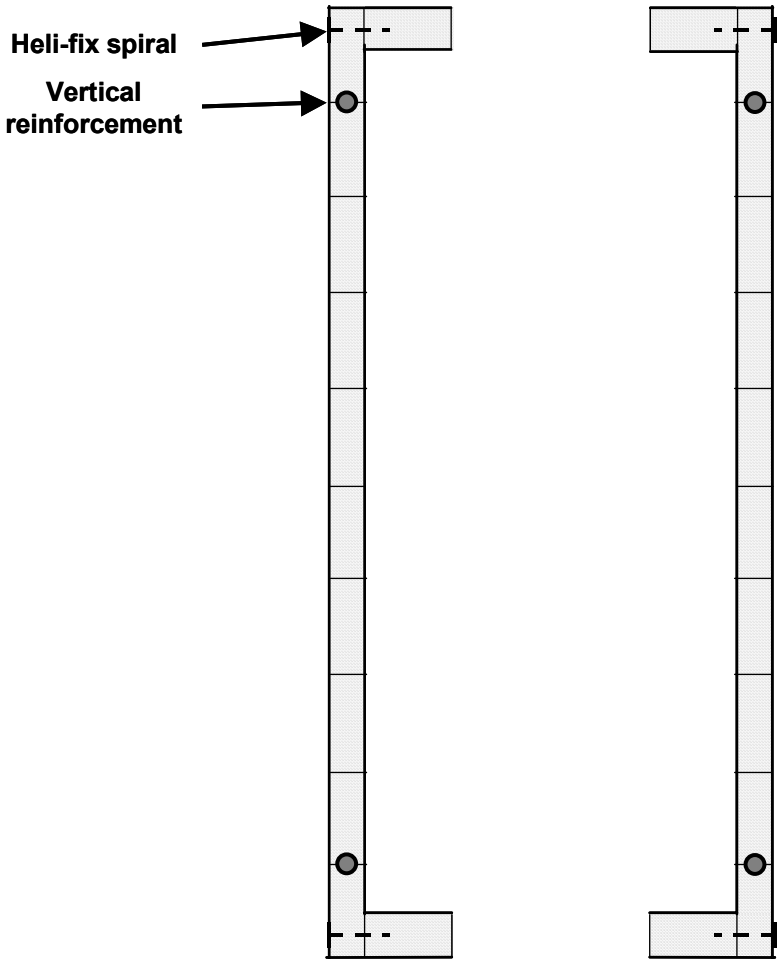

Figure 4.3: Connection detail for web-to-flange connection

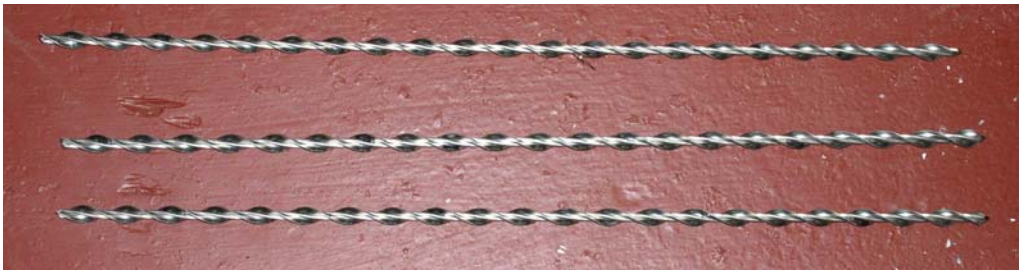

Figure 4.4: Heli-fix spiral anchors

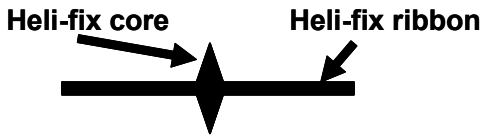

Figure 4.5: Cross-section of Heli-fix spiral anchor

4.2.3 Floor System

A maximum potential diaphragm width was 16 ft (4.9 m); for this case the maximum wall length would be reduced to 12 ft (3.7 m). The 20 ft (6.1 m) assemblage was selected to meet the design goal of forcing flexural behavior in a squat wall.

Typical AAC floor systems are panels with reinforcement placed in grouted keys. The panels may be oriented either parallel or perpendicular to the applied load. Plan and elevation views of floor panels oriented perpendicular to the walls are presented in Figure 4.6 and Figure 4.7. In Figure 4.6, a "Detail A" is identified, that same detail is referred to elsewhere (for example Figure 4.7 and Figure 4.11). The reinforcement in the grouted keys is anchored into the bond beam (see Detail A in Figure 4.11).

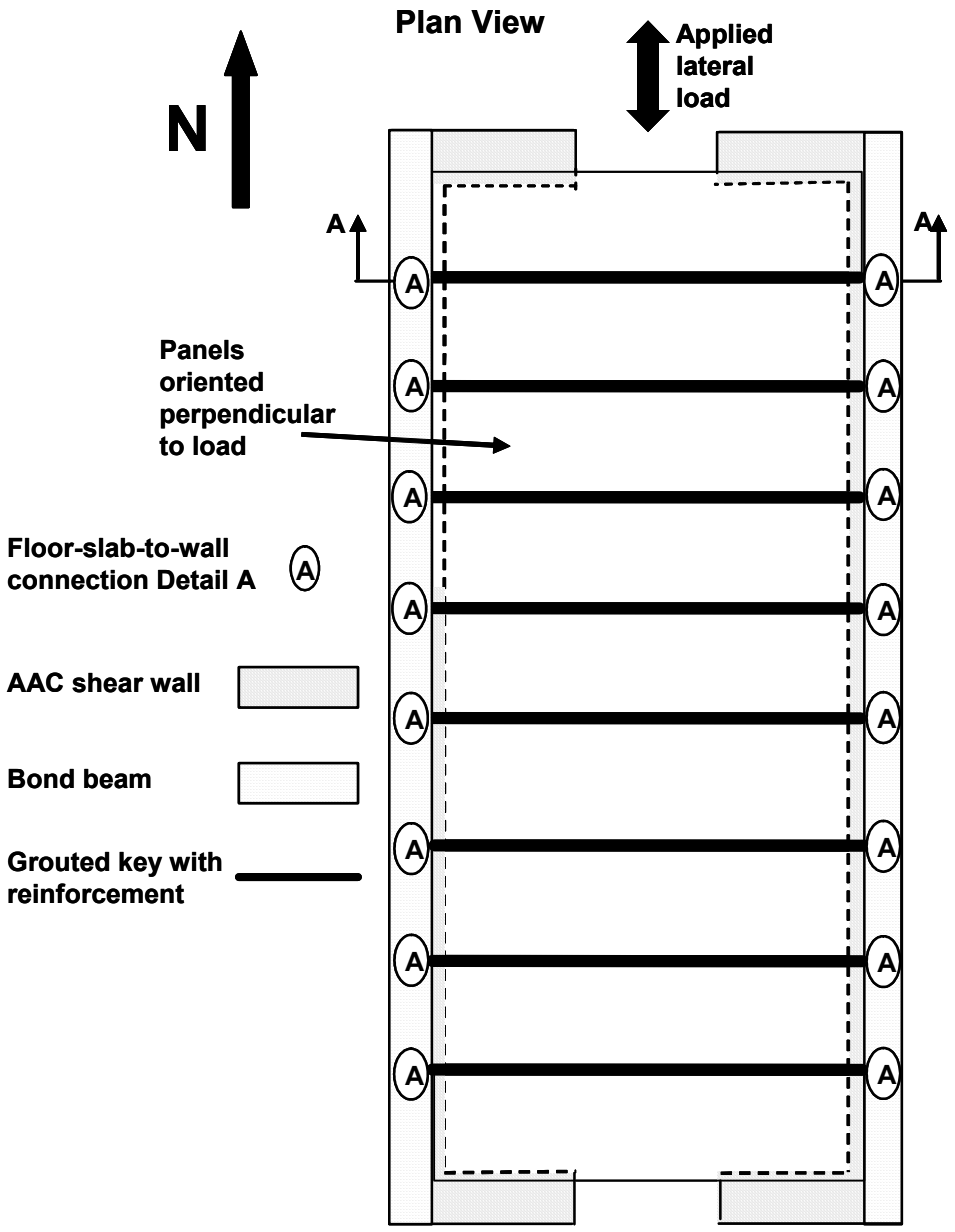

Figure 4.6: Floor plan for panels oriented perpendicular to applied load

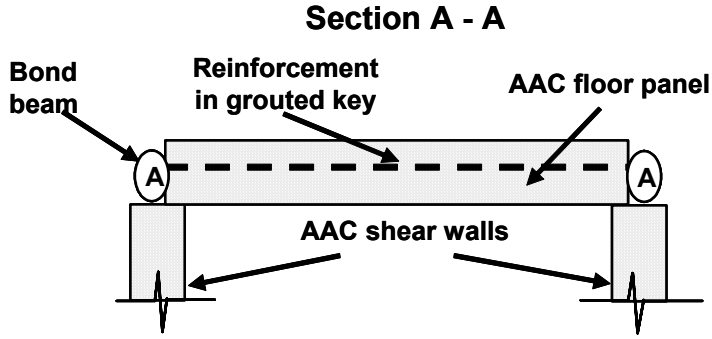

Figure 4.7: Elevation of Section A-A, floor slab-shear wall connection (panels oriented perpendicular to the direction of loading)

In a real structure, seismic lateral loads can act in any plan direction. Therefore, for testing purposes, lateral load transfer should be verified for panels parallel and perpendicular to the direction of loading. Floor panels oriented perpendicular to the direction of the loading were selected in the first elevated floor level (Figure 4.6 and Figure 4.7), and floor panels oriented parallel to the applied load were selected for the second elevated floor level.

Plan view and elevations of the second floor are presented in Figure 4.8 through Figure 4.14. The interior panels of the second floor that did not rest entirely on the wall flanges were shored during construction. Bond beams were constructed in both the north-south and east-west directions. The grouted key reinforcement was anchored into the two east-west bond beams. Connection Details A and B are presented in Figure 4.11 and Figure 4.14 of Section 4.2.4. Specimen details and dimensions are presented in Appendix A. Shear transfer was expected to be critical in the second-floor slab, due to the lack of continuous reinforcement perpendicular to the applied lateral load.

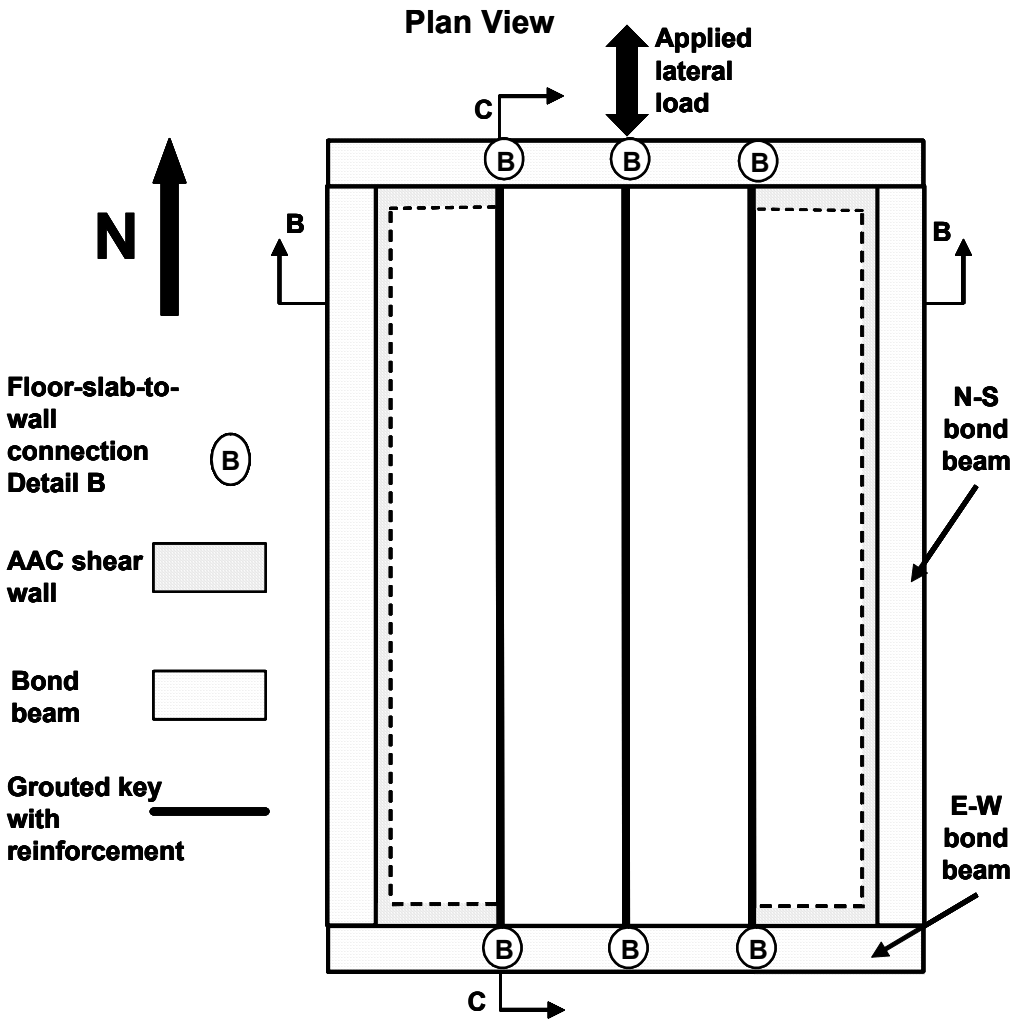

Figure 4.8: Floor slab for second story (panels oriented parallel to the direction of loading)

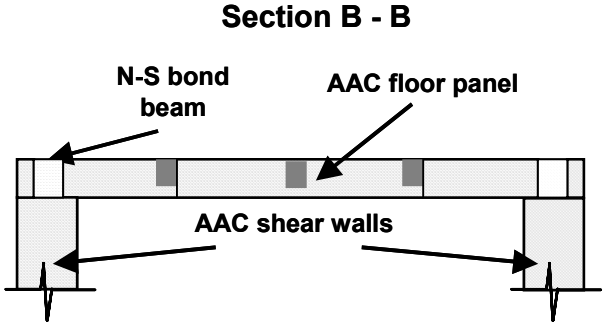

Figure 4.9: Elevation of Section B-B, second story floor slab-shear wall connection (panels oriented parallel to the direction of loading)

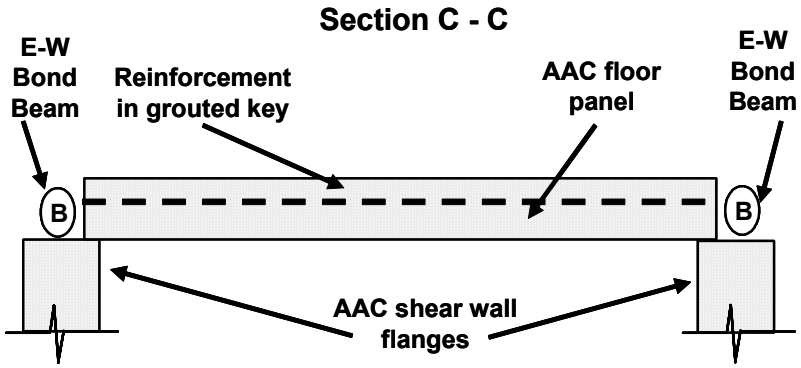

Figure 4.10: Section through connections between second-story floor slab, with longitudinal reinforcement, and bond beam (section rotated so floor is horizontal)

4.2.4 Connections between Wall and Floor Slab

Detail A, a connection between the bond beam and floor panels defined in Figure 4.6 and Figure 4.7, is shown in Figure 4.11. The reinforcement in the grouted key consists of a standard 90 degree hook bent around the longitudinal reinforcement and oriented in a vertical plane.

In cases where a vertical reinforcing bar was present in Detail A (Figure 4.12), the detail was modified as shown in Figure 4.13. Detail B, a connection

between the floor panels defined in Figure 4.8 and Figure 4.9, is shown in Figure 4.14.

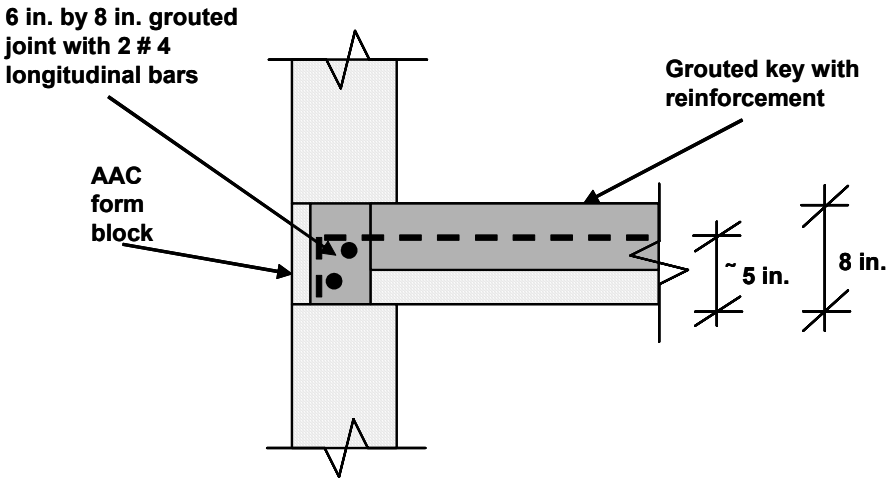

Figure 4.11: Detail A, anchorage of reinforcement in grouted keys for panels oriented perpendicular to the direction of loading

Figure 4.12: Photograph of Detail A, at intersection with vertical bar

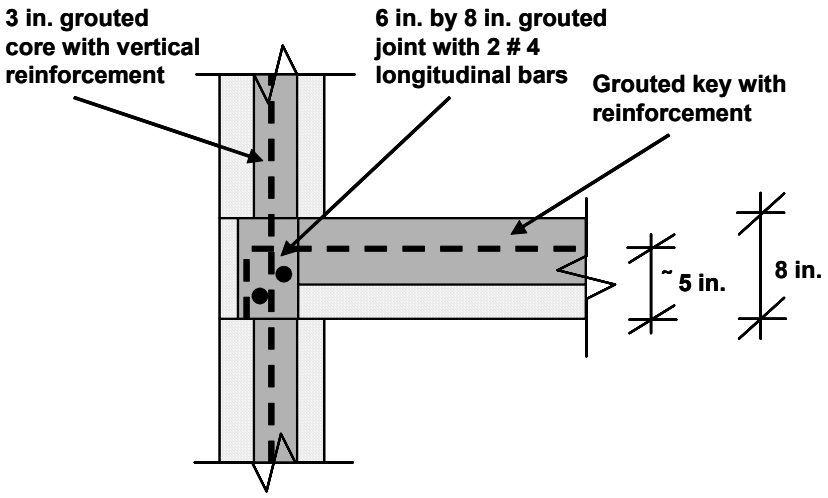

Figure 4.13: Detail A, at intersection with vertical bar

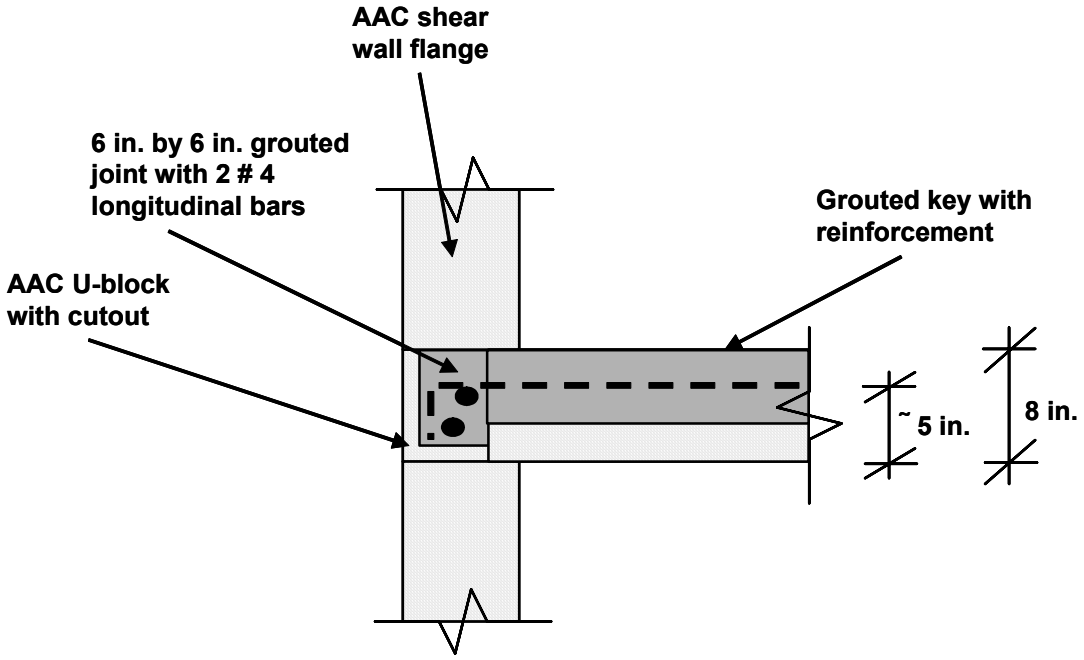

Figure 4.14: Detail B, anchorage of reinforcement in grouted keys for panels oriented parallel to the direction of loading

4.2.5 Lateral Load Transfer in Floor Slab for Panels Oriented Perpendicular to Direction of Loading

In a building subject to seismic loading, concentrated inertial forces are generated in areas of concentrated mass, usually the floor slabs. Forces generated in floor slabs must be transferred to shear walls. Lateral load applied perpendicular to the panels was designed to be transferred through dowel action of perpendicular reinforcement in grouted keys. Based on dowel action, the capacity of a connection between a floor slab and a shear wall is 35.6 kips (158 kN), which is 1.4 times the load corresponding to nominal flexural capacity.

4.2.6 Connections between Wall and Floor Slab for Panels Oriented Parallel to Direction of Loading

Lateral load generated in the floor slab must be transferred to the base of the structure through the shear walls. Shear transfer is critical in the case of panels oriented parallel to the direction of load, due to the lack of continuous reinforcement perpendicular to the applied load. This shear transfer can occur through adhesion between the panels and through a truss mechanism. These methods are discussed independently in the following sections.

4.2.6.1 Shear transfer through adhesion between joints

The second story of the Two-story Assemblage Specimen was designed based on shear transfer through adhesion. The critical sections in the second story floor slab are Section D-D and Section E-E, since no steel is oriented perpendicular to these paths (Figure 4.15). In panel-to-panel connections, Section D-D, the adhesion depends on both the thin-bed mortar and grouted key adhesion (Figure 4.16). In panel-to-bond beam connections the adhesion depends primarily on grout and a small section of thin-bed mortar (Figure 4.17).

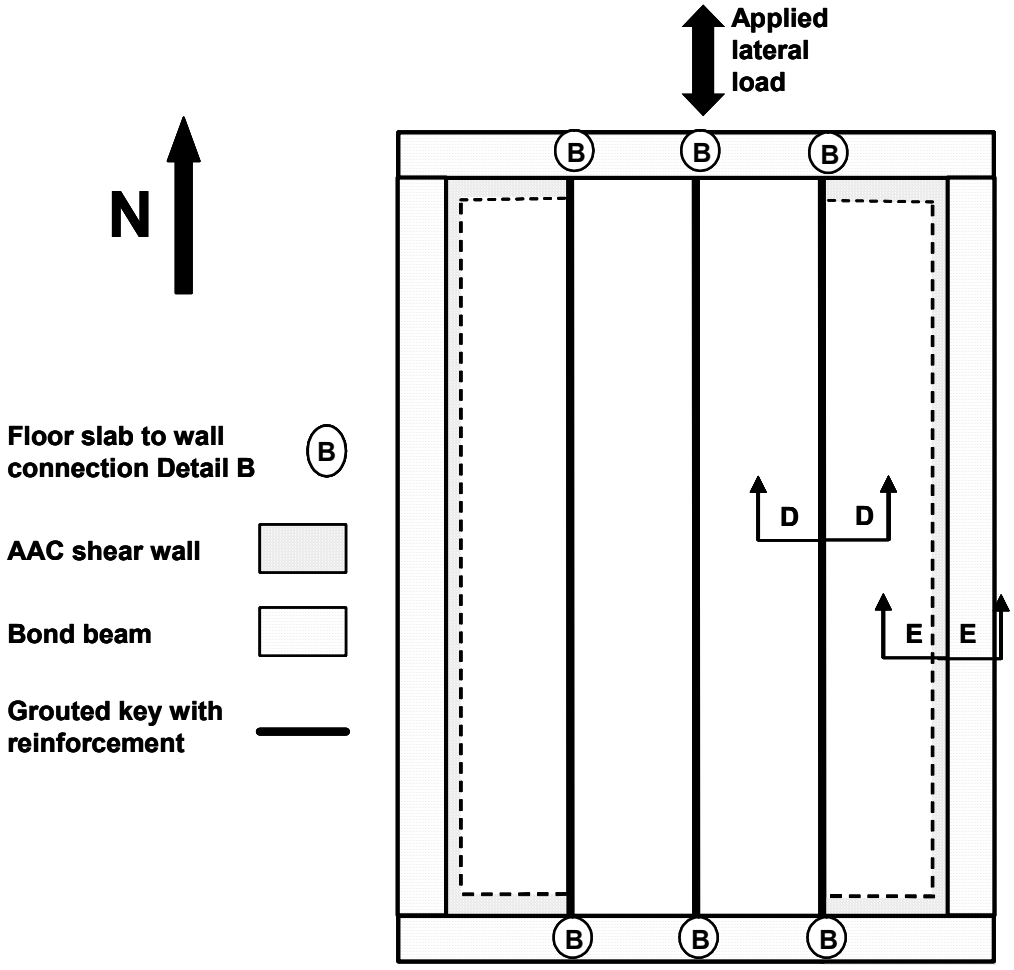

Figure 4.15: Plan view of second story floor panels

The panel-to-panel joints were constructed by applying thin-bed mortar at the panel joint below the grouted key and clamping adjacent panels. The grouted key was cleaned with compressed air and pre-wetted prior to placing grout. The grout was vibrated during placement. The same construction process is proposed for all panel-to-panel joints. Based on the average shear strengths and the corresponding lengths of grout and thin-bed mortar, the shear capacity is 60.5 kips

(270 kN) for each joint, 2.4 times the predicted load at each joint for the nominal flexural capacity.

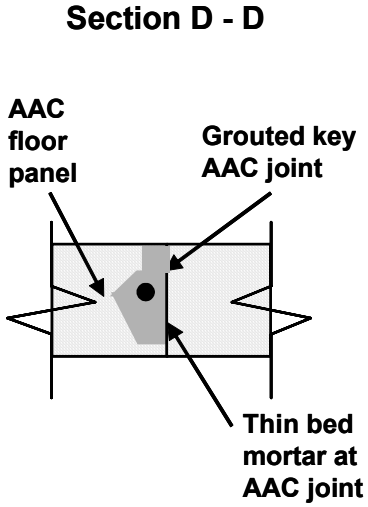

Figure 4.16: Elevation of Section D-D, panel-panel connection

The joints between panels and bond beams were constructed by applying thin-bed mortar at the bed joint between panels and the slab. In some cases a gap existed between the top of the vertical panel and the floor panel due to differences in the height of the leveling bed, which caused different heights at the top of panels. For this reason, the thin-bed mortar area was conservatively neglected. The bond beam was cleaned with compressed air and pre-wetted prior to placing grout. The grout was vibrated during placement. The same construction process is proposed for all panel-to-bond beam joints. Based on the average shear strength of grout and AAC the shear capacity is 69.1 kips (310 kN) for each joint, 2.8 times the load in each joint at the nominal flexural capacity.

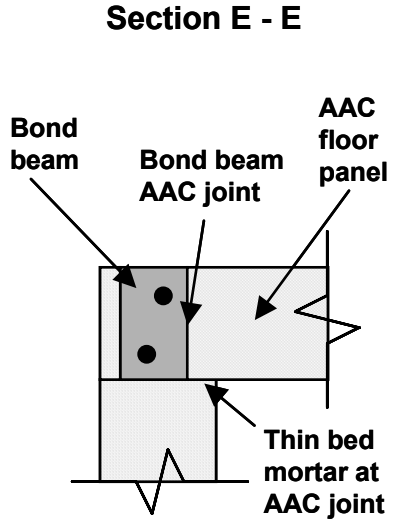

Figure 4.17: Elevation of Section E-E, panel-bond beam connection

If a failure occurred in the second-story slab, load could no longer be applied to the second story and the shear walls could not have been tested to failure. Due to the lack of redundancy in the system combined with the brittle nature of an adhesion failure, reinforcement was used across the joint. A plan view of deformed reinforcing bars oriented along a diagonal is shown in Figure 4.18. In this configuration the deformed reinforcement works efficiently in tension. Strain gages were applied to the bars to indicate the tensile force, which is related to the shear resistance through geometry. AAC panels were modified to permit this by cutting with a masonry blade on a rotary saw (Figure 4.19).

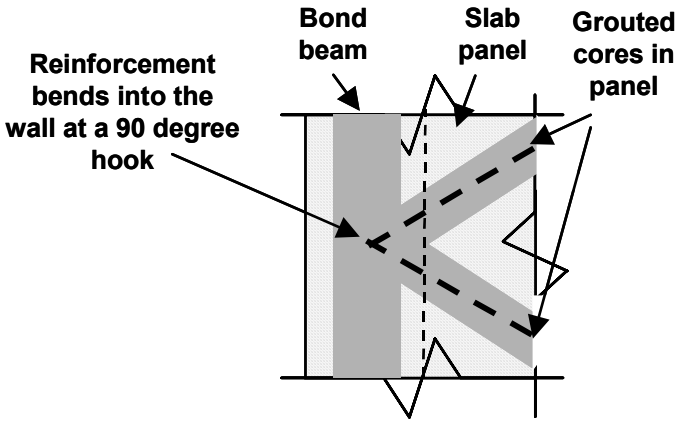

Figure 4.18: Incorporation of diagonal steel across joint parallel to the direction of load in Two-story Assemblage Specimen

Figure 4.19: Picture of diagonal reinforcement across the joint parallel to the direction of load in Two-story Assemblage Specimen

4.2.6.2 Shear transfer through truss mechanism

Shear transfer may also be applied through a truss mechanism, which follows the principles of a strut-and-tie model. Compression is transferred through the panels in the form of struts. The reinforcement in the grouted keys

serves as tension ties, which must be tied into the bond beam by 90-degree standard hooks bent around the longitudinal reinforcement in the tension ties and oriented in a vertical plane.

The strut-and-tie model used to design the diaphragm (Figure 4.20) has a capacity of 77.1 kips (343 kN), 1.5 times the load in the diaphragm at nominal flexural capacity. This model is discussed in Section 9.4.6.

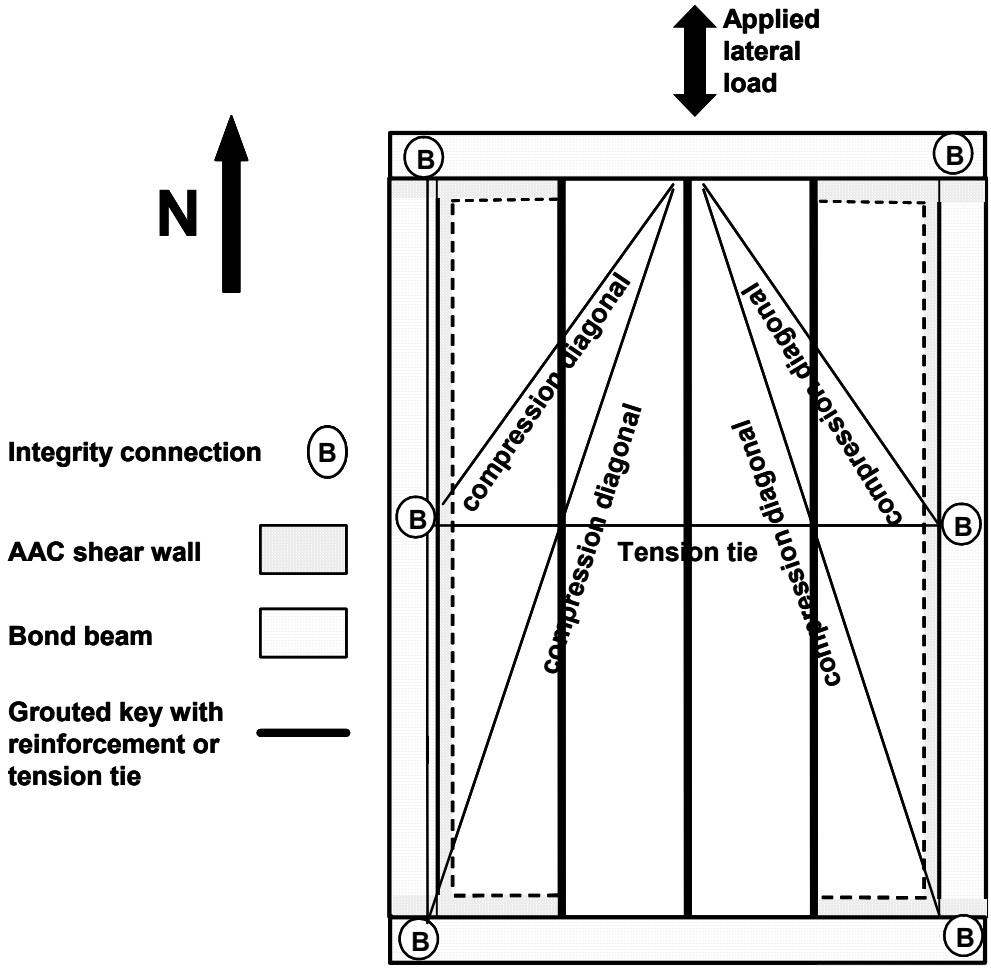

Figure 4.20: Truss mechanism for transferring lateral load parallel to the orientation of the panels

4.2.7 Connection between First- and Second-Story Wall

The first- and second-story walls were connected through the vertical reinforcement and the bond beam. If the surface of the grouted joint at the floor slab level was rough, a leveling bed was used between the joint and the AAC shear wall. The vertical reinforcement was spliced in the second-story wall above the first-story floor slab (Figure 4.11, Figure 4.13 and Figure 4.14).

4.2.8 Longitudinal Reinforcement in the Two-story AAC Assemblage Specimen

The in-plane behavior of an AAC shear wall depends on its plan configuration, reinforcement, and axial load. The selected reinforcement and location affects the shear force that causes yielding of the flexural reinforcement, the nominal flexural capacity, and the sliding shear capacity. Flexural reinforcement shown in Figure 4.21 was selected so that the wall behavior would be governed by flexure rather than shear.

The nominal flexural capacity was determined using the proposed flexural design provisions (Argudo 2003). The expected flexural capacity was 1.25 times the nominal flexural capacity, because of material overstrength and strain hardening. The nominal flexural capacities were converted to nominal base shear capacities based on the relationship between moment and shear found using the vertical distribution of lateral forces proposed in Section 4.3.3. A tested compressive strength of 1025 psi (7.07 MPa) found in previous Class 4 material from Babb was used in the calculations. Elasto-plastic behavior of the steel was assumed, with a yield strength of 75 ksi (517 MPa), based on mill test reports for the vertical reinforcement used in the AAC shear wall specimens.

The design web-shear capacity using the appropriate strength-reduction factors (ϕ) from ACI 318-02 was greater than the nominal flexural capacity with 1 #4 bar at 2 ft. (0.7 m) from the ends of the wall for the design axial load of 30 kips (133 kN) per shear wall. The capacity as governed by web-shear cracking was based on equations proposed and calibrated at The University of Texas at Austin, and described in Chapter 8 of this dissertation. The tested splitting tensile strength for the Babb units in the previous shipment, 88 psi (0.61 MPa), was used for this prediction.

Three additional #5 dowels were placed at the base and at the first elevated floor slab to increase the design sliding-shear capacity (Figure 4.21).

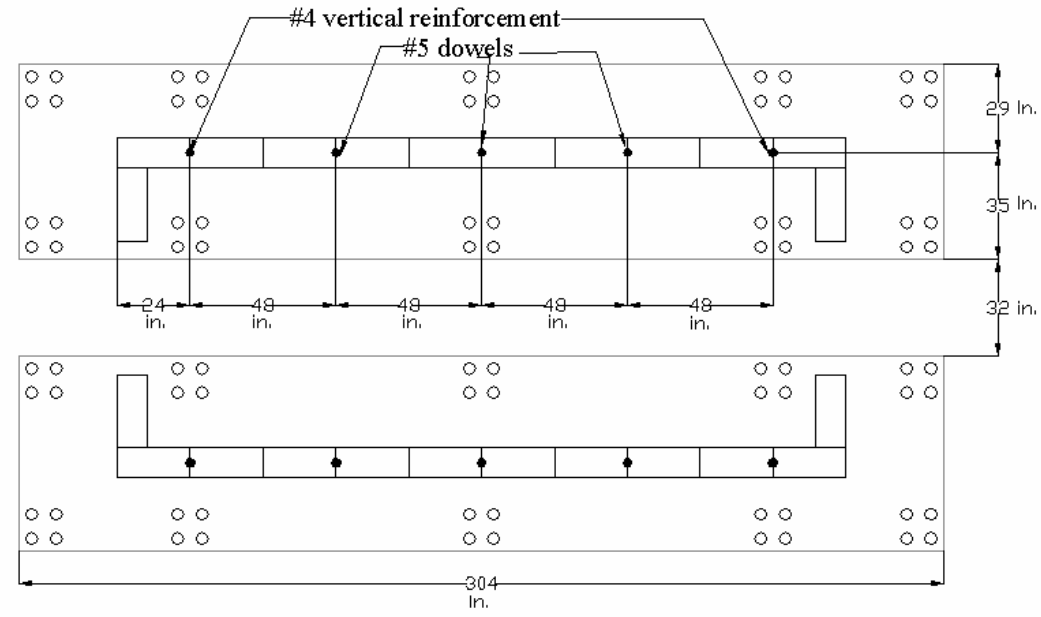

Figure 4.21: Plan view of base beams

4.3 TEST SETUP

4.3.1 Base Beam

Individual rectangular concrete base beams, reinforced and post-tensioned, were cast as foundations for each wall. The foundation size, 304 in. (7.7 m) by 64 in. (1.6 m) by 16 in. (0.41 m), was dictated by the geometry of the lab tie-downs. For a 20 ft. (6.1 m) long wall, using tie-downs only at the ends of the wall will result in large stresses, which may induce cracking of the slab. The foundations and tie-down holes are shown in Figure 4.21.

4.3.2 Application of Lateral Load

The lateral load was applied to the floor slabs through reinforced concrete loading beams attached to the slabs. The loading beams themselves were longitudinally post-tensioned. Two loading beams, one above and one below each floor slab, were clamped together by vertical rods. The loading beams were 16 in. (400 mm) by 20 in. (500 mm) by 256 in. (6.5 m). The lateral load was applied through the frictional resistance between the concrete loading beam and the AAC floor slab. The required clamping force was based on the predicted maximum lateral load. The size of the loading beam and location of vertical post-tensioning rods were determined using a linear elastic finite element model. Principal tensile stresses were determined to avoid cracking either the loading beams or AAC floor slab. Plan and elevation details for the loading beam–floor slab connection are shown in Figure 4.22 and Figure 4.23. In the case of panels oriented parallel to the direction of loading, the panels could not carry the weight of the loading beam. A loading slab spanning the entire width of the floor slab and resting directly on the top of the shear walls was selected to transfer the load to the shear walls, and to carry the weight of the lower loading beam. Since these sections were half the height of the loading beams in the first story, additional

vertical rods were used to distribute the clamping force. An elevation of this system is shown in Figure 4.24.

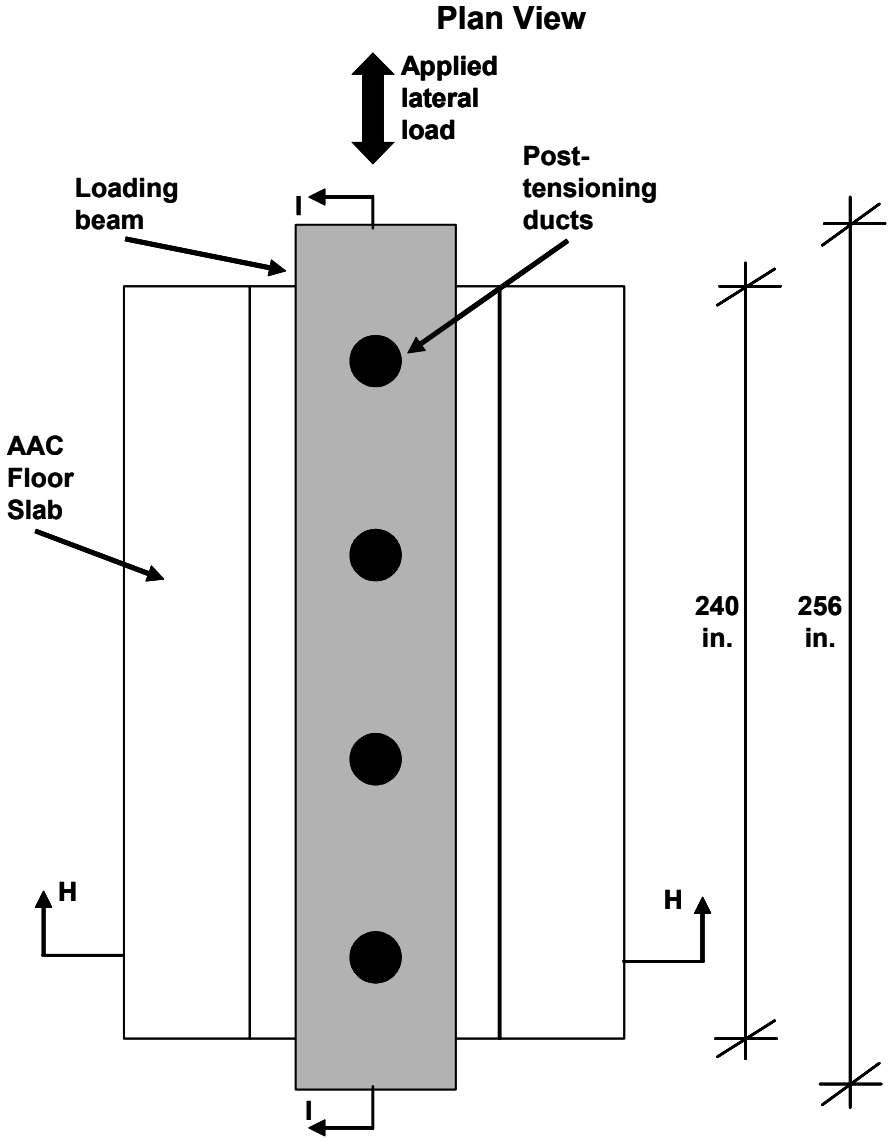

Figure 4.22: Plan view of loading beam attachment to the floor slab

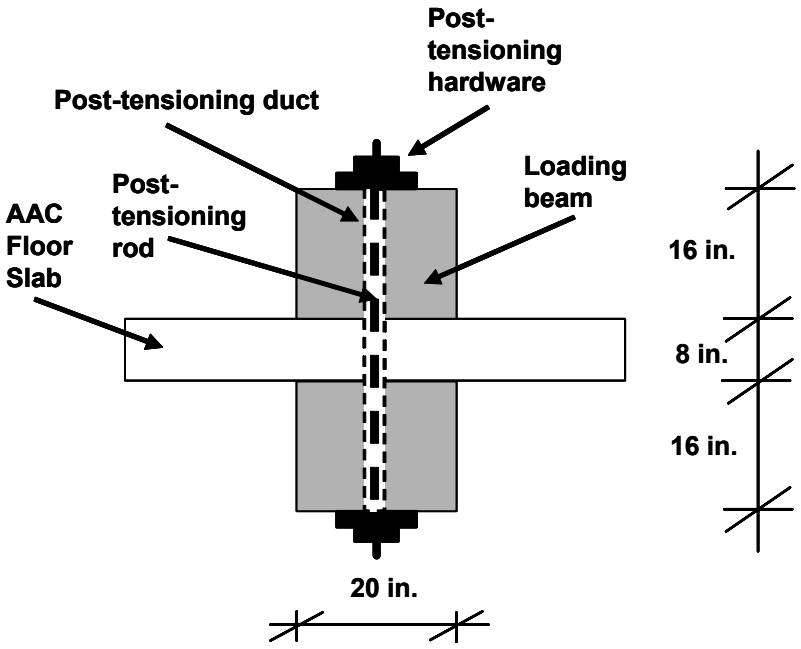

Figure 4.23: Elevation of Section H-H, loading beam attachment to the floor slab

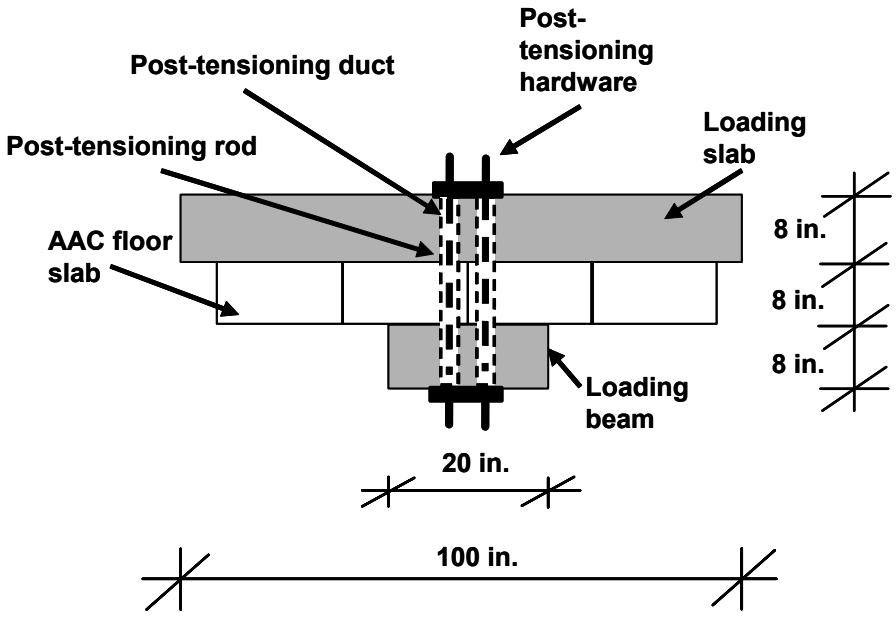

Figure 4.24: Modification of Section H-H for loading slab

The loading beams were also post-tensioned longitudinally. The connection between the rams and loading beam is shown in Figure 4.25. The vertical post-tensioning rods are omitted for clarity. For panels oriented parallel to the direction of loading, the loading slab and loading beam contained two internal post-tensioning ducts. Although the risk for cracking due to non-concentric loading is increased, the calculated stresses are below the cracking load. This system is shown in Figure 4.26.

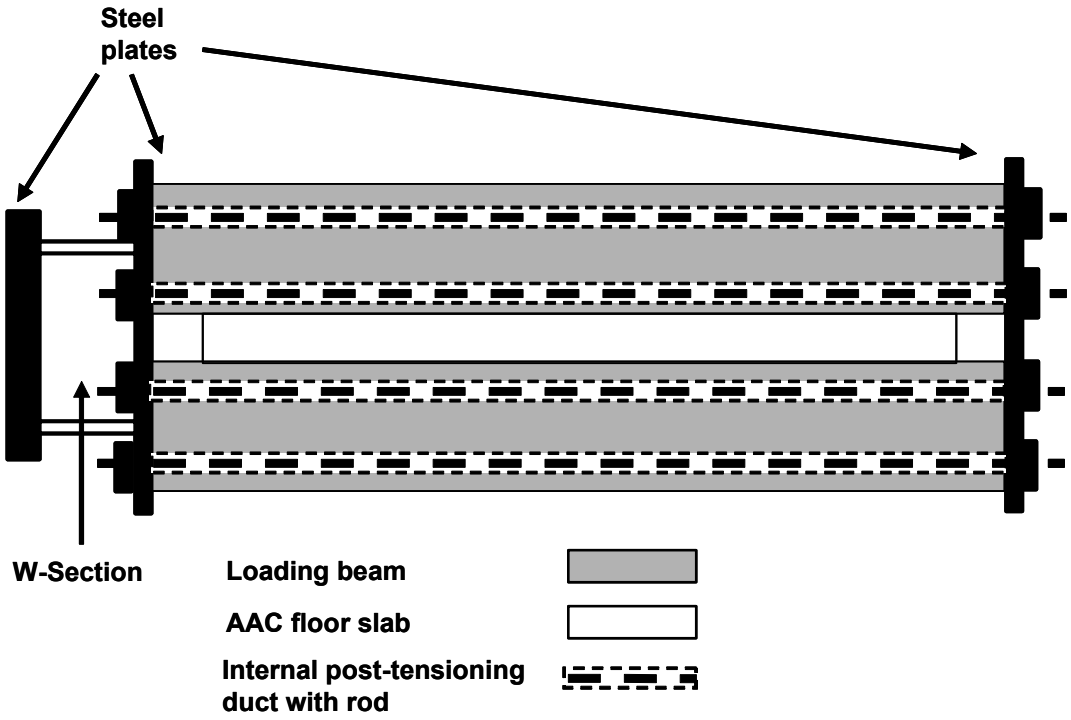

Figure 4.25: Elevation of Section I-I, loading beam-ram connection

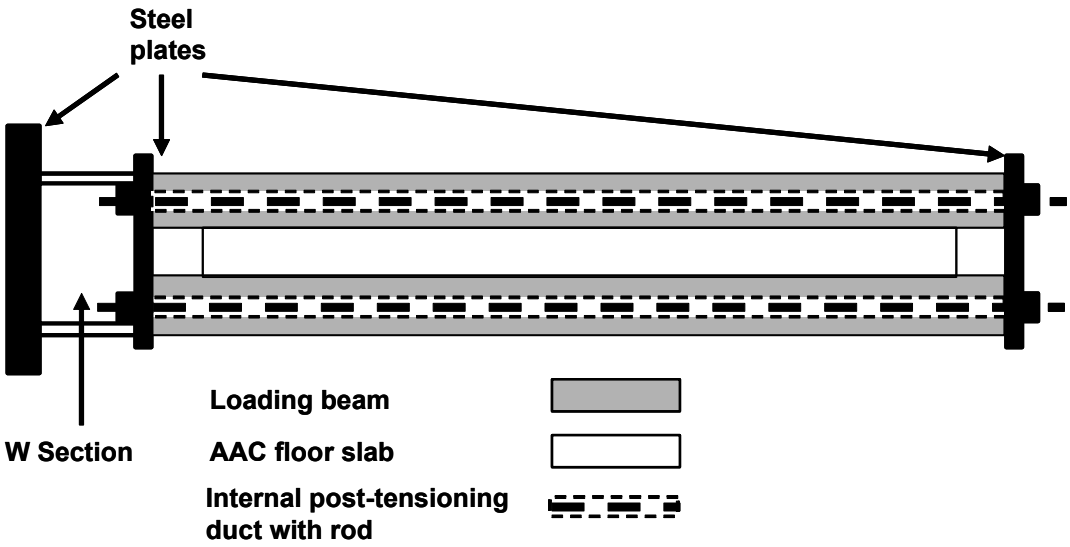

Figure 4.26: Modification of Section I-I for loading slab

During construction of the concrete loading slab, the cross-section was concave down. To transfer gravity loads to the wall, shims were placed between the exterior edges of the concrete loading slab and the bond beam (Figure 4.27). The center of the loading slab was bearing on the AAC slab, while the edges of the loading slab were bearing the grouted beam through the action of the shims. Based on this configuration part of the loading slab weight was transferred to the shear walls and another part was transferred through the AAC floor slab. Due to the gaps present in Figure 4.27 the clamping force from the slab is only transferred at the center of the slab. A free body diagram of the clamping force transferred to the floor system is shown in Figure 4.28. The lateral load is expected to be transferred to the AAC floor slab at this location. It is improbable that lateral load was transferred through friction from the weight of the loading slab. Even if this were true, the lateral load transfer would be limited by the low coefficient of friction between the plastic shims and the concrete loading slab.

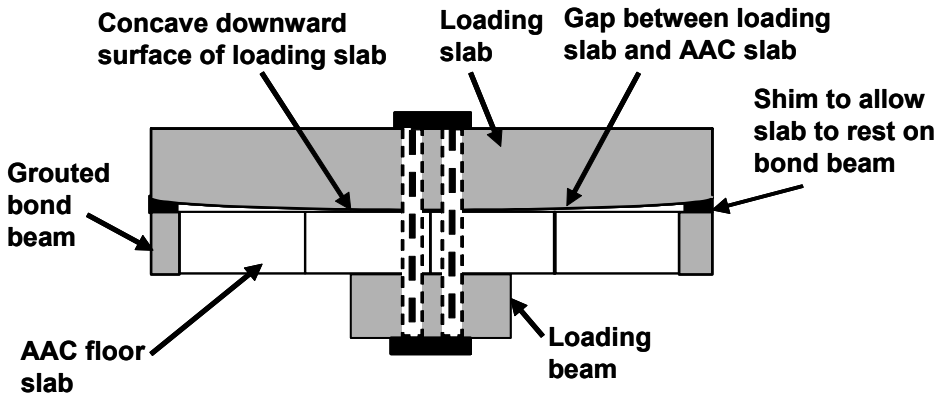

Figure 4.27: Cross-section of as built upper loading slab including shims

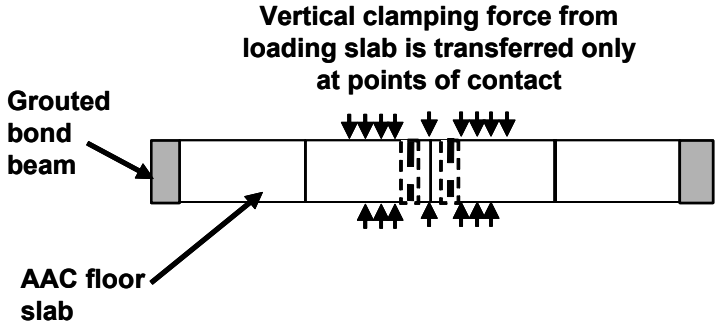

Figure 4.28: Free-body diagram of clamping force on AAC floor slab

4.3.3 Vertical Distribution of Lateral Load

The vertical distribution of seismic lateral load over the height of the building could take many forms. For design of the assemblage specimen, two specific distributions are considered, a triangular distribution and a uniform distribution (equal load at each floor). Those distributions are shown in Figure 4.29 and Figure 4.30 respectively.

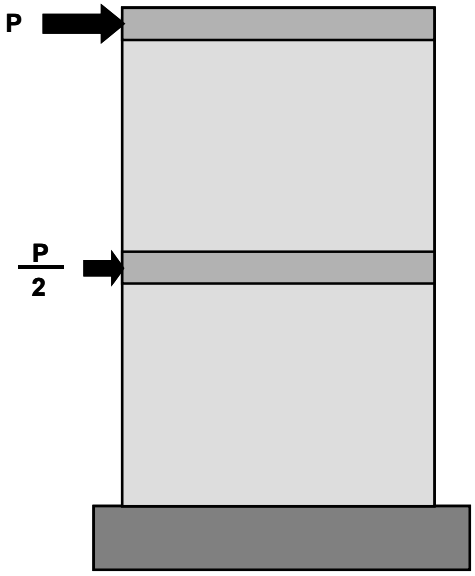

Figure 4.29: Vertical distribution of lateral forces for triangular load distribution

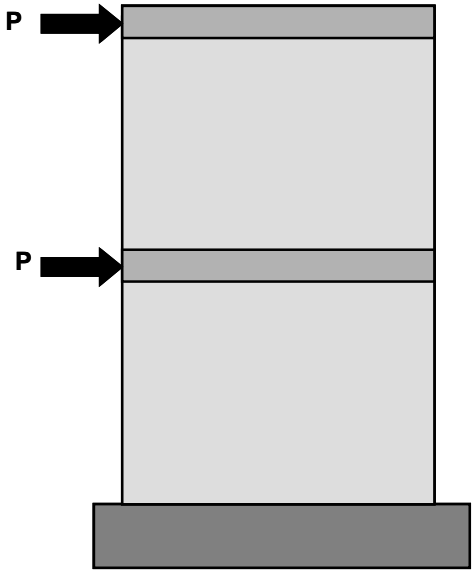

Figure 4.30: Vertical distribution of lateral forces for uniform load distribution

The triangular load distribution follows the IBC 2000 equivalent lateral force procedure for low-rise buildings. The uniform vertical load distribution applies equal loads to each story and was thought to be more representative of the actual distribution in the inelastic range of behavior. It is justified below. It is important to represent this vertical distribution of loads accurately, because the triangular distribution that is often assumed actually has a smaller base shear for the same base shear overturning moment, and can therefore suppress potential shear-dominated behavior.

To estimate the most reasonable vertical distribution of lateral loads, several non-linear analyses were performed using CANNY99 (CANNY99). A single wall with the geometry and reinforcement was modeled using the observed behavior of Shear Wall Specimen 13, the first flexure-dominated AAC shear wall tested at UT Austin. The wall was subject to ground motion records from California earthquakes (PEER 2002). For these ground motions, the structure remained elastic; the earthquakes were then scaled up to force yielding of the flexural reinforcement. The ratio of the maximum moment in the structure (M_{max}) to the moment at yielding of the flexural reinforcement (M_{yield}) is also presented in Table 4.1. The forces generated at each level as a function of time for the Arleta 1 ground motion are presented in Figure 4.31. Prior to flexural yielding at the base of the wall, the force generated at the second story was larger than the forge generated at the second story. After flexural yielding at the base of the wall, the forces in each story are nearly equal.

Two procedures were used to quantify the ratio of story forces. In the first procedure, the ratio of second-story forces (F_2) to first-story forces (F_1) was

calculated at times corresponding to the generation of maximum base shear in the structure. Results are presented in Table 4.1. The average ratio of forces was 1.1 and the COV was 11%. The Canoga Park 2 ground motion resulted in a large negative base shear at the very end of the analysis. This anomalous result was associated with second-mode behavior and the next largest negative base shear was used for the analysis.

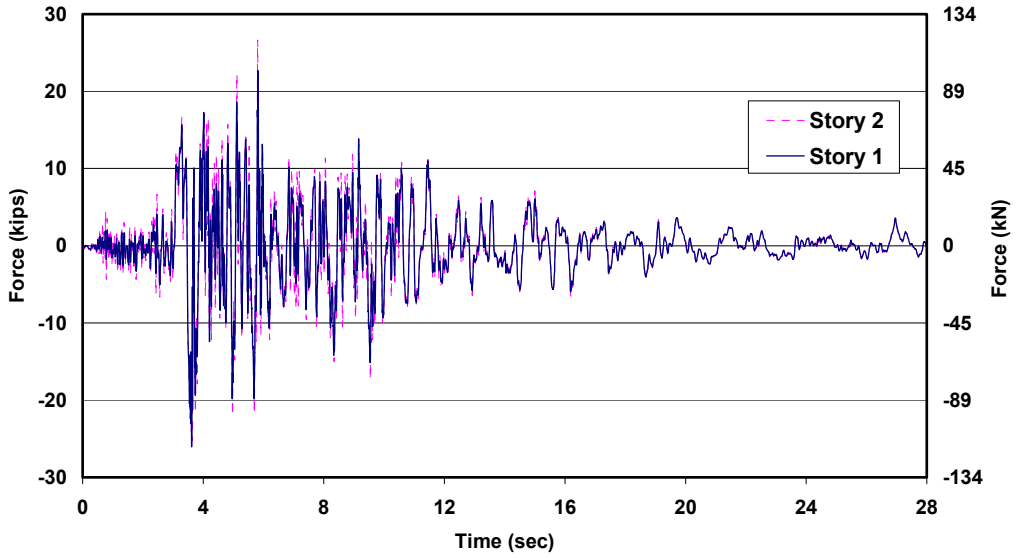

Figure 4.31: Lateral loads in the first and second elevated levels as a function of time for the Arleta 1 record

Table 4.1: Ratio of lateral force at second elevated force to force at first elevated level for maximum positive and negative peaks of base shear

Location (Date)	Station	Record	M_{max}/M_{yield}	Positive F_2/F_1	Negative F_2/F_1
Corralitos 1 (1989)	57007	CLS000	1.164	1.22	1.05
Corralitos 2 (1989)	57007	CLS090	1.206	1.08	1.01
Gilroy #1 2 (1989)	47379	GO1000	1.004	1.05	1.11
Gilroy #1 1 (1989)	47379	GO1090	1.029	1.40	1.01
Canoga Park 1 (1994)	90053	CNP106	1.003	1.07	0.87
Canoga Park 2 (1994)	90053	CNP196	1.123	1.13	0.88
Arleta 1 (1994)	24087	ARL090	1.007	1.14	1.17
Arleta 2 (1994)	24087	ARL360	1.017	1.09	1.05
Canyon Country 1 (1994)	90057	LOS000	1.003	1.27	1.04
Canyon Country 2 (1994)	90057	LOS270	1.003	1.04	1.11
Mendocino (1992)	89005	CMP000	1.006	0.971	0.90
Mendocino (1992)	89005	CMP090	1.006	0.997	0.95

In the second procedure, a more rigorous approach was used to verify the ratio of forces in the second story to forces in the first story during the duration of the earthquake ground motion. A minimum value of base shear was selected, V_{min}. For any point in the time history analysis when the total base shear exceeded the minimum selected base shear (V_{min}) the ratio of forces in each story was determined. The average of all of the ratios of forces after yielding of the flexural reinforcement was calculated along with the COV for these data points. As the minimum base shear increased, the average ratio of forces approaches 1.1 and the COV decreases. The results of the ratio of forces versus V_{min} are presented in Figure 4.32 and Figure 4.34 for Northridge and Loma Prieta earthquakes respectively. The COV's that correspond to these ratios of forces are plotted in Figure 4.33 and Figure 4.35. This information is also presented in tabular format in Table 4.2 and Table 4.3. These findings indicate that the ratio of

forces is approximately 1.1 for the peak base shear and for values approaching the peak base shear.

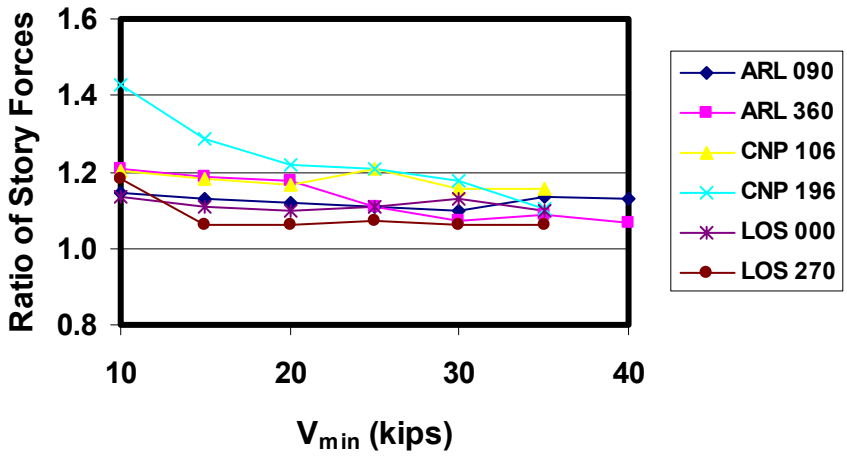

Figure 4.32: Ratio of forces versus V_{min} for Northridge records

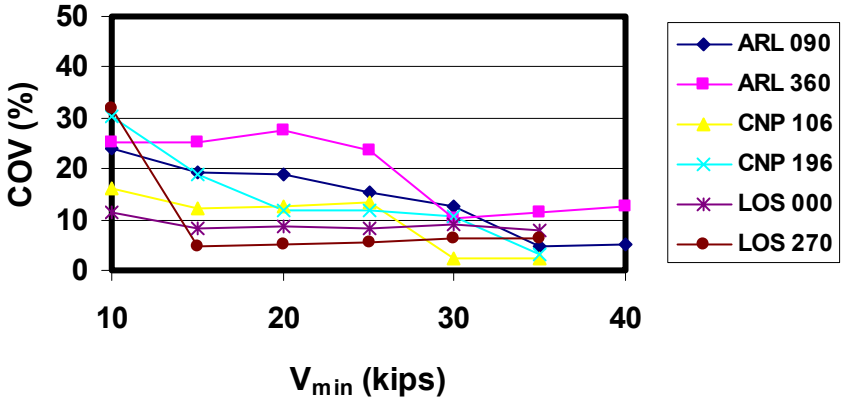

Figure 4.33: Corresponding COV's for ratio of forces versus V_{min} for Northridge records

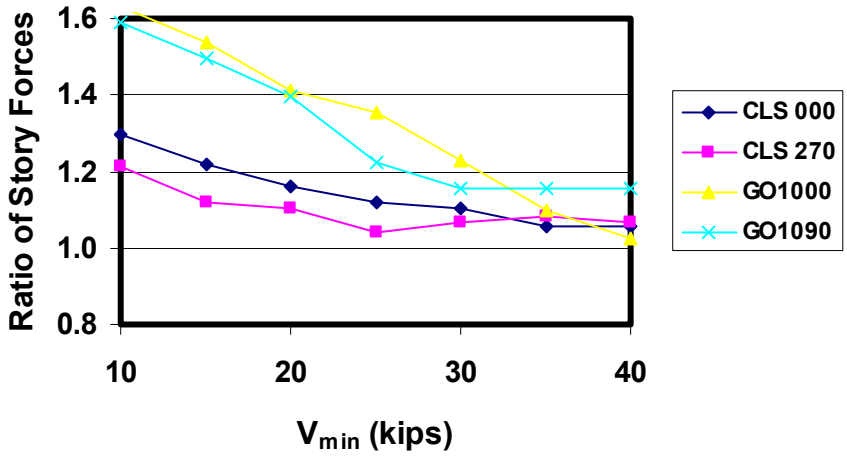

Figure 4.34: Ratio of forces versus V_{min} for Loma Prieta records

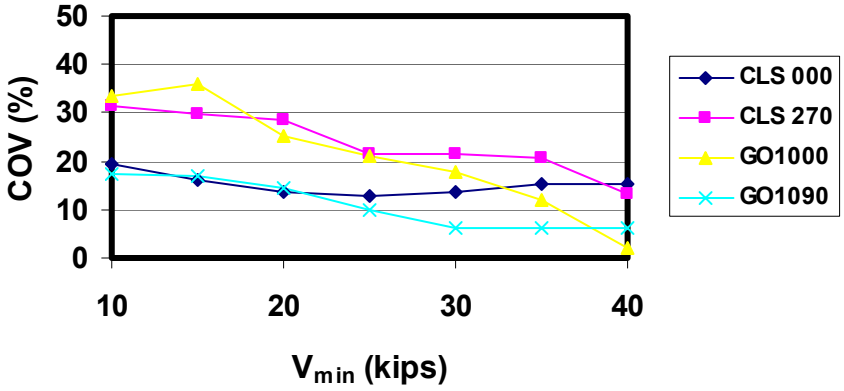

Figure 4.35: Corresponding COV's for ratio of forces versus V_{min} for Loma Prieta records

Table 4.2: Ratio of forces versus V_{min}, for different records

V_{min}	ARL 90	ARL 360	CNP 106	CNP 196	LOS 000	LOS 270	CLS. 000	CLS 270	GO 1000	GO 1090
10	1.15	1.21	1.20	1.43	1.13	1.18	1.30	1.21	1.63	1.59
15	1.13	1.19	1.18	1.29	1.11	1.08	1.22	1.12	1.54	1.50
20	1.12	1.18	1.17	1.22	1.10	1.07	1.16	1.10	1.41	1.39
25	1.11	1.11	1.21	1.21	1.11	1.06	1.12	1.04	1.35	1.22
30	1.10	1.07	1.16	1.18	1.13	1.05	1.10	1.07	1.23	1.16
35	1.14	1.09	1.16	1.10	1.10	1.05	1.06	1.08	1.10	1.16
40	1.13	1.06				1.06	1.06	1.07	1.02	1.16

Table 4.3: Corresponding COV's for ratio of forces versus V_{min}, for different records

V_{min}	ARL 90	ARL 360	CNP 106	CNP 196	LOS 000	LOS 270	CLS. 000	CLS 270	GO 1000	GO 1090
10	24.2	25.0	16.0	30.3	11.5	27.70	19.5	31.4	33.4	17.4
15	19.3	25.4	12.1	19.0	8.2	8.10	15.9	29.9	35.9	16.9
20	19.1	27.5	12.7	11.9	8.6	6.30	13.6	28.4	25.2	14.4
25	15.4	23.4	13.3	11.9	8.3	5.20	13.0	21.6	20.9	10.1
30	12.7	10.3	2.2	10.5	9.1	5.40	13.5	21.5	18.0	6.0
35	4.9	11.4	2.2	3.3	7.9	5.70	15.1	20.8	11.8	6.0
40	5.3	12.8				6.30	15.1	13.2	2.0	6.0

Based on both of these analyses, equal lateral loads were applied at each floor of the assemblage specimen. This is justified since the calculated ratio of forces of 1.1 is close to 1.0. The ratio is significantly lower than 2.0, which corresponds to the ratio of forces for a triangular distribution. The selected vertical distribution of forces subjected both orientations of floor panels to the same lateral load. This load was applied through identical hydraulic rams at each floor level supplied by an air-powered hydraulic pump, controlled manually. The loading equipment previously used in the shear wall specimens was used in the assemblage tests as well.

4.3.4 Overview of Assemblage Specimen

The Two-story Assemblage Specimen was constructed between June and July 2002 and was tested on August 12, 2002. A picture of the in-plane walls including the rams is presented in Figure 4.36. A picture of the flanges and loading beams is shown in Figure 4.37.

Figure 4.36 Elevation view of assemblage specimen (North-South direction)

Figure 4.37 Elevation view of assemblage specimen (East-West direction)

4.4 LOADING HISTORY

The planned in-plane loading history for the shear wall specimens, shown in Figure 4.38, consisted of a series of reversed cycles to monotonically increasing maximum load. Lateral loads were manually controlled using a hydraulic actuator. The predetermined target values (PV) were based on the predicted load to produce significant changes in the behavior of the specimen such as flexural cracking and yielding of the flexural reinforcement. After

yielding of the flexural reinforcement load was applied by controlling the displacements, a minimum of one cycle at each displacement level was applied. The proposed loading history is shown in Figure 4.38.

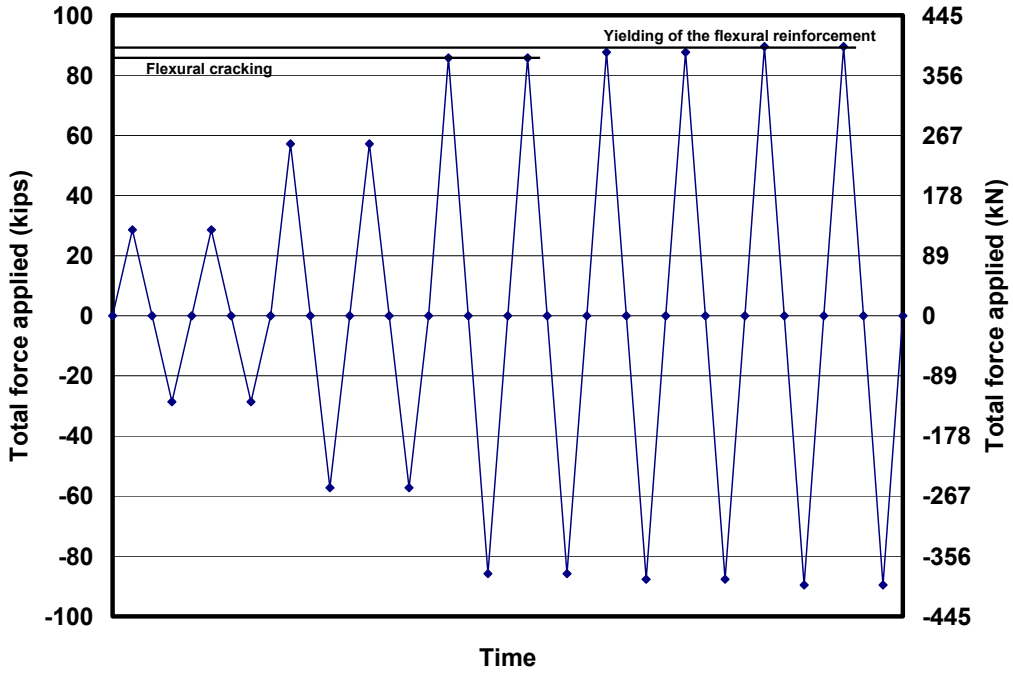

Figure 4.38: Proposed loading history

4.5 AXIAL LOAD

Axial load on the assemblage specimen comes from the weight of the assemblage itself and the loading equipment. The total axial load per wall is 30.2 kips (133 kN).

4.6 TRANSVERSE STABILITY

The flanges were also intended to enhance the out-of-plane stability of the assemblage specimen by increasing the stiffness of the assemblage about its weak axis. No external supports were used.

4.7 INSTRUMENTATION

The purpose of instrumentation was to determine the behavior of the assemblage. This instrumentation was selected to measure global and local behavior of the assemblage.

4.7.1 Global Behavior

The global behavior of the assemblage specimen is characterized by its overall force-displacement behavior in the direction of loading. The horizontal displacement of each wall was measured at each floor level using string potentiometers. The applied load was measured using the same pin load cells as in the shear wall tests. Pressure transducers were used to verify those load-cell readings.

4.7.2 Local Behavior

The local behavior of the assemblage was described in terms of the deformation patterns of individual components. The following measurements were recorded for both stories of the east and west shear wall:

- vertical displacement of wall;
- vertical displacement through mid-height of wall;
- diagonal deformation of wall;
- horizontal deformation along transverse length of floor slab; and
- slip between elements.

The vertical deformations were measured using string potentiometers mounted to the wall. The diagonal deformations indicate the shear deformation in each wall, using string potentiometers mounted to wooden blocks mounted to the specimen (Figure 4.39). The displacement of each slab was measured to determine abnormal deformation patterns or indicate slip between floor panels on the second elevated slab. Possible slip between adjacent elements was measured

using a linear potentiometer mounted between the adjacent elements. This was done to detect any relative movement between the loading beam and the floor slabs, between the base of the wall and the foundation, and between the foundation and the laboratory floor. For other locations slip was determined visually, observing any offset in a line drawn perpendicular to the interface between adjacent elements (Figure 4.40 through Figure 4.42). Slip was monitored during the tests; if the line was no longer continuous, the slip was quantified based on manual readings. This technique was used where slip was not probable, or was possible along several planes:

- vertical panel connections;
- bond beam-wall connection;
- floor slab panel joints; and
- loading beam-floor slab joints.

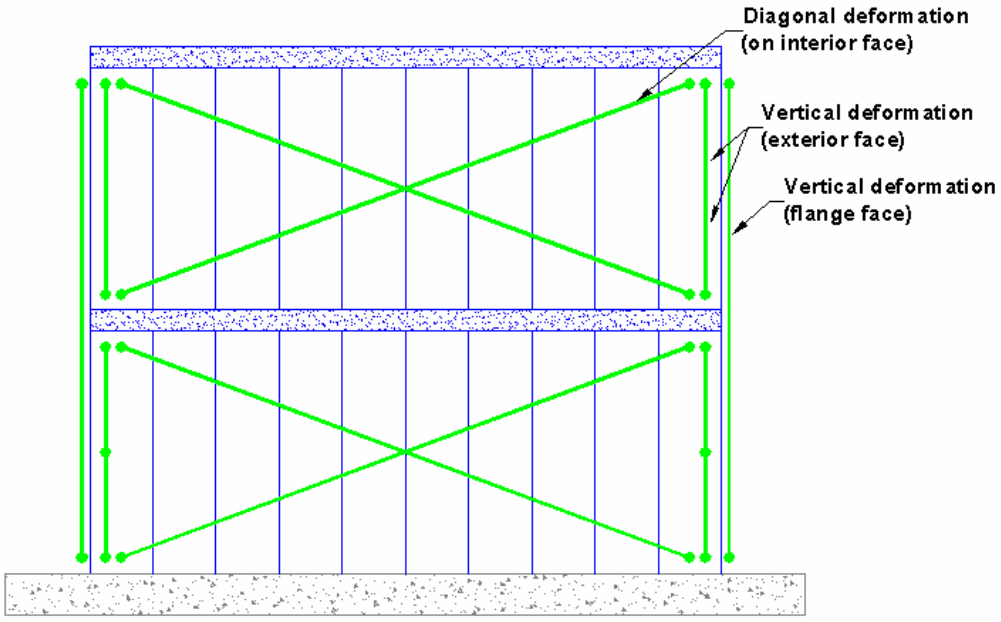

Figure 4.39: Displacement transducers to measure vertical and diagonal deformation in each shear wall

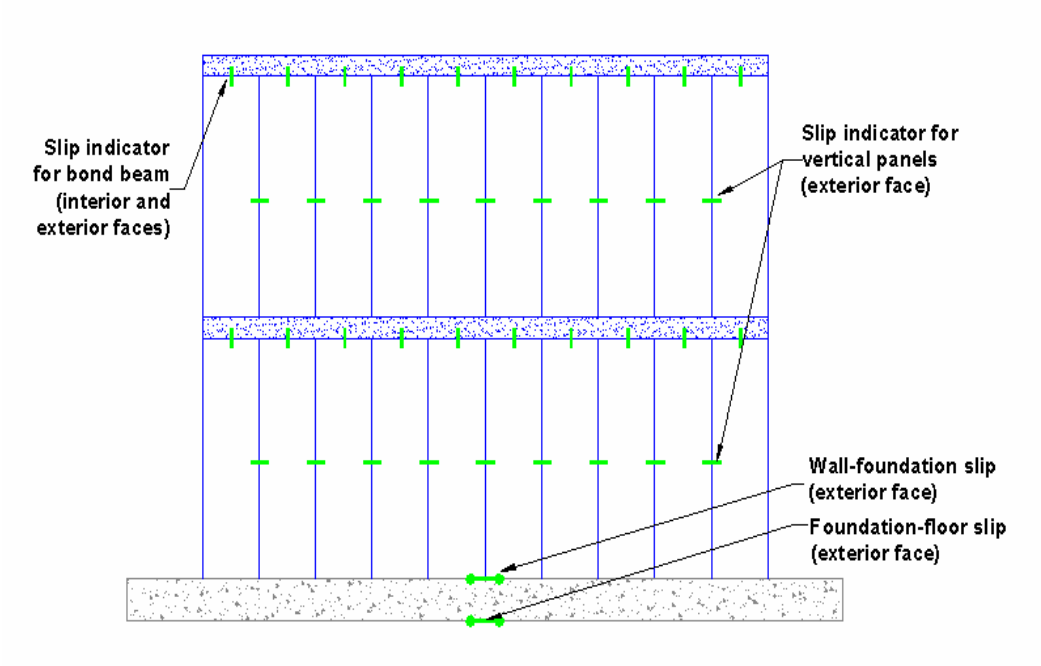

Figure 4.40: Measurement of relative slip for wall elevation

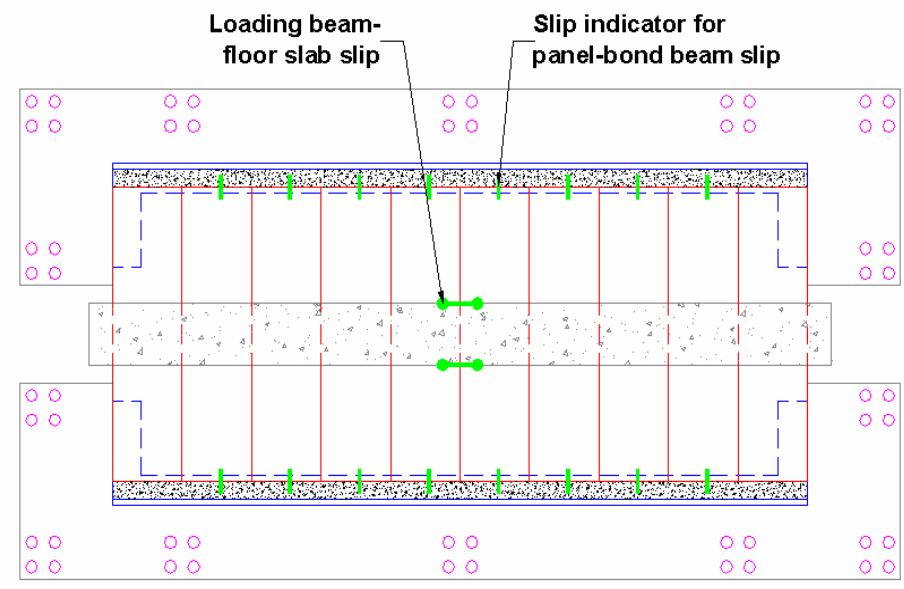

Figure 4.41: Measurement of relative slip at first story

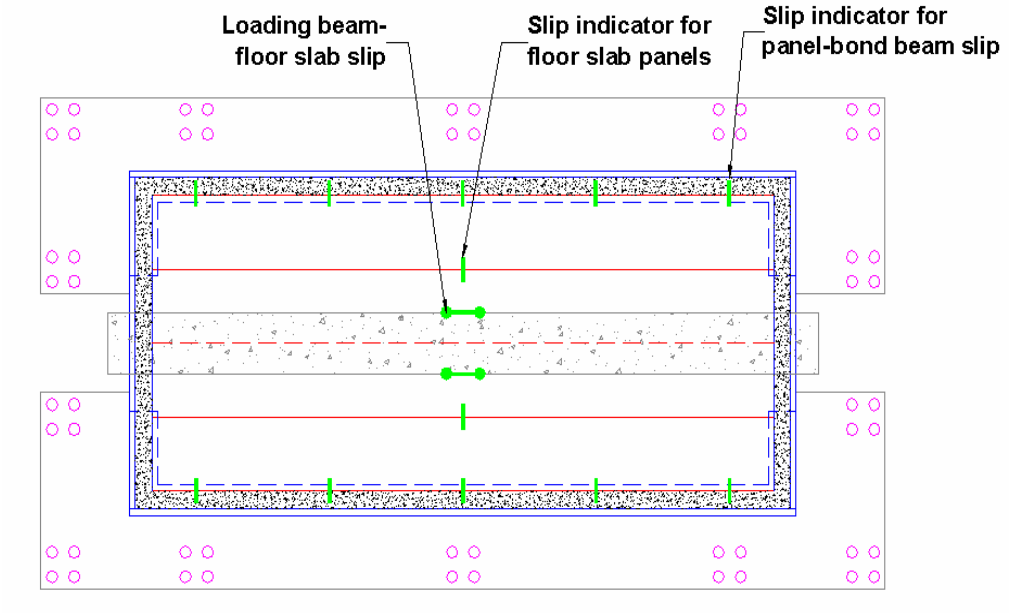

Figure 4.42: Measurement of relative slip at second story

4.7.3 Data Acquisition

Data were acquired in real time using a HP 3852 scanner. Analog-to-digital conversion was carried out by a National Instruments card in a Windows-based microcomputer, running under Measure, a National Instruments add-on for the Microsoft Excel spreadsheet program. Once in Excel format, data were plotted conventionally.

CHAPTER 5
Test Results for Shear-dominated AAC Shear Wall Specimens

The primary objective of this chapter is to describe the results of each shear-dominated AAC shear wall tested at UT Austin. This chapter also presents for each specimen the design objectives, actual loading history, major events, history of crack formation and hysteretic behavior. A section on the behavior that had been predicted for each specimen identifies several conditions that represent a change in strength or stiffness for each shear wall specimen. The sequence of behavior based on the interaction diagram justifies the geometry and prescriptive reinforcement for each shear wall specimen. The actual loading and displacement histories are also presented. The sequence of damage in the wall is presented for each specimen, along with quantification of the observed versus predicted behavior of each specimen.

5.1 DESIGN OBJECTIVES OF EACH AAC SHEAR WALL SPECIMEN

The basic design approach for AAC shear wall specimens involved the following steps:

1) Select the desired behavior mode. In design of real AAC structures, the desired behavior mode would be flexure-dominated behavior in the case of inelastic response, or either flexure- or shear-dominated behavior in the case of elastic response. In design of AAC shear wall specimens, the desired failure mode for each specimen depended on the test objectives for that specimen.

2) Prepare an interaction diagram for the wall showing the capacity as governed by each possible failure mode, as a function of axial load. In design of real AAC structures, for which the design axial loads are known, the failure mode can be controlled by controlling the walls aspect ratio and flexural reinforcement. In design of AAC shear wall specimens, the axial load could also be controlled.

This section presents the process for selecting the wall geometry, reinforcement and axial load for Shear Wall Specimen 1. The selection of the wall geometry and reinforcement for the remaining specimens is included with the results of each specimen. In an actual building the geometry and selection of the reinforcement may be changed to force the desired behavior in an interaction diagram.

The behavior of Shear Wall Specimen 1 was predicted prior to testing. An interaction diagram is presented in Figure 5.1 for the prediction of flexural cracking, web-shear cracking, sliding shear, crushing of the diagonal strut, and the nominal flexural capacity of Shear Wall Specimen 1, based on the proposed equations of Chapter 8. Two levels of axial load are represented in this figure by dashed horizontal lines, 80 kips (356 kN) and 156 kips (694 kN). At an axial load of 80 kips (356 kN), as the base shear increases the expected sequence of behavior is flexural cracking; web-shear cracking; sliding shear and crushing of the diagonal strut. Web-shear cracking was not observed in the specimen when the wall began to slide at the foundation at a load of 80 kips (356 kN). To stop the sliding the axial load was increased three times, to a final load of 156 kips (694 kN). The anomalously high splitting tensile strength of the AAC material used in Shear Wall Specimen 1 caused a discrepancy between the web-shear

cracking capacity predicted using the equations developed in Chapter 7 and the observed web-shear cracking capacity in Shear Wall Specimen 1. If this final axial load would have been used during the entire test, the predicted sequence of events would have been web-shear cracking, flexural cracking, and simultaneous crushing of the diagonal strut and sliding shear.

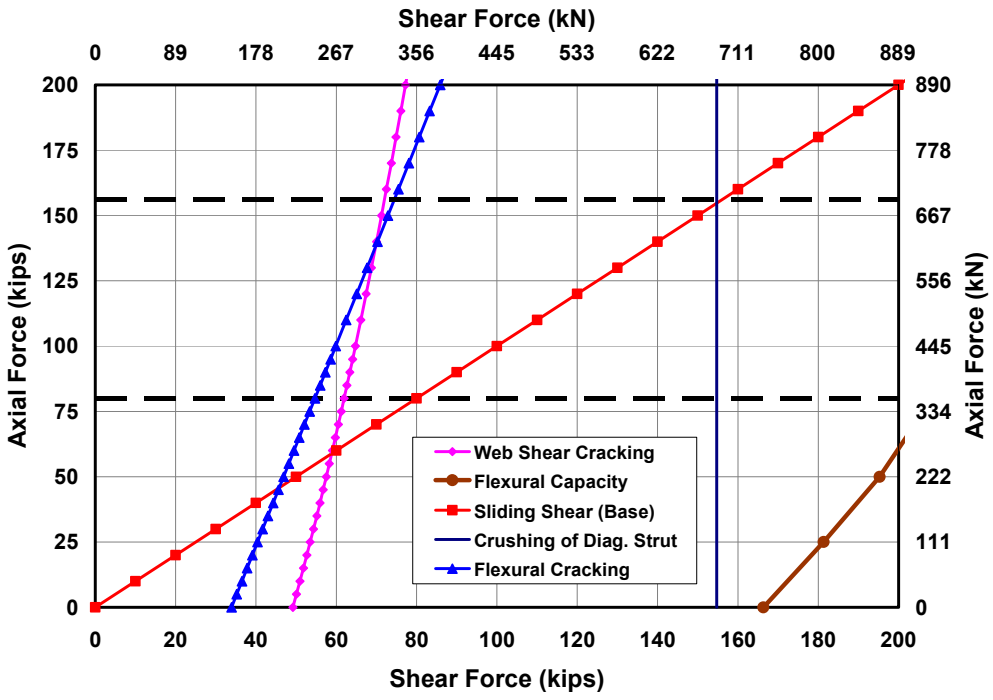

Figure 5.1: Interaction diagram for Shear Wall Specimen 1 based on predictions of Chapter 8

5.2 SHEAR WALL SPECIMEN 1

The predicted behavior of this specimen at the initial and final axial loads is discussed in Section 5.1.

5.2.1 Loading History and Major Events for Shear Wall Specimen 1

The actual loading and displacement histories for Shear Wall Specimen 1 are presented in Figure 5.2. Monotonically increasing load point numbers are assigned for each set of data recorded during the test. Data are classified into cycles with maximum loads and drift ratios for each cycle (Table Table 5.1). Loading to the south is considered positive; loading to the north, negative. In this test the wall was loaded first to the north and then to the south, so that the load history curve and hysteresis curve would begin with negative values. In Cycles 15, 20 and 23 the wall was loaded to the north and then reloaded to the north. Since the axial load changed during the test, a summary of the applied axial load in each cycle is presented in Table 5.2.

Cycles are further classified by the direction of loading in terms of "a" and "b." For Shear Wall Specimen 1, "a" refers to loading to the north, and "b" refers to loading to the south. In future tests, specimens were loaded first to the south.

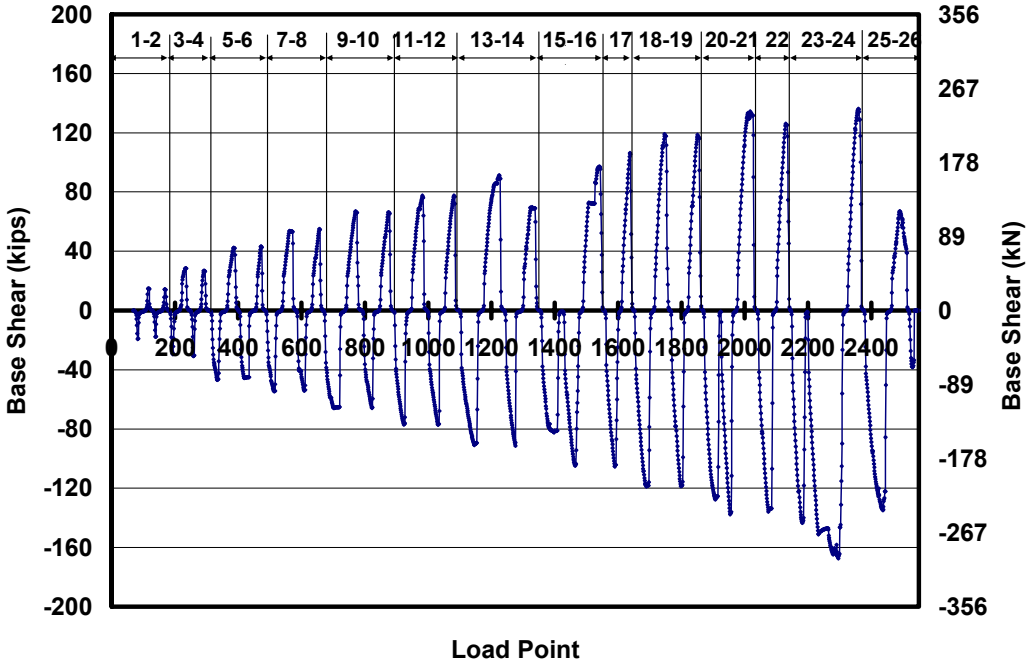

Figure 5.2: Actual loading history for Shear Wall Specimen 1 (numbers at the top designate cycle numbers)

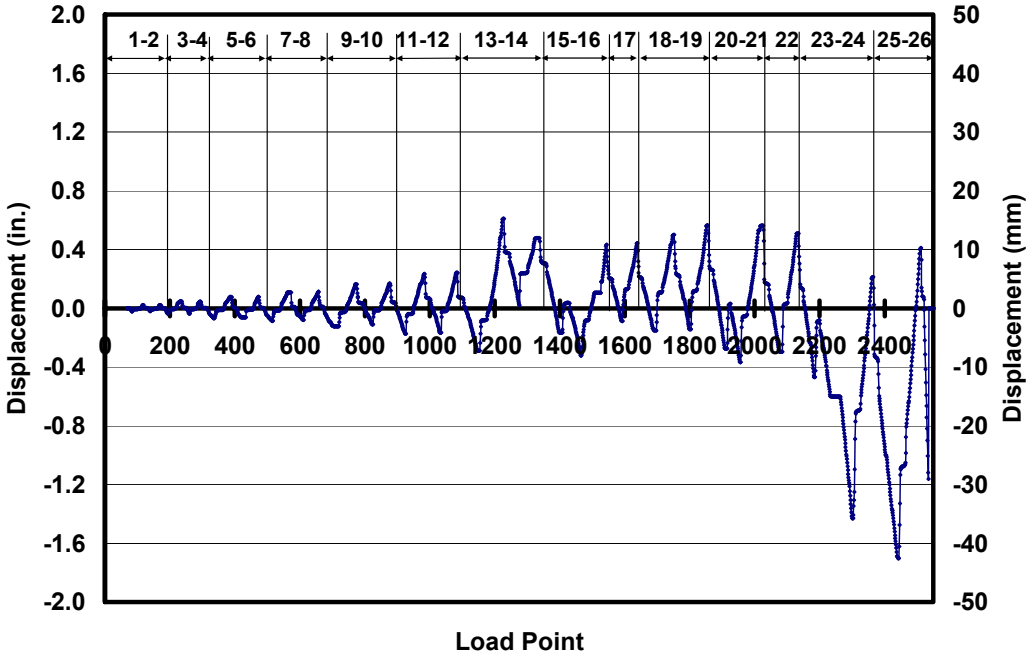

Figure 5.3: Actual tip displacement history for Shear Wall Specimen 1 (numbers at the top designate cycle numbers)

Table 5.1: Load points, maximum load and drift ratios for each cycle for Shear Wall Specimen 1

Cycle	Load Points	Maximum Applied Load kips (kN)	Max. Drift Ratio (%)	Cycle	Load Points	Minimum Applied Load kips (kN)	Min. Drift Ratio (%)
1a	68-106	-19.3 (86)	0.013	1b	107-128	14.8 (66)	0.015
2a	129-158	-17.9 (79)	0.012	2b	159-180	14.2 (63)	0.013
3a	181-213	-29.4 (131)	0.023	3b	214-247	28.4 (126)	0.032
4a	248-278	-30.9 (137)	0.021	4b	279-309	26.9 (-120)	0.03
5a	310-361	-46.8 (208)	0.039	5b	362-400	42.3 (188)	0.052
6a	401-447	-45.6 (203)	0.036	6b	448-485	43.2 (192)	0.055
7a	486-535	-54.7 (243)	0.045	7b	536-582	53.8 (239)	0.073
8a	583-629	-54.0 (240)	0.042	8b	630-668	55.0 (245)	0.074
9a	669-737	-65.8 (292)	0.056	9b	738-790	67.0 (298)	0.099
10a	791-844	-65.9 (293)	0.05	10b	845-889	66.2 (295)	0.088
11a	890-944	-77.1 (343)	0.069	11b	945-996	68.9 (307)	0.11
12a	997-1049	-77.2 (343)	0.071	12b	1050-1095	77.7 (346)	0.14
13a	1096-1170	-90.9 (404)	0.11	13b	1170-1240	91.3 (406)	0.19
14a	1241-1295	-91.3 (406)	0.11	14b	1296-1353	69.9 (311)	0.15
15a	1354-1424	-82.3 (366)	0.095				
16a	1425-1486	-104.8 (466)	0.13	16b	1487-1553	97.2 (432)	0.19
17a	1554-1608	-105.3 (465)	0.10	17b	1609-1648	106.3 (473)	0.20
18a	1649-1711	-118.9 (529)	0.13	18b	1712-1764	119.1 (530)	0.23
19a	1765-1819	-118.6 (528)	0.12	19b	1820-1868	118.6 (528)	0.25
20a	1869-1924	-127.6 (568)	0.15				
21a	1925-1973	-137.6 (612)	0.16	21b	1974-2038	133.4 (593)	0.32
22a	2039-2097	-133.9 (595)	0.16	22b	2098-2145	126.2 (561)	0.31
23a	2146-2197	-143.4 (638)	0.20				
24a	2198-2319	-167.6 (745)	0.51	24b	2320-2375	136.1 (605)	0.42
25a	2376-2460	-134.9 (598)	0.69	25b	2461-2517	67.0 (298)	0.83
26a	2518	-38.4 (171)	0.18				

Table 5.2: Axial load throughout the test

Axial Load kips (kN)	Load Points	Cycles
80 (356)	68 - 1424	1-15
100 (445)	1425 - 1553	16
128 (569)	1554 - 1648	17
140 (623)	1649 - 1924	18-20
156 (694)	1925 - 2518	21-25

5.2.2 Sequence of Crack Formation for Shear Wall Specimen 1

The sequence of crack formation in Shear Wall Specimen 1 is described in terms of major events: points during the test when either the condition of the specimen changed (for example, flexural cracking or shear cracking), or the applied axial force was increased. Table 5.3 lists the major events and the load point at which they occurred.

Table 5.3: Description of major events for Shear Wall Specimen 1

Major Event	Load Point	Physical Description
1	1218	Sliding on leveling bed joint, loading south
2	1275	Formation of horizontal crack, loading north
3	1396	Sliding on leveling bed joint, load north
4	1424	Increasing axial load to 100 kips
5	1541	Sliding on leveling bed joint
6	1556	Increasing axial load to 128 kips
7	1648	Increasing axial load to 140 kips
8	1924	Increasing axial load to 156 kips
9	2233	Minor crushing of diagonal strut
10	2275	Sliding on leveling bed joint
11	2296	Web-shear cracking
12	2360	Web-shear cracking
13	2361-2518	Crushing of the diagonal strut

5.2.2.1 Cracks formed prior to testing Shear Wall Specimen 1

Prior to testing, shrinkage cracks had already formed along the base of the wall through the leveling bed mortar joint. Additional cracks had formed during testing of Shear Wall Pilot Specimen 2, at locations where the panels had been patched due to minor spalling during shipping. These are also shown in gray in Figure 5.4. The cracks did not affect the stiffness or strength of the wall, nor the cracking pattern observed in Shear Wall Specimen 1.

5.2.2.2 Formation of horizontal crack and observed sliding in Shear Wall Specimen 1

During Cycle 13b it was clear the wall had slid at the base at a load of 85 kips (378 kN) between Load Points 1210 and 1218; at Load Point 1228 thin metal plates were first placed between the wall and buttress to restrain movement. When the horizontal crack formed at the south toe during Load Point 1275 (Figure 5.4), it became clear that the wall was no longer free to move vertically, and the plates were removed since they were causing local damage at the toe. As the wall was loaded to the north sliding was observed at a load of 81 kips (360 kN) between Load Points 1388 and 1408, the wall was allowed to slide in order to begin the next cycle with a displacement close to zero. Both cases of sliding are shown in the hysteretic behavior of Cycles 13-15 (Section 5.2.3).

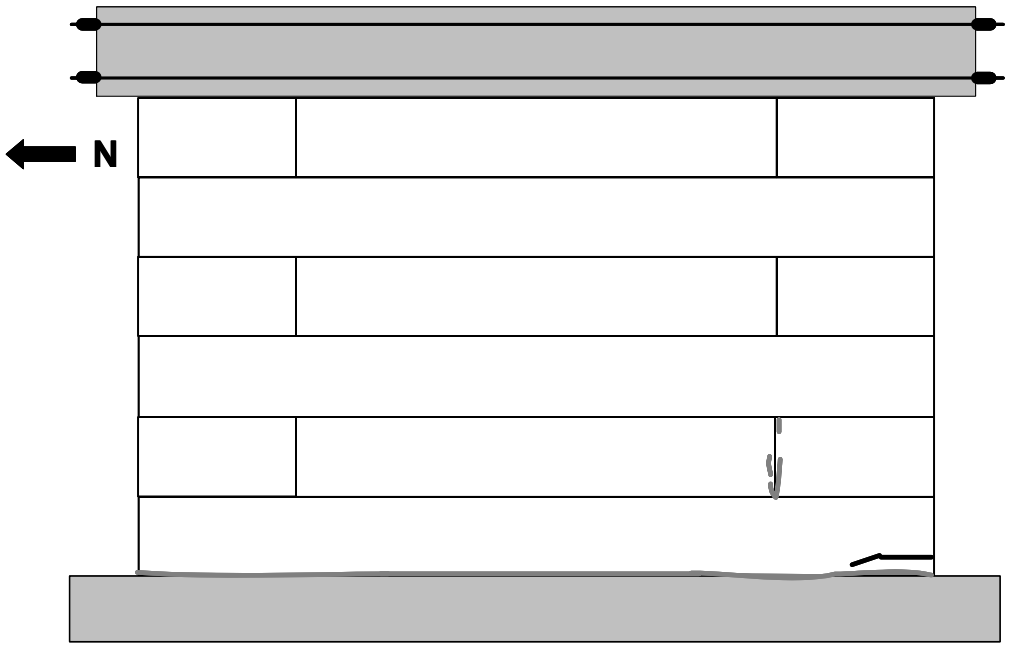

Figure 5.4: Formation of horizontal crack at south toe in Shear Wall Specimen 1

To suppress sliding and provoke web-shear cracking or another major event, the axial load was increased to 100 kips (445 kN) at Load Point 1424 (Major Event 4). Sliding was observed again between Load Points 1539 and 1543 at a base shear 97 kips (418 kN). The specimen was cycled at an axial load of 100 kips (445 kN). As it became apparent that sliding was imminent, the axial load was increased to 128 kips (569 kN), 140 kips (623 kN) and 156 kips (694 kN).

5.2.2.3 Formation of cracks at the compression toes in Shear Wall Specimen 1

During Load Point 2010 at a base shear of 133 kips (593 kN), a vertical crack propagated from the horizontal crack at the south toe; during Cycle 22b minor spalling occurred at the base of the wall. While loading to the north, at Load Point 2185 and a load of 143.4 kips (638 kN), the inverted V-shaped crack

and the curved section of spalling shown in Figure 5.5 formed. The wall was unloaded and reloaded to the north because the crushing indicated that a major event was imminent. At a load of 151.2 kips (673 kN) to the north (Load Point 2233), a horizontal crack formed, inducing minor spalling over 4 ft. (1.2 m) of the first panel. As the load increased to 164.9 kips (734 kN), the spalling increased. Figure 5.6 presents the corresponding cracking pattern in the north half of the lower two panels. Although spalling occurred on both faces of the wall, the locations of spalling were not always located symmetrically with respect to the plan centerline of the wall. This could be due to interference with the instrumentation, or because the cracks were not always visible on both faces of the wall.

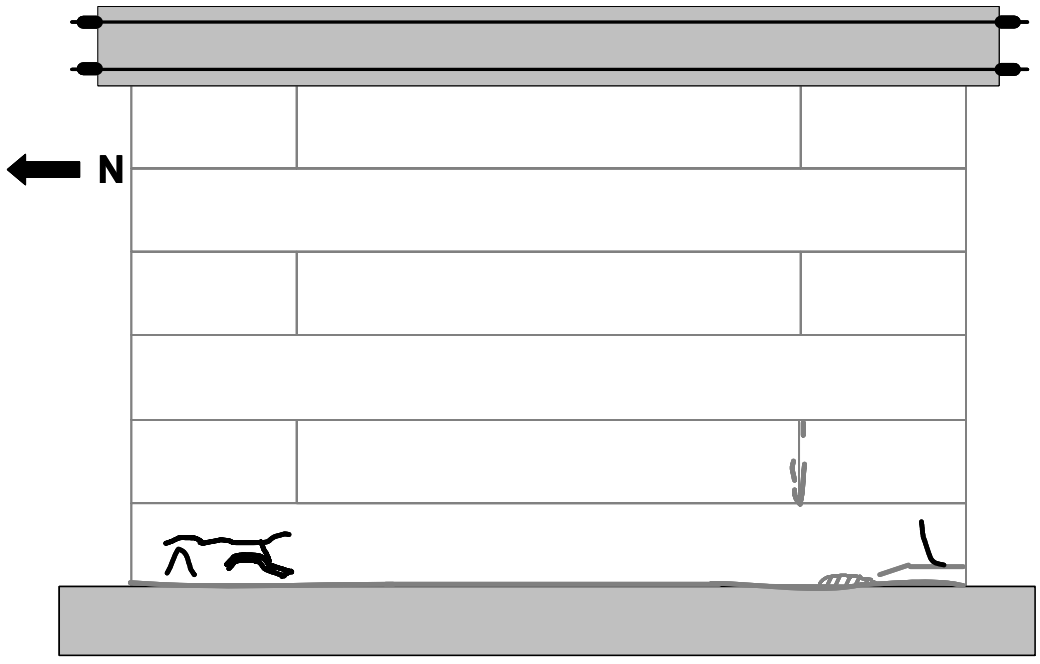

Figure 5.5: Formation of cracks in compression toes in Shear Wall Specimen 1

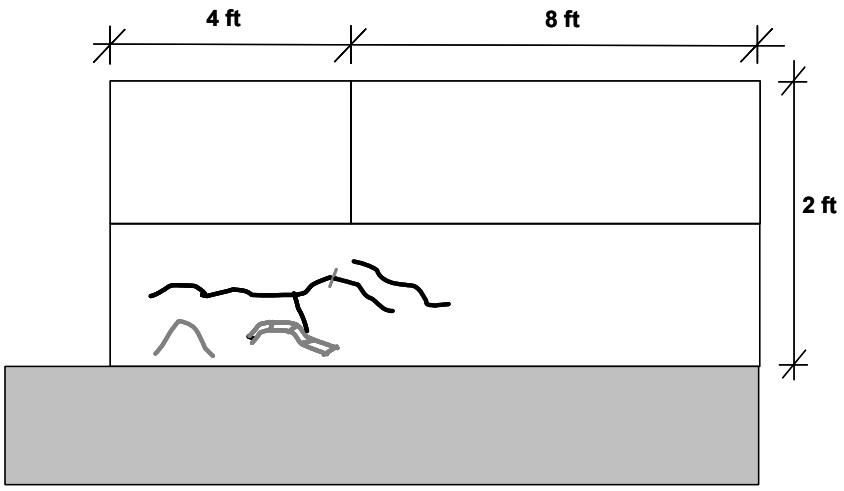

Figure 5.6: Formation of cracks in spalled zone in Shear Wall Specimen 1

5.2.2.4 Formation of web-shear cracks in Shear Wall Specimen 1

Almost immediately after cracks at the wall toes formed (Load Point 2296), the two parallel web-shear cracks shown in Figure 5.7 formed at the maximum load of 164.2 kips (730 kN). The cracks are inclined except at the intersection of bed or head joints, where the crack temporarily follows the joint. In addition, further propagation of the horizontal crack at the north toe indicates the widening of the compression zone to a length of 65 in. (1.65 m). The initial prediction for web-shear cracking was 127.7 kips (568 kN). This specimen exhibited a value of web-shear cracking significantly higher than the predicted value and is anomalous with respect to the remaining shear dominated specimens as shown in Section 8.3.

Next, the wall was reloaded to the south to a load of 136.1 kips (605 kN). Another web-shear crack formed at the same location as the previous web-shear crack, at the same time that the existing cracks propagated in the south toe (Figure 5.7).

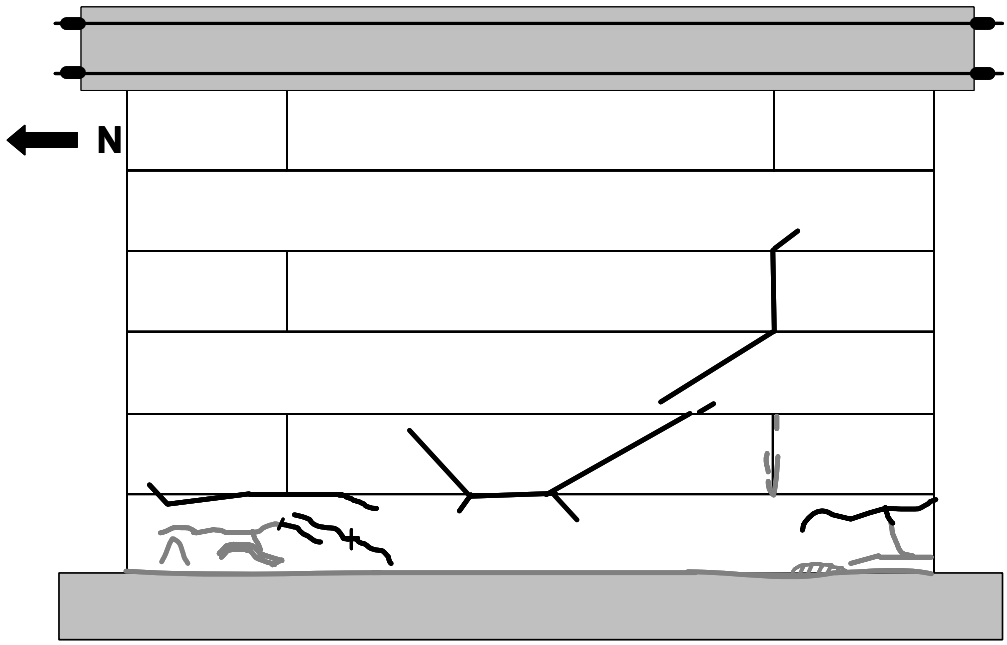

Figure 5.7: Web-shear cracking in Shear Wall Specimen 1

5.2.2.5 Crushing of the diagonal strut in Shear Wall Specimen 1

Throughout Cycle 25a, the horizontal cracks at the base extended to the center of the wall. As shown in Figure 5.8, the spalling of the AAC cover at the north end had reduced the capacity of the compression strut, which continued to move toward the center of the wall.

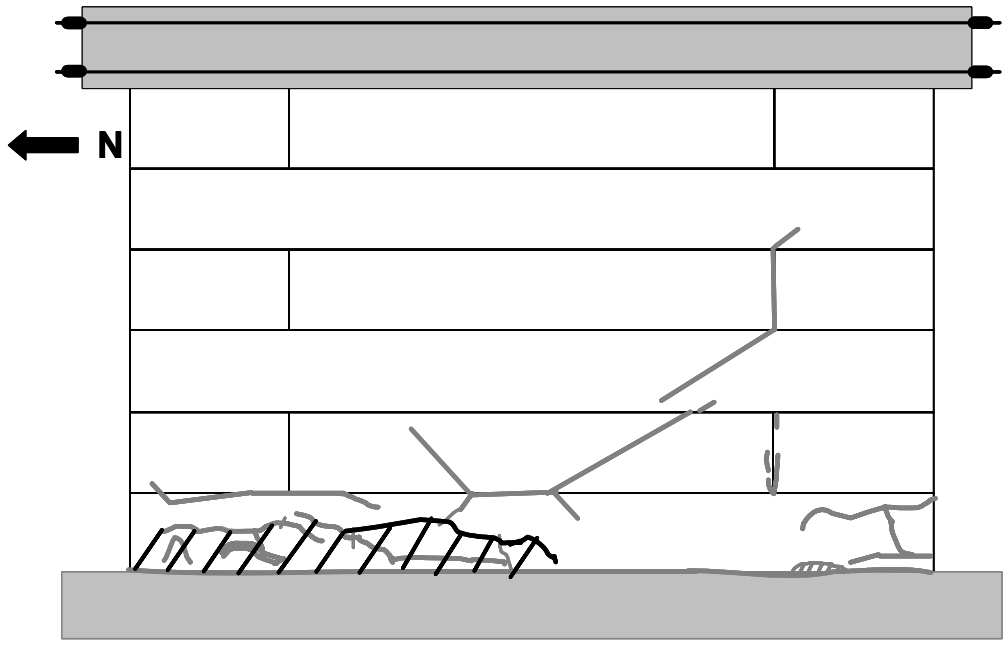

Figure 5.8: Crushing of the diagonal strut while loading to the north in Shear Wall Specimen 1

Similar events occurred in Cycle 25b. The extent of crushing shown in Figure 5.9 was not as severe, however, because the peak loads were 134.6 kips (598 kN) and 67 kips (298 kN) respectively for Cycles 25a and 25b. The zone of spalling was much larger at the north end, probably due to the larger loads applied in that direction throughout the test. The model for crushing of the diagonal strut in Section 8.6 was based on the observed behavior of this specimen. In the event of very large nominal flexural or web-shear cracking capacities, crushing of the diagonal strut can govern the behavior of an AAC shear wall.

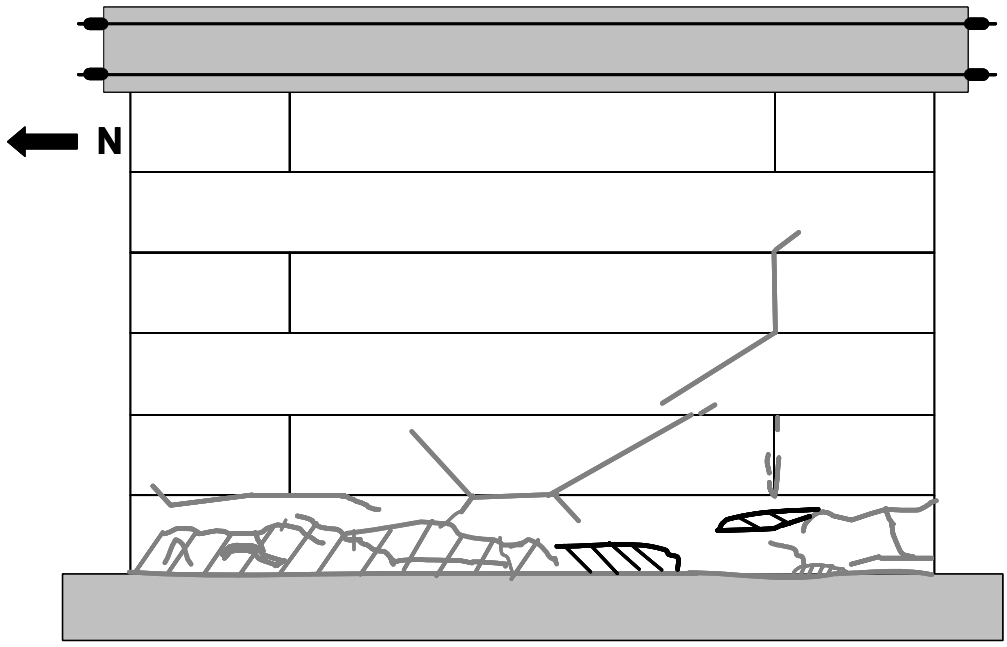

Figure 5.9: Crushing of the diagonal strut while loading to the south in Shear Wall Specimen 1

The wall did not show an increase in capacity. As it was subjected to further loading, a complete loss of cover occurred, leading to buckling of the welded wire reinforcement (Figure 5.10).

Figure 5.10: Buckling of vertical welded wire reinforcement in Shear Wall Specimen 1

5.2.3 Load-Displacement Behavior for Shear Wall Specimen 1

The load-displacement relationship of Shear Wall Specimen 1 is presented in terms of the non-dimensional drift ratio, and is non-linear elastic for the first 12 cycles (Figure 5.11). If the slip were removed from the specimen the maximum and minimum drift ratios would be 0.14% and 0.07%, respectively. The slip was removed from displacement data for this specimen by subtracting the measured slip from the measured horizontal displacement at every load point. The stiffnesses observed at various points in the loading history are described in Varela (2003).

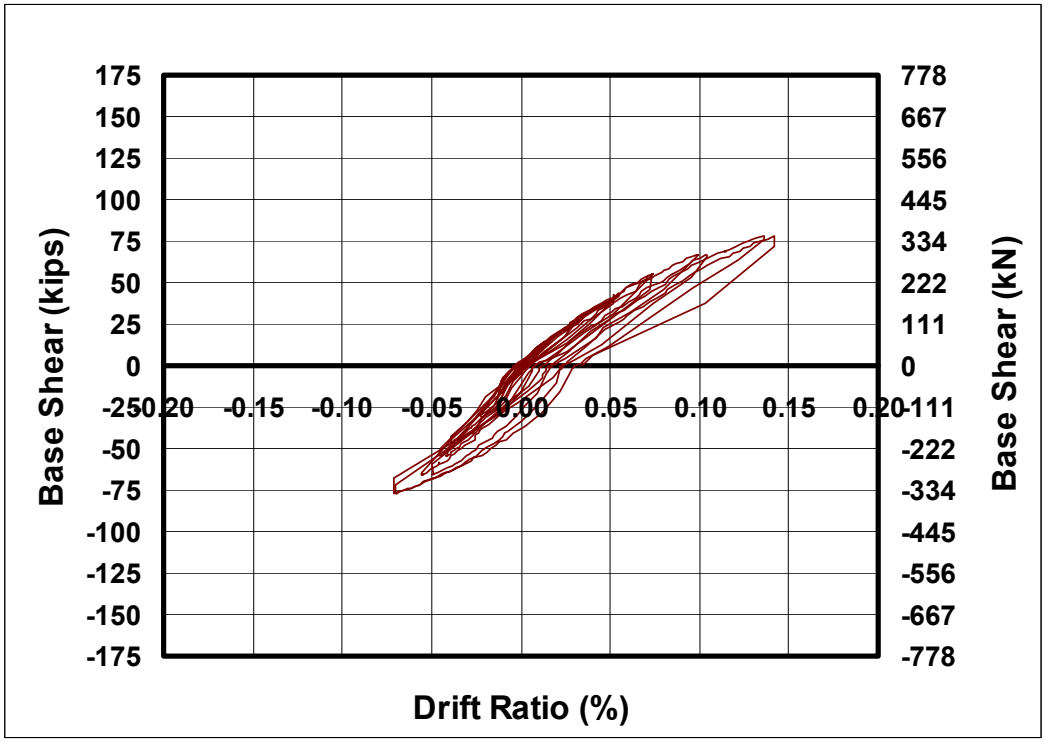

Figure 5.11: Load-displacement relationship for Cycles 1 through 12 based on recorded drift ratios

Cycles 13 through 15 were characterized by sliding between the first course and the Type S leveling bed mortar. This was observed twice in these cycles when the load-displacement curve was horizontal, at loads of 80 kips (356 kN) and 85 kips (378 kN). The hysteretic behavior for the slip removed in these specimens is presented along with the general hysteretic behavior for these cycles in Figure 5.12. Both of these curves have been corrected to remove the displacement present at the start of Cycle 13.

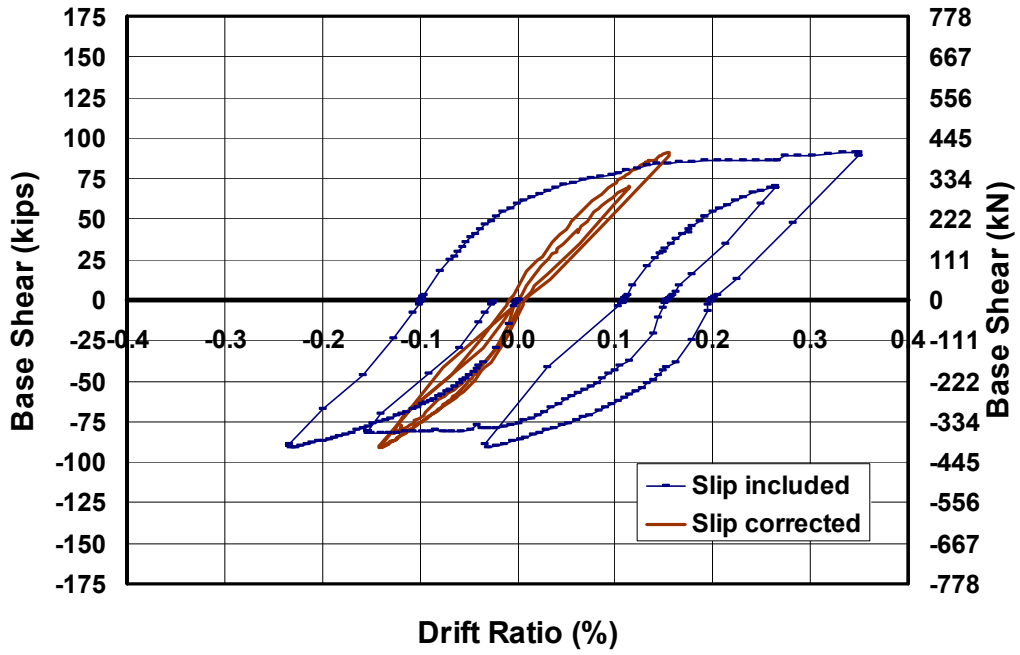

Figure 5.12: Load-displacement relationship for Cycles 13 through 15 including and excluding slip, with a correction for offset at the start of Cycle 13 in Shear Wall Specimen 1

Cycle 16 also indicates clear sliding by a horizontal portion of the load-displacement relationship, at a load of 97 kips (418 kN). The hysteretic behavior for the slip removed in these specimens is presented along with the general hysteretic behavior for these cycles in Figure 5.13. Both of these curves have been corrected to remove the displacement present at the start of Cycle 16.

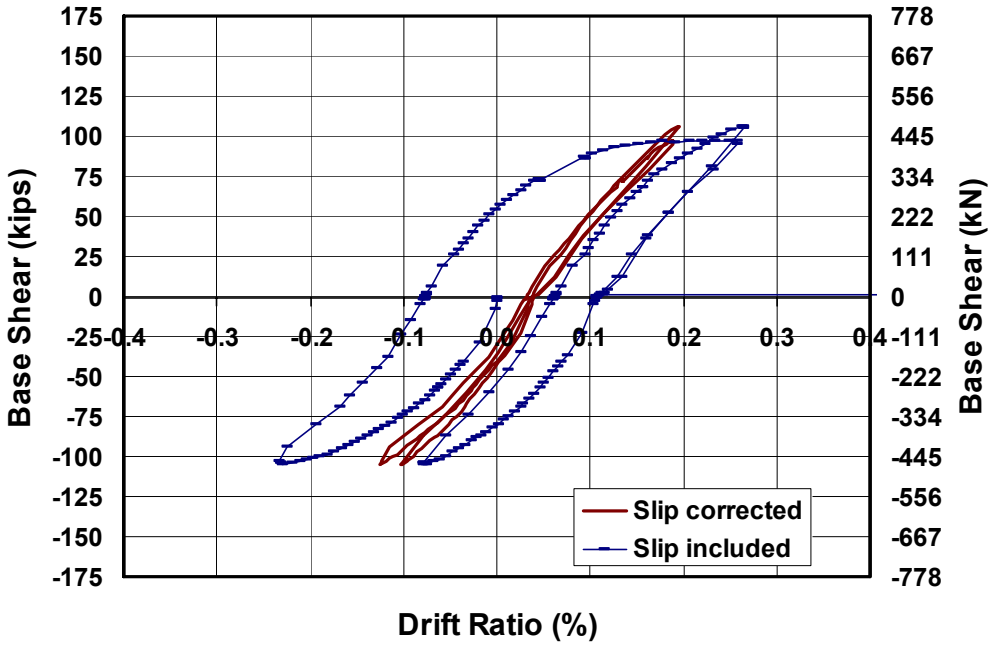

Figure 5.13: Load-displacement relationship for Cycles 16 and 17 including and excluding slip, with a correction for offset at the start of Cycle 16 in Shear Wall Specimen 1

The load-displacement relationship from Cycle 18 through the end of the test is presented in Figure 5.14. Slip has been removed from the specimen and the graph is corrected to remove any displacement offset present at the start of Cycle 18. The original load-displacement relationship including slip is presented in Figure 5.15. The coefficient of friction between AAC and Type S leveling bed mortar of Section 8.5.2 is based on the results of this specimen.

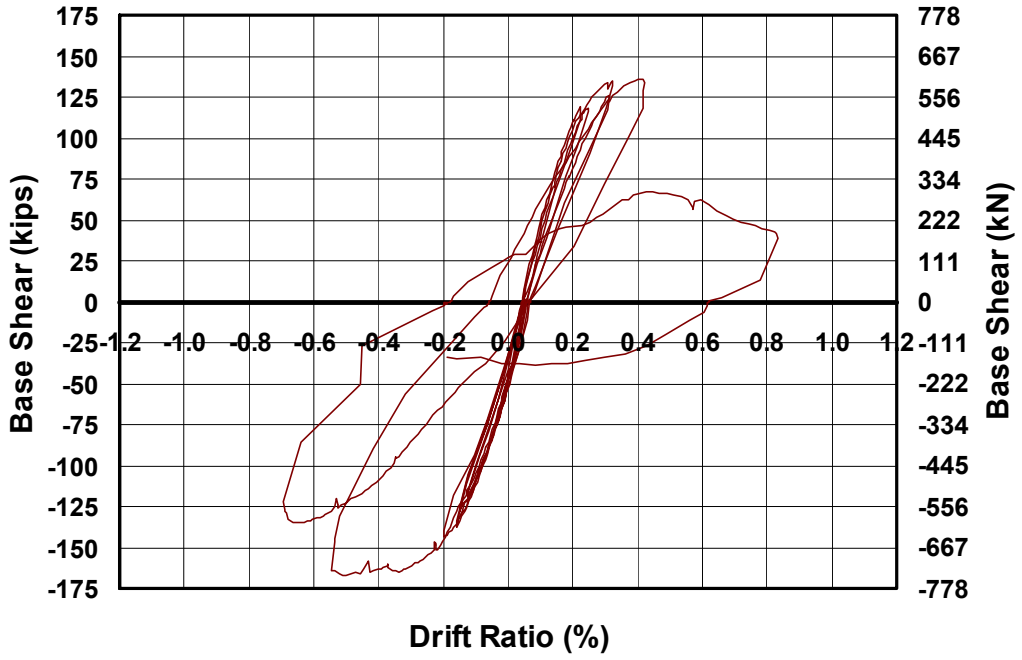

Figure 5.14: Load-displacement relationship from Cycle 18 through the end of the test excluding slip, with a correction for offset at the start of Cycle 18 in Shear Wall Specimen 1

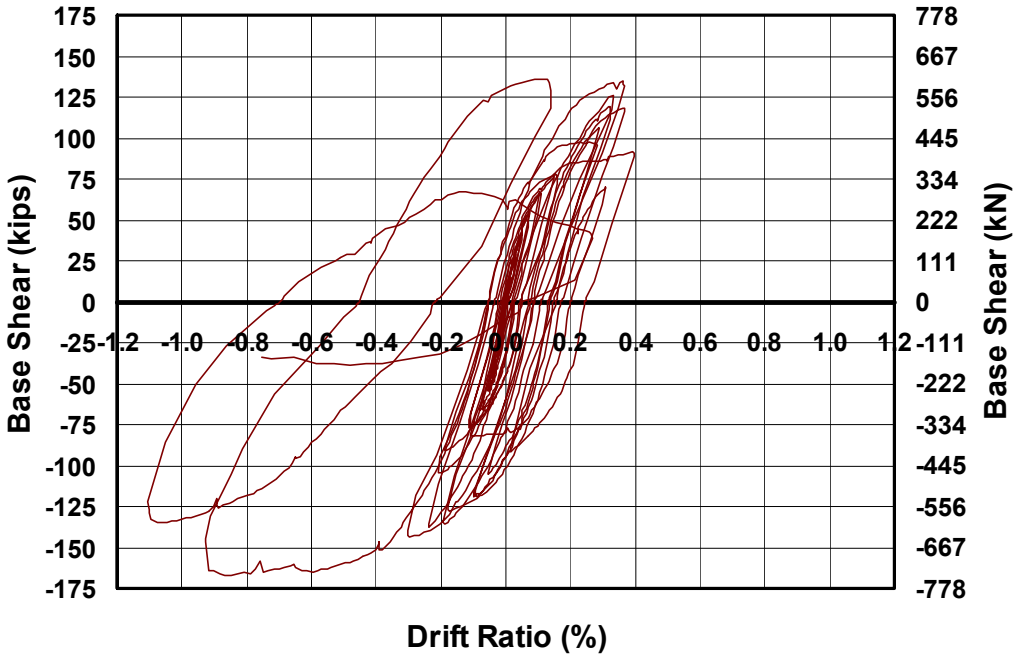

Figure 5.15: Load-displacement relationship throughout Shear Wall Specimen 1 with slip retained

5.3 SHEAR WALL SPECIMEN 2

An interaction diagram for base shear capacity as a function of axial load for Shear Wall Specimen 2 is presented in Figure 5.16. The axial load applied to Shear Wall Specimen 2 was 156 kips (694 kN), as shown by a dashed horizontal line in Figure 5.16. At this level of axial load the following major events are predicted in order of occurrence: web-shear cracking; flexural cracking; crushing of the diagonal strut; and sliding shear. This specimen was designed to observe flexural cracking and web-shear cracking.

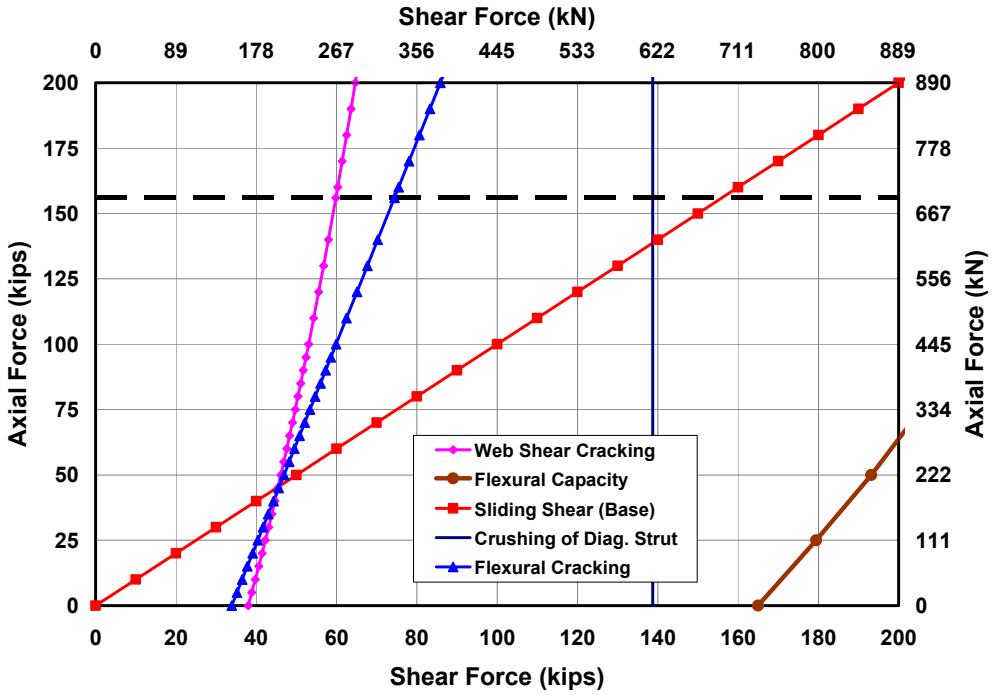

Figure 5.16: Predicted behavior of Shear Wall Specimen 2

5.3.1 Loading History and Major Events for Shear Wall Specimen 2

The actual load and displacement histories for Shear Wall Specimen 2 are presented in Figure 5.17 and Figure 5.18. Monotonically increasing load point numbers are assigned for each set of data recorded during the test. Data are classified into cycles with maximum loads and drift ratios for each cycle (Table 5.4). Loading to the south is considered positive; loading to the north, negative.

Cycles are further classified by the direction of loading in terms of "a" and "b." For Shear Wall Specimen 2 and all remaining specimens, "a" refers to loading to the south, and "b" refers to loading to the north.

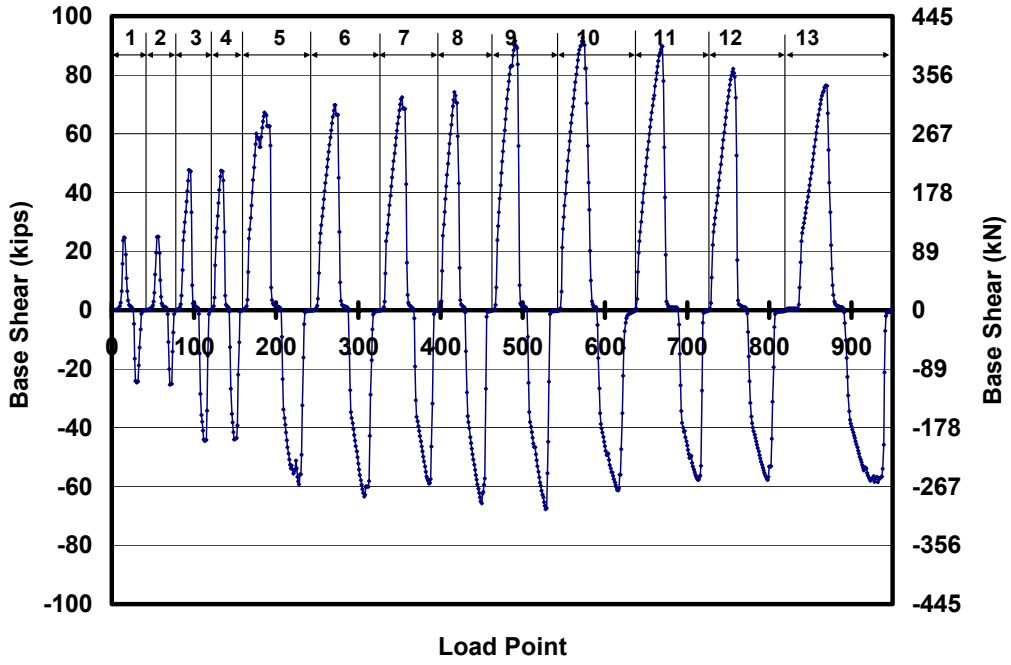

Figure 5.17: Actual loading history for Shear Wall Specimen 2 (numbers at the top designate cycle numbers)

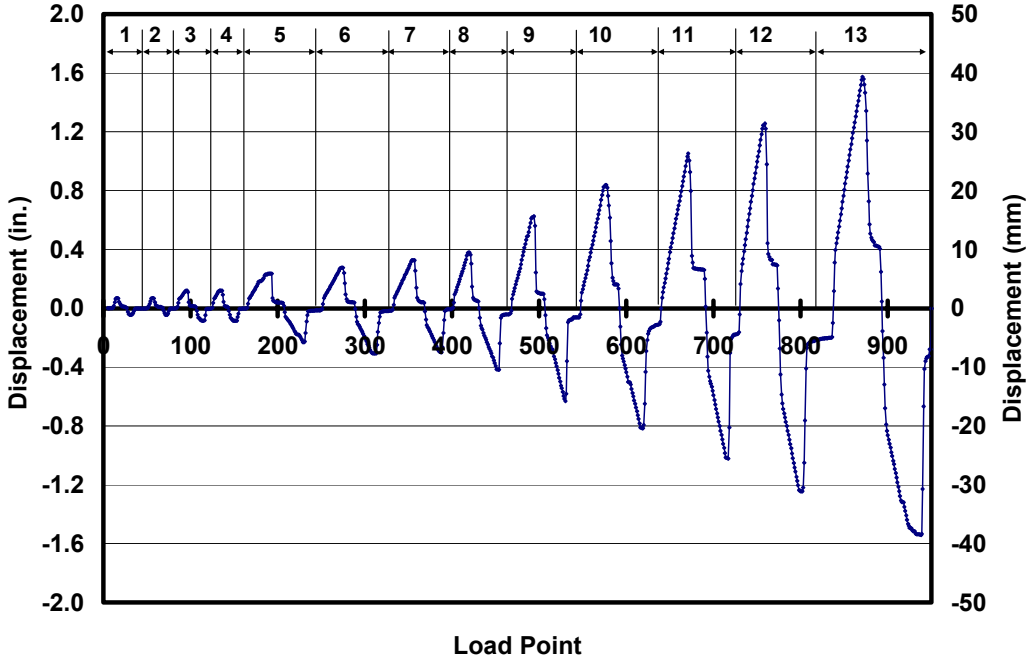

Figure 5.18: Actual tip displacement history for Shear Wall Specimen 2 (numbers at the top designate cycle numbers)

Table 5.4: Load points, maximum load and drift ratios for each cycle for Shear Wall Specimen 2

Cycle	Load Points	Maximum Applied Load, kips (kN)	Max. Drift Ratio (%)	Cycle	Load Points	Min. Applied Load, kips (kN)	Min. Drift Ratio (%)
1a	1-26	24.7 (110)	0.04	1b	27-41	24.6	0.03
2a	42-67	25 (111)	0.04	2b	68-78	25.3	0.03
3a	79-105	47.7 (212)	0.08	3b	106-120	44.9	0.06
4a	121-142	47.4 (211)	0.08	4b	143-158	43.9	0.06
5a	159-205	67.2 (299)	0.15	5b	206-245	59.3	0.15
6a	246-287	69.8 (310)	0.18	6b	288-327	63.4	0.19
7a	328-367	72.3 (322)	0.21	7b	368-396	59.0	0.19
8a	397-429	74.1 (330)	0.25	8b	430-464	65.7	0.27
9a	465-505	91.4 (407)	0.40	9b	506-544	67.7	0.41
10a	545-590	92.7 (413)	0.52	10b	591-637	61.3	0.53
11a	638-689	89.9 (400)	0.67	11b	690-726	57.8	0.66
12a	727-772	82.1 (365)	0.82	12b	773-820	57.8	0.81
13a	821-890	76.5 (340)	1.02	13b	891-949	58.4	1.00

5.3.2 Sequence of Crack Formation for Shear Wall Specimen 2

The sequence of crack formation in Shear Wall Specimen 2 is described in terms of major events: points during the test when either the condition of the specimen changed (for example, flexural cracking or web-shear cracking), or the applied axial force was increased. Table 5.5 lists the major events and the load point at which they occurred. In each section where crack maps are presented, preexisting cracks are shown in gray, and new cracks are shown in black.

Table 5.5: Description of major events for Shear Wall Specimen 2

Major Event	Load Point	Physical Description
1	176	Vertical crack formed at the center line of wall dividing the wall into two walls, loading south
2	188	Flexural cracks formed at north end of each wall section, loading south
3	221	Flexural crack formed at south ends of both walls with a simultaneous vertical crack that propagated into diagonal cracks, loading north
4	270, 272, 307 and 353	Continued vertical, flexural and diagonal cracks formed with propagation of existing cracks
5	417, 450	Formation of diagonal cracks at both ends of the wall and some propagation
6	491, 529	Minor spalling, vertical cracks formed at toes of wall, wall uplift, additional propagation
7	573, 616	New cracks formed in south section of wall and propagation of existing
8	670, 716, 798, 870	Small cracks formed and existing cracks propagated, minor spalling
9	934	Crack was observed between panels 9 and 10 continued spalling

5.3.2.1 Vertical, flexural and diagonal cracking in Shear Wall Specimen 2

In Shear Wall Specimen 2, two vertical shrinkage cracks formed prior to testing. Major Event 1 consists of the formation of a vertical crack at the panel joints in the center of the wall at Load Point 176, at a base shear and drift ratio of 60.1 kips (267 kN) and 0.1% respectively. This crack divided the specimen into individual walls. As load continued to be applied flexural cracks formed at the north end of each section, at a load of 66.3 kips (267 kN) and a drift ratio of 0.15%. These cracks are shown in black in Figure 5.19 and the preexisting vertical cracks are shown in gray.

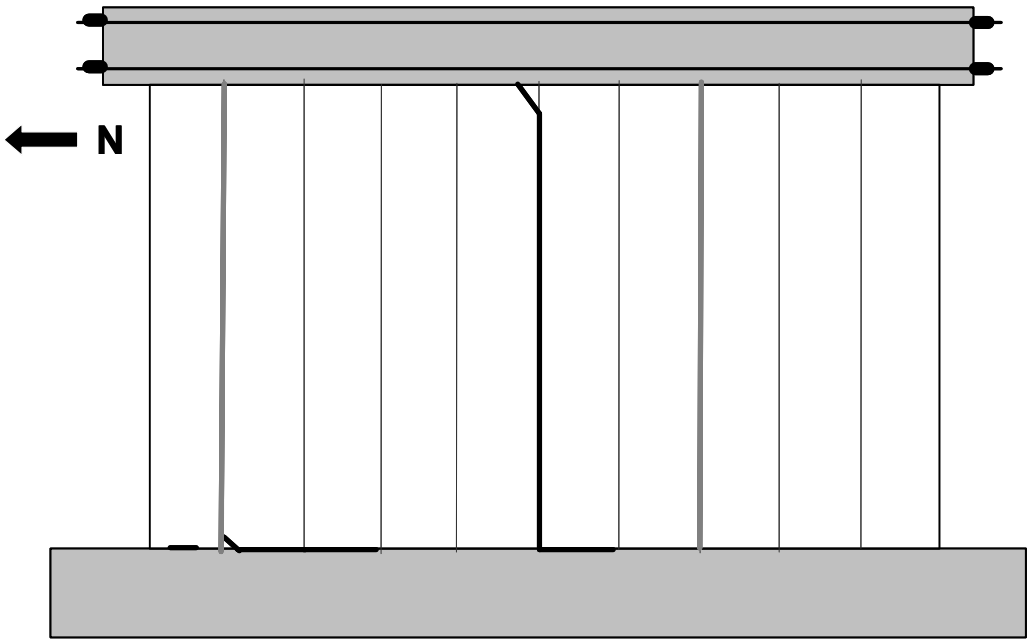

Figure 5.19: Vertical crack and flexural cracks at Major Events 1 and 2 in Shear Wall Specimen 2

As the wall was loaded to the north, dual flexural cracks formed at Load Point 221. A vertical crack between the third and fourth panels from the north formed and propagated into a diagonal crack, when the base shear and drift ratio in the specimen were 55.6 kips (247 kN) and 0.11% respectively. These events, shown in Figure 5.20, constitute Major Event 3. In future crack descriptions for Shear Wall Specimen 2, the panel number will be referenced from the north end of the wall.

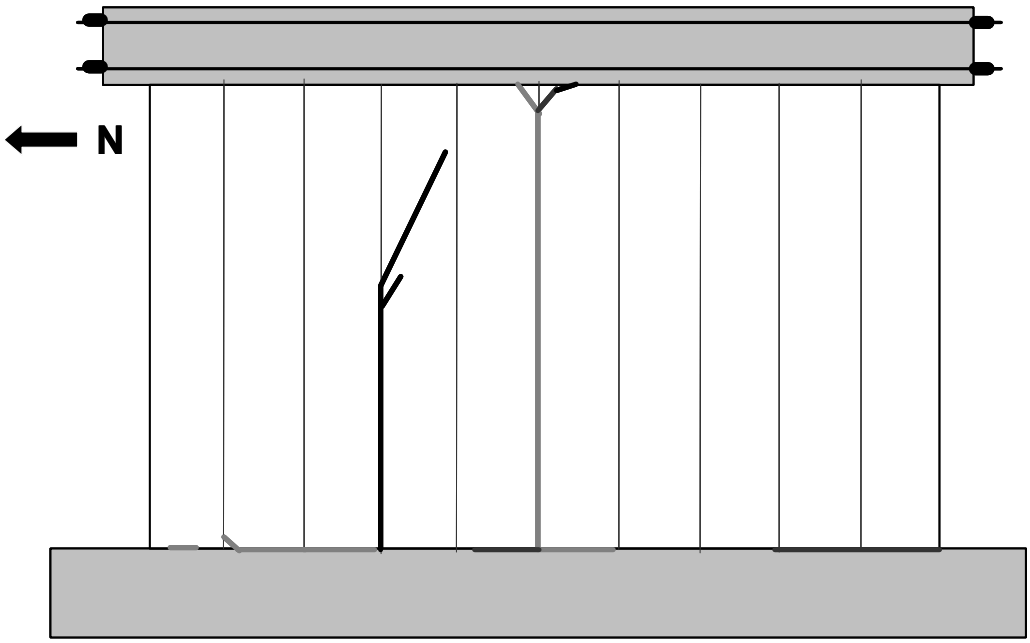

Figure 5.20: Simultaneous flexural cracking, vertical cracking and diagonal cracking occurred in Shear Wall Specimen 2

5.3.2.2 Additional vertical, flexural and diagonal cracking in Shear Wall Specimen 2

Major Event 4 corresponds to the formation of additional vertical flexural and diagonal cracks in Shear Wall Specimen 2. It includes Load Points 270, 272, 307 and 353. While loading to the south, at Load Point 270, a vertical crack formed between the sixth and seventh panels. It propagated into a diagonal crack near the base of the wall. Shortly afterwards, at Load Point 272, a flexural crack formed in the fourth panel. The base shears for Load Points 270 and 272 are 67.8 kips (302 kN) and 69.8 kips (310 kN) respectively. The corresponding drift ratios are 0.16% and 0.18%. While loading to the north, at Load Point 307, a diagonal crack propagated from both the top and bottom of the vertical crack formed in Load Point270 and the diagonal cracks of Load Point 221 propagated at a base

shear and drift ratio for this load point of 62.8 kips (280 kN) and 0.2% respectively. Additional diagonal cracks formed in the third, fourth and seventh panels while loading to the south (Load Point 353). The corresponding base shear and drift ratio were 72.3 kips (322 kN) and 0.21%. All of these cracks are shown in Figure 5.21.

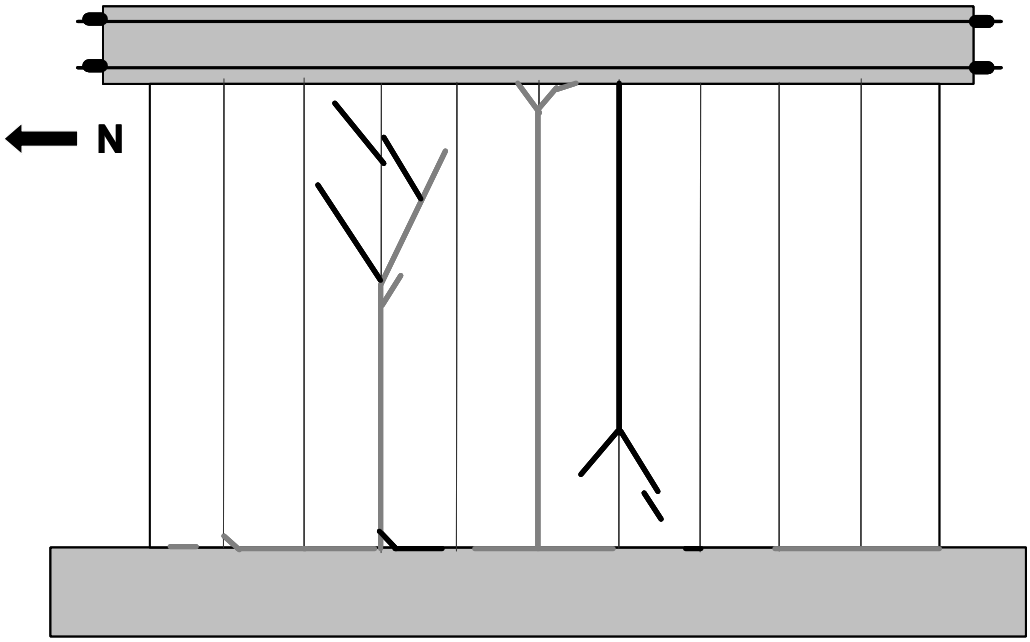

Figure 5.21: Formation of additional vertical, flexural and diagonal cracks in Major Event 4 of Shear Wall Specimen 2

Major Event 5 corresponds to the formation of additional vertical flexural and diagonal cracks in Shear Wall Specimen 2. While loading to the south, a web-shear crack formed in the ninth and tenth panels at Load Point 417 at a base shear of 74.1 kips (330 MPa) and a drift ratio of 0.23%. Smaller diagonal cracks formed in the third, fifth and seventh panels. While loading to the north an additional vertical crack formed between the second and third panels with diagonal cracks propagating from this crack and in the sixth panel (Load Point

450). The base shear and drift ratio were 65.7 kips (292 kN) and 0.25%. The cracks observed in Major Event 5 are shown in Figure 5.22.

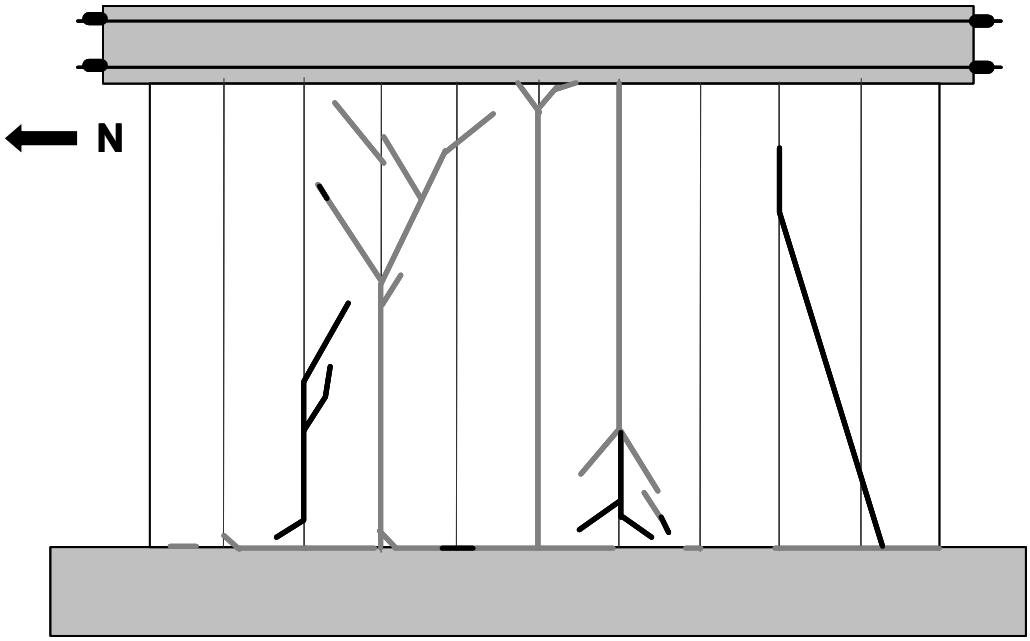

Figure 5.22: Formation of web-shear crack, vertical crack and diagonal cracks in Major Event 5 of Shear Wall Specimen 2

Major Events 6 and 7 consist of Load Points 491 and 573 while loading to the south and Load Points 529 and 616 while loading to the north. The base shears were 91.5 kips (407 kN), 92.7 kips (413 kN), 66.6 kips (296 kN) and 61.3 kips (273 kN) for Load Points 491, 573, 529 and 616 respectively. The respective drift ratios are 0.4%, 0.52%, 0.37% and 0.53%. Cracks formed in Load Point 491 include the T-crack in the tenth panel. Cracks formed in Load Point 573 include the web-shear cracks parallel to the existing web-shear crack in the ninth panel. The propagation of cracks with the same inclination in the second and third panels formed in either Load Point 491 or 573. The remaining cracks in the second and third panels formed in Load Point 529 along the cracks in the upper section of the

third and fourth panels. The web-shear cracks in the fourth and fifth panels formed during Load Point 616 along with the diagonal cracks in the same direction in the seventh through the tenth panels. The damage in the specimen at the end of Major Events 6 and 7 is shown in Figure 5.23.

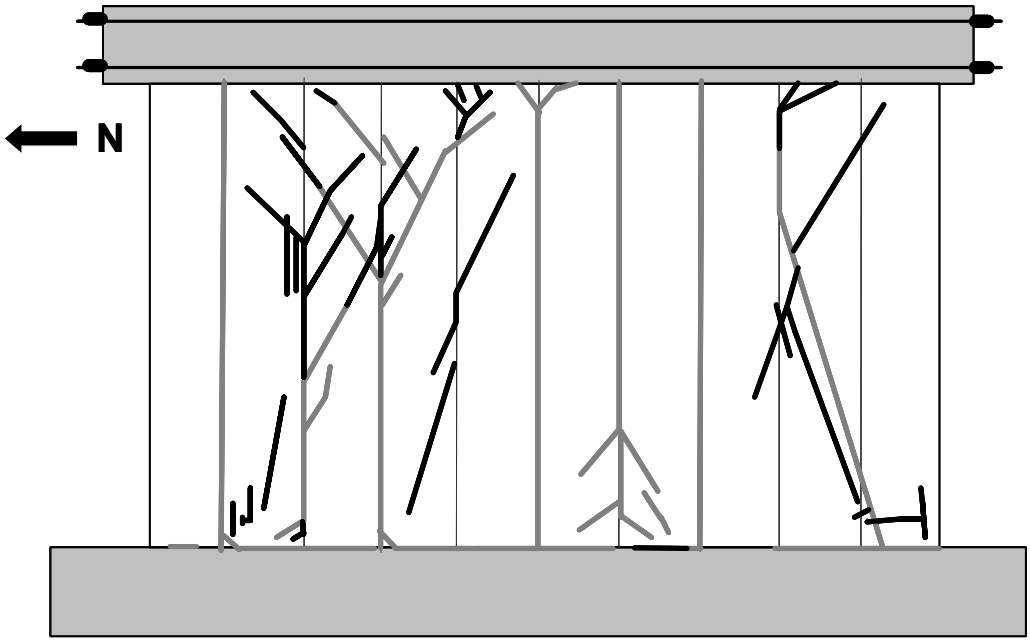

Figure 5.23: Formation of additional cracks in Major Events 6 and 7 of Shear Wall Specimen 2

Major Event 8 consists of Load Points 670 and 870 while loading to the south and Load Points 716 and 798 while loading to the north. The base shears were 89.6 kips (399 kN), 76.4 kips (340 kN), 56.3 kips (250 kN) and 57.8 kips (257 kN) for Load Points 670, 870, 716 and 798 respectively. The respective drift ratios are 0.67%, 0.89%, 0.66% and 0.8%. During this major event preexisting cracks continued to propagate. The first panel underwent out-of-plane buckling at an observed displacement of 0.18 in. (10 mm) at mid-height of the panel. An additional series of cracks formed between Panels 9 and 10 at Load Point 934. The test was terminated due to the onset of spalling in the specimen.

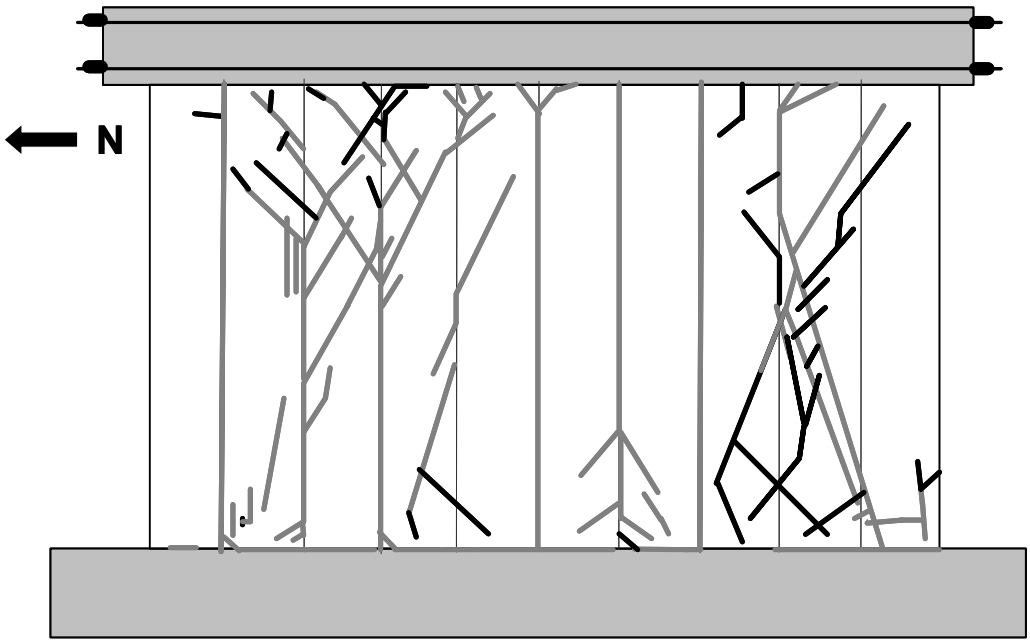

Figure 5.24: Formation of additional cracks in Major Events 8 and 9 of Shear Wall Specimen 2

5.3.3 Load-Displacement Behavior for Shear Wall Specimen 2

The load-displacement relationship of Shear Wall Specimen 2 is presented in terms of the non-dimensional drift ratio in Figure 5.25. The stiffnesses observed at various points in the loading history are described in Varela (2003).

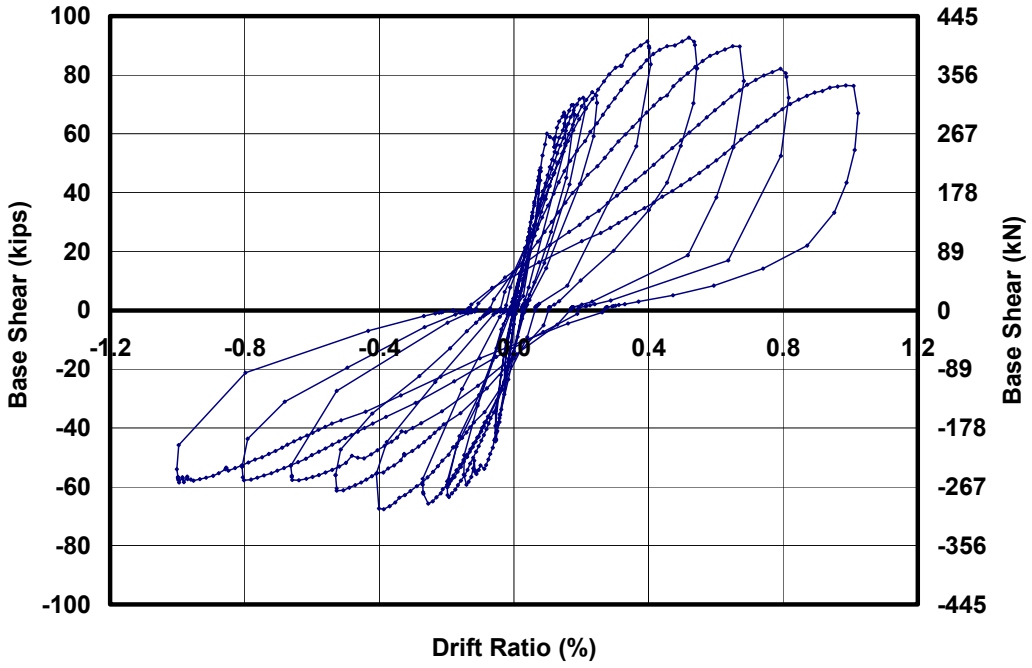

Figure 5.25: Load-displacement relationship for Shear Wall Specimen 2

5.4 SHEAR WALL SPECIMEN 3

An interaction diagram for base shear capacity as a function of axial load for Shear Wall Specimen 3 is presented in Figure 5.26. The axial load applied to Shear Wall Specimen 3 was 120 kips (534 kN), as shown by a dashed horizontal line in Figure 5.26. At this level of axial load the following major events are predicted in order of occurrence: simultaneous flexural cracking and web-shear cracking; sliding shear; and crushing of the diagonal strut. This specimen was not expected to reach nominal flexural capacity.

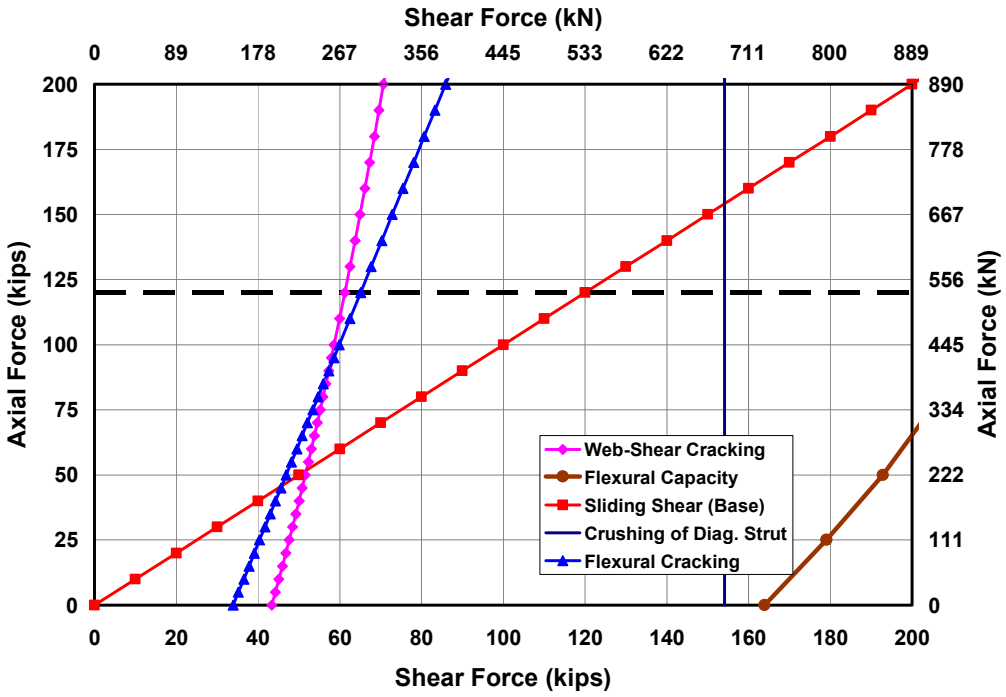

Figure 5.26: Prediction of behavior for Shear Wall Specimen 3

5.4.1 Loading History and Major Events for Shear Wall Specimen 3

The actual loading and displacement histories for Shear Wall Specimen 3 are presented in Figure 5.27 and Figure 5.28. Monotonically increasing load point numbers are assigned for each set of data recorded during the test. Data are classified into cycles with maximum loads and drift ratios for each cycle (Table 5.6). Loading to the south is considered positive; loading to the north, negative.

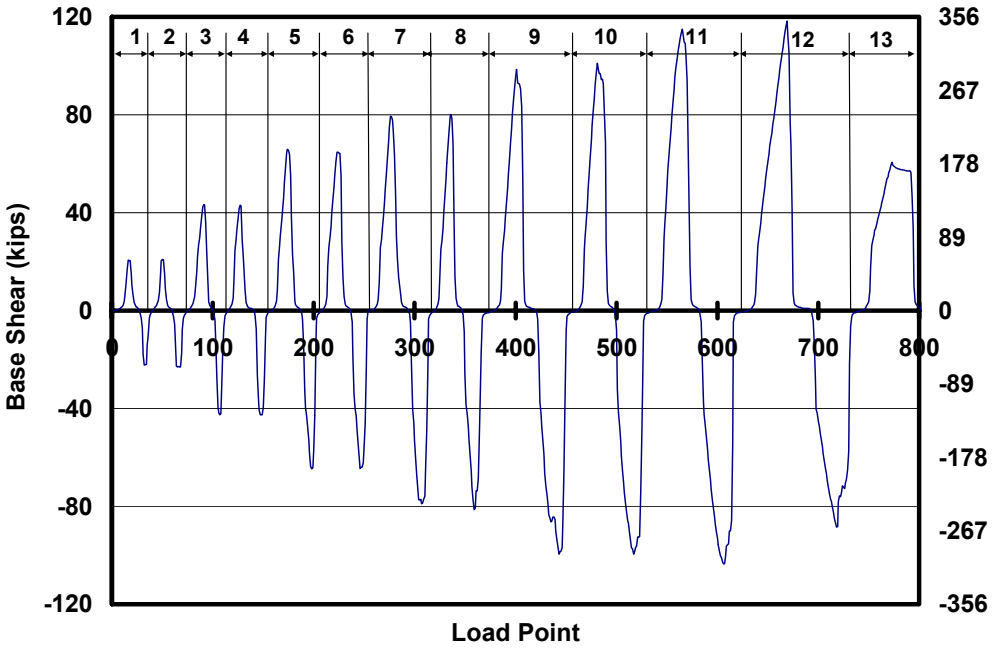

Figure 5.27: Actual loading history for Shear Wall Specimen 3 (numbers at the top designate cycle numbers)

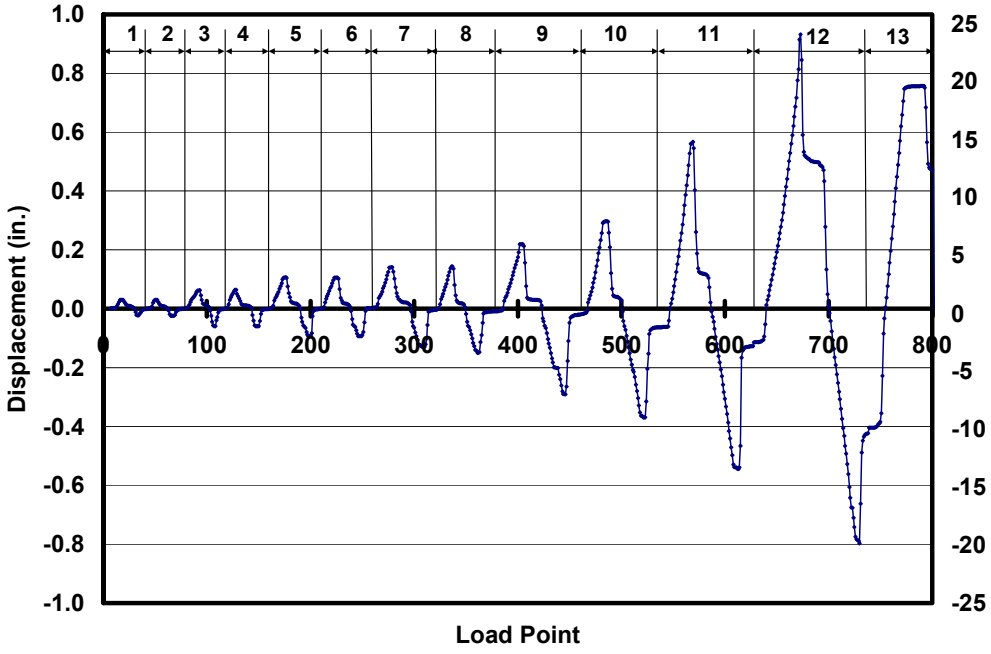

Figure 5.28: Actual tip displacement history for Shear Wall Specimen 3 (numbers at the top designate cycle numbers)

Table 5.6: Load points, maximum load and drift ratios for each cycle for Shear Wall Specimen 3

Cycle	Load Points	Maximum Applied Load, kips (kN)	Max. Drift Ratio (%)	Cycle	Load Points	Minimum Applied Load, kips (kN)	Min. Drift Ratio (%)
1a	1-26	20.7(92)	0.020	1b	27-39	-22.3(99)	0.015
2a	40-59	20.9(93)	0.020	2b	60-74	-23.1(103)	0.016
3a	75-100	43.3(193)	0.040	3b	101-115	-42.6(190)	0.038
4a	116-140	43.0(191)	0.042	4b	141-158	-42.6(190)	0.039
5a	159-187	65.9(293)	0.069	5b	188-208	-64.7(282)	0.061
6a	209-236	64.8(288	0.069	6b	237-254	-64.5(287)	0.060
7a	255-293	79.4(353)	0.091	7b	294-319	-78.9(351)	0.084
8a	320-347	80.2(357)	0.093	8b	348-379	-81.3(362)	0.097
9a	380-420	98.4(348)	0.142	9b	421-461	-99.5(443)	0.189
10a	462-497	101.0(449)	0.193	10b	498-539	-99.6(443)	0.239
11a	540-582	115.0(512)	0.368	11b	583-630	-103.5(461)	0.353
12a	631-693	118.3(526)	0.605	12b	694-743	-88.4(393)	0.518
13a	744-801	60.6(269)	0.492				

5.4.2 Sequence of Crack Formation for Shear Wall Specimen 3

The sequence of crack formation in Shear Wall Specimen 3 is described in terms of major events: points during the test when either the condition of the specimen changed (for example, flexural cracking or web-shear cracking), or the applied axial force was increased. Table 5.7 lists the major events and the load point at which they occurred. In each section where crack maps are presented, preexisting cracks are shown in gray, and new cracks are shown in black.

Table 5.7: Description of major events for Shear Wall Specimen 3

Major Event	Load Point	Physical Description
1	174, 276	Flexural cracking, loading south
2	307	Flexural cracking, loading north
3	359	Web-shear crack formed, loading north
4	401	Web-shear crack formed, loading south
5	442, 481	Additional web-shear cracks formed
6	517	Additional web-shear cracks formed
7	565	Additional web-shear cracks formed along with spalling
8	607	Spalling at south toe, with additional web-shear cracking
9	669, 690	Spalling at north toe, with additional web-shear cracking
10	726	Additional web-shear cracking

5.4.2.1 Flexural cracking in Shear Wall Specimen 3

Major Events 1 and 2 correspond to flexural cracking. At Load Point 174, a 2 in. (51 mm) flexural crack formed while loading to the south at a load of 65.9 kips (293 kN) and a drift ratio of 0.07%. This crack propagated to 30 in. (76.2 mm) at a load of 79.4 (353 kN) and a drift ratio of 0.09% (Load Point 276). A flexural crack formed while loading to the north at Load Point 307 when the base shear in the specimen was 78.9 kips (351 kN) and the drift ratio was 0.083%. The predicted base shear at flexural cracking using the average tensile bond strength of Section 8.1.1 is 65.1 kips (306 kN). The ratios of observed to predicted flexural cracking capacity are 1.0 and 1.2 while loading to the south and north respectively.

5.4.2.2 Web-shear cracking in Shear Wall Specimen 3

Major Events 3 and 4 correspond to the formation of web-shear cracking while loading to the north and south respectively. A web-shear crack formed along the entire height of the wall while loading to the north along with a smaller parallel web-shear crack at Load Point 359 (Figure 5.29), at a base shear and drift ratio of 81.3 kips (362 kN) and 0.09%, respectively. The prediction for web-shear

cracking based on Equation (8.11) at the corresponding axial load is 61 kips (273 kN). The ratio of observed to predicted web-shear cracking capacity is 1.33. This ratio exceeds 1.0 because the proposed predictive equations were calibrated to lower fractiles of observed capacities. This ratio exceeds 1.0 because the proposed predictive equations were calibrated to lower fractiles of observed capacities.

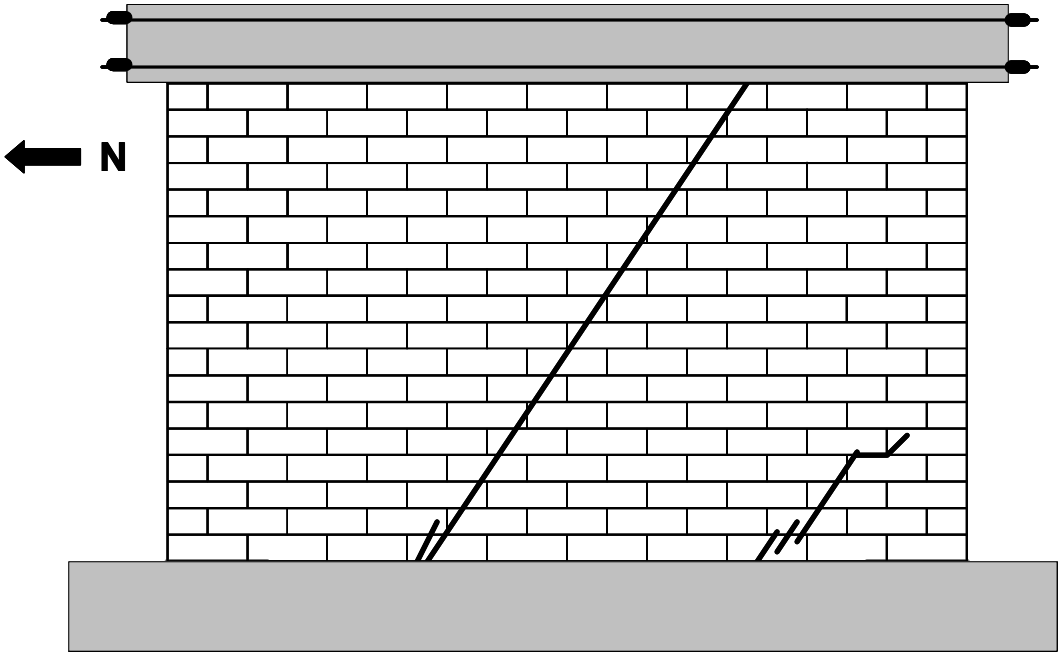

Figure 5.29: Formation of web-shear crack while loading to the north in Shear Wall Specimen 3

While loading to the south, a similar web-shear crack formed at Load Point 401 at a base shear of 98.4 kips (438 MPa) and a drift ratio of 0.12% (Figure 5.30). An additional flexural crack formed at the base of this web-shear crack and the flexural crack at the north end of the wall closed, indicating a separation of the north corner from the rest of the wall.

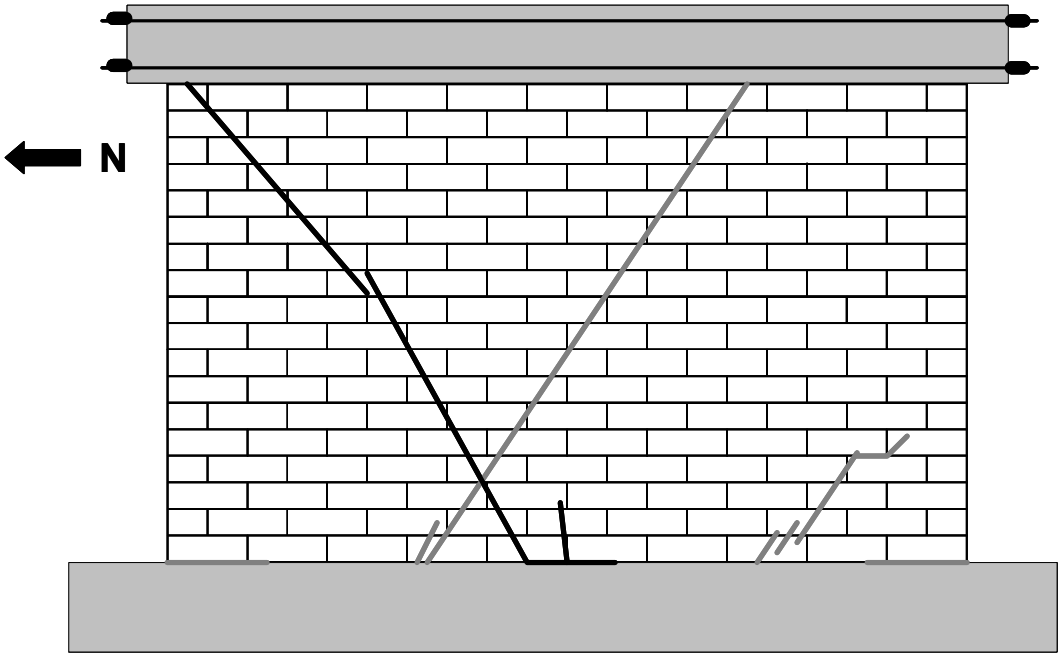

Figure 5.30: Formation of web-shear crack while loading to the south in Shear Wall Specimen 3

5.4.2.3 Additional web-shear cracking in Shear Wall Specimen 3

Major Events 5 through 7 correspond to the development of additional web-shear cracks in the specimen. The base shears were 98.6 kips (431 kN) and 101 kips (449 kN) for Load Points 442 (loading north) and 481 (loading south) respectively and the drift ratio was 0.26% for both. Damage in the specimen at the end of Major Event 5 is shown in Figure 5.31. Major Event 6 occurred at Load Point 517 (Figure 5.32), when the base shear was 115 kips (512 kN) and the drift ratio was 0.32%. Major Event 7 occurred at Load Point 565 and includes distributed web-shear cracking, combined with spalling and vertical cracks in the compression toe (Figure 5.33).

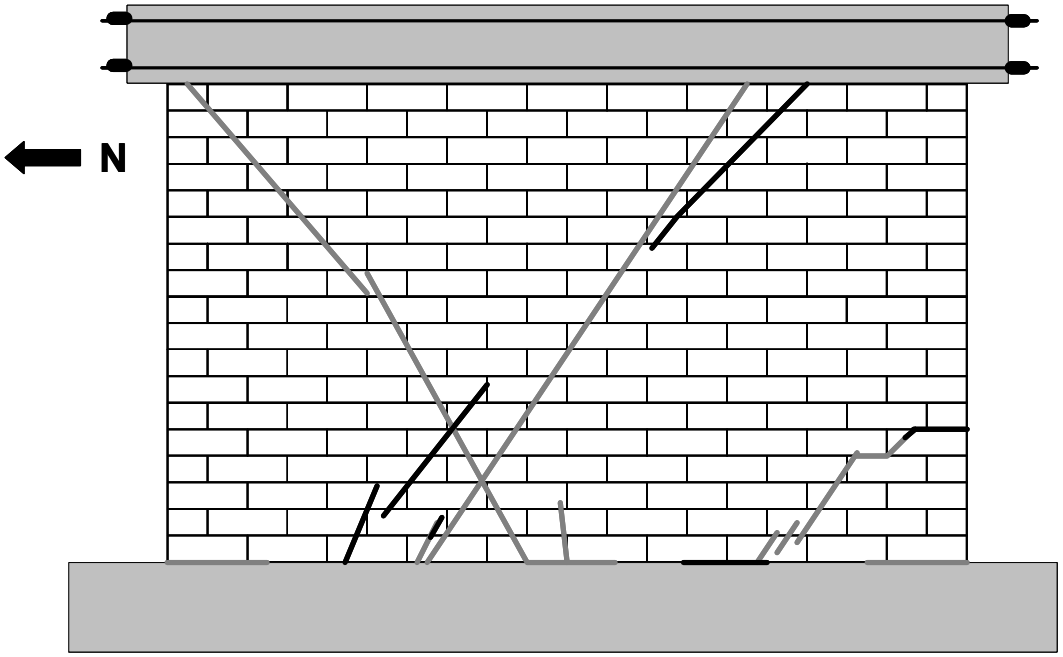

Figure 5.31: Additional web-shear cracking in Shear Wall Specimen 3 for Major Event 5

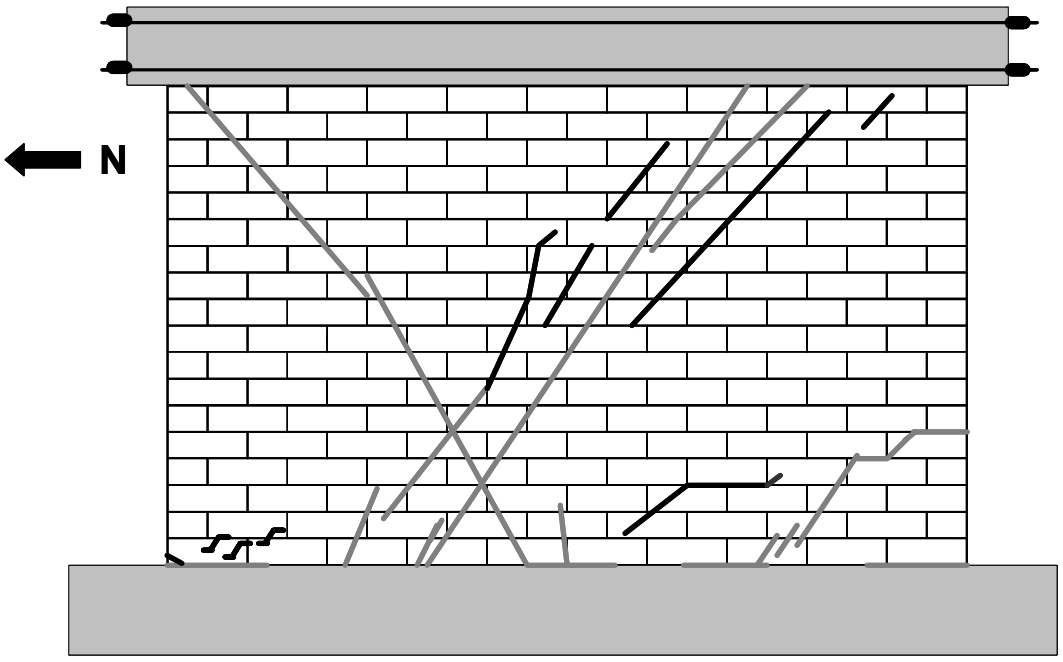

Figure 5.32: Additional web-shear cracking in Shear Wall Specimen 3 for Major Event 6

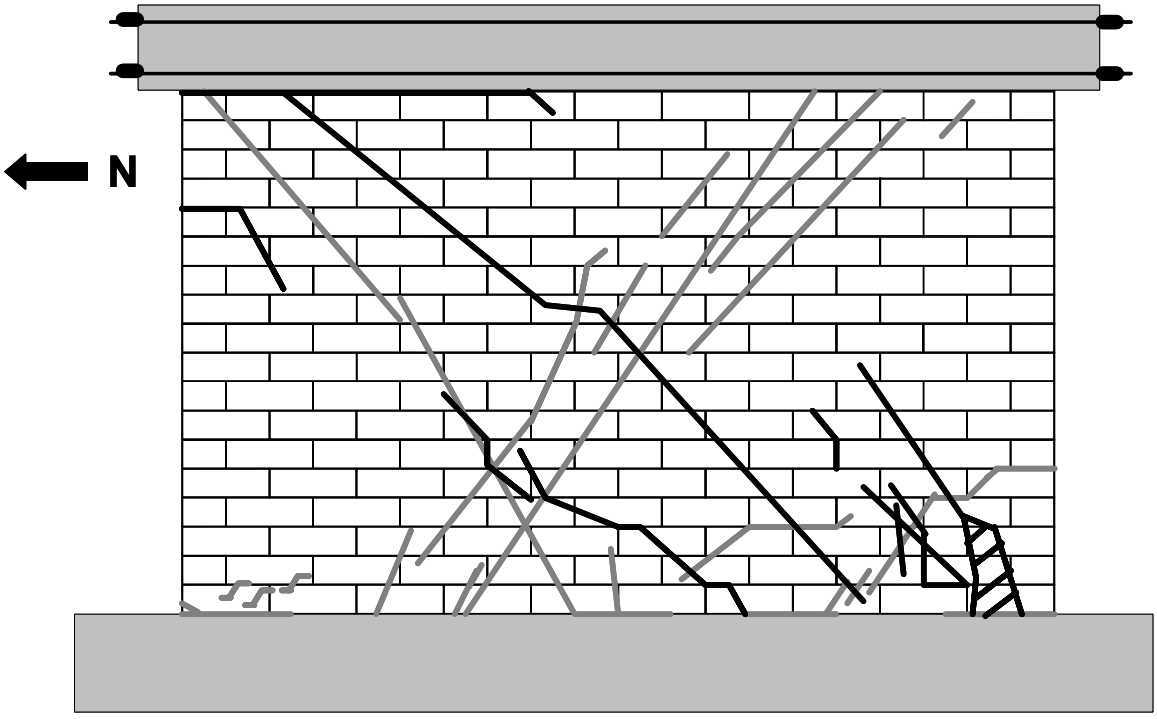

Figure 5.33: Additional web-shear cracking in Shear Wall Specimen 3 for Major Event 7

5.4.2.4 Spalling of the compression toe and distributed web-shear cracking in Shear Wall Specimen 3

In Major Events 8 and 9, spalling at the compression toe was observed. In Major Event 9 vertical cracks were observed at the upper north corner (loading south), which indicated that load was being transferred through a diagonal strut. In Major Event 10 vertical cracks were observed along the compression diagonal (loading south). All three major events were characterized by additional distributed web-shear cracking, as shown in the combined crack map of Figure 5.34.

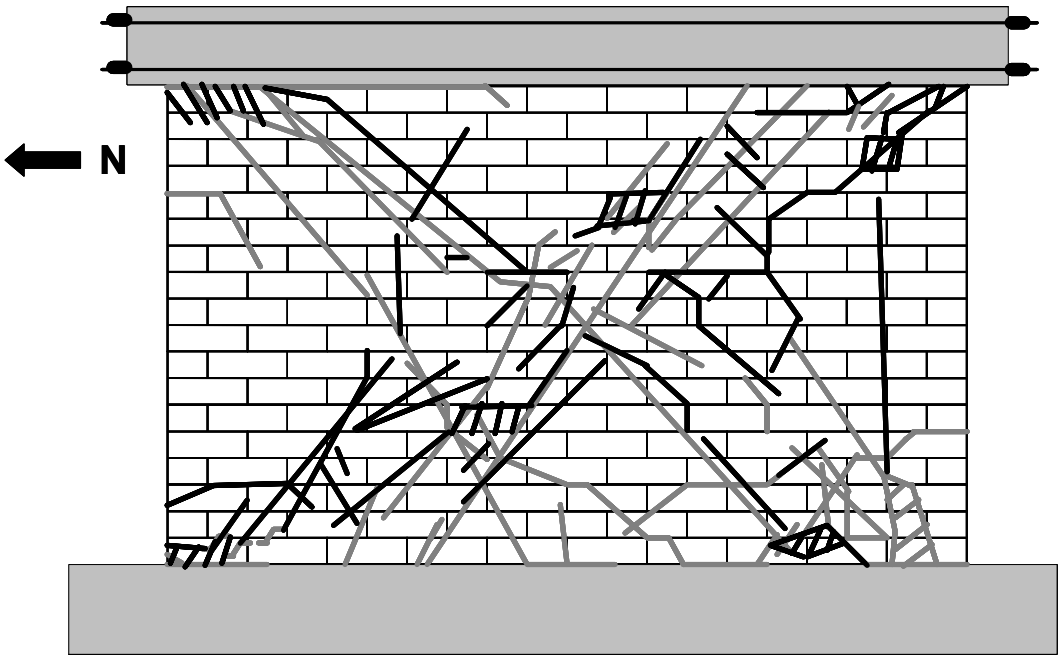

Figure 5.34: Observed cracks in Shear Wall Specimen 3 for Major Events 8-10

5.4.3 Load-Displacement Behavior for Shear Wall Specimen 3

The load-displacement relationship of Shear Wall Specimen 3 is presented in terms of the non-dimensional drift ratio in Figure 5.35. The stiffnesses observed at various points in the loading history are described in Varela (2003).

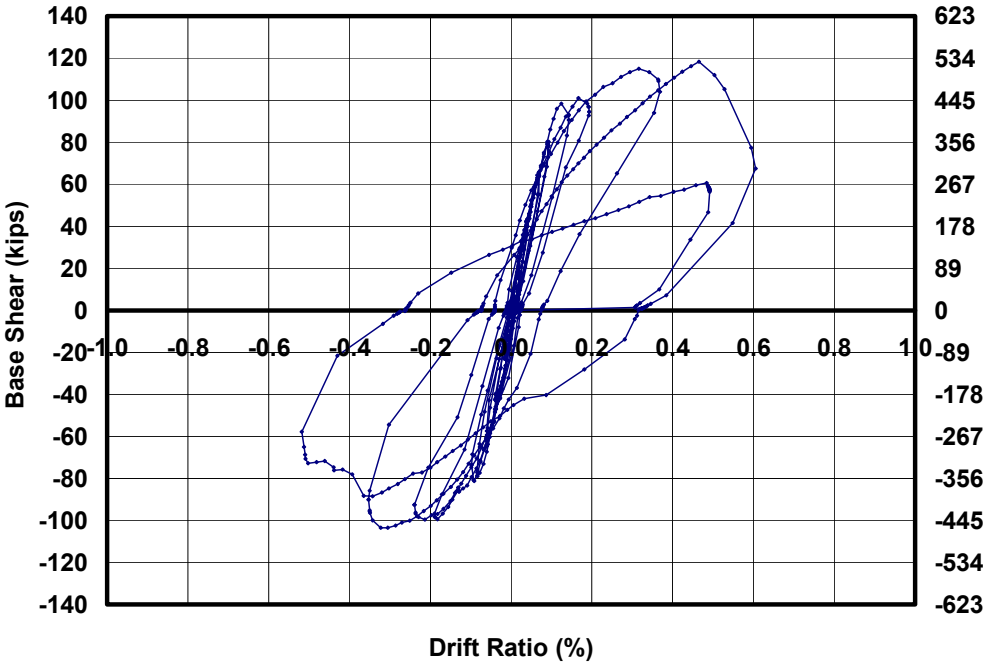

Figure 5.35: Load-displacement relationship for Shear Wall Specimen 3

5.5 SHEAR WALL SPECIMEN 4

An interaction diagram for base shear capacity as a function of axial load for Shear Wall Specimen 4 is presented in Figure 5.36. The axial load applied to Shear Wall Specimen 4 was 120 kips (534 kN), as shown by a dashed horizontal line in Figure 5.36. At this level of axial load the following major events are predicted in order of occurrence: flexural cracking; web-shear cracking; and sliding shear. This specimen was not expected to reach crushing of the diagonal strut or nominal flexural capacity.

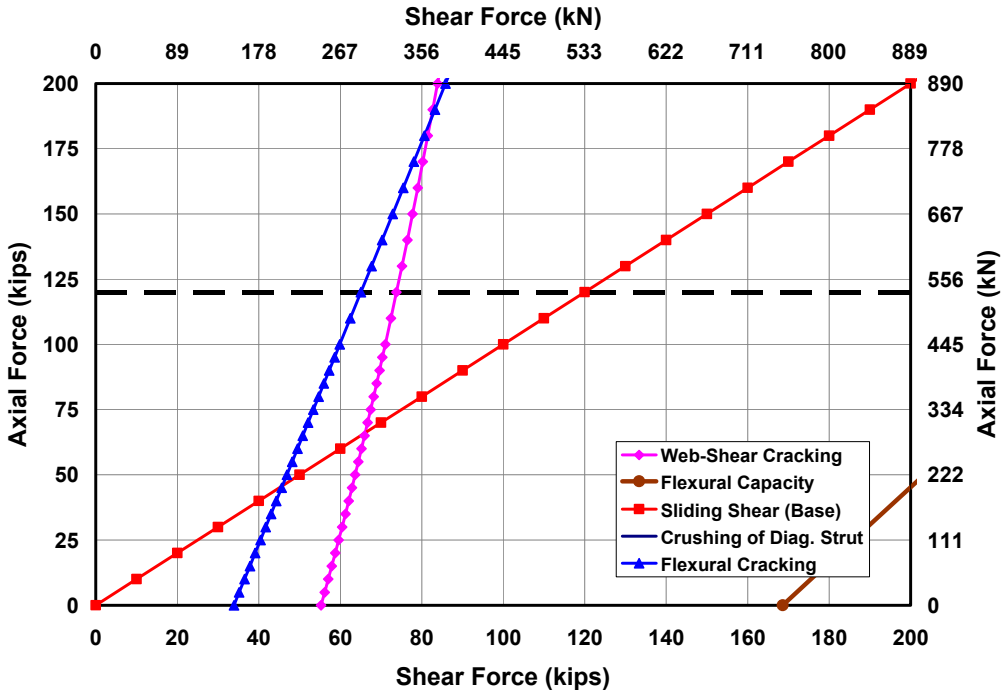

Figure 5.36: Prediction of behavior for Shear Wall Specimen 4

5.5.1 Loading History and Major Events for Shear Wall Specimen 4

The actual loading and displacement histories for Shear Wall Specimen 4 are presented in Figure 5.37 and Figure 5.38. Monotonically increasing load point numbers are assigned for each set of data recorded during the test. Data are classified into cycles with maximum loads and drift ratios for each cycle (Table 5.8). Loading to the south is considered positive; loading to the north, negative.

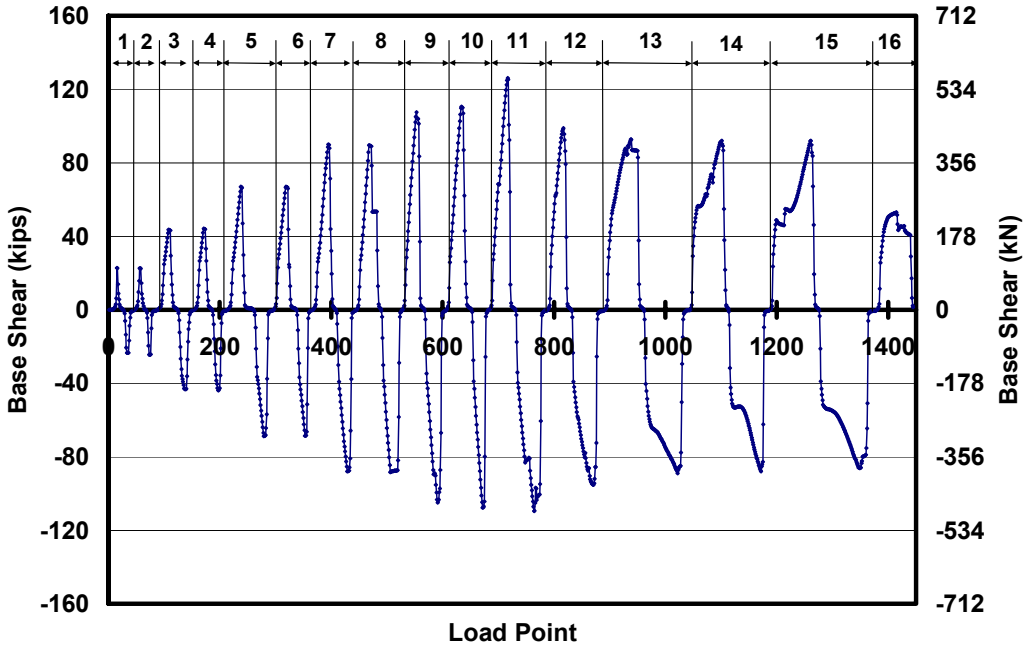

Figure 5.37: Actual loading history for Shear Wall Specimen 4 (numbers at the top designate cycle numbers)

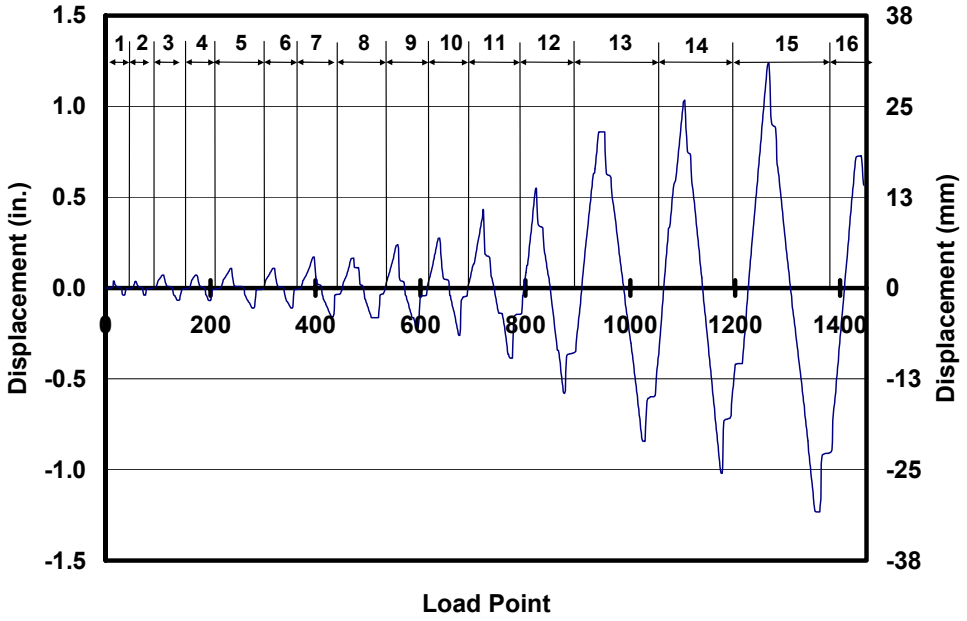

Figure 5.38: Actual tip displacement history for Shear Wall Specimen 4 (numbers at the top designate cycle numbers)

Table 5.8: Load points, maximum load and drift ratios for each cycle for Shear Wall Specimen 4

Cycle	Load Points	Maximum Applied Load, Kips (kN)	Max. Drift Ratio (%)	Cycle	Load Points	Minimum Applied Load, Kips (kN)	Min. Drift Ratio (%)
1a	1-26	22.8(101)	0.025	1b	27-48	-23.5(104)	0.025
2a	49-66	22.6(101)	0.024	2b	67-88	-24.4(109)	0.026
3a	89-123	43.5(194)	0.046	3b	124-153	-43.1(192)	0.043
4a	154-184	44.1(196)	0.047	4b	185-213	-43.8(195)	0.045
5a	214-258	67.0(298)	0.070	5b	259-297	-68.9(306)	0.072
6a	298-336	66.9(298)	0.070	6b	337-367	-68.6(305)	0.072
7a	368-407	90.0(400)	0.111	7b	408-446	-87.9(391)	0.103
8a	447-488	89.7(399)	0.107	8b	489-528	-88.4(393)	0.106
9a	529-567	107.6(479)	0.155	9b	568-608	-105.0(467)	0.144
10a	609-652	110.5(491)	0.179	10b	653-684	-107.7(479)	0.170
11a	685-730	126.2(561)	0.281	11b	731-788	-109.5(487)	0.251
12a	789-831	98.8(440)	0.357	12b	832-891	-95.3(424)	0.377
13a	892-961	92.8(413)	0.558	13b	962-1044	-88.9(396)	0.548
14a	1045-1113	92.0(409)	0.671	14b	1114-1188	-88.0(391)	0.663
15a	1189-1275	91.9(409)	0.804	15b	1276-1380	-86.2(383)	0.800
16a	1381-1445	53.1(236)	0.473				

5.5.2 Sequence of Crack Formation for Shear Wall Specimen 4

The sequence of crack formation in Shear Wall Specimen 4 is described in terms of major events: points during the test when either the condition of the specimen changed (for example, flexural cracking or web-shear cracking), or the applied axial force was increased. Table 5.9 lists the major events and the load point at which they occurred. In each section where crack maps are presented, preexisting cracks are shown in gray, and new cracks are shown in black.

Table 5.9: Description of major events for Shear Wall Specimen 4

Major Event	Load Point	Physical Description
1	395	Flexural crack formed, loading south
2	423	Flexural crack formed, loading north
3	634	Web-shear crack and horizontal crack formed, loading south
4	672	Web-shear crack formed, loading north
5	717	Web-shear cracks formed, horizontal crack propagated and local spalling occurred, loading south
6	749, 764	Web-shear cracks formed, horizontal crack propagated and local spalling occurred, loading north
7	817	Diagonal cracks formed in compression toe with opening of head joint, loading south
8	871	Major spalling with diagonal cracking in north compression toe, loading north
9	930	Major spalling at north toe, additional opening of head joint, loading south
10	1260	Severe spalling with opening of head joint, loading south
11	1340	Severe spalling with opening of head joint, loading north

5.5.2.1 Flexural cracking in Shear Wall Specimen 4

Major Events 1 and 2 correspond to the observance of flexural cracking. At Load Point 395 a flexural crack was observed while loading to the south at a load of 90.0 kips (400 kN) and a drift ratio of 0.11%. It is probable that the crack formed prior to this observation, because the crack was approximately 6 ft. (1.8 m) long. A flexural crack formed while loading to the north at Load Point 423, when the base shear in the specimen was 71.5 kips (318 kN) and the drift ratio was 0.07%. This crack propagated to 6 ft. (1.8 m) at Load Point 429 at a corresponding base shear and drift ratio of 87.9 kips (300 kN) and 0.1% respectively. These cracks propagated without other damage between Load Points 429 and 536 and are shown in gray in Figure 5.39.

The predicted base shear at flexural cracking using the average bond tensile strength of Section 8.1.1 is 65.1 kips (289 kN). The ratios of observed to predicted flexural cracking capacity are 1.4 and 1.1 while loading to the south and

north respectively. The high ratio of observed to predicted flexural capacity while loading to the north supports the possibility that the crack formed prior to the observation at Load Point 395. In addition the base shear and drift ratios measured when the observed flexural crack was 6 ft. (1.8 m) long in both directions also supports this theory.

5.5.2.2 Web-shear cracking in Shear Wall Specimen 4

Major Event 3 corresponds to the formation of a horizontal crack and a web-shear crack while loading to the south at Load Point 634 at a base shear of 110.5 kips (491 kN) and a drift ratio of 0.18%. Major Event 4 consisted of a two web-shear cracks that formed in the center of the wall at Load Point 672 at a base shear of 108 kips (479 MPa) and a drift ratio of 0.16%. The damage in these Major Events is shown in Figure 5.39.

The prediction for web-shear cracking based on Equation (8.11) at the corresponding axial load is 73 kips (324 kN). The ratio of observed to predicted web-shear cracking capacity is 1.5. This ratio exceeds 1.0 because the proposed predictive equations were calibrated to lower fractiles of observed capacities.

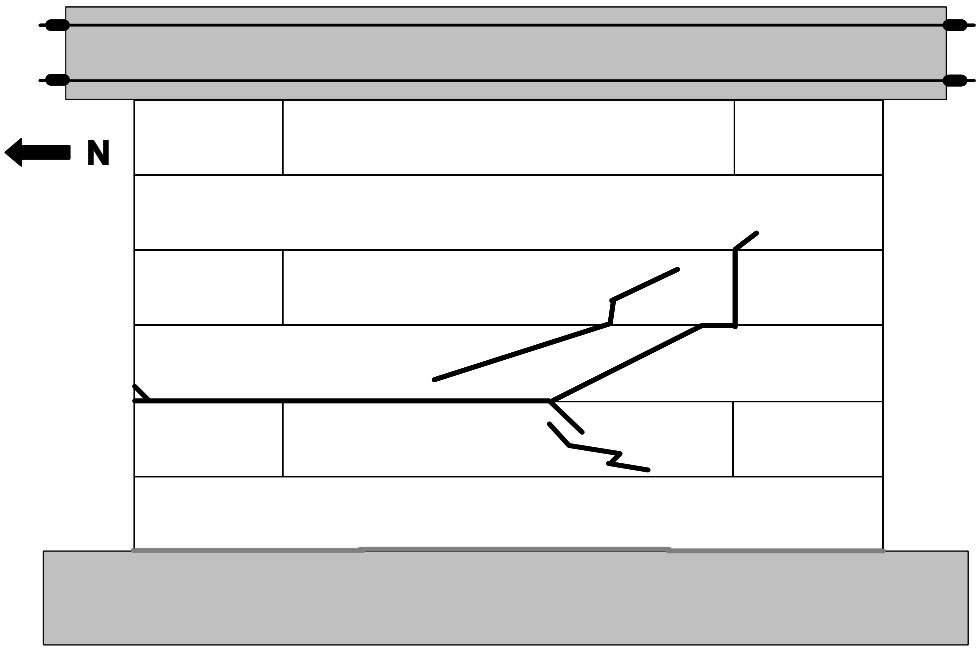

Figure 5.39: Formation of web-shear cracks in Shear Wall Specimen 4

5.5.2.3 Additional web-shear cracking in Shear Wall Specimen 4

While loading to the south, another series of web-shear cracks formed throughout the specimen (Load Point 717). Local spalling in the south compression toe and the center of the wall occurred simultaneously with these web-shear cracks. In addition, the horizontal crack of Load Point 634 propagated an additional 3 ft. (0.91 m). At Load Point 717 the base shear was 126.2 kips (561 kN) and the drift ratio was 0.25%. Similar damage occurred while loading to the north at Load Points 749 and 764. Two web-shear cracks formed in the north end of the wall at Load Point 749. At Load Point 764 additional web-shear cracks formed in the north and south ends of the wall, combined with propagation of the horizontal crack to the end of the wall. Local spalling was observed above the horizontal crack at the south end of the wall. The base shears were 82.4 kips (366 kN) and 109.5 kips (487 kN) for Load Points 749 and 764 respectively, with

corresponding drift ratios of 0.09% and 0.19% respectively. While loading to the south in the next cycle additional diagonal cracks formed in the south compression toe (Load Point 817). A 0.25 in. (6 mm) gap was observed in the south head joint in the second course. This indicates that sliding occurred between the second and third course. The damage shown in Figure 5.40 occurred in Major Events 5 through 7.

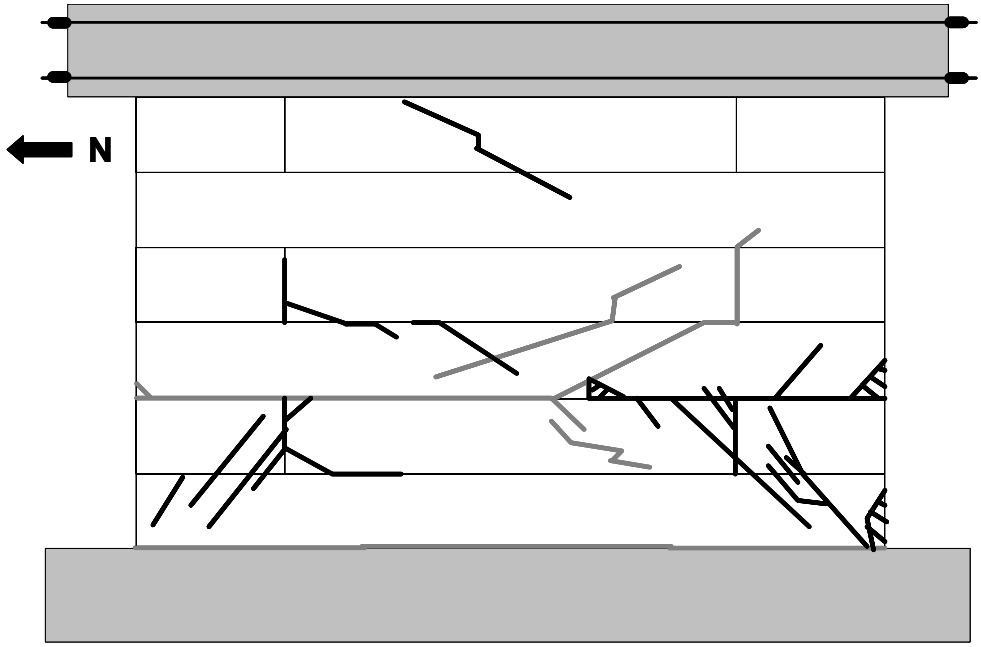

Figure 5.40: Formation of Additional web-shear cracks, propagation of horizontal cracks and local spalling in Shear Wall Specimen 4

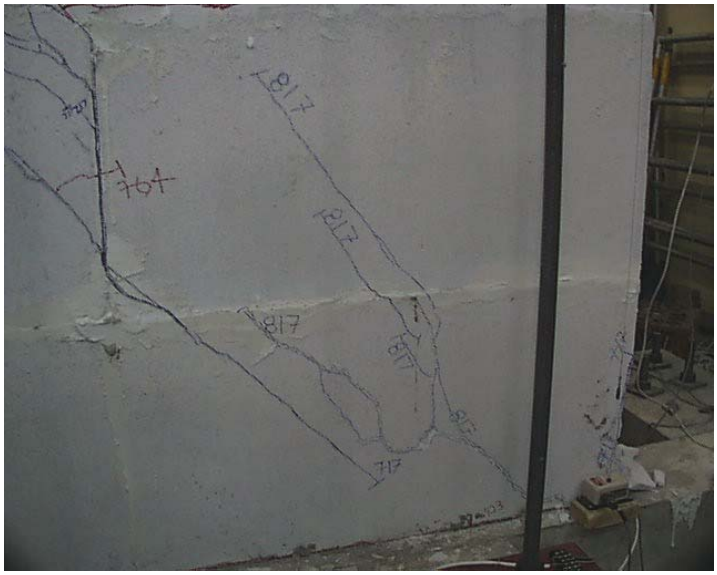

Figure 5.41: Gap in head joint of second course indicating sliding in Shear Wall Specimen 4

5.5.2.4 Severe spalling of the compression toe in Shear Wall Specimen 4

Major Events 8 and 9 consisted of severe spalling in the compression toes at Load Points 871 and 930. While loading to the north, at Load Point 871 the base shear and drift ratio were 91.7 kips (408 kN) and 0.78% respectively. While loading to the south, at Load Point 930 the base shear and drift ratio were 86.2 kips (383 kN) and 0.75% respectively. The area affected by the spalling is shown in Figure 5.42; front and side views of the spalling observed in Load Point 871 are shown in Figure 5.43. The spalling may be exasperated by the sliding observed in at the bed joint. A 0.5 in. (12 mm) gap was observed in the south head joint of the second course at Load Point 939.

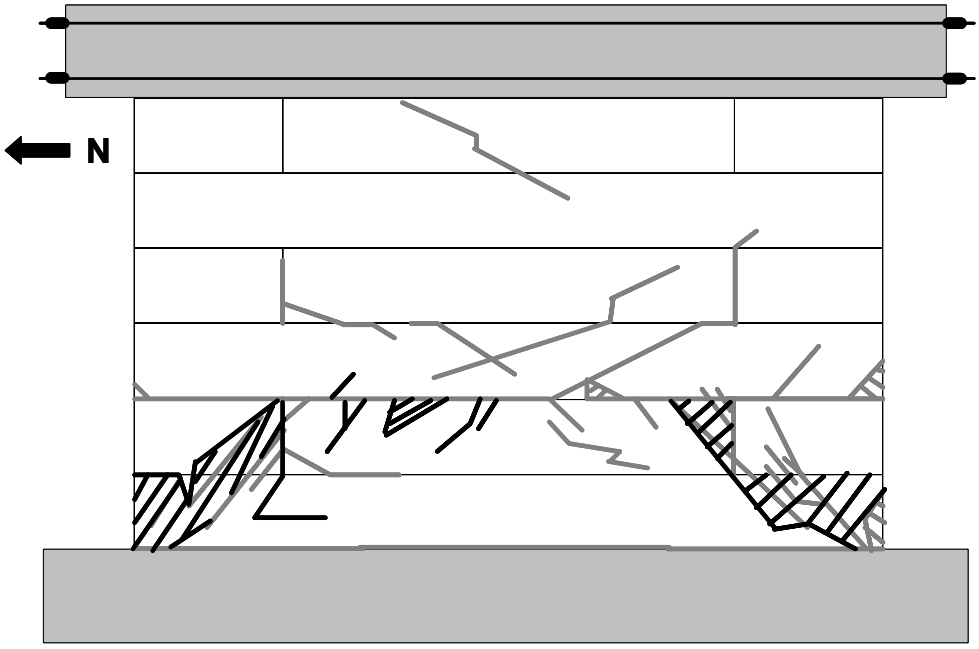

Figure 5.42: Major spalling in Shear Wall Specimen 4 for Major Events 8 and 9

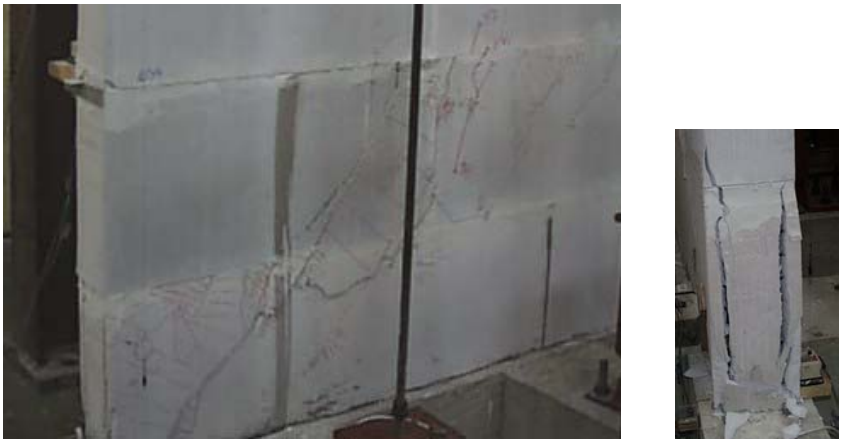

Figure 5.43: Front and side views of spalling at Load Point 871 in Shear Wall Specimen 4

The wall was loaded for 3 more cycles. In each cycle the damage increased. At Load Points 1260 and 1340 the cover was lost from all of the areas

shown in Figure 5.44. Views of the compression corners of the specimen without cover are shown in Figures Figure 5.45 and Figure 5.46. Additional evidence of sliding of the panels at the horizontal crack is shown by the displacement of the third course at the end of the wall (Figure 5.45). The test was ended due to instability of the compression toe combined with a decrease in lateral load capacity.

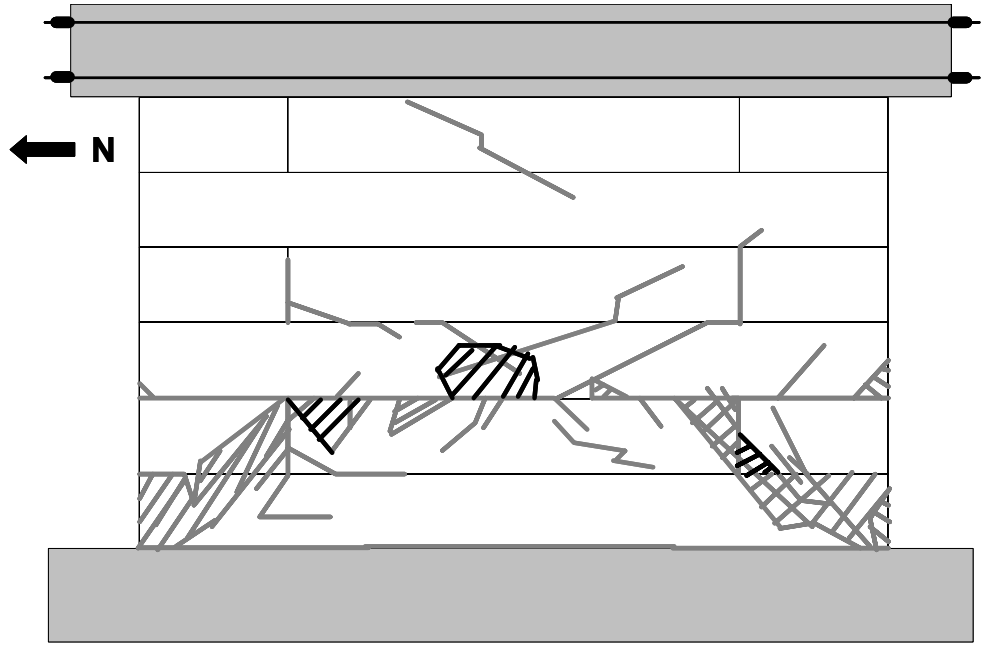

Figure 5.44: Zones with a loss of cover in Shear Wall Specimen 4 for Major Events 10 and 11

Figure 5.45: Loss of cover in the south end of Shear Wall Specimen 4

Figure 5.46: Loss of cover in the north end of Shear Wall Specimen 4

5.5.3 Load-Displacement Behavior for Shear Wall Specimen 4

The load-displacement relationship of Shear Wall Specimen 4 is presented in terms of the non-dimensional drift ratio in Figure 5.47. The stiffnesses observed at various points in the loading history are described in Varela (2003).

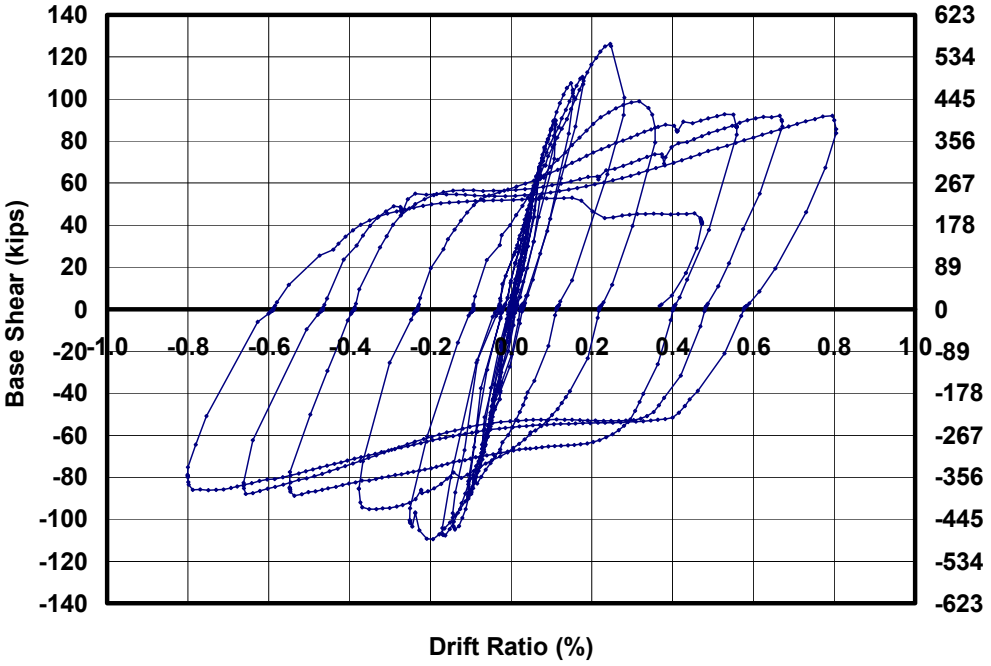

Figure 5.47: Load-displacement relationship for Shear Wall Specimen 4

5.6 SHEAR WALL SPECIMEN 5

An interaction diagram for base shear capacity as a function of axial load for Shear Wall Specimen 5 is presented in Figure 5.48. The axial load applied to Shear Wall Specimen 5 was 60 kips (267 kN), as shown by a dashed horizontal line in Figure 5.48. At this level of axial load, flexural cracking is predicted to occur first followed by simultaneous web-shear cracking and sliding shear. This

specimen was not expected to reach crushing of the diagonal strut or nominal flexural capacity.

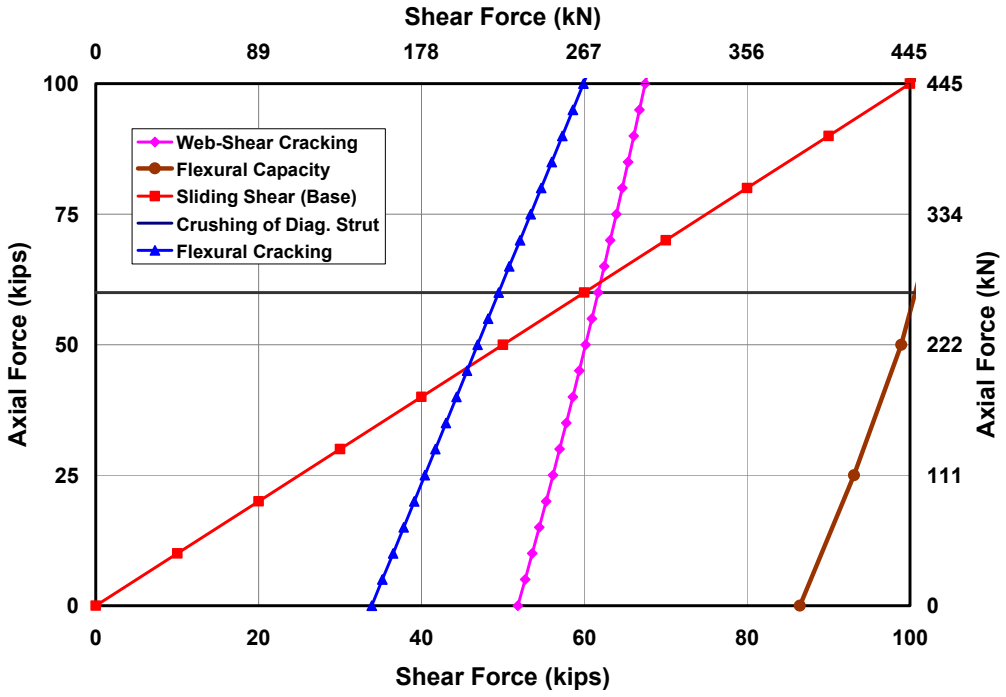

Figure 5.48: Prediction of behavior for Shear Wall Specimen 5

5.6.1 Loading History and Major Events for Shear Wall Specimen 5

The actual loading and displacement histories for Shear Wall Specimen 5 are presented in Figure 5.49 and Figure 5.50. Monotonically increasing load point numbers are assigned for each set of data recorded during the test. Data are classified into cycles with maximum loads and drift ratios for each cycle (Table 5.10). Loading to the south is considered positive; loading to the north, negative.

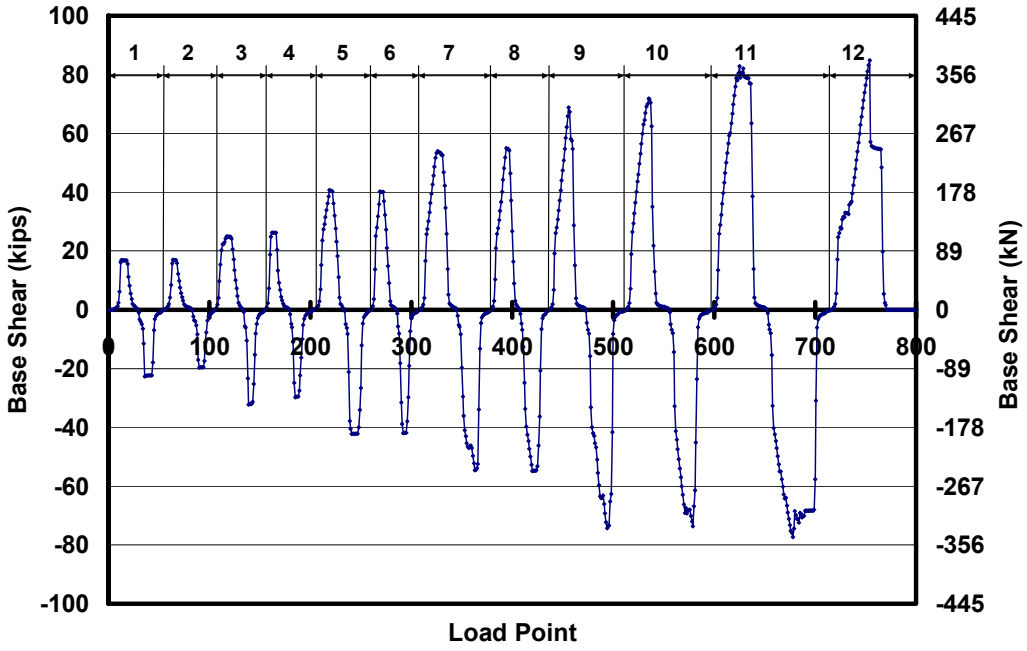

Figure 5.49: Actual loading history for Shear Wall Specimen 5 (numbers at the top designate cycle numbers)

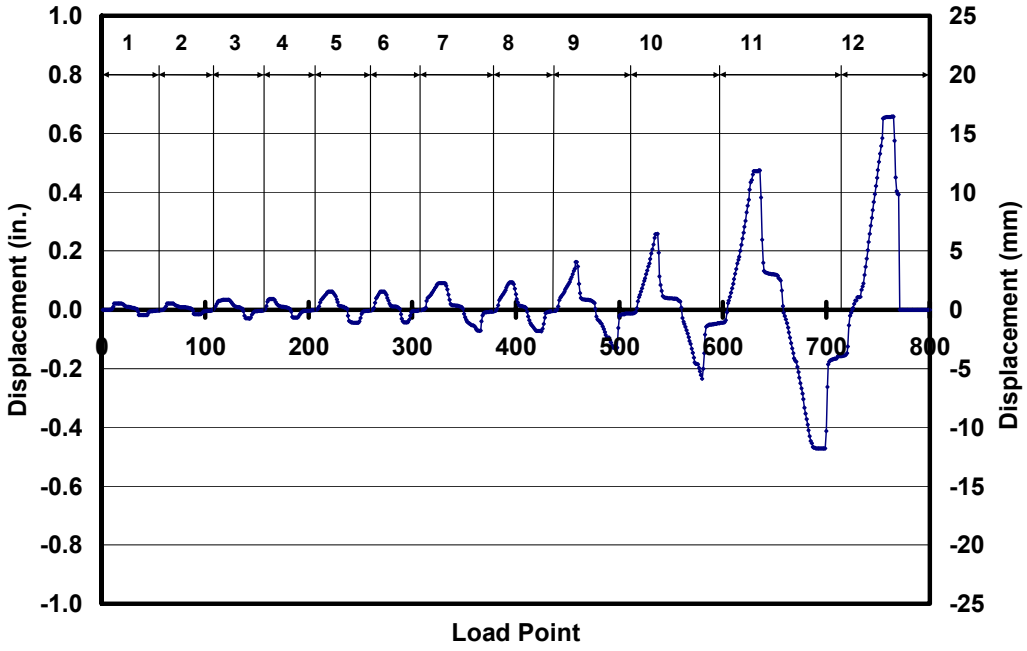

Figure 5.50: Actual tip displacement history for Shear Wall Specimen 5 (numbers at the top designate cycle numbers)

Table 5.10: Load points, maximum load and drift ratios for each cycle for Shear Wall Specimen 5

Cycle	Load Points	Maximum Applied Load, kips (kN)	Max. Drift Ratio (%)	Cycle	Load Points	Minimum Applied Load, kips (kN)	Min. Drift Ratio (%)
1a	1-28	16.9 (75)	0.014	1b	20-55	-22.7 (101)	0.012
2a	56-79	17.0 (75.6)	0.014	2b	80-106	-19.6 (87)	0.01
3a	107-133	25.0 (111)	0.022	3b	134-155	-32.3 (144)	0.019
4a	156-179	26.3 (117)	0.023	4b	180-202	-29.7 (132)	0.017
5a	203-233	40.7 (181)	0.04	5b	234-260	-42.3 (188)	0.028
6a	261-285	40.2 (179)	0.04	6b	286-308	-42.0 (187)	0.028
7a	309-345	53.9 (240)	0.059	7b	346-379	-54.6 (243)	0.046
8a	380-407	55.0. (254)	0.061	8b	408-437	-54.8 (244)	0.047
9a	438-472	68.8 (306)	0.105	9b	473-514	-74.3 (330)	0.089
10a	515-554	71.9 (320)	0.17	10b	555-598	-73.7 (328)	0.15
11a	599-652	82.8 (368)	0.31	11b	653-716	-77.3 (344)	0.31
12a	717-770	84.8 (377)	0.43				

5.6.2 Sequence of Crack Formation for Shear Wall Specimen 5

The sequence of crack formation in Shear Wall Specimen 5 is described in terms of major events: points during the test when either the condition of the specimen changed (for example, flexural cracking or web-shear cracking), or the applied axial force was increased. Table 5.11 lists the major events and the load point at which they occurred. In each section where crack maps are presented, preexisting cracks are shown in gray, and new cracks are shown in black.

Table 5.11: Description of major events for Shear Wall Specimen 5

Major Event	Load Point	Physical Description
1	326	Flexural cracking, loading south
2	363	Flexural cracking, loading north
3	454	Web-shear cracks formed at base of wall, loading south
4	457	Web-shear crack formed along height of wall, loading south
5	482, 488	Web-shear crack formed at toe of wall and propagated into flexural crack, loading north
6	494	Additional web-shear cracks formed at base of wall, loading north
7	535	Additional web-shear cracks formed with a flexural crack at the fourth course, loading south
8	579	Web-shear crack formed along height of wall, loading north
9	625, 629	Additional web-shear cracks formed, loading south
10	670	Additional web-shear crack at north end of wall, loading north
11	689	Additional web-shear crack at south end of wall accompanied by compression toe damage, loading north
12	754	Additional web-shear crack formed at center of wall, crushing of diagonal strut, loading south

5.6.2.1 Flexural cracking in Shear Wall Specimen 5

Major Events 1 and 2 correspond to the observance of flexural cracking. At Load Point 326 a flexural crack formed while loading to the south at a load of 53.9 kips (240 kN) and a drift ratio of 0.06%. A flexural crack formed while loading to the north at Load Point 363, when the base shear and the drift ratio in the specimen were 54.6 kips (243 kN) and 0.05% respectively. Both of these cracks, shown in gray in Figure 5.51, propagated throughout the remainder of the test.

The predicted base shear at flexural cracking using the average tensile bond strength of Section 8.1.1 is 49.5 kips (220 kN), which corresponds to a ratio of observed to predicted flexural cracking capacity of 1.1 for loading in both directions.

5.6.2.2 Web-shear cracking in Shear Wall Specimen 5

Major Events 3 and 4 correspond to the formation of web-shear cracks while loading to the south. A series of web-shear cracks formed in the lower north corner at Load Point 454 at a base shear of 62.2 kips (277 MPa) and a drift ratio of 0.07%. The prediction for web-shear cracking based on Equation (8.11) at the corresponding axial load is 64.6 kips (287 kN), which corresponds to a ratio of observed to predicted web-shear cracking capacity of 0.96.

As the load increased, Load Point 457, a web-shear crack formed along the entire height of the wall as shown in Figure 5.51. The corresponding base shear and drift ratio were 67.4 kips (300 kN) and 0.09%.

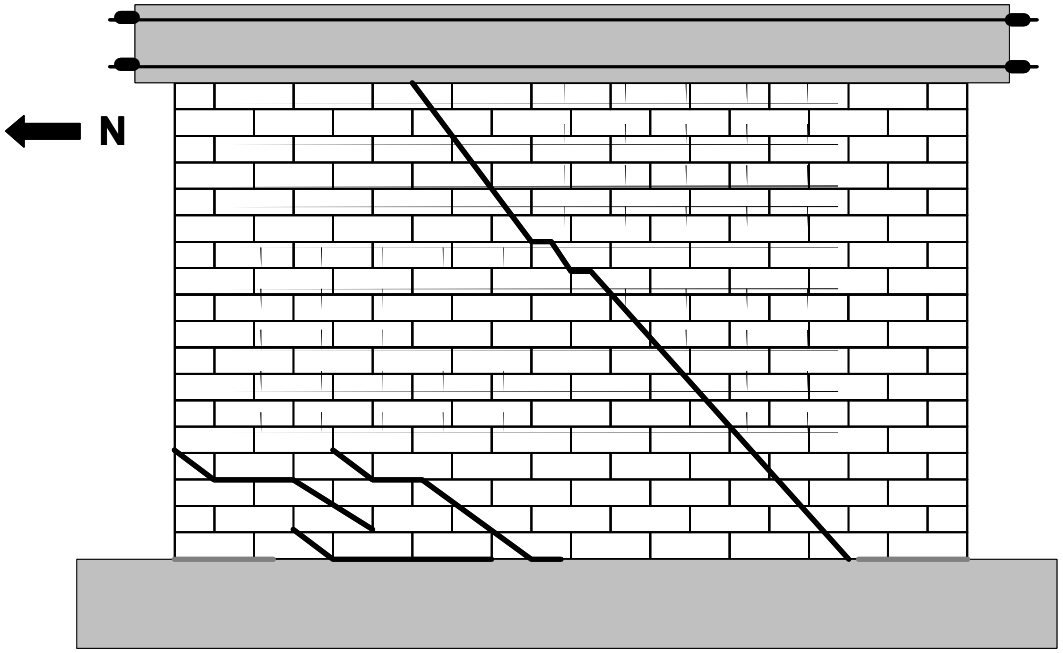

Figure 5.51: Formation of web-shear crack while loading to the south in Shear Wall Specimen 5

While loading to the north, another series of shear cracks formed in the lower south corner of the specimen. Major Event 5 corresponds to the formation

of a flexural crack that propagated into a flexure-shear crack. The base shears were 45.4 kips (202 kN) and 64.1 kips (285 kN) for Load Points 482 and 488 respectively with corresponding drift ratios of 0.03% and 0.06%. A series of web-shear cracks formed at a base shear of 74.3 kips (330 MPa) and a drift ratio of 0.08%. All of these cracks are shown in Figure 5.52.

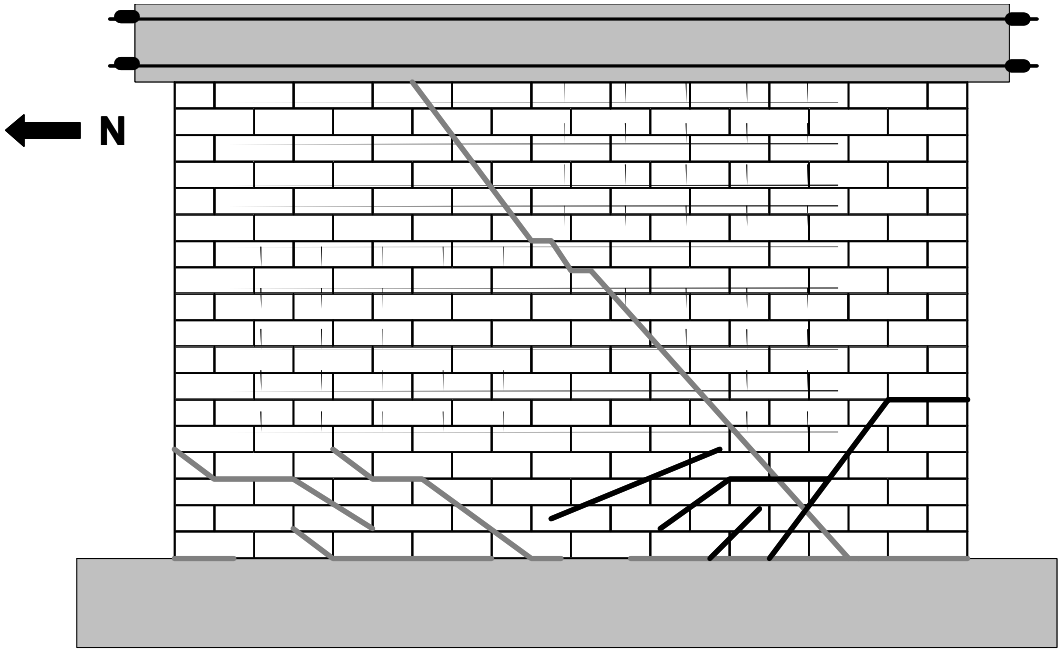

Figure 5.52: Formation of web-shear crack while loading to the north in Shear Wall Specimen 5

5.6.2.3 Additional web-shear cracking in Shear Wall Specimen 5

Major Events 7 through 10 correspond to the development of additional web-shear cracks in the specimen. At Load Point 535, additional web-shear cracks formed along with a flexural crack above the fourth course. These cracks occurred while loading to the south at a base shear of 71.9 kips (320 kN) with a corresponding drift ratio of 0.17% At Load Point 579, addition web-shear cracks

formed while loading to the north, when the base shear and drift ratio were 73.7 kips (328 kN) and 0.14% respectively. These load points represent Major Events 7 and 8; the damage that occurred during these load points is shown in Figure 5.53.

At Load Points 625 and 629 additional web-shear cracks formed while loading to the south. The corresponding base shears were 82.8 kips (368 kN) and 82.1 kips (365 kN) and the corresponding drift ratios were 0.24% and 0.3%. Major Event 9 occurred at Load Point 670. The base shear and drift ratio at the formation of this additional web-shear crack are 64.2 kips (286 kN) and 0.11%. The damage observed in Load Points 625, 629 and 670 is shown in Figure 5.54.

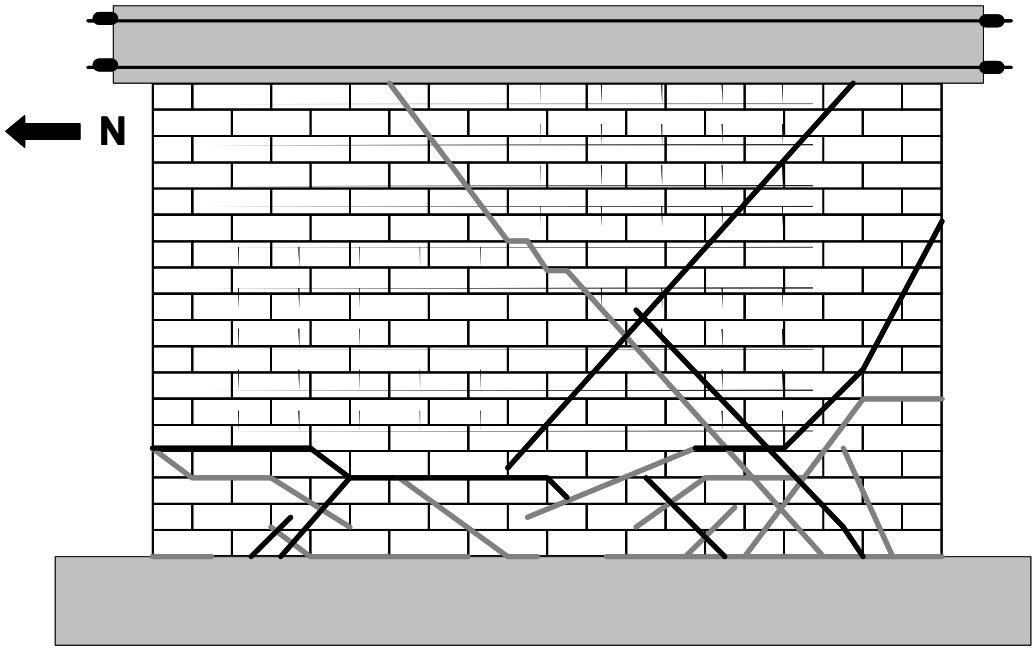

Figure 5.53: Additional web-shear cracking in Shear Wall Specimen 5 for Major Events 7 and 8

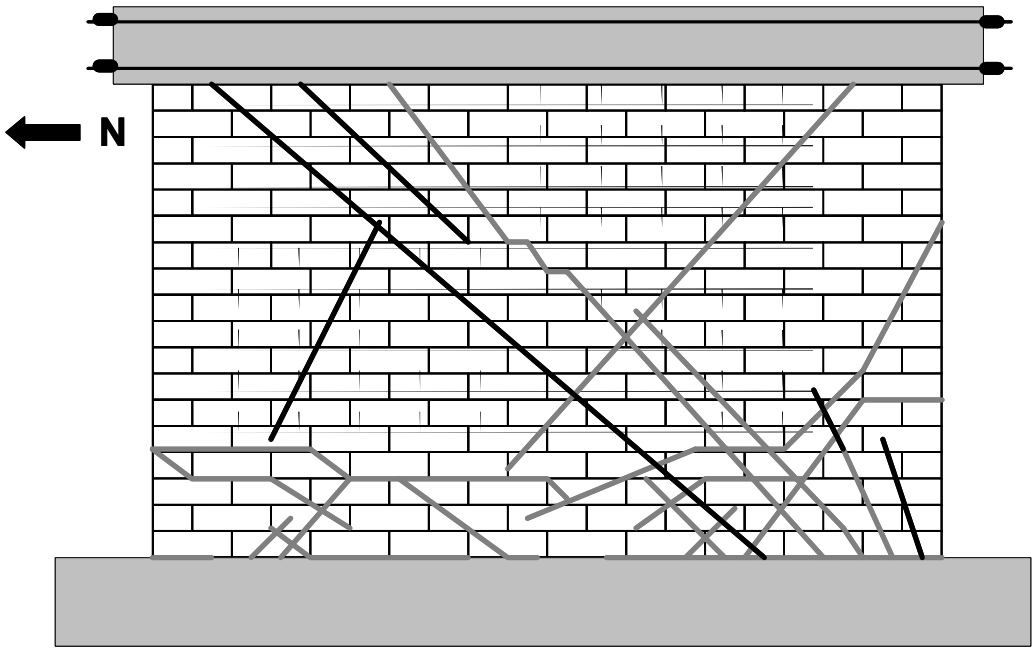

Figure 5.54: Additional web-shear cracking in Shear Wall Specimen 5 for Major Events 9 and 10

5.6.2.4 Spalling of the compression toe and distributed web-shear cracking in Shear Wall Specimen 5

Major Events 11 and 12 were additional web-shear cracks combined with vertical cracking and spalling in the compression toe. As the load continued to increase to the north, a web-shear crack, vertical cracks in the compression toe and spalling of the compression toe occurred at a base shear of 70.1 kips (312 kN) at a drift ratio of 0.31% (Load Point 689). Similar damage occurred while loading to the south at a base shear of 84.8 kips (377 kN) at a drift ratio of 0.38% (Load Point 754). This damage was also combined with crushing in the upper north end of the wall indicating that load was transferred through a diagonal compression strut. A 0.25 in. (6 mm) gap was observed in the web-shear crack that formed at

Load Point 457 (Figure 5.51). The test was ended due to an abrupt decrease in strength after this damage occurred.

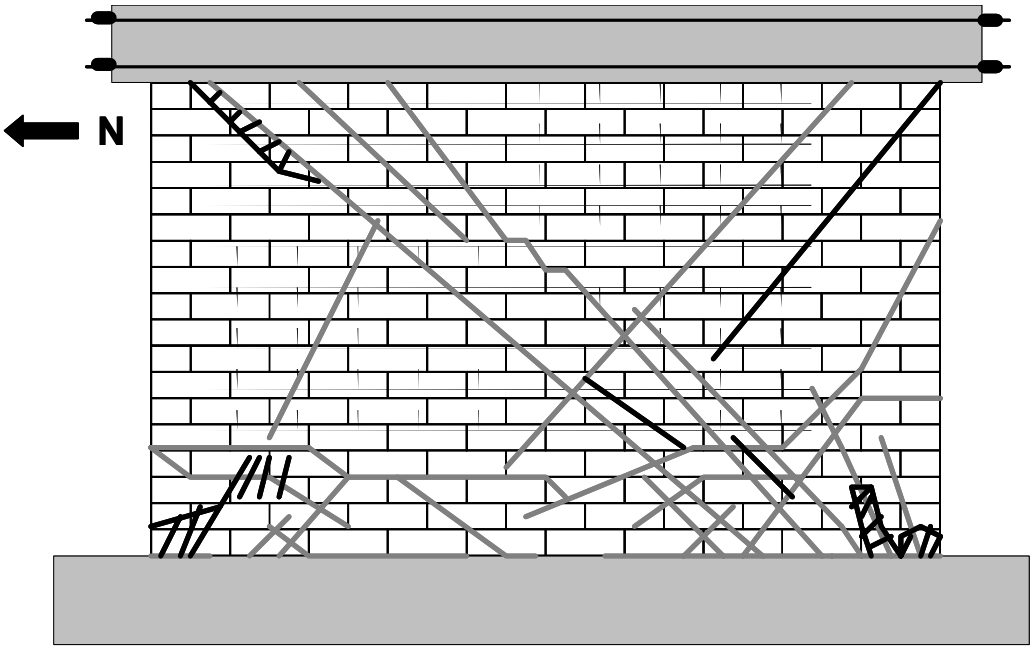

Figure 5.55: Additional web-shear cracking in Shear Wall Specimen 5 for Major Events 11 and 12

5.6.3 Load-Displacement Behavior for Shear Wall Specimen 5

The load-displacement relationship of Shear Wall Specimen 5 is presented in terms of the non-dimensional drift ratio in Figure 5.56. The stiffnesses observed at various points in the loading history are described in Varela (2003).

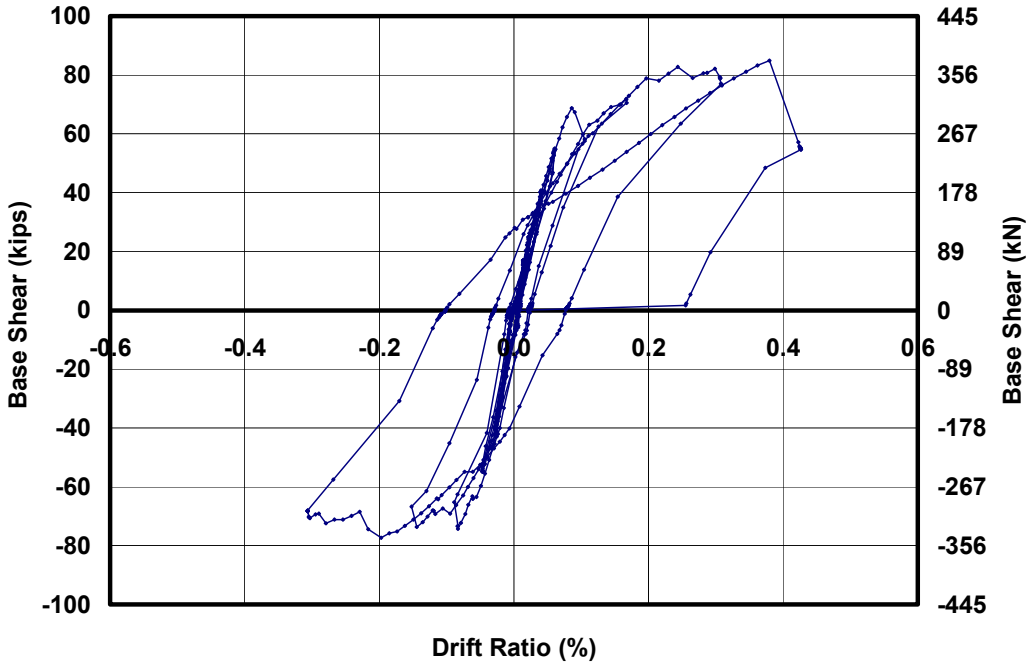

Figure 5.56: Load-displacement relationship for Shear Wall Specimen 5

5.7 SHEAR WALL SPECIMENS 6, 8, 10 AND 12

An additional four shear-dominated shear wall specimens were proposed: Shear Wall Specimen 6, 8, 10 and 12. These specimens were not tested because sufficient data on shear-dominated specimens was obtained through Shear Wall Specimens 1, 2, 3, 4, 5, 7, 9 and 11 combined with the data from other sources presented in Section 7.3.

5.8 SHEAR WALL SPECIMEN 7

An interaction diagram for base shear capacity as a function of axial load for Shear Wall Specimen 7 is presented in Figure 5.60. The axial load applied to Shear Wall Specimen 7 was 80 kips (236 kN), as shown by a dashed horizontal line in Figure 5.60. At this level of axial load the following major events are

predicted in order of occurrence: flexural cracking; web-shear cracking; sliding shear; and crushing of the diagonal strut. This specimen was not expected to reach nominal flexural capacity.

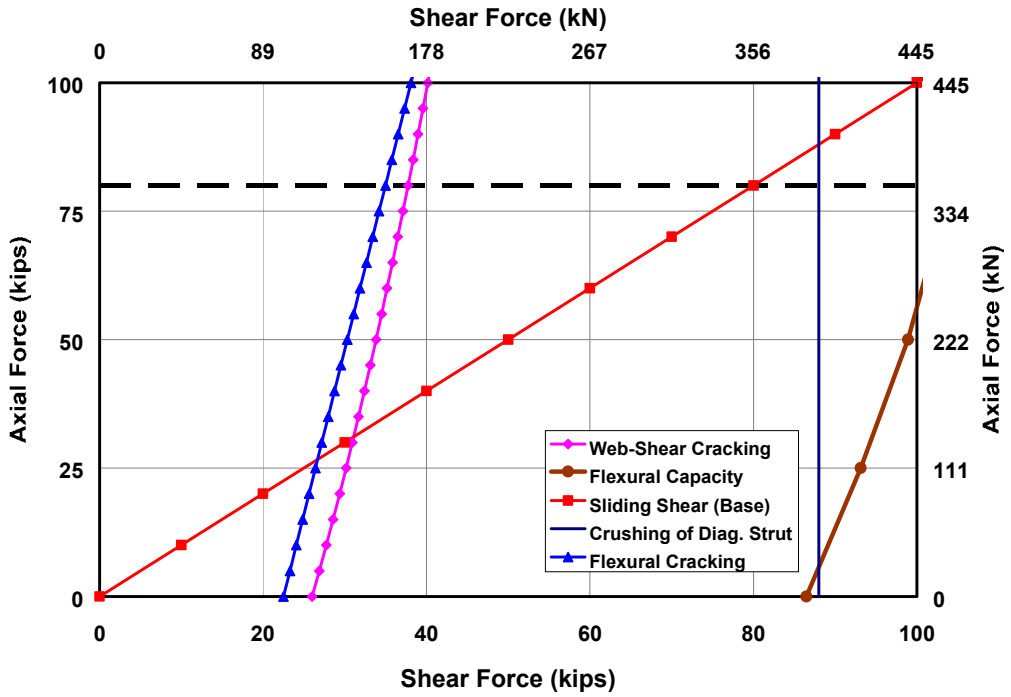

Figure 5.57: Prediction of behavior for Shear Wall Specimen 7

5.8.1 Loading History and Major Events for Shear Wall Specimen 7

The actual loading and displacement histories for Shear Wall Specimen 7 are presented in Figure 5.58 and Figure 5.59. Monotonically increasing load point numbers are assigned for each set of data recorded during the test. Data are classified into cycles with maximum loads and drift ratios for each cycle (Table 5.12). Loading to the south is considered positive; loading to the north, negative.

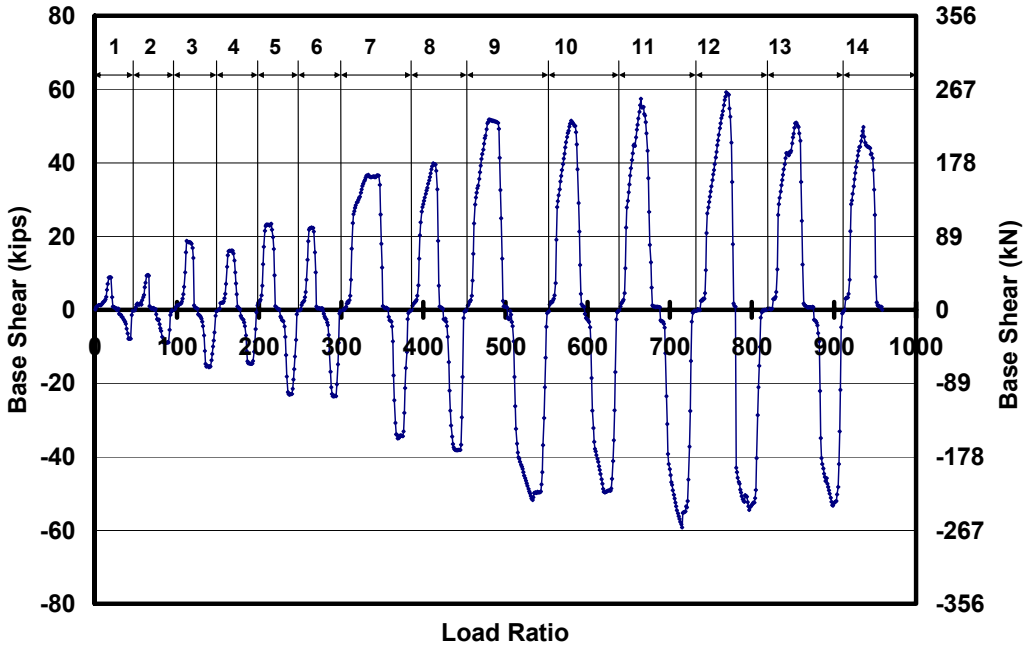

Figure 5.58: Actual loading history for Shear Wall Specimen 7 (numbers at the top designate cycle numbers)

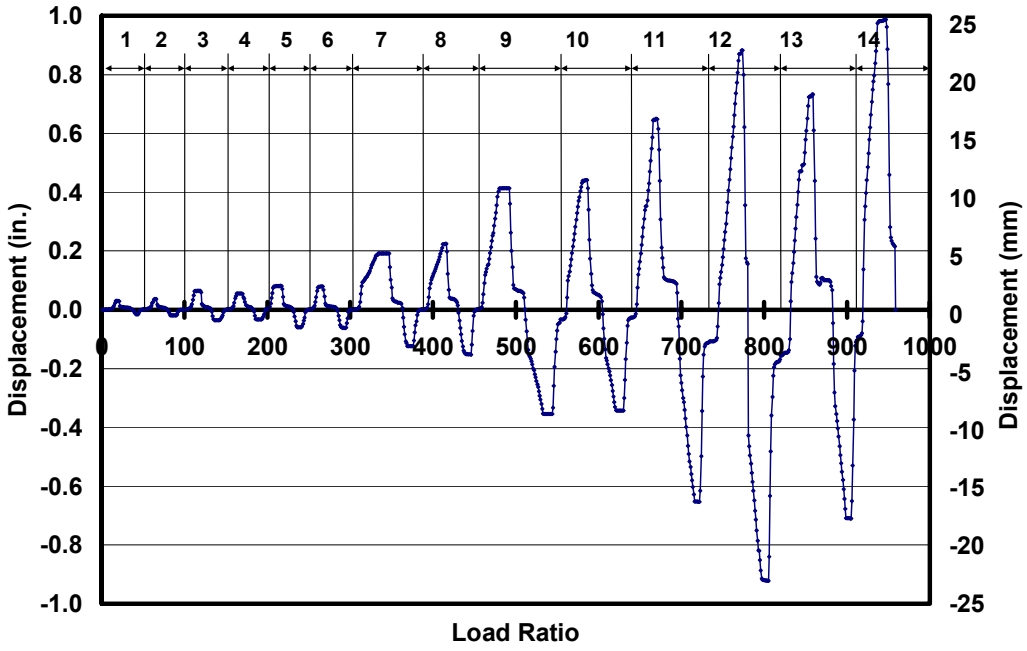

Figure 5.59: Actual tip displacement history for Shear Wall Specimen 7 (numbers at the top designate cycle numbers)

Table 5.12: Load points, maximum load and drift ratios for each cycle for Shear Wall Specimen 7

Cycle	Load Points	Maximum Applied Load, kips (kN)	Max. Drift Ratio (%)	Cycle	Load Points	Minimum Applied Load, kips (kN)	Min. Drift Ratio (%)
1a	1-38	8.8(39)	0.020	1b	39-48	-7.8(35)	0.010
2a	49-73	9.5(42)	0.023	2b	74-95	-9.0(40)	0.012
3a	96-125	18.7(83)	0.042	3b	126-149	-15.6(69)	0.023
4a	150-177	16.1(72)	0.036	4b	178-196	-14.7(65)	0.021
5a	197-225	23.4(104)	0.053	5b	226-250	-23.1(103)	0.039
6a	251-277	22.4(99)	0.051	6b	278-300	-23.6(105)	0.040
7a	301-357	36.7(163)	0.124	7b	358-385	-35.0(156)	0.080
8a	386-424	39.8(177)	0.146	8b	425-452	-38.2(170)	0.099
9a	453-502	51.8(230)	0.269	9b	503-553	-51.7(230)	0.230
10a	554-596	51.4(229)	0.286	10b	597-638	-49.7(221)	0.223
11a	639-688	57.4(255)	0.421	11b	689-733	-59.2(263)	0.424
12a	734-779	59.2(263)	0.573	12b	780-822	-59.2(263)	0.599
13a	823-875	51.0(227)	0.475	13b	875-912	-53.3(237)	0.461
14a	912-958	49.7(221)	0.641				

5.8.2 Sequence of Crack Formation for Shear Wall Specimen 7

The sequence of crack formation in Shear Wall Specimen 7 is described in terms of major events: points during the test when either the condition of the specimen changed (for example, flexural cracking or web-shear cracking), or the applied axial force was increased. Table 5.13 lists the major events and the load point at which they occurred. In each crack map, preexisting cracks are shown in gray, and new cracks are shown in black.

Table 5.13: Description of major events for Shear Wall Specimen 7

Major Event	Load Point	Physical Description
1	320	Flexural cracking, loading south
2	366	Flexural cracking, loading north
3	490-623	Propagation of flexural cracks and flexural rocking
4	665	Web-shear cracking, loading south
5	715	Web-shear cracking, loading north
6	772	Spalling at the south toe and additional web-shear cracking
7	803	Spalling at the north toe and additional web-shear cracking
8	859	Propagation of web-shear cracks in Load Point 772
9	903	Additional diagonal cracks formed with toe crushing, loading north
10	935	Additional diagonal cracks formed with toe crushing, loading south

5.8.2.1 Flexural cracking in Shear Wall Specimen 7

Major Events 1 and 2 correspond to the observance of flexural cracking. At Load Point 320 a flexural crack formed while loading to the south at a load of 29.4 kips (131 kN) and a drift ratio of 0.07%. A flexural crack formed while loading to the north at Load Point 366, when the base shear in the specimen was 30.8 kips (137 kN) and the drift ratio was 0.05%. These cracks propagated throughout Load Points 490-623 as the wall underwent flexural rocking for the next three cycles. Local damage, consisting of two vertical cracks, was observed at the base of the wall at Load Points 583 and 490. All of these cracks are shown in gray in Figure 5.60. The predicted base shear at flexural cracking using the average tensile bond strength of Section 8.1.1 is 24.7 kips (110 kN). The ratios of observed to predicted flexural cracking capacity are 1.2 and 1.25 while loading to the south and north respectively.

5.8.2.2 Web-shear cracking in Shear Wall Specimen 7

Major Events 4 and 5 correspond to the formation of web-shear cracking while loading to the south and north respectively. A web-shear crack formed along the entire height of the wall at Load Point 665 at a corresponding base shear and drift ratio of 57.4 kips (255 kN) and 0.38% respectively. While loading to the north, a similar web-shear crack formed at Load Point 715 at a base shear of 59.2 kips (263 MPa) and a drift ratio of 0.41%. Although additional localized cracks formed at the base of the wall in Load Point 715, the crack patters were symmetric (Figure 5.60).

The prediction for web-shear cracking based on Equation (8-11) at the corresponding axial load is 38 kips (168 kN). The ratio of observed to predicted web-shear cracking capacity is 1.5. This ratio exceeds 1.0 because the proposed predictive equations were calibrated to lower fractiles of observed capacities.

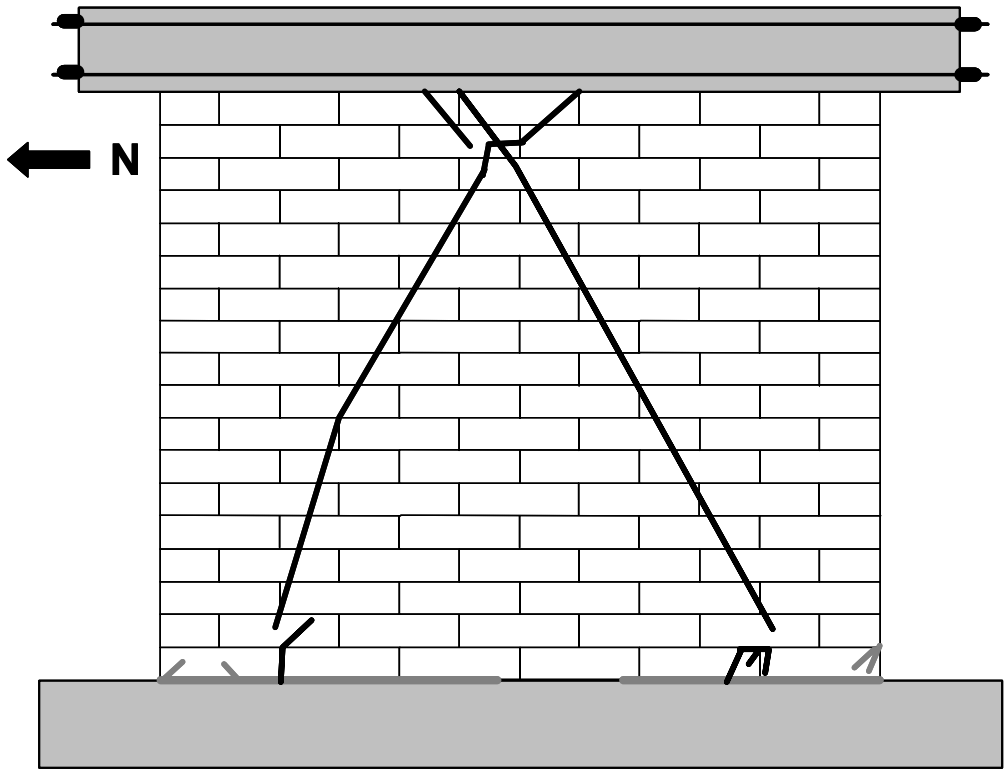

Figure 5.60: Formation of web-shear crack in Shear Wall Specimen 7

5.8.2.3 Spalling and Additional Web-shear Cracking in Shear Wall Specimen 7

Major Events 6 and 7 correspond to the development of additional web-shear cracks in the specimen combined with spalling at the compression toe. The base shears were 58.5 kips (260 kN) and 52.4 kips (233 kN) for Load Points 772 (loading south) and 802 (loading north) respectively. The corresponding drift ratios were 0.57% and 0.6%. Major Event 8 is the propagation of diagonal cracks that formed in Major Event 6. The base shear was 46.0 kips (204 kN) at a drift ratio of 0.48%. The damage in the specimen at the end of Major Event 8 is shown in Figure 5.61.

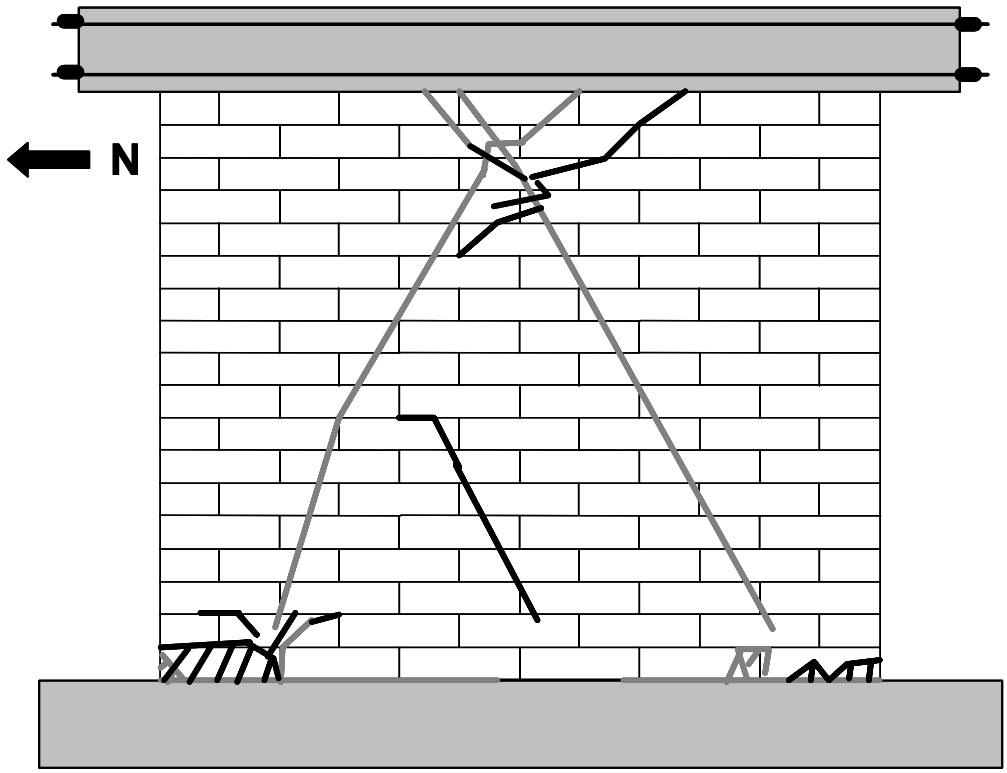

Figure 5.61: Spalling and additional web-shear cracking in Shear Wall Specimen 7

5.8.2.4 Toe crushing and additional web-shear cracking in Shear Wall Specimen 7

Major Events 9 and 10 occurred at Load Points 903 and 935. Both events include distributed web-shear cracking with combined crushing in the compression toe (Figure 5.62). The respective base shears are 52.0 kips (231 kN) and 48.6 kips (216 kN) at drift ratios of 0.46% and 0.57%. The test was unloaded and discontinued after Load Point 935 due to crushing of the south compression toe and opening of the web-shear crack of 0.75 in. (19 mm). This damage is shown in Figure 5.63.

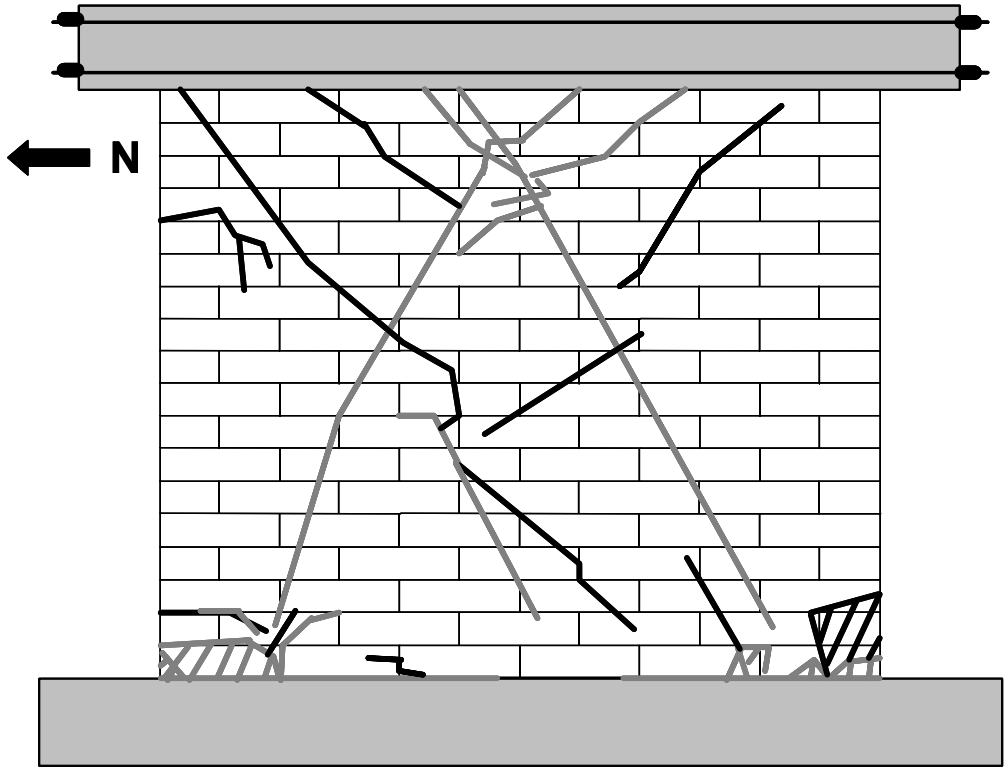

Figure 5.62: Toe crushing and additional web-shear cracking in Shear Wall Specimen 7

Figure 5.63: Toe crushing and opening of web-shear crack in Shear Wall Specimen 7

5.8.3 Load-Displacement Behavior for Shear Wall Specimen 7

The load-displacement relationship of Shear Wall Specimen 7 is presented in terms of the non-dimensional drift ratio in Figure 5.64. The stiffnesses observed at various points in the loading history are described in Varela (2003).

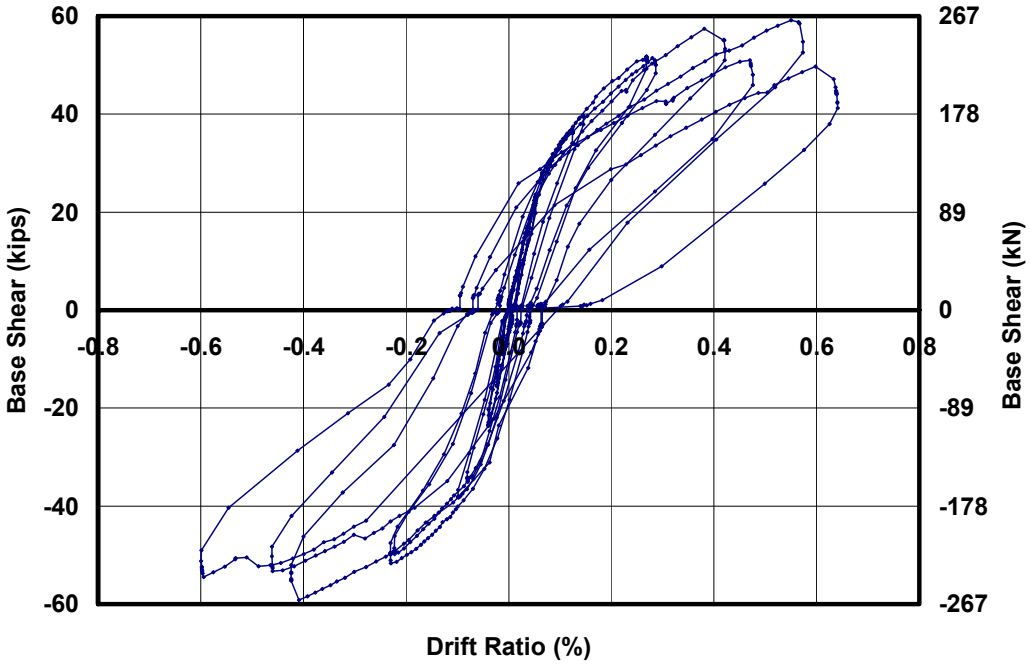

Figure 5.64: Load-displacement relationship for Shear Wall Specimen 7

5.9 SHEAR WALL SPECIMEN 9

An interaction diagram for base shear capacity as a function of axial load for Shear Wall Specimen 9 is presented in Figure 5.65. The axial load applied to Shear Wall Specimen 9 was 60 kips (267 kN), as shown by a dashed horizontal line in Figure 5.65. At this level of axial load the following major events are predicted in order of occurrence: flexural cracking; web-shear cracking; and sliding shear. This specimen was not expected to reach crushing of the diagonal strut or nominal flexural capacity.

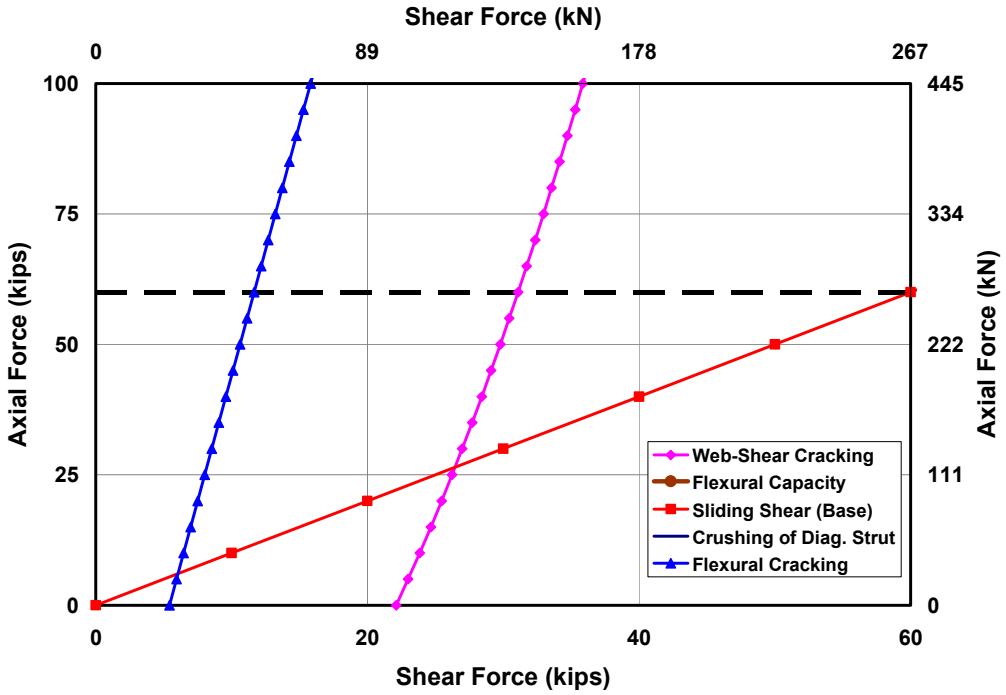

Figure 5.65: Prediction of behavior for Shear Wall Specimen 9

5.9.1 Loading History and Major Events for Shear Wall Specimen 9

The actual loading and displacement histories for Shear Wall Specimen 9 are presented in Figure 5.66 and Figure 5.67. Monotonically increasing load point numbers are assigned for each set of data recorded during the test. Data are classified into cycles with maximum loads and drift ratios for each cycle (Table 5.14). Loading to the south is considered positive; loading to the north, negative.

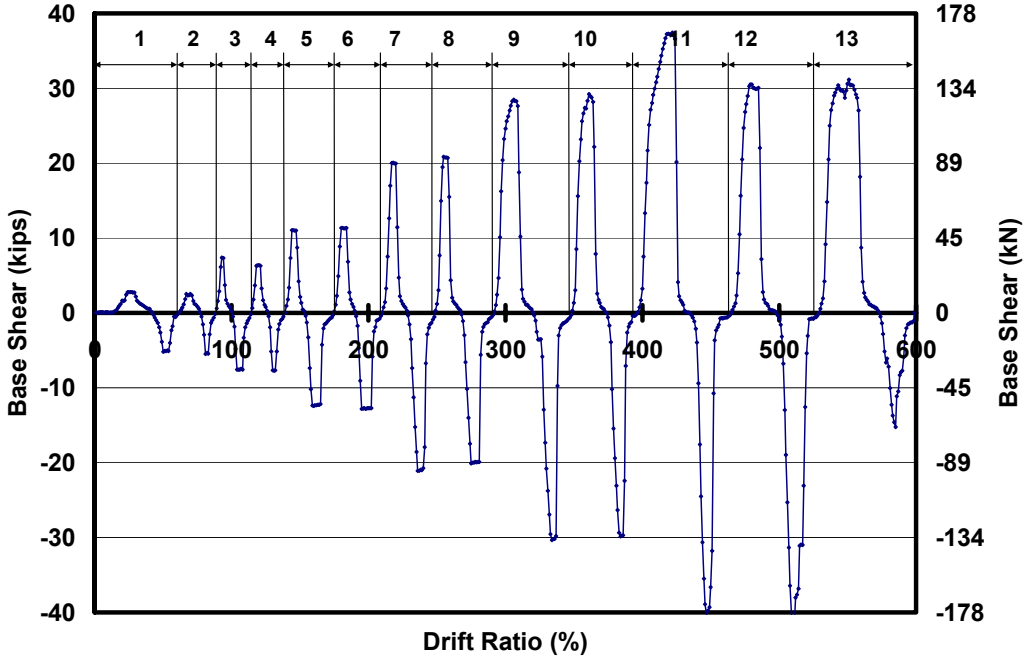

Figure 5.66: Actual loading history for Shear Wall Specimen 9 (numbers at the top designate cycle numbers)

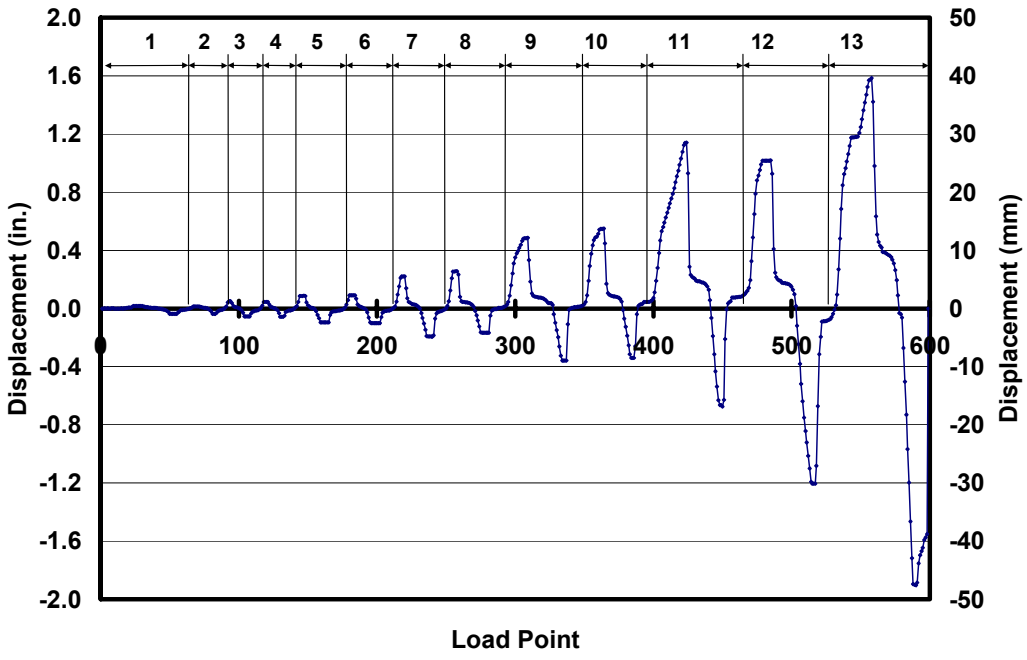

Figure 5.67: Actual tip displacement history for Shear Wall Specimen 9 (numbers at the top designate cycle numbers)

Table 5.14: Load points, maximum load and drift ratios for each cycle for Shear Wall Specimen 9

Cycle	Load Points	Maximum Applied Load, kips (kN)	Max. Drift Ratio (%)	Cycle	Load Points	Minimum Applied Load, kips (kN)	Min. Drift Ratio (%)
1a	1-41	2.8 (12.3)	0.011	1b	42-61	-5.2 (23.0)	0.024
2a	62-77	2.5 (11.1)	0.008	2b	78-88	-5.4 (24.3)	0.025
3a	89-100	7.4 (32.7)	0.032	3b	101-114	-7.6 (33.7)	0.036
4a	115-126	6.4 (28.3)	0.029	4b	127-138	-7.7 (34.4)	0.038
5a	139-153	11.1 (49.2)	0.056	5b	154-174	-12.4 (54.9)	0.062
6a	175-190	11.4 (50.5)	0.059	6b	191-209	-12.8 (56.9)	0.065
7a	210-228	20.0 (89)	0.14	7b	229-248	-21.1 (93.6)	0.13
8a	249-268	20.8 (92.6)	0.17	8b	269-291	-20.1 (89.3)	0.11
9a	292-320	28.5 (127)	0.31	9b	321-349	-30.4 (135)	0.23
10a	350-374	29.2 (130)	0.36	10b	375-396	-29.9 (133)	0.22
11a	397-434	37.3 (166)	0.74	11b	435-464	-40.2 (179)	0.44
12a	465-498	30.5 (135)	0.66	12b	499-529	-42.4 (189)	0.80
13a	530-573	31.1 (138)	1.03	13b	573-600	-15.3 (68)	1.24

5.9.2 Sequence of Crack Formation for Shear Wall Specimen 9

The sequence of crack formation in Shear Wall Specimen 9 is described in terms of major events: points during the test when either the condition of the specimen changed (for example, flexural cracking or web-shear cracking), or the applied axial force was increased. Table 5.15 lists the major events and the load point at which they occurred. In each crack map, preexisting cracks are shown in gray, and new cracks are shown in black.

Table 5.15: Description of major events for Shear Wall Specimen 9

Major Event	Load Point	Physical Description
1	160	Flexural cracking, loading north
2	180	Flexural cracking, loading south
3	198-360	Propagation of flexural cracks and rocking of wall under flexural behavior
4	361	Minor crushing of south toe, vertical splitting at end of panel
5	422	Web-shear crack at base of wall, spalling of south toe
6	447	Spalling at north toe
7	510	Diagonal crack formed in lower three panels, spalling at north toe
8	554	Diagonal crack propagated from crack in head joint
9	578	Increased axial load in load maintainer

5.9.2.1 Flexural cracking and rocking in Shear Wall Specimen 9

Major Events 1 and 2 correspond to the observance of flexural cracking. At Load Point 160, the formation of a flexural crack was observed while loading to the north at a base shear of 12.4 kips (55.1 kN) and a drift ratio of 0.06%. A flexural crack formed while loading to the south at Load Point 180. The base shear in the specimen was 11.4 kips (50.5 kN) and the drift ratio was 0.06%. Both of these cracks were less than 4 in. (104 mm) long at the time of observation. The predicted base shear at flexural cracking using the average tensile bond strength of Section 8.1.1 is 31.1 kips (137 kN). The ratios of observed to predicted flexural cracking capacity are 1.1 and 1.0 while loading to the north and south respectively.

The flexural cracks propagated throughout Load Points 198-360 and the wall underwent flexural rocking for the next three cycles before minor crushing was observed. Vertical displacements at the base of the wall reached 0.25 in. (5mm). All of these cracks are shown in gray in Figure 5.68.

5.9.2.2 Spalling and web-shear cracking in Shear Wall Specimen 9

Major Event 4 corresponds to minor spalling of the south compression toe at Load Point 361. The corresponding base shear is 29.2 kips (130 kN) at a drift ratio of 0.35%. This is defined as Major Event 4.

The area of spalling increased at Load Point 422 and spalling in the north compression toe occurred at Load Point 447 (Figure 5.68). The corresponding base shears are 37.4 kips (166 kN) and 40.3 kips (179 kN) at drift ratios of 0.73% and 0.41%. Vertical cracks were observed in the width of the end of the wall. These load points are also defined as Major Events 5 and 6. A web-shear crack formed in the first panel during Load Point 447 (Figure 5.68). The prediction for web-shear cracking based on Equation (8.11) is 31.1 kips (137 kN). The ratio of observed to predicted web-shear cracking capacity is 1.2.

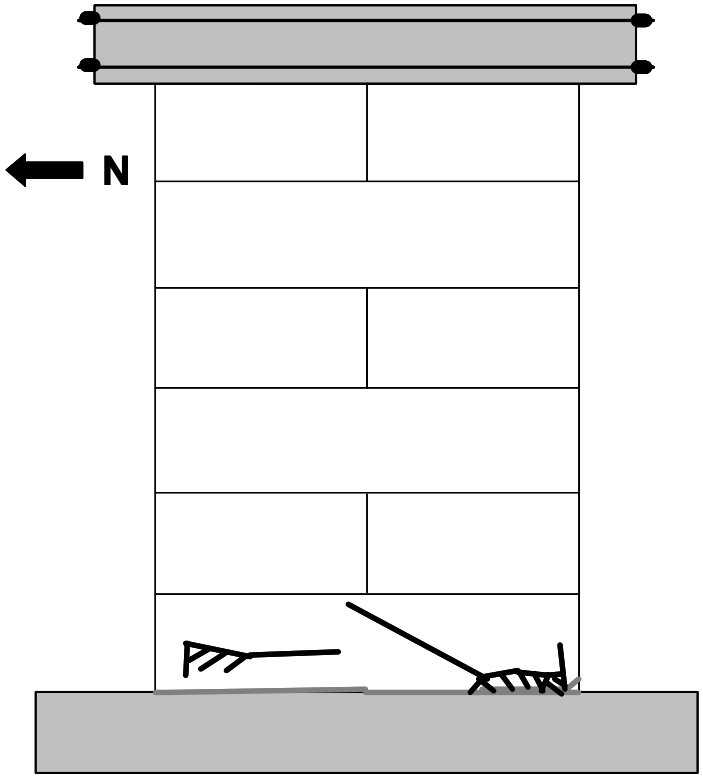

Figure 5.68: Spalling of the compression toes in Shear Wall Specimen 9 with simultaneous web-shear cracking

Figure 5.69: Vertical cracks at the base of the south and north ends of Shear Wall Specimen 9

5.9.2.3 Additional spalling of the compression toes and web-shear cracking in Shear Wall Specimen 9

At Load Points 510 and 554, Major Events 7 and 8, additional spalling and web-shear cracks occurred at the base of the wall (Figure 5.70). The respective base shears were 42.4 kips (188 kN) and 30.3 kips (135 kN) at drift ratios of 0.55% and 0.95%. At Major Event 8, the welded wire reinforcement began to buckle causing sufficient vertical displacement to eliminate all post-tensioning in the external threaded rods.

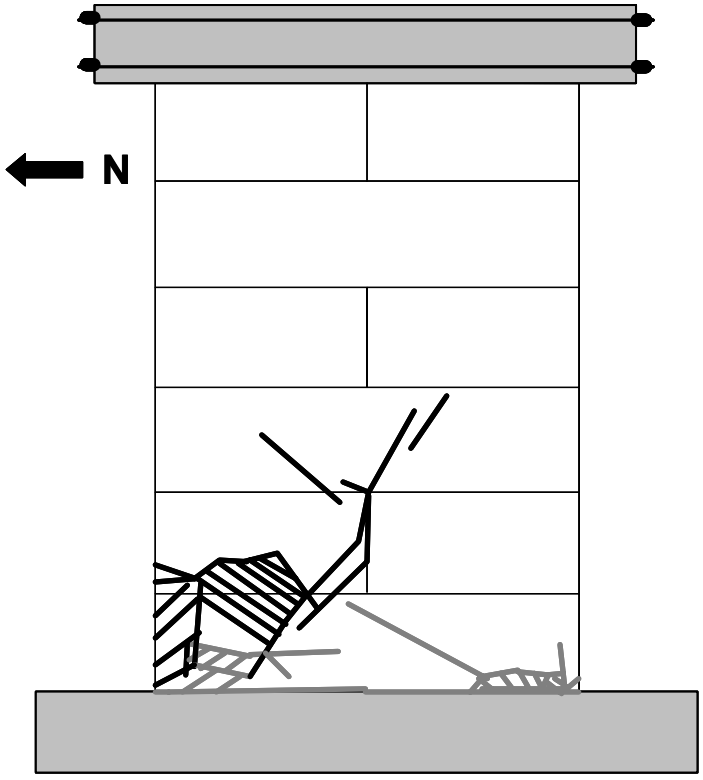

Figure 5.70: Formation of web-shear crack while loading to the south in Shear Wall Specimen 9

Figure 5.71: Buckling of welded-wire reinforcement in Shear Wall Specimen 9

5.9.3 Load-Displacement Behavior for Shear Wall Specimen 9

This load-displacement relationship of Shear Wall Specimen 9 is presented in terms of the non-dimensional drift ratio in Figure 5.72. The stiffnesses observed at various points in the loading history are described in Varela (2003).

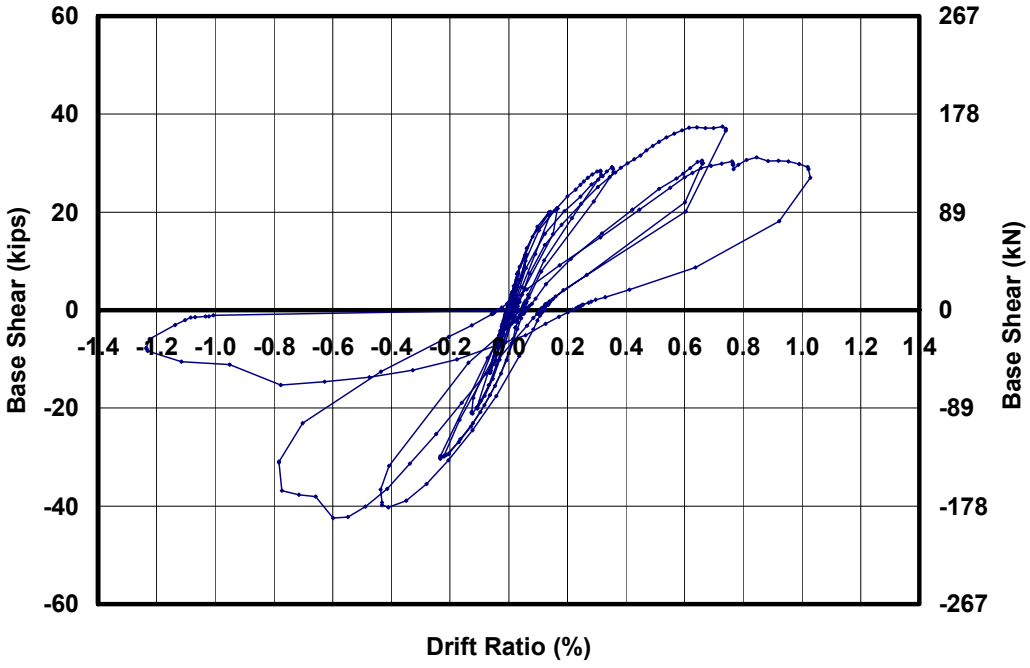

Figure 5.72: Load-displacement relationship for Shear Wall Specimen 9

5.10 SHEAR WALL SPECIMEN 11

An interaction diagram for base shear capacity as a function of axial load for Shear Wall Specimen 11 is presented in Figure 5.73. The axial load applied to Shear Wall Specimen 11 was 25 kips (111 kN), as shown by a dashed horizontal line in Figure 5.73. At this level of axial load the following major events are predicted in order of occurrence: flexural cracking; web-shear cracking; and simultaneous crushing of the diagonal strut and sliding shear. This specimen was not expected to reach nominal flexural capacity.

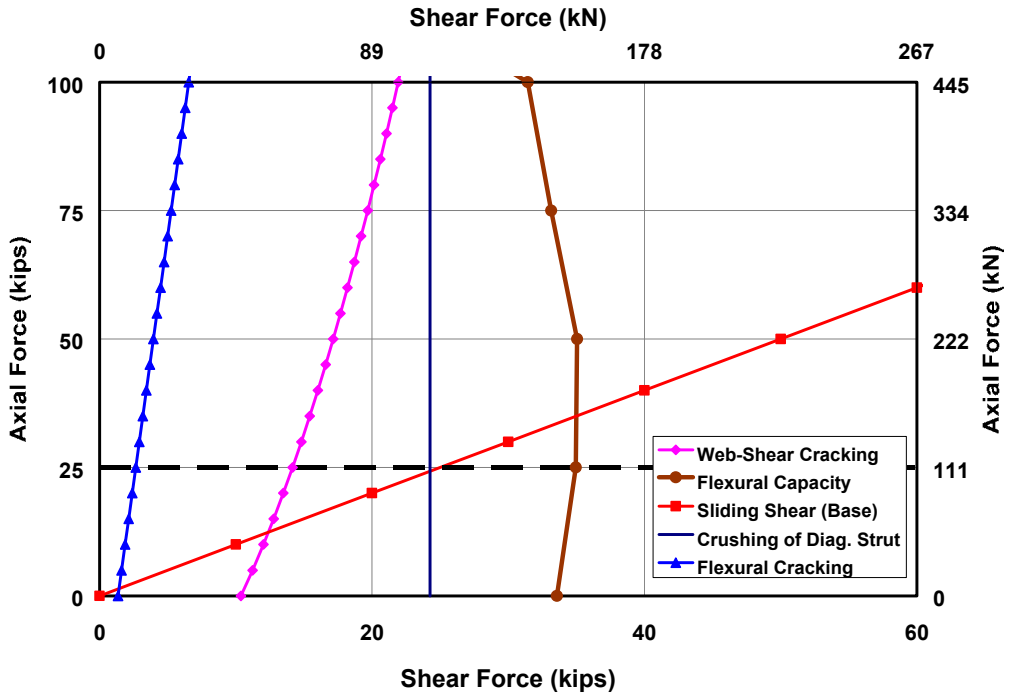

Figure 5.73: Prediction of behavior for Shear Wall Specimen 11

5.10.1 Loading History and Major Events for Shear Wall Specimen 11

The actual loading and displacement histories for Shear Wall Specimen 11 are presented in Figure 5.74 and Figure 5.75. Monotonically increasing load point numbers are assigned for each set of data recorded during the test. Data are classified into cycles with maximum loads and drift ratios for each cycle (Table 5.16). Loading to the south is considered positive; loading to the north, negative.

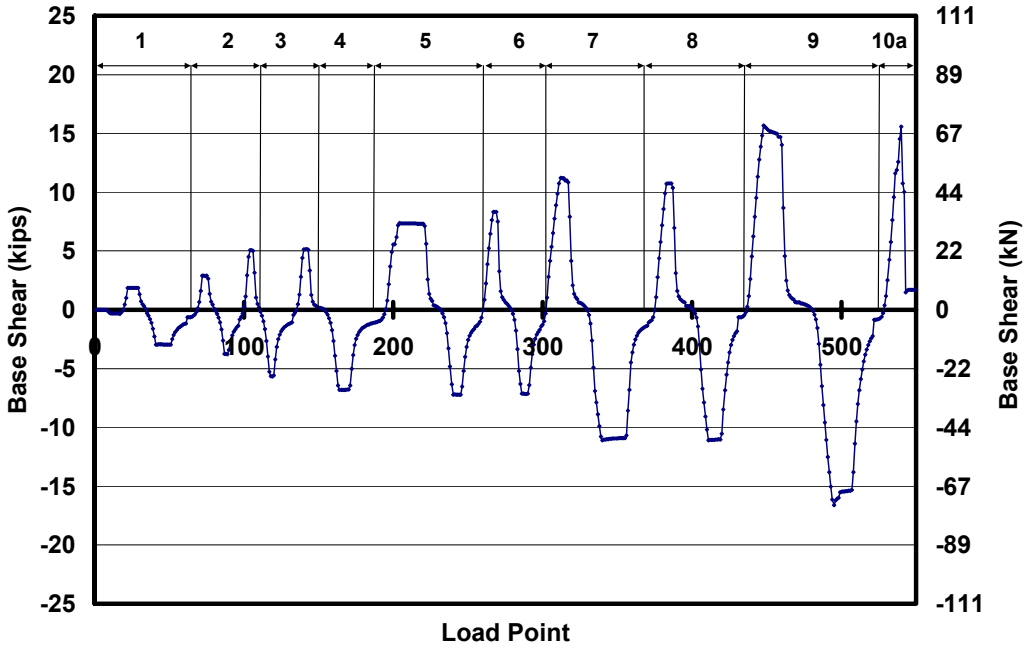

Figure 5.74: Actual loading history for Shear Wall Specimen 11 (numbers at the top designate cycle numbers)

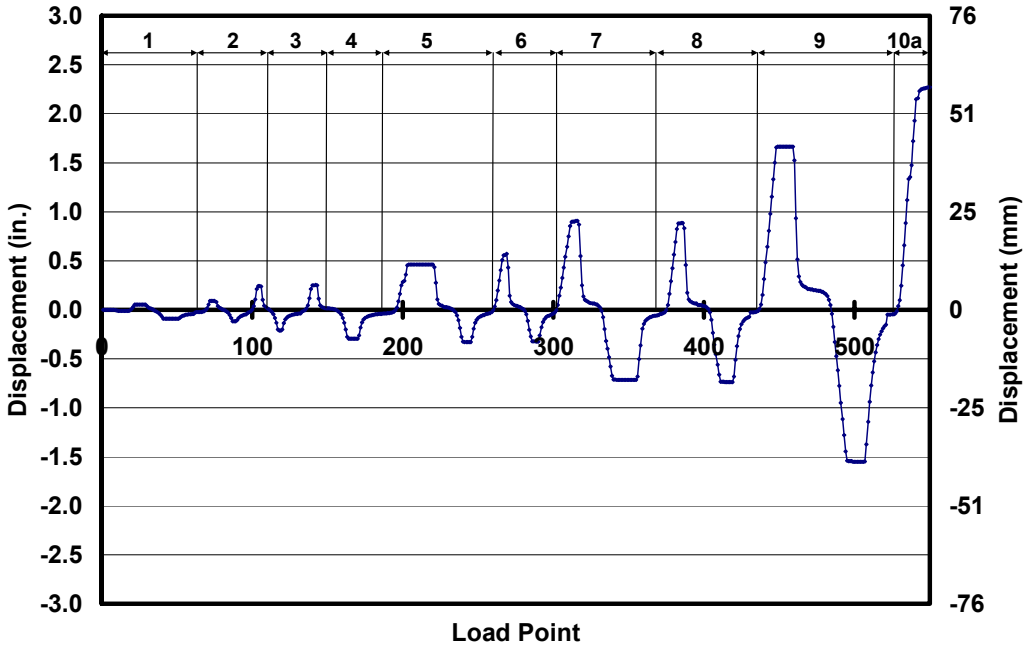

Figure 5.75: Actual tip displacement history for Shear Wall Specimen 11 (numbers at the top designate cycle numbers)

Table 5.16: Load points, maximum load and drift ratios for each cycle for Shear Wall Specimen 11

Cycle	Load Points	Maximum Applied Load, kips (kN)	Max. Drift Ratio (%)	Cycle	Load Points	Minimum Applied Load, kips (kN)	Max. Drift Ratio (%)
1a	1-33	1.9(8)	0.035	1b	19-33	-3.0(13)	-0.059
2a	34-68	2.9(13)	0.060	2b	69-80	-3.8(17)	-0.077
3a	81-99	5.1 (23)	0.158	3b	100-110	-5.7(25)	-0.139
4a	111-135	5.2(23)	0.164	4b	135-153	-6.8(30)	-0.192
5a	154-194	7.4(33)	0.300	5b	195-231	-7.2(32)	-0.215
6a	232-260	8.3(37)	0.370	6b	261-278	-7.1(32)	-0.211
7a	279-302	11.2(50)	0.589	7b	303-329	-11.1(49)	-0.465
8a	330-375	10.8(48)	0.576	8b	376-400	-11.1(49)	-0.479
9a	401-437	15.7(70)	1.082	9b	438-480	-16.6(74)	-1.008
10a	481-529	15.6(69)	1.498				

5.10.2 Sequence of Crack Formation for Shear Wall Specimen 11

The sequence of crack formation in Shear Wall Specimen 11 is described in terms of major events: points during the test when either the condition of the specimen changed (for example, flexural cracking or web-shear cracking), or the applied axial force was increased. Table 5.17 lists the major events and the load point at which they occurred. In each crack map, preexisting cracks are shown in gray, and new cracks are shown in black.

Table 5.17: Description of major events for Shear Wall Specimen 11

Major Event	Load Point	Physical Description
1	168	Flexural cracking, loading north
2	199	Flexural cracking, loading south
3	205-446	Propagation of flexural cracking and flexural rocking
4	447	Minor spalling at compression toe, loading south
5	495	Minor spalling at compression toe, loading north
6	540	Web-shear crack formed, loading south

5.10.2.1 Flexural cracking and local cracking at the base in Shear Wall Specimen 11

Major Events 1 and 2 correspond to the observance of flexural cracking. At Load Point 168 a flexural crack formed was observed while loading to the north at a base shear of 6.8 kips (30.0 kN) and a drift ratio of 0.19%. A flexural crack formed while loading to the south at Load Point 199 when the base shear and drift ratio in the specimen were 4.9 kips (21.9 kN) and 0.16% respectively. Both of these cracks were 24 in. (61 mm) at the time of observation. The predicted base shear at flexural cracking using the average tensile bond strength of Section 8.1.1 is 2.7 kips (12 kN). The ratios of observed to predicted flexural cracking capacity are 2.5 and 1.8. It is possible that the flexural cracks formed prior to the time they were observed since they had propagated half the length

These cracks propagated throughout Load Points 205-340 and the wall underwent flexural rocking for the next five cycles before significant damage was observed. At Load Points 313 and 340 these cracks were 38 in. (97 mm) long. A local crack formed at Load Point 240 at a base shear of 7.2 kips and a drift ratio of 0.21%. All of these cracks are shown in gray, in Figure 5.76 of Section 5.10.2.2.

5.10.2.2 Minor spalling in Shear Wall Specimen 11

Minor spalling occurred in the compression toes while loading to the south and north at Load Points 447 and 449. The corresponding base shears are 14.8 kips (65.9 kN) and 16.6 kips (73.9 kN). At both events the drift ratio was 1.0%. These load points are defined as Major Events 4 and 5.

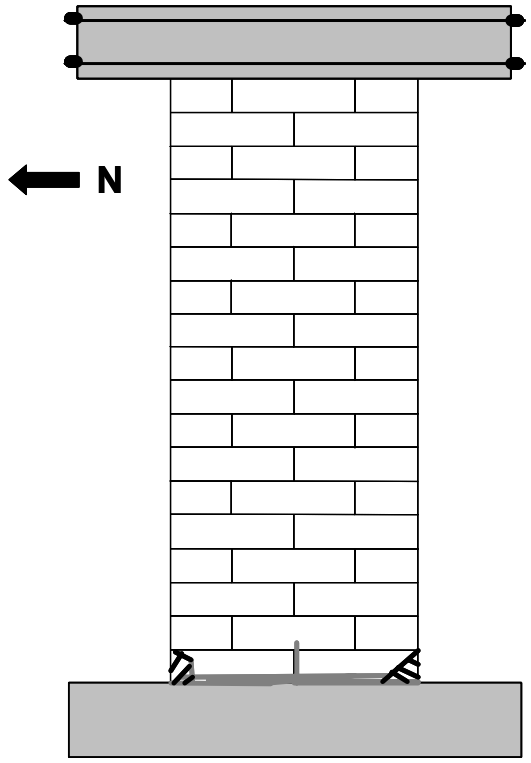

Figure 5.76: Spalling of the compression toes in Shear Wall Specimen 11

5.10.2.3 Web-shear cracking in Shear Wall Specimen 11

At Load Point 540, Major Event 6, a web-shear crack formed along the height of the wall. Immediately prior to the formation of this crack a smaller diagonal crack formed at the compression toe (Figure 5.77). The base shear and drift ratio at this Major Event were 15.6 kips (69.3 kN) and 1.3%. The lower

north corner of the wall became loose but was restrained by the testing equipment. The test was completed after loosing this integral part of the wall.

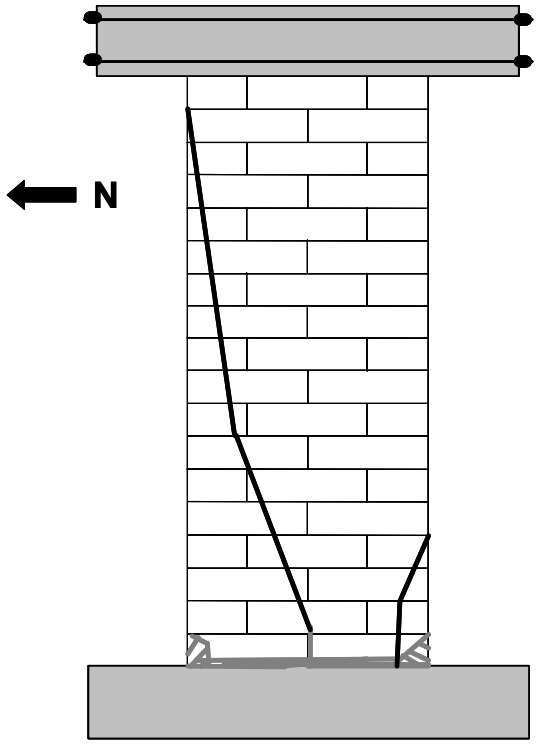

Figure 5.77: Formation of web-shear crack while loading to the south in Shear Wall Specimen 11

5.10.3 Load-Displacement Behavior Shear Wall Specimen 11

The load-displacement relationship of Shear Wall Specimen 11 is presented in terms of the non-dimensional drift ratio in Figure 5.25. The stiffnesses observed at various points in the loading history are described in Varela (2003).

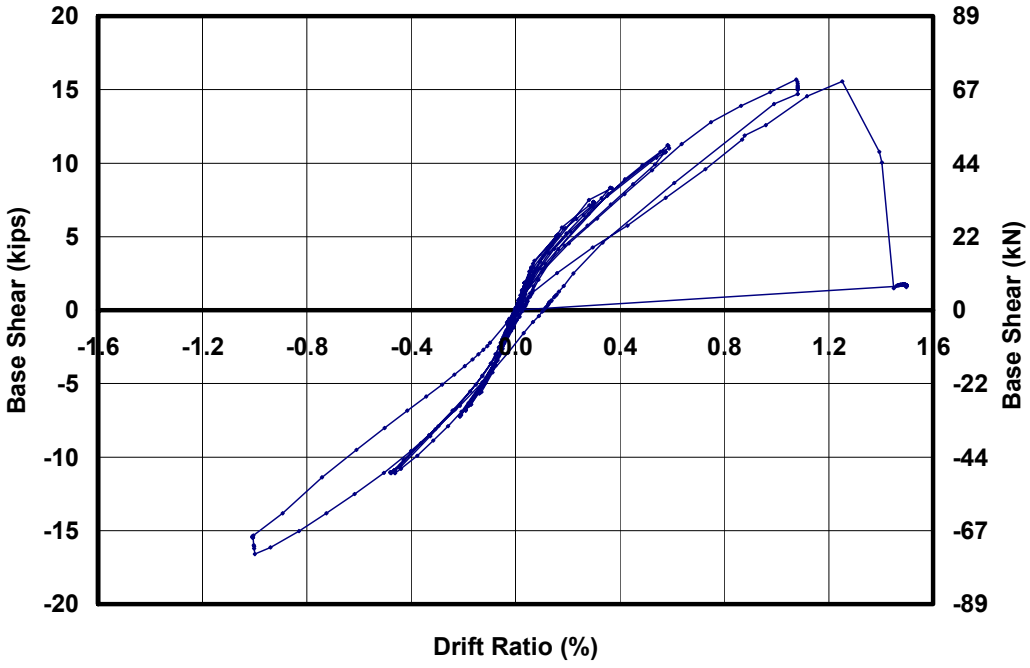

Figure 5.78: Load-displacement relationship for Shear Wall Specimen 11

CHAPTER 6
Test Results for Flexure-dominated AAC Shear Wall Specimens

The primary objective of this chapter is to describe the results of each flexure-dominated AAC shear wall tested at UT Austin. This chapter also presents for each specimen the design objectives, actual loading history, major events, crack formation, and hysteretic behavior. A section on the predicted behavior identifies several conditions that represent a change in strength or stiffness for each shear wall specimen. The sequence of predicted behavior justifies the geometry and prescriptive reinforcement for each shear wall specimen. The actual loading and displacement histories are also presented. The sequence of damage in the wall is presented for each specimen along with quantification of the observed versus predicted behavior for each specimen.

6.1 DESIGN OBJECTIVES OF EACH AAC SHEAR WALL SPECIMEN

The basic design approach for AAC shear wall specimens starts with selecting the desired behavior mode. The wall geometry and flexural reinforcement are selected considering possible behavior modes. The capacity of each shear-dominated specimen is predicted for each behavior mode. An interaction diagram for base shear capacity as a function of axial load is constructed for any shear wall. The axial load is selected based on the interaction diagram. If necessary, any modifications are presented to the original geometry and selection of the reinforcement. This section presents the process for selecting the wall geometry, reinforcement and axial load for Shear Wall Specimen 13. The selection of the wall geometry and reinforcement for the remaining specimens is included with the results of each specimen.

The behavior of Shear Wall Specimen 13 was predicted prior to testing. In Figure 5.1 an interaction diagram is presented for predicting flexural cracking, flexure-shear cracking, sliding shear, web-shear cracking, and the nominal flexural capacity of Shear Wall Specimen 13, based on the proposed equations of Chapter 8. The axial load applied to Shear Wall Specimen 13 was 25 kips (111 kN), as shown by a dashed horizontal line in Figure 5.1. At this level of axial load the following major events are predicted in order of occurrence: flexural cracking; flexure-shear cracking; and nominal flexural capacity. This specimen was not expected to exhibit web-shear cracking or sliding shear.

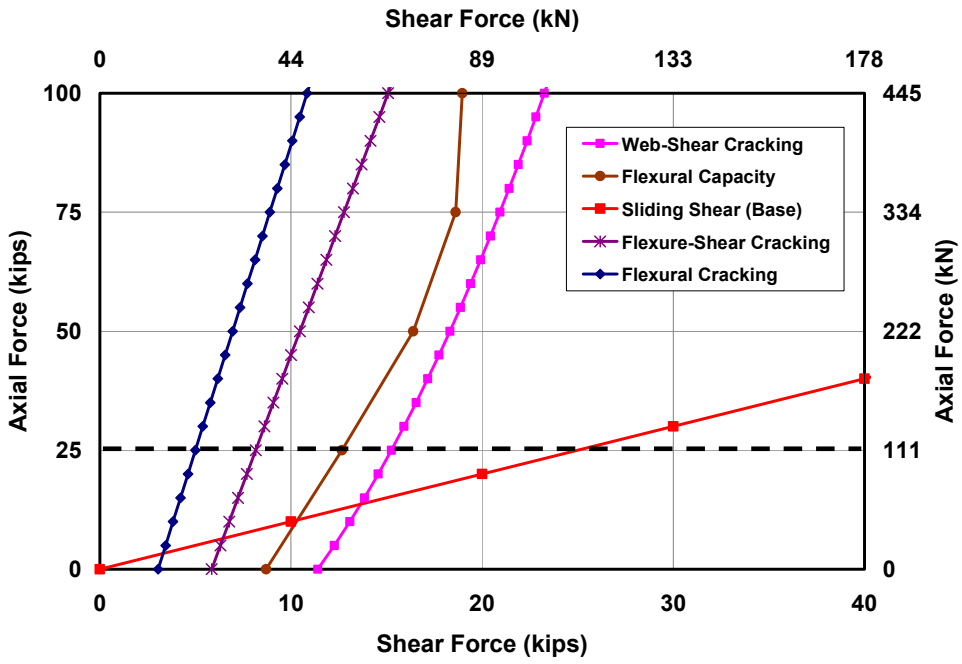

Figure 6.1: Interaction diagram for Shear Wall Specimen 13 based on predictions of Chapter 8

6.2 SHEAR WALL SPECIMEN 13

The predicted behavior of this specimen at the initial and final axial loads is discussed in Section 6.1.

6.2.1 Loading History and Major Events for Shear Wall Specimen 13

The actual loading and displacement histories for Shear Wall Specimen 13 are presented in Figure 5.2 and Figure 6.3. Monotonically increasing load point numbers are assigned for each set of data recorded during the test. Data are classified into cycles with maximum loads and drift ratios for each cycle (Table 5.1). Loading to the south is considered positive; loading to the north, negative.

Cycles are further classified by the direction of loading in terms of "a" and "b." For Shear Wall Specimen 13, "a" refers to loading to the north, and "b" refers to loading to the south. In future tests, specimens were loaded first to the south.

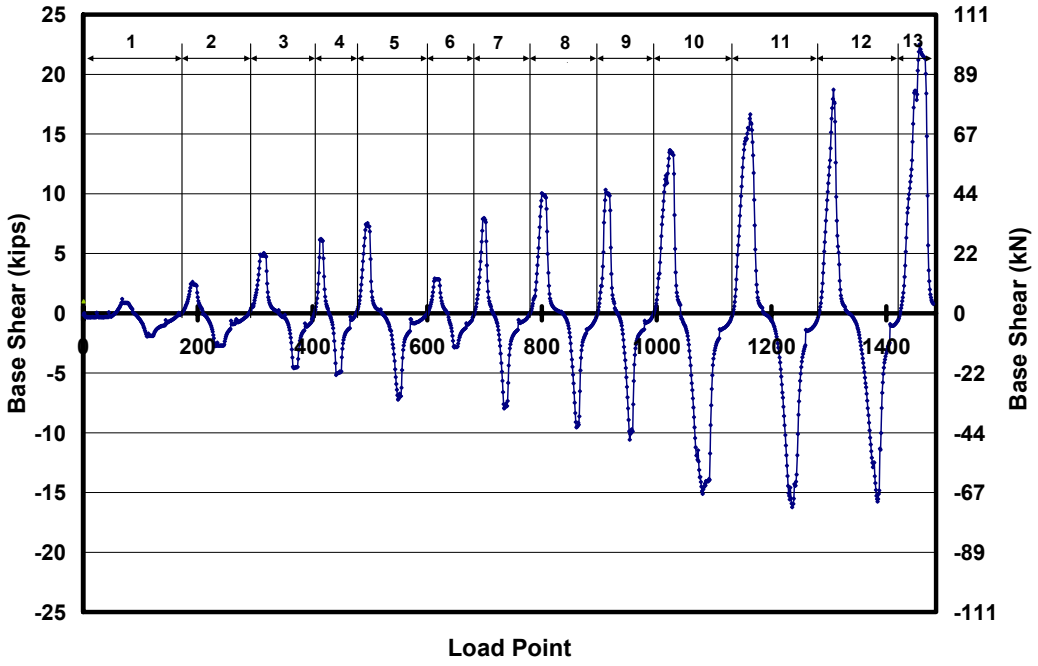

Figure 6.2: Actual loading history for Shear Wall Specimen 13 (numbers at the top designate cycle numbers)

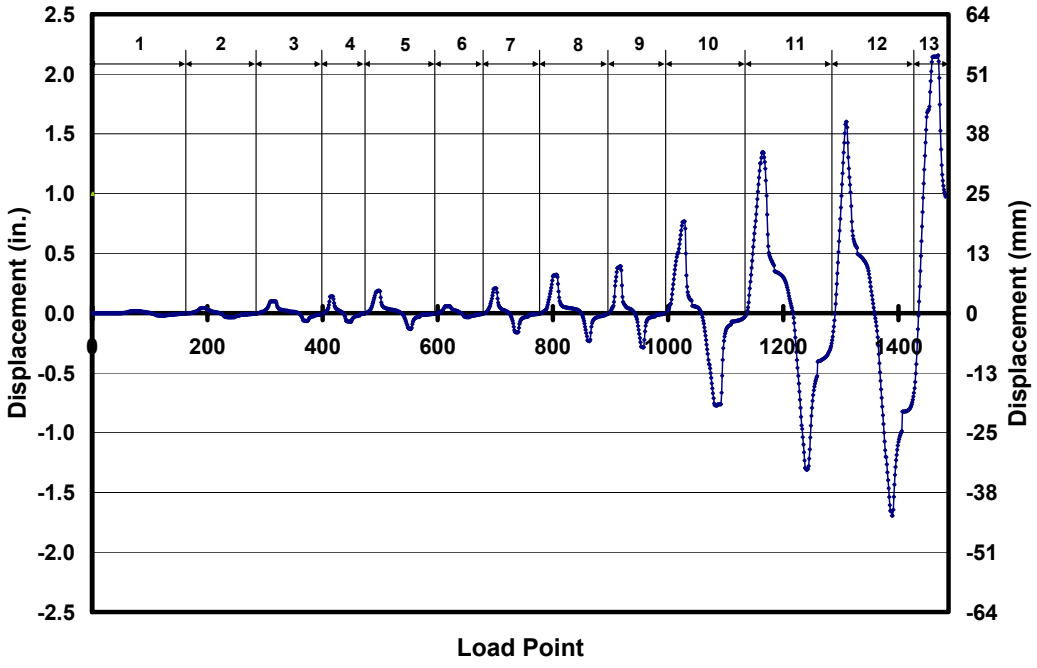

Figure 6.3: Actual tip displacement history for Shear Wall Specimen 13 (numbers at the top designate cycle numbers)

Table 6.1: Load points, maximum load and drift ratios for each cycle for Shear Wall Specimen 13

Cycle	Load Points	Maximum Applied Load kips (kN)	Max. Drift Ratio (%)	Cycle	Load Points	Minimum Applied Load kips (kN)	Min. Drift Ratio (%)
1a	0 - 80	2.0 (9)	0.01	1b	81 - 125	-2.7 (-12)	0.01
2a	126 - 205	3.5 (15)	0.03	2b	206 - 255	-3.9 (-17)	0.02
3a	256 - 330	5.6 (25)	0.06	3b	331 - 380	-6.2 (-28)	0.04
4a	381 - 425	7.0 (31)	0.09	4b	426 - 455	-6.7 (-30)	0.05
5a	456 - 515	8.0 (35)	0.12	5b	516 - 565	-7.4 (-33)	0.09
6a	566 - 630	4.1 (18)	0.04	6b	631 - 655	-4.6 (-20)	0.02
7a	656 - 712	9.1 (40)	0.13	7b	713 - 755	-9.0 (-40)	0.10
8a	756 - 825	10.9 (49)	0.21	8b	826 - 875	-10.6 (-47)	0.15
9a	876 - 927	11.6 (52)	0.25	9b	928 - 970	-11.3 (-50)	0.19
10a	971 - 1040	14.2 (63)	0.50	10b	1041 - 1110	-16.0 (-71)	0.50
11a	1111 - 1183	17.6 (78)	0.88	11b	1184 - 1260	-17.7 (-79)	0.85
12a	1261 - 1328	21.1 (94)	1.04	12b	1329 - 1405	-17.4 (-77)	1.10
13a	1406 - 1485	23.4 (104)	1.40				

6.2.2 Sequence of Crack Formation for Shear Wall Specimen 13

The sequence of crack formation in Shear Wall Specimen 13 is described in terms of major events: points during the test when either the condition of the specimen changed (for example, flexural cracking or shear cracking), or the applied axial force was increased. Table 5.3 lists the major events and the load point at which they occurred.

Table 6.2: Description of major events for Shear Wall Specimen 13

Major Event	Load Point	Physical Description
1	494	Flexural cracking at base, loading south
2	549	Flexural cracking at base, loading north
3	800	Flexural cracking at first bed joint, loading south
4	860	Flexural cracking at first bed joint, loading north
5	911	Propagation of flexural crack, loading south
6	953	Propagation of flexural crack, loading north
7	1016-1163	Distributed flexural cracks and flexure-shear cracks, both directions
8	1023, 1232	Vertical cracks formed, both directions
9	1385	Crushing of north toe
10	1468	Spalling at south toe

6.2.2.1 Formation of flexural cracks in Shear Wall Specimen 13

Major Events 1 and 2 correspond to the observance of flexural cracking. At Load Point 494 a 30 in. (0.8 m) flexural crack formed while loading to the south at a load of 7.3 kips (36 kN) and a drift ratio of 0.12%. A 20 in. (0.5 m) long flexural crack formed while loading to the north at Load Point 549. The base shear in the specimen was 7.2 kips (32 kN) and the drift ratio was 0.08%. The predicted base shear at flexural cracking was 8.2 kips (36.5 kN) which corresponds to a ratio of observed to predicted flexural cracking capacity of 0.9 while loading in both directions.

6.2.2.2 Formation of flexure-shear cracks in Shear Wall Specimen 13

Major Event 3 corresponds to the formation of the flexural portion of a flexure-shear crack in the first panel at a height of 22 in. (0.55 m). The corresponding base shear and drift ratio were 10.1 kips (45 kN) and 0.2% respectively. Major Event 4 corresponds to the formation of the flexural portion of a flexure-shear crack in the first bed joint. The corresponding base shear and drift ratio were 9.5 kips (42 kN) and 0.15% respectively. The predicted loads for

flexural cracks at heights of 22 in. (0.55 m) and 24 in. (0.6 m) are 8.2 kips (36 kN) and 8.0 kips (34 kN) respectively. This corresponds to ratios of observed to predicted flexural cracking capacities of 1.2 and 1.3 while loading to the south and north respectively.

At Load Points 911 and 953 the flexural cracks propagated diagonally, and flexural cracks formed in the second bed joint while loading to the south and north respectively. The corresponding base shear for these load points are 10.3 kips (46 kN) and 10.6 kips (47 kN); the corresponding drift ratios for these load points are 0.22% and 0.18%. The cracks that formed during Major Events 1 through 4 are shown in gray in Figure 5.6, while the cracks that formed during Major Events 5 and 6 are shown in black in Figure 5.6.

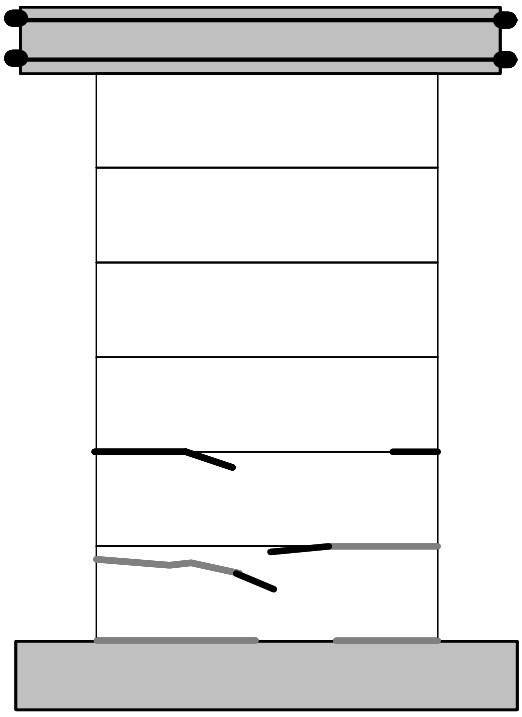

Figure 6.4: Formation of flexure-shear cracks in Shear Wall Specimen 13

6.2.2.3 Additional cracking in Shear Wall Specimen 13

During Load Points 1016 and 1163 additional flexure-shear cracks formed throughout the height of the specimen. These cracks are shown in Figure 5.7.

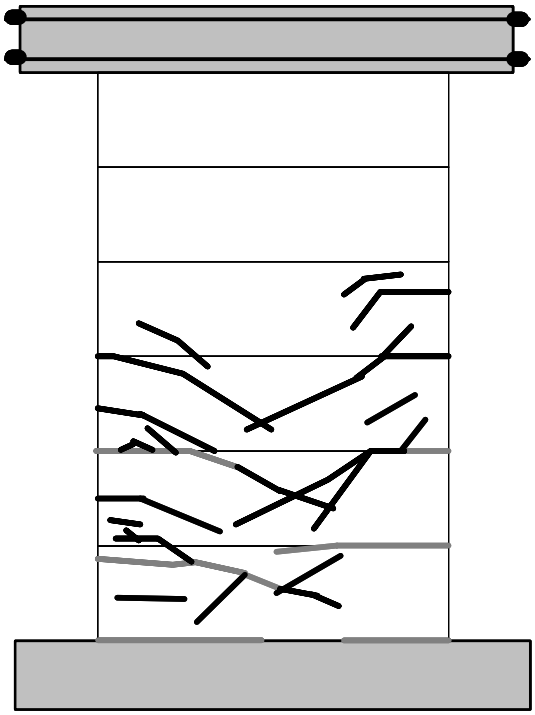

Figure 6.5: Distributed flexure-shear cracking in Shear Wall Specimen 13

At Load Points 1023 and 1232 vertical cracks formed at the location of vertical reinforcement, which constituted Major Event 8. The base shear and drift ratio at Load Point 1023 were 13.6 kips (61 kN) and 0.45% respectively. The base shear and drift ratio at Load Point 1232 were 15.6 kips (69 kN) and 0.61% respectively. Crushing was observed at the north and south toes during Load Points 1385 and 1468. The corresponding drift ratios were 1.0% and 1.4%. The cracks observed in Major Event 8 through the end of the test are shown in Figure 5.9. The test was ended due to instability of the north compression toe (Figure 6.7).

Figure 6.6: Toe crushing and additional damage in Shear Wall Specimen 13

Figure 6.7: Instability of the north compression toe

6.2.3 Load-Displacement Behavior for Shear Wall Specimen 13

The force-displacement behavior of Shear Wall Specimen 13 is presented in terms of the non-dimensional drift ratio in Figure 5.25. The stiffnesses observed at various points in the loading history are described in Varela (2003).

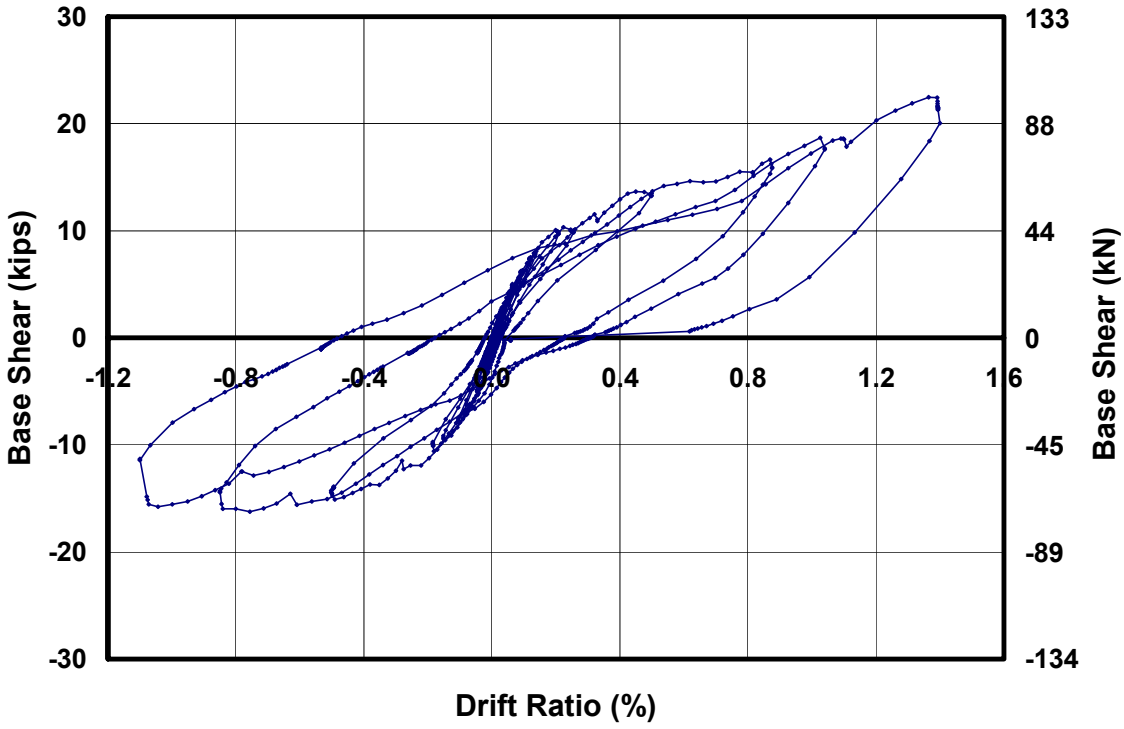

Figure 6.8: Load-displacement relationship for Shear Wall Specimen 13

6.3 SHEAR WALL SPECIMEN 14A

An interaction diagram for base shear capacity as a function of axial load for Shear Wall Specimen 14a is presented in Figure 6.9. The axial load applied to Shear Wall Specimen 14a was 25 kips (111 kN), as shown by a dashed horizontal line in Figure 6.9. At this level of axial load the following major events are

predicted in order of occurrence: flexural cracking; flexure-shear cracking; and simultaneous sliding at the base and nominal flexural capacity.

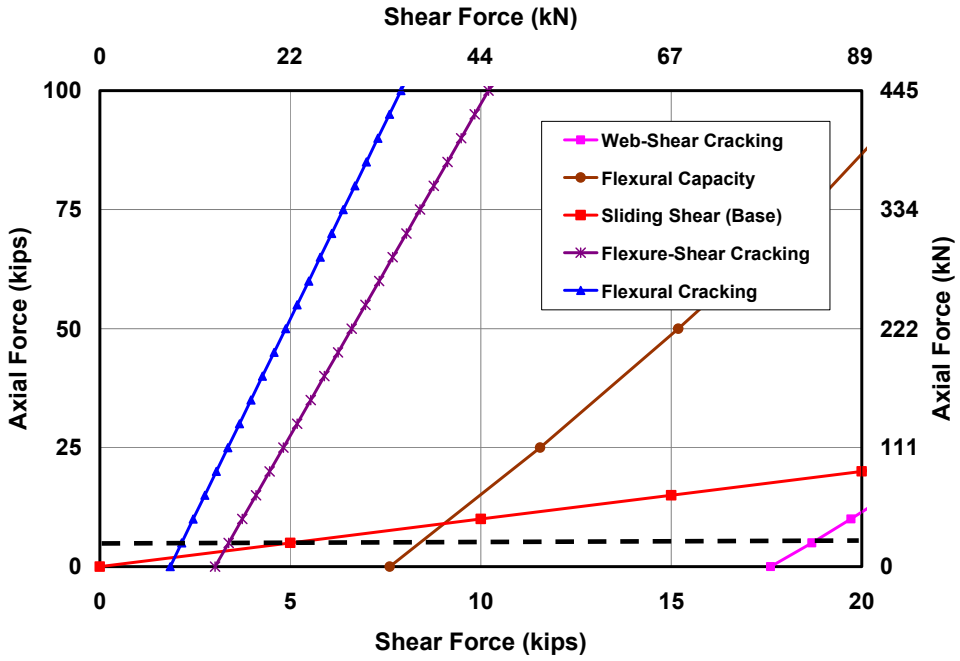

Figure 6.9: Prediction of behavior for Shear Wall Specimen 14a and 14b

6.3.1 Loading History and Major Events for Shear Wall Specimen 14a

The actual load and displacement histories for Shear Wall Specimen 14a are presented in Figure 6.10 and Figure 6.11. Monotonically increasing load point numbers are assigned for each set of data recorded during the test. This test was subject to lateral cyclic load through Load Point 231. The test changed to a monotonic test and the load point numeration began with Load Point 400. Data are classified into cycles with maximum loads and drift ratios for each cycle (Table 5.1). Loading to the south is considered positive; loading to the north, negative.

Cycles are further classified by the direction of loading in terms of "a" and "b." For Shear Wall Specimen 14a and all remaining specimens, "a" refers to loading to the south, and "b" refers to loading to the north.

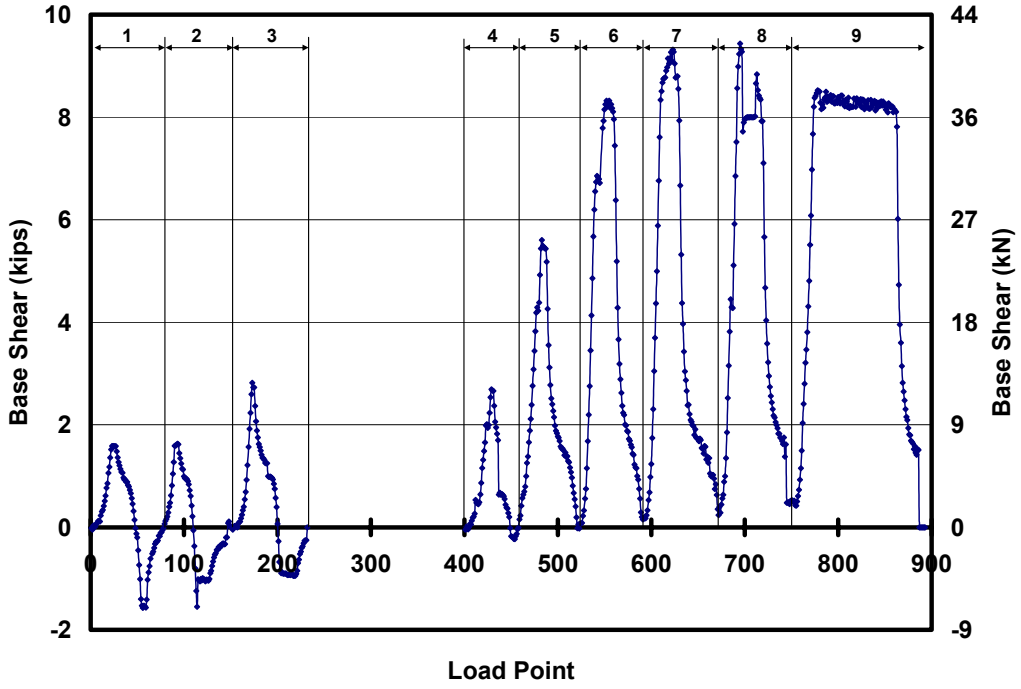

Figure 6.10: Actual loading history for Shear Wall Specimen 14a (numbers at the top designate cycle numbers)

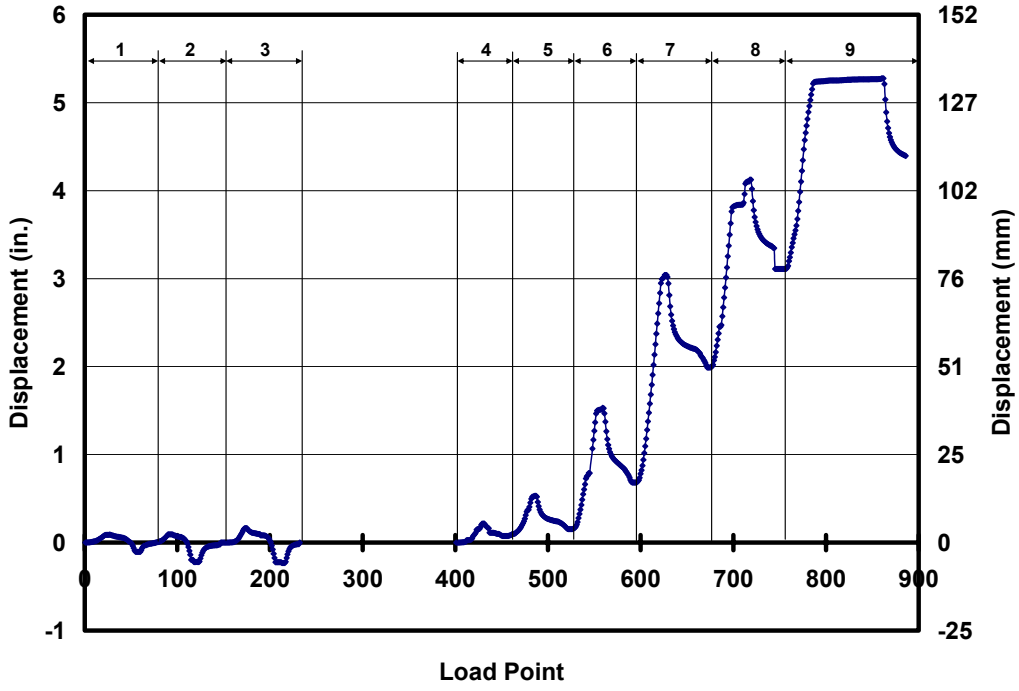

Figure 6.11: Actual tip displacement history for Shear Wall Specimen 14a (numbers at the top designate cycle numbers)

Table 6.3: Load points, maximum load and drift ratios for each cycle for Shear Wall Specimen 14a

Cycle	Load Points	Maximum Applied Load, kips (kN)	Max. Drift Ratio (%)	Cycle	Load Points	Minimum Applied Load, kips (kN)	Min. Drift Ratio (%)
1a	1-48	1.6 (7)	0.06	1b	49-76	-1.6 (7)	0.07
2a	77-110	1.6 (7)	0.06	2b	111-146	-1.1 (5)	0.14
3a	147-200	2.8 (14)	0.10	3b	201-231	-0.9 (4)	0.15
4a	400-450	2.7 (12)	0.14	4b	-	-	-
5a	451-520	5.6 (25)	0.34	5b	-	-	-
6a	521-590	8.3 (37)	0.98	6b	-	-	-
7a	591-660	9.3 (41)	1.9	7b	-	-	-
8a	661-745	9.4 (42)	2.2	8b	-	-	-
9a	746-890	8.5 (38)	3.4	9b	-	-	-

6.3.2 Sequence of Crack Formation for Shear Wall Specimen 14a

The sequence of crack formation in Shear Wall Specimen 14a is described in terms of major events: points during the test when either the condition of the specimen changed (for example, flexural cracking or web-shear cracking), or the applied axial force was increased. Table 5.5 lists the major events and the load point at which they occurred. In each section where crack maps are presented, preexisting cracks are shown in gray, and new cracks are shown in black.

Table 6.4: Description of major events for Shear Wall Specimen 14a

Major Event	Load Point	Physical Description
1	114	Flexural crack, loading north
2	173	Flexural crack, loading south
3	200-231	Pullout failure of threaded longitudinal reinforcement at south end
4	400	Testing proceeded as a monotonic specimen, loading south
5	478	Formation of flexural cracks at the base of the third and fourth courses
6	483	Formation of flexure-shear crack in the first course
7	542	Formation of addition flexure-shear cracks and a vertical splitting crack
8	713	Crushing of compression toe

6.3.2.1 Observed behavior in cyclic test in Shear Wall Specimen 14a

Prior to testing, this specimen had a flexural crack on the west face of the wall due to flexural tensile stresses generated by an out-of-plane displacement at the top of the wall. This displacement was necessary to align the rams with the loading beam. At Load Point 114 a flexural crack was observed on the east side of the wall at a base shear of 1.6 kips (7 kN) and a drift ratio of 0.09%. This load is lower than the predicted load due to the reduced section of the uncracked wall. At Load Point 173 a flexural crack was observed at the first course of the west side of the wall. Since the crack was not observed on the east side of the wall it is believed to be from tensile stresses from out-of-plane loading and in-plane loading.

While loading to the north during the second cycle, the wall no longer resisted load after 1.5 kips (6.7 kN) as shown in Figure 5.19. At a drift ratio of 0.15% and vertical displacement at the base of the wall of at least 0.1 in. (3 mm) it was suspected that the threaded vertical reinforcement had pulled out of the inserts placed in the foundation. This hypothesis was verified based on data from strain gages and visual inspection of the damaged threads (after disassembling the

wall). Since the tensile reinforcement on the south end of the wall did not work properly the wall was tested monotonically to the south. The load point numeration began at Load Point 400.

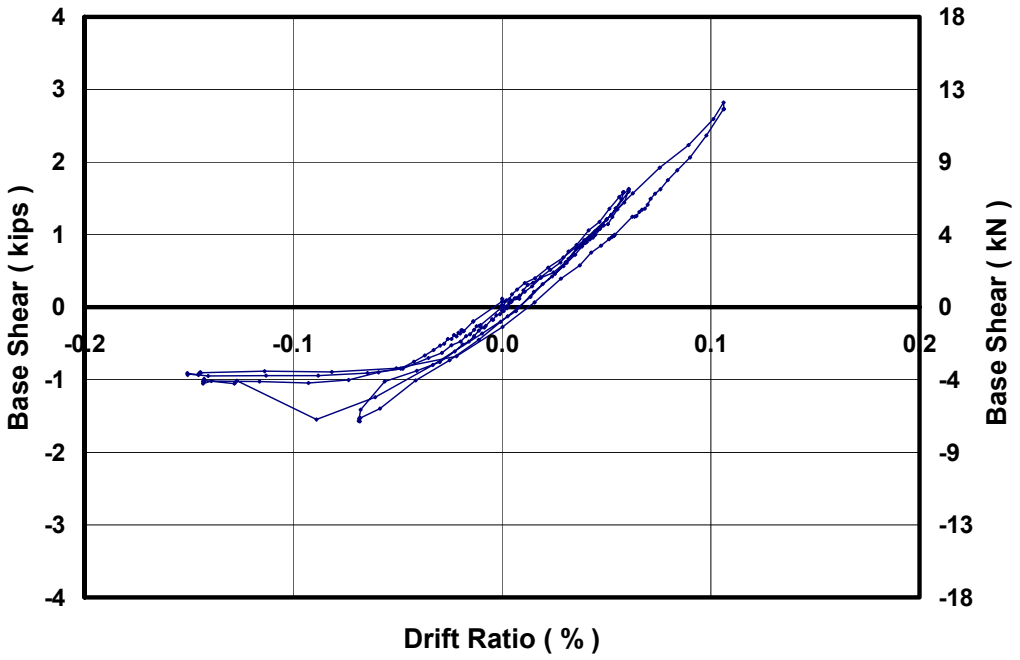

Figure 6.12: Force displacement behavior observed in the cyclic portion of Shear Wall Specimen 14a

6.3.2.2 Damage observed in the monotonic testing of Shear Wall Specimen 14a

Flexural cracks were observed at the first and second bed joints in Load Point 478 at a base shear of 4.3 kips (19 kN) and corresponding drift ratio of 0.24%. A flexure-shear crack formed in the AAC material in the first bed joint at a base shear of 5.6 kips (25 kN) and a drift ratio of 0.34%. At Load Point 542 additional flexure-shear cracks formed along the height of the wall along with a vertical crack at the location of the north longitudinal reinforcement. Similar

flexure-shear and vertical cracks formed throughout the testing of the wall. Concentrated vertical cracks formed in the compression toe during Load Points 555 and 624. All of these cracks observed in Shear Wall Specimen 14a are shown in Figure 5.21. The test was ended after crushing of the compression toe was observed at Load Point 713 (Figure 6.14).

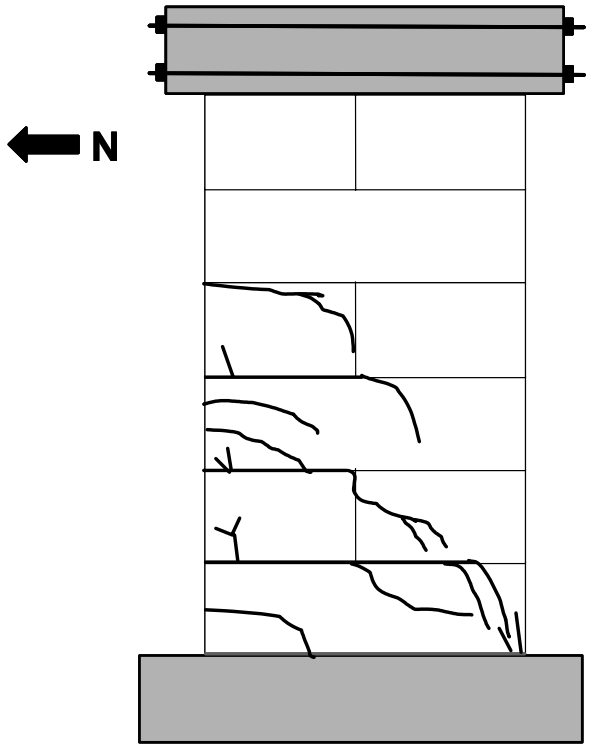

Figure 6.13: Observed crack pattern of Shear Wall Specimen 14a

Figure 6.14: Crushing of the compression toe in Shear Wall Specimen 14a

6.3.3 Load-Displacement Behavior for Shear Wall Specimen 14a

The force-displacement relationship of Shear Wall Specimen 14a is presented in terms of the non-dimensional drift ratio in Figure 5.25. The stiffnesses observed at various points in the loading history are described in Varela (2003).

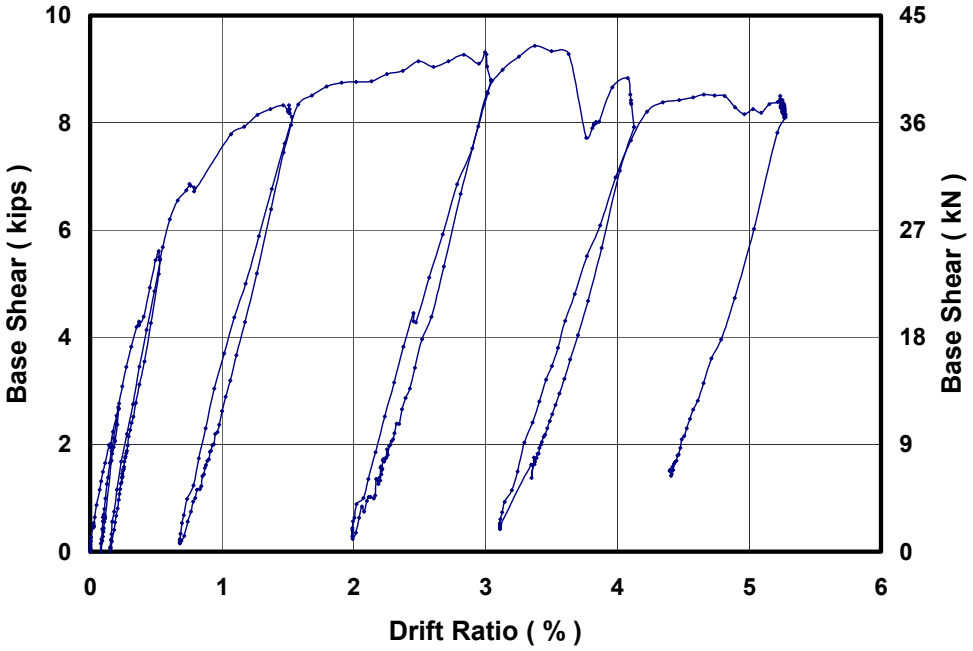

Figure 6.15: Force-displacement relationship for Shear Wall Specimen 14a

6.4 SHEAR WALL SPECIMEN 14B

Shear Wall Specimen 14b is a replica of Shear Wall Specimen 14a. The predicted behavior of this specimen is described in Section 6.3.

6.4.1 Loading History and Major Events for Shear Wall Specimen 14b

The actual loading and displacement histories for Shear Wall Specimen 14b are presented in Figure 5.27 and Figure 5.28. Monotonically increasing load point numbers are assigned for each set of data recorded during the test. Data are classified into cycles with maximum loads and drift ratios for each cycle (Table 5.6). Loading to the south is considered positive; loading to the north, negative.

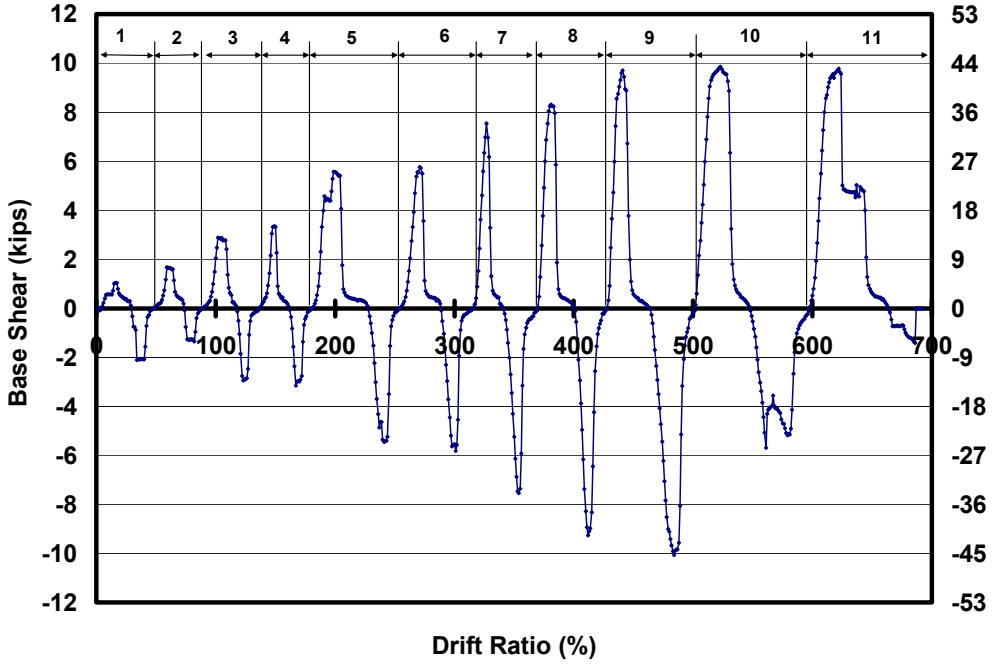

Figure 6.16: Actual loading history for Shear Wall Specimen 14b (numbers at the top designate cycle numbers)

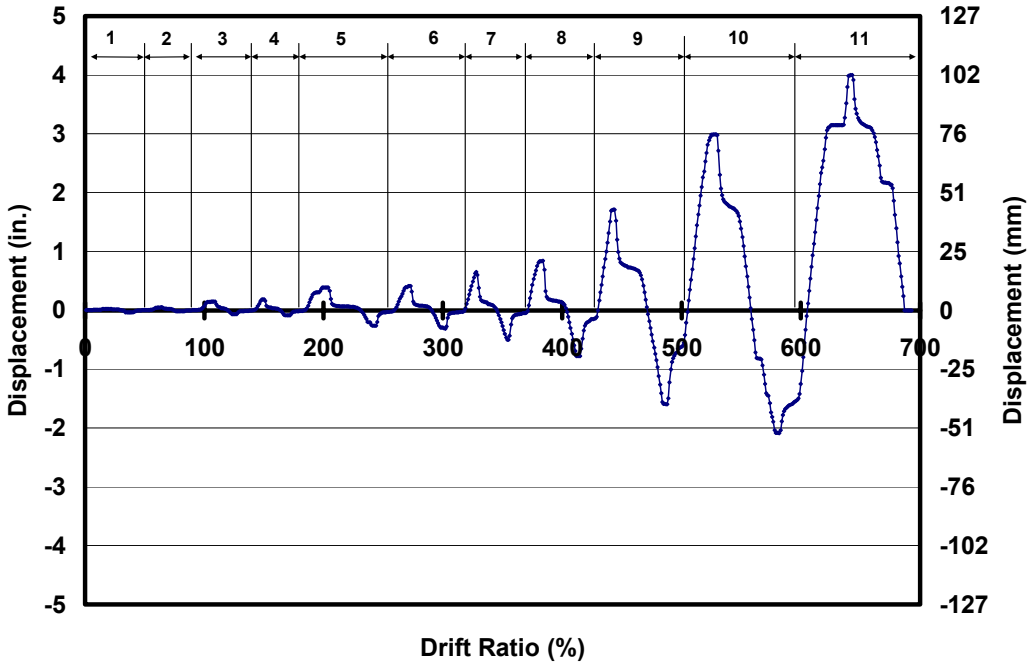

Figure 6.17: Actual tip displacement history for Shear Wall Specimen 14b (numbers at the top designate cycle numbers)

Table 6.5: Load points, maximum load and drift ratios for each cycle for Shear Wall Specimen 14b

Cycle	Load Points	Maximum Applied Load, kips (kN)	Max. Drift Ratio (%)	Cycle	Load Points	Minimum Applied Load, kips (kN)	Min. Drift Ratio (%)
1a	1 - 28	1.0 (5)	0.02	1b	29 - 50	-2.1 (-9)	0.02
2a	51 - 73	1.7 (7)	0.03	2b	74 - 90	-1.3 (-6)	0.01
3a	91 - 116	2.9 (13)	0.10	3b	117 - 135	-2.9 (-13)	0.04
4a	136 - 160	3.3 (15)	0.12	4b	161 - 180	-3.2 (-14)	0.06
5a	181 - 226	5.6 (25)	0.25	5b	227 - 252	-5.5 (-24)	0.17
6a	253 - 288	5.8 (26)	0.27	6b	289 - 312	-5.8 (-26)	0.20
7a	313 - 340	7.5 (34)	0.42	7b	341 - 370	-7.5 (-34)	0.33
8a	371 - 400	8.3 (37)	0.55	8b	401 - 428	-9.3 (-41)	0.51
9a	429 - 460	9.7 (43)	1.11	9b	461 - 500	-10.1 (-45)	1.04
10a	501 - 546	9.9 (44)	1.94	10b	547 - 598	-5.7 (-25)	1.36
11a	599 - 664	9.8 (43)	2.60	11b	665 - 686	-1.4 (-6)	0.04

6.4.2 Sequence of Crack Formation for Shear Wall Specimen 14b

The sequence of crack formation in Shear Wall Specimen 14b is described in terms of major events: points during the test when either the condition of the specimen changed (for example, flexural cracking or web-shear cracking), or the applied axial force was increased. Table 5.7 lists the major events and the load point at which they occurred. In each section where crack maps are presented, preexisting cracks are shown in gray, and new cracks are shown in black.

Table 6.6: Description of major events for Shear Wall Specimen 14b

Major Event	Load Point	Physical Description
1	102	Flexural crack, loading south
2	123	Flexural crack, loading north
3	191	Flexural crack at first, second and third bed joint, loading south
4	237	Flexural crack at first, second and third bed joint, loading north
5	271	Propagation of flexural cracks and diagonal propagation, loading south
6	301	Propagation of flexural cracks and diagonal propagation, loading north
7	326	Additional flexure-shear cracks with a vertical splitting crack
8	442	Splitting crack, loading south
9	487	Splitting crack, loading north
10	624	Crushing of toe

6.4.2.1 Flexural cracking in Shear Wall Specimen 14b

Major Events 1 and 2 correspond to the observance of flexural cracking. At Load Point 102 a 36 in. (0.9 m) flexural crack formed while loading to the south at a load of 2.9 kips (13 kN) and a drift ratio of 0.09%. A 60 in. (1.5 m) long flexural crack formed while loading to the north at Load Point 123. The base shear in the specimen was 2.9 kips (13 kN) and the drift ratio was 0.07%. The predicted base shear at flexural cracking was 2.2 kips (9.6 kN) which corresponds to a ratio of observed to predicted flexural cracking capacity of 1.35 while loading in both directions.

6.4.2.2 Flexure-shear cracking in Shear Wall Specimen 14b

Major Events 3 and 4 correspond to the formation of the flexural portion of a flexure-shear crack in the first three courses while loading to the north and south (Figure 5.29). The corresponding base shears were 4.6 kips (20 kN) and 4.9 kips (21 kN) with drift ratios of 0.18% and 0.2%, respectively. The predicted load for the flexural cracks at the first course is 4.8 kips (21 kN) which

corresponds to ratios of observed to predicted strength of 0.96 and 1.0 while loading to the south and north respectively.

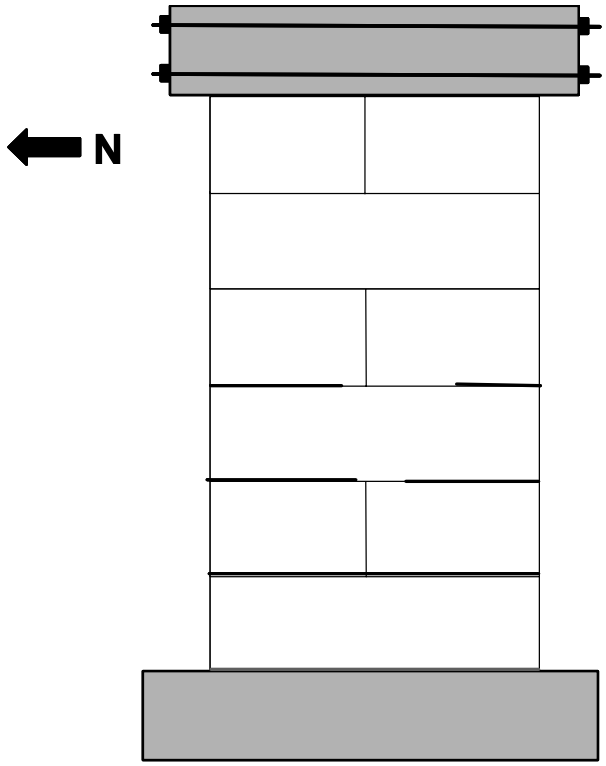

Figure 6.18: Formation of flexural cracks in the first three courses in Shear Wall Specimen 14b

Major Events 5 and 6 correspond to the diagonal propagation of the flexural cracks that had previously formed in the wall at Load Points 271 and 301. The base shear at both major events was 5.8 kips (26 kN). Additional flexural shear cracks formed at a base shear of 7 kips (31 kN) during Load Point 326 (Major Event 7). A vertical crack at the location of the longitudinal reinforcement also formed. All of the cracks that formed in Major Events 5 through 7 are shown in Figure 5.30. Additional flexure-shear cracks formed throughout the remainder of the test.

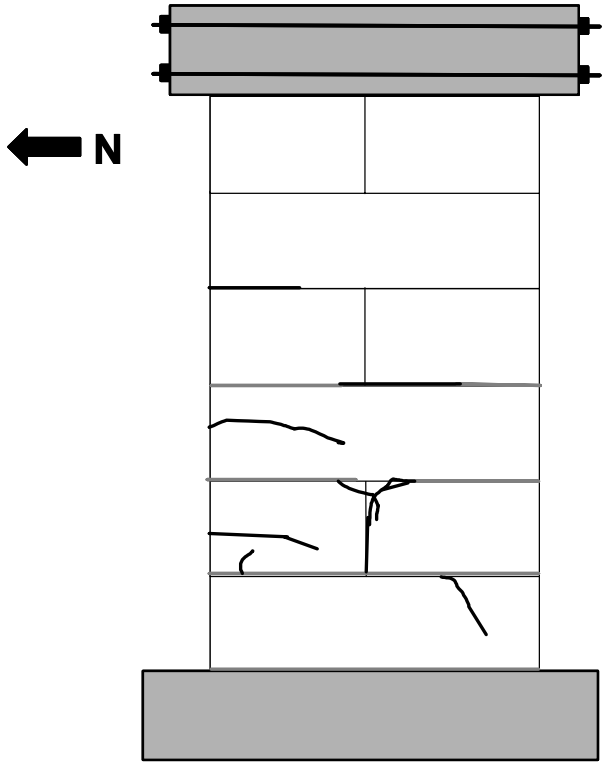

Figure 6.19: Propagation of flexure-shear cracks in Shear Wall Specimen 14b

6.4.2.3 Additional cracking in Shear Wall Specimen 14b

Major Event 8 and 9 consist of splitting cracks observed in the specimen. The vertical cracks propagated in the specimen throughout the remained of the test. Sliding along the first and second courses was observed in Load Points 514 to 527 (Major Event 10). Crushing of the north compression toe was observed at Load Point 624. As the crushing increased the lateral load dropped from 9.6 kips (43 kN) to 5.0 kips (22 kN). The drift ratio increased from 2% to 2.5% as the crushing occurred. The damage observed in Major Event 8 through the end of the test is shown in Figure 5.31. A picture of the permanent displacement and the crushing observed in the specimen is shown in Figure 5.32.

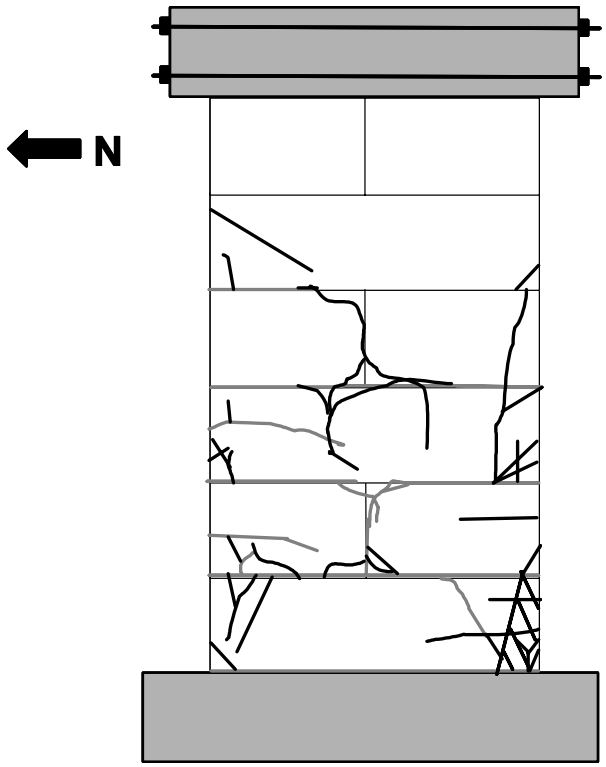

Figure 6.20: Additional shear cracking in Shear Wall Specimen 14b

Figure 6.21: Shear Wall Specimen 14b at the end of the test

6.4.3 Load-Displacement Behavior for Shear Wall Specimen 14b

The force-displacement relationship of Shear Wall Specimen 14b is presented in terms of the non-dimensional drift ratio in Figure 5.35. The stiffnesses observed at various points in the loading history are described in Varela (2003).

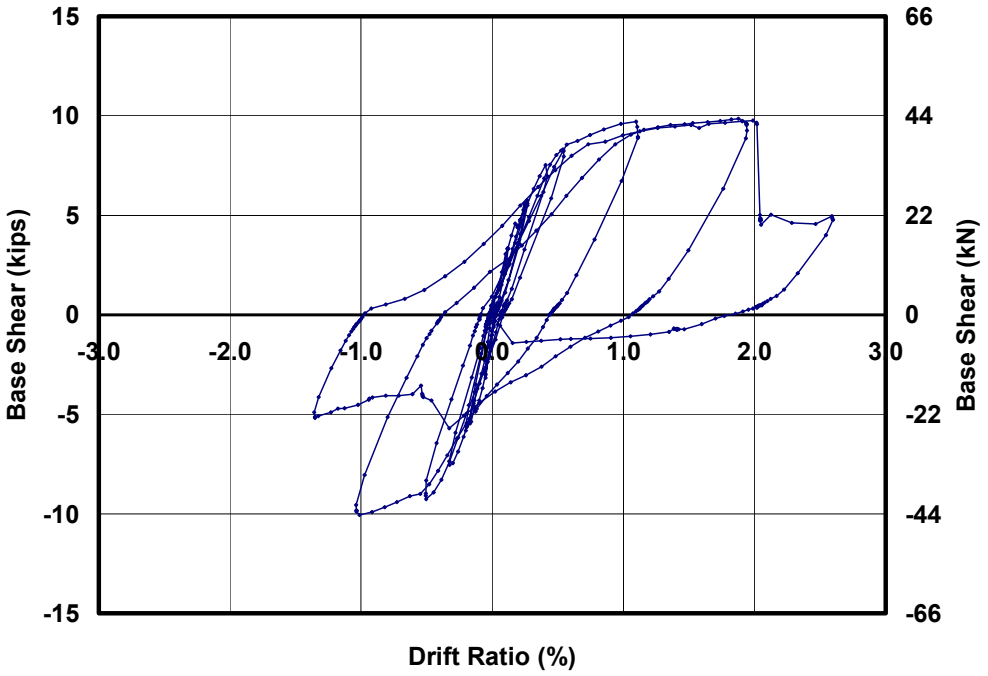

Figure 6.22: Load-displacement relationship for Shear Wall Specimen 14b

6.5 SHEAR WALL SPECIMEN 15A

An interaction diagram for base shear capacity as a function of axial load for Shear Wall Specimen 15a is presented in Figure 6.37. The axial load applied in Shear Wall Specimen 15a was 25 kips (111 kN), as shown by a dashed horizontal line in Figure 6.23. At this level of axial load the following major events are predicted in order of occurrence: flexural cracking; flexure-shear cracking; and simultaneous sliding at the base and nominal flexural capacity.

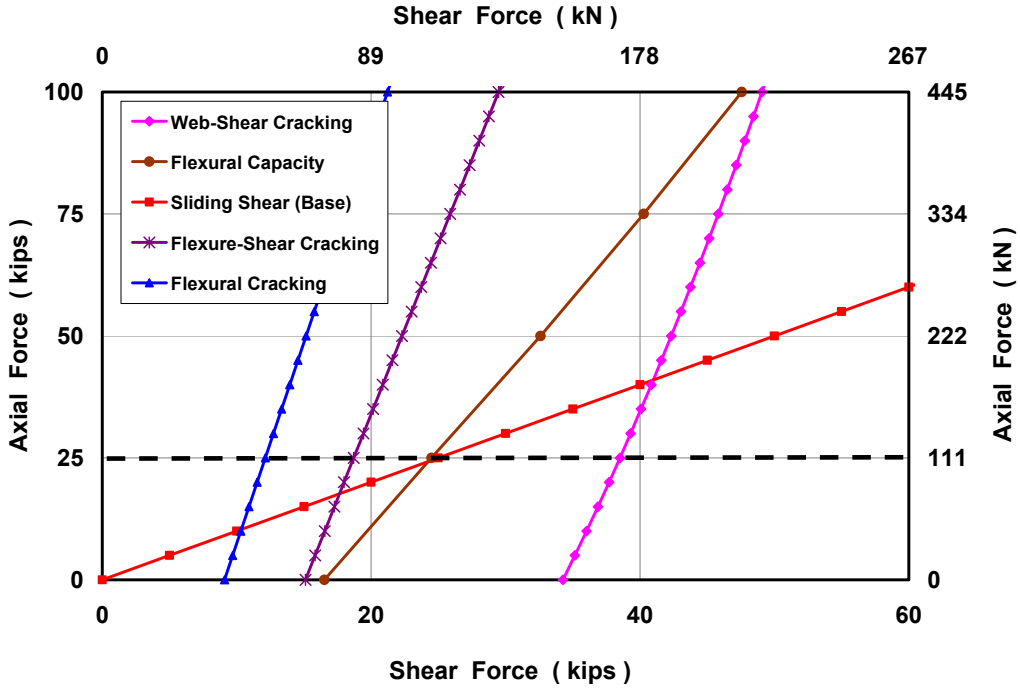

Figure 6.23: Prediction of behavior for Shear Wall Specimen 15a and 15b

6.5.1 Loading History and Major Events for Shear Wall Specimen 15a

The actual loading and displacement histories for Shear Wall Specimen 15a are presented in Figure 5.37 and Figure 5.38. Monotonically increasing load point numbers are assigned for each set of data recorded during the test. Data are classified into cycles with maximum loads and drift ratios for each cycle (Table 5.8). Loading to the south is considered positive; loading to the north, negative.

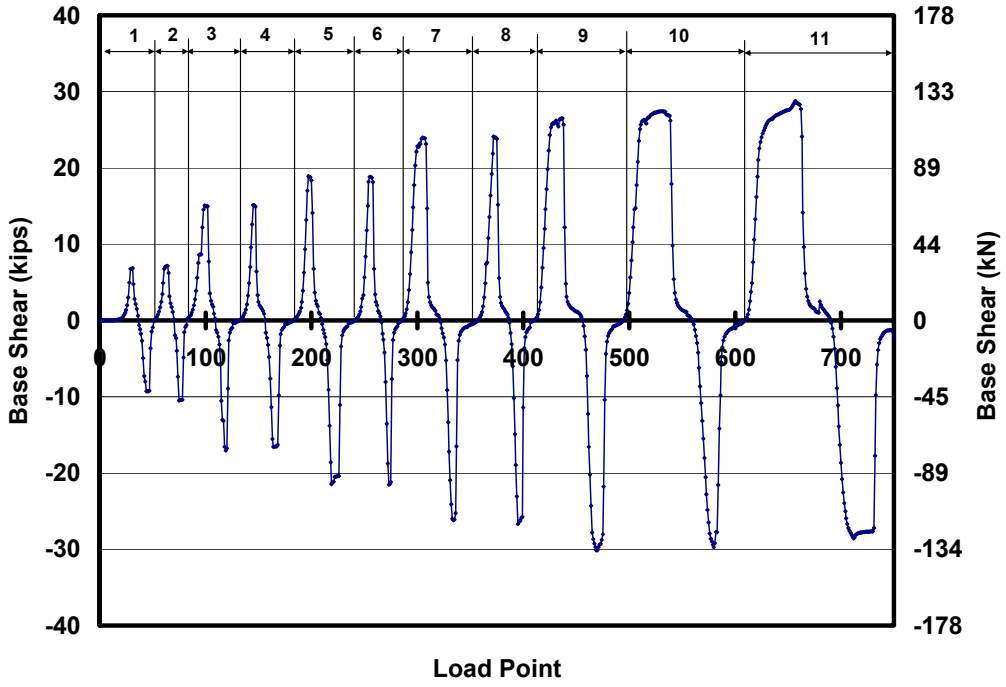

Figure 6.24: Actual loading history for Shear Wall Specimen 15a (numbers at the top designate cycle numbers)

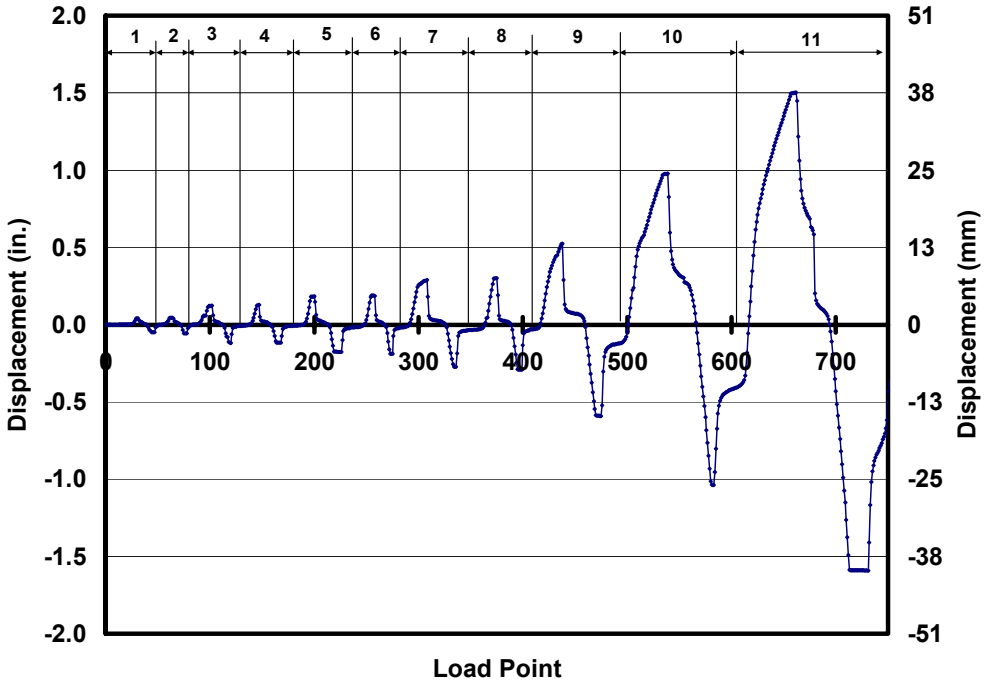

Figure 6.25: Actual tip displacement history for Shear Wall Specimen 15a (numbers at the top designate cycle numbers)

Table 6.7: Load points, maximum load and drift ratios for each cycle for Shear Wall Specimen 15a

Cycle	Load Points	Maximum Applied Load, Kips (kN)	Max. Drift Ratio (%)	Cycle	Load Points	Minimum Applied Load, Kips (kN)	Min. Drift Ratio (%)
1a	1 - 36	6.8 (30)	0.03	1b	37 - 52	-9.3 (-41)	0.03
2a	53 - 70	7.1 (32)	0.03	2b	71 - 82	-10.5 (-47)	0.04
3a	83 - 110	15.0 (67)	0.08	3b	111 - 130	-17.1 (-76)	0.08
4a	131 - 156	15.1 (67)	0.08	4b	157 - 180	-16.6 (-74)	0.08
5a	181 - 210	18.9 (84)	0.12	5b	211 - 240	-21.5 (-96)	0.11
6a	241 - 265	18.8 (84)	0.12	6b	266 - 285	-21.5 (-96)	0.12
7a	286 - 322	24.0 (107)	0.19	7b	323 - 350	-26.2 (-117)	0.18
8a	351 - 386	24.1 (107)	0.20	8b	387 - 410	-26.7 (-119)	0.19
9a	411 - 456	26.5 (118)	0.34	9b	457 - 490	-30.1 (-134)	0.38
10a	491 - 560	27.4 (122)	0.64	10b	561 - 600	-29.8 (-132)	0.67
11a	601 - 690	28.8 (128)	0.98	11b	691 - 750	-28.6 (-127)	1.03

6.5.2 Sequence of Crack Formation for Shear Wall Specimen 15a

The sequence of crack formation in Shear Wall Specimen 15a is described in terms of major events: points during the test when either the condition of the specimen changed (for example, flexural cracking or web-shear cracking), or the applied axial force was increased. Table 5.9 lists the major events and the load point at which they occurred. In each section where crack maps are presented, preexisting cracks are shown in gray, and new cracks are shown in black.

Table 6.8: Description of major events for Shear Wall Specimen 15a

Major Event	Load Point	Physical Description
1	94	Flexural cracking, loading south
2	115	Flexural cracking, loading north
3	219	Flexure-shear crack, loading north
4	305	Flexure-shear crack, loading south
5	334-581	Additional flexure-shear cracks
6	530	Vertical crack, loading north
7	581	Vertical crack, loading south

6.5.2.1 Flexural cracking in Shear Wall Specimen 15a

Major Events 1 and 2 correspond to the observance of flexural cracking. At Load Point 94 a flexural crack was observed while loading to the south at a load of 8.6 kips (38 kN) and a drift ratio of 0.04%. A flexural crack formed while loading to the north at Load Point 115 at a base shear of 10.6 kips (47 kN) and a drift ratio of 0.04%. The predicted base shear at flexural cracking was 9.1 kips (40 kN) which corresponds to ratios of observed to predicted strength of 0.95 and 1.16 while loading to the south and north respectively.

These cracks propagated without other damage between Load Points 119 and 219. All of these cracks are shown in gray in Figure 5.39.

6.5.2.2 Flexure-shear cracking in Shear Wall Specimen 15a

Major Event 3 corresponds to the formation of a horizontal crack that propagated diagonally to form a flexure-shear crack while loading to the north. The damage occurred at Load Point 219 at a base shear of 21.5 kips (96 kN) and a drift ratio of 0.11%. Major Event 4 consisted of a flexure-shear crack that formed at Load Point 305 at a base shear of 24 kips (107 MPa) and a drift ratio of 0.11%. The damage in these major events is shown in Figure 5.39. The prediction for flexure-shear cracking at the first joint based on Section 8.2.2 is 18.7 kips (83 kN). The ratios of observed to predicted flexural cracking capacity are 1.12 and

1.28 for loading to the north and south respectively. If the height of the flexural portion of the crack is raised from 24 in. (0.6 m) to 48 inches (1.2 m) the predicted load for the flexural crack increases to 22.9 kips (101 kN) which decreases the ratio of observed to predicted capacity to 0.95.

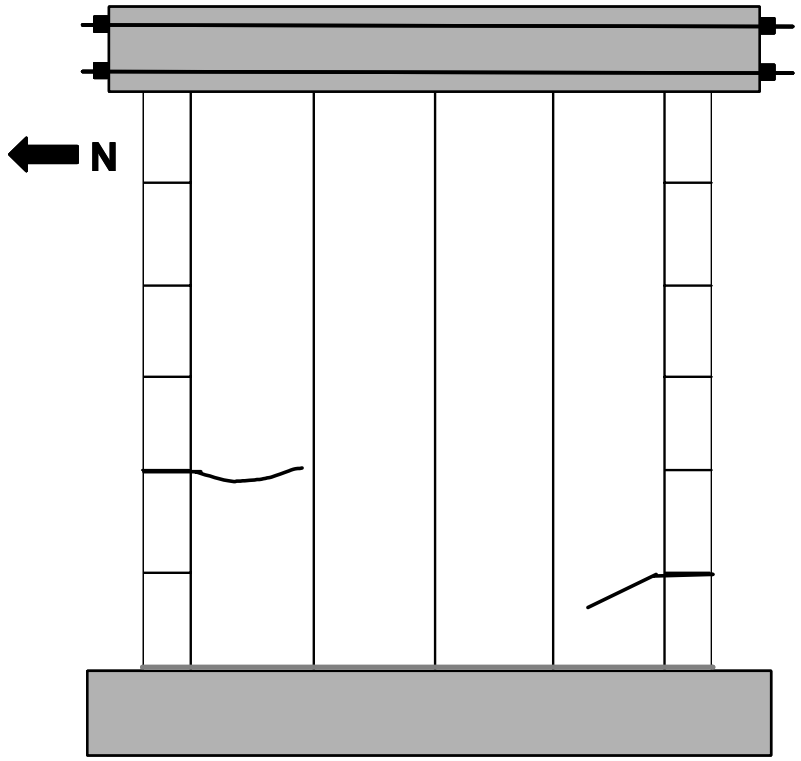

Figure 6.26: Formation of initial flexure-shear cracks in Shear Wall Specimen 15a

6.5.2.3 Additional cracking in Shear Wall Specimen 15a

Additional flexure-shear cracks formed throughout the specimen (Load Points 334 through 581). A vertical crack at the location of the reinforcement at the south end of the wall formed at the base of the wall in Load Point 474. At Load Point 538 another vertical crack formed at the location of the reinforcement

on the north end at midheight of the wall. The combined cracks comprise Major Events 5 through 7 and the damage is shown in Figure 5.40.

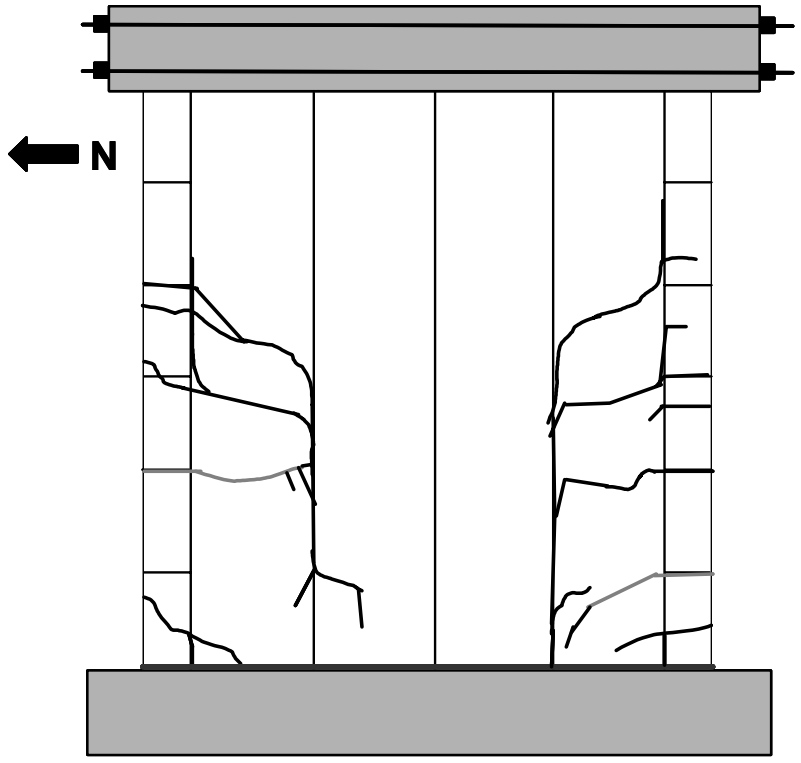

Figure 6.27: Formation of additional cracks in Shear Wall Specimen 15a

The test was terminated due to the separation of a section of the compression toes after vertical cracks at the location of the reinforcement intersected with the flexural cracks. This damage for the north and south sides of the wall is shown in Figure 6.28.

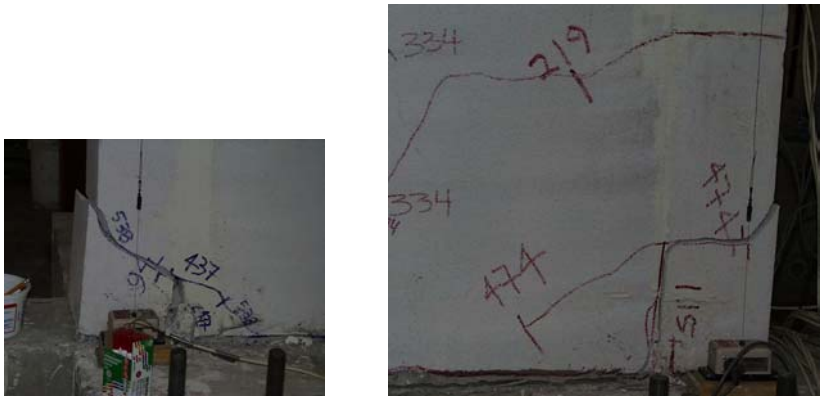

Figure 6.28: Loss of material in the north and south compression toes of Shear Wall Specimen 15a

6.5.3 Load-Displacement Behavior for Shear Wall Specimen 15a

The force-displacement relationship of Shear Wall Specimen 15a is presented in terms of the non-dimensional drift ratio in Figure 5.47. The stiffnesses observed at various points in the loading history are described in Varela (2003).

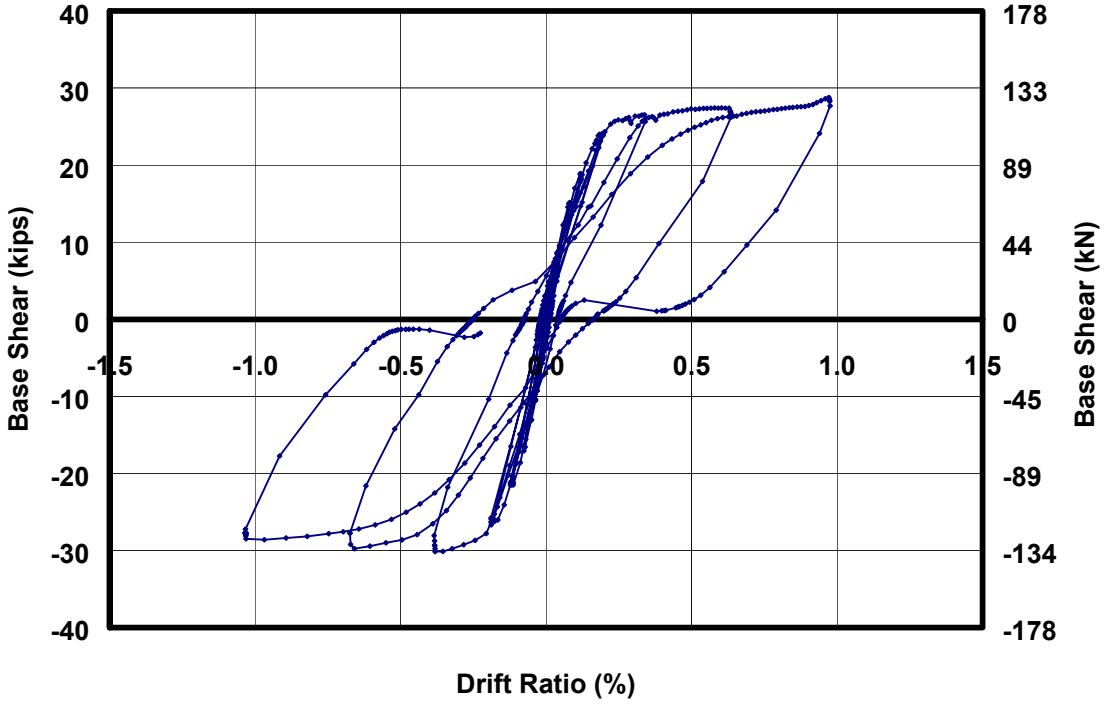

Figure 6.29: Force-displacement relationship for Shear Wall Specimen 15a

6.6 SHEAR WALL SPECIMEN 15B

Shear Wall Specimen 15b is a replica of Shear Wall Specimen 15a. The predicted behavior of this specimen is described in Section 6.5.

6.6.1 Loading History and Major Events for Shear Wall Specimen 15b

The actual loading and displacement histories for Shear Wall Specimen 15b are presented in Figure 5.49 and Figure 5.50. Monotonically increasing load point numbers are assigned for each set of data recorded during the test. Data are classified into cycles with maximum loads and drift ratios for each cycle (Table 5.10). Loading to the south is considered positive; loading to the north, negative.

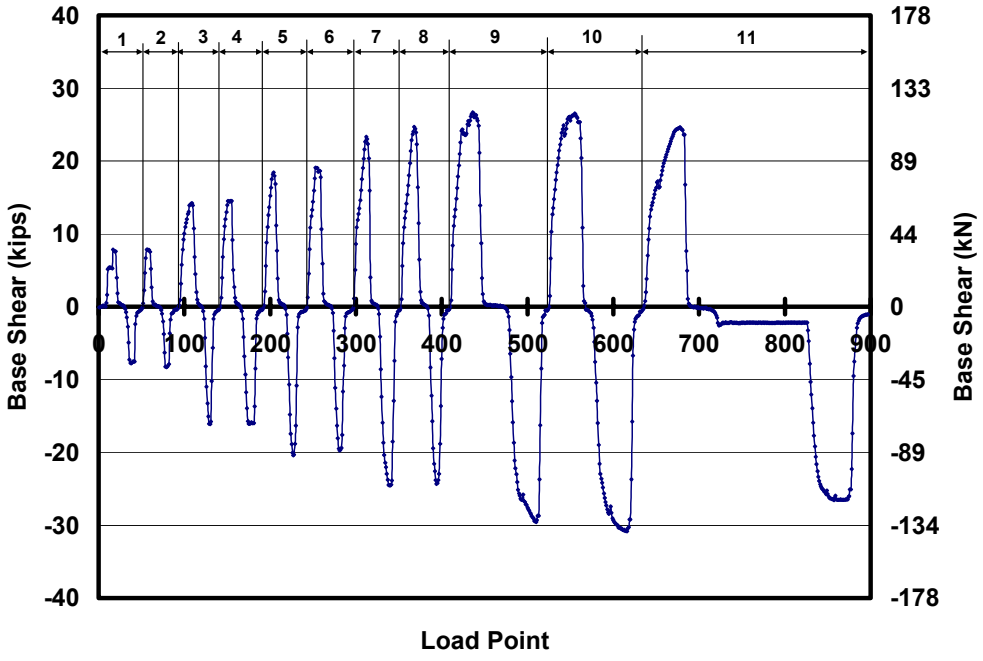

Figure 6.30: Actual loading history for Shear Wall Specimen 15b (numbers at the top designate cycle numbers)

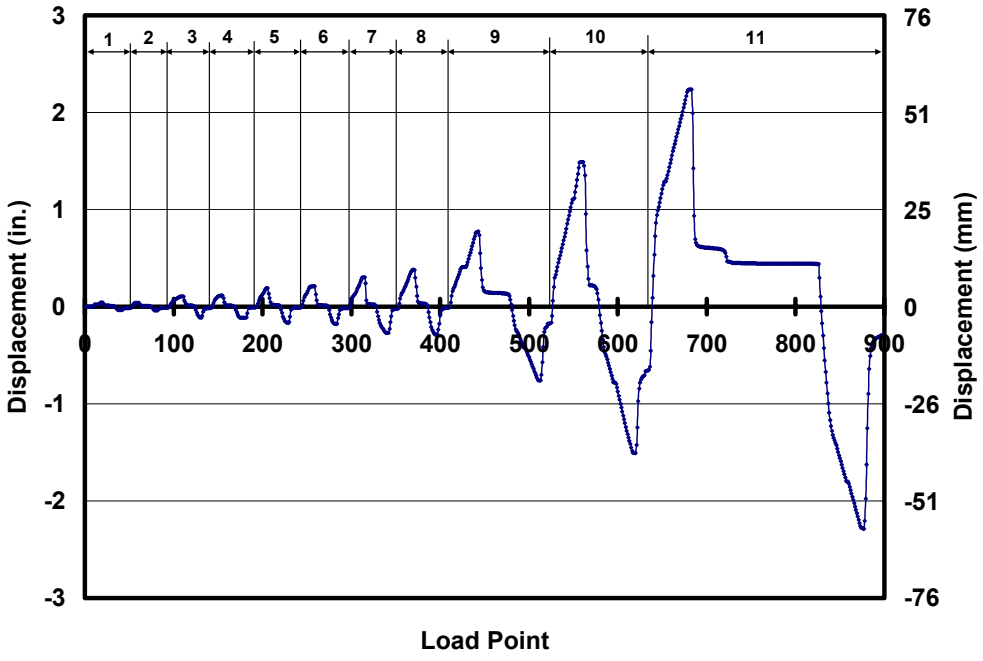

Figure 6.31: Actual tip displacement history for Shear Wall Specimen 15b (numbers at the top designate cycle numbers)

Table 6.9: Load points, maximum load and drift ratios for each cycle for Shear Wall Specimen 15b

Cycle	Load Points	Maximum Applied Load, kips (kN)	Max. Drift Ratio (%)	Cycle	Load Points	Minimum Applied Load, kips (kN)	Min. Drift Ratio (%)
1a	1 - 22	7.8 (35)	0.03	1b	23 – 44	-7.8 (-35)	0.02
2a	45 - 63	7.8 (35)	0.03	2b	64 – 85	-8.3 (-37)	0.03
3a	86 - 116	14.2 (63)	0.07	3b	117 - 135	-16.1 (-72)	0.07
4a	136 - 160	14.5 (65)	0.07	4b	161 - 188	-16.1 (-72)	0.08
5a	189 - 210	18.4 (82)	0.12	5b	211 - 234	-20.4 (-91)	0.11
6a	235 - 264	19.1 (85)	0.14	6b	265 - 290	-19.7 (-88)	0.12
7a	291 - 320	23.3 (104)	0.20	7b	321 - 350	-24.5 (-109)	0.18
8a	351 - 378	24.7 (110)	0.25	8b	379 - 408	-24.3 (-108)	0.19
9a	409 - 460	26.7 (119)	0.50	9b	461 - 522	-29.5 (-131)	0.49
10a	523 - 570	26.5 (118)	0.97	10b	571 - 635	-30.9 (-137)	0.98
11a	636 - 690	24.6 (110)	1.45	11b	691 - 900	-26.6 (-118)	1.48

6.6.2 Sequence of Crack Formation for Shear Wall Specimen 15b

The sequence of crack formation in Shear Wall Specimen 15b is described in terms of major events: points during the test when either the condition of the specimen changed (for example, flexural cracking or web-shear cracking), or the applied axial force was increased. Table 5.11 lists the major events and the load point at which they occurred. In each section where crack maps are presented, preexisting cracks are shown in gray, and new cracks are shown in black.

Table 6.10: Description of major events for Shear Wall Specimen 15b

Major Event	Load Point	Physical Description
1	59	Flexural cracking, loading south
2	79	Flexural cracking, loading north
3	202	Flexure-shear crack, loading south
4	226	Flexure-shear crack, loading north
5	255, 311	Additional flexure-shear cracks and vertical cracks, loading south
6	338	Additional flexure-shear cracks and vertical cracks, loading north
7	442-615	Additional splitting and flexure-shear cracking
8	651, 681	Vertical crack at joint, loading south
9	875	Damage at top of wall

6.6.2.1 Flexural cracking in Shear Wall Specimen 15b

Major Events 1 and 2 correspond to the observance of flexural cracking. At Load Point 59 a flexural crack formed while loading to the south at a load of 7.8 kips (34 kN) and a drift ratio of 0.03%. A flexural crack formed while loading to the north at Load Point 79. The base shear in the specimen was 8.3 kips (37 kN) and the drift ratio was 0.03%. The predicted base shear at flexural cracking was 9.1 kips (40 kN) which corresponds to ratios of observed to predicted strength of 0.86 and 0.91 while loading to the south and north respectively.

These cracks propagated to the middle of the wall at Load Points 109 and 130, as shown by the gray line in Figure 5.51

6.6.2.2 Flexure-shear cracking in Shear Wall Specimen 15b

Major Events 3 and 4 correspond to the formation of flexure-shear cracks while loading to the south and north respectively. A flexure-shear crack formed in the lower north corner at Load Point 202 at a base shear of 17.5 kips (78 kN) and a drift ratio of 0.1%. This crack propagated upwards at the location of the

vertical reinforcement. While loading to the north at Load Point 226, a flexure-shear crack formed, as shown in Figure 5.51. The corresponding base shear and drift ratio were 20 kips (89 kN) and 0.1%. The prediction for flexure-shear cracking at the first joint based on Section 8.2.2 is 18.7 kips (83 kN). The ratios of observed to predicted cracking are 0.95 and 1.07 for loading to the south and north respectively.

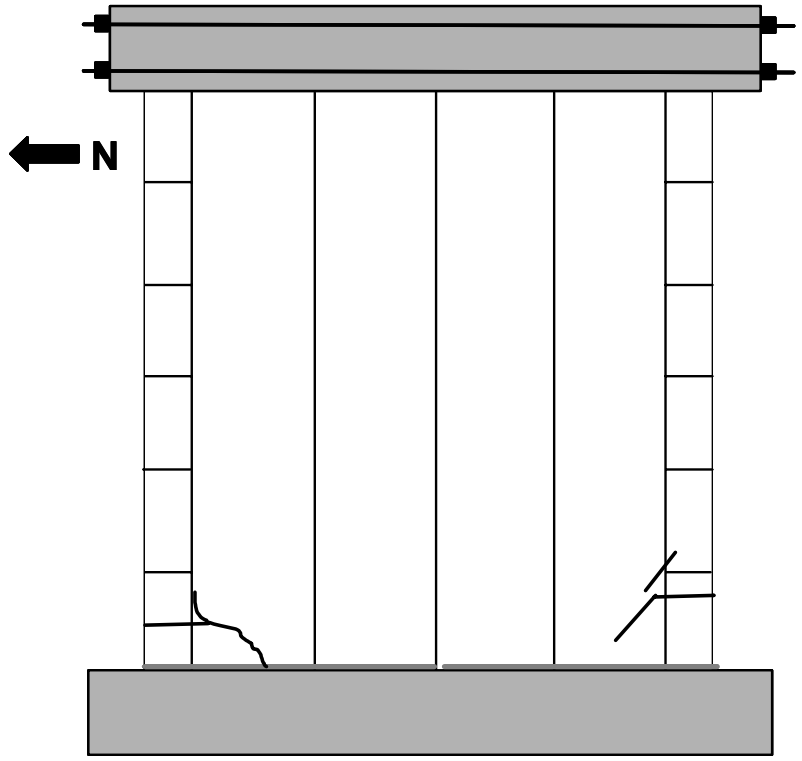

Figure 6.32: Formation of initial flexure-shear cracks in Shear Wall Specimen 15b

While loading to the south, additional flexure-shear cracks and vertical cracks formed in the lower north corner of the specimen. Major Event 5 corresponds to the formation of these cracks at Load Points 255 and 311. Additional flexure-shear cracks and vertical cracks formed in the lower south

corner of the specimen at Load Point 338 (Major Event 6). All of these cracks are shown in Figure 5.52.

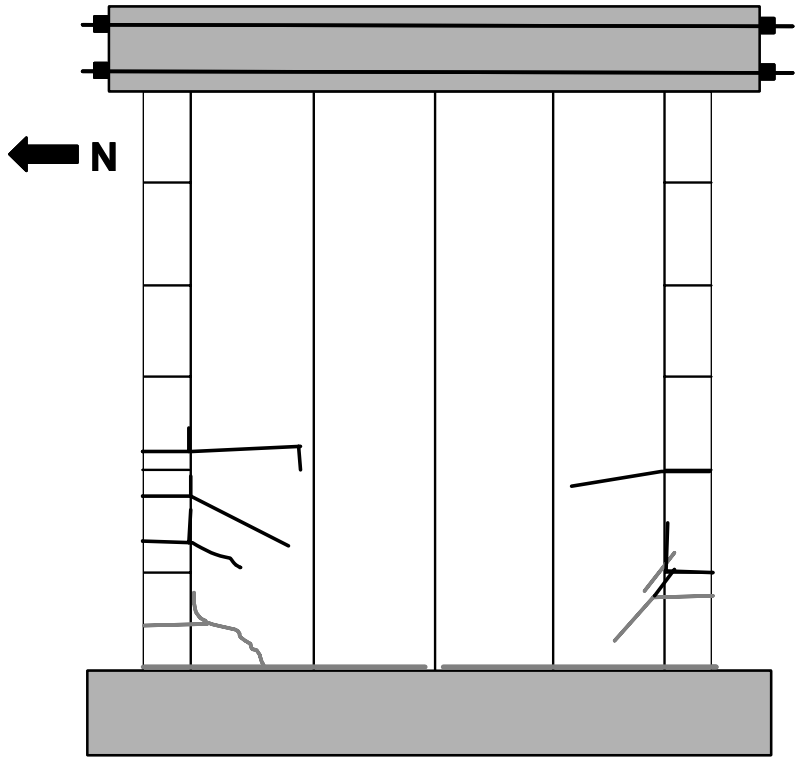

Figure 6.33: Formation of additional flexure-shear cracks in Shear Wall Specimen 15b

6.6.2.3 Additional cracking in Shear Wall Specimen 15b

Major Events 7 through 9 correspond to the development of additional cracks in the specimen. Between Load Points 442 and 615, additional flexure-shear cracks formed along with vertical cracks between the vertical panels and modular blocks. These events are classified as Major Event 7. Major Event 8 consists of vertical cracks at the joints between the two north vertical panels or the between the two south vertical panels. Propagation of these vertical cracks and

damage in the upper south corner of the specimen occurred at Load Point 875; this constitutes Major Event 9. The damage that occurred during these load points is shown in Figure 5.53.

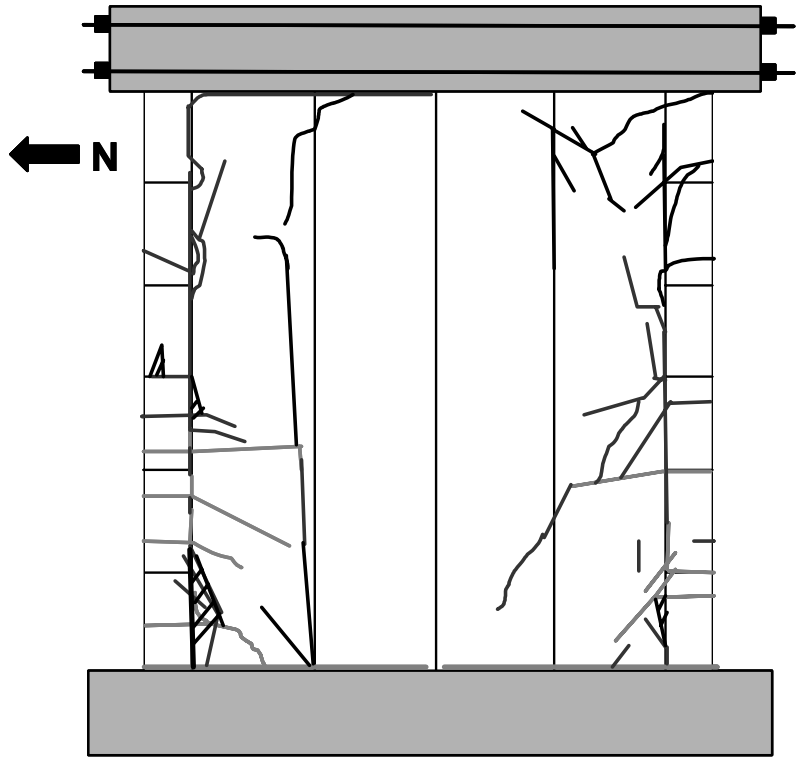

Figure 6.34: Additional cracking in Shear Wall Specimen 15b for Major Events 7 through 9

The test was ended due to a separation of both columns of modular blocks accompanied by buckling of the vertical reinforcement as shown in Figure 6.35.

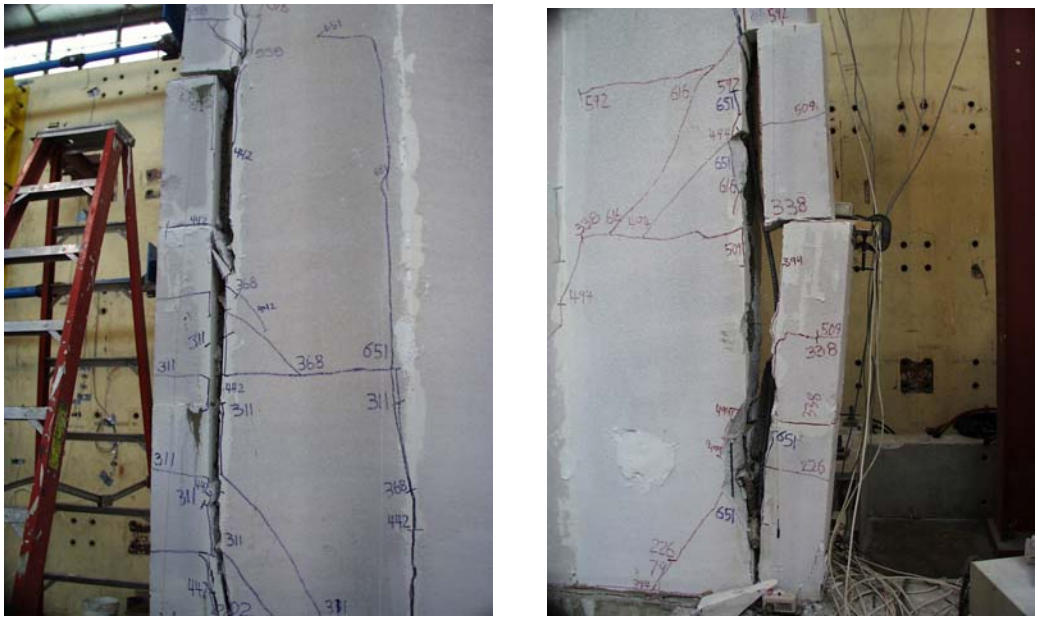

Figure 6.35: Loss of modular block columns on the north and south ends of Shear Wall Specimen 15b

6.6.3 Load-Displacement Behavior for Shear Wall Specimen 15b

This section is dedicated to presenting the hysteretic behavior of Shear Wall Specimen 15b. The force-displacement relationship is presented in terms of the non-dimensional drift ratio in Figure 5.56. The stiffnesses observed at various points in the loading history are described in Varela (2003).

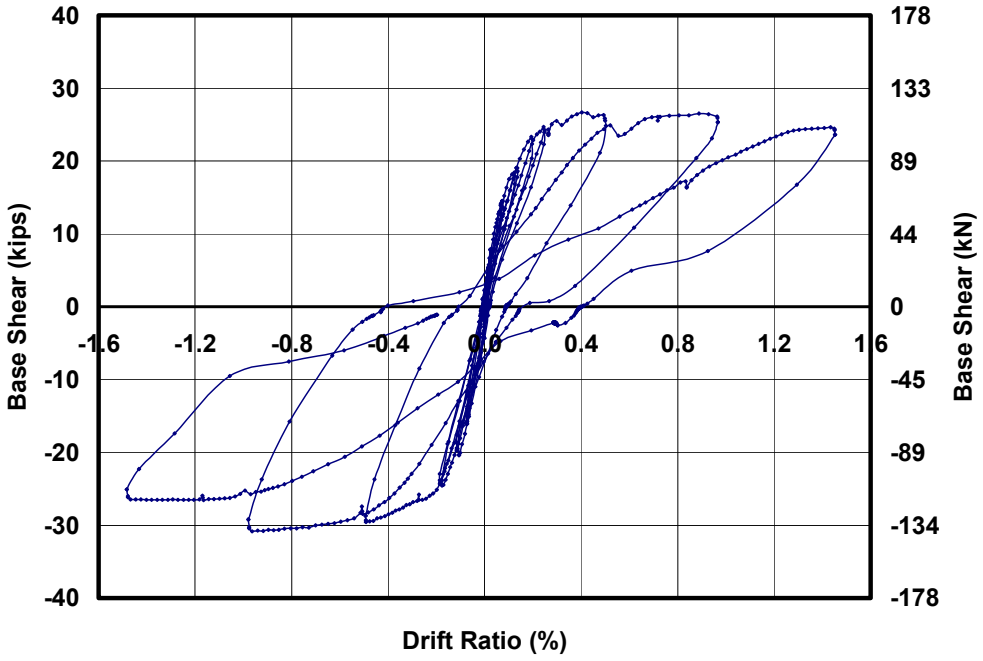

Figure 6.36: Force-displacement relationship for Shear Wall Specimen 15b

6.7 SHEAR WALL SPECIMEN 16

An interaction diagram for base shear capacity as a function of axial load for Shear Wall Specimen 16 is presented in Figure 6.37. The axial load applied to Shear Wall Specimen 16 was 25 kips (111 kN), as shown by a dashed horizontal line in Figure 6.37. At this level of axial load the following major events are predicted in order of occurrence: flexural cracking; flexure-shear cracking; and simultaneous sliding at the base and the nominal flexural capacity.

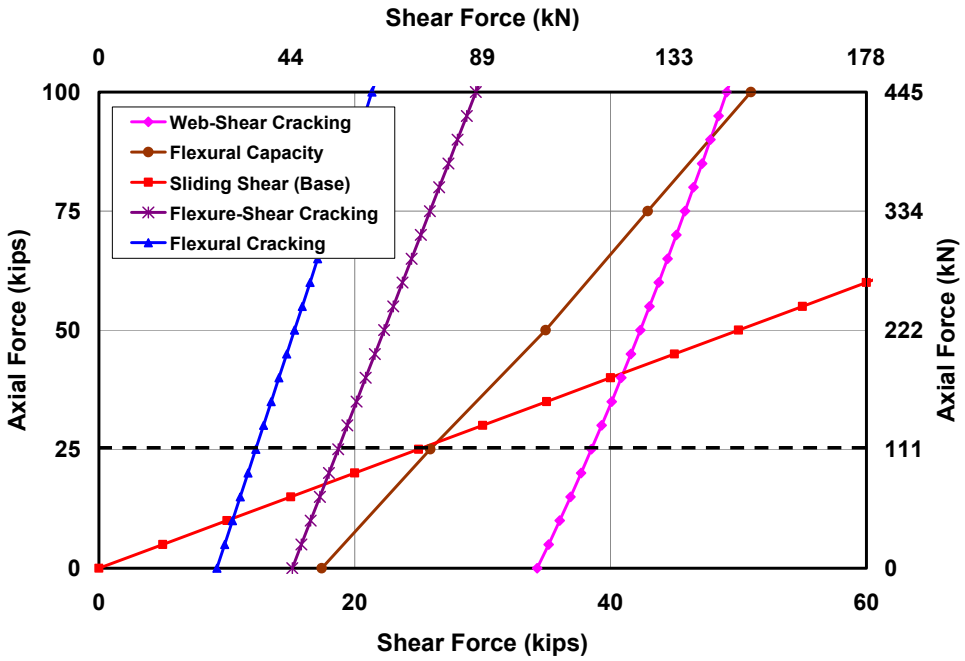

Figure 6.37: Prediction of behavior for Shear Wall Specimen 16

6.7.1 Loading History and Major Events for Shear Wall Specimen 16

The actual loading and displacement histories for Shear Wall Specimen 16 are presented in Figure 5.58 and Figure 5.59. Monotonically increasing load point numbers are assigned for each set of data recorded during the test. Data are classified into cycles with maximum loads and drift ratios for each cycle (Table 5.12). Loading to the south is considered positive; loading to the north, negative.

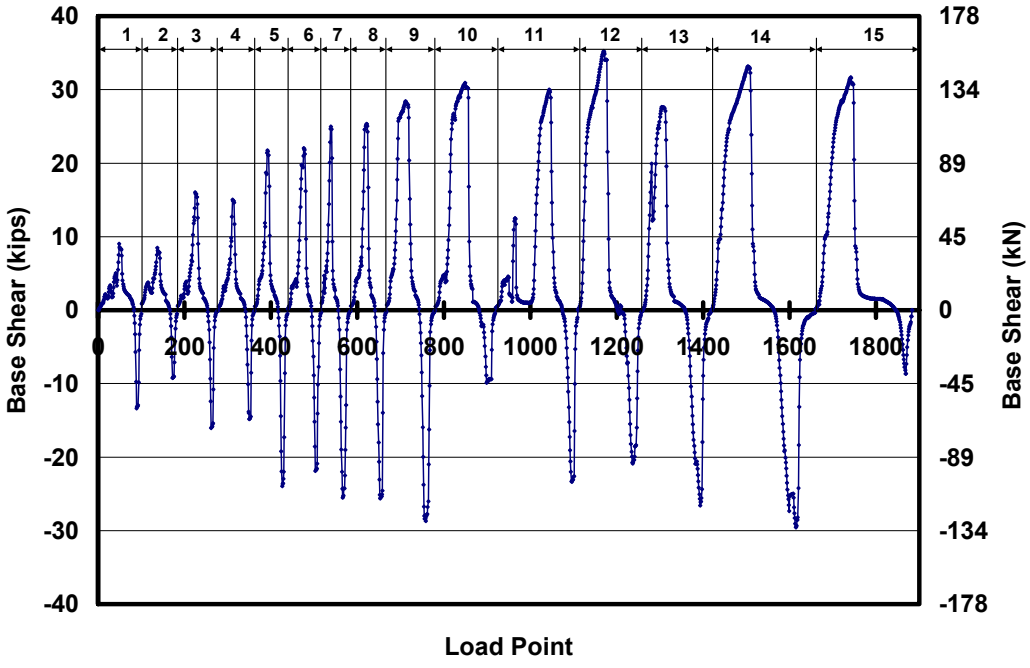

Figure 6.38: Actual loading history for Shear Wall Specimen 16 (numbers at the top designate cycle numbers)

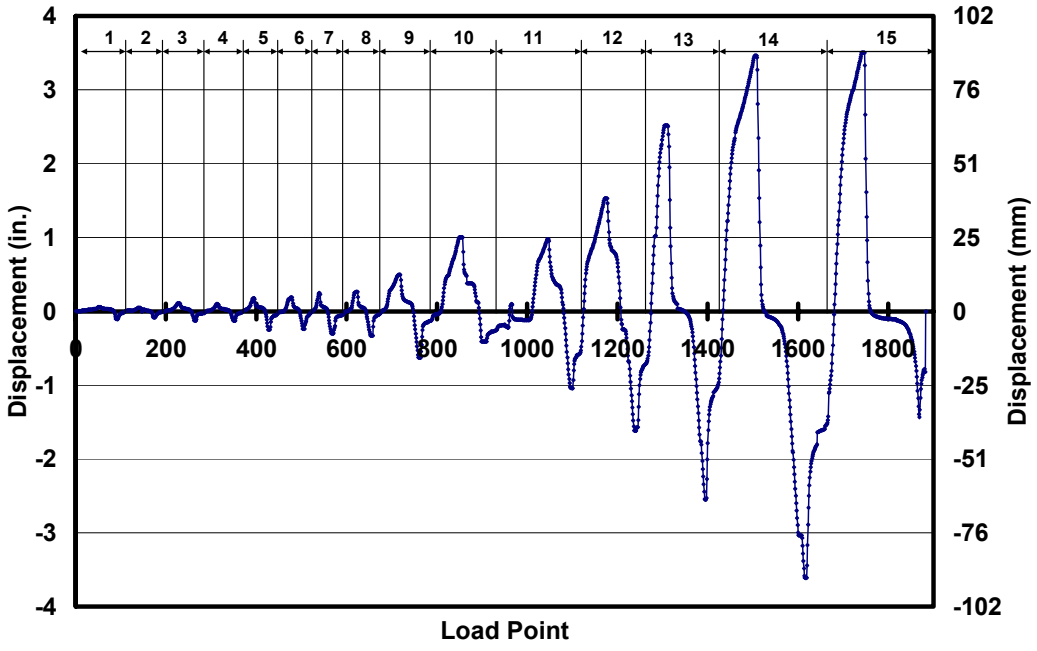

Figure 6.39: Actual tip displacement history for Shear Wall Specimen 16 (numbers at the top designate cycle numbers)

Table 6.11: Load points, maximum load and drift ratios for each cycle for Shear Wall Specimen 16

Cycle	Load Points	Maximum Applied Load, kips (kN)	Max. Drift Ratio (%)	Cycle	Load Points	Minimum Applied Load, kips (kN)	Min. Drift Ratio (%)
1a	0-83	9.0 (40)	0.04	1b	84-105	-13.4 (-60)	-0.07
2a	106-164	8.5 (38)	0.03	2b	165-185	-9.3 (-41)	-0.05
3a	186-253	16.1 (71)	0.07	3b	254-278	-16.1 (-71)	-0.08
4a	279-340	15.1 (67)	0.06	4b	341-362	-14.8 (-66)	-0.08
5a	363-418	21.8 (97)	0.11	5b	419-440	-24.0 (-107)	-0.16
6a	441-490	22.1 (98)	0.12	6b	491-520	-21.9 (-97)	-0.15
7a	521-555	25.0 (111)	0.16	7b	556-585	-25.5 (-114)	-0.20
8a	586-640	25.3 (113)	0.17	8b	641-670	-25.6 (-114)	-0.21
9a	671-742	28.4 (126)	0.32	9b	743-780	-28.7 (-128)	-0.41
10a	779-880	30.9 (138)	0.65	10b	881-920	-9.9 (-44)	-0.27
11a	921-1075	30.0 (134)	0.64	11b	1076-1112	-23.3 (-104)	-0.68
12a	1113-1210	35.2 (157)	0.99	12b	1211-1260	-20.9 (-93)	-1.05
13a	1261-1368	27.6 (123)	1.64	13b	1369-1425	-26.6 (-118)	-1.66
14a	1426-1565	33.2 (147)	2.25	14b	1566-1662	-29.5 (-131)	-2.35
15a	1663-1850	31.7 (141)	2.28	15b	1851-1880	-8.7 (-38)	-1.00

6.7.2 Sequence of Crack Formation for Shear Wall Specimen 16

The sequence of crack formation in Shear Wall Specimen 16 is described in terms of major events: points during the test when either the stiffness or the condition of the specimen changed. Table 5.13 lists the major events and the load point at which they occurred. In each crack map, preexisting cracks are shown in gray, and new cracks are shown in black.

Table 6.12: Description of major events for Shear Wall Specimen 16

Major Event	Load Point	Physical Description
1	31	Flexural cracking, loading south
2	93	Flexural cracking, loading north
3	392	Flexure-shear cracking, loading south
4	426	Flexure-shear cracking, loading north
5	566-760	Formation of additional flexure-shear cracks and vertical cracks at joint
6	824, 834	Web-shear cracking, loading south
7	1210	Vertical crack formed between panels after unloading
8	1225, 1238	Damage in compression toe vertical cracks propagated, loading north
9	1284	Fracture of north bar, loading south
10	1297-1385	Vertical cracks at south bar, loading both directions
11	1458	Crushing at south toe
12	1668	Loss of grouted column

6.7.2.1 Flexural cracking in Shear Wall Specimen 16

Major Events 1 and 2 correspond to the observance of flexural cracking. At Load Point 31 a 2 in. (51 mm) flexural crack formed while loading to the south at a load of 2.4 kips (11 kN) and a drift ratio of 0.01%. A flexural crack formed while loading to the north at Load Point 92. The base shear in the specimen was 13.1 kips (58 kN) and the drift ratio was 0.07%. The predicted base shear at cracking using an average tensile bond strength is 12.3 kips (55 kN), which corresponds to a ratio of tested to predicted strength of 1.06.

These flexural cracks propagated throughout Load Points 112-392 until the flexural crack at the base extended through the entire length of the wall. The wall underwent flexural rocking for the next 3 cycles.

6.7.2.2 Flexure-shear cracking in Shear Wall Specimen 16

Major Events 3 and 4 correspond to the formation of flexure-shear cracking while loading to the south and north respectively. A flexure-shear crack

formed at Load Point 392. The corresponding base shear and drift ratio were 21.8 kips (97 kN) and 0.11%. While loading to the north, a similar flexure-shear crack formed at Load Point 426 at a base shear of 24 kips (107 MPa) and a drift ratio of 0.17%. The cracks were nearly symmetric about the centerline of the wall as both cracks propagated along the head joint between the modular blocks and vertical panels and included additional flexural cracks (Figure 5.60). The prediction for flexure-shear cracking at an axial load of 25 kips (111 kN) based on Section 8.1.1 is 18.7 kips (83 kN). The ratios of observed to predicted cracking capacity are 1.15 and 1.3 for loading to the south and north respectively.

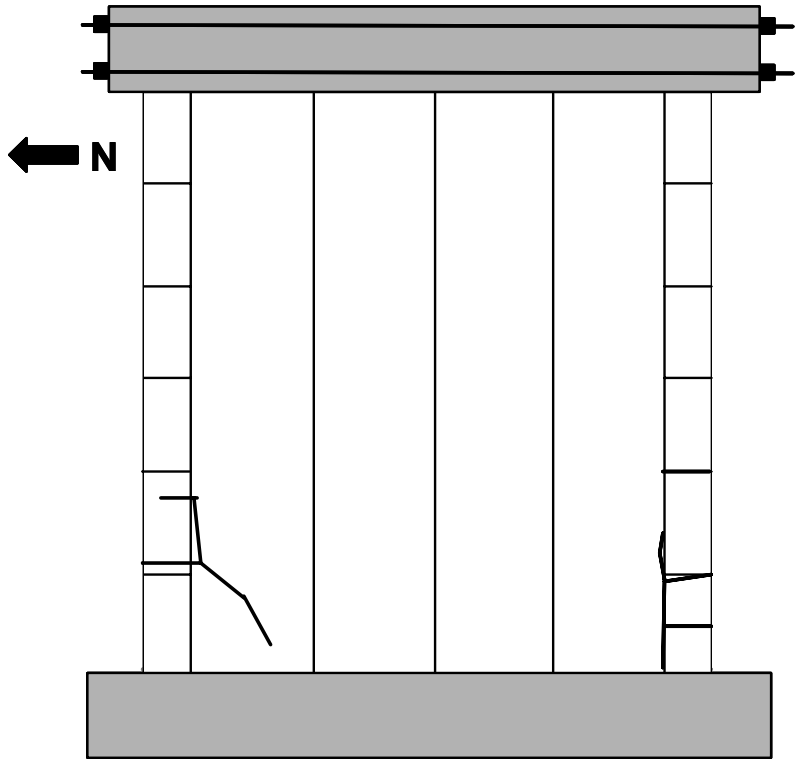

Figure 6.40: Formation of flexure-shear cracks in Shear Wall Specimen 16

Major Event 5 corresponds to the development of additional flexure-shear cracks in the specimen and vertical cracks along the head joint. This damage occurred throughout Load Points 566 and 760. Major Event 6 is characterized by

the formation of diagonal cracks while loading to the south at Load Points 824 and 834. The damage from Major Events 5 and 6 is shown in Figure 5.61.

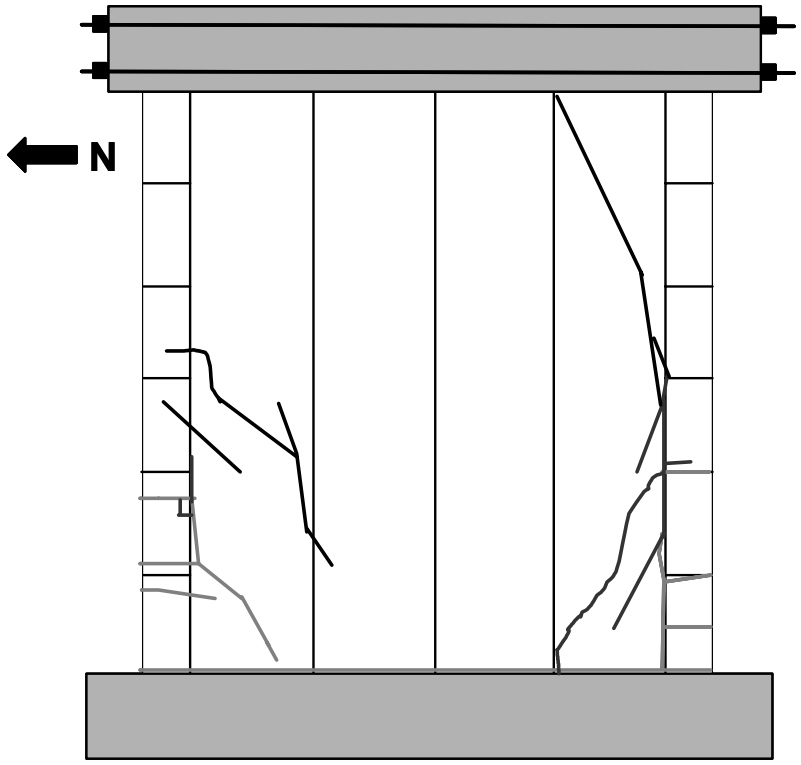

Figure 6.41: Formation of additional flexure-shear cracks in Shear Wall Specimen 16

6.7.2.3 Final damage in Shear Wall Specimen 16

While unloading at Load Point 1210 a vertical crack formed between the two north vertical panels along with vertical cracks at the north toe (Major Event 7). Major Event 8 corresponds to the crushing of the north toe and propagation of the vertical crack through the top of the wall at the south head joint. While loading to the south an abrupt drop in stiffness was observed at Load Point 1284. It was later determined that the north deformed reinforcement fractured, which is defined as Major Event 9. The impact of this event is discussed in Section 7.7.5.

The wall continued to be loaded to complete Cycles 12 through 15. Damage in the grouted columns was observed in Loading Points 1297 through 1385 (Major Event 10). Crushing of the south toe was observed during Load Point 1458 which constitutes Major Event 11. Major event 12 constituted the end of the test, when the grouted column failed.

A summary of the cracks observed during Major Events 7 through 12 is shown in Figure 5.62. The damage to the grouted column including the buckled reinforcement is shown in Figure 5.63 and Figure 6.44.

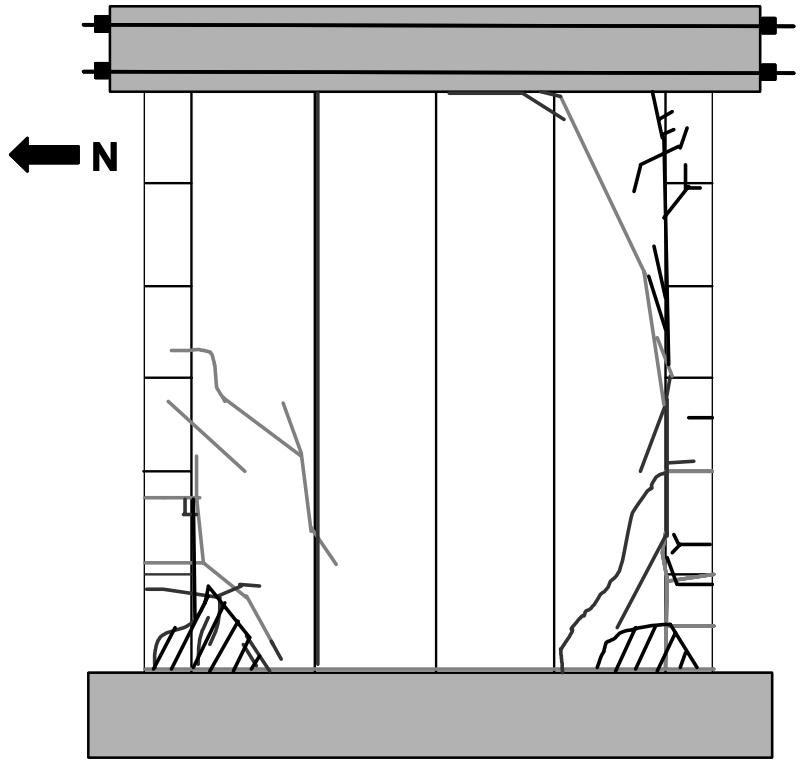

Figure 6.42: Toe crushing and additional damage in Shear Wall Specimen 16

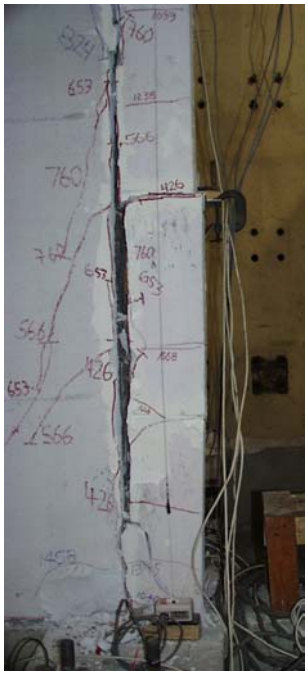

Figure 6.43: Loss of the grouted column in Shear Wall Specimen 16

Figure 6.44: Buckled reinforcement in Shear Wall Specimen 16

6.7.3 Load-Displacement Behavior for Shear Wall Specimen 16

The force-displacement relationship of Shear Wall Specimen 16 is presented in terms of the non-dimensional drift ratio in Figure 5.64. An abrupt drop in stiffness corresponding to a base shear of 20 kips (89 kN) and a drift ratio of 0.06% was observed at the time when the north bar fractured. Stiffnesses observed at various points in the loading history are described in Varela (2003).

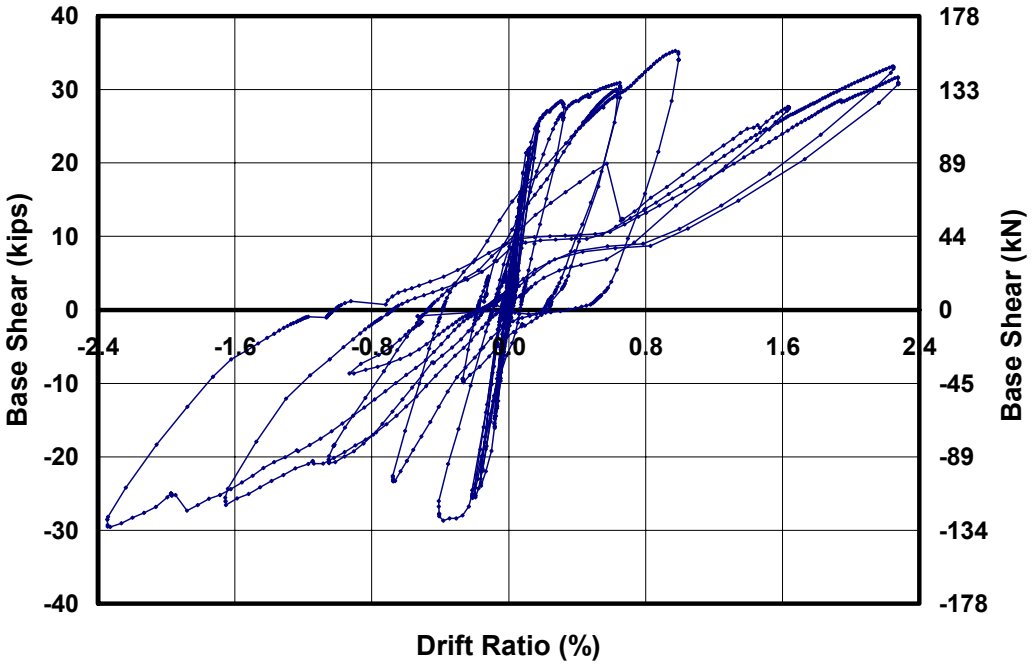

Figure 6.45: Force-displacement relationship for Shear Wall Specimen 16

6.7.4 Evaluation of Specimen Behavior after the Fracture of the Vertical Bar in for Shear Wall Specimen 16

The vertical bar at the north end of the wall fractured at Load Point 1284 (Cycle 14a). Although this fracture was not observed until the end of the test the noise associated with the fracture of the bar is recorded in the test notes. In

addition, an abrupt decrease in strength is observed along with a change in stiffness at that point (Figure 5.64). After this event the base shear continued to increase to a maximum of 33.2 kips (148 kN) despite the loss of internal vertical reinforcement. This value is significantly larger than the capacity of an unreinforced wall, 7 kips (31 kN). After the test the following hypotheses were investigated: error in the load cells; potential lateral restraint from the safety chains; or lateral bracing system and error in the axial load system. The first hypothesis was discarded after a calibration of the load cell indicated the cell was functioning properly. The lateral bracing system is not capable of resisting the lateral load reached in Cycles 14a-16a. There was no evidence of physical movement of the safety chains and the load applied is over twice the safe working load for these chains. The only remaining hypothesis is a change in the axial load, despite a constant pressure reading from the load maintainer. The axial load system is analyzed in detail in Section 6.7.5

6.7.5 Analysis of Axial Load System

The axial load system is shown in Figure 6.46. An elevation of the system shows a transverse beam connected through hinges to rods that supply the axial load. The transverse beam is simply supported at the center; thus a force applied to one rod must be the same as the other rod to maintain equilibrium (Figure 6.47). The force in the rods is controlled by a single ram connected to a load maintainer. It is possible for the piston to retract fully into the ram casing. This can cause the piston to bear on the casing and change the force from the originally intended force supplied by the pressure of the hydraulic fluid, causing an increase in axial load as the piston retracts fully into the ram casing. Both a free-body diagram of the ram piston and ram schematics of these cases are shown in Figure 6.48. If the ram “bottoms out” (the piston fully retracts into the ram casing), the

force in the rods can exceed that supplied by the load maintainer. Due to the hinges in the axial load system, any vertical displacement of the wall without additional elongation of the rods will result in a retraction of the piston (Figure 6.49). If the vertical displacement at the location of the ram exceeds one-half of the initial ram stroke, the ram will bottom out (the piston retracts fully into the ram causing an unintended increase in axial load). After this point, the ram is no longer able to compensate for the vertical displacement, and the rod force will increase. The end result is an unintended increase in force based on displacement compatibility as a result of the ram bottoming out (or fully retracting into the ram casing).

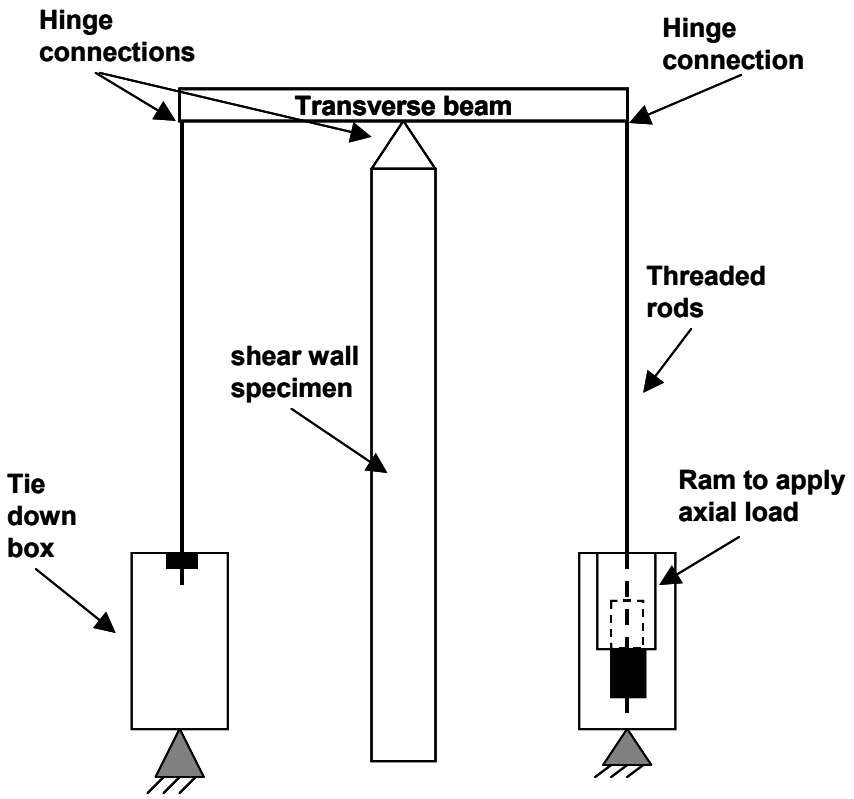

Figure 6.46: Schematic of the axial load system

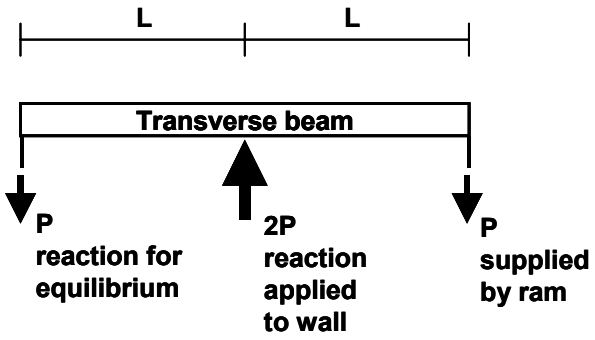

Figure 6.47: Free-body diagram of forces in wall and rods

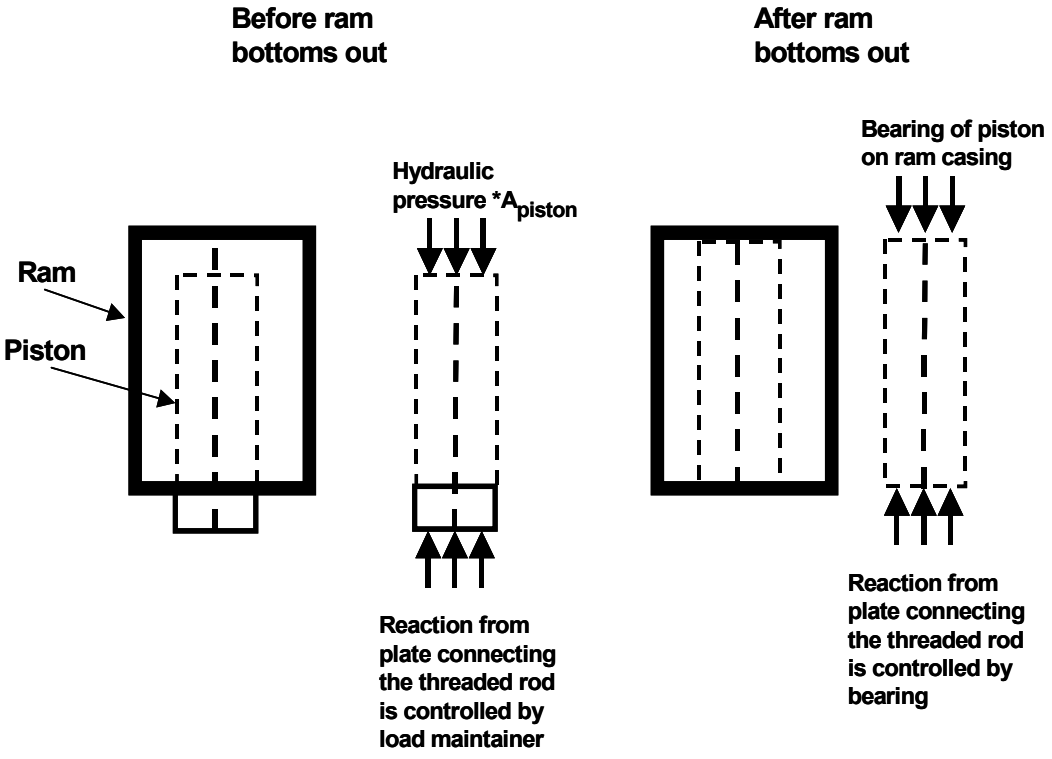

Figure 6.48: Free body diagram of piston inside ram

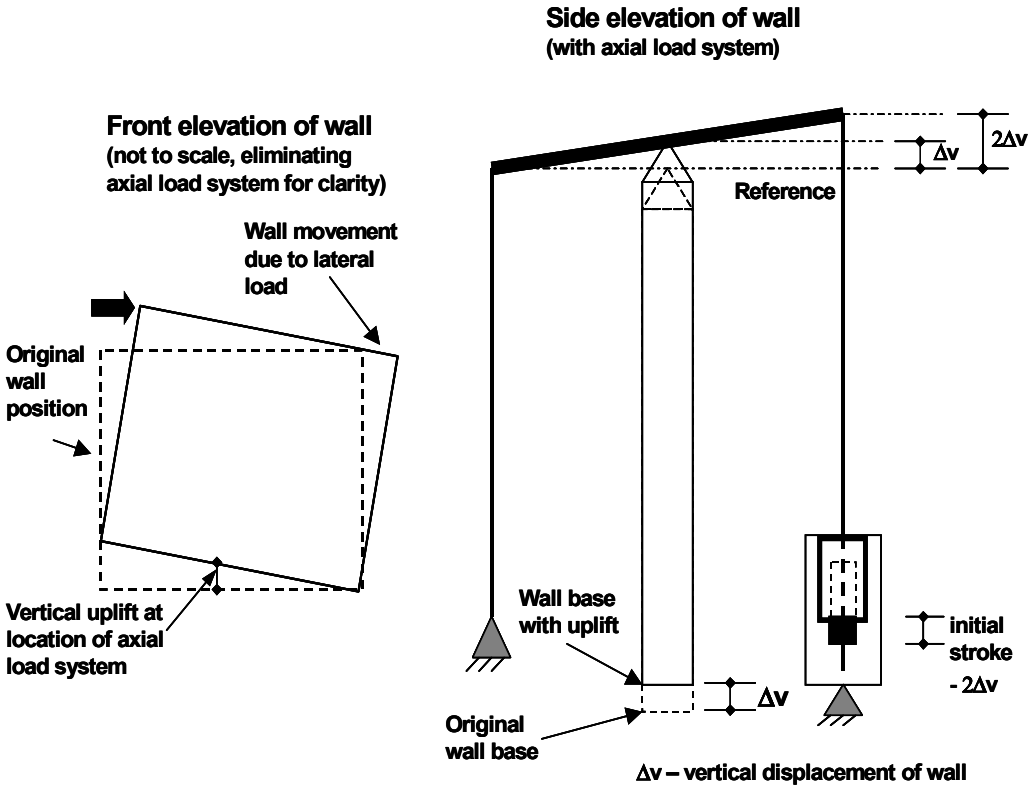

Figure 6.49: Vertical compatibility of the axial load system

6.7.5.1 Evaluation of axial load in Shear Wall Specimen 16

Since the bar fractured at Load Point 1284, the wall was unreinforced while loading to the south from this time forward. The axial load was determined based on the flexural capacity of an unreinforced wall for Cycles 14a-16a. The critical vertical displacement is one half of the initial stroke (Δ_{cr}). This was determined to be 0.5 in. (12 mm) based on a photograph of the wall. The following steps were performed in order to determine the axial load for each load point:

1. Determine the vertical displacement (Δ_v) at the location of the ram;

2. Determine if Δ_v exceeds the critical vertical displacement (Δ_{cr}) for bottoming out the ram (or fully retracting the piston); and
3. If Δ_{cr} was exceeded back-calculate the axial load (N_{total}) based on flexural theory for an unreinforced shear wall (Figure 6.50).

The axial load was back calculated based on the preceding sequence of steps. The graph of Figure 6.50 shows the axial load versus load point after the south bar fractured. In this graph, axial load is 25 kips (111 kN) if the vertical displacement is less than the critical displacement of 0.5 in. (12 mm) or while loading to the north. This graph indicates that during three cycles the axial load was exceeded.

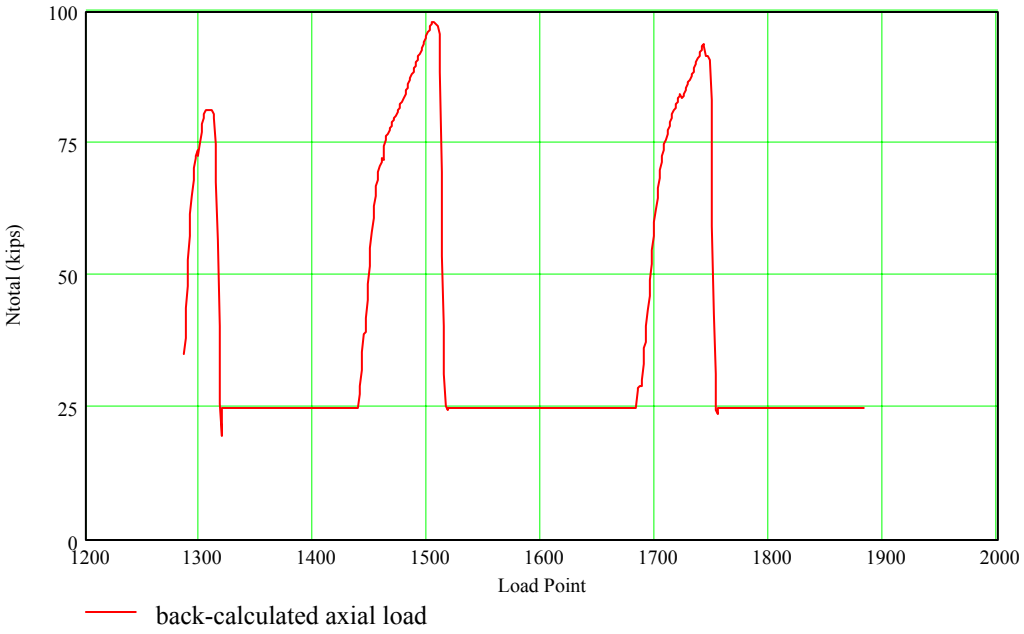

Figure 6.50: Back-calculated axial load for Cycles 14a-16a in Shear Wall Specimen 16

For each cycle, the increase in axial load is plotted versus the additional increase in rod deformation. Each cycle is represented by a different marker; the elastic loading portion is represented by solid markers, while the inelastic or unloading portion is represented by open markers. In the elastic portion the average slope is 115.5 kips/in. with a COV of 1.5%. The inelasticity seen in Cycles 15a and 16a is due to toe crushing observed at the peak load of each of these cycles. The presence of toe crushing indicates that the critical vertical displacement will increase throughout the test.

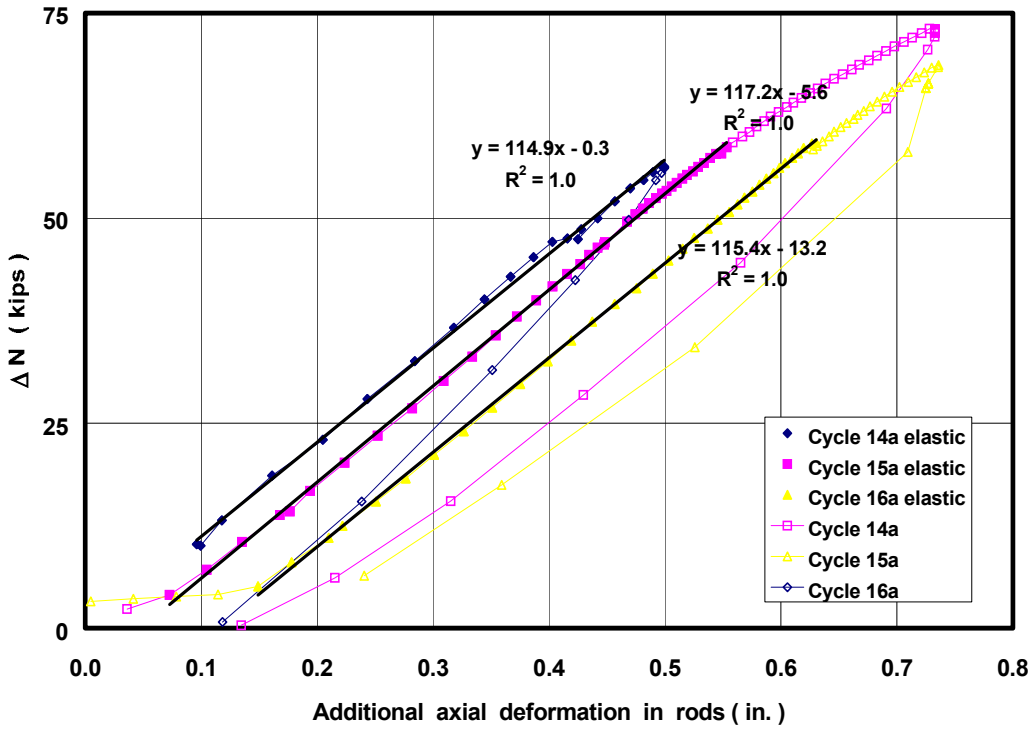

Figure 6.51: Linear regression of Cycles 14a, 15a and 16a in Shear Wall Specimen 16 for initial stroke of 0.5 in. (13 mm)

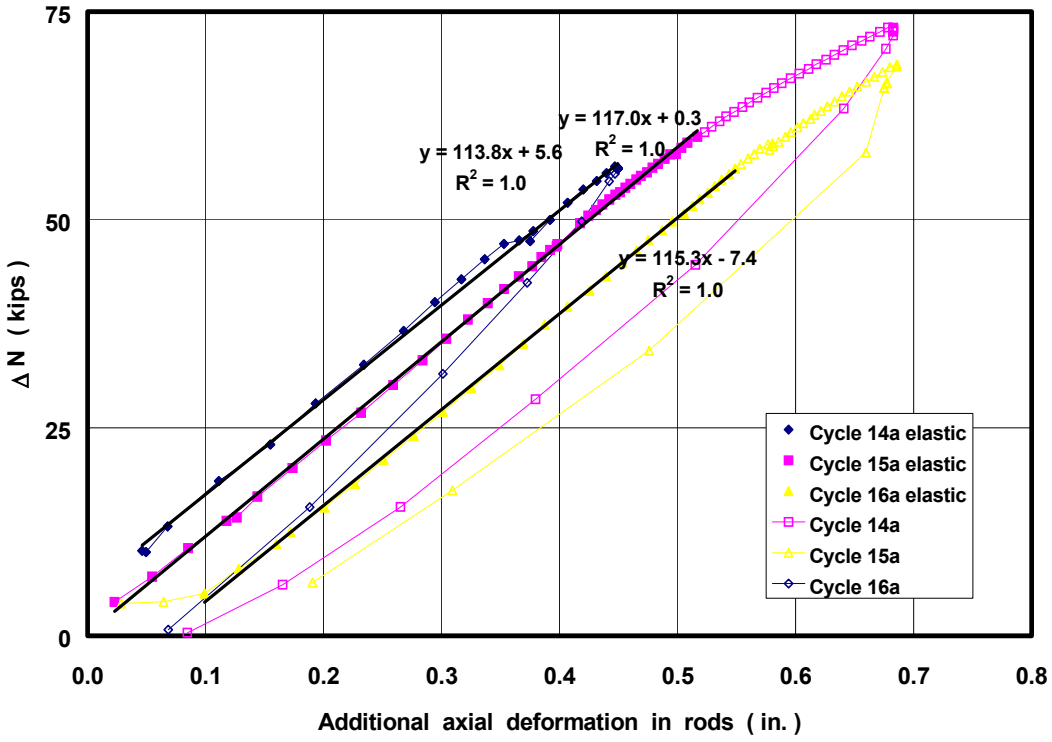

Figure 6.52: Linear regression of Cycles 14a, 15a and 16a in Shear Wall Specimen 16 for initial stroke of 0.6 in. (15 mm)

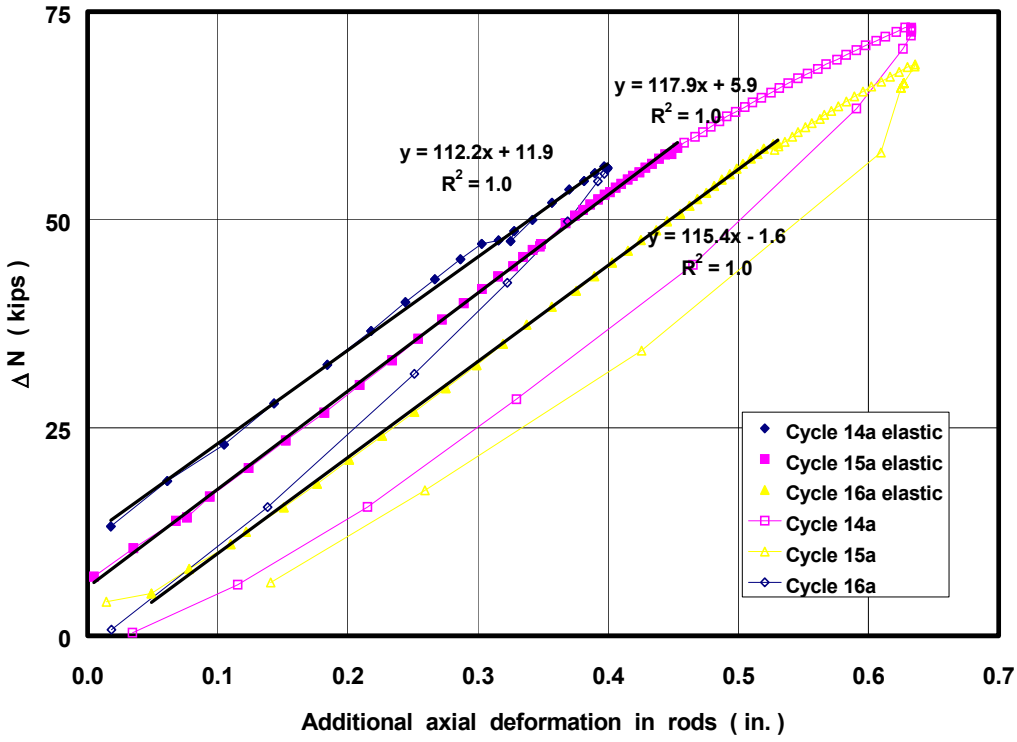

Figure 6.53: Linear regression of Cycles 14a, 15a and 16a in Shear Wall Specimen 16 for initial stroke of 0.7 in. (18 mm)

Using Equation (6.1), the increase in axial load, ΔN, was calculated based on a measured increase in vertical displacement. The new axial load, N_{total}, was determined using Equation (6.2), where N_o is the initial applied axial load. This procedure was applied to the cycles loading to the north. For each cycle where the critical vertical displacement was exceeded, a change in axial load was determined. The base shear was back-calculated based on the new axial load and the tensile force in the south bar. The tensile force remained constant throughout the analysis and it considers the effect of strain hardening. Since the critical vertical displacement is changing, this must be reflected in the analysis. The

critical vertical displacement of each cycle loading to the south will remain the same for each cycle loading to the north. The increase in ram stroke for each cycle is 0.1 in. (3 mm) for each cycle. While loading to the north, the axial load changed during load points 1384-1400 and 1591-1628. The difference in base shear determined using flexural theory based on an increase in axial load for these points is shown in Figure 6.54. Highlights of those cycles are shown in Figure 6.55 and Figure 6.56.

$$\Delta N = 115.5\left(\Delta_v - \Delta_{cr}\right) \qquad \text{Equation (6.1)}$$

$$N_{total} = N_o + \Delta N \qquad \text{Equation (6.2)}$$

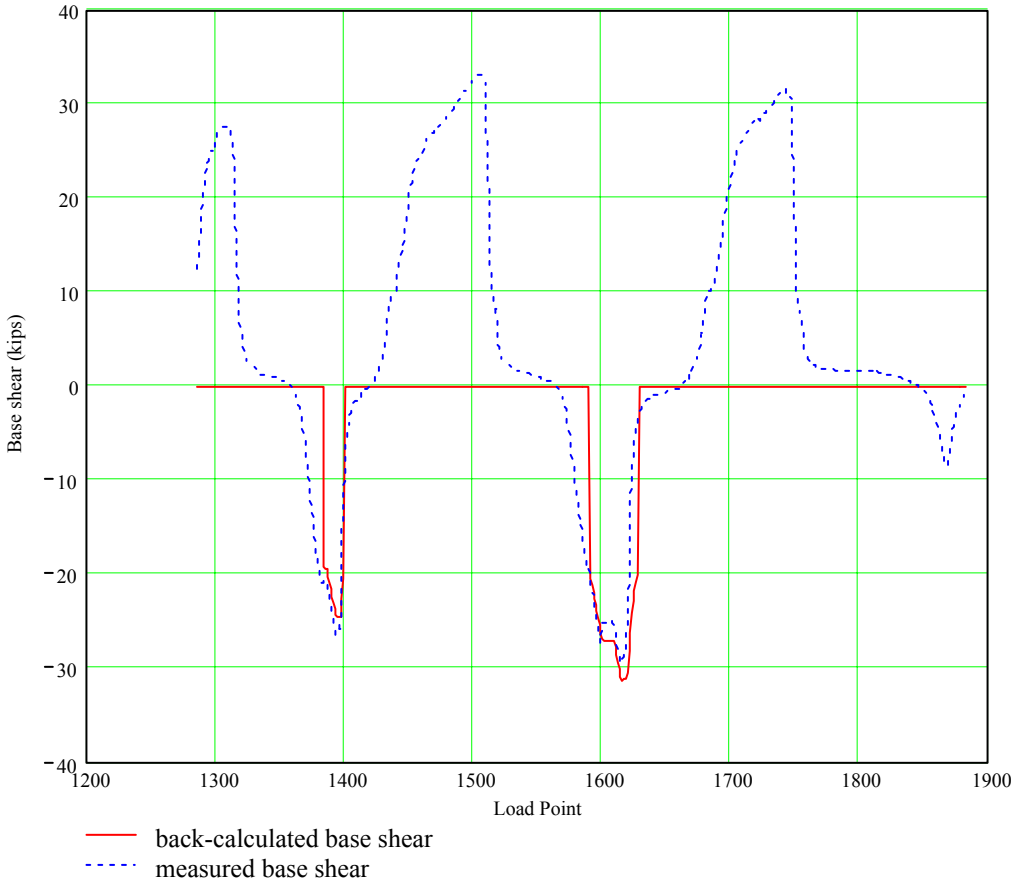

Figure 6.54: Difference in calculated base shear using calculated increase in axial load and measured base shear for Shear Wall Specimen 16

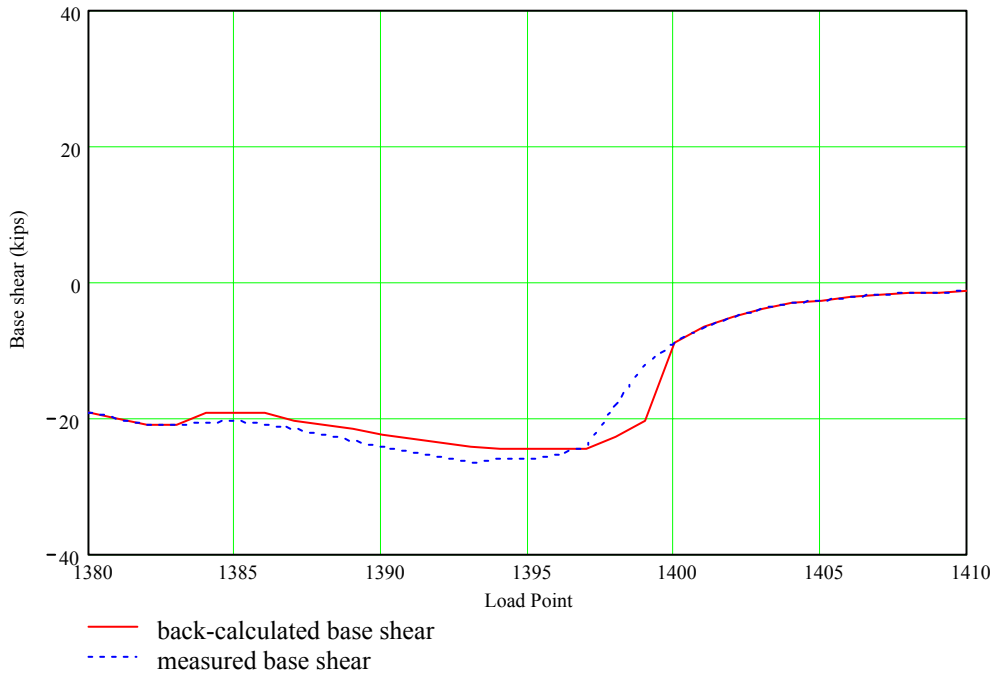

Figure 6.55: Load Points 1384 through 1400 in Shear Wall Specimen 16

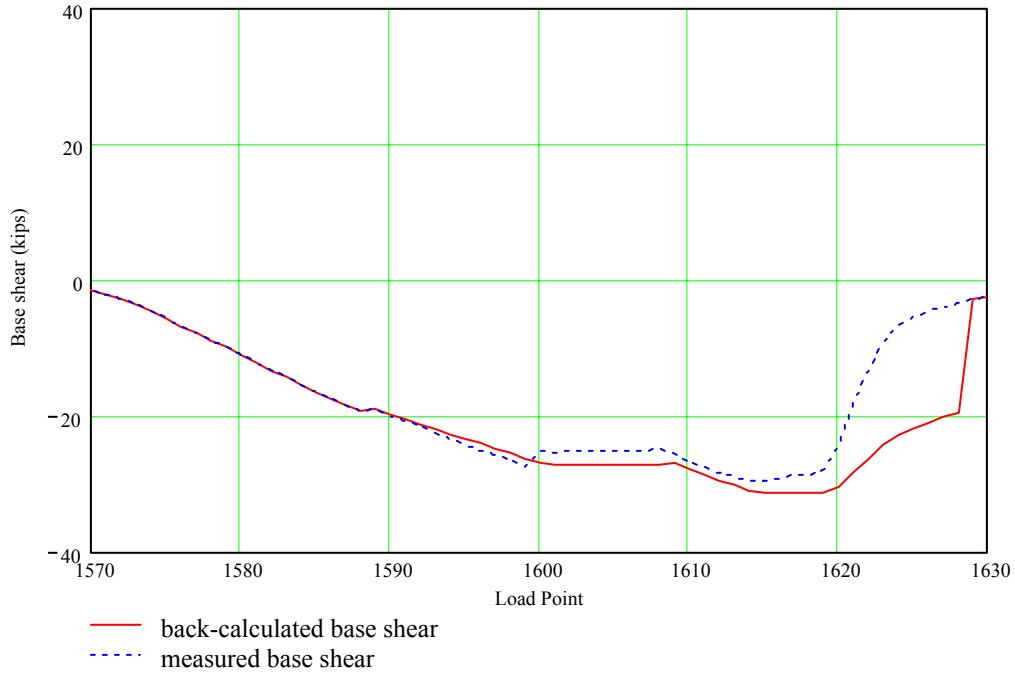

Figure 6.56: Load Points 1591 through 1628 in Shear Wall Specimen 16

6.7.5.2 Potential increase in axial load in other Shear Wall Specimens

Increasing the axial load could occur in any of the shear wall specimens if the rams bottomed out (corresponding to a full retraction of the piston into the ram casing); this section presents the results of the investigation at UT Austin. The potential for increase in axial load of the shear-dominated specimens is reduced due to the smaller vertical displacements observed in each specimen. The probability of an increase in axial load for the flexure-dominated specimens is higher due to the larger vertical displacements induced by rocking of the specimen. Each group of specimens are discussed individually in this section.

An analysis of each shear-dominated specimen was performed. This consisted of determining the vertical displacement of the wall at the location of

the ram for the load maintainer. The vertical displacement was calculated based on a linear displacement gradient between the two vertical string pots. The vertical displacement is multiplied by 2 (Figure 6.46) in order to convert this displacement into a required initial stroke to avoid bottoming out the ram. The results of this analysis for the shear-dominated specimens are presented in Table 6.13. The maximum required stroke was 0.6 in. (15 mm) in Shear Wall Specimen 1. The remaining shear wall specimens have required initial strokes less than 0.4 in (10 mm). The initial stroke will consist of the axial elongation of the threaded rods and tie downs, flexural deformation of the transverse loading beam, and any additional slop in the system such as oversized holes in the pin connections. It is unlikely that the initial stroke was less than the required value. Despite that, the values for web-shear cracking are well below a known minimum, the total axial elongation of the system.

Table 6.13: Required initial stroke for each shear-dominated specimen

Shear Wall Specimen	Load Maintainer	Required initial stroke in. (mm)	Required initial stroke for WSC in. (mm)	Total axial elongation in. (mm)
1	Y	0.57 (15)	NA	0.30 (8)
2	Y	0.36 (9)	NA	0.28 (7)
3	Y	0.38 (10)	0.04 (1)	0.17 (4)
4	Y	0.11 (3)	0.11 (3)	0.17 (4)
5	Y	0.32 (8)	0.03 (1)	0.04 (1)
7	Y	0.26 (7)	0.21 (5)	0.23 (6)
9	Y	0.11 (3)	0.11 (3)	0.01 (0)
11	N	NA	NA	NA

The flexure-dominated specimens that have been tested are listed in Table 6.14. Of the flexural specimens tested to date, Shear Wall Specimen 13 and 16 are affected by an increase in axial load. Shear Wall Specimen 14a was not

affected because the axial load was supplied by gravity. No evidence of an increase in axial load exists for Shear Wall Specimen 15a. The observed base shear at yield agreed with the predicted base shear at yield. After yielding almost no increase in base shear was observed (Figure 5.47).

Table 6.14: Probability of increased axial load in the flexure-dominated specimens

Shear Wall Specimen	Load maintainer used	Evidence of increase in axial load
13	Y	Yes, unexplained increase in flexural capacity
14a	N	NA
14b	N	NA
15a	Y	No, no increase observed in flexural capacity beyond yield
15b	Y	Was tested with sufficient initial stroke
16	Y	Yes, unexplained increase in flexural capacity
17	Y	Shall be tested with sufficient initial stroke

6.7.5.3 Increase in axial load in Shear Wall Specimen 13

The section is dedicated to an analysis of Shear Wall Specimen 13. The predicted base shear capacity was exceeded in Cycles 10-13 (Table 5.1)

The formula derived for Shear Wall Specimen 16 was applied to Shear Wall Specimen 13. The axial load was applied at two locations. Only one ram will reflect an increase in axial load, this means the load is no longer concentric. The eccentricity was considered in calculating the base shear capacity. The assumed initial stroke is 0.5 in. (13 mm) for each ram. This analysis uses the same assumptions present in the analysis for Shear Wall Specimen 16:

- a linear relationship between vertical displacement and increase in axial load (Equation (6.1));
- a constant value for the force in the internal reinforcement, including strain hardening; and
- an increase in stroke of 0.1 in. (3 mm) for each cycle.

The calculated lateral load based on an analysis using flexural theory with the increased axial load is presented in Figure 6.57. Agreement is achieved for Cycles 10, 11, and 12b. The difference in readings for Cycles 12a and 13a are potentially due to further increases in strain hardening of the internal reinforcement.

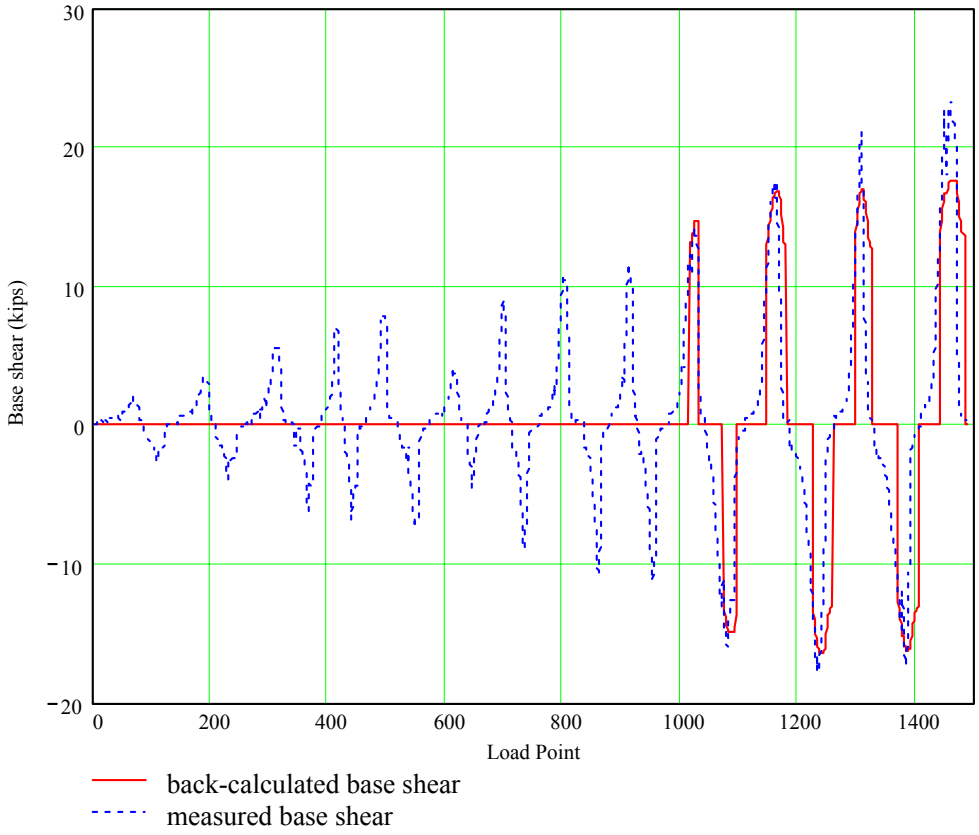

Figure 6.57: Difference in calculated base shear using calculated increase in axial load and measured base shear for Shear Wall Specimen 13

6.7.5.4 Conclusion of increase in axial load

The increase in axial load only affected two specimens. For these two specimens, after the ram bottoms out (or the piston retracts fully inside the ram casing), the amount of reinforcement effectively increases. The behavior changes from a lightly reinforced wall to a heavily reinforced wall, approaching the balance point. The increase in axial load does not affect the drifts achieved in the wall. It does increase the base shear capacity; this implies that Shear Wall Specimens 13 and 16 would have performed equally well or better as a lightly reinforced wall.

CHAPTER 7

Observed Versus Predicted Behavior of AAC Shear Wall Specimens

In the suite of 14 AAC shear wall specimens, 8 were designed as shear-dominated specimens and 6 were designed as flexure-dominated specimens. The wall geometry, prescriptive reinforcement and axial load were selected to force the desired failure mode. The behaviors observed in the shear wall specimens were: flexural cracking; flexure-shear cracking; web-shear cracking; shear strength provided by the reinforcement; sliding shear; crushing of the diagonal strut; nominal flexural capacity; and vertical cracking at the longitudinal reinforcement. All of the shear wall specimens with modular blocks in running bond and panels oriented horizontally behaved as a monolithic wall.

The behavior of Shear Wall Specimen 2, with panels oriented vertically, was distinct due to the formation of vertical cracks. AAC panels oriented vertically have potential planes of failure along continuous head joints. These cracks may be attributed to shrinkage or weak joints, where the thin-bed mortar is not in contact with both panel faces. The presence of vertical cracks can change the behavior of a shear wall specimen. This observed behavior in Shear Wall Specimen 2 is discussed in Section 7.8. Theoretical representations and design methodologies for determining the capacities in flexure and shear are presented in Section 7.10. Sections 7.11 and 7.12 of the Chapter apply these design methodologies to the shear wall specimens constructed of vertical panels.

7.1 FLEXURAL CRACKING

Based on the test data from the shear wall specimens tested at UT Austin, a tensile bond strength of 50 psi (0.34 MPa) is used in the proposed design design provisions. The following sections present the background and justification for this value.

7.1.1 Background Information of Flexural Cracking

In flexural cracking of AAC shear walls, a flexural crack forms at the base of the tensile side of the wall, between the AAC and the leveling bed of ASTM C270 Type S mortar. When the tensile stresses exceed the modulus of rupture of the AAC material or the tensile bond strength of the interface between the AAC material and the leveling bed, a flexural crack forms (Figure 7.1).

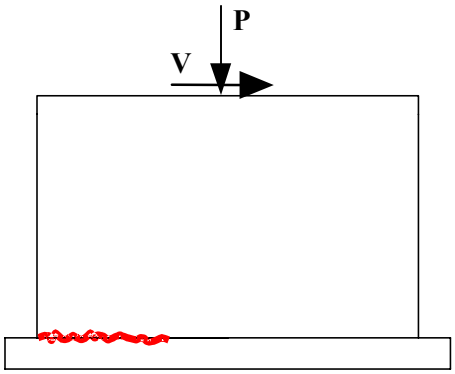

Figure 7.1: Flexural crack

The general form of the proposed equation for flexural cracking is based on principal tensile stresses. A crack will form when the net tensile stress, given by Equation (7.1), exceeds the tensile strength of the material.

$$\frac{M}{S_x} \pm \frac{P}{A_n} > f_r \qquad \text{Equation (7.1)}$$

7.1.2 Test Results for Flexural Cracking

Flexural cracking was observed in 11 shear-wall specimens tested at UT Austin. Flexural cracking is governed by the modulus of rupture of the AAC, or by the tensile bond strength across a leveling bed joint if such a joint is present in the element under consideration. In all cases, these flexural cracks formed between the AAC and the masonry leveling bed. The observed smooth failure surface indicates that the failure was a bond failure rather than an AAC material failure. The flexural cracks occurred in both ends of the wall because the walls were subject to reversed cyclic load. General agreement exists between the lateral load at the first and second occurrence of flexural cracking (V_{cr}). The lateral loads at which flexural cracking was observed and back-calculated tensile bond strengths for each shear wall are listed in Table 7.1.

Table 7.1: Calculated modulus of rupture of AAC shear walls tested at UT Austin

Specimen	Axial Load kips (kN)	First tested V_{cr} kips (kN)	Second tested V_{cr} kips (kN)	First calc. f_{bond} psi (MPa)	Second calc. f_{bond} psi (MPa)
3	120 (534)	65.9 (293)	78.9 (351)	67.1 (0.47)	92.6 (0.64)
4	120 (534)	90.0 (400)	71.5 (318)	117.9 (0.82)	80.9 (0.56)
5	60 (267)	53.9 (240)	54.5 (243)	74.8 (0.52)	75.9 (0.53)
7	80 (356)	29.4 (131)	30.8 (137)	91.1 (0.63)	98.8 (0.69)
9	60 (267)	12.4 (55)	11.4 (51)	77.5 (0.54)	64.7 (0.45)
11	25 (111)	6.8 (30)	4.9 (22)	269.5 (1.87)	175.7 (1.22)
13	25 (111)	7.0 (31)	5.9 (26)	111.7 (0.78)	88.0 (0.61)
14b	5 (22)	2.9 (13)	2.9 (13)	76.5 (0.53)	76.5 (0.53)
15a	5 (22)	8.5 (38)	10.6 (47)	40.3 (0.28)	55.8 (0.39)
15b	25 (111)	7.8 (35)	8.3 (37)	35.1 (0.24)	38.8 (0.27)
16	25 (111)	13.1 (58)	2.4 (11)	74.2 (0.52)	NA
Assemblage	30 (134)	40.8 (0)	36.5 (162)	62.7 (0.44)	54.6 (0.38)
				Mean	68.3
				COV (%)	33

Shear Wall Specimens 4 (first occurrence) and 11 (both occurrences) show the highest modulus of rupture. In both specimens, at least one flexural crack was not observed until it had propagated more than one-quarter the plan length of the wall. Those specimens were not included in the mean calculation and coefficient of variation (COV) because it is probable the flexural crack occurred prior to the observation. The mean tensile bond strength is 68 psi (0.46 MPa), and the COV is 33%. The high COV may be due to differences in amount of water in the leveling bed mortar or different curing conditions of the bed joint. The corresponding 20% fractile is 49.4 psi (0.34 MPa). The lower fractile of 20% is selected because the modulus of rupture is used to determine whether the wall has cracked, and whether its flexural stiffness should be reduced from the gross value to the cracked value. It is generally conservative to underestimate the modulus of rupture, so a lower fractile of 20% was selected. The proposed design value for modulus of rupture should not exceed 50 psi (0.34 MPa) if a leveling bed joint is present in the AAC element. In Table 7.1 data are not presented for three shear-wall specimens. Shear Wall Specimen 1 and Shear Wall Specimen 14b had shrinkage cracks along the bedding mortar joint prior to testing, and multiple flexural cracks had formed in Shear Wall Specimen 2.

7.2 FLEXURE-SHEAR CRACKING

Flexure-shear cracking was observed in the flexure-dominated shear wall specimens. Although the formation of flexure-shear cracks can be predicted, no design provisions are proposed for this behavior because it did not constitute a limit state in the testing program at UT Austin. The following sections present the background and justification for this conclusion.

7.2.1 Background Information for Flexural Shear Cracking of AAC Shear Walls

A flexural shear crack begins as a horizontal crack at a height of about one-half the plan length of the wall (l_w) above the base of the wall, and then propagates diagonally through the center of the wall, as shown in Figure 7.2.

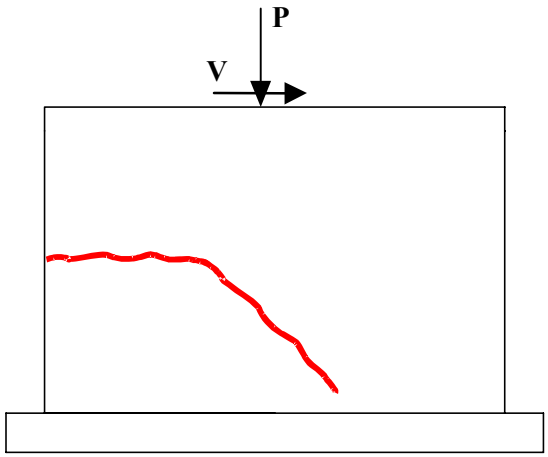

Figure 7.2: Flexural shear cracking

The formation of the horizontal portion of this crack is governed by the flexural tensile stress in the wall (Equation (7.3)).

$$\sigma = \frac{M}{S_x} \pm \frac{P}{A_n} \qquad \text{Equation (7.2)}$$

Based on experiments with reinforced concrete shear walls, the controlling horizontal crack develops at a height of about $l_w/2$. Therefore, the moment at the crack, M_{flcr} is expressed by Equation (7.2).

$$M_{flcr} = M - \frac{Vl_w}{2}$$ Equation (7.3)

In Equation (7.3), M is the moment at the base. Equation (7.4) presents the semi-empirical flexure-shear capacity in US customary units, that forms the basis of Equation (11-30) in ACI 318-02.

$$V_c = \frac{S_x \cdot \left(f_t + \frac{P}{l_w t} \right)}{\left(\frac{M}{V} - \frac{l_w}{2} \right)} + 0.6 \cdot \sqrt{f'_c} \cdot td$$ Equation (7.4)

ACI 318-02 uses a conservative (low) flexural tensile strength of $6\sqrt{f'_c}$ (US customary units); experiments have shown an additional force of $0.6\sqrt{f'_c} \cdot td$ is required to develop the crack (ASCE-ACI Task Committee 426 1973). Therefore, ACI 318-02 uses Equation (7.6) for the flexural shear cracking capacity.

$$V_c = \left[0.6\sqrt{f'_c} + \frac{l_w \left(1.25\sqrt{f'_c} + 0.2\frac{P}{l_w t} \right)}{\frac{M}{V} - \frac{l_w}{2}} \right] \cdot td$$ Equation (7.5)

For AAC the tensile strength calculated using Equation (3.11) can be substituted into Equation (7.5).

7.2.2 Technical Justification for Flexure-Shear Cracking of AAC Shear Walls

Flexure-shear cracking was observed in the six flexure-dominated shear wall specimens. In every case the flexural portion of the flexure-shear crack formed first in the horizontal joint. Flexure-shear cracking was not observed in the eight shear-dominated shear wall specimens tested at UT Austin because the exterior unbonded reinforcement (threaded rods) prevents vertical tensile stresses from forming at the base of the wall after flexural cracking (Figure 4.13).

Based on the location of the flexural crack, the predicted load can be determined based on Equation (7.4) (Table 7.2). For AAC the modulus of rupture was calculated using Equation (3.11) and the tested splitting tensile strength. This value was used in Equation (7.4). For flexure-dominated shear wall specimens, with the exception of Shear Wall Specimen 14a, the ratio of observed load versus predicted load ranges from 0.6 to 1.3. The mean ratio is 0.86 with a COV of 36%.

The observed load is lower than the predicted load because the failure occurred in the joint between the AAC and the thin-bed mortar, rather than in the AAC material itself. A relationship for the tensile bond strength, f_{bond}, between AAC and thin-bed mortar was determined based on tests performed at UAB (Appendix A). Equation (7.6) presents the tensile bond strength for AAC densities greater than 32 pcf (2 kg/m^3). This indicates that for mid- to high-density AAC the tensile bond strength will be lower than the modulus of rupture. The tensile bond strength of the material in the flexure-dominated specimens, except Shear Wall Specimen 13, is 94 psi (0.7 MPa) based on a density of 39.9 pcf (2.5 kg/m^3). Shear Wall Specimen 13 had a density below the limit of 32 pcf (2 kg/m^3); therefore the modulus of rupture will govern the formation of a

flexure-shear crack. The results of using the tensile bond strength rather than the modulus of rupture in Equation (7.4) for the remaining specimens are presented in Table 7.3. With the exception of Shear Wall Specimen 14a, the ratios of observed to predicted strength range from 1.0 to 1.3 with a mean of 1.15 and a COV of 6.5%.

Shear Wall Specimen 14a exhibited flexural cracks at the base of the wall prior to testing. These cracks are presumed to have occurred while moving the top of the wall (out-of-plane) approximately 1 in. (25 mm) to the east to align the rams and loading beam. This would be expected to cause premature out-of-plane flexural cracks on the west side of the wall, which is where the first flexure-shear cracks did in fact occur.

$$f_{bond} = 1.5\rho + 34$$

ρ in lb/ft^3 Equation (7.6)

f_{bond} in lb/in.^{2}

$$f_{bond} = 0.04 f_{AAC} + 66$$ Equation (7.7)

f_{AAC} and f_{bond} in lb/in.^{2}

Table 7.2: Results for flexure-shear cracking of AAC flexure-dominated shear wall specimens

Specimen	f_r psi (MPa)	P kips (kN)	Tested V_{flcr} North kips (kN)	Predicted V_{flcr} North kips (kN)	Tested V_{flcr} South kips (kN)	Predicted V_{flcr} South kips (kN)	Observed V_{flcr} / Predicted V_{flcr} North kips (kN)	Observed V_{flcr} / Predicted V_{flcr} South kips (kN)
13	110 (0.8)	25 (111)	9.6 (43)	8.2 (36)	10.1 (45)	8.0 (36)	1.18	1.26
14a	178 (1.2)	5 (22)	N/A	N/A	2.8 (12)	7.4 (33)	N/A	0.38
14b	178 (1.2)	5 (22)	4.9 (22)	7.4 (33)	4.6 (20)	7.4 (33)	0.66	0.62
15a	178 (1.2)	25 (111)	21.5 (96)	31.9 (142)	24.0 (107)	39.1 (174)	0.71	0.61
15b	178 (1.2)	25 (111)	20.0 (89)	17.9 (80)	17.5 (78)	17.1 (76)	0.66	0.60
16	178 (1.2)	25 (111)	24.0 (107)	31.9 (142)	21.8 (97)	32.4 (144)	0.75	0.67
							Mean	0.86
							COV (%)	36.1

Table 7.3: Results for flexure-shear cracking of AAC flexure-dominated shear wall specimens using tensile bond strength of AAC material

Specimen	f_{bond} psi (MPa)	P kips (kN)	Tested V_{flcr} North kips (kN)	Predicted V_{flcr} North kips (kN)	Tested V_{flcr} South kips (kN)	Predicted V_{flcr} South kips (kN)	Observed V_{flcr} / Predicted V_{flcr} North kips (kN)	Observed V_{flcr} / Predicted V_{flcr} South kips (kN)
13	110 (0.8)	25 (111)	9.6 (43)	8.2 (36)	10.1 (45)	8.0 (36)	1.18	1.26
14a	94 (0.7)	5 (22)	N/A	N/A	2.8 (12)	4.1 (18)	N/A	0.68
14b	94 (0.7)	5 (22)	4.9 (22)	4.1 (18)	4.6 (20)	4.1 (18)	1.19	1.11
15a	94 (0.7)	25 (111)	21.5 (96)	18.7 (83)	24.0 (107)	22.9 (102)	1.15	1.05
15b	94 (0.7)	25 (111)	20.0 (89)	17.9 (80)	17.5 (78)	17.1 (76)	1.12	1.02
16	94 (0.7)	25 (111)	24.0 (107)	18.7 (83)	21.8 (97)	19.0 (84)	1.28	1.15
							Mean	1.15
							COV (%)	6.5

The predictions of Table 7.3 can be repeated with the equivalent equation in terms of compressive strength using Equation (7.7). The resulting average ratio of observed V_{flcr} to predicted V_{flcr} is 1.1, with a COV of 14%.

Design provisions are not proposed for flexure-shear cracking, because that behavior does not constitute a limit state. The formation of the flexural portion of flexure-shear cracks was not accompanied by a decrease in strength or stiffness of the specimens. Examples of the hysteretic behavior are shown in Figure 7.3 through Figure 7.7. In each case at least one load cycle was completed before a significant loss of stiffness was observed. Furthermore, vertical reinforcement was sufficient to maintain shear capacity after flexure-shear

cracking. Based on these observations, no design equations are proposed for flexure-shear cracking.

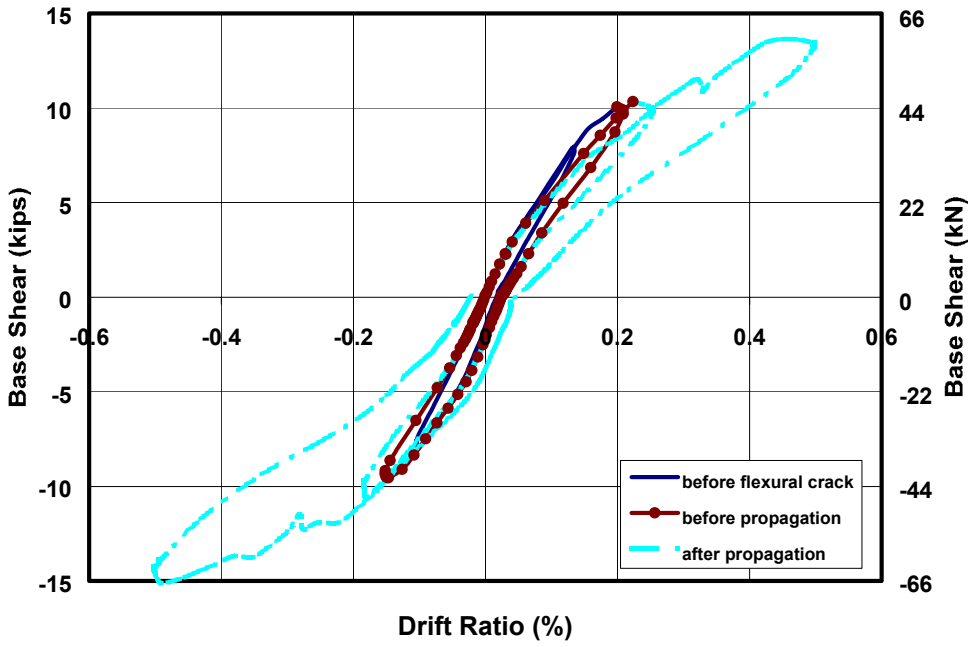

Figure 7.3: Hysteretic behavior of Shear Wall Specimen 13 before and after flexure-shear cracking

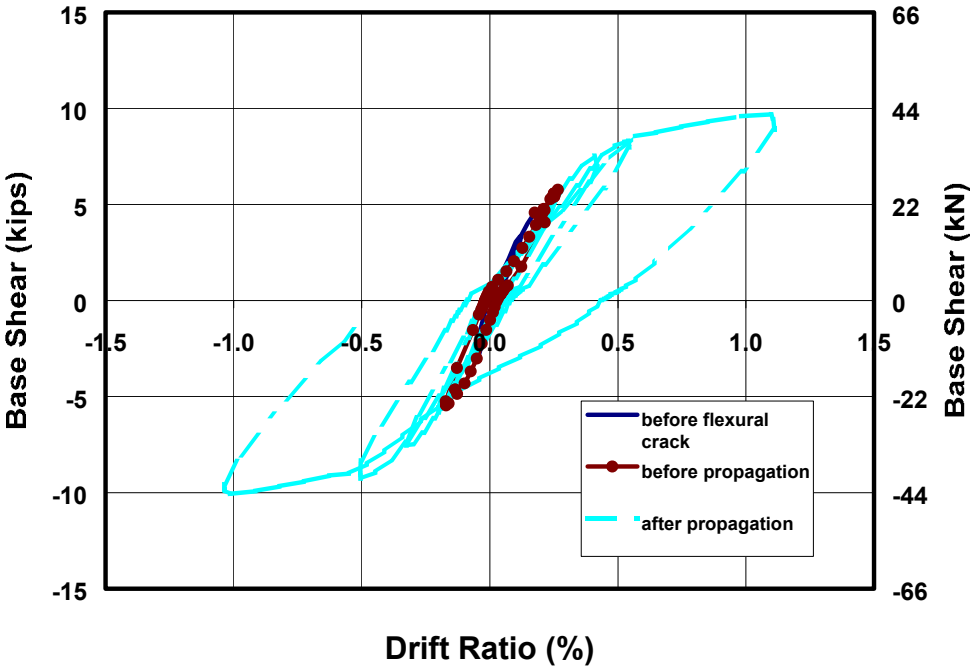

Figure 7.4: Hysteretic behavior of Shear Wall Specimen 14b before and after flexure-shear cracking

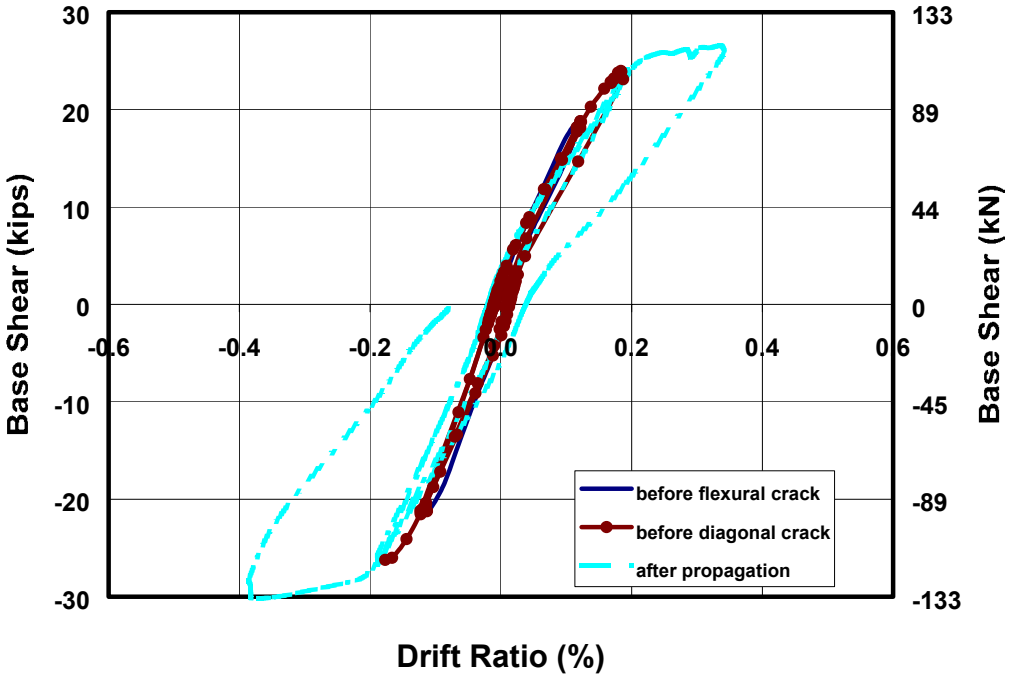

Figure 7.5: Hysteretic behavior of Shear Wall Specimen 15a before and after flexure-shear cracking

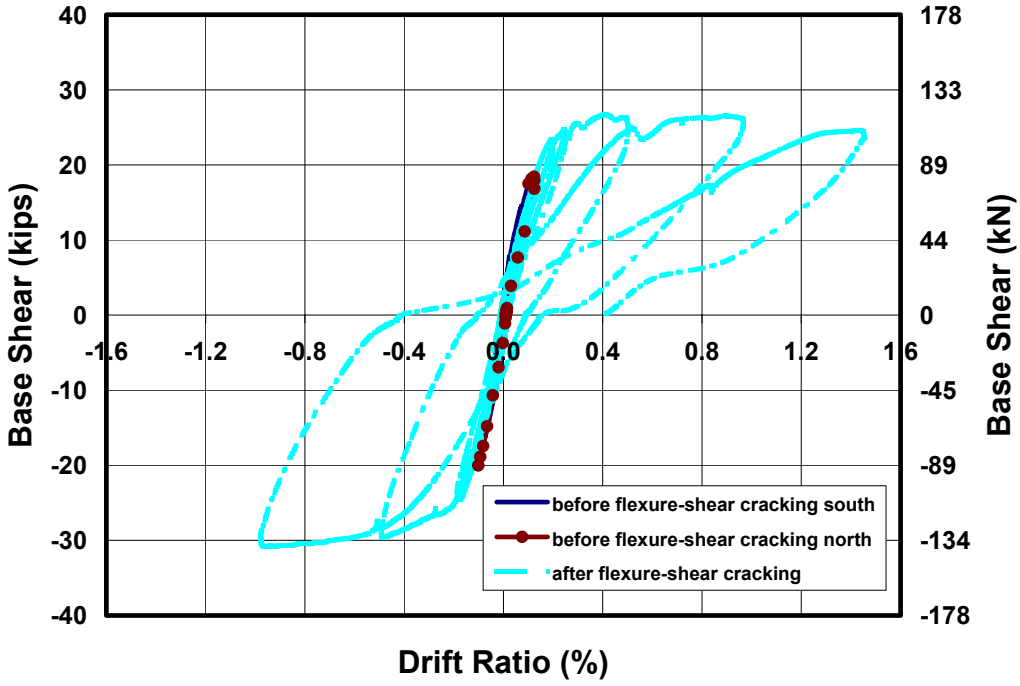

Figure 7.6: Hysteretic behavior of Shear Wall Specimen 15b before and after flexure-shear cracking

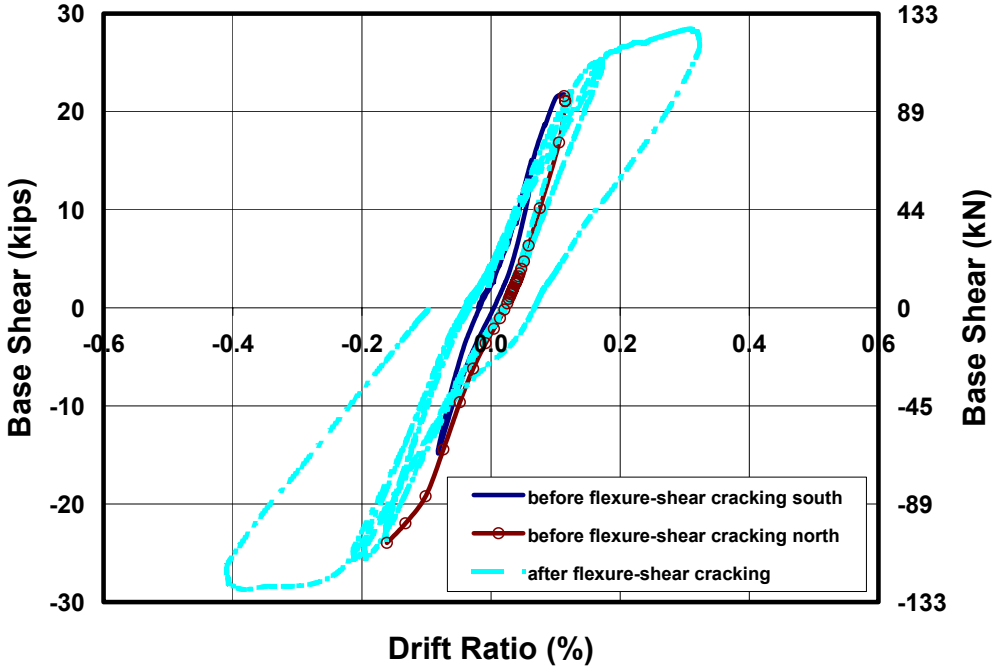

Figure 7.7: Hysteretic behavior of Shear Wall Specimen 16 before and after flexure-shear cracking

7.3 WEB-SHEAR CRACKING

Web-shear cracks formed in the shear wall specimens tested at UT Austin. This data combined with the results of tests performed elsewhere form the basis for design equations to predict web-shear cracking in shear wall specimens constructed of any panel orientation and shear wall specimens constructed of modular blocks with unmortared head joints. The discussion on web-shear cracking begins with an equation to determine the base shear when the maximum principal tensile stresses reach the splitting tensile strength of the material (Section 7.3.1). This equation is modified based on the results of shear wall

specimen tests (Sections 7.3.2 and 7.3.3). The final results based on the proposed equation for web-shear cracking correspond to an average ratio of observed to predicted web-shear cracking capacity of 1.27 with a COV of 17% (Table 7.7 and Figure 7.12).

7.3.1 Background Information for Web-Shear Cracking

Web-shear cracking is the formation of an inclined crack in the web of a shear wall, as shown in Figure 7.8. The crack forms when the principal tensile stresses in the wall exceed the tensile strength of the AAC.

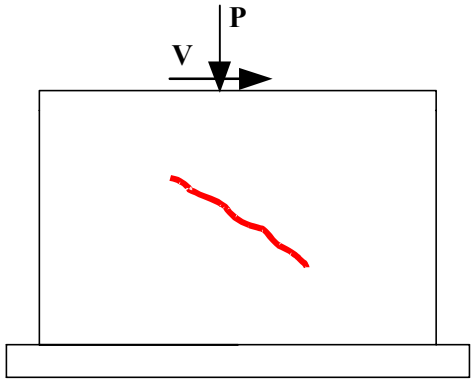

Figure 7.8: Web-shear cracking

This inclined crack forms when the principal tensile stress in the web exceeds the tensile strength of the AAC. That principal stress is given by Equation (7.8), where the normal stress in the wall is *n* and the maximum shear stress in the center of the web is *v*.

$$f_t = \sqrt{\left[\left(\frac{n}{2}\right)^2 + \left(v^2\right)\right]} - \frac{n}{2} \quad \text{where} \quad v = \frac{3V}{2l_w t} \quad \text{and} \quad n = \frac{P}{l_w t} \qquad \text{Equation (7.8)}$$

Substituting the equations for shear stress and axial stress into the above equation, and solving for the base shear, the corresponding shear capacity is given by Equation (7.9).

$$V_m = \frac{2 l_w t}{3} f_t \cdot \left[1 + \left(\frac{P}{f_t l_w t} \right) \right]^{0.5} \qquad \text{Equation (7.9)}$$

For reinforced concrete shear walls, ACI 318-02 uses a conservative (low) tensile capacity of $4\sqrt{f'_c}$ (US customary units) to develop a conservative, semi-empirical equation for capacity as governed by web-shear cracking.

7.3.2 Additional Test Results for Web-Shear Cracking

Results from a suite of 12 shear-wall tests performed by Hebel (Germany) provide additional information[10]. Each of those walls measured 8.2 ft (2.5 m) long, 8.2 ft (2.5 m) tall and 9.5 in. (0.24 m) thick and was constructed of modular blocks. The aspect ratio of each specimen is 1.0. The test set up is shown in Figure 7.9. Additional physical details for each Hebel specimen are presented in Table 7.4.

[10] Personal communication, Violandi Vratsanou, Hebel AG, Germany, November 2000

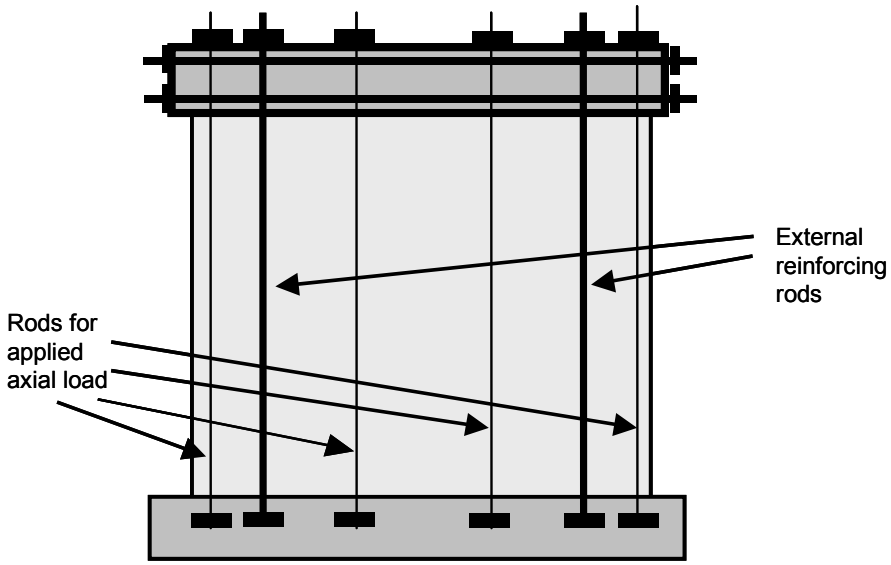

Figure 7.9: Test setup for shear wall specimens at Hebel (Germany)

Table 7.4: Details of shear wall specimens tested by Hebel (Germany)

Specimen	AAC Units	Mortared Head Joints	Type of Running Bond
3.3	Blocks	No	one-half
3.2	Blocks	No	one-half
3.4	Blocks	No	one-half
3.5	Blocks	No	one-fifth
3.6	Blocks	Yes	one-fifth
4.3	Blocks	No	one-half
4.4	Blocks	No	one-half
4.1	Blocks	No	one-half
4.5	Blocks	No	one-fifth
4.6	Blocks	No	one-fifth
4.7	Blocks	Yes	one-fifth
4.8	Blocks	Yes	one-fifth

In the Hebel tests, axial load was applied using uniformly spaced, external post-tensioning rods. This axial load was monitored and was kept constant. Two

additional 1 in. (25 mm) diameter rods on each side of the wall, with initial pre-tension less than 0.5 kip (2 kN), were used as external reinforcement. As the wall displaces laterally in its own plane, tensile forces increase in the external reinforcement on the tension side. The rods on the compressive side of the wall are not initially post-tensioned, so the force in them does not decrease as the force in the tension rods increases. Increasing the force in the tension rods without decreasing the force in the compression rods is equivalent to applying an additional compressive axial load to the wall. Therefore, the axial load in the Hebel specimens changed as the lateral load changed. The axial load used to evaluate the behavior of the Hebel specimens at each state is the initial axial load (including weight of loading equipment) plus the summation of tensile forces in the rods at that state.

7.3.3 Test Results for Web-Shear Cracking

Web-shear cracking was observed in all AAC shear wall specimens tested at The University of Texas at Austin except Shear Wall Specimen 2 (constructed of vertical panels). In addition, the tests performed by Hebel (Germany) provide corroborating data on shear strength as controlled by web-shear cracking.

The relationship between splitting tensile strength and compressive strength is expressed by Equation (3.6). The theoretical equation including this substitution is presented in Equation (7.10). To further evaluate the effects of mortared head joints, the AAC shear-walls tested at UT Austin and by Hebel (Germany) are divided into two groups: those with fully mortared head joints, and those with unmortared head joints. The observed and predicted web-shear cracking capacities based on Equation (7.10) are presented in Table 7.5 and Table 7.6 for fully and partially mortared specimens respectively.

$$V_{AAC} = 1.6\ \ell_w\ t\ \sqrt{f_{AAC}}\ \sqrt{1+\frac{P_u}{2.4\sqrt{f_{AAC}}\ \ell_w\ t}}$$ Equation (7.10)

Table 7.5: Initial predictions of capacity as governed by web-shear cracking for fully- mortared specimens

Specimen	Axial load, P kips (kN)	Observed V_{AAC} kips (kN)	Predicted V_{AAC} kips (kN)	Observed V_{AAC} / Predicted V_{AAC}
1 (UT)	156.0 (694)	164.2 (730)	127.7 (568)	1.29
3 (UT)	120.0 (534)	81.3 (362)	111.4 (495)	0.73
4 (UT)	120.0 (534)	110.5 (492)	132.5 (589)	0.83
5 (UT)	60.0 (267)	62.2 (277)	117.4 (522)	0.53
7 (UT)	80.0 (356)	57.4 (255)	68.7 (305)	0.84
9 (UT)	60.0 (267)	37.7 (168)	55.9 (249)	0.67
11 (UT)	25.0 (111)	15.6 (69)	26.9 (120)	0.58
Assemblage (UT)	25.0 (111)	52.0 (231)	96.7 (430)	0.54
3.6 (Hebel)	36.8 (164)	27.7 (123)	39.3 (175)	0.71
4.7 (Hebel)	62.4 (277)	46.7 (208)	57.7 (256)	0.81
4.8 (Hebel)	178.2 (792)	61.5 (273)	80.3 (357)	0.77
			Mean	0.70
			COV (%)	16.8

Table 7.6: Initial predictions of capacity as governed by web-shear cracking for partially-mortared specimens

Specimen	Axial load, P kips (kN)	Observed V_{AAC} kips (kN)	Predicted V_{AAC} kips (kN)	Observed V_{AAC} / Predicted V_{AAC}
3.3 (Hebel)	60.0 (267)	18.3 (81)	36.2 (161)	0.50
3.2 (Hebel)	26.2 (116)	20.6 (92)	42.0 (187)	0.49
3.4 (Hebel)	49.7 (221)	24.4 (109)	52.2 (232)	0.47
3.5 (Hebel)	89.8 (399)	18.2 (81)	36.7 (163)	0.49
4.3 (Hebel)	30.3 (135)	23.7 (105)	49.4 (220)	0.48
4.4 (Hebel)	30.3 (135)	32.1 (143)	62.7 (279)	0.51
4.1 (Hebel)	85.5 (380)	25.1 (112)	76.7 (341)	0.33
4.5 (Hebel)	153.9 (685)	21.3 (95)	48.5 (216)	0.44
4.6 (Hebel)	33.5 (149)	29.9 (133)	74.5 (331)	0.40
			Mean	0.46
			COV (%)	13.1

The ratios of observed to predicted capacities, shown in Table 7.5, indicate that the ratio of observed strength to predicted strength of Shear Wall Specimen 1 (UT Austin) is significantly greater than that for the other specimens, and can be considered an anomaly with respect to the rest of the tests. The remaining specimens show lower observed than predicted strengths, indicating that Equation (7.10) is unconservative.

The range of ratios of observed V_{AAC} to predicted V_{AAC} is 0.53 to 1.29 for the fully-mortared specimens, and 0.33 to 0.51 for the partially-mortared specimens. For the specimens with fully mortared head joints, the mean ratio of observed to predicted V_{AAC} is 0.70, with a coefficient of variation of 17%. For the specimens with unmortared head joints, corresponding values are 0.46 and 13%.

These data can be plotted in

Figure 7.10 and Figure 7.11. In each figure, the mean ratio of observed capacity to that predicted using the theoretical Equation (7.9) is represented by a solid horizontal line. Also plotted on each figure is the normal distribution with the same mean and COV as the test data. The lower 10% fractile of that distribution, shown by a dashed horizontal line, has a value of 0.55 for the fully mortared specimens and 0.38 for the partially mortared ones.

Equation (7.10) was therefore modified so that it would correspond to the lower 10% fractiles of the ratios of observed to predicted capacities. This lower fractile is selected based on the low COV of test results and the number of specimens. In carrying out that reduction, fully-mortared and partially-mortared specimens were considered separately. Equation (7.10) was multiplied by 0.55 to

obtain proposed Equation (7.11) for fully-mortared specimens. In the same way, Equation (7.10) was multiplied by 0.38 to obtain proposed Equation (7.12) for partially-mortared specimens. These equations are expressed in terms of the specified compressive strength based on Equation (3.6) (Equation (7.13) and Equation (7.14)).

$$V_{AAC} = 0.37\,\ell_w\,t\,f_t\sqrt{1+\frac{P_u}{2.4\sqrt{f'_{AAC}}\,\ell_w\,t}} \qquad \text{Equation (7.11)}$$

$$V_{AAC} = 0.25\,\ell_w\,t\,f_t\sqrt{1+\frac{P_u}{2.4\sqrt{f'_{AAC}}\,\ell_w\,t}} \qquad \text{Equation (7.12)}$$

$$V_{AAC} = 0.9\,\ell_w\,t\sqrt{f'_{AAC}}\sqrt{1+\frac{P_u}{2.4\sqrt{f'_{AAC}}\,\ell_w\,t}} \qquad \text{Equation (7.13)}$$

$$V_{AAC} = 0.6\,\ell_w\,t\sqrt{f'_{AAC}}\sqrt{1+\frac{P_u}{2.4\sqrt{f'_{AAC}}\,\ell_w\,t}} \qquad \text{Equation (7.14)}$$

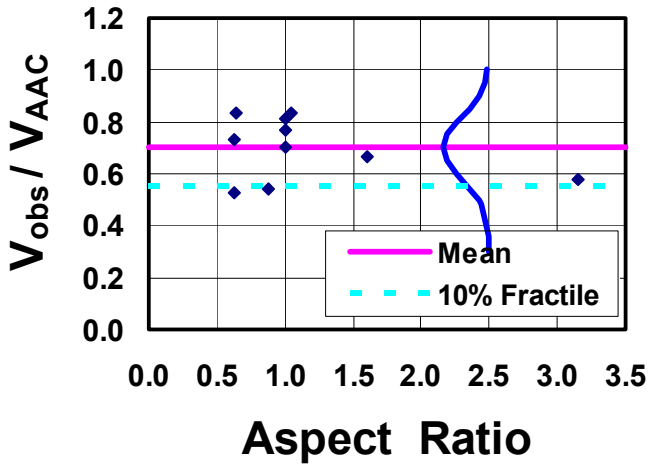

Figure 7.10: Ratios of observed to predicted (Equation (7.11)) web-shear cracking capacities for AAC shear-wall specimens with fully-mortared head joints

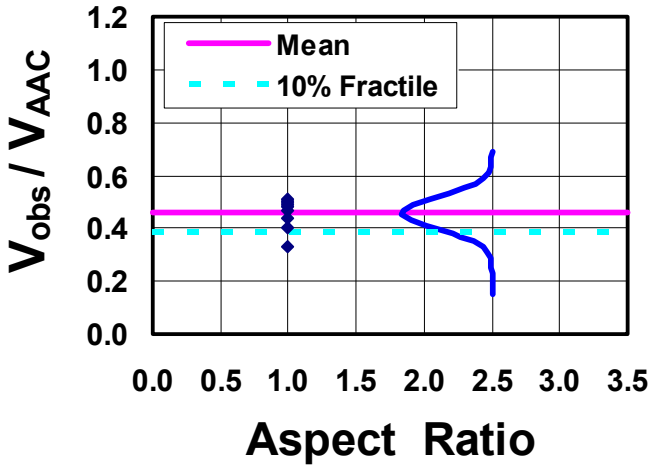

Figure 7.11: Ratios of observed to predicted (Equation (7.12)) web-shear cracking capacities for AAC shear-wall specimens with partially-mortared head joints

The predicted V_{AAC} using Equation (7.11) and Equation (7.12) are presented in Table 7.7 and Table 7.8 for all specimens that exhibited web-shear cracking. Ratios of observed V_{AAC} versus predicted V_{AAC} using Equation (7.11) and Equation (7.12) based on the tested compressive strength are presented graphically in Figure 7.12. In that figure, a solid diagonal line represents perfect agreement between observed and predicted shear capacities. The proposed equations are very close, or have slight errors in the direction of conservatism, for the specimens tested. If the ACI 318-02 equation for web-shear cracking is used directly for AAC (substituting f_{AAC} for f_c), the predicted capacity is greater than that observed, and hence unconservative. This is also true if the ACI 318-02 equation for web-shear cracking is used with equivalent expressions for the tensile strength of concrete and for AAC. The web-shear cracking capacity will

be further reduced by using the specified compressive strength rather than the tested compressive strength.

Table 7.7: Prediction of capacity as governed by web-shear cracking for fully-mortared specimens using Equation (7.11) with tested compressive strength

Specimen	Axial load, P kips (kN)	Observed V_{AAC} kips (kN)	Predicted V_{AAC} kips (kN)	Observed V_{AAC} / Predicted V_{AAC}
1 (UT)	156.0 (694)	164.2 (730)	70 (312)	2.34
3 (UT)	120.0 (534)	81.3 (362)	61 (273)	1.33
4 (UT)	120.0 (534)	110.5 (492)	73 (324)	1.52
5 (UT)	60.0 (267)	62.2 (277)	65 (287)	0.96
7 (UT)	80.0 (356)	57.4 (255)	38 (168)	1.52
9 (UT)	30.0 (267)	37.7 (168)	31 (137)	1.22
11 (UT)	25.0 (111)	15.6 (69)	15 (66)	1.05
Assemblage (UT)	26.0 (116)	52.0 (231)	53 (237)	0.98
3.6 (Hebel)	36.8 (164)	27.7 (123)	22 (96)	1.28
4.7 (Hebel)	62.4 (277)	46.7 (208)	32 (141)	1.47
4.8 (Hebel)	178.2 (792)	61.5 (273)	44 (197)	1.39
			Mean	1.27
			COV (%)	16.8

Table 7.8: Prediction of capacity as governed by web-shear cracking for unmortared head joints using Equation (7.12) with tested compressive strength

Specimen	Axial load, P kips (kN)	Observed V_{AAC} kips (kN)	Predicted V_{AAC} kips (kN)	Observed V_{AAC} / Predicted V_{AAC}
3.3 (Hebel)	26.2 (116)	18.3 (81)	14 (61)	1.33
3.2 (Hebel)	49.7 (221)	20.6 (92)	16 (71)	1.29
3.4 (Hebel)	89.8 (399)	24.4 (109)	20 (88)	1.23
3.5 (Hebel)	26.6 (118)	18.2 (81)	14 (62)	1.30
4.3 (Hebel)	30.3 (135)	23.7 (105)	19 (84)	1.26
4.4 (Hebel)	85.5 (380)	32.1 (143)	24 (106)	1.35
4.1 (Hebel)	153.9 (685)	25.1 (112)	29 (130)	0.86
4.5 (Hebel)	33.5 (149)	21.3 (95)	18 (82)	1.15
4.6 (Hebel)	158.1 (703)	29.9 (133)	28 (126)	1.06
			Mean	1.21
			COV (%)	13.1

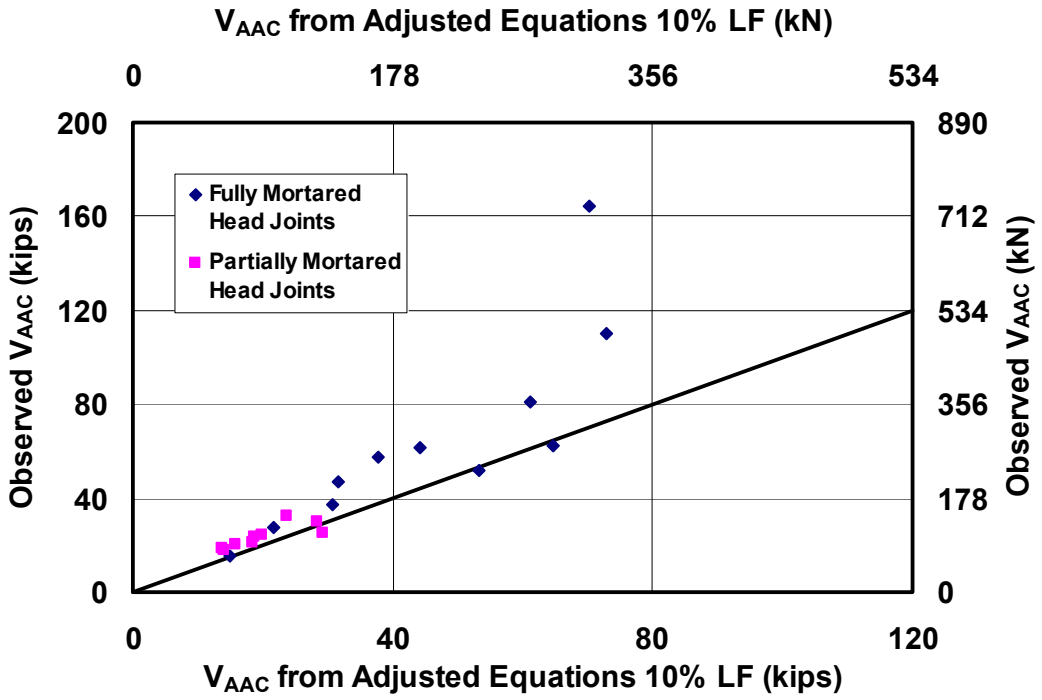

Figure 7.12: Observed versus predicted capacities as governed by web-shear cracking (Equation (7.11) and Equation (7.12)) using tested compressive strength

7.4 Shear Strength Provided by the Reinforcement in Horizontal Panels

The proposed design provisions permit the contribution of deformed horizontal reinforcement that is embedded in grout. They conservatively neglect the contribution of all other horizontal reinforcement embedded in AAC, based on the observed behavior of shear wall specimens tested at UT Austin and elsewhere. The following sections present background information on shear reinforcement,

development of a model for shear reinforcement in AAC and technical justification based on test results of AAC shear walls.

7.4.1 Background Information of Shear Reinforcement

In conventional reinforced concrete design, the contribution of shear reinforcement, V_s, is included by adding it directly to the nominal shear cracking capacity of the concrete, as in Equation (7.15).

$$V_n = V_c + V_s \qquad \text{Equation (7.15)}$$

This approach is based on the observations that the nominal shear capacity due to concrete is not less than that required to produce the shear crack in the first place, and that the bond between concrete and reinforcing steel is strong enough to permit the shear reinforcement to yield.

In masonry, the general form of the above approach is preserved, with slightly different equations for evaluating V_m, and an effectiveness factor of ½ for the shear reinforcement to reflect the non-uniform strain in the shear reinforcement over the height of the shear crack.

In AAC shear walls, the above approach is questionable, for the following reasons:

1) Because the fracture surfaces at shear cracks in AAC are smoother than for conventional concrete, and because those surfaces degrade more readily in friction than those of conventional concrete, the nominal shear

capacity of AAC may decrease below the value of shear originally required to produce shear cracking.

2) Because the bond strength and crushing capacity of AAC are much lower than those of conventional concrete, the capacity of shear reinforcement may be less than its yield strength.

7.4.2 Proposed Mechanism for Shear Resistance of Shear Reinforcement in AAC Elements

AAC panels are reinforced with a welded wire fabric that has horizontal and vertical wires. In horizontally oriented AAC panels, the horizontal wire is available to provide some shear capacity. Capacity of the shear reinforcement is limited by yielding of the horizontal wires and bearing of the vertical wires on the AAC. If the vertical spacing of horizontal wires is small compared to the horizontal spacing of cross wires, the capacity of the shear reinforcement can be governed by crushing of the AAC under the cross wires.

A free-body diagram for a single layer of welded wire fabric used in horizontal AAC panels is shown in Figure 7.13. The capacity of the horizontal wires is limited by the bearing capacity of the AAC supporting the vertical wires. Bond strength of the horizontal wire is conservatively neglected, because of the gaps that exist between the wires and AAC (due to porosity of the AAC) combined with the smooth, corrosion-resistant coating on the wires.

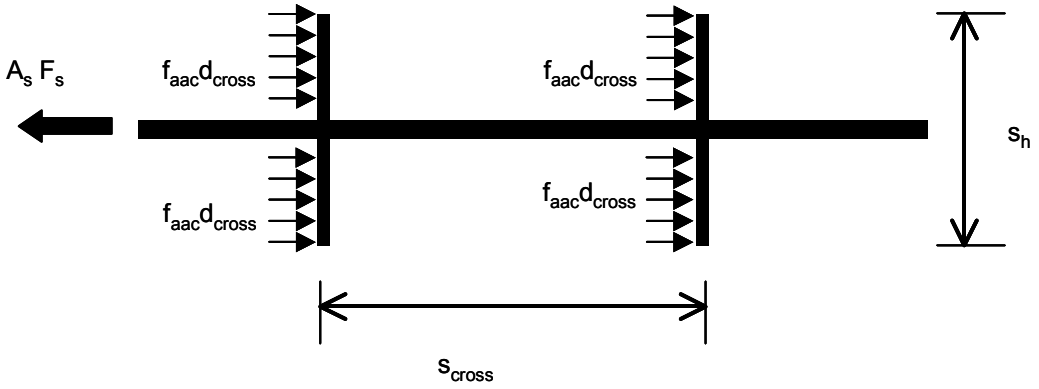

Figure 7.13: Forces acting on welded wire fabric in an AAC panel

Based on horizontal equilibrium, the maximum stress in the horizontal wire can be determined using Equation (7.16). If this stress is smaller than the yield stress, bearing on the AAC controls.

$$f_s = n_{cross} s_h \frac{d_{cross}}{A_s} f_{AAC} \qquad \text{Equation (7.16)}$$

The number of vertical wires that contribute to bearing resistance depends on the panel length and location. For each panel, a minimum number of cross wires exists to provide bearing resistance to equilibrate the force in the horizontal wires. This number of vertical cross wires can be computed based on the hypothetical crack location and the layout of the panels comprising the wall. Because it is simplest, first consider the stack-bonded wall shown in Figure 7.14, depicting a 20 ft. by 12 ft. shear wall with a 45-degree crack passing through the lower compression corner. The capacity of each horizontal wire depends on its minimum (critical) length on either side of the hypothetical shear crack. The

average number of vertical cross wires that can bear against the AAC is the average critical length divided by the spacing of the vertical cross wires.

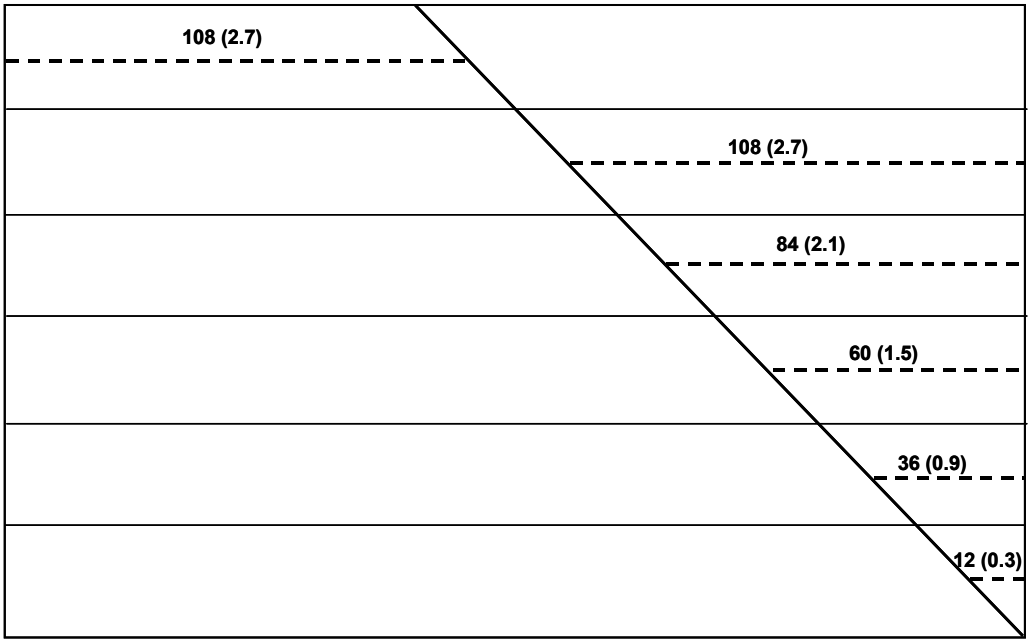

Figure 7.14: Critical lengths in in. and (m) for a 20 ft (6.3 m) AAC shear wall composed of 2 ft (0.6 m) high stack-bonded panels

Once the maximum stress in the horizontal wires is determined, the corresponding lateral capacity, V_s is calculated by Equation (7.17). Equation (7.18) represents the final equation to predict the additional shear capacity as governed by bearing stresses under vertical cross wires.

$$V_s = n_h f_s A_v \qquad \text{Equation (7.17)}$$

$$V_s = L_{avg} \cdot \frac{s_h}{s_{cross}} \cdot \frac{d_{cross}}{A_s} \cdot f_{AAC} \cdot n \cdot A_v$$

Equation (7.18)

Equation (7.18) is an upper bound to the shear capacity. The following factors can decrease the effectiveness of the contribution of the horizontal steel:

- bond pattern or angle of crack formation;
- cyclic load; and
- variation in wire strain over wall height.

Each is discussed in the following sections.

7.4.2.1 Loss of effectiveness of shear reinforcement due to panel bond pattern or angle of crack formation

Panels placed in running bond can have shorter critical lengths than panels placed in stack bond. An offset bond pattern results in a longer effective length than a perfect (half) running bond pattern. The panel length will also change the critical length. The concept of decreased average critical lengths for running bond patterns can be seen in the example of Figure 7.15 (with 4 ft. small panels and 12 ft. medium panels) where average critical lengths are shown for different angles and location of crack formation. The critical lengths for the same angle and crack locations on walls oriented in a stack bond pattern are listed in Figure 7.15.

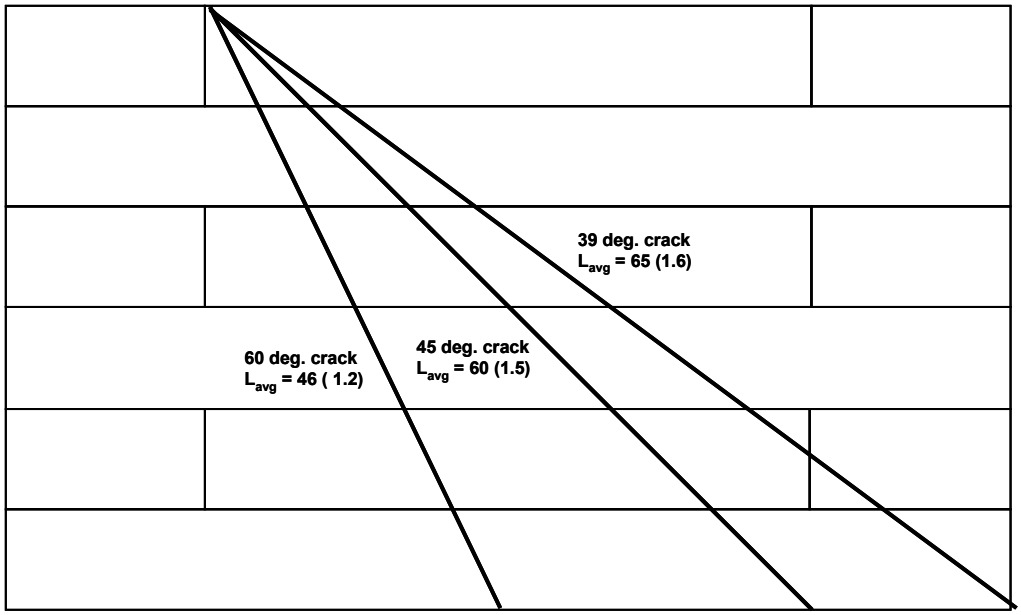

Figure 7.15: Average critical length calculations for different crack angles for a wall with offset running bond

Table 7.9: Critical lengths for stack bond pattern versus offset running bond pattern

Crack Angle degrees	L_{avg} for offset running bond in. (m)	L_{avg} for stack bond in. (m)	Ratio of L_{avg} for running bond to L_{avg} stack bond
60	46 (1.2)	70 (1.8)	0.66
45	60 (1.5)	84 (2.1)	0.71
39	65 (1.7)	89 (2.3)	0.73

7.4.2.2 Loss of effectiveness of shear reinforcement due to cyclic loading

When AAC fails in bearing, it deforms by crushing of voids. In the particular case of shear reinforcement, crushing of AAC ahead of the vertical cross wires is associated with displacement of the cross wires with respect to the

surrounding AAC matrix. When the AAC ahead of the cross wires crushes, a void forms behind the cross wires (Figure 7.16). Under reversed cyclic loading voids form ahead of and behind the cross wires (Figure 7.17). Until the lateral drift ratio of the wall increases enough for the cross wires to move through this void and again bear on the AAC, the shear resistance due to horizontal reinforcement is negligible.

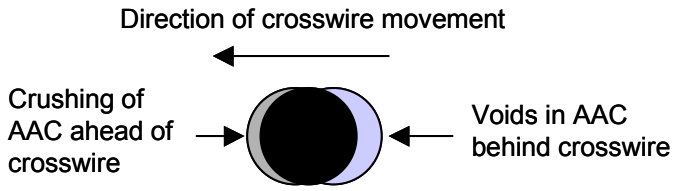

Figure 7.16: Voids caused by the crushing of AAC under monotonic loading

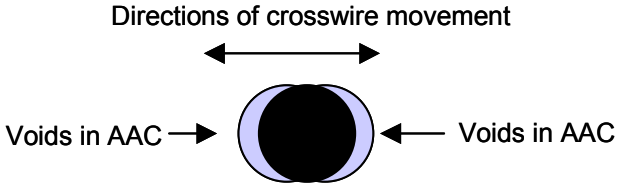

Figure 7.17: Voids caused by the crushing of AAC under cyclic loading

7.4.2.3 Loss of effectiveness of shear reinforcement due to wire participation

The horizontal wires may not all be subject to the same longitudinal strain. For example, a diagonal shear crack can be wider at the top than the bottom.

7.4.3 Test Results for Shear Reinforcement

Three shear-dominated wall specimens, tested at UT Austin, were made of horizontal panels with welded-wire reinforcement. One test performed at Hebel (Germany)[11], Test Specimen 5.2, includes the influence of horizontal reinforcement. This specimen was not included in the web-shear cracking predictions presented earlier in this report, because the data to determine the axial load at cracking was unreported. The difference between their maximum shear capacity (V_n) and the base shear at web-shear cracking (V_{AAC}) provides an estimate of the contribution of the welded-wire reinforcement. The observed contribution of the welded-wire reinforcement can be predicted by Equation (7.11). The predicted shear strength contribution can be determined based on Equation (7.16). This data with the resulting ratios of observed V_s to predicted V_s are presented Table 7.10.

Table 7.10: Observed increase in shear capacity based on contribution of dowels

Specimen	Maximum Capacity V_n kips (kN)	Observed V_{AAC} kips (kN)	Observed V_s (V_n-V_{AAC}) kips (kN)	Predicted V_s kips (kN)	Ratio of observed V_s to predicted V_s
1	167.6 (746)	164.2 (731)	3.4 (15)	27.0 (120)	0.13
4	126.4 (562)	110.5 (492)	15.2 (72)	130.2 (580)	0.12
9	42.4 (189)	37.7 (168)	4.7 (21)	34.5 (153)	0.14
5.2 Hebel	59.4 (264)	29.5 (131)	29.9 (133)	17.3 (77)	1.73

The ratios of observed V_s to predicted V_s range from 0.13 to 1.73. The contribution of the welded-wire reinforcement is limited to 0.13 in three of the four specimens. An alternate method to determine the contribution of the welded

[11] Personal communication, Violandi Vratsanou, Hebel AG, Germany, July 1999.

wire reinforcement is to calculate an average bond strength associated with bearing of the cross-wires on the AAC. The estimate depends on the following assumptions:

- All cross-wires in a critical length of panel bear on the AAC with a maximum stress equal to the compressive strength of the AAC; and
- All cross-wires that cross the web-shear crack participate equally.

Furthermore, the transfer of shear across the web-shear crack is unknown. The average bond strength can be estimated for two limiting conditions: 1) all of V_{AAC} is resisted by shear across the crack; and 2) none of V_{AAC} is resisted by shear across the crack. The results of for each shear wall specimen are presented in Table 7.11.

Table 7.11: Calculated range of bond strengths for welded-wire fabric based on shear walls tested at UT Austin

Specimen	Maximum Capacity V_n kips (kN)	Observed V_{AAC} kips (kN)	u with V_{AAC} psi (kPa)	u without V_{AAC} psi (kPa)
1	167.6 (746)	164.2 (731)	1.7 (12)	86 (592)
4	126.4 (562)	110.5 (492)	2.9 (20)	23 (157)
9	42.4 (189)	37.7 (168)	3.2 (22)	29 (200)
5.2 Hebel	59.4 (264)	29.5 (131)	23 (156)	45 (310)

The average bond stresses range from nearly 2 psi (12 kPa) to 23 psi (156 kPa) considering the contribution of shear transfer across the web-shear crack. The average bond stresses range from 23 psi (157 kPa) to 86 psi (592 kPa). The low results where the contribution of the AAC is included indicate that little shear is transferred along the interface of the web-shear crack or the contribution of welded-wire fabric is negligible.

Another possibility for increased shear strength is the redistribution of load in a shear wall after web-shear cracking, as observed in Shear Wall Specimen 3, an unreinforced specimen. This specimen was identical to Shear Wall Specimen 4; each specimen had the same geometry and an axial load of 120 kips (534 kN). Shear Wall Specimen 3 was unreinforced while Shear Wall Specimen 4 was constructed with horizontal panels with wire reinforcement. For Shear Wall Specimen 3, the lateral load at web-shear cracking and the maximum lateral load are 81.3 kips (362 kN) and 118.3 kips (526 kN). For Shear Wall Specimen 4, the corresponding values are 110.5 kips (492 kN) and 126.4 kips (562 kN). It is not clear how much of the strength beyond shear cracking in Shear Wall Specimen 4 is due to the horizontal reinforcement, since a similar unreinforced wall (Shear Wall Specimen 3) showed almost the same increase in strength after web-shear cracking.

At this time, the reduction in V_s, while potentially significant, cannot be quantified due to its dependence on loading history. The conservative recommendation for design is to neglect the contribution of horizontal reinforcement to shear capacity, unless the horizontal reinforcement is in the form of deformed reinforcement embedded in grout.

7.5 SLIDING SHEAR CAPACITY

Resistance to sliding shear in a shear wall may be provided by axial load and dowel action of reinforcement perpendicular to the plane of sliding. Tests performed at UT Austin indicate the effectiveness of the dowel action decreases as the level of damage around a dowel increases. The final conclusion is to conservatively neglect the contribution of the dowels in determining the sliding

shear capacity. The following sections present background information on sliding shear mechanisms and a technical justification based on test results of Shear Wall Specimen 4 and the Two-story Assemblage Specimen.

7.5.1 Background Information for Sliding Shear Capacity

An AAC shear wall of horizontal panels or masonry-type blocks exhibits a bed-joint crack when the shear stress on the bed joints exceeds the interface shear capacity, ν. An AAC shear wall subject to sliding shear across a horizontal bed joint is presented in Figure 7.18. After the crack forms the shear is resisted by the vertical reinforcement and frictional forces due to the axial load.

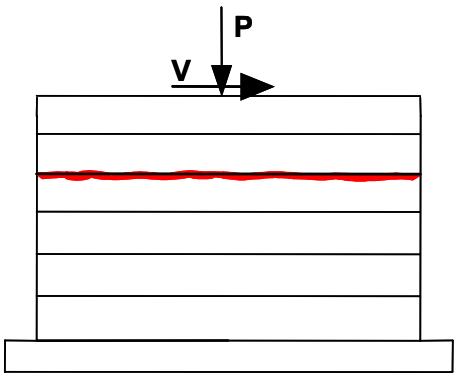

Figure 7.18: Formation of bed-joint crack in an AAC shear wall with horizontal panels

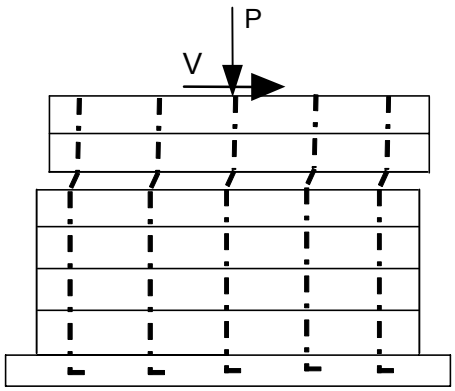

Figure 7.19: Sliding shear mechanism in an AAC shear wall with horizontal panels

After the crack forms, some resistance will be provided by shear friction across the bed joints:

$$V_{ss} = \mu\left(A_v f_s + P_u\right) \qquad \text{Equation (7.19)}$$

Sliding shear resistance is the product of the coefficient of friction across an interface, and the force acting perpendicular to that interface. This mechanism is referred to as "shear friction" in ACI 318. This resistance can come from reinforcement crossing the interface, and from applied axial load.

In the traditional shear friction mechanism, sliding over a rough joint causes one section of the crack to lift upwards; this results in yielding of the vertical reinforcement, which provides additional clamping force. Under reversed cyclic loading of AAC, the roughness of the bed joints can decrease, and resistance to sliding shear is provided by dowel action of reinforcement crossing the bed joints. This contribution to V_{ss} is the product of the area of the

reinforcement perpendicular to the crack and the shear resistance of the bars, $0.6f_y$. This contribution to the sliding shear mechanism is shown in Figure 7.21.

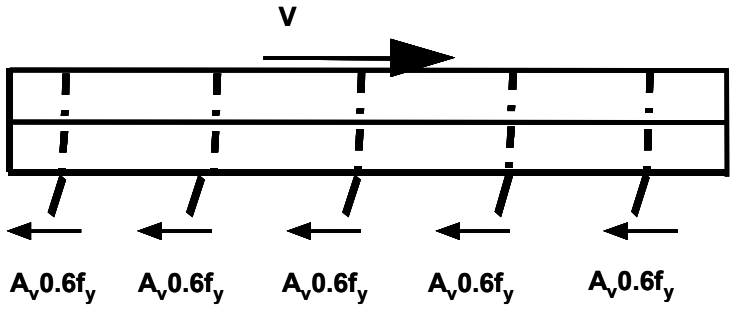

Figure 7.20: Internal lateral forces generated by dowel action along plane of sliding shear mechanism

Frictional resistance is the second component of resistance due to sliding shear. Figure 7.21 is a free-body diagram showing the horizontal equilibrium under frictional forces. Although sliding is associated with gradual deterioration of the interface, it is not associated with the crushing described in Section 7.6.

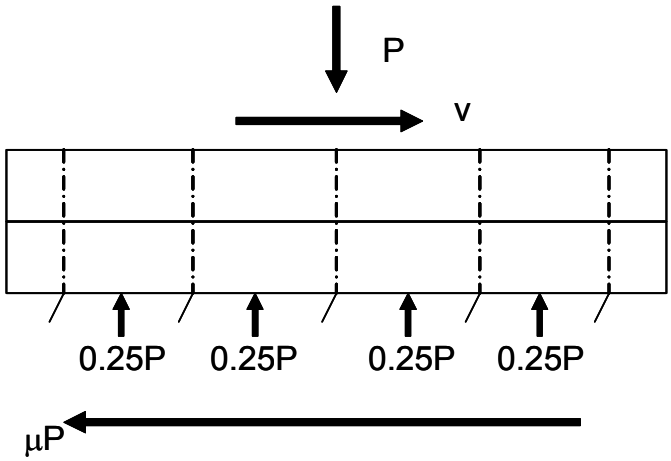

Figure 7.21: Internal lateral forces generated by friction along plane of sliding for sliding shear mechanism

$$V_{ss} = \mu P_u + 0.6 A_s f_y \qquad \text{Equation (7.20)}$$

7.5.2 Test Results for Sliding Shear Capacity

Sliding was observed at four times during the testing of Shear Wall Specimen 1 (UT Austin). Since no vertical reinforcement was present in the wall, the sliding shear resistance came from axial load alone. At each occurrence of sliding the axial load was increased, providing four data points for sliding shear resistance between the leveling bed and the AAC shear wall. The coefficient of friction was calculated by dividing the lateral load by the corresponding applied axial load at each occurrence of sliding. The average of the four coefficients of friction is 1.0, with a COV of 4%.

In subsequent specimens, the clamping force P was determined such that the shear capacity will be limited by web-shear cracking or flexure-shear

cracking, rather than bed-joint sliding. Sliding shear was avoided in 12 out of the remaining 14 specimens; it was observed in Shear Wall Specimen 4 and the Two-story Assemblage Specimen. Since the specimens were designed to avoid sliding shear, sufficient dowels were placed to ensure that V_{ss} was significantly greater the V_{AAC}. In four specimens, V_{max} was greater than V_{AAC}. Shear Wall Specimen 3 and Shear Wall Specimen 5 were both overdesigned in sliding shear. The load did not reach the sliding shear capacity because the specimen capacities were limited by distributed web-shear cracking. Shear Wall Specimen 4 and the Two-story Assemblage Specimen are used to determine the effectiveness of Equation (7.20).

The hysteretic behavior of the Two-story Assemblage Specimen is shown in Figure 7.22. The total base shear and sliding shear capacity for the specimen versus Load Point is presented in Figure 7.23. The design sliding shear capacity is presented for the contribution of axial load and dowels (Equation (7.20)) and the contribution of axial load only. A coefficient of friction of 1.0 was used since the sliding plane occurred between the vertical panels and the leveling bed mortar. The entire axial load was applied through gravity; therefore, the axial load remained constant throughout the test. In this specimen the longitudinal steel and dowels contribute significantly to the capacity for several cycles. Damage around the dowels began at Load Point 677 and continued throughout the test. Each loading cycle was accompanied by increasing damage. The cumulative damage at each cycle is accompanied by a continually decreasing base shear, as shown in load points above 700 in Figure 7.23.

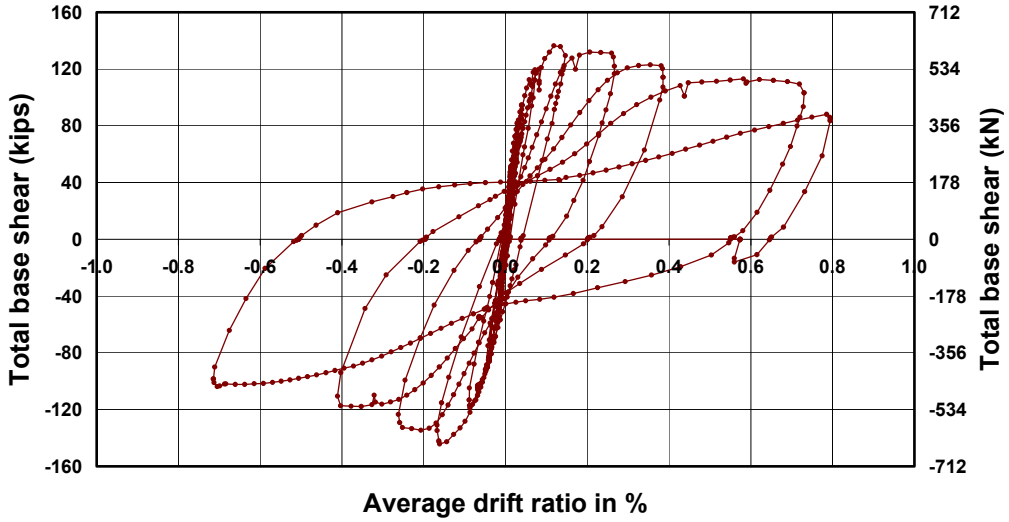

Figure 7.22: Hysteretic behavior of Two-story Assemblage Specimen

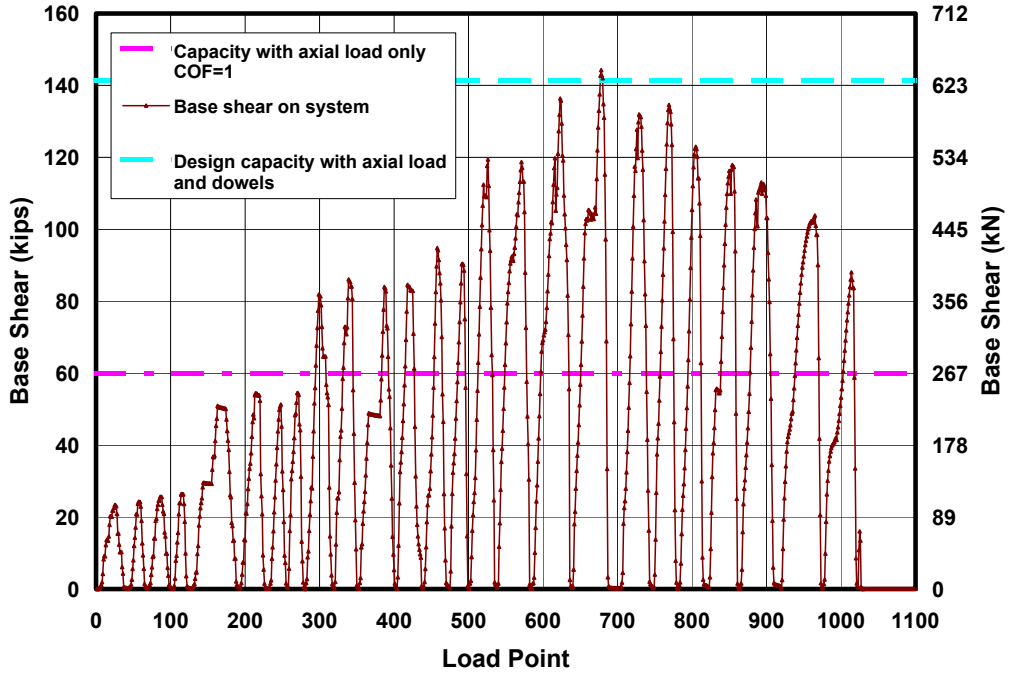

Figure 7.23: Base shear and sliding shear capacity versus Load Point for Two-story Assemblage Specimen

Sliding was observed in two adjacent panels in Shear Wall Specimen 4. A horizontal crack formed along the bed joint between the second and third courses. This crack formed in three stages, corresponding to Load Points 634, 717 and 764. The final crack propagation occurred after the maximum base shear was reached. A graph of base shear versus load point for Shear Wall Specimen 4 is shown in Figure 7.24. Since the sliding occurred between panels, a coefficient of friction of 0.75 was used to predict the capacity. The applied base shear increased beyond the sliding shear resistance for the level of axial load that was applied to the specimen. Several diagonal cracks formed at the compression toes of the walls. Spalling between these cracks occurred at Load Point 871.

The axial load consisted of three portions: gravity load from loading equipment; load applied through the load maintainer; and post-tensioning force in the rods. The pressure in the load maintainer system was checked during testing. It did not change, nor did the contribution of axial load due to gravity. Any decrease in axial load would therefore have to have occurred due to a loss of post-tensioning. This was observed in the spalling of the compression toe that occurred at Load Point 871. The loss of post-tensioning decreased the applied axial load and thus decreased the sliding shear capacity.

The measured axial load capacity of Figure 7.25 includes the unchanged axial load and the measured force in the external rods. As the base shear increases, a slight increase is also observed in the axial load (Load Point 1080 through 1110). This is the increase in load in the axial rods caused by the in-

plane rotation of the wall about its compression toe. At later load points, at points of zero base shear the force in the rods decreases due to toe crushing. This can be observed in the difference between measured axial loads at two points where the base shear is zero. For example, at Load Point 830 the measured axial load is 91 kips (405 kN); at Load Point 890 it decreases to 87 kips (387 kN); and at Load Point 960 it further decreases to 82 kips (365 kN).

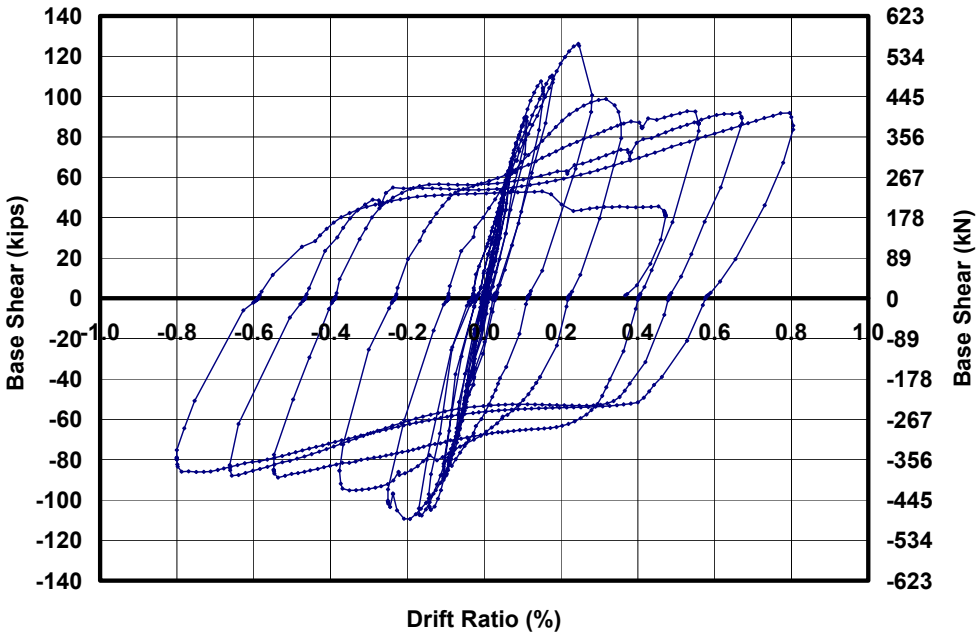

Figure 7.24: Hysteretic behavior of Shear Wall Specimen 4

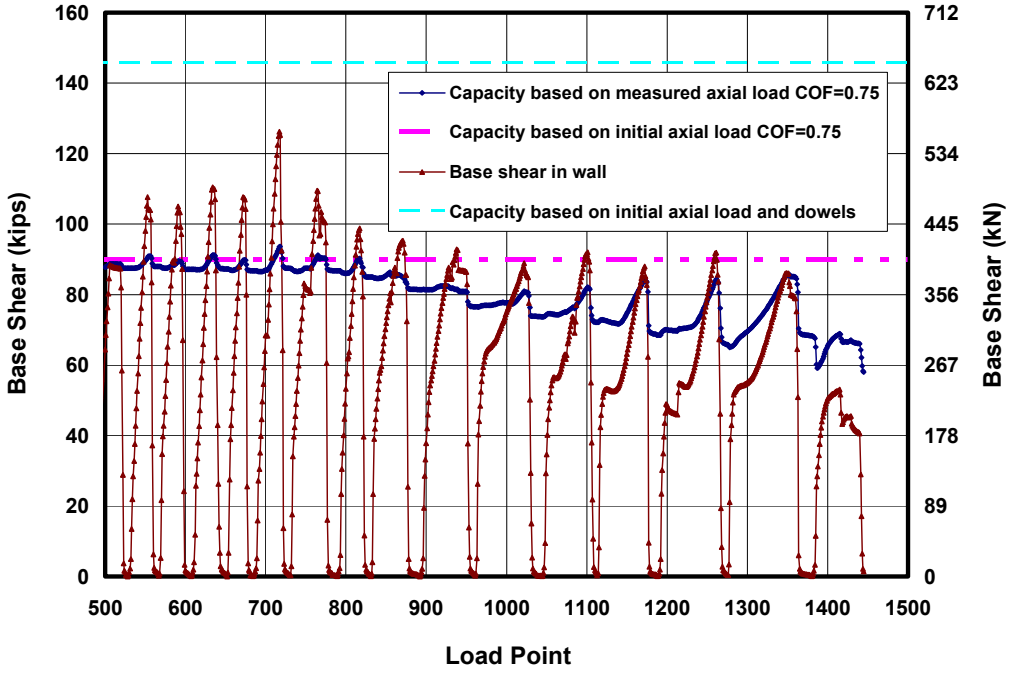

Figure 7.25: Base shear and sliding shear capacity versus Load Point for Shear Wall Specimen 4

For load points beyond 700 the base shear capacity decreases. This was also observed in the Two-story Assemblage Specimen. This is a further indication that as damage increases the effectiveness of the dowel action decreases. As the damage increases, the resistance provided by bearing on the dowel is reduced. For this reason, the proposed design provisions conservatively neglects the contribution of the dowels as shown in Equation (7.21).

$$V_{ss} = \mu P_u \qquad \text{Equation (7.21)}$$

Structures with small axial load may have low sliding shear capacity. In these cases the interface shear strength between AAC and thin-bed mortar may be

used. Based on the direct shear tests performed at UT Austin, the average interface shear strength between AAC and thin-bed mortar was 64 psi (441 kPa), with a COV of 44%. Based on this larger COV, a lower 5% fractile is proposed, for design, reducing the interface shear strength to 18 psi (117 kPa). This value is conservative compared to test results of 45 psi (310 kPa) to 82 psi (565 kPa) determined in shear tests performed at the University of Alabama at Birmingham (Argudo 2003).

The measured axial load in Figure 7.25 does not include the tensile forces in the internal reinforcement. Although those forces were not measured, they were estimated based on flexural calculations. The wall instrumentation indicates that the longitudinal reinforcement in the wall had yielded at the bed joint where sliding occurred. When the lateral load is removed and the bed-joint gap closes, the bars will be subject to compression. Based on an assumed debonded bar length, the compressive forces can be estimated. The solid vertical lines at points of zero lateral load, show the revised axial load considering compressive stresses in longitudinal reinforcement (Figure 7.26).

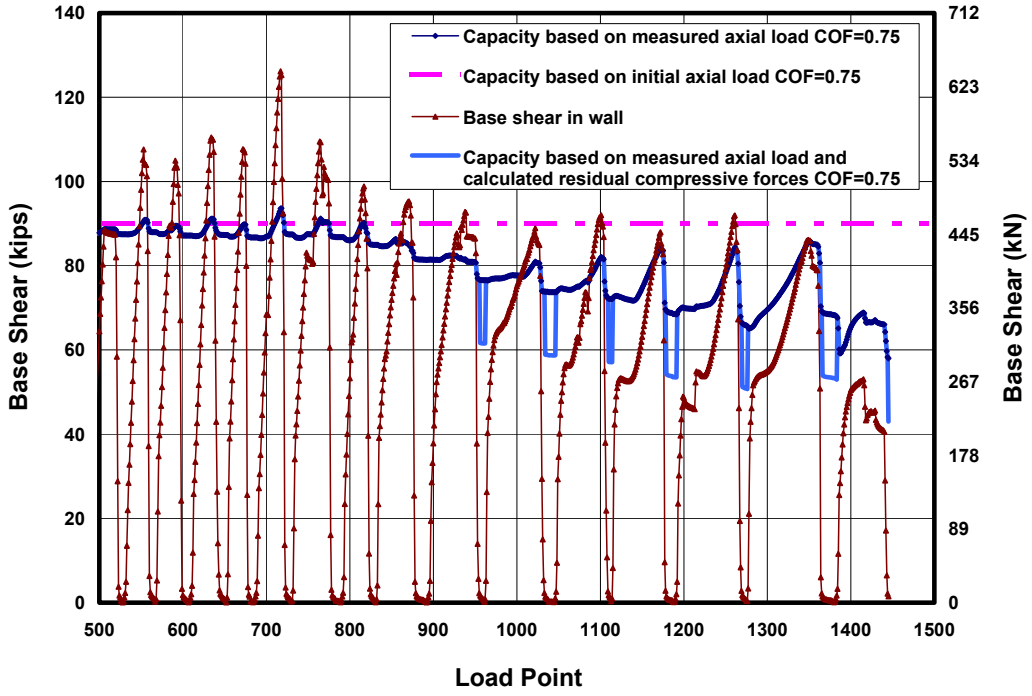

Figure 7.26: Base shear and reduced sliding shear capacity versus Load Point for Shear Wall Specimen 4

7.5.3 Sliding Shear Capacity for Capacity Design of AAC Shear Wall Specimens

A capacity design requires that the shear capacity exceed the shear corresponding to 125% of the nominal flexural capacity. This value based on current R/C and masonry design codes represents the overstrength in the reinforcement plus some strain hardening. This design, included in the current MSCJ and ACI seismic design provisions, ensures the behavior will be governed by flexure in the event of overstrength in flexure. The intent of a capacity design is to force ductile failures and avoid brittle failures. Although some degradation

from the dowels was observed, sliding shear resistance based on axial load is reliable. Since sliding shear dissipates energy, it may be acceptable in a high-magnitude earthquake. The permanent displacement that occurs with sliding may result in a complete loss of building function but does not threaten life safety. For this reason, sliding should be permitted, but only if the nominal capacity is exceeded due to unanticipated overloads. The proposed design provisions do not require a sliding check when calculating the shear capacity corresponding to 125% of the nominal flexural capacity.

7.6 CRUSHING OF THE DIAGONAL STRUT

7.6.1 Background information of Crushing of the Diagonal Strut

A shear wall can transfer load through the formation of a diagonal strut. The resultant of the applied lateral load and vertical forces acting on wall is transferred along a diagonal strip in the wall (Figure 7.27). The compressive force transferred along the diagonal strut is equilibrated at the base of the wall by the frictional resistance and vertical component of compression in the diagonal strut. The proposed design provisions and justification for this theory are presented in the following sections.

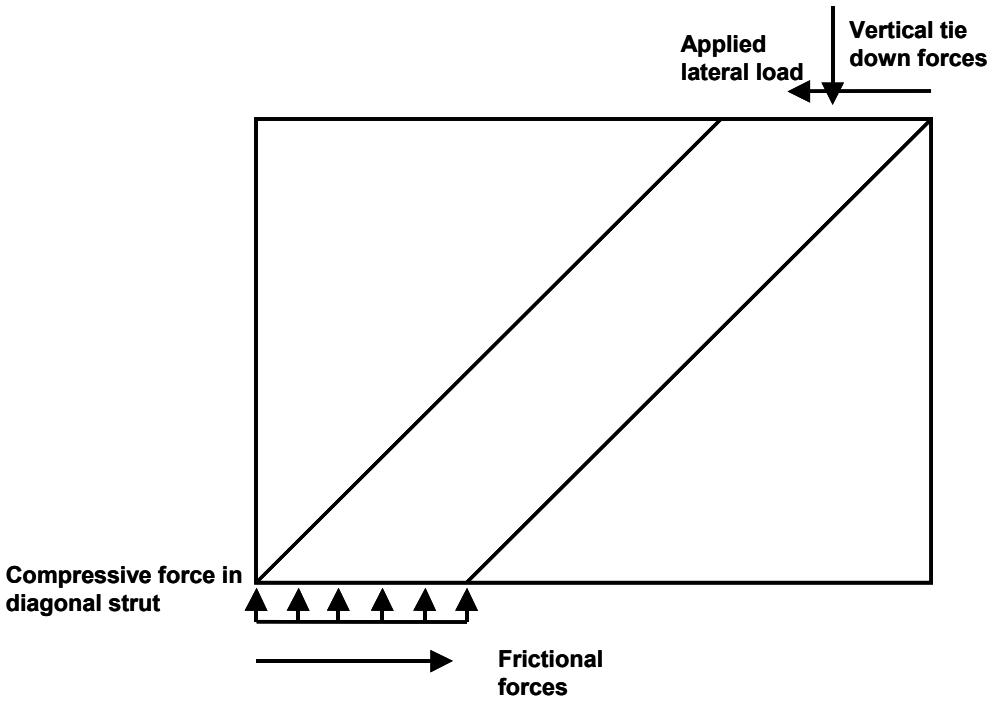

Figure 7.27: Diagonal compressive strut in an AAC shear wall

As axial load increases, the shear capacity of an AAC shear wall as governed by web-shear cracking also increases. If these axial loads are

accompanied by significant shear, as in a low-rise wall, the wall's shear capacity may be limited by crushing along the compression diagonal. Diagonal crushing can be predicted using a strut-and-tie model consisting of two elements: a diagonal compression strut (F_{strut}); and a tension tie-down force (T). The compressive force in the diagonal strut is the resultant of the vertical tie-down forces and the applied horizontal load. Because the system is statically determinate, the vertical component is the summation of the force in the tie-down rods, and the horizontal component is the applied lateral load (V).

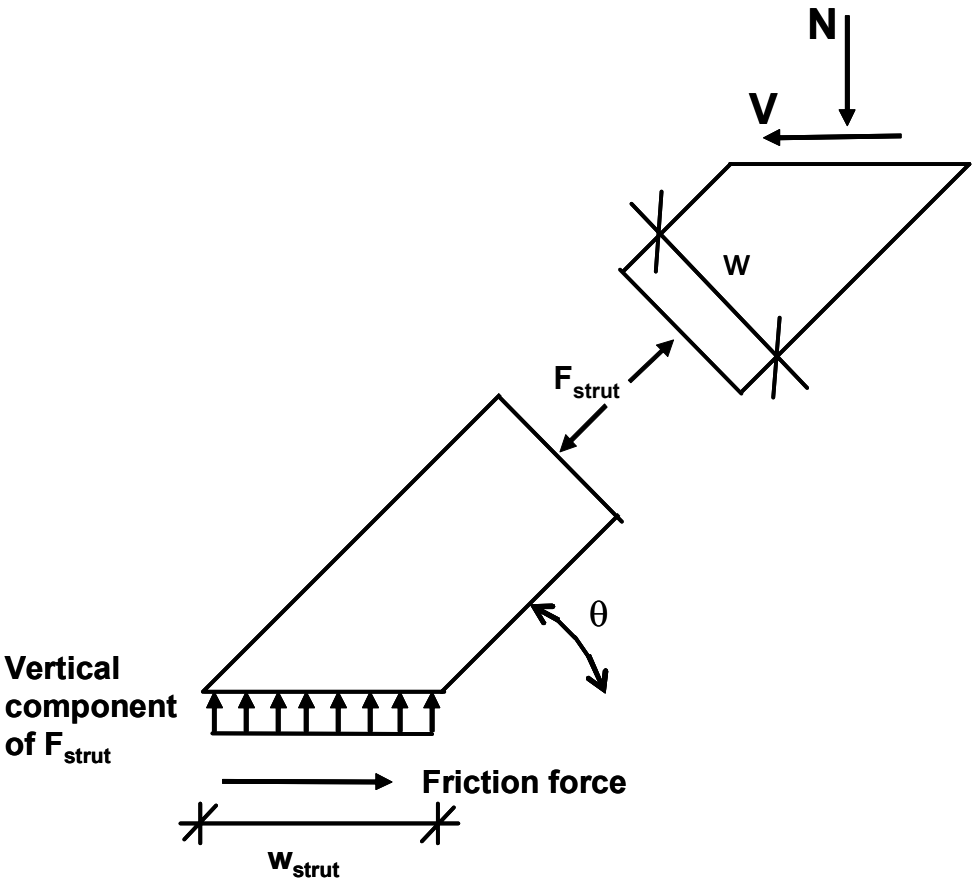

Figure 7.28: Forces acting on diagonal strut in an AAC shear wall

A free-body diagram of the compressive strut is shown in Figure 7.29. The free-body diagram on the right shows the forces at the ends of the strut, while the center free-body diagram shows the force inside the strut. The force in the strut is a function of the geometry of the wall and horizontal projection of the diagonal strut. The geometry of a shear wall specimen with aspect ratio of 0.6 and horizontal projection of the strut (l_{strut}) equal to one-quarter of the plan length of the wall, is shown in the left side of Figure 7.29. From geometry, the force in the strut will be 1.7 times the vertical reaction (ratio of diagonal leg to vertical leg of equivalent triangle). For a squat wall, the diagonal strut can crush at lateral loads smaller than those corresponding to the nominal flexural capacity. Because of the inclination of the strut, the force in the compression diagonal of a squat wall can be much higher than the flexural compression in the wall toe.

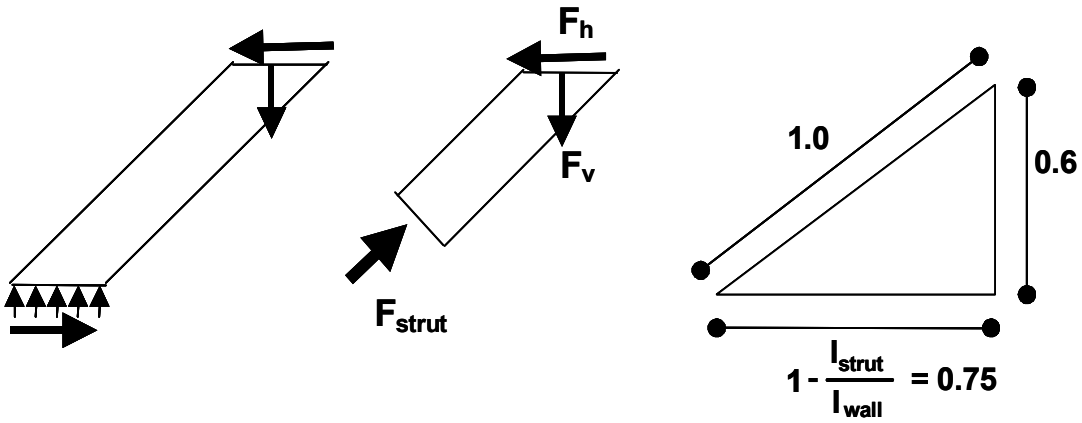

Figure 7.29: Relationship of forces in the diagonal strut

Crushing of the diagonal strut was observed in Shear Wall Specimen 1. The length of crushing extended one quarter of the plan length of the wall. Based on the applied load at crushing and the geometry of the wall Equation 8.22a was

calibrated. It represents the horizontal force (V) at crushing based on equilibrium of horizontal forces at the base of the diagonal strut.

The derivation can be shown in Equation (7.22) to Equation (7.27). The limiting force in the diagonal strut is based on a uniform compressive stress acting over the smallest area of the strut, as shown in Equation (7.5). The maximum applied lateral load is related by geometry to the force in the strut. Likewise, the minimum width of the strut can be related to the horizontal width of the diagonal strut. By substitution, the lateral load of Equation (7.28) can be expressed in terms of the wall geometry and horizontal width of the strut (Equation (7.25) Equation (7.26) and Equation (7.27)). The proposed equation uses a width of the compression strut of $0.25l_w$.

$$F_{strut} = w \cdot t \cdot f_{AAC} \qquad \text{Equation (7.22)}$$

$$V_{ds} = F_{strut} \cdot \cos(\theta) \qquad \text{Equation (7.23)}$$

$$w = \sin(\theta) \cdot w_{strut} \qquad \text{Equation (7.24)}$$

$$\cos(\theta) = \frac{l_w - w_{strut}}{\left[h^2 + (l_w - w_{strut})^2\right]^{0.5}} \quad , \quad \sin(\theta) = \frac{h}{\left[h^2 + (l_w - w_{strut})^2\right]^{0.5}} \qquad \text{Equation (7.25)} \quad \text{Equation (7.26)}$$

$$V_{ds} = w_{strut} \cdot t \cdot f_{AAC} \cdot \cos(\theta) \cdot \sin(\theta) \qquad \text{Equation (7.27)}$$

$$V_{ds} = f_{AAC} \cdot t \cdot w_{strut} \left[\frac{h \cdot (l_w - w_{strut})}{h^2 + (l_{wall} - w_{strut})^2} \right] \qquad \text{Equation (7.28)}$$

$$V_{ds} = 0.9 \cdot f_{AAC} \cdot t \cdot w_{strut} \left[\frac{h \cdot (\frac{3}{4} l_w)}{h^2 + (\frac{3l_w}{4})^2} \right] \qquad \text{Equation (7.29)}$$

7.6.2 Test Results for Crushing of the Diagonal Compressive Strut

Shear Wall Specimen 1 (UT Austin) confirmed this proposed model for crushing of the diagonal strut. Minor spalling was present in the toe at a load of 152 kips (676 kN). Major spalling occurred at a load of 167.6 kips (745 kN). Based on damage, the observed horizontal width of the diagonal strut was approximately one-quarter of the plan length. Using the Equation (7.26) crushing of the diagonal strut for Shear Wall Specimen 1 was predicted at a lateral load of 185.1 kips (823 kN). The maximum load was 90% of the load predicted by the model for crushing of the diagonal strut. Since, the model for crushing of the diagonal strut was unconservative in this case, it is multiplied by a factor of 0.9. The results of the predicted lateral load at crushing of the diagonal strut, for an assumed strut width of one-quarter of the plan length, are presented along with the maximum lateral load in Table 7.12.

Table 7.12: Predicted shear wall capacities as governed by crushing of the diagonal strut

Specimen	V_{ds} kips (kN)	$0.9V_{ds}$ kips (kN)	Maximum V kips (kN)	$0.9\ V_{ds}$ – Maximum V	Maximum V / $0.9\ V_{ds}$
1	185 (824)	167 (741)	168 (745)	-1 (-4)	1.01
3	154 (683)	138 (615)	118 (526)	20 (89)	0.86
4	315 (1403)	284 (1262)	126 (561)	158 (701)	0.44
5	246 (1093)	221 (984)	85 (377)	136 (607)	0.38
7	89 (394)	80 (355)	59 (263)	21 (91)	0.74
9	98 (436)	88 (392)	42 (189)	46 (204)	0.48
11	23 (100)	20 (90)	17 (74)	4 (16)	0.82
13	21 (93)	19 (84)	22.5 (100)	-4 (-16)	1.19
14a	36 (162)	33 (146)	9.9 (44)	23 (102)	0.30
14b	36 (162)	33 (146)	10.1 (45)	23 (101)	0.31
15a	121 (537)	109 (483)	30.1 (134)	79 (350)	0.28
15b	121 (537)	109 (483)	30.9 (137)	78 (346)	0.28
16	121 (537)	109 (483)	35.2 (157)	73 (327)	0.32

In the remaining shear wall specimens crushing of the diagonal strut was avoided by limiting the axial load. The validity of Equation (7.29) was indirectly determined by avoiding crushing. In Shear Wall Specimen 13, the maximum lateral load was higher than the proposed equation for the design provisions without observing crushing of a diagonal strut. One reason for the discrepancy is that the assumed width of the diagonal strut of one-quarter of the plan length of the wall is no longer valid. The aspect ratio of Shear Wall Specimen 13 is two. Since the model was adequate for walls with aspect ratios less than two, that aspect ratio is used as an upper limit to the proposed equation for design provisions.

This equation may be uncoservative because it was based on AAC panels with a splitting tensile strength higher than the tested splitting tensile strength of modular blocks from the same shipment. If the realationship between splitting

tensile strength and compressive strength is preserved this equation may be unconservative.

7.7 NOMINAL FLEXURAL CAPACITY

The nominal flexural capacity of AAC shear walls can be determined based on equilibrium of a cross section. General assumptions for flexural behavior, were verified in the flexure-dominated shear wall specimens. The following sections present the concept of an equivalent compressive stress block and the test results for the observed nominal flexural capacity in the flexure-dominated shear wall specimens.

7.7.1 Equivalent Compressive Stress Block

Using the proposed design provisions, the nominal flexural capacity of AAC shear walls can be predicted using conventional flexural theory. The sum of the tensile force is the longitudinal reinforcement and the axial load determine the magnitude of the compressive force in the wall. The anchorage detail for the longitudinal steel and the application of the lateral load are presented in Appendix B. The compressive zone is determined based on a linear strain relationship, using a maximum useful compressive strain in the AAC of 0.003 (RILEM 1993 and Section 3.6.1), and an equivalent rectangular stress block whose height is $0.85f'_{AAC}$ (or $0.85f'_m$), and whose depth is $\beta_1 c$, where $\beta_1 = 0.67$ (Figure 7.30). The value of β_1 is selected to maintain equilibrium between the equivalent stress block and a triangular compressive stress distribution based on tested stress-strain results of Section 3.6.1 (Argudo 2003).

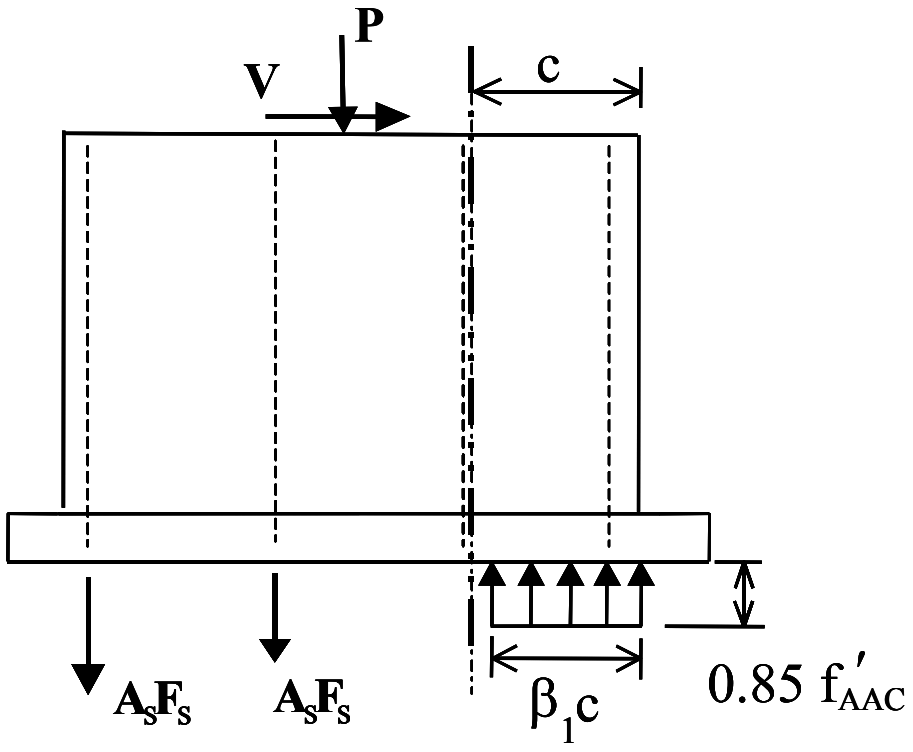

Figure 7.30: Equilibrium of an AAC shear wall at nominal flexural capacity

7.7.2 Test Results for Nominal Flexural Capacity

Observed versus predicted nominal flexural capacities can be compared for flexure-dominated Shear Wall Specimen 14a, 14b, 15a and 15b. During the test of Shear Wall Specimen 13 and Shear Wall Specimen 16, the actuators used to apply the constant axial load inadvertently reached the end of their travel. As increasing lateral drifts were applied, axial load on the wall inadvertently increased. To successfully interpret those test results, the probable axial load applied to the walls was back-calculated from the predicted flexural capacity,

removing those two tests from consideration for verifying observed versus predicted flexural capacity.

The nominal flexural capacity was calculated using a steel yield strength of 75 ksi (490 MPa), based on mill reports, along with the assumptions of 8.8.2. The ratios of observed to predicted strength range from 1.11 to 1.29, with an average of 1.19 and a COV of 5.8%. A refined analysis was performed considering strain hardening using RCCOLA (RCCOLA). The effect of strain hardening will increase the nominal flexural capacity as shown in the results of Table 7.14. With this refinement the range of observed to predicted nominal flexural capacity ranges from 0.95 to 1.13. The average is 1.03 with a COV of 6.2%. The degree of strain hardening in the flexural reinforcement is based on the bar strain. The strain is a function of the vertical displacement at the location of tensile reinforcement divided by the unbonded length of the tensile reinforcement. The unbonded length decreases as the bar size decreases, and can result in yielding and strain-hardening of small-diameter bars even at low drift levels.

Table 7.13: Observed versus predicted nominal shear capacities based on nominal flexural capacity

Specimen	Predicted V_{Mn} kips (kN)	Observed V_{Mn} South kips (kN)	Observed V_{Mn} North kips (kN)	Observed / Predicted V_{Mn} South	Observed / Predicted V_{Mn} North
14a	8.5 (38)	9.4 (42)	NA	1.11	NA
14b	8.5 (38)	9.9 (44)	10.1 (45)	1.16	1.19
15a	23.9 (106)	28.8 (128)	30.1 (134)	1.21	1.26
15b	23.9 (106)	26.7 (119)	30.9 (137)	1.12	1.29
				Average	1.19
				COV (%)	5.8

Table 7.14: Observed versus predicted nominal shear capacities based on nominal flexural capacity with strain hardening included

Specimen	Predicted V_{Mn} kips (kN)	Observed V_{Mn} South kips (kN)	Observed V_{Mn} North kips (kN)	Observed / Predicted V_{Mn} South	Observed / Predicted V_{Mn} North
14a	9.9 (44)	9.4 (42)	NA	0.95	NA
14b	9.9 (44)	9.9 (44)	10.1 (45)	1.00	1.02
15a	27.4 (122)	28.8 (128)	30.1 (134)	1.05	1.10
15b	27.4 (122)	26.7 (119)	30.9 (137)	0.97	1.13
				Average	1.03
				COV (%)	6.2

7.8 LONGITUDINAL CRACKS AT THE LOCATION OF VERTICAL REINFORCEMENT

In each of the flexure-dominated specimens vertical (longitudinal) cracks formed along the grouted cores and the surrounding AAC. In the following sections the observed load at which these cracks formed is presented, along with

two analyses to determine if the cracks occurred before yielding of the flexural reinforcement. The effect of these longitudinal cracks is presented, along with design recommendations intended to prevent their formation.

7.8.1 Background Information on Cracks along Longitudinal Reinforcement in AAC Shear Walls

After the initial adhesion between the reinforcement and concrete is broken, load is transferred from deformed reinforcement to the surrounding concrete or grout by the deformations (lugs). The axial component of the force transferred by the lugs to a vertical core is the difference in force (ΔT) in a section of vertical reinforcement (Figure 7.31). The associated radial component of that force also acts on the surrounding grout (Figure 7.31). The resultant forces generally act at about 45 degrees to the axis of the reinforcement, so that the resultants of the radial and axial component of the forces are equal. The radial forces generated per length of the bar equal the change in force in the bar over that same length. The pressure generated by the radial forces in the longitudinal bar can be determined by dividing the radial forces by the product of the circumference of the deformed bar and the length of the section of the bar, Δx, as shown in Figure 7.31. The diameter of the longitudinal bar is denoted by d_{bar}.

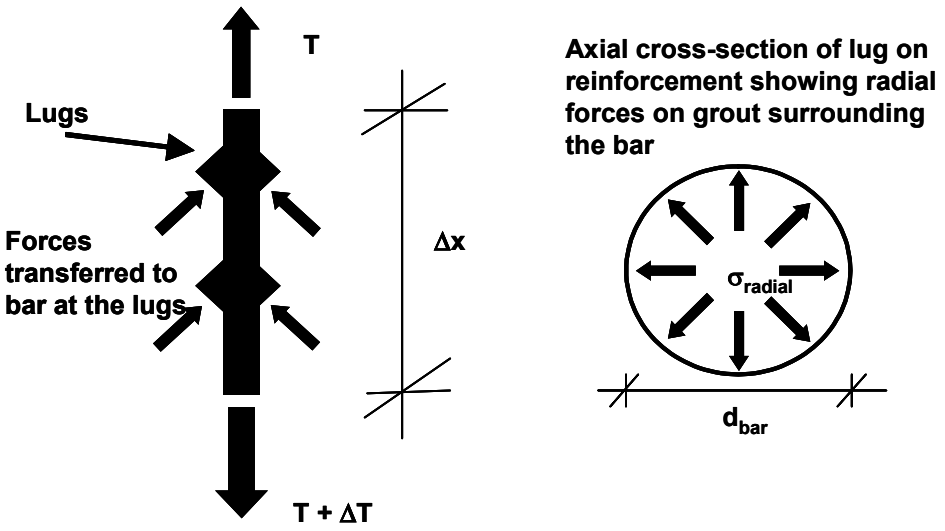

Figure 7.31: Free-body diagram of longitudinal bar with all load transferred through lugs and pressure generated in the surrounding grout

These radial forces cause splitting tensile stresses along a section through the wall at the center of the grouted core. Because the AAC has only about 15% of the splitting tensile strength of the grout, its tensile strength is neglected. A uniform distribution of splitting stresses across any section through the diameter of the grout core is assumed as shown in Figure 7.32a. Since the radial stresses are symmetric about the centerline of the core (Figure 7.32a), the net resultant of those radial stresses perpendicular to the centerline is zero. The splitting tensile stresses are resisted by the splitting tensile capacity of a section of grout, whose area is the length of grout shown in Figure 7.32b, multiplied by the length of a section Δx. The resistance to the splitting tensile stresses is expressed in Equation (7.30). The resistance is increased by increasing the diameter of the core, decreasing the diameter of the bar, or increasing the tensile strength of the grout.

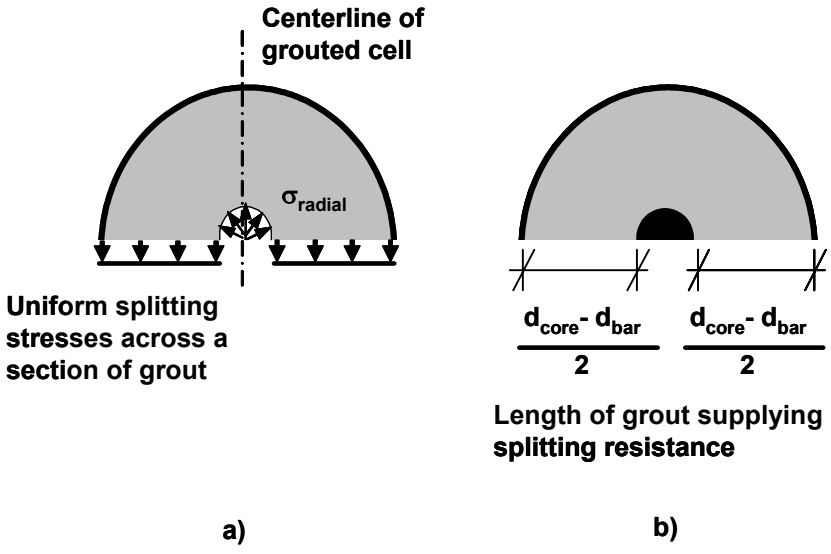

Figure 7.32: Stresses generated perpendicular to a cut along the diameter of a grouted cell

$$F_{resis\tan ce} = f_t(d_{core} - d_{bar})\Delta x \qquad \text{Equation (7.30)}$$

7.8.2 Formation of Cracks along Longitudinal Bars in AAC Shear Walls

The base shears at which cracks formed along longitudinal reinforcement formed are presented in Table 7.15. The base shear at which the first and second cracks formed along the vertical reinforcement is presented in Column 2 of that table. No second observed vertical crack data are presented for Shear Wall Specimen 14a, because that wall was tested in one direction only. The base shear at the expected flexural capacity (nominal capacity increased by steel overstrength) is presented in Column 3.

Table 7.15: Ratio of base shear at formation of vertical cracks to base shear at expected flexural capacity (including overstrength) in the flexure-dominated shear wall specimens

AAC Shear Wall Specimen	Base shear at first and second observed vertical crack, kips (kN)	Base shear at expected flexural capacity (fs=1.25fy) Vmax kips (kN)	Ratio of base shear at observed crack to Vmax (fs=1.25fy)
13	13.6 (60) – first 15.6 (69) - second	13.0 (58)	1.05 – first 1.20 – second
14a	6.9 (31) – first NA – second	8.3 (37)	0.83 – first NA – second
14b	7.0 (31) – first 9.8 (44) - second	8.3 (37)	0.84 – first 1.18 – second
15a	26.5 (118) – first 27.3 (128) - second	23.8 (106)	1.11 – first 1.15 – second
15b	17.5 (78) – first 24.5 (109) - second	23.8 (106)	0.74 – first 1.03 – second
16	24.0 (107)– first 28.0 (125) - second	25.5 (113)	0.94 – first 1.10 – second

The ratios of base shear at the observed crack to the base shear at the expected flexural capacity range from 0.74 to 1.20, with an average of 1.02 and a COV of 16%. Longitudinal cracks were observed in three specimens at 74% to 84% of the expected flexural capacity. The ratios of base shear at cracking to expected flexural capacity, along with a corresponding normal distribution, are shown in Figure 7.33. As shown in that figure, it is highly probable that an AAC shear wall will reach between 74% and 84% of its expected flexural capacity in a moderate to strong earthquake, and therefore highly probable that such longitudinal cracks would form.

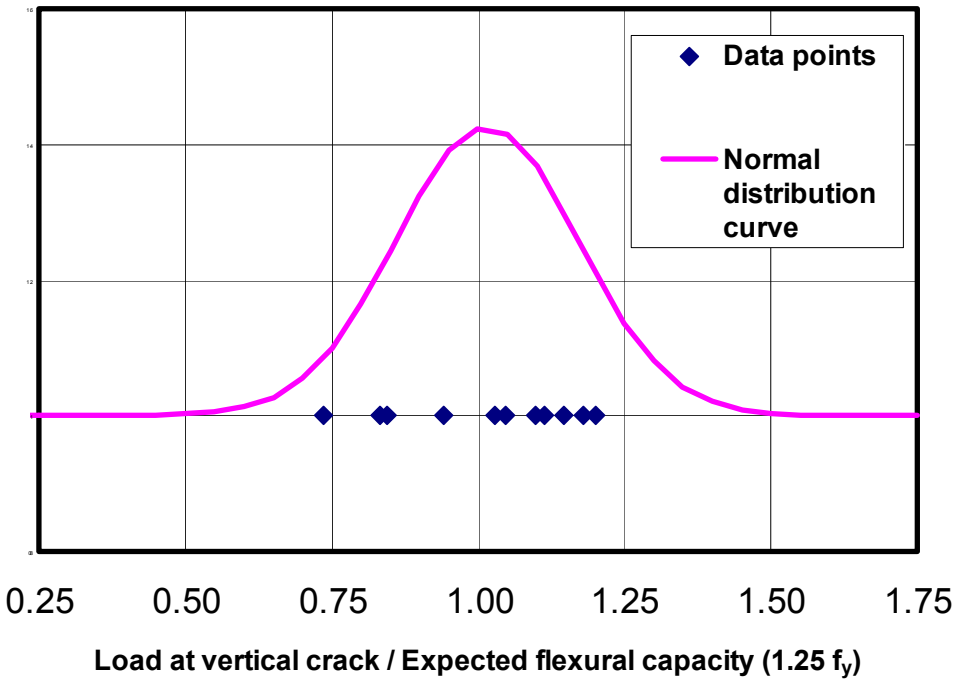

Figure 7.33: Ratio of base shear at observed longitudinal crack to base shear at expected flexural capacity (f_s=1.25 f_y)

For lower base shears, a similar analysis can be performed. The results of Table 7.15 are reproduced based on nominal moment capacity (rather than expected), and are presented in Table 7.16. In this case the ratios of base shear at longitudinal cracking to base shear at nominal capacity range from 0.84 to 1.42, with an average of 1.2 and a COV of 15.5%. These data are illustrated graphically in Figure 7.34. The ratio of 1.0 between base shear at longitudinal cracking to base shear at nominal flexural capacity, corresponds to a 16% lower fractile. A 5% lower fractile corresponds to a ratio of 0.88. Based on these results, 5% of shear walls would exhibit longitudinal cracking at the factored

nominal flexural capacity. To further determine if vertical cracks would occur at service loads, analyses were performed to determine if the cracks formed prior to yielding, and are presented in the following section.

Table 7.16: Ratio of base shear at observed vertical cracking to the nominal flexural capacity (without overstrength) in flexure-dominated AAC shear wall specimens

Specimen	Base shear at first and second observed vertical crack kips (kN)	Base shear at design flexural capacity V_{Mn} kips (kN)	Ratio of base shear at first observed crack to V_{Mn}
13	13.6 (60) – first 15.6 (69) - second	11.4 (51)	1.19 – first 1.37 – second
14a	6.9 (31) – first NA – second	6.9 (31)	1.00 – first NA – second
14b	7.0 (31) – first 9.8 (44) - second	6.9 (31)	1.01 – first 1.41 – second
15a	26.5 (118) – first 27.3 (128) - second	20.9 (93)	1.27 – first 1.31 – second
15b	17.5 (78) – first 24.5 (109) - second	20.9 (93)	0.84 – first 1.17 – second
16	24.0 (107) – first 28.0 (125) - second	22.2 (99)	1.08– first 1.26 – second

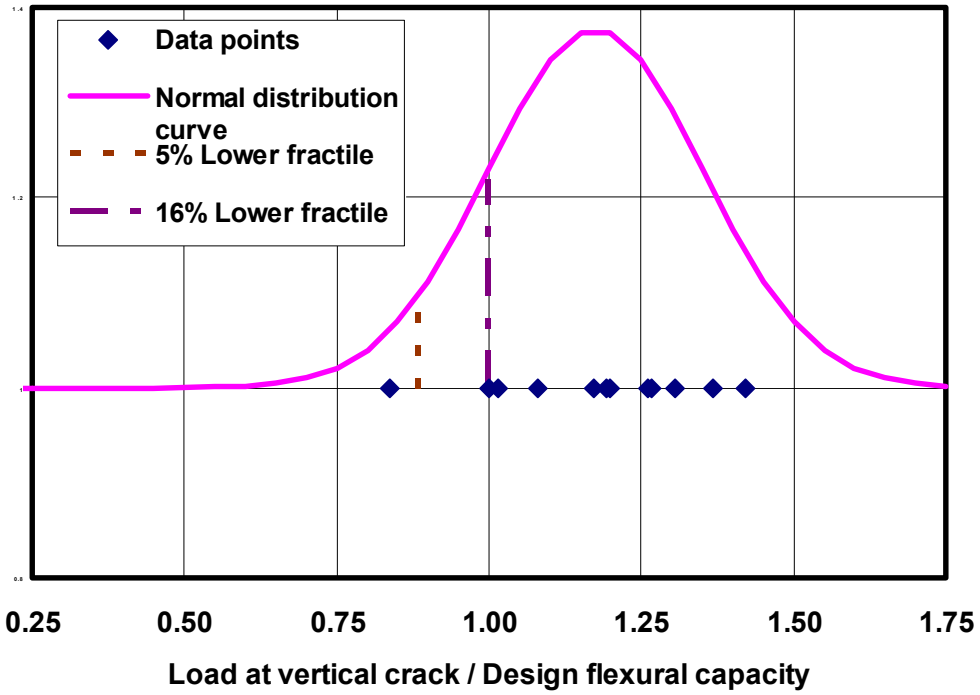

Figure 7.34: Ratio of base shear at observed longitudinal crack to base shear at nominal flexural capacity without overstrength

7.8.3 Analysis to Determine if Longitudinal Cracks Formed Prior to Yielding

Additional analysis was performed to determine if longitudinal cracks formed before or after the vertical reinforcement yielded. If the vertical cracks formed prior to yielding, then those cracks might also be present in walls at factored design loads. If the vertical cracks formed after yielding, it can be assumed that they would occur only during overloading beyond the nominal capacity.

Strain was measured by three strain gages on the longitudinal reinforcement at each end of the wall. If one strain gage indicated strains beyond yield and another strain gage indicated strains near but not exceeding yield, this was assumed to denote yielding. The base shear and load points at the formation of longitudinal cracks in each specimen, while loading to the south and to the north, are recorded in Column 2 of Table 7.17. In Shear Wall Specimen 13, strain gage data were not available; for this reason, in Column 2 both the South and North loading directions are labeled "NA." The base shear and load points at the yielding of the flexural reinforcement are presented in Column 3. Since load points are assigned in ascending order, the first event (either longitudinal cracking or yielding of longitudinal reinforcement) has the lowest-numbered load point. The event that occurred first for each loading direction is presented in Column 4. If the load-point numbers did not vary by more than 5, it was assumed that longitudinal cracking occurred simultaneously with yielding of flexural reinforcement, and was therefore associated with that yielding. For example, in Shear Wall Specimen 14a while loading to the south, longitudinal cracking was observed at Load Point 542, and the longitudinal reinforcement was determined to have yielded at Load Point 539. Since these load points do not vary by more than 5, it was concluded that the longitudinal cracking and yielding of the reinforcement occurred simultaneously, as indicated in Column 4. Finally, the ratio of base shear at longitudinal cracking to base shear at yielding is presented in Column 5.

Table 7.17: Estimation of order of vertical cracking and yielding of longitudinal reinforcement, based on strain gages

Specimen	Base shear at observed vertical crack, loading south and loading north, Kips (kN) Load point	Base shear at yielding of flexural reinforcement, loading south and loading north, kips (kN) Load point	Estimated order of yielding of reinforcement and longitudinal cracking	Ratio of base shear at formation of longitudinal crack of base shear at yielding of flexural reinforcement
13	13.6 (60) LP 1023 – S 15.6 (69) LP 1232 - N	NA – S NA – N	NA – S NA – N	NA – S NA – N
14a	6.9 (31) LP 542 – S NA – N	6.2 (27.6) LP 539 – S NA – N	Together – S NA – N	1.1 – S NA – N
14b	7.0 (31) LP 326 – S 9.8 (25) LP 487 - N	7.5 (33) LP 327 – S 8.9 (40) LP 410 – N	Together – S Yielding – N	0.9 – S 1.1 – N
15a	28.8 (128) LP 437 – S 27.3 (121) LP 528 – N	22.1 (98) LP 299 – S 26.0 (116) LP 333 – N	Yielding – S Yielding – N	1.3 – S 1.1 – N
15b	17.5 (78) LP 202 – S 24.5 (109) LP 338 – N	23.7 (102) LP 363 – S 24.5 (109) LP 340 – N	Cracking – S Together – N	0.7 – S 1.0 – N
16	28.0 (125) LP 716 – S 24.0 (107) LP 426 - N	27.0 (120) LP 704 – S 26.8 (119) LP 754 – N	Yielding – S Cracking – N	1.0 – S 0.9 – N

In four cases, yielding occurred before longitudinal cracking; and in two cases, it occurred afterwards. In the remaining cases these events probably occurred simultaneously. In both cases where the flexural reinforcement yielded after longitudinal cracks were observed, the ratio of base shear at formation of longitudinal cracking to base shear at yielding was also less than 1. This further supports the conclusion that if #5 bars are used in 3-in. grouted cores, longitudinal cracks may form prior to yielding of the flexural reinforcement. The ratio of base shear at longitudinal cracking to base shear at yielding is less than 1.25 for all of the specimens, which indicates that longitudinal cracks will probably form prior to reaching the nominal flexural capacity considering a strain hardening factor of 1.25. This analysis does not consider the height at which the vertical crack

formed. If the crack formed at a height of 48 in. (1.2 m) the stress in the reinforcement could be significantly below yield. The impact of crack height is considered in a separate analysis.

An additional analysis was performed to estimate the stress in the flexural reinforcement at longitudinal cracking, using elastic flexural stresses calculated based on a cracked transformed section (Table 7.18). The applied base shear was converted to an applied moment at the location of the crack by multiplying by the height of the wall minus the crack height. The stress in the longitudinal tensile reinforcement was computed using Equation (7.31). The contributions from the axial load are not presented in Table 7.18 because they were less than 2 ksi (14 MPa). The distance from the neutral axis to the centroid of the tensile reinforcement is denoted by y_{As}; the modular ratio between steel and AAC is denoted by n; and the cracked transformed moment of inertia is denoted by I_{crtr}. The results indicate that in 6 of the 11 cases, calculated stresses at longitudinal cracking exceeded the expected yield strength of 75 ksi (10.9 GPa). This indicates that approximately half of the vertical cracks occurred prior to or simultaneously with yielding of the flexural reinforcement.

$$\sigma_{As} = \frac{My_{As}n}{I_{crtr}} - \frac{Pn}{A_{tr}} \qquad \text{Equation (7.31)}$$

Table 7.18: Calculated stresses in tensile reinforcement based on elastic theory for vertical cracks on the south and north sides of the specimen

Specimen	Base shear at observed vertical crack, loading south and loading north kips (kN)	Height of the vertical crack in. (m)	Cracked transformed moment of inertia in.^{4} (m^4)	yAs, distance from the area of tensile steel to the neutral axis in. (m)	Calculated stress in tensile reinforcement for first observed vertical crack ksi (GPa)
13	13.6 (60) – S 15.6 (69) – N	24 (0.6) – S 24 (0.6) – N	64900 (0.027)	45 (1.1)	96 (0.67) – S 111 (0.79) – N
14a	6.9 (31) – S NA – N	48 (1.2) – S NA – N	46100 (0.019)	39 (1.0)	49 (0.35) – S NA – N
14b	7.0 (31) – S 9.8 (44) – N	24 (0.6) – S 48 (1.2) – N	46100 (0.019)	39 (1.0)	61 (0.44) – S 70 (0.50) – N
15a	28.8 (128) – S 27.3 (121) – N	48 (1.2) – S 0 (0) – N	226800 (0.094)	86 (2.2)	91 (0.65) – S 127 (0.90) – N
15b	17.5 (78) – S 24.5 (109) – N	12 (0.3) – S 24 (0.6) – N	226800 (0.094)	86 (2.2)	74 (0.53) – S 95 (0.68) – N
16	28.0 (125) – S 24.0 (107) – N	0 (0) – S 24 (0.6) – N	309100 (0.129)	94 (2.4)	104 (0.73) – S 75 (0.54) - N

7.8.4 Implications of the Formation of Longitudinal Cracks

The above evaluations show that longitudinal cracks are highly probable in real AAC shear walls subject to lateral loads. This section is devoted to explaining the probable consequences of those cracks and providing design recommendations for preventing them.

Cracks along reinforcement in a grouted core are inherently undesirable, because they provide an opportunity for air and water to enter the core, and

thereby increase the probability of corrosion of that reinforcement. Longitudinal cracks along the height of the wall, combined with horizontal cracks, can cause the end blocks to spall and crush sooner than in otherwise identical walls without longitudinal cracks (Figure 7.35). Longitudinal cracks can also lead to buckling of the longitudinal reinforcement in the compression toe (Figure 7.36). As the load is reversed, the previously buckled longitudinal reinforcement may fracture, effectively reducing the wall's flexural capacity to zero. Examples of the undesirable consequences of loss of the compression toe are shown by Shear Wall Specimen 15b and Shear Wall Specimen 16.

Figure 7.35: Loss of end block on compression toe in Shear Wall Specimen 16

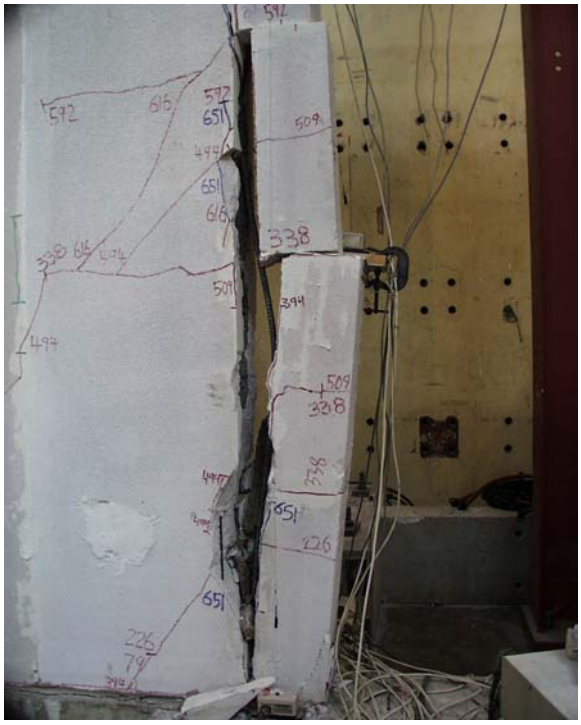

Figure 7.36: Loss of end blocks and buckling of compression reinforcement in Shear Wall Specimen 15b

Resistance to cracks along longitudinal reinforcement could be increased. Longitudinal splitting cracks could be prevented by increasing the size of grouted core or decreasing the bar diameter. This is equivalent to limiting the ratio of area of the longitudinal reinforcement to area of core (area ratio).

The area ratio of a #5 (17 mm) bar in a 3-in. (76 mm) diameter grouted core (4.4%) was observed to produce splitting along longitudinal bars in plastic hinge zones. This is inherently undesirable for AAC shear walls. Such cracking has not been observed with #4 bars in 3-in. grouted cores, even at splices. A #4 (12 mm) bar in a 3 in. (76 mm) core corresponds to an area ratio of 2.8%. For that reason, the proposed design provisions for AAC masonry and reinforced

AAC panels limit the maximum ratio of the area of reinforcement to the area of the grouted core containing that reinforcement, to 3% in plastic hinge zones. This limit is discussed further in Section 10.5.

7.9 OBSERVED FLEXURAL CRACKING AND WEB-SHEAR CRACKING OF SHEAR WALL SPECIMEN 2 (PANELS ORIENTED VERTICALLY)

In Shear Wall Specimen 2, two vertical cracks formed prior to testing. Shortly after flexural cracks formed, another two vertical cracks formed and separated the wall into smaller sections. The initial cracks are indicated by gray lines and the cracks formed during testing are indicated by black lines in Figure 7.37. The first diagonal crack formed at a load of 55.6 kips (247 kN). As the load increased, additional vertical and diagonal cracks formed in the specimen (Figure 7.38).

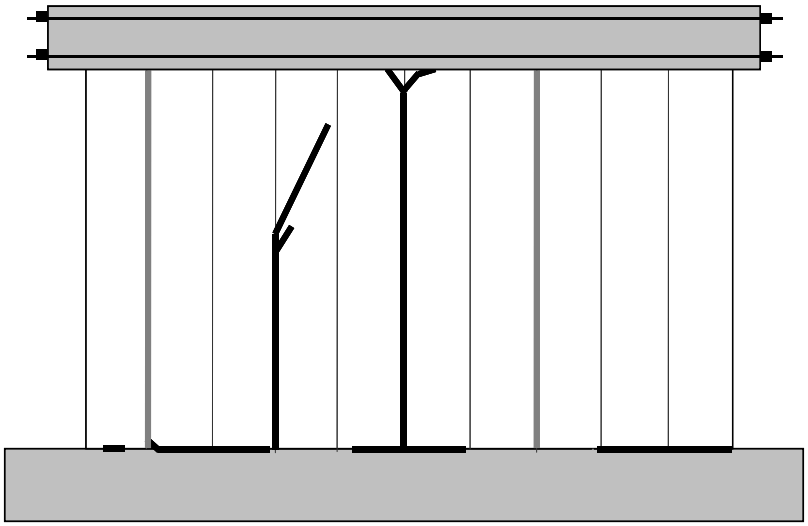

Figure 7.37: Formation of first diagonal crack in Shear Wall Specimen 2

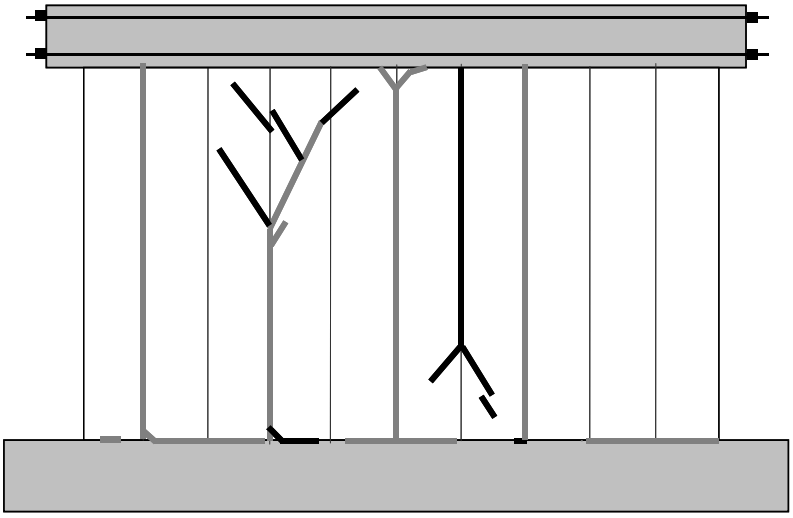

Figure 7.38: Formation of additional cracks in Shear Wall Specimen 2

7.10 General Behavior of Shear Wall Specimens Constructed With Vertical Panels

Distinct behavior was observed in Shear Wall Specimen 2, constructed of panels oriented vertically. Based on this behavior, design models were constructed and compared to the behavior of other tests with panels oriented vertically. The results of this analysis are proposed design provisions that consider the potential formation of vertical cracks at panel joints. The following sections present models for the behavior of shear wall specimens with panels oriented vertically, verification of the observed behavior in shear wall specimens with panels oriented vertically and design provisions that consider the construction methods used in the results obtained at UT Austin.

7.10.1 Modeling of Shear Wall Specimens with Panels Oriented Vertically

In the case of monolithic behavior, the wall behaves as a cantilever (Figure 7.39). In the case of individual panels, the stiffness of the loading beam is

large compared to a single panel, and the loading beam restrains the wall at the top (Figure 7.40).

If the wall behaves monolithically, the shear capacity will remain the same as presented in Section 7.1 through 7.8 and the flexural design will be conventional. If the panels are separated by vertical cracks at the head joints, however, the behavior will change. The predicted behavior as governed by flexure and shear are discussed in Sections 7.10.2 and 7.10.3.

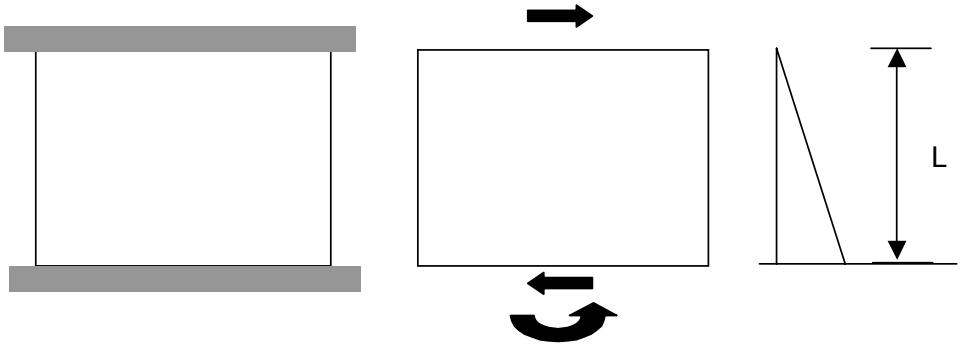

Figure 7.39: Behavior of monolithic AAC shear wall

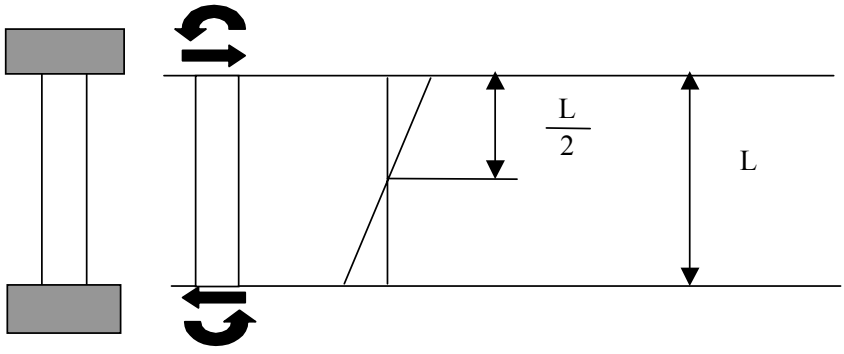

Figure 7.40: Behavior of individual panel for an AAC shear wall

7.10.2 Behavior of Individual Panels as Governed by Flexure

The most critical case would be panels with vertical cracks at every section. The flexural capacity can be predicted based on the sum of the capacity of the individual panels (Equation (7.32)). An interaction diagram for a single panel can be calculated and the flexural capacity of each panel can be determined based on the axial load in the respective panel; a value that depends on the forces acting on the wall. The lateral load produces a series of axial loads in each panel that vary linearly based on the wall geometry. The applied axial load per panel will be the total axial load divided by the number of panels (Figure 7.41).

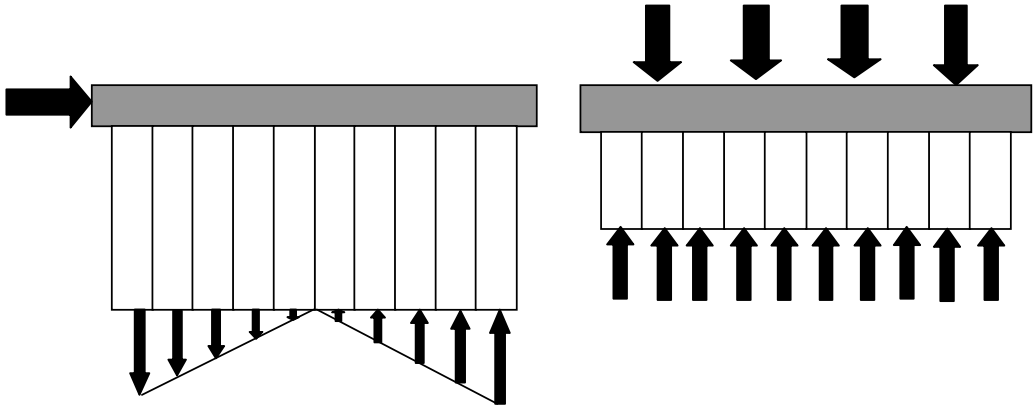

Figure 7.41: Distribution of axial loads for laterally loaded condition and axially loaded condition

If the net axial load applied to each panel is within the straight-line portion of the interaction diagram for a single panel, the total wall capacity will be the capacity at the axial load in a single panel, multiplied by the number of panels, as shown in Equation (7.33).

$$M_{wall} = \Sigma M_{panels} \qquad \text{Equation (7.32)}$$

$$M_{wall} = n_{panels} M_{panels(averageP)}$$ Equation (7.33)

7.10.3 Behavior of Individual Panels as Governed by Shear

If the wall behaves as individual panels, the aspect ratio of each panel becomes large; each panel behaves as a beam subject to compressive and lateral loads. The total wall capacity as governed by shear is expressed by Equation (7.34). The shear capacity of individual panels can be predicted using the shear equations for beams.

$$V_{wall} = \Sigma V_{panels}$$ Equation (7.34)

Equations for beam shear capacity, exist in ACI 318-02 and the Masonry Standards Joint Committee design provisions (ACI 530-02/ASCE 5-02/TMS 402-02). Equation 11-4 of ACI 318-02 is a design equation for the cracking shear strength of reinforced concrete beams including axial load that is defined as Equation (7.35) in this dissertation. The MSJC design provisions uses a similar Equation (7.37) to determine the shear capacity of a masonry beam. Equation (7.37) is MSCJ Equation (3-21), conservatively simplified by using the maximum required ratio of shear span to depth ($M/Vd_v=1$). Equation (7.38) can be produced by substituting the relationship between splitting tensile strength and compressive strength into Equation (7.37). Both equations are expressed as a function of the splitting tensile strength (f_t) of concrete by substituting the relationship between splitting tensile strength and compressive strength ($6\sqrt{f_c'}$ in US customary units) as shown in Equation (7.36) and Equation (7.38).

$$V_c = \left(1 + \frac{P_u}{2000 A_g}\right) 2\sqrt{f_c'} b_w d$$

Equation (7.35)

Equation (11-4) in ACI 318-02

$$V_c = \left(1 + \frac{P_u}{2000 A_g}\right) \frac{f_t}{3} b_w d$$

Equation (7.36)

$$V_m = 2.25\sqrt{f'_{AAC}}\, A_n + 0.25 P_u$$

Equation (7.37)

Equation (3-21) in ACI 530-02/ASCE 5-02/TMS 402-02

$$V_m = \left[\frac{2.25 f_t}{6}\right] A_n + 0.25 P_u$$

Equation (7.38)

In Equation (7.36) and Equation (7.38), the first term represents the web-shear cracking capacity, while the second term represents the beneficial effect of compressive axial load, which is significantly smaller in Equation (7.36) than in Equation (7.38). Equation (7.38), applied to Shear Wall Specimen 2, predicts a shear capacity that exceeds the predicted capacity of an otherwise identical monolithic AAC shear wall using Equation (8.11), an indication that Equation (7.38) should not be applied directly to AAC shear walls. This coefficient in front of the second term in Equation (7.38) was reduced from 0.25 to 0.05 based on the results of Shear Wall Specimen 2. It is especially important to reduce this factor since it is not known reliably, because axial load was not varied for AAC shear walls composed of vertical panels. A detailed discussion of this issue is presented in Section 7.11.2.

Equation (7.39)

$$V_{AAC} = \left[\frac{2.25 f_t}{6}\right] A_n + 0.05 P_u$$

$$V_{AAC} = 0.8\left(1 + \frac{P_u}{2000 A_g}\right) f_t b_w d \qquad \text{Equation (7.40)}$$

$$V_{AAC} = 0.9\sqrt{f'_{AAC}}\, A_n + 0.05 P_u \qquad \text{Equation (7.41)}$$

V_{AAC} and P_u in lb, f_{AAC} in psi

7.11 VERIFICATION OF BEHAVIOR OF SHEAR WALL SPECIMEN 2

The following behaviors were observed in Shear Wall Specimen 2: flexural cracking; diagonal cracking and the base shear capacity. All of these behaviors are compared to the predicted capacity considering the effect of vertical cracks separating the specimen into smaller walls.

7.11.1 Flexural Cracking in Shear Wall Specimen 2

The presence of vertical cracks prior to testing separated Shear Wall Specimen 2 into individual sections. This was confirmed by the presence of dual flexural cracks that formed while loading to the south and north (Figure 7.42 and Figure 7.43). These flexural cracks formed at a load of 66.3 kips (295 kN) and 55.6 kips (247 kN) while loading to the south and north respectively. The predicted base shear at cracking for two walls, one consisting of 4 vertical panels and another consisting of 5 vertical panels, corresponding to the axial load present in Shear Wall Specimen 2 is 61 kips (271 kN). The ratios of observed to predicted load for the observed flexural cracks in this specimen are 1.1 and 0.9 while loading to the south and north respectively. These calculations indicate that the specimen was functioning as individual walls made of one or more panels.

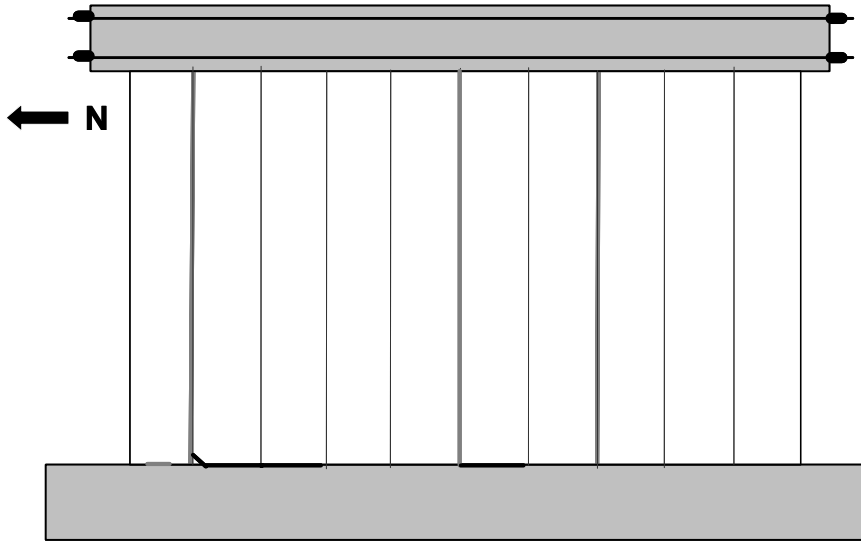

Figure 7.42: Flexural cracks that formed at edges of individual wall sections while loading to the south in Shear Wall Specimen 2

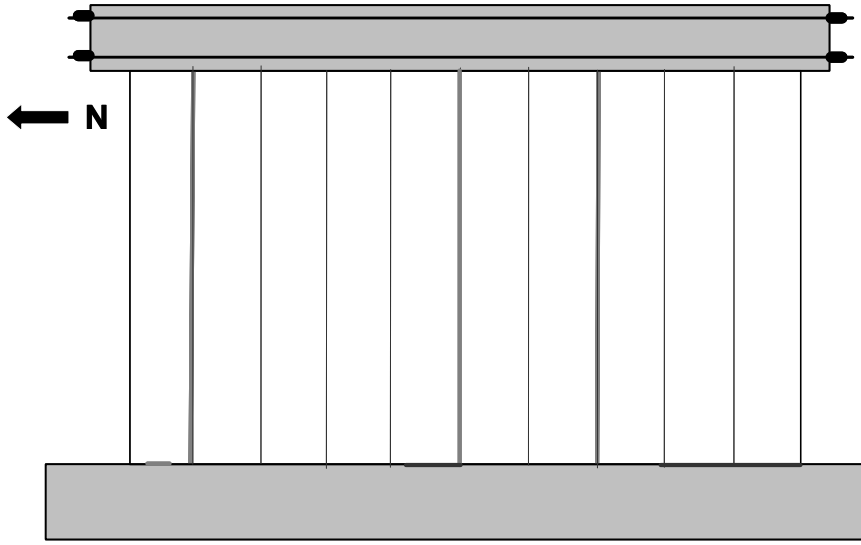

Figure 7.43: Flexural cracks that formed at edges of individual wall sections while loading to the north in Shear Wall Specimen 2

7.11.2 Shear Cracking and Base Shear Capacity of Shear Wall Specimen 2

An interaction diagram that combines the individual panel design equations and the monolithic wall equations of Sections 7.1 through 7.7 is shown in Figure 7.44. The shear capacity for individual panels is based on Equation (7.36). The first diagonal crack shown in Figure 7.37 formed at a load of 55.6 kips (247 kN). This base shear and axial load in the specimen are represented as a diamond and dashed horizontal line. The base shear is between the base shear for individual panels and for the monolithic wall but closer to the results for the monolithic wall. This indicates that Equation (7.36) is conservative.

The load continued to increase throughout the test as distributed cracking occurred in the specimen. The maximum load of 92 kips (409 kN) is also represented as a diamond in Figure 7.44. This shear capacity of the wall falls between the flexural capacity of individual panels and the flexural capacity of a monolithic wall considering the sum of the individual panels. In this interaction diagram the external rods were considered in the monolithic case and were not considered in the individual panel case. If the pair of external rods is used as tensile reinforcement for an individual panel the section is overreinforced. As a general design rule to determine the flexural capacity of an individual panel, the internal bonded reinforcement should be included in calculating the flexural capacity if it is located on the tensile side of the panel.

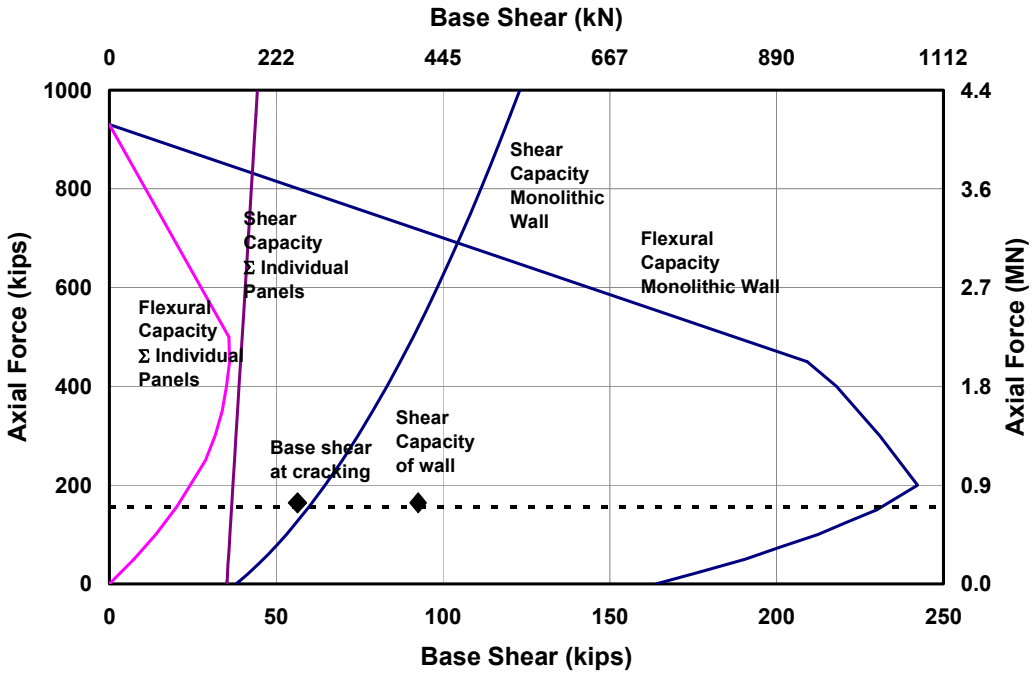

Figure 7.44: Base shear capacity for Shear Wall Specimen 2 considering individual panel behavior using Equation (7.36) and monolithic wall behavior

An interaction diagram that combines the individual panel design equations using the shear capacity for individual panels is based on Equation (7.38) is shown in Figure 7.45. The first diagonal crack formed at a load of 55.6 kips (247 kN) is closer to the prediction of base shear using Equation (7.39).

Equation (7.38) predicts a shear capacity of 79 kips for Shear Wall Specimen 2. This exceeds the predicted capacity of an otherwise identical monolithic AAC shear wall using Equation (7.11), an indication that Equation (7.38) should not be applied directly to AAC shear walls. The effectiveness factor associated with that term is not known reliably, because axial load was not

varied for AAC shear walls composed of vertical panels. Based on the available data, an effectiveness factor of 0.2 would give a computed base shear capacity, governed by web-shear cracking, of 47.8 kips (213 kN). This corresponds to a ratio of observed V_{AAC} to predicted V_{AAC} of 1.2, which is believed to be acceptable. Applying the effectiveness factor to Equation (7.38) produces Equation (7.39). The observed base shear is closer to the results for the monolithic wall, indicating that Equation (7.39) is conservative.

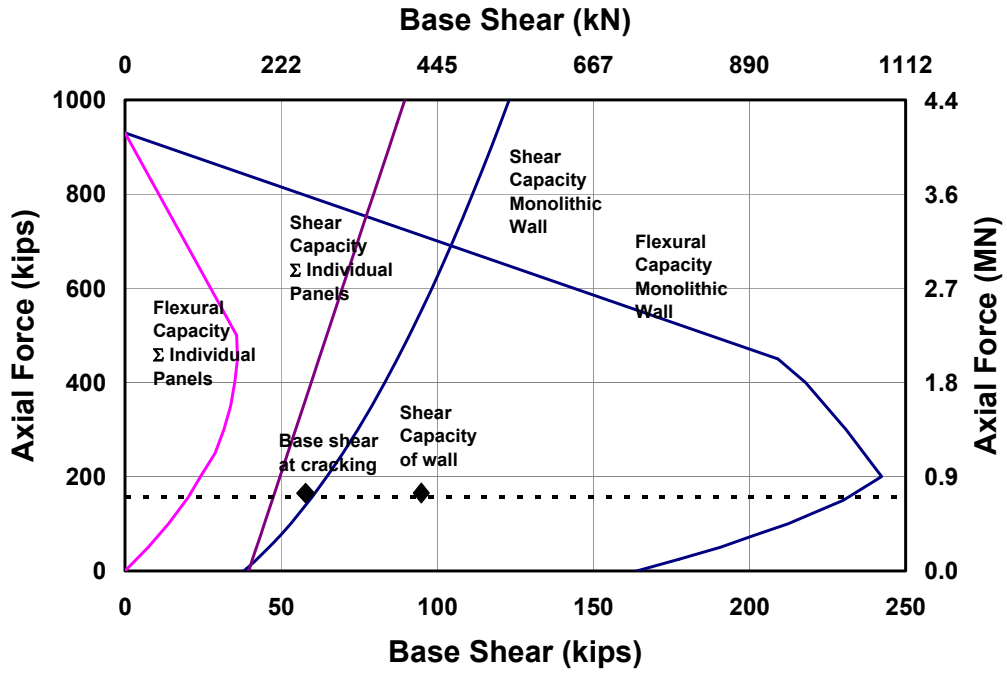

Figure 7.45: Base shear capacity for Shear Wall Specimen 2 considering individual panel behavior using Equation (7.39)and monolithic wall behavior

7.12 BEHAVIOR OF REMAINING SPECIMENS WITH VERTICAL PANELS

In the remaining specimens constructed of vertical panels (Shear Wall Specimens 15a, 15b, 16 and the Two-story Assemblage Specimen), vertical

cracks at the joints were not observed until the end of the test when the wall stiffness was reduced due to prior cracks. Furthermore, the cracks left at least three panels joined together. In this section the construction methods for the shear wall specimens are considered and design recommendations are proposed.

7.12.1 Construction Methods for Vertical Panel Specimens

In Shear Wall Specimen 2 the panel faces were prepared and pressure was applied perpendicular to the joint, parallel to the plane of the wall. Initially, the joints were not mortared on both faces. After a lack of coverage was observed in several joints, the panel was removed, cleaned and re-installed with mortar applied to both faces of the joint. This procedure was applied thereafter. The joint was clamped at the base (using one clamp on each wall face) and at the top (using one clamp at the centerline of the wall). The construction process used in Shear Wall Specimen 2 indicated that several conditions can increase the strength of the head joint between vertical panels:

- Cleaning and wetting the panel face prior to application of the thin-bed mortar increases the adhesion.
- Applying mortar to both faces of the vertical joint increases the extent of bond at the joint.
- Clamping adjacent panels applies pressure and increases the adhesion.

7.12.2 Proposed Design Criteria Using Improved Construction Methods

The three previous construction recommendations were used in the shear wall specimens where vertical cracks along the joints were not a problem. Pressure was applied to the joint using four clamps, one clamp on each wall face, both at the bottom and top of the wall. The proposed design recommendation is

to relax the individual panel requirements to groups of three panels connected together for walls meeting the design criteria of Section 7.12.1.

The base shear versus axial load interaction diagram including the capacities as governed by flexure and shear for groups of panels are included in Figure 7.46. Equation (8.11) was used to predict web-shear cracking was used for panel groups with an aspect ratio less than or equal to two. Equation (7.36) was used to predict the capacity of individual panels. The resulting interaction diagram is close to the observed shear cracking capacity, while the flexural capacity is conservative with respect to the observed flexural capacity.

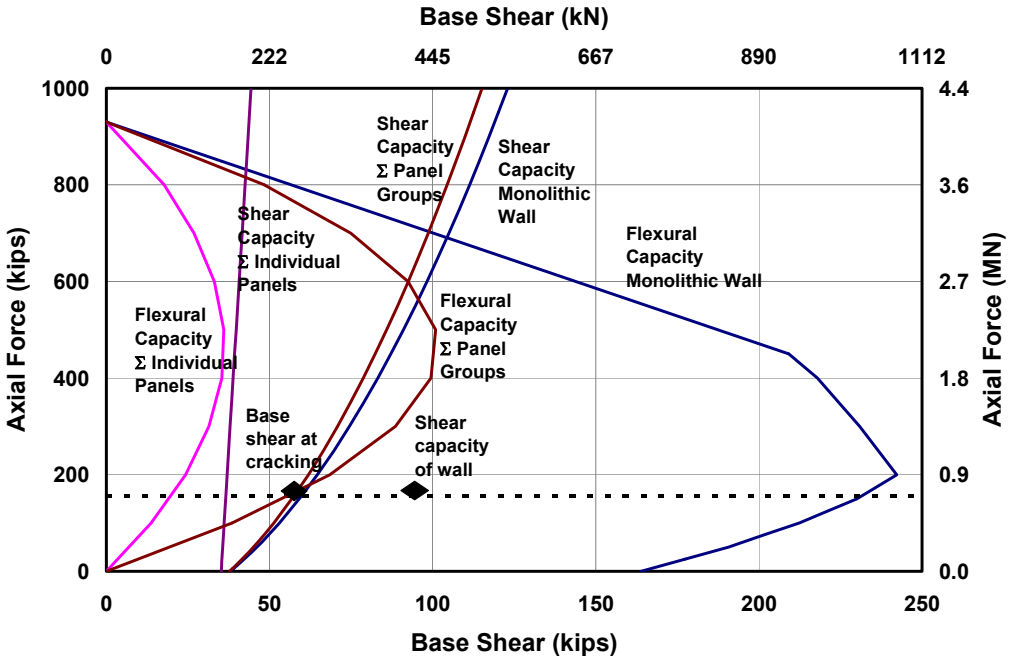

Figure 7.46: Base shear capacity for Shear Wall Specimen 2 considering individual panel behavior using Equation (7.36), behavior of panel groups and monolithic wall behavior

A base shear versus axial load interaction diagram for Shear Wall Specimen 15a is shown in Figure 7.47. In this specimen the internal reinforcement is included in the flexural capacity of individual panels. The range of axial load is 100 kips (445 kN) is intended to represent potential design axial loads in a shear wall. This example illustrates the increase in shear and flexural capacity of groups of three panels versus individual panel behavior. In conclusion, the effect of vertical cracks in panels can be accounted for theoretically. Design provisions exist in order to account for potential separation between vertical panels. Based on construction techniques the design restrictions can be relaxed if vertical cracks are not expected in a shear wall.

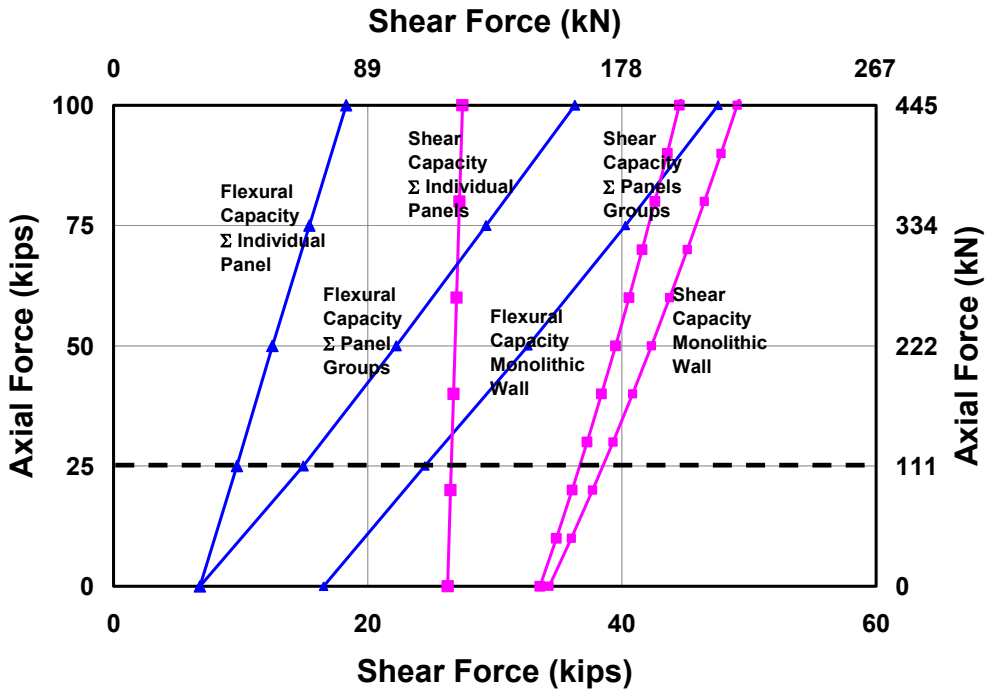

Figure 7.47: Base shear capacity for Shear Wall Specimen 15 considering individual panel behavior using Equation (7.36), behavior of panel groups and monolithic wall behavior

CHAPTER 8

Observed Versus Predicted Behavior of AAC Two-story Assemblage Specimen

The primary objective of this chapter is to describe the behavior of the Two-story Assemblage Specimen tested at UT Austin on August 12, 2002. This chapter presents the design objectives, actual loading history, actual displacement history, major events, history of crack formation, and sequence of hysteretic behavior. Finally, the observed behavior is compared with that predicted.

8.1 PREDICTED BEHAVIOR OF TWO-STORY ASSEMBLAGE SPECIMEN

The in-plane behavior of the AAC shear walls in the Two-story Assemblage Specimen depends on the plan configuration, reinforcement and axial load. The reinforcement was selected so that the wall behavior would be governed by flexure rather than shear.

The in-plane capacity of each of the two shear walls comprising the Two-story Assemblage Specimen was predicted prior to testing. An interaction diagram for the initial prediction of flexural cracking, sliding shear, web-shear cracking, yielding of the flexural reinforcement, and the nominal flexural capacity of each individual wall based on the proposed equations of Chapter 8, are presented in Figure 5.1. The contribution of the dowels is included in the initial prediction for sliding-shear capacity. The flexural cracking capacity was larger than the nominal flexural capacity. To prevent potentially unstable behavior at flexural cracking, a bond breaker (consisting of plastic sheeting between the leveling bed mortar and the AAC wall panels) was used between the flanges and a 12 in. (0.3 m) section of the shear wall. This reduced the flexural cracking

capacity below the nominal flexural capacity. The axial load applied to each wall in the Two-story Assemblage Specimen was 30.2 kips (133 kN) shown by a dashed horizontal line in Figure 5.1. At this level of axial load the following major events are predicted in order of occurrence: flexural cracking; yielding of the flexural reinforcement; and nominal flexural capacity. This specimen was not expected to exhibit web-shear cracking or sliding shear.

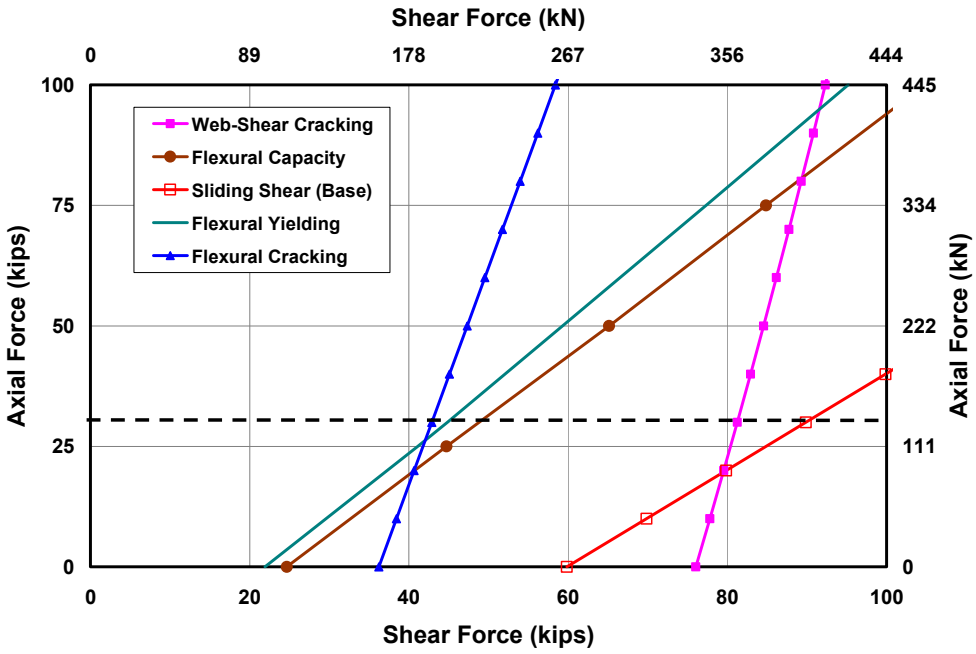

Figure 8.1: Initial prediction of the interaction diagrams for a single shear wall in Two–story Assemblage Specimen based on previous shipment of Class 4 AAC

The initial predictions were based on the tested strength of material from the Class 4 AAC from Babb. ASTM C1006 splitting tensile strength tests performed prior to testing indicated that the splitting tensile strength of 53 psi

(0.36 MPa) was significantly below the splitting tensile strength of 85 psi (0.58 MPa) from the previous shipment of Class 4 AAC from the same manufacturer. The observed tensile strength of 53 psi (0.36 MPa) was not used in the initial prediction of assemblage strength because the moisture content was 25%, which would cause a decrease in material properties. Further material testing conducted at C1386 yielded a compressive strength of 495 psi (3.4 MPa) and a splitting tensile strength of 45 psi (0.31 MPa), both of which fall below the tested strengths of the prior Babb shipment of Class 4 AAC material as described in Section 3.7. Interaction diagrams based on the actual tested strengths are shown in Figure 8.2. While the flexural capacity does not vary significantly, the web-shear cracking capacity will decrease proportionally with splitting tensile strength. In this specimen the revised web-shear cracking capacity decreases by a factor of the actual splitting tensile strength divided by the assumed splitting tensile strength (85/45) or two. Because of the unexpected non-complying material, the assemblage showed unexpected web-shear cracking. This did not appear to affect the flexural behavior of the Two-story Assemblage Specimen. It may have slightly reduced its drift and ductility capacities.

The prediction of major events based on the tested material strengths is simultaneous flexural cracking, web-shear cracking and yielding of the flexural reinforcement followed by nominal flexural capacity. As with the initial prediction, sliding shear was not expected.

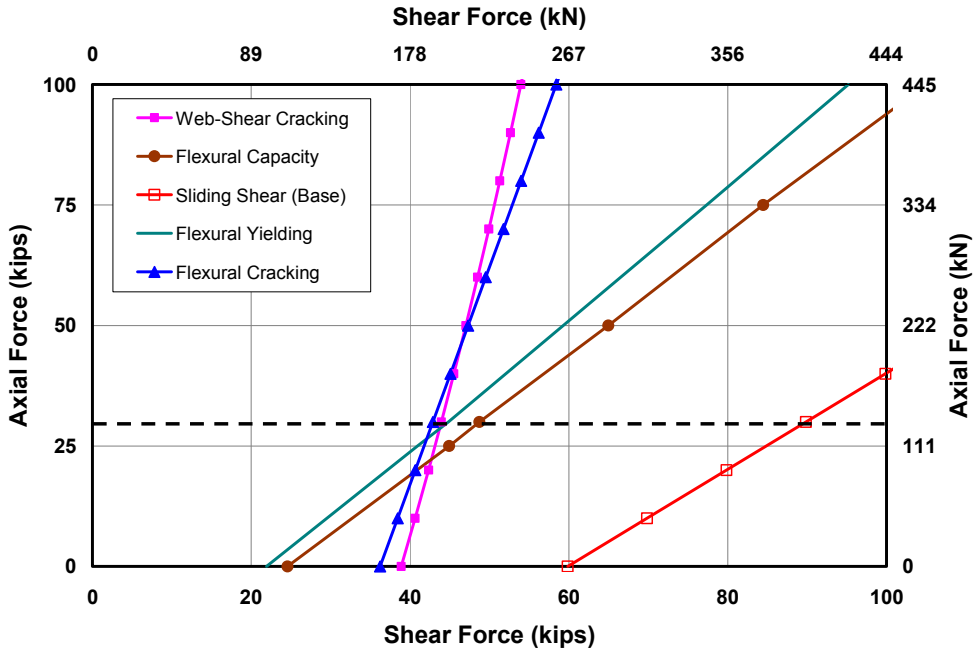

Figure 8.2: Interaction diagrams for a single shear wall in Two–story Assemblage Specimen based on tested material strengths

8.2 LOADING HISTORY

The actual loading history for the Two-story Assemblage Specimen is presented in Figure 8.3. The loading protocol described in Chapter 4 was initially force-controlled based on predicted major events. To limit degradation of the compression toe only two cycles at each load were performed. The actual displacement histories at the top and midheight of the structure are presented in Figure 8.4 and Figure 8.5. After yielding of the flexural reinforcement the wall was loaded to target displacement values. One cycle at each displacement level was selected to avoid degradation of the compression toe. Strength degradation was defined as occurring whenever the maximum ordinate of the displacement

envelope of the specimen in any particular cycle was less than the maximum ordinate if the envelope in the corresponding direction in the previous cycle. Monotonically increasing load point numbers are assigned for each set of data recorded during the test. Data are classified into cycles with maximum loads and drift ratios for each cycle (Table 8.1). Loading to the south is considered positive; loading to the north, negative.

Cycles are further classified by the direction of loading in terms of "a" and "b," where "a" refers to loading to the south, and "b" refers to loading to the north.

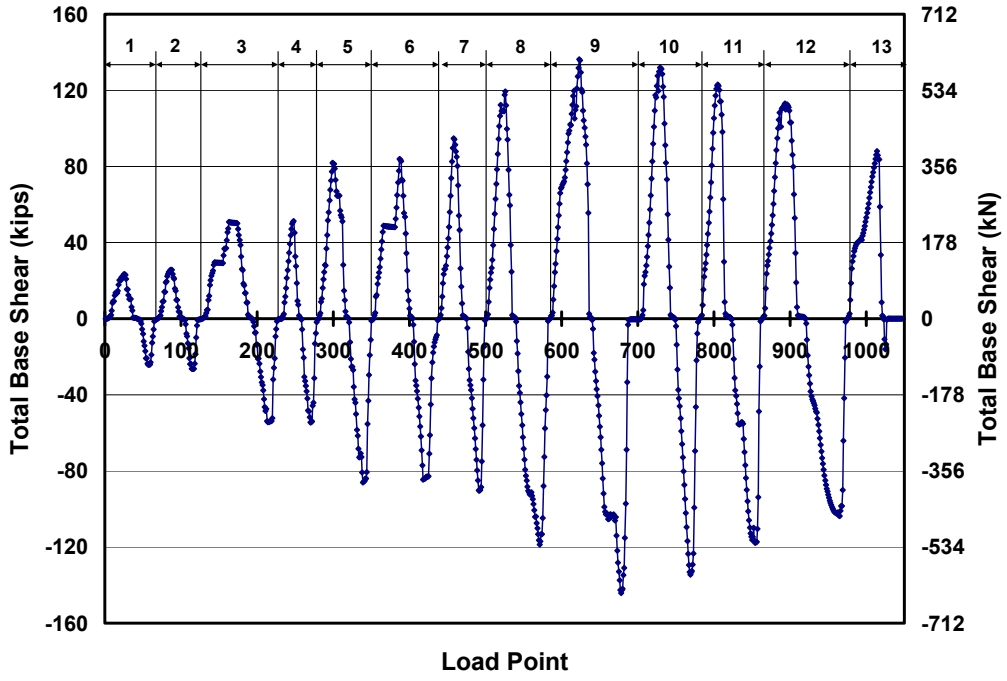

Figure 8.3: Actual loading history for Two-story Assemblage Specimen (numbers at top designate cycle numbers)

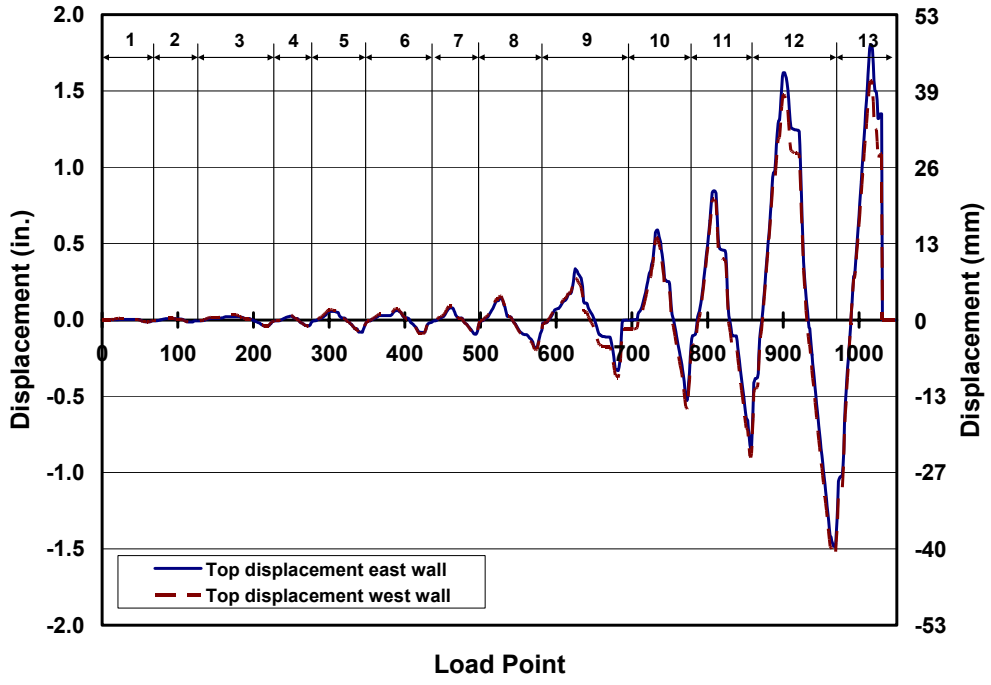

Figure 8.4: Actual displacement history at the top of the Two-story Assemblage Specimen (numbers at top designate cycle numbers)

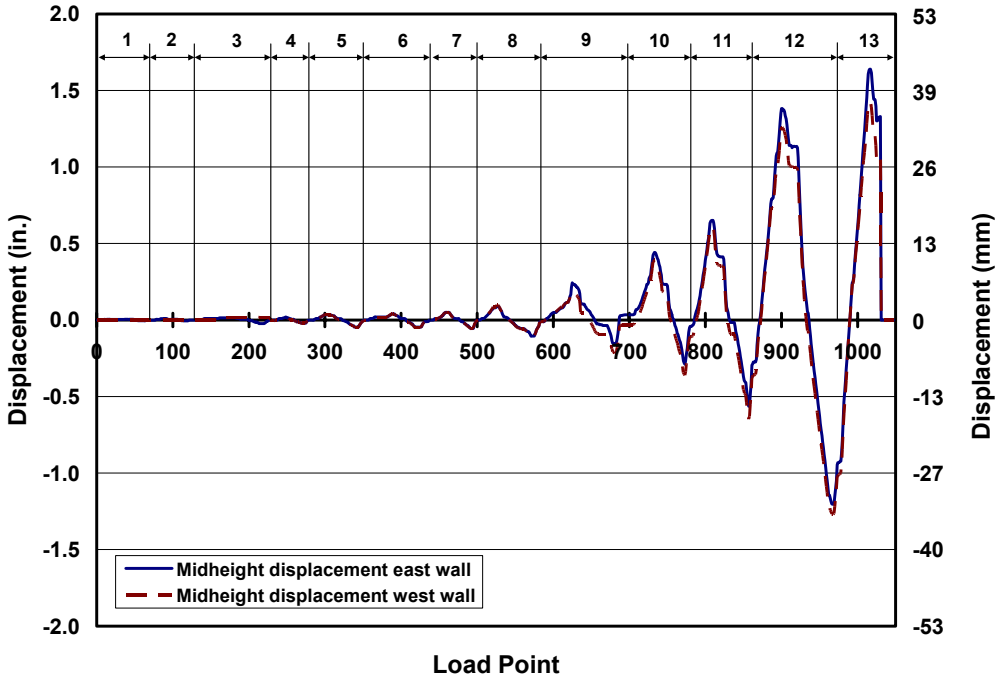

Figure 8.5: Actual displacement history at midheight of the Two-story Assemblage Specimen (numbers at top designate cycle numbers)

Table 8.1: Load points, maximum load and drift ratios for each cycle for the Two-story Assemblage Specimen

Cycle	Load Points	Maximum Applied Load kips (kN)	Max. Drift Ratio (%)	Cycle	Load Points	Minimum Applied Load kips (kN)	Min. Drift Ratio (%)
1a	1 - 40	23.4 (104)	0.00	1b	41 - 70	-24.3 (-108)	0.01
2a	71 - 101	25.6 (114)	0.01	2b	102 - 126	-26.4 (-118)	0.01
3a	127 - 192	50.9 (226)	0.01	3b	193 - 230	-54.4 (-242)	0.02
4a	231 - 258	51.3 (228)	0.01	4b	259 - 280	-54.5 (-243)	0.02
5a	281 - 320	81.9 (364)	0.03	5b	321 - 352	-86.1 (-383)	0.04
6a	353 - 403	84.0 (374)	0.03	6b	404 - 440	-84.6 (-376)	0.04
7a	441 - 472	94.8 (422)	0.04	7b	473 - 500	-90.4 (-402)	0.05
8a	501 - 538	119.4 (531)	0.07	8b	539 - 585	-118.7 (-528)	0.09
9a	586 - 638	136.3 (607)	0.15	9b	639 - 700	-144.3 (-642)	0.17
10a	701 - 746	131.9 (587)	0.27	10b	747 - 782	-134.6 (-599)	0.26
11a	783 - 820	122.9 (547)	0.39	11b	821 - 865	-117.8 (-524)	0.41
12a	866 - 915	113.0 (503)	0.73	12b	916 - 975	-103.8 (-462)	0.71
13a	976 - 1022	88.0 (392)	0.79	-	-	-	-

8.3 SEQUENCE OF CRACK FORMATION AND MAJOR EVENTS FOR TWO-STORY ASSEMBLAGE SPECIMEN

This section presents the observed damage in the Two-story Assemblage Specimen. The crack formation in the shear walls and the loading slabs are treated independently. The sequence of crack formation is described in terms of major events: points during the test when either the stiffness or testing conditions of the specimen changed (for example, flexural cracking or web-shear cracking). Table 8.2 lists the major events and the load point at which they occurred.

Table 8.2: Major events in Two-story Assemblage Specimen

Major Event	Load Point	Physical Description
1	173	Flexural cracking west wall, loading south
2	211	Flexural cracking west wall, loading north
3	300	Flexural cracking east wall, loading south
4	334	Flexural cracking east wall, loading north
5	418, 458	Local vertical cracking in both walls
6	520	Diagonal cracks around dowels in west wall, loading south
7	565	Diagonal cracks around dowels in west wall, loading north,
8	571	Diagonal cracks around dowels in east wall, Yielding of reinforcement in east wall, and web-shear cracking in both walls, loading north
9	615	Diagonal cracks around dowels in east wall, Yielding of reinforcement in east wall, and web-shear cracking in both walls, loading south
10	621	Yielding of reinforcement in west wall, loading south
11	675	Yielding of reinforcement in west wall, loading north
12	624-732	Distributed web-shear cracking
13	623-806	Sliding of web, with damage around dowels
14	772-890	Vertical cracks formed near panel joints
15	833, 856	Cracks formed in flanges
16	856-966	Spalling around the dowels and in the flanges
17	966, 1031	Vertical cracks formed in the west wall and as load was applied the crack opened enough to lose the flange

8.3.1 Formation of Flexural Cracks in Shear Walls of the Two-story Assemblage Specimen

Flexural cracks formed first in the west wall at Load Point 173 (loading south) and Load Point 211 (loading north). The corresponding base shears and drift ratios are 50.2 kips (223 kN), 48.5 kips (216 kN), 0.016% and 0.015%. Flexural cracks formed in the east wall at Load Point 300 (loading south) and Load Point 334 (loading north). The corresponding base shears and drift ratios are 81.6 kips (363 kN), 72.9 kips (324 kN), 0.026% and 0.028%. The formation of flexural

cracks, ranging from 20 in.(0.5 m) to 24 in. (0.6 m) in length, comprised Major Events 1 through 4.

8.3.2 Formation of Vertical Cracks and Local Damage to Shear Walls of Two-story Assemblage Specimen

Major Event 5 consists of vertical cracks that formed in the west and east walls at Load Points 418 and 458, when the base shear was 84.6 kips (376 kN) and 94.8 kips (422 kN) respectively. The drift ratio was 0.039% for both load points.

In Major Event 6 and 7 diagonal cracks formed around the dowels at Load Points 520 and 565, when the base shear was 112.4 kips (500 kN) and 104.2 kips (463 kN) respectively. The corresponding drift ratios were 0.058% and 0.06%. The damage from the beginning of the test through Major Event 7 is shown in gray in Figure 8.6 and Figure 8.7.

8.3.3 Formation of Web-shear Cracks and Yielding of the Flexural Reinforcement in the Shear Walls of Two-story Assemblage Specimen

Loading to the south at Load Point 571 the following events occurred in the Two-story Assemblage Specimen: web-shear cracking in both walls; diagonal cracking around the dowels in the east wall; and yielding of the reinforcement in the east wall. All of these events are included in Major Event 7. The corresponding base shear and drift ratio are 118.7 kips (528 kN) and 0.087%. Major Event 8 consists of the same events while loading to the north at Load Point 615. The corresponding base shear and drift ratio are 117 kips (521 kN) and 0.075%. Major Event 10 consists of yielding of the flexural reinforcement in the west wall while loading to the south. The corresponding base shear and drift ratio are 127.3 kips (566 kN) and 0.096%. At Major Event 11 the strain gages at 5 in.

(127 mm) and 8 in. (203 mm) from the base of the wall yielded. The corresponding base shear and drift ratio are 132.9 kips (591 kN) and 0.11%. It is probable that the base of the bar yielded prior to this load point; the global hysteretic behavior for the west wall of the structure indicates that first yield occurred at a drift ratio of 0.094%. The damage in Major Events 8 and 9 is shown in black in Figure 8.6 and Figure 8.7; damage in Major Events 1-7 is shown in gray.

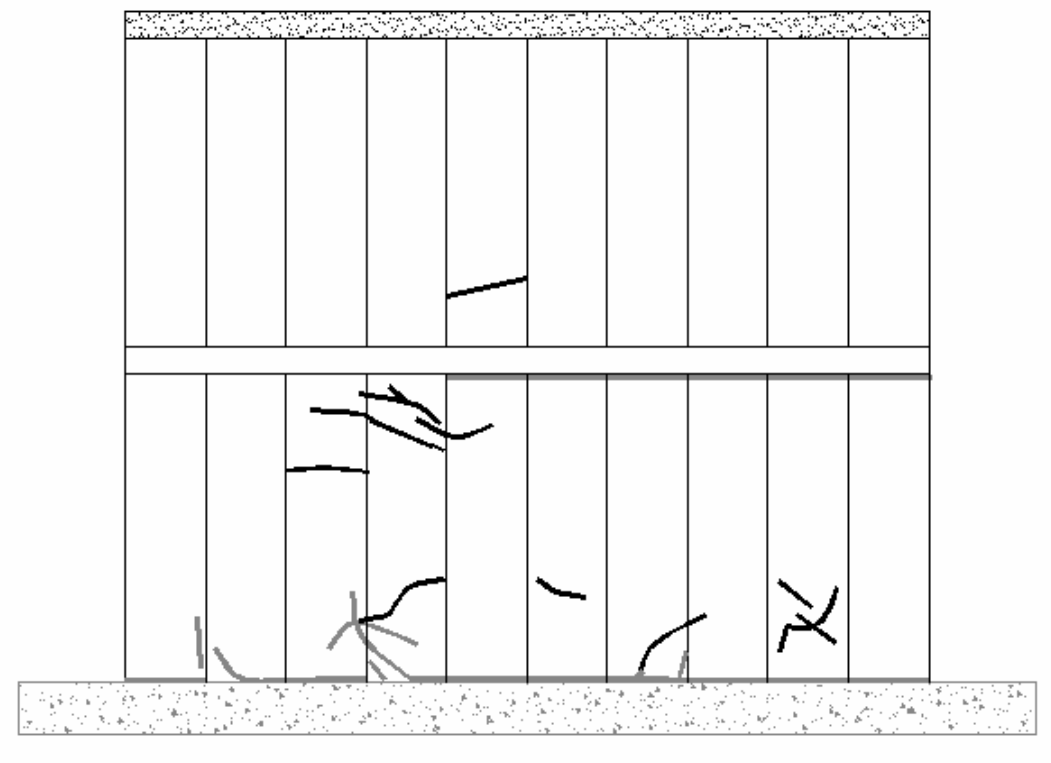

Figure 8.6: Cracking in the west wall after Major Event 8

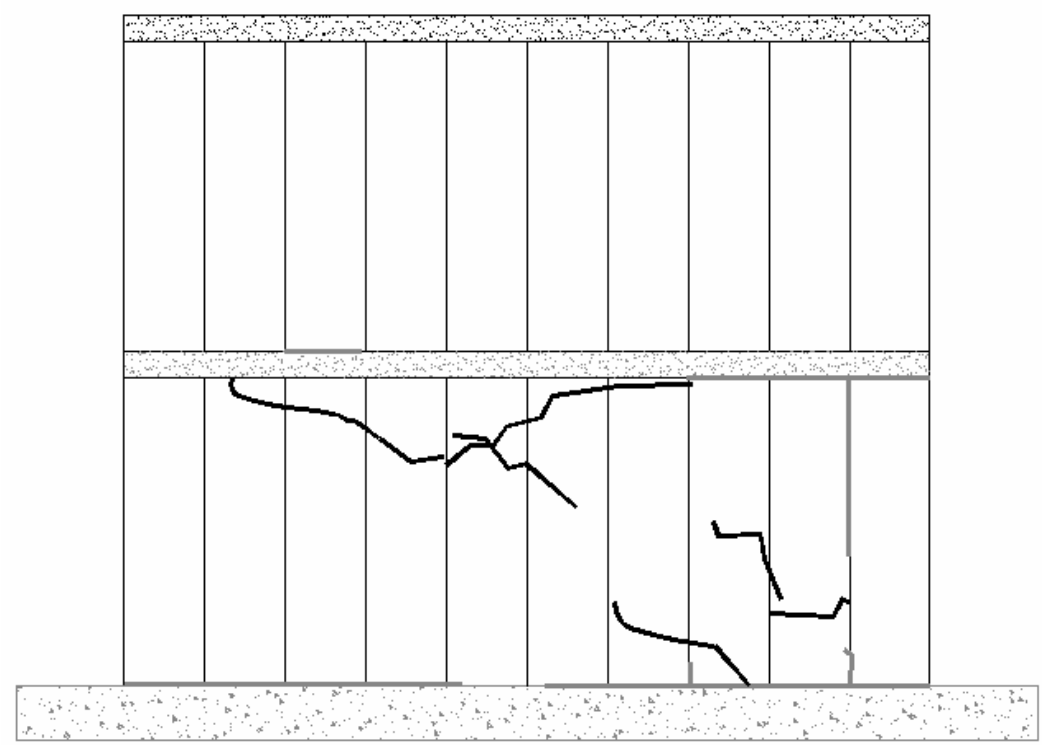

Figure 8.7: Cracking in the east wall after Major Event 8

8.3.4 Formation of Additional Cracks in Shear Walls of Two-story Assemblage Specimen

As the test continued, distributed web-shear cracking was observed during Load Points 624 through 732 (Major Event 12). The maximum loads of 136.4 kips (606 kN) and 144.3 kips (642 kN) were reached at Load Points 623 (loading south) and 678 (loading north) respectively. At these load points a slip of 0.02 in. (0.5 mm) or greater was observed between the shear wall and foundation. This slip and accompanying damage around the dowels constitutes Major Event 13. This damage includes the formation of diagonal cracks around the dowels, separating those dowels from the webs of the AAC shear walls (Figure 8.8).

After 3 cycles of flexural rocking to drift ratios of 0.32% (loading south) and 0.24% (loading north), vertical cracks began to form at the interfaces between the webs and the flanges between Load Points 772 and 890 (Major Event 14). Diagonal cracks formed in the flanges at Load Points 833 and 856 (Major Event 15). Further degradation of dowel action is also identified by spalling of AAC around the diagonal cracks (Figure 8.8) which constituted Major Event 16.

Figure 8.8: Example of diagonal cracks and spalling at dowel location

As the displacements increased, the flange panel did not slide with the web in the direction of loading, resulting in local damage to the flange and finally in instability of the flange at both the north and south ends of the specimen. At the north end, the flange damage was accompanied by a wide vertical crack in the east web at Load Point 966. As the wall was loaded to the north in the next cycle the vertical crack propagated and opened to a displacement of one in. (26 mm) at Load Point 1031 (Figure 8.9 and Figure 8.10), which halted the testing of the Two-story AAC Assemblage Specimen. Final cracking patterns for each exterior faces of the specimen are shown in Figure 8.11 through Figure 8.14. Cracks previously shown are in gray; subsequent cracks are shown in black.

Figure 8.9: Vertical crack at north end of east wall (top of first story wall)

Figure 8.10: Vertical crack at north end of east wall (base of first story wall)

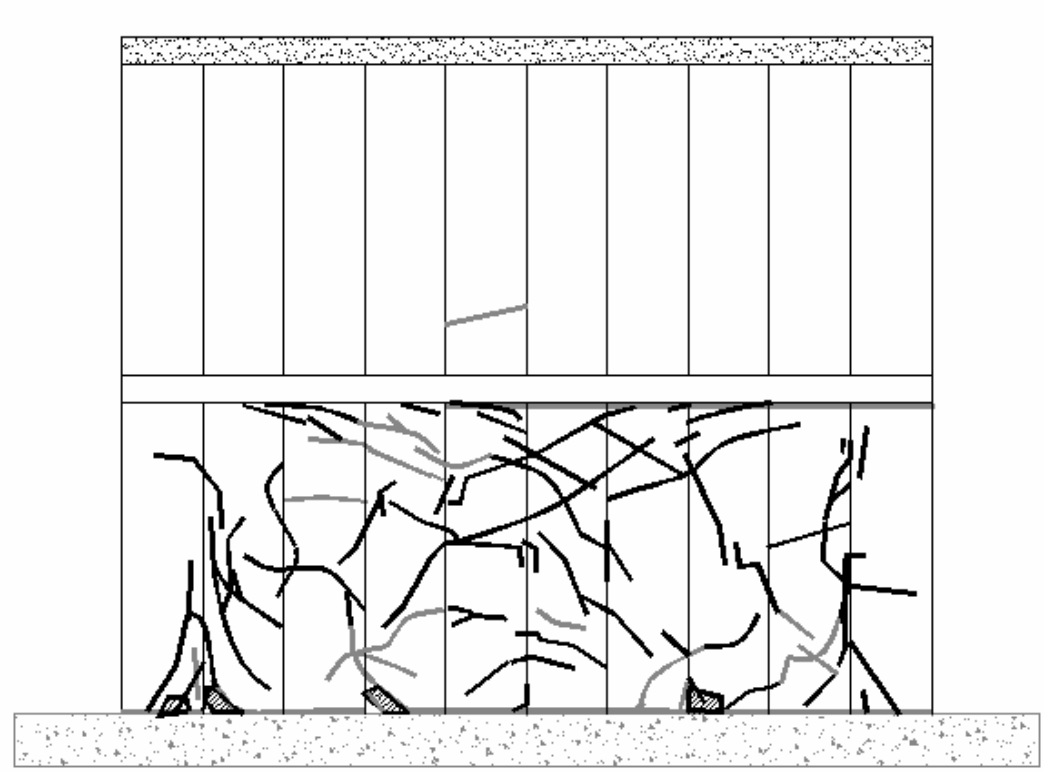

Figure 8.11: Cracks in the west wall at end of assemblage test

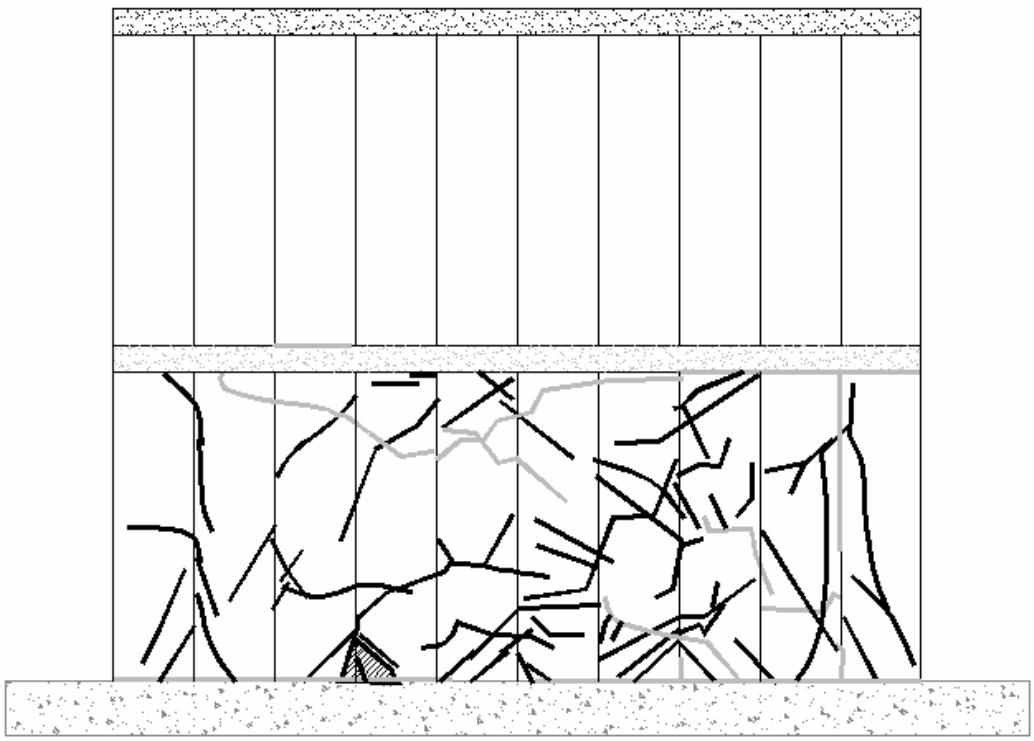

Figure 8.12: Cracks in the east wall at end of assemblage test

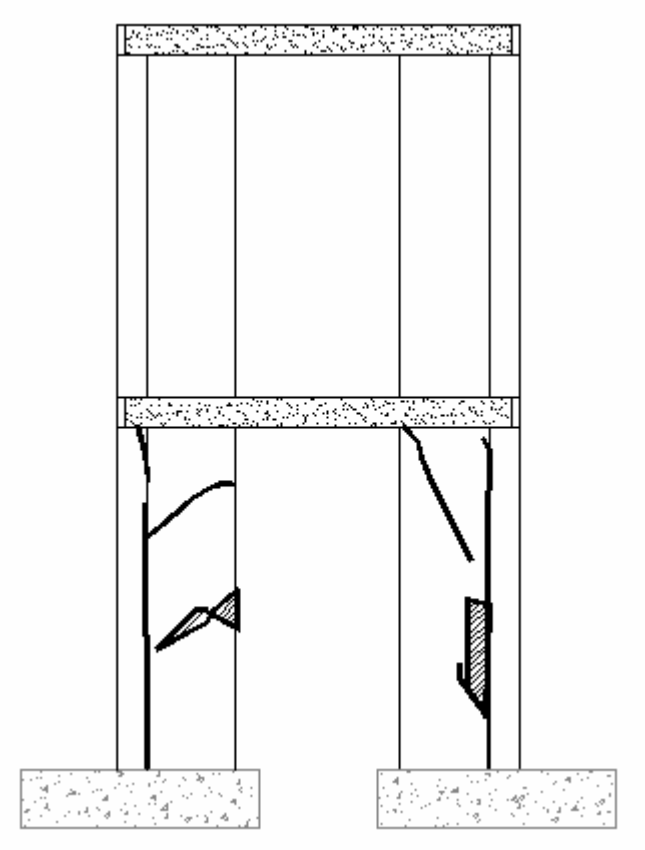

Figure 8.13: Cracks in the south wall at end of assemblage test

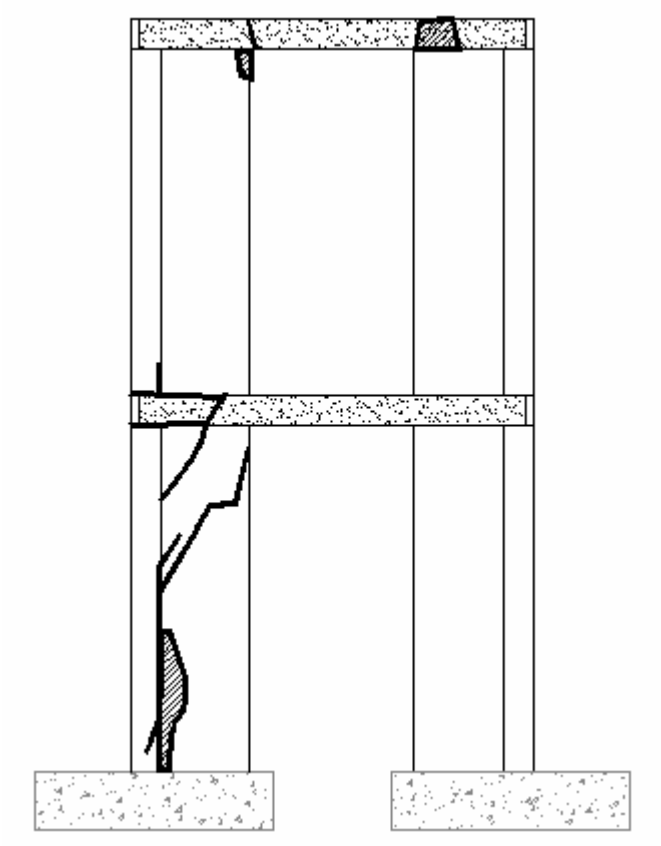

Figure 8.14: Cracks in the north wall at end of assemblage test

8.3.5 Crack Formation in Slab of the Two-story Assemblage Specimen

A shear crack formed in the north bond beam at the second level. At the location of the bond beam the loading slab was supported almost entirely on the bond beam. The capacity of the bond beam was exceeded which caused the damage shown in Figure 8.15.

Cracks were not observed in either floor diaphragm. Inspection of the specimen after the test did not reveal cracks between floor panels or between

panel-to-bond beam joints. This identifies that shear was transferred entirely through adhesion at these locations. Inspection of the strain gage readings in the diagonal slab reinforcement (Section 5.2.6.1) indicates that during the entire test the strain in 24 of the 30 strain gages on the diagonal reinforcement was below 100 με, or is 4% of the yield strain. This indicates that the diagonal reinforcement was not participating in the lateral load resistance. In three of the gages the strain reached 300 με at a single load point; again, this is much less than the yield strain. Two additional gages drifted during the test, reaching maximum strains of 400 με and 1000 με. All of these results confirm that the diagonal reinforcement was not working in tension.

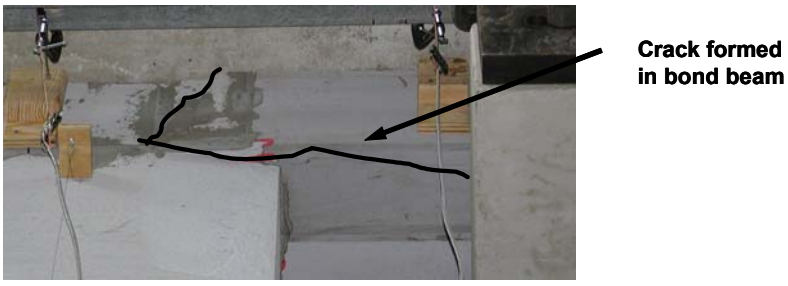

Figure 8.15: Damage to the bond beam on the second level of assemblage

8.4 DISCUSSION OF OBSERVED BEHAVIOR

The following behaviors observed in the Two-story Assemblage Specimen can be predicted based on the predictions of Chapter 8:

- flexural cracking at the base;
- web-shear cracking in the webs of both walls in the lower story;
- yielding of the flexural reinforcement at all four corners of the assemblage; and
- sliding at the base of the specimen.

In the following sections these behaviors are compared to the predicted behavior defined in Chapter 8.

8.4.1 Flexural Cracking

Flexural cracking was observed at the base of the west wall at total base shears of 48.4 kips (215 kN) and 50.2 kips (223 kN) while loading to the south and north respectively. Flexural cracking was observed at the base of the east wall at a total base shear of 81.6 kips (364 kN) and 72.9 kips (324 kN) while loading to the south and north respectively. The predicted flexural cracking capacity of each wall is 42.9 kips (191 kN), corresponding to a flexural cracking capacity of the assemblage of 85.8 kips (382 kN). The ratios of observed to predicted flexural cracking capacity for the west wall are 0.56 (loading south) and 0.59 (loading north). The ratios of observed to predicted flexural cracking capacity for the east wall are 0.95 (loading south) and 0.85 (loading north). The low ratio of observed to predicted flexural cracking capacity in the west wall could be attributed to shrinkage cracking at the leveling bed, or to a reduced area of leveling-bed mortar. The bond-strength data from the Two-story Assemblage Specimen, combined with data from the shear walls, gave an average tensile bond strength of 68 psi (0.46 MPa) and a COV of 33%.

8.4.2 Vertical Cracking

The vertical cracking did not significantly affect the in-plane lateral strength or stiffness of the Two-story Assemblage Specimen. If the in-plane lateral stiffness of the specimen had been dominated by flexure, such cracks would have significantly decreased the stiffness and strength of the specimen. For this specimen, the ratio of shear stiffness to flexural stiffness is 1.35. Since this value is close to one, the shearing and flexural deformations contribute about equally to the flexibility of the specimen. Because the in-plane lateral stiffness of

the specimen was influenced about equally by shear and by flexure, the stiffness did not change much as a result of the vertical crack. Also, since the crack occurred two feet from the flange, the loss of flexural stiffness was less than it would have been had the crack occurred near the middle of the web.

8.4.3 Web-shear Cracking

Web-shear cracking was observed in both shear walls at a total base shear of 119 kips (530 kN) while loading to the north, and 117 kips (520 kN) while loading to the south. This is lower than the web-shear capacity of 157 kips (700 kN) predicted based on the splitting tensile strength from a previous shipment of Babb material from the same class. After the Two-story Assemblage Specimen was tested, tests conducted to confirm the splitting tensile strength gave an average value of 45 psi (0.3 MPa) with a COV of 15%. This corresponds to a total base shear capacity of 88 kips (391 MPa) at a total axial load of 60 kips (267 kN). This predicted value is based on the lower 10% fractile of the test results (Equation (8.11)). The ratio of observed to predicted web-shear cracking capacity is approximately 1.3 for both walls. If the web-shear cracking capacity were based on the average results for the tested shear wall specimens rather then the lower 10% fractile used for design, the ratio of observed to predicted web-shear cracking capacity would be 0.92.

8.4.4 Yielding of the Flexural Reinforcement and Nominal Flexural Capacity

Based on strain gage readings, the flexural reinforcement in the east wall yielded at a total base shear of 118 kips (525 kN) while loading to the north and to the south. The flexural reinforcement in the west wall yielded at a base shear of about 130 kips (580 kN) in each direction. These readings agree with the initial

decrease in stiffness observed in the hysteretic behavior (Figure 8.21), or first yield observed in the structure.

The initially predicted total base shear at flexural yielding at the base of each wall, excluding the effect of dowels, under the applied axial load of 60 kips (267 kN), was 90 kips (344 kN). The base shear is determined by dividing the flexural capacity by the effective height or M/V ratio. This method is illustrated in Figure 8.16. The increase in observed capacity is due to the dowels. The base shear at yielding can be predicted based on the flexural capacity at two critical sections:

- at the base, considering the contribution of the dowels to the flexural capacity, and
- at a critical section just above the ends of the dowels.

Including the contribution of the dowels would significantly increase the flexural capacity at the base. Assuming that the critical section is at the base, the base shear capacity at yield would be determined by calculating the flexural capacity at yield, including the dowel contribution, and converting it to an equivalent base shear yield capacity by dividing by the M/V ratio presented in Figure 8.16. Assuming that the critical section is at the point where the dowels end, the flexural capacity would be calculated without the dowels, and would be converted to a base shear yield capacity by dividing by the reduced lever arms between each load and the critical section. The results of these calculations are expressed in Table 8.3. The base shear at yielding of the flexural reinforcement falls between the limiting cases defined by the two critical sections noted above.

The flexural capacity was calculated using a yield strength of 75 ksi (520 GPa) based on mill reports of the longitudinal steel in the shear wall specimens.

Tests performed on the #4 bars in the Two-story Assemblage Specimen revealed a two distinct yield strengths 65 ksi (450 MPa) and 75 ksi (520 MPa), indicating that the longitudinal steel did not come from the same heat (Section 3.9).

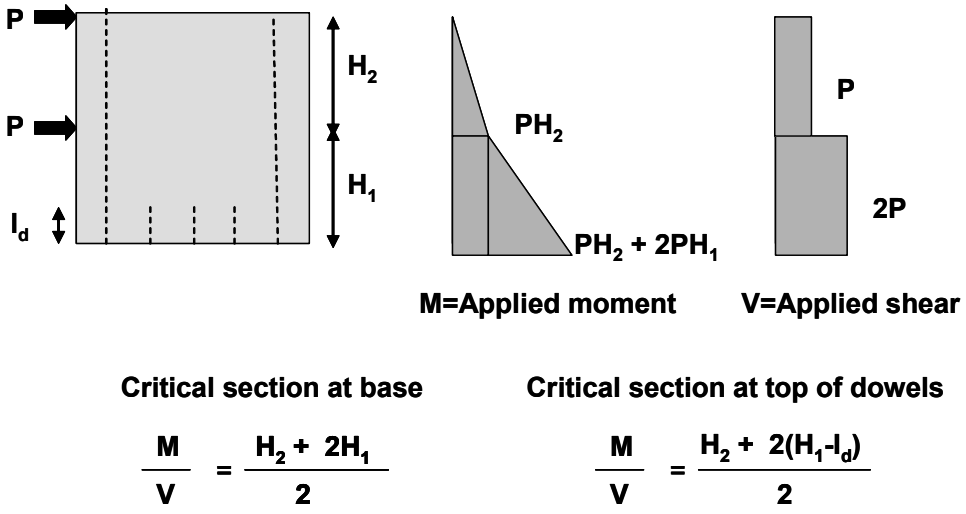

Figure 8.16: Shear span used to calculate the base shear capacity of a wall corresponding to a given flexural capacity

Table 8.3: Base shear capacity for the Two-story Assemblage Specimen for yielding of the flexural reinforcement and nominal flexural capacity

	Critical Section	
	Base of Wall	**Top of Dowels**
Base shear at flexural yield, kips (kN)	145 (644)	107 (477)
Base shear at nominal flexural capacity, kips (kN)	197 (877)	117 (521)

After the flexural reinforcement yielded, both walls exhibited flexural behavior, consisting largely of rigid-body rocking. Vertical displacements were observed at the wall bases on the tension side, due to yielding and bond deterioration of the tensile reinforcement. Crushing of the compression toe was

avoided, due to their lateral support by the flanges. The maximum loads observed in each wall was 136 kips (605 kN) loading to the south and 144 kips (641 kN) while loading to the north. The observed nominal flexural capacity falls between the bounds presented in Table 8.3.

8.4.5 Sliding Shear

Sliding was observed in the shear walls of the Two-story Assemblage Specimen. The sliding was measured through 2 in. (51 mm) linear potentiometers fixed to the foundation. The results of the sliding for each shear wall are shown in Figure 8.17. The observed sliding is equal for both the east and west shear walls. Near the end of the test at Load Point 900 (Cycle 12a), the instrument used to measure slip in the east wall reached the end of its stroke. Since the west instrument did not reach the end of its stroke, the slip measured in the west instrument was used to determine the slip in the east wall. While loading to the north at Load Point 957 (Cycle 12b), the spalling in the dowel area caused the bearing plate for the instrument to separate, signifying that accurate readings were no longer measured. From this point on, the slip in the west wall was considered equal to the measured slip in the east wall. After Load Point 1007 the east instrument also exceeded its available stroke. The displacement in the east wall after this point was assumed to be one-half of the total displacement, because this is consistent with the ratio of displacement to slip measured in the previous cycle loading to the south (Cycle 12a).

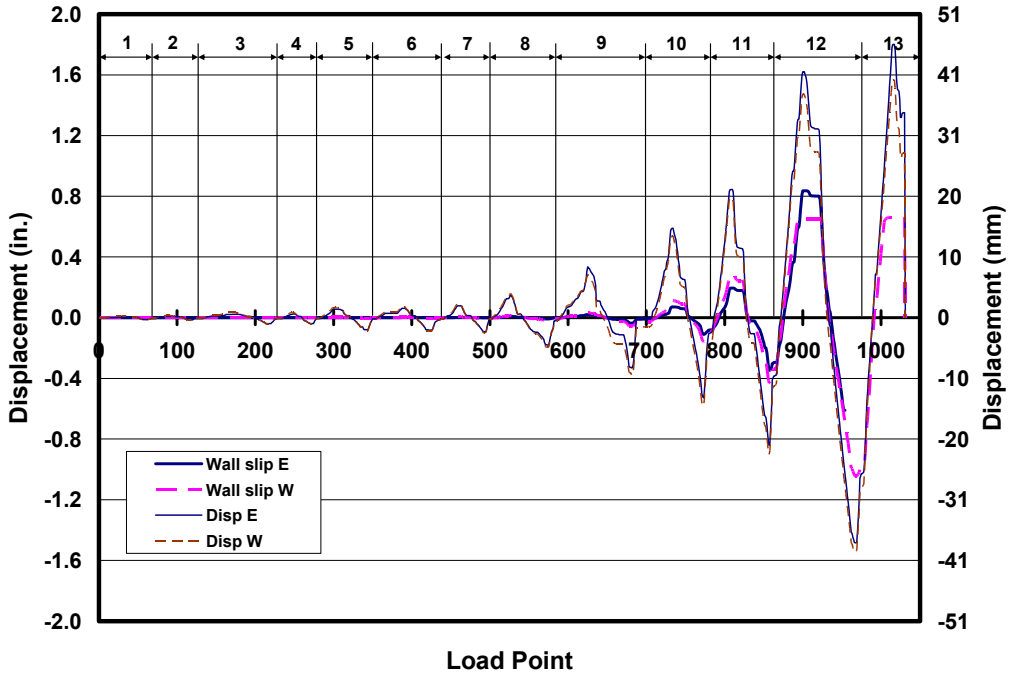

Figure 8.17: Displacement and corrected slip between shear walls and foundation of the Two-story Assemblage Specimen

The total base shear and sliding shear capacity for the specimen versus Load Point is presented in Figure 7.23 (reproduced from Chapter 8). The design sliding shear capacity is presented for the contribution of axial load and dowels (Figure 7.23) and the contribution of axial load only, using a coefficient of friction of 1.0. Initially, total lateral capacity based on the contribution of friction plus the dowel action of the longitudinal steel and dowels is accurate until Load Point 677. As described in Section 8.5.2, as damage around the dowels increases (Load Point 677 through the end of the test) the dowel contribution decreases, thus decreasing the total lateral capacity of the Two-story Assemblage Specimen.

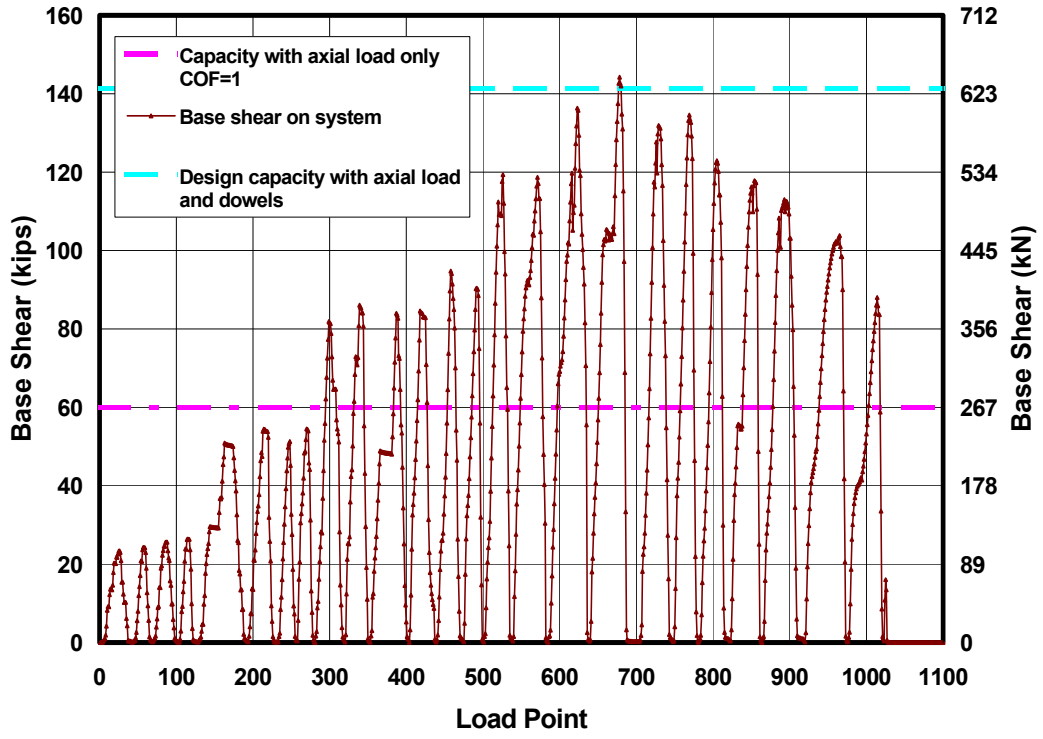

Figure 8.18: Base shear and sliding shear capacity versus Load Point for Two-story Assemblage Specimen

8.4.6 Diaphragm Behavior

The diaphragm behavior of the Two-story Assemblage Specimen is presented individually for the first and second elevated level.

This configuration of panels oriented perpendicular to the direction of load was tested in the first story of the Two-story Assemblage Specimen. The maximum applied load at this story of 72.1 kips (321 kN) corresponds to a load of 36.1 kips (160 kN) at each diaphragm to shear wall connection. The shear

strength of the reinforcement in the grouted keys working in dowel action is 39.6 kips (176 kN). No distress was observed at the joints, which indicates that load could have also been transferred through adhesion.

The upper diaphragm in the Two-story Assemblage Specimen was governed by adhesion, as indicated by the observed behavior presented in Section 8.3.5. The capacity of the AAC panel to grouted bond beam joint is 69.1 kips (310 kN) for each joint, 1.9 times the maximum applied load per joint of 36.1 kips (160 kN). The capacity of the AAC panel to AAC panel joint is 60.5 kips (270 kN) for each joint, 1.7 times the maximum applied load at each joint of 36.1 kips (160 kN). This further confirms that the proposed design provisions based on adhesion are conservative. Using the strut-and-tie model of Section 5.2.6.2 the diaphragm capacity is 77.1 kips (343 kN), 1.0 times the applied load. This strut-and-tie model is not proposed for design based on the discussion of Section 10.3.

8.5 LOAD-DISPLACEMENT BEHAVIOR

The overall hysteretic behavior of the Two-story Assemblage Specimen is summarized in Figure 8.21. Total base shear is the summation of the equal shears applied to each floor level. Positive displacements are to the south; negative, to the north. The load-displacement relationships for the east and west walls are shown separately in Figure 8.22. The load corresponds to the force applied to each floor slab (one half of the total load) or the load in each shear wall.

The tip displacement in each wall, corrected for the respective values of slip, is shown in Figure 8.19. The correction for slip in each wall was carried out by subtracting the slip at every load point from the measured displacement at every load point. The uncorrected slip data versus load point is shown in Figure 8.20. All

of the assumptions regarding slip are discussed in Section 8.4.5. While loading to the south, the difference in recorded displacement for each wall was 0.3 in. (7 mm) and 0.4 in. (10 mm) in Cycles 12a and 13a, respectively (Figure 8.22). This indicates that the east wall was subject to larger displacements. Similar differences in displacement exist in the hysteretic behavior for slip (Figure 8.19).

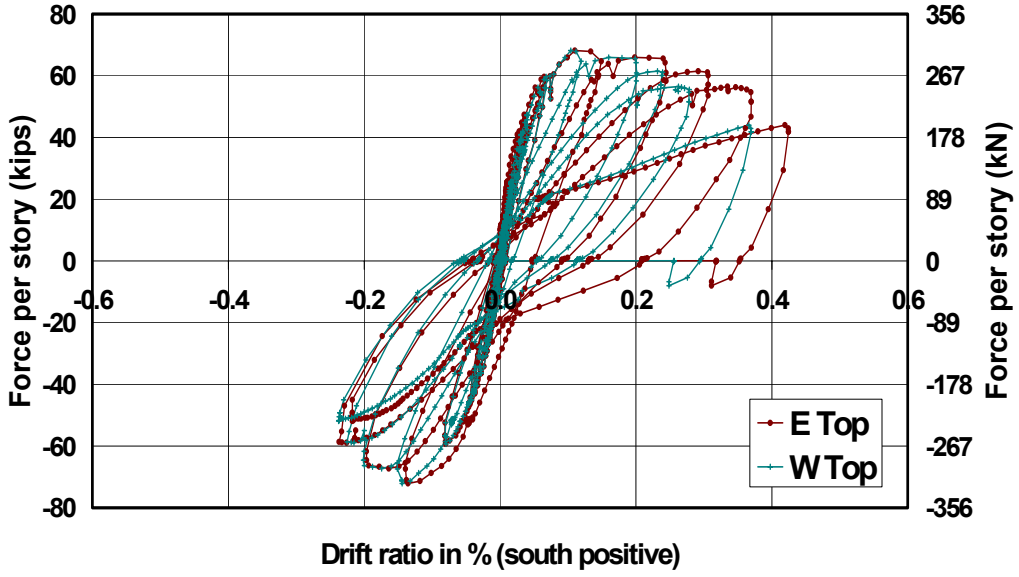

Figure 8.19: Hysteretic behavior of Two-story AAC Assemblage Specimen with slip removed (force per story)

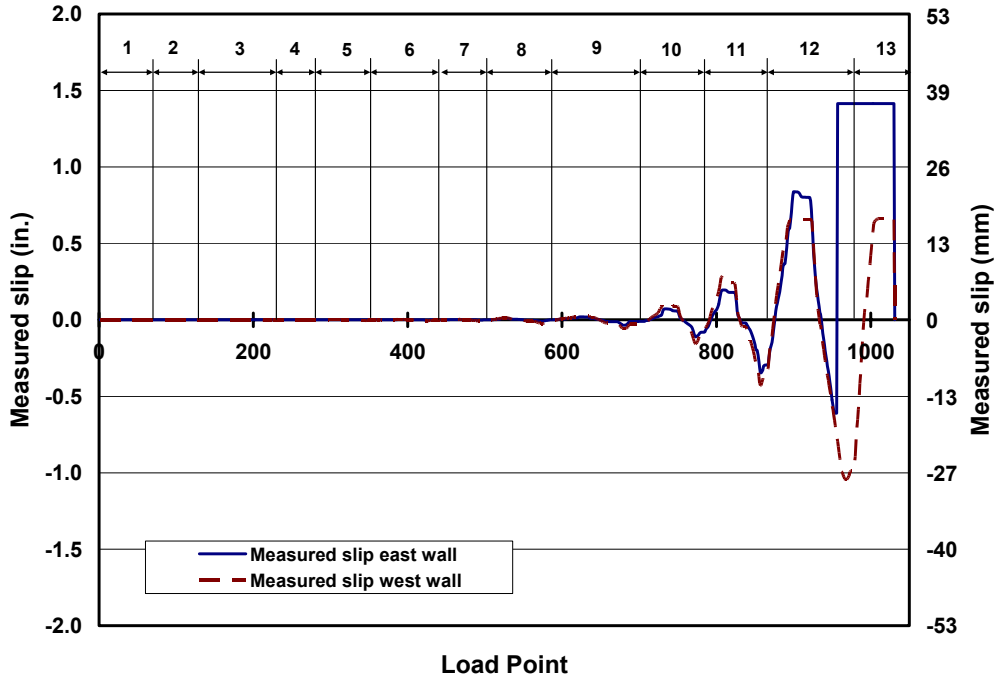

Figure 8.20: Uncorrected slip data for each wall in the Two-story Assemblage Specimen

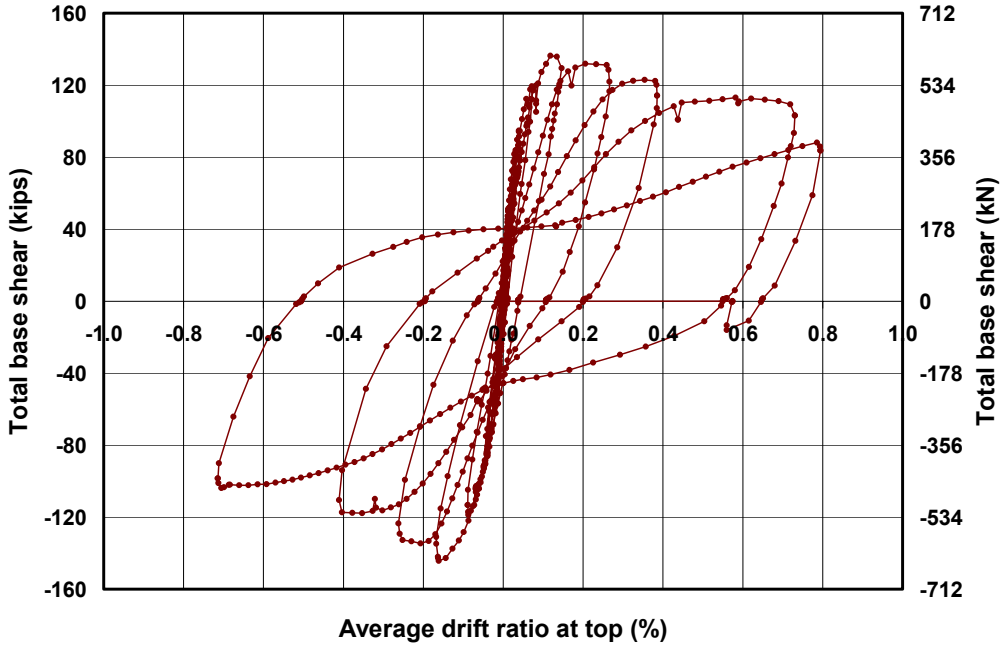

Figure 8.21: Overall hysteretic behavior of Two-story AAC Assemblage Specimen

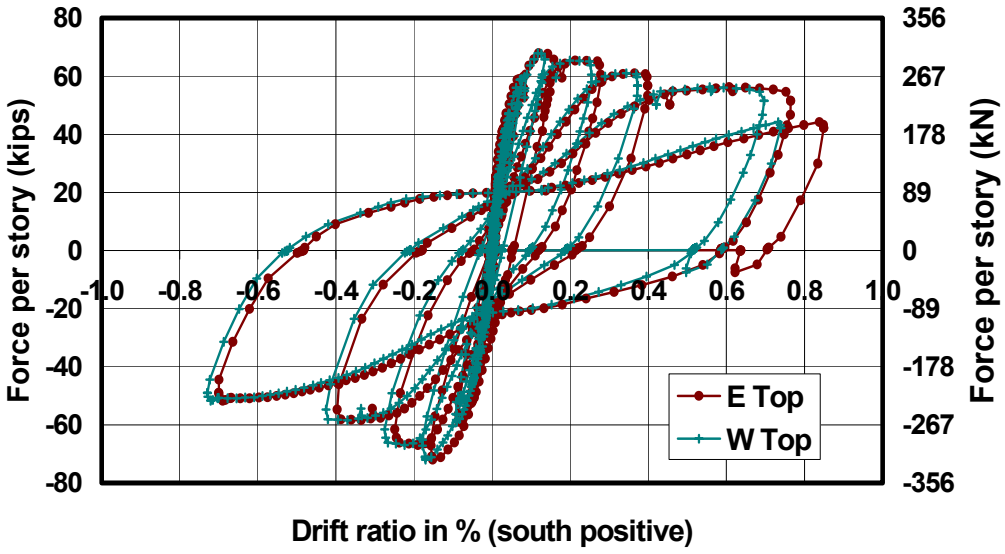

Figure 8.22: Hysteretic behavior of Two-story AAC Assemblage Specimen (force per story)

The force-displacement behavior is initially linear elastic. Stable flexural hysteretic loops are presented with a decrease in peak load less than 10% of the previous cycle until the final cycle, despite the presence of web-shear cracks. The hysteretic behavior would have improved if the web-shear cracks had not formed.

The effect of sliding in the Two-story Assemblage Specimen can be removed through Cycle 12b to evaluate the ductility and flexural performance of an AAC shear wall. After removing the base slip, the Two-story Assemblage Specimen reached drift ratios between 0.24% and 0.42%, and final displacement ductilities ranged from 2.5 to 6 (Table 8.4). The correction for slip in the final

cycle of the east wall includes an assumption for the slip. If this cycle were eliminated the drift would decrease to 5.3, a 10% difference.

Table 8.4: Drift ratios and displacement ductilities for each wall, with base slip removed

Shear wall / Direction of loading	Displacement ductility	Drift ratio at yield (%)	Drift ratio (%)
East wall / south	6	0.07	0.42
East wall / north	3.1	0.075	0.24
West wall / south	3.9	0.098	0.37
West wall / north	2.5	0.13	0.24

Including base slip, the Two-story Assemblage Specimen reached drift ratios between 0.7% and 0.85%. Final displacement ductilities (final displacement divided by the displacement at yielding of the flexural reinforcement), ranged from 7.8 to 12 (Table 8.5).

Table 8.5: Drift ratios and displacement ductilities for each wall, including base slip

Shear wall / Direction of loading	Displacement ductility	Drift ratio at yield (%)	Drift ratio (%)
East wall / south	12	0.07	0.85
East wall / north	9.2	0.075	0.70
West wall / south	7.8	0.098	0.74
West wall / north	7.8	0.13	0.73

8.6 CONCLUSIONS OF TWO-STORY ASSEMBLAGE SPECIMEN TEST

The assemblage test met the required objectives. The shear walls conformed to the predictive models for flexural cracking and web-shear cracking. Although the nominal flexural capacity was influenced by the presence of the

dowels, the actual load was bounded by the cases of full dowel participation and zero dowel participation. The knowledge of sliding in AAC shear wall specimens was improved in this specimen. It was used to confirm that the sliding shear capacity can be reliably predicted based on axial load multiplied by the coefficient of friction. Sliding occurs when the applied load exceeds μP. If the axial load is due entirely to self-weight W, the potential frictional resistance is simply μW, and sliding will occur when the response spectral ordinate exceeds μ. Since μ is 1.0 for this specimen, sliding will occur when spectral ordinates exceed 1.0 g. This is expected only in areas of high seismic risk.

Sliding shear resistance based on applied axial load is reasonably well understood based on the use of Shear Wall Specimen 4, the Two-story Assemblage Specimen and the direct shear tests to determine the appropriate coefficient of friction between AAC and leveling bed mortar or between AAC and AAC. Sliding shear resistance can be increased temporarily by thin-bed mortar or dowels but the effectiveness is degraded by flexural cracks at bed joints and by cycling, respectively. Unlike conventional reinforced concrete, AAC cannot be provided with enough reinforcement crossing the sliding shear interface to generate more resistance by shear friction. As a result, the sliding shear capacity of AAC structures is limited by friction alone. For low-rise AAC structures, sliding shear resistance can limit base shear capacity.

Damage did not occur in the floor slabs or connections, verifying that the behavior of the specimen was governed by the behavior of the shear walls. These combined results indicate that other AAC buildings can be designed based on the proposed design provisions of Chapter 9.

Although the Two-story assemblage specimen exhibited web-shear cracking, stable hysteretic loops were achieved. Displacement ductilities, with the effects of sliding removed, ranged from 2.5 to 6. For design purposes, these results justify the assumption of an available displacement ductility of at least 2.5. Although this ductility is slightly less that the ductility proposed in the R and C_d study, it would have been improved if web-shear cracking had not occurred. It is reasonably consistent with that observed in previous tests of flexure-dominated AAC shear walls at UT Austin (Varela 2003). This test confirms that the design objective of forcing flexure-dominated failures can be successful even in relatively squat walls.

CHAPTER 9
Proposed Design Provisions

The purpose of this chapter is to organize the proposed design provisions, provide a technical justification of them, and discuss special topics not included in the test results. The proposed design provisions of Appendix E are intended to be a separate document used in conjunction with the design provisions of ACI 318-02. These provisions are referred to as "ACI 3xx" throughout this dissertation. The provisions of ACI 318-02 are intended as the default, and are augmented, modified or replaced by the provisions of ACI 3xx. The proposed MSJC design provisions address field-reinforced AAC masonry. The proposed ACI 3xx design provisions address factory-reinforced AAC panels. The complete proposed design provisions and commentary for the MSJC code and for ACI 3xx are presented in Appendix D and Appendix E, respectively.

In this chapter the justification behind proposed design provisions for AAC structural systems and wall elements subject to in-plane lateral loads are summarized. Justification for the proposed design provisions for AAC panels loaded out of plane are discussed in Argudo (2003). All proposed code language is expressed in mandatory form and presented in indented italics. In many cases, equations are labeled with the chapter and "xx" indicating that some numbering system will be selected upon approval.

9.1 Proposed Design Provisions Regarding Mechanical Properties

The mechanical properties of AAC as discussed in Chapter 3 are introduced into the proposed design provisions of ACI 3xx (Sections 8.5.1, 8.13,

and 11.7.4.3) and the proposed MSJC design provisions (Section 1.8.2.3 and Section 8.1.8). The splitting tensile strength, modulus of rupture, masonry direct shear strength, shear strength of joints and tensile bond strength are defined. Since the language is identical for both the proposed ACI 3xx and MSJC design provisions, only code language for the proposed MSJC design provisions is presented as follows:

8.1.8 *Material properties*

8.1.8.2 *Masonry splitting tensile strength – The splitting tensile strength f_{tAAC} shall be determined by Equation 8-xx.*

$$f_{tAAC} = 2.4\sqrt{f'_{AAC}} \qquad \text{(8-xx)}$$

8.1.8.3 *Masonry modulus of rupture -- The modulus of rupture, f_{rAAC}, for AAC masonry elements shall be taken as two times the masonry splitting tensile strength, f_{tAAC}. If a section of AAC contains a horizontal leveling bed, the value of f_{rAAC} shall not exceed 50 psi (345 kPa) at that section. If a section of AAC contains a bed joint between thin-bed mortar and AAC the value of f_{rAAC} shall not exceed 80 psi (552 kPa) at that section.*

8.1.8.4 *Masonry direct shear strength – The direct shear strength f_v shall be determined by Equation 8-xx.*

$$f_v = 0.15 f'_{AAC} \qquad \text{(8-xx),}$$

f'_{AAC} and f_v in psi

8.1.8.5 *Shear strength of joints in AAC masonry – The shear strength of a joint between AAC and grout shall be 36 psi (0.25 MPa). The shear strength of a joint between AAC and thin-bed mortar shall be 18 psi (0.13 MPa).*

8.1.8.6 *Coefficient of friction – The coefficient of friction between AAC and AAC shall be 0.75. The coefficient of friction between AAC and leveling-bed mortar shall be 1.0.*

The sections describing technical justification for each mechanical property are presented in Chapter 3 and the specific reference for each mechanical property is presented in Table 9.1.

Table 9.1: Specific section describing technical justification for each mechanical property

Mechanical property	Section of technical justification in dissertation
Modulus of elasticity	Section 3.6
Splitting tensile strength	Section 3.7.1
Modulus of rupture	Section 3.7.2
Direct shear strength	Appendix A
Shear strength of a joint	Section 3.8.3, 3.8.4 and 3.8.5
Coefficient of friction	Section 3.8.6

9.2 PROPOSED DESIGN PROVISIONS FOR AAC SHEAR WALLS

Design provisions for AAC shear walls are proposed in this section along with a brief technical justification. A detailed technical justification is included in Chapter 7. Design provisions are presented first for monolithic AAC shear walls and special considerations for AAC shear walls that have continuous head joints along the height of the shear wall.

9.2.1 Proposed Design Provisions for Monolithic AAC Shear Walls

The proposed code language addresses the following behavior mechanisms: flexural cracking; flexure-shear cracking; nominal flexural capacity; web-shear cracking; sliding shear; and crushing of the diagonal strut. Each behavior mode is addressed independently in the following sections.

9.2.1.1 Flexural cracking

The formation of flexural cracks decreases the stiffness in a shear wall specimen. To predict the stiffness, the flexural cracking capacity must be calculated. For AAC shear walls the load at flexural cracking is presented in Section 8.1. The proposed code language addresses the formation of flexural

cracking in ACI 3xx and MSJC by identifying the modulus of rupture between various layers present in an AAC shear wall. Examples of different layers include joints between AAC and thin-bed mortar or AAC and leveling mortar.

9.2.1.2 Flexure-shear cracking

Design provisions for flexure-shear cracking are not proposed because this cracking does not constitute a limit state for design. No decrease in strength or stiffness was observed after the formation of web-shear cracking in AAC shear walls.

9.2.1.3 Nominal flexural capacity

The nominal flexural capacity calculations for AAC are quite similar to those for conventional concrete. The β_1 factor is reduced to 0.67 to reflect the effect of a nearly linear stress-strain relationship on the equivalent stress block. All other assumptions remain unchanged in both ACI 3xx and the MSJC design codes.

9.2.1.4 Web-shear cracking

Web-shear cracking is undesirable due to the brittle nature of the mechanism. The proposed design provisions for web-shear cracking of fully mortared specimens are the same in ACI 3xx and the MSJC design provisions. In the proposed MSJC provisions, separate equations are presented in Section 8.2.4.1.2.1 for masonry with mortared head joints and unmortared head joints:

> ***8.2.4.1.2.1*** *Nominal masonry shear strength as governed by web-shear cracking — Nominal masonry shear strength as governed by web-shear cracking, V_{AAC} , shall be computed using Eq. (8-21a) for AAC masonry with mortared head joints, and Eq. (8-21b) for AAC masonry with unmortared head joints:*

$$V_{AAC} = 0.9\,\ell_w\,t\,\sqrt{f'_{AAC}}\,\sqrt{1+\frac{P_u}{2.4\sqrt{f'_{AAC}}\,\ell_w\,t}} \qquad (8\text{-}21a)$$

$$V_{AAC} = 0.6\,\ell_w\,t\,\sqrt{f'_{AAC}}\,\sqrt{1+\frac{P_u}{2.4\sqrt{f'_{AAC}}\,\ell_w\,t}} \qquad (8\text{-}21b)$$

In all equations (8-21), V_{AAC} shall be expressed in lb and f'_{AAC} shall be expressed in psi.

9.2.1.5 Crushing of the diagonal strut

The crushing of a diagonal strut can cause premature brittle failure for AAC shear wall specimens subject to high axial loads. The proposed design provisions for crushing of the diagonal strut in the proposed MSJC design provisions read as follows:

> ***8.2.4.1.2.2*** *Nominal shear strength as governed by crushing of diagonal compressive strut — For walls with $M/Vd_v < 1.5$, nominal shear strength, V_{AAC}, as governed by crushing of a diagonal strut, shall be computed as follows:*
>
> $$V_{AAC} = 0.17 f'_{AAC} t \frac{h \cdot l_w^{\,2}}{h^2 + (\frac{3}{4} l_w)^2} \qquad (8\text{-}22a)$$
>
> *For walls with M/Vd_v equal to or exceeding 1.5, capacity as governed by crushing of the diagonal compressive strut need not be calculated.*

An identical equation exists for crushing of the diagonal strut in the proposed Section 11.10 of ACI 3xx. This equation replaces the current ACI 318-02 equation for flexure-shear cracking in a reinforced concrete shear wall.

9.2.1.6 Sliding shear

The sliding shear capacity of an AAC shear wall is discussed in Section 8.5 of this dissertation. This capacity at an unbonded interface is governed by friction after crushing around the longitudinal reinforcement. At a leveling bed

mortar joint, this initial adhesion may not be present after flexural cracking. At an interface where thin-bed mortar is present, the nominal sliding shear capacity may be based on the greater of the strength of the initial adhesion or the frictional capacity. This is expressed in Section 8.2.4.1.2.3.

> ***8.2.4.1.2.3*** *Nominal shear strength as governed by sliding shear – – At an unbonded interface, nominal shear strength as governed by sliding shear, V_{AAC}, shall be as follows:*
>
> $$V_{AAC} = \mu P_u \qquad (8\text{-}22b)$$
>
> *At an interface where uncracked thin-bed mortar is present, the nominal sliding shear capacity shall be calculated as the greater of the capacity calculated by Section 8.1.8.5, and that calculated by Eq. 8-22b. At an interface where leveling-bed mortar is present, the nominal sliding shear capacity shall be calculated by Eq. 8-22b. In an AAC shear wall, it shall also be permitted to include the force in the tensile steel at a given cross-section ($A_s f_s$) in the axial load.*

The same provisions are presented in Section 11.7.4.1 of ACI 3xx. The coefficient of friction is found in Section 11.7.4.3.

9.2.1.7 Shear reinforcement in walls

The reduced effectiveness of welded wire fabric in AAC shear walls is discussed in Section 8.4. The design provisions in both MSJC and ACI 3xx limit the contribution of shear reinforcement to deformed reinforcement embedded in grout. This is found in Section 8.2.4.1.2 (MSJC) and Section 11.10.9.1 (ACI 3xx). The last sentence of Section 8.2.4.1.2 of the proposed MSJC design provisions reads as follows:

> *Nominal shear strength provided by reinforcement, V_s , shall include only deformed reinforcement embedded in grout for AAC shear walls.*

9.2.1.8 Anchorage of longitudinal reinforcement

AAC reinforcement consists of factory-reinforced AAC panels or field-reinforced AAC masonry. AAC panels may also be field reinforced. The anchorage requirements for field-reinforced AAC elements do not vary from those used for conventional reinforced concrete. The anchorage requirements for the current MSJC and ACI 318-02 design provisions therefore also apply to field-installed reinforcement in AAC structural systems. A discussion of the contribution of factory-installed reinforcement in AAC panels under monotonic loading conditions is presented by Argudo (2003).

9.2.1.9 Summary of technical justification for each behavior mode in an AAC shear wall

Technical justification for proposed design provisions addressing each behavior mode in AAC shear walls is presented in Chapter 7. The specific section describing each behavior mode is presented in Table 9.2.

Table 9.2: Specific section describing technical justification for provisions addressing each behavior mode in AAC shear walls

Behavior mode	Location of technical justification in dissertation
Flexural cracking	Section 8.1
Flexure-shear cracking	Section 8.2
Web-shear cracking	Section 8.3
Crushing of diagonal strut	Section 8.6
Sliding shear	Section 8.5
Shear reinforcement in walls	Section 8.4

9.2.2 Prescriptive Reinforcement Requirements in Shear Wall Specimens

Prescriptive requirements for horizontal and vertical reinforcement exist in both ACI 318-02 and the current MSJC design provisions. The shear wall specimen tests performed at UT Austin indicate that the lateral capacity of an AAC shear wall can be predicted reliably, and can be designed to behave elastically or in a flexure-dominated manner with vertical reinforcement concentrated at the ends of a specimen. These reinforcement requirements are addressed individually in each set of design provisions.

9.2.2.1 Prescriptive reinforcement requirements for AAC shear walls in ACI 3xx

Sections 14.3, 16.4.2, 16.5.1.3 and 21.7 of ACI 318-02 require prescriptive reinforcement in shear walls. Section 14.2.1 requires walls to be designed for eccentric load and any lateral loads. In the new document proposed for AAC, the proposed reinforcement requirements are limited to reinforcement around openings, as indicated by Section 14.3.7 of ACI 3xx, which replaces Sections 14.3.1 through 14.3.6 and 16.4.2 of ACI 318-02; it reads as follows:

> ***14.3.7*** *In addition to the minimum reinforcement required by 14.2.1, not less than one No. 4 bar shall be provided around all window and door openings. Such bars shall be extended to develop the bar beyond the corners of the openings but not less than 24 in.*

Proposed Section 16.5.1.3 of ACI 3xx considers vertical tension ties in precast elements. These ties generally exist in columns, wall panels and concrete foundations. Proposed ACI 3xx design provisions for AAC do not allow AAC columns due to the low compressive strength of AAC. Longitudinal reinforcement must be provided to resist design moments. Additional longitudinal reinforcement is required at shear wall intersections; it must be anchored into the floor slab and continuous at wall intersections to provide

structural continuity. The proposed ACI 3xx provisions that address these issues read as follows:

> ***16.5.1.3 —*** *Vertical tension tie requirements of 7.13.3 shall apply to all vertical structural members, except cladding., and shall be achieved by providing connections at horizontal joints in accordance with the following:*
> *(a) Precast columns shall not be made of AAC;*
> *(b) Precast wall panels that comprise shear walls shall be connected at wall intersections, at locations of longitudinal reinforcement;*
> *(c) When design forces result in no tension at the base, the ties required by 16.5.1.3(b) shall be permitted to be anchored into an appropriately reinforced concrete slab on grade.*
> ***16.5.2.5*** *Continuous vertical reinforcement in AAC shear walls shall be sufficient to resist the design moments.*

The proposed ACI 3xx provisions in Chapter 21 of ACI 3xx for seismic design of AAC structural systems are discussed in Section 9.4.2 of this dissertation.

9.2.2.2 Prescriptive reinforcement requirements for AAC shear walls in MSJC design provisions

The current MSJC strength design provisions require prescriptive reinforcement in Section 1.13.2. The minimum reinforcement requirements of Section 1.13.2.2.2.1 would be replaced in the new proposed MSJC design provisions of Section 1.13.2.2.7 and 13.2.2.8:

> ***1.13.2.2.7*** *Detailed plain AAC masonry shear walls – Design of detailed plain (unreinforced) AAC masonry shear walls shall comply with the requirements of Section 8.3 and the requirements of Section 1.13.2.2.7.1*
> ***1.13.2.2.7.1*** *Minimum reinforcement requirements for members of the lateral force-resisting system in AAC masonry – Vertical reinforcement of at least 0.2 in.^{2} shall be provided within 24 in. of each side of openings, within 8 in. of movement joints, and within 24 in. of the ends of walls. Reinforcement adjacent to openings need not be provided for*

openings smaller than 16 in. unless the minimum reinforcement requirements are interrupted by such openings.

1.13.2.2.8 *Ordinary reinforced AAC masonry shear walls – Design of ordinary reinforced AAC masonry shear walls shall comply with the requirements of Section 8.2 and the requirements of Section 1.13.2.2.7.1.*

The proposed MSJC design provisions for seismic design are discussed in Sections 9.4.2 of this dissertation.

9.2.3 Proposed Design Provisions for AAC Shear Walls with Continuous Head Joints

Based on the observed behavior of AAC shear walls with vertical panels, independent provisions have been developed to address the potential formation of vertical cracks. A complete technical justification for these design provisions is found in Sections 8.9 through 8.12 of this dissertation. In ACI 3xx these proposed provisions would apply directly to vertical panels. In the proposed MSJC design provisions the observed behavior in vertical panels may also apply to walls constructed of stack-bonded masonry or masonry configuration other than running bond. For simplicity the proposed MSJC design provisions simply address masonry in other than running bond as defined in Section 8.2.4.1.3 of the proposed MSJC design provisions:

8.2.4.1.3 *Special provisions for shear walls with AAC laid in other than running bond — Nominal shear strength and flexural strength shall be determined assuming that vertical cracks exist at each head joint. It shall be permitted to design with vertical cracks at every third joint, using Equation (8-21a), if the following construction techniques are met: each panel shall be cleaned and wet prior to applying the thin-bed mortar; mortar shall be applied to both faces of the vertical joint; and pressure shall be applied perpendicular to the vertical joint through clamps.*

The proposed MSJC provisions are included at the end of Section 8.2.4.1.2.1 as follows:

> *For AAC masonry in other than running bond, nominal masonry shear strength as governed by web-shear cracking, V_{AAC} , shall be computed using Eq. (8-21c):*
>
> $$V_{AAC} = 0.9\sqrt{f'_{AAC}}\, A_n + 0.05 P_u \qquad \text{(8-21c)}$$
>
> *In all equations (8-21), V_{AAC} shall be expressed in lb and f'_{AAC} shall be expressed in psi.*

The same language is expressed for vertically oriented panels in Section 11.10.7 of ACI 3xx with a reference to Equation (11-4) to determine the shear capacity of single panels or groups of two panels. The proposed construction requirements for vertical panels are given in Section 5.7.

9.3 PROPOSED DESIGN PROVISIONS FOR AAC FLOOR SLABS

In AAC structures, floor diaphragms must transfer load through in-plane flexure and shear to the AAC shear walls comprising the lateral force-resisting system. Since flexure-dominated behavior of AAC floor diaphragms is not directly addressed by ACI381-02 or current MSJC design provisions, no corresponding additional requirements are specified. The critical function of AAC floor slabs is to transfer lateral load to AAC shear walls. This can be accomplished through adhesion at joints, through dowel action of reinforcement perpendicular to the direction of load, or through a truss mechanism for panels oriented parallel to the direction of load based on a strut and tie model. Additional structural integrity connection requirements are reviewed in Section 9.3.2.

9.3.1 Design Provisions for Lateral Load Transfer in AAC Diaphragms

Lateral load transfer in AAC diaphragm design may be based on adhesion, dowel action, adhesion, or a truss mechanism. These concepts are presented in Chapter 4 and discussed further in Sections 9.3.1.2 and 9.3.1.3.

9.3.1.1 General design requirements for connections between AAC floor diaphragms and AAC shear walls in ACI 3xx

Chapter 16 of the proposed design provisions for ACI 3xx addresses connections between AAC floor slabs and shear walls. The proposed design is based on the orientation of the panels with respect to the lateral load. Provisions for each orientation are referenced in Section 16.5.1.2.1.

> ***16.5.1.2 —*** *Where precast AAC elements form floor or roof diaphragms, the minimum provisions of Section 16.5.1.2.1 through 16.5.1.2.4 shall apply in addition to the requirements of Section 7.13.3.*
>
> ***16.5.1.2.1 —*** *Nominal shear strength for AAC floor and roof diaphragms subject to lateral load parallel to the direction of panels shall be calculated based on Section 16.5.1.2.2 or Section 16.5.1.2.3. Nominal shear strength for AAC floor and roof diaphragms subject to lateral load perpendicular to the direction of panels shall be calculated based on Section 16.5.1.2.2 or Section 16.5.1.2.4.*

9.3.1.2 Proposed design provisions for AAC floor diaphragm to shear wall connection for panels oriented perpendicular to the direction of load

Shear transfer in AAC slabs with panels oriented perpendicular to the direction of load was tested in the Two-story Assemblage Specimen. The test results indicate that load was transferred through adhesion rather than dowel action. In the proposed design provisions, both of these mechanisms are permitted for panels oriented perpendicular to the direction of load.

For joints depending on adhesion, the proposed design margin of safety is 1.5. This factor is introduced as a strength reduction factor of 0.67, applied to the nominal interface shear capacity of AAC joints as governed by adhesion. The proposed strength reduction factor for adhesion is incorporated in Section 9.3.2.8 of ACI 3xx. This safety factor, combined with a nominal strength based on a lower fractile of the observed shear strength, provides an adequately conservative model for a brittle failure. Design provisions based on adhesion are provided in proposed Section 16.5.1.2.2 of ACI 3xx.

> ***16.5.1.2.2 —*** *Nominal shear strength shall be based on adhesion at diaphragm joints, and shall be computed as the product of the contact area of grout and AAC and the shear strength of a grout and AAC joint plus the product of the contact area of thin-bed mortar and AAC and the shear strength of thin-bed mortar. The shear strengths of joints between thin-bed mortar and AAC and grout and AAC are defined in Section 8.14.4.*

Although dowel action was not tested in this specimen, this mechanism has been successfully used in traditional masonry construction. Justification exists for relying on dowel action here, when it was not reliable at the base of the wall. Lateral load is transferred through dowel action of the reinforcement embedded in the grouted key. Strength degradation based of the dowel action of the reinforcement is not expected if the surrounding AAC is not damaged. AAC damage is minimal because the load transfer at the connection occurs entirely within the grouted bond beam. Proposed design provisions for this design based on dowel action are addressed in Section 15.6.1.2.4.

> ***16.5.1.2.4 —*** *Nominal shear strength shall be based on dowel action of reinforcement in the grouted keys perpendicular to the lateral load. The nominal shear strength shall be computed as the product of 60 percent of the cross-sectional area of the reinforcement and the specified yield strength of the reinforcement.*

9.3.1.3 Proposed design requirements for connections between AAC floor diaphragm and AAC shear walls for panels oriented parallel to the direction of load

Panels oriented parallel to the direction of lateral load may be designed based on adhesion or a truss mechanism. The design provisions for adhesion are the same as those presented in Section 9.3.1.3 for panels oriented parallel to the direction of lateral load.

The truss mechanism for shear transfer functions as a secondary resistance mechanism and follows the principles of a strut-and-tie model (Figure 9.1). Compression is transferred through the panels in the form of struts. The reinforcement in the grouted keys serves as tension ties, which must be tied into the bond beam by 90-degree standard hooks bent around the longitudinal reinforcement in the tension ties and oriented in a vertical plane. The mechanical connection of the hook allows the grouted key reinforcement to bear on the perpendicular reinforcement in the bond beam, increasing the integrity of the connection.

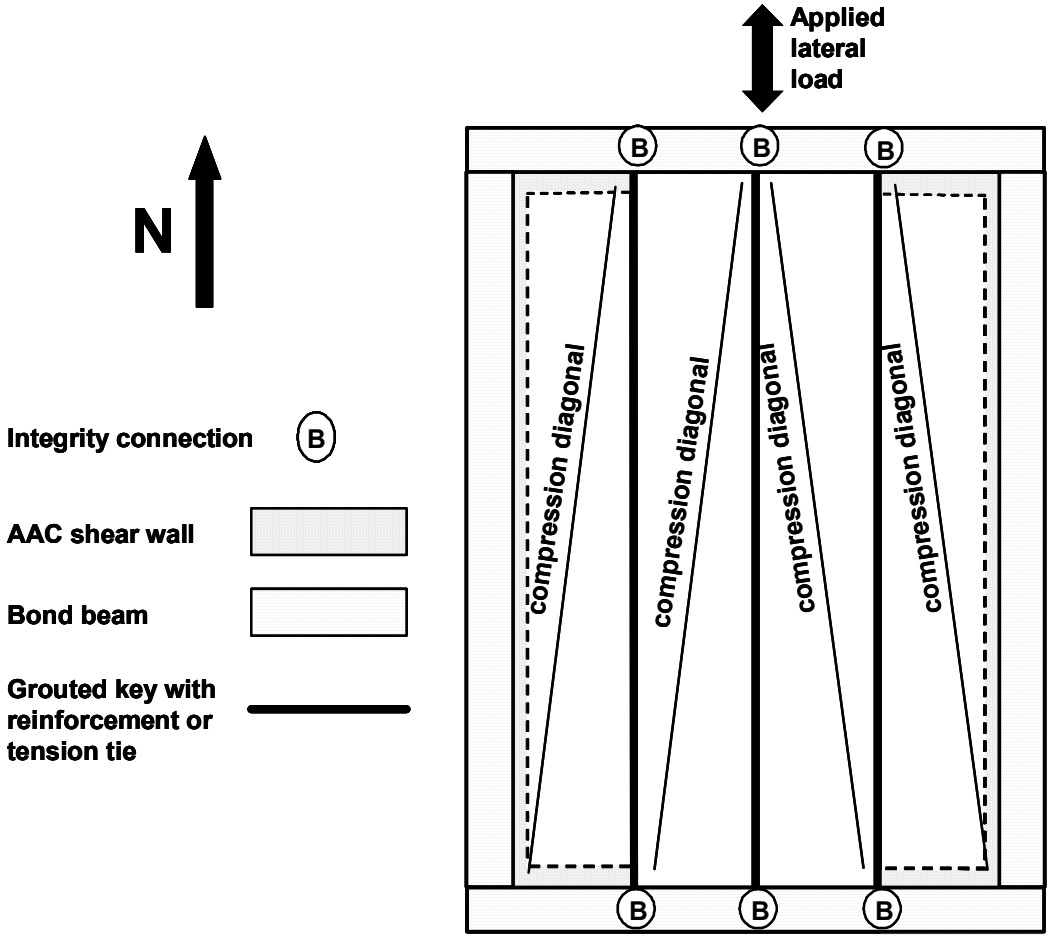

Figure 9.1: Truss mechanism for transferring lateral load parallel to the orientation of the panels

Since the compression diagonals do not cross the panel joints, the capacity of the compression struts will not be decreased if the panel joints crack. If each compression strut remains within an individual panel the angle between the compression strut and the vertical tie is a function of the length of the panel and the panel height. This angle is clearly smaller than the minimum angle of 25 degrees between a strut element and a tie element defined in Appendix A of ACI

318-02. The limit placed on a strut-and-tie model is to reduce damage by enforcing compatibility at the node. The use of a smaller angle is justified here because in the proposed model for the proposed ACI 3xx and MSJC design provisions, the tie performance is not limited by interface panel cracking, and therefore the angle is not critical.

The proposed width of the compression strut is 6 in. (153 mm), one-quarter of the panel width. The depth of the strut is the thickness of the panel. The nodal forces will not limit the design in this case because the compressive strength of the grout is approximately 4 times the compressive strength of the AAC. The code language to express these concepts is as follows:

> ***16.5.1.2.3 —*** *Nominal shear strength of AAC floor and roof diaphragms shall be based on a truss mechanism subject to the minimum provisions of Section 16.5.1.2.3.1 through Section 16.5.1.2.3.4.*
> ***16.5.1.2.3.1 —*** *Compression struts shall not be permitted to cross panel joints and shall intersect with tension ties in grouted keys and tension ties (chords) in bond beams.*
> ***16.5.1.2.3.2 —*** *Tension ties shall consist of the reinforcement in grouted keys or in a bond beam. The reinforcement in the grouted keys shall be hooked around the longitudinal reinforcement in the bond beam with standard 90-degree hooks oriented in a vertical plane.*
> ***16.5.1.2.3.3 —*** *Compression struts shall be defined within the panel. Their dimension perpendicular to the plane of the panel shall be taken equal to the thickness of the panel. Their dimension in the plane of the panel, measured perpendicular to the axis of the strut, shall be taken as 6 in. The nominal strength of compression struts shall be calculated as the product of 85 percent of the specified compressive strength of the AAC, multiplied by the cross-sectional area of the strut.*
> ***16.5.1.2.3.4 —*** *The strength of the tension ties shall not exceed the product of the cross-sectional area of the reinforcement and the specified yield strength of the reinforcement.*

9.3.1.4 Discussion regarding performance of AAC slab with panels oriented parallel to the direction of loading

An alternate strut-and-tie model was initially used to design the diaphragm (Figure 5.18). Based on that model, the nominal design capacity was 77.1 kips (343 kN), and the design capacity was 57.9 kips (257 kN), slightly less than the observed capacity. That alternate model is not proposed for design, for the following reasons:

- cracks at the panel interfaces could decrease the capacity of the compression strut; and
- additional steel is required to provide a transverse tension tie at the center of the diaphragm.

Using the strut-and-tie model of the proposed ACI 3xx and MSJC design provisions, the computed nominal shear capacity of the diaphragm (second level) is 22.5 kips (100 kN). This is only 31% of the maximum load carried by the diaphragm in the assemblage test, which suggests that the strut-and-tie model is certainly conservative. If necessary, the nominal capacity calculated using the strut-and-tie model could be increased by increasing the bar size in the grouted key. The required ratio of reinforcing bar area to cell area of Section 8.2.3.1 may be relaxed because splitting cracks between panels will not reduce the strength of the model.

9.3.1.5 Proposed MSJC design requirements for connectors between AAC floor diaphragm and AAC shear walls

The proposed MSJC requirements for connections between an AAC floor diaphragm and AAC shear walls are identical to those proposed for ACI 3xx. The strength reduction factor for adhesion is incorporated in Section 8.2.7 of the proposed MSJC design design provisions.

9.3.2 Additional Structural Integrity Requirements

The proposed structural integrity provisions of Section 16.5.2 in ACI 3xx are addressed in this section. The vertical reinforcement restriction of ACI 318-02 Section 16.5.2.5 is relaxed and replaced with equally or more-stringent diaphragm reinforcement requirements. The following code language expresses this change:

> ***16.5.2*** *— For precast autoclaved aerated concrete bearing wall structures three or more stories in height, the minimum provisions of 16.5.2.1 through 16.5.2.5 shall apply.*
> ***16.5.2.1*** *— Longitudinal and transverse ties shall be provided in floor and roof systems to provide a nominal strength of 1500 lb per ft of width or length, and shall be designed to transfer shear to lateral force-resisting elements. Ties shall be provided over interior wall supports and between members and exterior walls. Ties shall be positioned in or within 2 ft of the plane of the floor or roof system. Longitudinal ties shall only be required parallel to the direction of span of the panels.*
> ***16.5.2.2*** *— Longitudinal ties parallel to floor or roof slab spans shall be spaced not more than 10 ft on centers. Provision shall be made to transfer forces around openings.*
> ***16.5.2.3*** *— Transverse ties perpendicular to floor or roof slab spans shall be spaced not greater than the bearing wall spacing.*
> ***16.5.2.4*** *— At each level, a bond beam shall be provided, and shall be reinforced with at least two longitudinal reinforcing bars, having a total cross-sectional area of at least 0.4 in.^{2} If floor diaphragms are made of AAC panels, those panels shall be connected to each other by grouted keys, each having at least 0.11 in.^{2} of reinforcement, anchored in the bond beam by a standard 90-degree hook, placed around the longitudinal reinforcement in the bond beam and oriented in a vertical plane.*
> ***16.5.2.5*** *Continuous vertical reinforcement in AAC shear walls shall be sufficient to resist the design moments.*

The longitudinal ties required by ACI 318-02 Section 16.5.2.1 are intended to support the diaphragm if a supporting bearing wall is removed from the structure (Schultz 1976). The ties are shown in Figure 9.2; the effect of losing

an interior wall is shown in Figure 9.3. Since the mechanism will only form in the direction parallel to the direction the slab is spanning, the ties are not required perpendicular to the direction a slab is spanning. The additional bond beam reinforcement provides general structural integrity and also serves as chord reinforcement to resist in-plane flexure in the slab. Vertical reinforcement requirements are relaxed based on the performance of the shear wall specimens and the Two-story Assemblage Specimen tested at UT Austin.

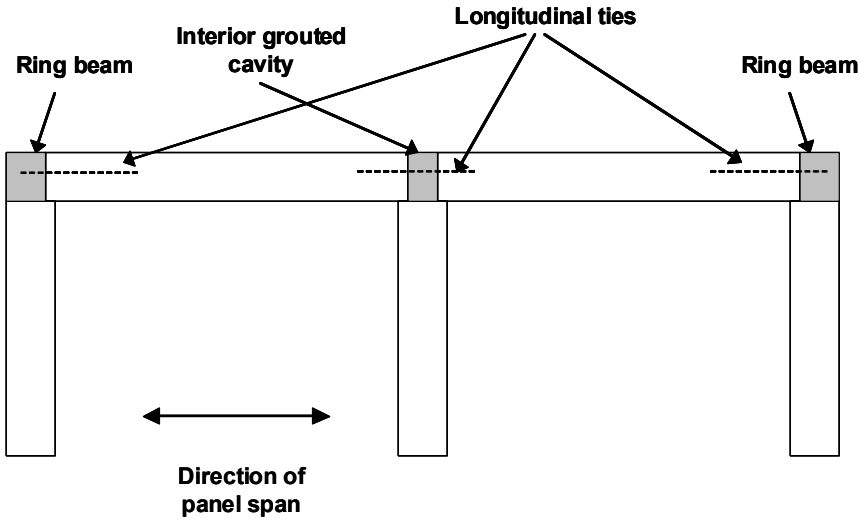

Figure 9.2: Elevation of two exterior shear walls and one interior shear wall with two interior panels connected by longitudinal ties

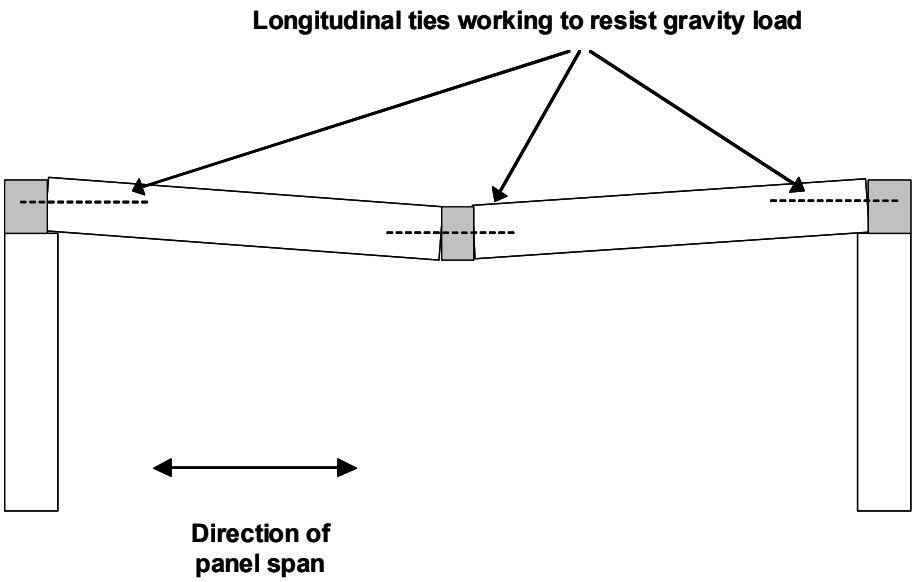

Figure 9.3: Elevation of shear walls with interior bearing wall missing and longitudinal ties serving as reinforcement

9.4 SPECIAL TOPICS CONSIDERED IN PROPOSED CODE LANGUAGE

This section covers design provisions that are worth additional justification beyond the commentaries provided in Appendices B and C. Items presented are provisions regarding seismic design, provisions regarding bearing area, and provisions regarding area of vertical reinforcement and area of grouted cell.

9.4.1 Proposed MSJC Provisions for Seismic Design of AAC

The proposed seismic design provisions in MSJC impose incrementally increasing categories, Seismic Design Categories A through E. Seismic Design Category A has the lowest seismic design hazard. Consistent with the current MSJC provisions, all structure types including ordinary plain structures

(unreinforced AAC) are permitted. Anchorage requirements between AAC floor diaphragms and shear walls can be addressed by any of the proposed design methods to transfer lateral load in a diaphragm (Sections 8.2.7.2.1.1, 8.2.7.2.1.2, and 8.2.7.2.2.1).

> ***1.13.3*** *Seismic Design Category A*
> *Structures in Seismic Design Category A shall comply with the requirements of Chapter 2, 3, 4 or 5. AAC masonry structures in Seismic Design Categories A shall comply with the requirements of Chapter 8.*
> ***1.13.3.3*** *Anchorage of masonry walls – Masonry walls shall be anchored to the roof and all floors that provide ... Exception: AAC masonry walls shall comply with the requirements of Section 1.13.3.4.*
> ***1.13.3.4*** *Anchorage of AAC masonry diaphragms -- The lateral load resistance of AAC diaphragms shall be determined according to Section 8.2.7.2.1.1, Section 8.2.7.2.1.2 or Section 8.2.7.2.2.1.*

Structures assigned to Seismic Design Category B are subject to an increased seismic hazard, reflected by additional prescriptive requirements for diaphragm reinforcement to provide additional continuity in AAC systems.

> ***1.13.4*** *Seismic Design Category B*
> ***1.13.4.1*** *Structures in Seismic Design Category B shall comply with the requirements of Seismic Design Category A and to the additional requirements of Section 1.13.4. AAC masonry structures shall comply with the requirements of 1.13.4.3.*
> ***1.13.4.2*** *Design of elements that are part of lateral force-resisting system -- The lateral force-resisting system shall be designed to comply with the requirements of Chapter 2, 3, or 4. Masonry shear walls shall comply with the requirements of ordinary plain (unreinforced) masonry shear walls, detailed plain (unreinforced) masonry shear walls, ordinary reinforced masonry shear walls, intermediate reinforced masonry shear walls, or special reinforced masonry shear walls.*
> ***1.13.4.3*** *Anchorage of floor and roof diaphragms in AAC masonry structures — Floor and roof diaphragms in AAC masonry structures shall be surrounded by a continuous grouted bond beam reinforced with at least two longitudinal reinforcing bars, having a total cross-sectional area of at least 0.4 in.^{2} If floor diaphragms are made of AAC panels, those panels shall be connected to each other by grouted keys, each*

having at least 0.11 in.^{2} of reinforcement, anchored in the bond beam by a standard 90-degree hook, placed around the longitudinal reinforcement in the bond beam and oriented in a vertical plane. Continuous longitudinal ties shall be provided over interior wall supports. The shear capacity of the diaphragm shall be determined according to Section 8.2.7.2.1.1, Section 8.2.7.2.1.2 or Section 8.2.7.2.2.1.

Seismic Design Category C reflects moderate seismic hazard. Due to the brittle nature of an adhesion failure, the proposed design provision prohibit lateral load transfer through adhesion. In addition, connections across a diaphragm and AAC shear wall are required to ensure a ductile failure.

1.13.5 *Seismic Design Category C*

1.13.5.1 *Structures in Seismic Design Category C shall comply with the requirements of Seismic Design Category B and to the additional requirements of Section 1.13.5*

1.13.5.2.3 *Reinforcement requirements -- Masonry elements listed in Section 1.13.5.2.2, except AAC masonry elements, shall be reinforced in either the horizontal or vertical direction in accordance with the following: . . .*

1.13.5.3 *Design of elements that are part of the lateral force-resisting system – Design of masonry columns and shear walls shall comply with the requirements of 1.13.5.3.1 and 1.13.5.3.2. Design of ordinary reinforced AAC masonry structures shall comply with the requirements of 1.13.5.3.3 and 1.13.5.3.4.*

1.13.5.3.3 *Anchorage of floor and roof diaphragms in AAC masonry structures — Lateral load between floor and roof diaphragms and AAC masonry shear walls shall be transferred through connectors embedded in grout in accordance with Section 2.1.8. Connectors shall be designed to transfer horizontal design forces acting either parallel or perpendicular to the wall but not less than 200 lb per lineal ft of wall. The maximum spacing between connectors shall be 4 ft.*

1.13.5.3.4 *Anchorage of floor and roof diaphragms in AAC masonry structures — Floor and roof diaphragms in AAC masonry structures shall comply with the requirements of Section 1.13.4.3. The shear capacity of the diaphragm shall be determined by Section 8.2.7.2.1.2 or Section 8.2.7.2.2.1.*

Seismic Design Category D reflects moderate to severe seismic hazard. The additional stipulations of Seismic Design Category C are applied to this case. The additional horizontal and vertical reinforcement requirements currently required in masonry shear walls are waived based on the performance of AAC shear wall tests and results of the assemblage specimen.

1.13.6 *Seismic Design Category D*

1.13.6.1 *Structures in Seismic Design Category D shall comply with the requirements of Seismic Design Category C and with the additional requirements of Section 1.13.6.*
Exception: AAC masonry elements shall comply with the requirements of 1.13.5.

1.13.6.2 *Design requirements -- Masonry elements, other than those covered by Section 1.13.5.2.2, shall be designed in accordance with the requirements of Sections 2.1 and 2.3, Chapter 2, Chapter 3, Chapter 4 or Chapter 8.*

1.13.6.3 *Minimum reinforcement requirements for masonry walls -- Masonry walls other than those covered by Section 1.13.5.2.3, and other than AAC masonry, shall be reinforced in both the horizontal and vertical direction. . . .*

The testing program used to verify the seismic performance of AAC structural systems included simulated loading histories representative of Seismic Design Categories E and F. For that reason, proposed requirements for Seismic Design Categories E and F are the same as in Seismic Design Category D. Furthermore, AAC shear walls can be designed for flexure-dominated behavior.

Through the use of a capacity design, AAC diaphragms can be designed to exceed the expected capacity of an AAC shear wall. Additional provisions are included to ensure that the AAC diaphragm is reliably connected to the shear walls.

9.4.2 Proposed Seismic Design Provisions for AAC in ACI 3xx

The seismic design provisions for AAC in ACI 3xx provide additional detailing requirements for a given element, depending on the amount of additional detailing the standards are designated intermediate or special. Specific requirements for AAC are proposed for AAC intermediate or special structural wall systems. In regions of moderate seismic risk intermediate or special structural wall systems are permitted in ACI 3xx. In regions of high seismic risk only special structural wall systems are permitted. These designations are introduced into the proposed design provisions of ACI 3xx in Sections 21.2.1.2 and 21.2.1.3. Intermediate and special structural wall systems include shear walls that are designed to fail in flexure. Ductile behavior is promoted even though the walls cannot be provided with the confined boundary elements required for special concrete walls. Special structural wall systems are also required to provide additional connectors between an AAC diaphragm and AAC shear wall. The word "system" is included because the requirements address floor diaphragms and bond beams as well as walls.

> ***21.2.1.2*** *– In regions of moderate seismic risk or for structures assigned to intermediate seismic performance or design categories, intermediate or special moment frames, ordinary, intermediate, or special structural walls, or intermediate or special AAC structural wall systems shall be used to resist forces induced by earthquake motions. Where the design seismic loads are computed using provisions for special concrete systems or intermediate or special AAC structural walls, the requirements of Chapter 21 for special systems, as applicable, shall be satisfied.*

21.2.1.3 *– In regions of high seismic risk for structures assigned to high seismic performance or design categories, special moment frames, special structural walls, special AAC structural wall systems, or diaphragms and trusses complying with 21.2 through 21.10 shall be used to resist forces induced by earthquake motions. Frame members not proportioned to resist earthquake forces shall comply with 21.11.*

In regions of moderate seismic risk, a capacity design approach is required to determine the design forces for floor diaphragms in ACI 318-02 and ACI 3xx. In ACI 3xx, these loads are not permitted to be transferred through adhesion due to the brittle nature of this failure. The horizontal and vertical reinforcement requirements of a shear wall are replaced by additional reinforcement requirements based on the use of a truss mechanism to resist lateral load in AAC floor panels oriented parallel to the direction of load. The performance of AAC shear walls and the assemblage specimen tested at UT Austin justifies relaxing the requirements for reinforcement in the shear wall itself, compared with conventional reinforced concrete.

21.14.1 *– The provisions of this section apply to design of intermediate AAC structural walls and their associated horizontal diaphragms to resist forces induced by earthquake motions. The design provisions of Chapters 1-18 shall apply except as modified in this Section.*

21.14.2 *– The design shear force V_e shall be determined from consideration of the maximum forces that can occur in an AAC element. Forces in the longitudinal reinforcement shall be determined assuming that the stress in the flexural tensile reinforcement is $1.25f_y$.*

21.14.3 *– The horizontal diaphragm shall be designed to resist the design shear force, V_e, of Section 21.14.2. Design according to Section 16.5.1.2.2 shall not be permitted.*

In the ACI 3xx, in regions of high seismic risk, the design requirements for intermediate seismic risk are applied. Connecting elements are also required

between all faces of a floor diaphragm and an AAC shear wall to ensure a ductile failure mode dominated by flexural behavior of the AAC shear walls. The additional provisions are as follows:

> ***21.15.1*** *– The design provisions of this section apply to special AAC structural walls and horizontal diaphragms to resist forces induced by earthquake motions.*
>
> ***21.15.2*** *– The design provisions of Chapters 1-18 and Section 21.14 shall apply except as modified in this Section.*
>
> ***21.15.3*** *– Lateral load between horizontal diaphragms and AAC structural walls shall be transferred through connectors embedded in grout in accordance with Section 16.*

9.4.3 Concentrated Loads

Special provisions have been proposed for the MSJC design provisions for concentrated loads. These provisions address the bearing area of AAC floor slabs resting on AAC shear walls, and read as follows:

> ***8.1.10*** *Concentrated Loads*
>
> ***8.1.10.3*** *Design bearing strength on AAC masonry shall not exceed ($\phi f'_{AAC} A_1$), where A_1 is the loaded area.*
>
> ***8.1.10.4*** *Bearing for simply supported precast floor and roof members on AAC shear walls — The following minimum requirements shall apply so that after the consideration of tolerances, the distance from the edge of the supporting wall to the end of the precast member in the direction of the span is not less than:*

For AAC floor panels	*2 in. (51 mm)*
For solid or hollow-core slabs	*2 in. (51 mm)*
For beams or stemmed members	*3 in. (76 mm)*

These provisions are identical to those in ACI 3xx. Current ACI 318-02 design provisions allow an increase in bearing area due to confinement. These

provisions have been removed in the proposed ACI 3xx and MSJC design provisions since the porous structure of AAC does not produce increased bearing capacity due to confinement.

9.4.4 Ratio between Area of Longitudinal Reinforcement and Area of Grouted Core

When the ratio of the area of longitudinal reinforcement to the ratio of a grouted core exceeds about 3% longitudinal splitting cracks (in an AAC shear wall) may form along the reinforcement at plastic hinge zones (Section 8.8 of this dissertation). The test results of the Two-story Assemblage Specimen tested at UT Austin show that no splitting cracks occur, in plastic hinge zones when the area ratio is 3%. The proposed design provisions limit the area ratio to 3% in Section 8.2.3.1 of the proposed MSJC design provisions and in the proposed Section 12.1.2 of ACI 3xx. Higher ratios (up to 4.5% are permitted if the reinforcement remains elastic. In this section, those proposed requirements are discussed.

9.4.4.1 Analysis of maximum permissible area ratio if the longitudinal reinforcement remains elastic

Area ratios of reinforcement up to 4.5% are permitted in ACI 3xx and the proposed MSJC design provisions, provided that radial (splitting) stresses can be limited by limiting the bond stress, which in turn means limiting the shear. The formation of radial stresses is explained in Section 8.8 of this dissertation, and briefly reviewed here.

For design convenience the bond stress can be expressed as a function of shear as shown in Equation (9.1). This relationship is valid in cases where the bond between grout and reinforcement remains intact. Generally bond is broken

after the reinforcement yields, therefore this development does not apply to cases where a plastic hinge may form. For practical reasons this analysis based on Equation (9.1) is limited to out-of-plane loading. Since the resultant force acting on the lugs acts at about 45 degrees, the radial stresses, σ_{radial} are also equal to the bond stress, u, as shown in Equation (9.2).

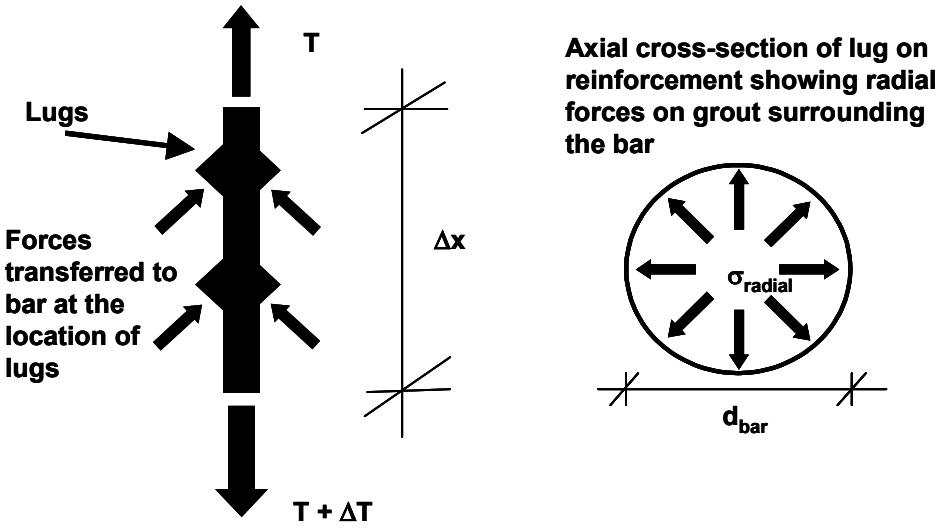

Figure 9.4: Free-body diagram of longitudinal bar with all load transferred through lugs and pressure generated in the surrounding grout

$$u = \frac{\Delta T}{\pi d_{bar} \cdot \Delta x} = \frac{\Delta M}{jd \cdot \pi d_{bar} \cdot \Delta x} = \frac{V}{jd \cdot \pi d_{bar}} \qquad \text{Equation (9.1)}$$

$$\sigma_{radial} = u = \frac{V}{jd \cdot \pi d_{bar}} \qquad \text{Equation (9.2)}$$

These radial forces cause splitting tensile stresses along any cut through the diameter of the core. A uniform distribution of splitting stresses across a

section of grout is shown in Figure 7.32a. The splitting tensile stresses are resisted by the splitting tensile capacity of a section of grout. The area of grout resisting splitting stresses is the length of grout shown in Figure 7.32b multiplied by the length of a section Δx. The resistance to the splitting tensile stresses is expressed in Equation (7.30).

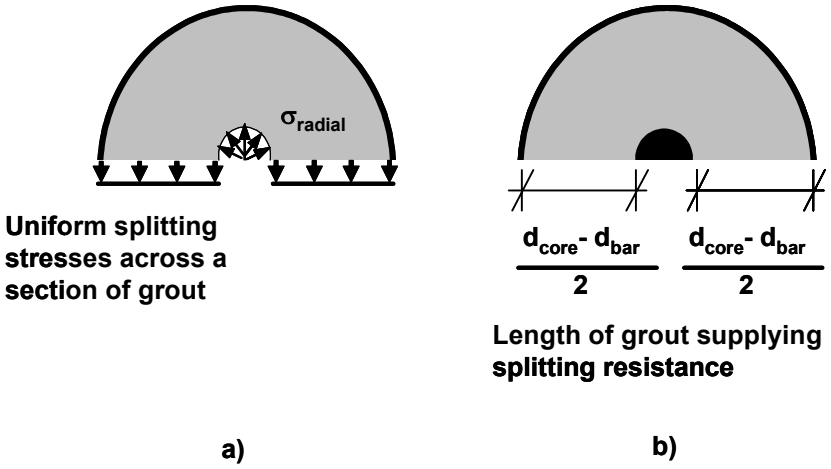

Figure 9.5: Stresses generated perpendicular to a cut along the diameter of a grouted cell

$$F_{resis\,\tan ce} = \sigma_{radial} d_{bar} \Delta x \qquad \text{Equation (9.3)}$$

The uniform splitting stress across a section of grout as shown in Figure 7.32a is calculated by integration. Figure 9.6a shows the radial stress acting at the interface between the bar and grout. The vertical component of stress which corresponds to a uniform splitting stress is calculated using geometry for a differential section of the arc, ds (Figure 9.6b). Integrating this expression for the vertical component of force between angles of 0 and π yields the expression for the total force generated by the splitting stress shown in Equation (9.4). If the

resultant of the uniform splitting tensile stress is set equal to the total force supplied by the resistance of the grout, Equation (9.5) is generated. The splitting tensile strength, f_t, and expressed in terms of the bond stress in Equation (9.6).

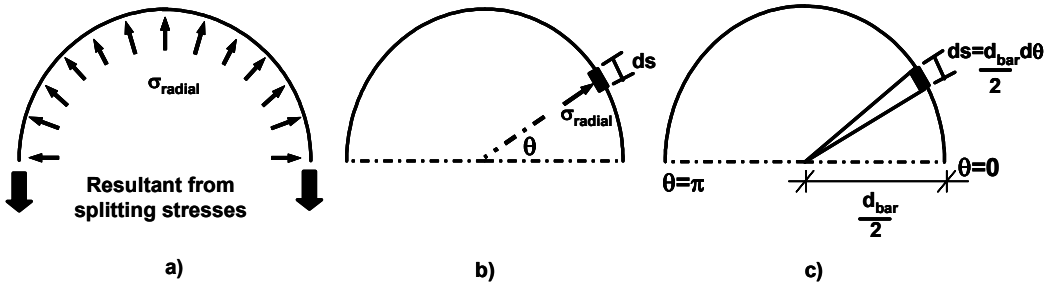

Figure 9.6: Calculation of force corresponding to the splitting tensile stresses across a section of grout

$$F_{splitting} = \int_0^{\pi} \sigma_{radial} \Delta x \sin\theta \cdot ds = \int_0^{\pi} \sigma_{radial} \Delta x \sin\theta \cdot \frac{d_{bar}}{2} d\theta = \sigma_{radial} d_{bar} \Delta x$$

Equation (9.4)

$$f_t (d_{core} - d_{bar}) \Delta x = \sigma_{radial} d_{bar} \Delta x \qquad \text{Equation (9.5)}$$

$$f_{t,reqd} = \frac{\sigma_{radial} d_{bar}}{(d_{core} - d_{bar})} = \frac{u d_{bar}}{(d_{core} - d_{bar})} = \frac{V d_{bar}}{jd \cdot d_{bar} \cdot (d_{core} - d_{bar})} \qquad \text{Equation (9.6)}$$

Based on this analysis, for reinforcement in the elastic stress range, the acting splitting tensile stress can be calculated. In such a case the area ratio of longitudinal steel may be increased beyond the proposed value of 3% for the design provisions of Section 8.8. These proposed ACI 3xx and MSJC design provisions permit area ratios of longitudinal steel to grouted core up to 4.5%, provided that the splitting tensile stress generated in the core (Equation (9.6)) is less than the available splitting tensile strength. A detailed example of these

calculations is presented in Appendix D for a particular design example involving walls subject to out-of-plane loading. The proposed code language in ACI 3xx is as follows:

> ***12.1.3 –*** *The maximum ratio of vertical reinforcement to area of a grouted cell shall be 3%. It shall be permitted to use ratios of vertical reinforcement up to 4.5% if the reinforcement remains elastic throughout its entire length and the available splitting tensile strength of the grout is greater than the acting splitting tensile strength as defined by Equation (12-xx)*
>
> $$f_t = \frac{Vd_{bar}}{jd \cdot d_{bar} \cdot (d_{core} - d_{bar})} \qquad \textit{Equation (12-xx)}$$
>
> *The splitting tensile strength of the grout shall be taken as* $4\sqrt{f_g'}$. *If* f_g' *is not specified it shall be permitted to be taken as 2000 psi.*

9.4.4.2 Analysis of the maximum permissible area ratio in a plastic hinge zone

If the reinforcement is located in a plastic hinge zone, compatibility of strains no longer exists between the reinforcement and the surrounding grout, and the splitting tensile stress cannot be determined using Equation (10.6). Based on the cracking observed along the flexural reinforcement in the flexure-dominated specimens (Section 8.8), the proposed design provisions limit the area ratio to 3% in areas where a plastic hinge may form.

CHAPTER 10
Summary, Conclusions and Recommendations

10.1 SUMMARY

This dissertation describes a research project whose objective was to develop design provisions for Autoclaved Aerated Concrete (AAC). Typical AAC construction uses AAC shear walls combined with AAC floor and roof diaphragms. Results from a testing program on AAC shear walls and an AAC assemblage specimen were used to prepare proposed code language, along with proposed commentary and underlying technical justification. The proposed design provisions for reinforced panels are in the form of a separate document, designated here as "ACI 3xx," whose format corresponds to that of ACI 318-02. Proposed design provisions for AAC masonry are referred to as the proposed MSJC design provisions. The development of R and C_d factors is addressed in Varela (2003).

The mechanical properties of a material are fundamental to the design process for structural elements made of that material. Mechanical properties of AAC were determined at the Ferguson Structural Engineering Laboratory, and were validated with the results of material tests performed at other laboratories. Based on the results of those tests, design-related equations for material properties were developed for use in design provisions.

A comprehensive testing program was developed. The first phase of that testing program was intended to determine the behavior of AAC shear walls

subjected to reversed cyclic lateral loads. Walls were made of a variety of AAC elements, including masonry-type units and reinforced panels, laid either horizontally or vertically. The aspect ratio of the specimens (ratio of height to base length) varied from 0.6 to 3, and each specimen was designed to fail in either shear or flexure. Because the behavior of flexure-dominated AAC shear walls is inherently easier to predict than that of shear-dominated walls, and because the prediction of shear capacity is very important in the capacity design of AAC shear walls, initial tests emphasized shear-dominated walls. Based on test results, procedures and corresponding design equations were developed to predict the behavior of AAC shear walls as governed by flexure, shear, and other limit states.

The second phase of the testing program involved the design, construction and testing, under reversed cyclic lateral loads, of a full-scale, two-story AAC assemblage specimen. Results from this second phase were used to validate the previously developed wall-design equations, to evaluate proposed procedures for the design of AAC floor systems and connections, and to evaluate the overall behavior of AAC structures.

10.2 CONCLUSIONS

1) Reliable relationships exist for the splitting tensile strength, modulus of rupture and modulus of elasticity expressed as a function of the compressive strength. In this context, "reliable" connotes low coefficients of variation (COV) and mean values close to or exceeding 1.0 for the ratios of observed material characteristics, to those predicted based on the specified compressive strength (strength class).

2) Less (but still sufficiently) reliable information exists on the coefficient of friction and tensile bond strength between AAC and leveling bed mortar, and on the coefficient of friction between AAC and AAC.

3) Based on tests conducted at UT Austin and elsewhere, reliable predictive models have been developed for the behavior of AAC shear walls with masonry-type units and horizontally oriented panels. In this context, "reliable" connotes low coefficients of variation and values close to or exceeding 1.0 for the ratios of observed capacity to the capacity predicted using equations based on the tested strength. These models have been used to develop design approaches and corresponding design equations for AAC shear walls with masonry-type units and horizontally oriented panels, addressing the following aspects of behavior:
   - flexural cracking;
   - web-shear cracking;
   - flexure-shear cracking;
   - sliding shear capacity;
   - flexural yielding;
   - nominal flexural capacity; and
   - crushing of the diagonal strut (observed for one specimen only).

4) In general, mean values of tested compressive strengths considerably exceed the specified values corresponding to each AAC strength class, with low coefficients of variation (COV) of about 35% for the ratios of tested to specified compressive strengths. As a result, the predictive equations referred to in Conclusions (1) and (3) above give even smaller

coefficients of variation (COV), and mean values close to 1.0, for the ratios of observed values to those predicted using equations based on the tested compressive strength.

5) In spite of the general validity of Conclusions (1), (3) and (4), it is clear that the Class 4 AAC material used for the Two-story Assemblage Specimen did not comply with the compressive strength specified by ASTM C1386 for that class. The reasons for this non-compliance are not known.

6) Sliding shear resistance based on applied axial load is reasonably well understood based on the use of Shear Wall Specimen 4, the Two-story Assemblage Specimen and the direct shear tests to determine the appropriate coefficient of friction between AAC and leveling bed mortar or between AAC and AAC. Sliding shear resistance can be increased temporarily by thin-bed mortar or dowels but the effectiveness is degraded by flexural cracks at bed joints and by cycling, respectively. Unlike conventional reinforced concrete, AAC cannot be provided with enough reinforcement crossing the sliding shear interface to generate more resistance by shear friction. As a result, the sliding shear capacity of AAC structures is limited by friction alone. For low-rise AAC structures, base shear capacity can be limited by frictional resistance.

7) Based on tests conducted at UT Austin, design approaches and equations have been developed for AAC shear walls made of vertically oriented panels. These models have been used to develop design approaches and

corresponding design equations for AAC shear walls made of vertically oriented panels, addressing the following aspects of behavior:

- flexural cracking;
- web-shear cracking;
- flexural yielding; and
- nominal flexural capacity.

8) Design approaches and equations have been developed to assess the contributions of factory-installed and field-installed reinforcement.

9) Construction requirements have been developed for AAC structures, based on the construction practices used in the shear wall specimen tests and assemblage specimen tests performed at UT Austin. Because those construction requirements are part of the technical justification for the proposed the design provisions, they constitute minimum life-safety requirements.

10) Design provisions have been developed for AAC floor diaphragms, based on the following experimentally validated mechanisms:

- adhesion between thin-bed mortar and AAC;
- adhesion between grout and AAC;
- dowel action of reinforcement perpendicular to the load;
- strut-and-tie mechanisms involving multiple floor panels; and
- adhesion, friction and dowel action for connecting AAC floor diaphragms to walls.

11) Additional requirements intended to ensure ductile failure have been proposed for use of AAC structural systems in seismic zones.

10.3 RECOMMENDATIONS FOR FUTURE RESEARCH

1) Additional research could be performed to refine the proposed design requirements for AAC floor and roof diaphragms to validate the use of strut-and-tie models that permit cracks to cross joints between AAC panels oriented parallel to the direction of load. These models could provide better predictions of capacity and permit refinements in prescriptive reinforcement and detailing requirements.

2) Additional information is required on the shear strength between AAC and grout. Insufficient data points exist to determine if the few samples tested in this study were statistically representative. The effect of construction techniques such as pre-wetting the AAC units could be investigated. Additional tests may also be performed on the shear strength between AAC and thin-bed mortar. If the total height of the direct shear specimens was reduced, the stresses due to the horizontal loads that developed at the base of the direct shear specimen will be minimized.

3) In the research described here, crushing of the diagonal strut was observed in one shear wall specimen only. Additional research could be conducted to prove or disprove the validity of this design limit state, and if valid, to refine the corresponding predictive design equation.

4) Additional experimental and analytical research could be conducted to develop design provisions for AAC infills. Infills could be a cost-effective application of AAC for passive fire protection, drift control, and added lateral strength in framed structures.

5) Because the design provisions that resulted from this study (the proposed MSJC and ACI 3xx design provisions) are intended to be consistent with the existing MSJC Code and Specification and with ACI 318-02 respectively, they consider shear capacity as the summation of a capacity due to AAC (V_{AAC}) and possibly a capacity due to V_s (deformed reinforcement in grouted, horizontally oriented bond beams). The capacity due to AAC is taken as the shear required to produce web-shear or flexure-shear cracking. This is conservative, but not as rational as an approach based on strut-and-tie mechanisms. Experimental and analytical research could be conducted to develop and validate strut-and-tie models for design of AAC elements, particularly AAC shear walls.

APPENDIX A:

TENSILE BOND STRENGTH AND DIRECT SHEAR STRENGTH OF AAC

This Appendix contains information on the tensile bond strength of thin-bed mortar joints and direct shear strength of AAC. This information is written by and presented in Argudo (2003).

A.1 TENSILE BOND STRENGTH OF JOINTS BETWEEN THIN-BED MORTAR AND AAC

The University of Alabama at Birmingham (UAB) conducted tests to evaluate the modulus of rupture in AAC specimens with thin-bed mortar joints, based on Method 2. Data are presented in Table A1. Each data point reflects the average of a group of specimens, usually 3 in number.

Table A1: Modulus of Rupture of AAC specimens with thin-bed mortar joints (UAB, Method 2)

Manufacturers Specifications		**Tensile stresses parallel to the direction of rise**	
Material	**ρ (pcf)**	**Measured Density ρ1386 (pcf)**	**Modulus of Rupture, fr (psi)**
Hebel-HG1	25	25.7	60
Ytong-YG1	25	28.9	71
Ytong-YG2	31	39.6	85
Ytong-YG3	40	44.0	39
Contec-CG1	25	31.3	80
Contec-CG2	32	34.7	87
Contec-CG3	38	39.2	101

Modulus of rupture tests from UAB on specimens with thin mortar joints showed tensile bond failures of the AAC material for low-strength material only. As the strength of the AAC increased, failure was governed by the tensile bond strength of the thin-bed mortar. If the failure is governed by the material the slope would be the same as the modulus of rupture. Figure A1 and Figure A2 show, however, that as the density increases the failure is governed by the thin-bed mortar joint. The limit tensile bond strength is 80 psi (0.55 MPa) for materials with f_{AAC} less than 700 psi (4.8 MPa). For materials with f_{AAC} less than 450 psi (3.1 MPa), the AAC unit failure governs, regardless of the type of mortar used and the extent of polymer modification of the mortar. Although the data fit is far from perfect, it does correlate with the results of flexural cracking (Section 7.2).

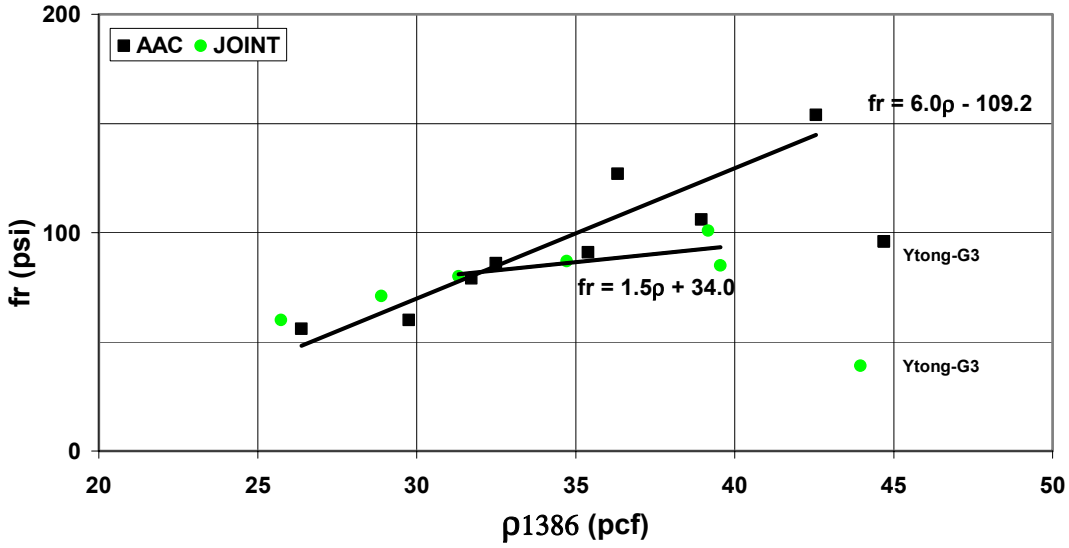

Figure A1: Tensile bond strength versus density

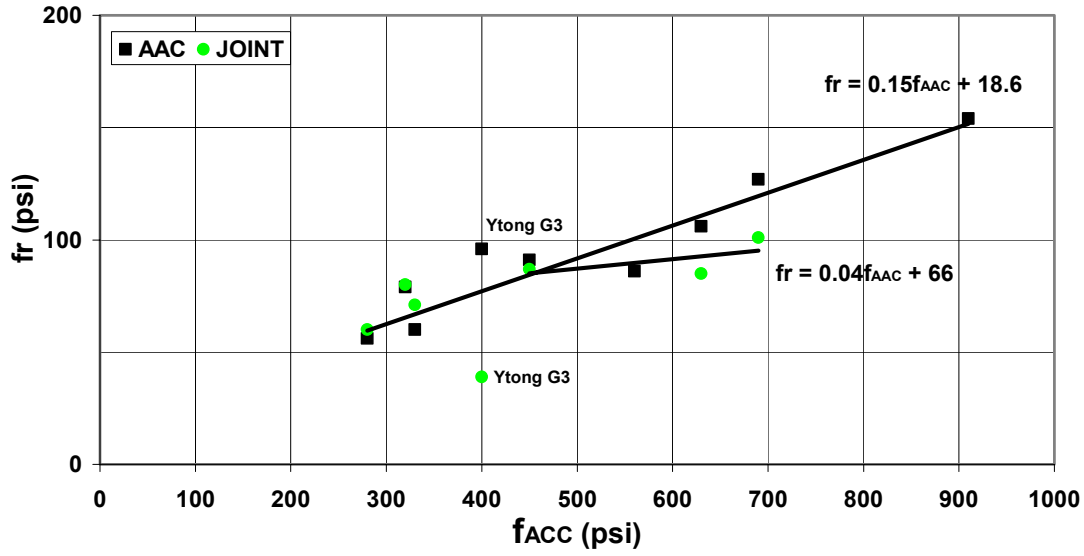

Figure A2: Tensile bond strength versus compressive strength

A.2 DIRECT SHEAR STRENGTH OF AAC

UAB conducted direct shear tests (at essentially zero moment and high shear) on plain AAC specimens. One group of specimens was oven-dried to a MC ranging from 8% to 12%. A second group of specimens was air-dried to a MC ranging from 15% to 25%. Data from such groups are referred as AAC-oven dry (MC=10%) and AAC-air dry (MC=20%) respectively. Researchers at UAB tested air-dried specimens to confirm that the shear strength of oven-dried specimens can be less than that of otherwise identical air-dried specimens because of micro-cracking produced by oven-drying. There are no shear tests on reinforced AAC elements.

The relationship between direct shear strength (f_v) and compressive strength (f_{AAC}) is shown in Figure A3, in which two points (f_{AAC} = 560 psi and 910 psi) show a significant decrease in shear strength from air-dried to oven-dried specimens. Because those points may be influenced by micro-cracking, it is debatable whether or not they should be included in the data analysis. Since field units are not expected to be oven-dried, Equation (A.1) is proposed to estimate the nominal direct shear capacity of AAC.

$$f_v = 0.15 f_{AAC} \qquad \text{Equation (A.1)}$$

f_{AAC} and f_v in psi

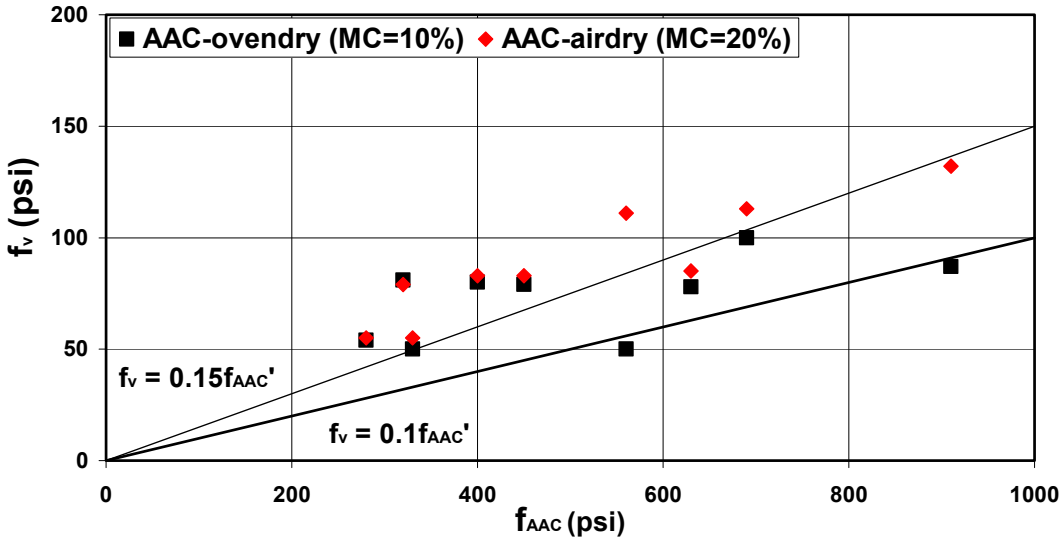

Figure A3: Relationship between direct shear strength (f_v) and compressive strength (f_{AAC})

APPENDIX B:

TESTING PROGRAM FOR AAC SHEAR WALL SPECIMENS

This Appendix contains the complete information on the testing program of AAC shear walls. This section was written by Varela (2003).

The experimental part of this dissertation consisted of two phases. Phase I involved testing 14 AAC shear wall specimens; and Phase II, testing a two-story assemblage specimen. This chapter describes the test setup for those AAC shear wall specimens, the objectives and fundamental characteristics of each test specimen, the loading equipment, instrumentation, and loading history. The test setup used in this test program was verified through two initial tests, AAC Shear Wall Pilot Specimen 1 and AAC Shear Wall Pilot Specimen 2 (Brightman 2000).

The test setup, objectives, loading equipment, instrumentation, and loading history of the assemblage specimen are described in Appendix A. A summary of the test setup and objectives of the assemblage specimen is presented in Chapter 4.

The first eight shear wall specimens described here were intended to represent AAC shear walls whose behavior is controlled by shear and the remaining six specimens by flexure. The specimen geometry, reinforcement, and axial loads were selected based on those objectives.

Eight shear-dominated walls were designed and tested to verify proposed design formulas for web-shear cracking, sliding shear, and crushing of the diagonal strut for AAC shear walls. Those specimens were also intended to provide experimental data to develop analytical models that represent the behavior of shear-dominated AAC walls subject to earthquake ground motions. The first four AAC shear-dominated wall specimens were also tested to determine

the differences in behavior of AAC shear-dominated walls with the same overall geometry, but constructed with different orientations of panel and block elements.

The geometry, flexural reinforcement, and axial force for each of the shear-dominated specimens were selected to force shear behavior. The geometry of the AAC shear-dominated specimens was selected to represent potential walls of AAC structures. The height of the shear-dominated specimens was 12 ft (3.6 m), and the length of the first shear dominated-specimens was 20 ft (6.1 m). This length was reduced in some specimens to study the effect of change in wall length in the capacity of the AAC walls as governed by web-shear cracking. The axial load was varied in some cases among the shear-dominated specimens to determine the influence of the axial force in the capacity of the AAC walls as governed by web-shear cracking.

Six flexure-dominated walls were designed and tested to verify proposed design formulas for flexural shear cracking, flexural capacity, and to provide experimental data to develop analytical models to predict the behavior of flexure-dominated AAC shear walls under earthquake ground motions, and to define appropriate values of drift ratio and displacement ductility capacities for AAC shear walls.

The geometry, flexural reinforcement, and axial force for each of the flexure-dominated specimens were selected to force flexural behavior. The wall geometry for the flexure-dominated specimen was selected to represent the aspect ratio (height divided by plan length) of walls of potential AAC structures whose behavior is dominated by flexure. The axial force in those specimens was varied to represent the range of compressive stresses found in shear walls located in the first story of potential AAC structures up to five stories high.

B.1 SUMMARY OF DETAILS OF SHEAR WALL SPECIMENS

For each of the fourteen shear wall specimens, the intended failure mode, AAC units used in construction, material supplier, and test date is summarized in Table B1. The geometry, amount and location of exterior and interior flexural reinforcement for each shear wall specimen are summarized in Table B2. Details of the axial load applied to each of the shear wall specimens are presented in Table B3. The measured average compressive strengths of AAC for the different AAC units used in the shear wall specimens are presented in Table B4. Detailed description for each of the shear wall specimens is presented in Section 3.2.

Table B1: Intended failure mode, AAC units used in construction, and material supplier for each AAC shear wall specimen

Specimen	Intended Failure Mode	AAC units	Material Supplier	Test Date
1	Shear	Horizontal Panels	Contec 1	6/15/2000
2	Shear	Vertical Panels	Ytong 1	7/26/2000
3	Shear	Blocks	Ytong 2	12/11/2000
4	Shear	Horizontal Panels	Matrix 1	10/21/2000
5	Shear	Blocks	Contec 2	5/15/2001
7	Shear	Blocks	Ytong 2	11/18/2000
9	Shear	Horizontal Panels	Matrix 1	2/6/2001
11	Shear	Blocks	Contec 2	4/10/2001
13	Flexure	Horizontal Panels	Ytong 1	07/03/2001
14a	Flexure	Horizontal Panels	Babb 1	12/10/2001
14b	Flexure	Horizontal Panels	Babb 1	03/07/02
15a	Flexure	Vertical Panels with Blocks	Babb 1	11/29/01
15b	Flexure	Vertical Panels with Blocks	Babb 1	03/28/02
16	Flexure	Vertical Panels with U-Blocks	Babb 1	1/17/02

In Table B1 the number following the material supplier refers to the shipment number of the material. For example, Babb-1 is the first shipment of AAC units received at the FSEL from Babb.

Table B2: Geometry, amount and location of exterior and interior flexural reinforcement for each shear wall specimen

Specimen	Length in. (m)	Height in. (m)	Thickness in. (m)	Exterior Reinforcement	Interior Reinforcement
1	240 (6.1)	154 (3.9)	8 (0.2)	2-B7 1 in. (25 mm) 24 in.(0.6 m) from ends	No
2	240 (6.1)	154 (3.9)	8 (0.2)	2-B7 1 in. (25 mm) 24 in.(0.6 m) from ends	No
3	240 (6.1)	152 (3.8)	8 (0.2)	2-B7 1 in. (25 mm) 24 in.(0.6 m) from ends	No
4	240 (6.1)	154 (3.9)	8 (0.2)	2-B7 1 in. (25 mm) 24 in.(0.6 m) from ends	#5 (16 mm) at 48 in. (1.2 m)
5	240 (6.1)	152 (3.8)	8 (0.2)	2-B7 1 in. (25 mm) 24 in.(0.6 m) from ends	No
7	144 (3.7)	152 (3.8)	8 (0.2)	2-B7 1 in. (25 mm) 24 in.(0.6 m) from ends	No
9	96 (2.4)	154 (3.9)	8 (0.2)	2-B7 1 in. (25 mm) right at wall ends	No
11	48 (1.2)	152 (3.8)	8 (0.2)	2-B7 1 in. (25 mm) right at wall ends	No
13	72 (2.1)	154 (3.9)	8 (0.2)	No	# 5 (16 mm) 12 in. (0.3 m) from ends
14a	56 (1.4)	154 (3.9)	10 (0.25)	No	# 5 (16 mm) 4 in. (0.1 m) from ends
14b	56 (1.4)	154 (3.9)	10 (0.25)	No	# 5 (16 mm) 4 in. (0.1 m) from ends
15a	112 (2.8)	154 (3.9)	10 (0.25)	No	# 5 (16 mm) 8 in. (0.2 m) from ends
15b	112 (2.8)	154 (3.9)	10 (0.25)	No	# 5 (16 mm) 8 in. (0.2 m) from ends
16	112 (2.8)	154 (3.9)	10 (0.25)	No	# 5 (16 mm) 8 in. (0.2 m) from ends

Table B3: Details of axial load applied to each shear wall specimen

Specimen	Axial Load (Exterior Reinforcement) kips (kN)	Axial Load (Load Maintainer) kips (kN)	Self Weight Loading Beam kips (kN)	Total Axial Load kips (kN)
1	32 (142.3)	116 (516.0)	8 (35.6)	156 (693.9)
2	40 (177.9)	108 (480.4)	8 (35.6)	156 (693.9)
3	48 (213.5)	64 (284.7)	8 (35.6)	120 (533.8)
4	48 (213.5)	64 (284.7)	8 (35.6)	120 (533.8)
5	36 (160.1)	16 (71.2)	8 (35.6)	60 (266.9)
7	40 (177.9)	35 (155.7)	5 (22.2)	80 (355.8)
9	50 (222.4)	5 (22.2)	5 (22.2)	60 (266.9)
11	20 (89.0)	0 (0.0)	5 (22.2)	25 (111.2)
13	0 (0.0)	20 (89)	5 (22.2)	25 (111.2)
14a	0 (0.0)	0 (0.0)	5 (22.2)	5 (22.2)
14b	0 (0.0)	0 (0.0)	5 (22.2)	5 (22.2)
15a	0 (0.0)	20 (90.0)	5 (22.2)	25 (111.2)
15b	0 (0.0)	20 (90.0)	5 (22.2)	25 (111.2)
16	0 (0.0)	20 (90.0)	5 (22.2)	25 (111.2)

Table B4: Measured compressive strength for different units used in shear wall specimens

Material	Measured Compressive Strength f_{AAC} psi (MPa)
Contec 1	781 (5.4)
Contec 2	1040 (7.2)
Babb 1	1140 (7.9)
Matrix 1	1330 (9.2)
Ytong 1	NA
Ytong 2	650 (4.5)

B.2 SHEAR WALL SPECIMENS

In the following sections, the geometry, type of AAC units used in construction, reinforcement, and axial force is presented in detail for each of the shear wall specimens.

B.2.1 Shear Wall Specimen 1

Shear Wall Specimen 1 was constructed with horizontal AAC panels placed in running bond (Figure B1). The wall measured 240 in. (6.1 m) long by 154 in. (3.91 m) high (top of base to line of load application) by 8 in. (203.2 mm) thick. The aspect ratio of the wall (height divided by plan length) was 0.64. An axial load of 80 kips (355.8 kN) was applied at the beginning of the test, and was increased throughout the test to a final axial load of 156 kips (693.9 kN). The axial load was increased during the test because sliding of the wall with respect to its base was observed. The increase in the axial load provided additional sliding shear capacity in the wall, to force web-shear cracking in the specimen. The first four panels of this specimen were previously used in AAC Shear Wall Pilot Specimen 2 (Brightman 2000); since the damage in that specimen was concentrated to the top two panels, these panels were replaced. The damaged panels were removed and the bed joint was carefully sanded and leveled to allow for full contact of the thin-bed mortar across the joint. The exterior flexural reinforcement of this wall consisted of two ASTM A193-B7 threaded rods 1 in. (25.4 mm) in diameter, placed 24 in. (0.6 m) from each wall end. This reinforcement was selected to force shear- rather than flexure-dominated behavior. Steel buttresses were attached to the base and to the loading beam at the ends of the wall to avoid slip for Shear Wall Specimen 1 (Brightman 2000). Steel buttresses were used in this shear wall specimen only. The AAC panels in Shear Wall Pilot Specimen 2 were supplied by Contec Mexicana (Monterrey, Mexico) and the thin-bed mortar was supplied by Ytong Florida, Ltd. (Haines City, Florida).

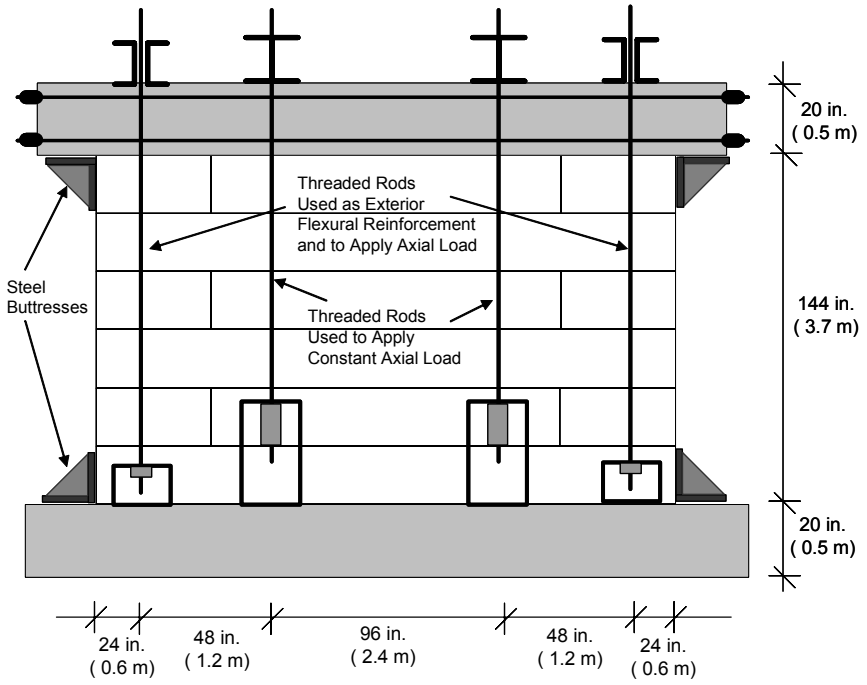

Figure B1: Layout of Shear Wall Specimen 1

B.2.2 Shear Wall Specimen 2

Shear Wall Specimen 2 was constructed with vertical AAC panels (Figure B2). The wall measured 240 in. (6.1 m) long by 154 in. (3.91 m) high (top of base to line of load application) by 8 in. (203.2 mm) thick. The aspect ratio of the wall was 0.64. A constant axial load of 156 kips (693.9 kN) was applied throughout the test. The exterior flexural reinforcement consisted of two ASTM A193-B7 threaded rods 1 in. (25.4 mm) in diameter, placed 24 in. (0.6 m) from each wall end. The AAC panels and the thin-bed mortar were supplied by Ytong Florida, Ltd. (Haines City, Florida).

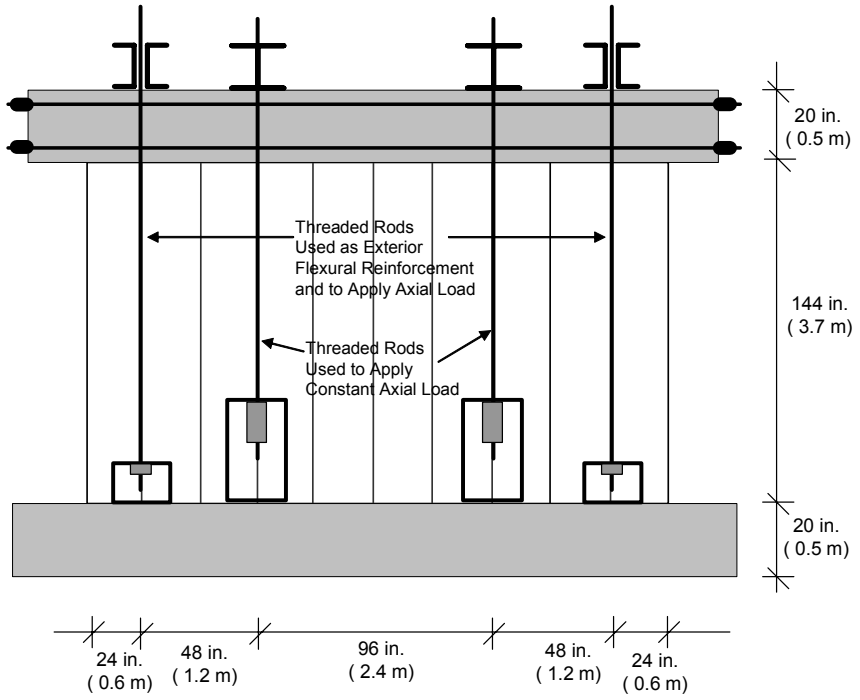

Figure B2: Layout of Shear Wall Specimen 2

B.2.3 Shear Wall Specimen 3

Shear Wall Specimen 3 was constructed with AAC masonry units placed in running bond (Figure B3). The wall measured 240 in. (6.1 m) long by 152 in. (3.86 m) high by 8 in. (203.2 mm) thick. The aspect ratio of the wall was 0.63, and a constant axial load of 120 kips (533.8 kN) was applied throughout the test. The exterior flexural reinforcement consisted of two ASTM A193-B7 threaded rods 1 in. (25.4 mm) in diameter, placed 24 in. (0.6 m) from each wall end. The AAC blocks and the thin-bed mortar were supplied by Ytong Florida, Ltd. (Haines City, Florida).

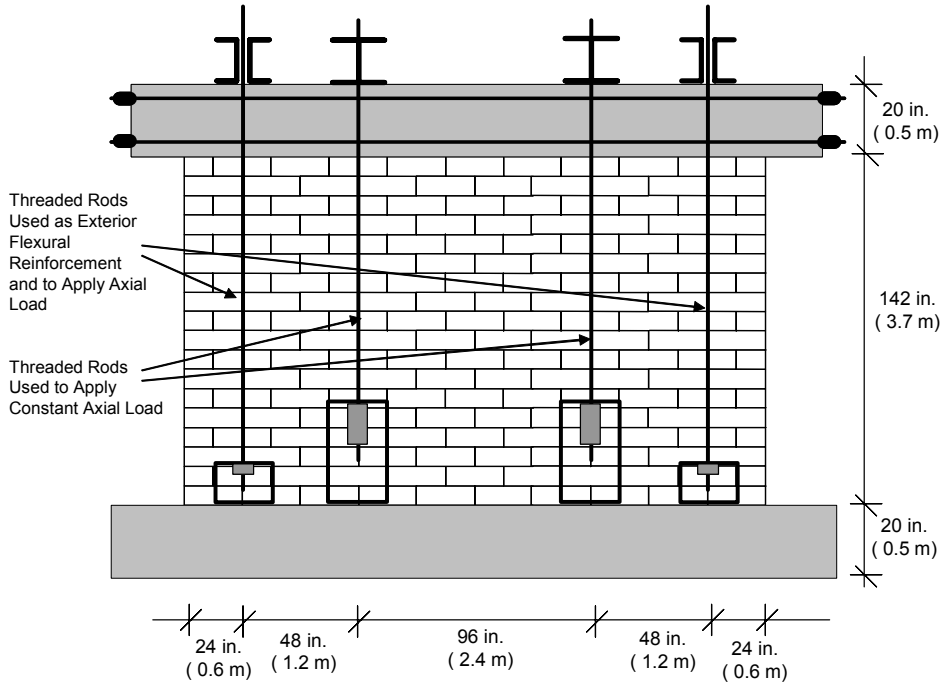

Figure B3: Layout of Shear Wall Specimen 3

B.2.4 Shear Wall Specimen 4

Shear Wall Specimen 4 was constructed with horizontal AAC panels placed in running bond (Figure B4). The geometry of the wall was the same as that of Shear Wall Specimen 1. An axial load of 120 kips (533.8 kN) was applied throughout the test. This specimen consisted of both exterior and interior flexural reinforcement. The exterior flexural reinforcement consisted of two A193-B7 threaded rods 1 in. (25.4 mm) in diameter, placed 24 in. (0.6 m) from each wall end, and the internal flexural reinforcement consisted of 1 # 5 (16 mm) bar spaced at every 48 in. (1.22 m) starting 24 in. (0.6 m) from the end of the wall. This internal flexural reinforcement was placed in 3 in. (76.2 mm) grouted cores. ASTM C 476 coarse grout by proportion was used to fill the grouted cores in this

specimen. The AAC panels and the thin-bed mortar were supplied by Hebel / Matrix (now Babb International, Inc.).

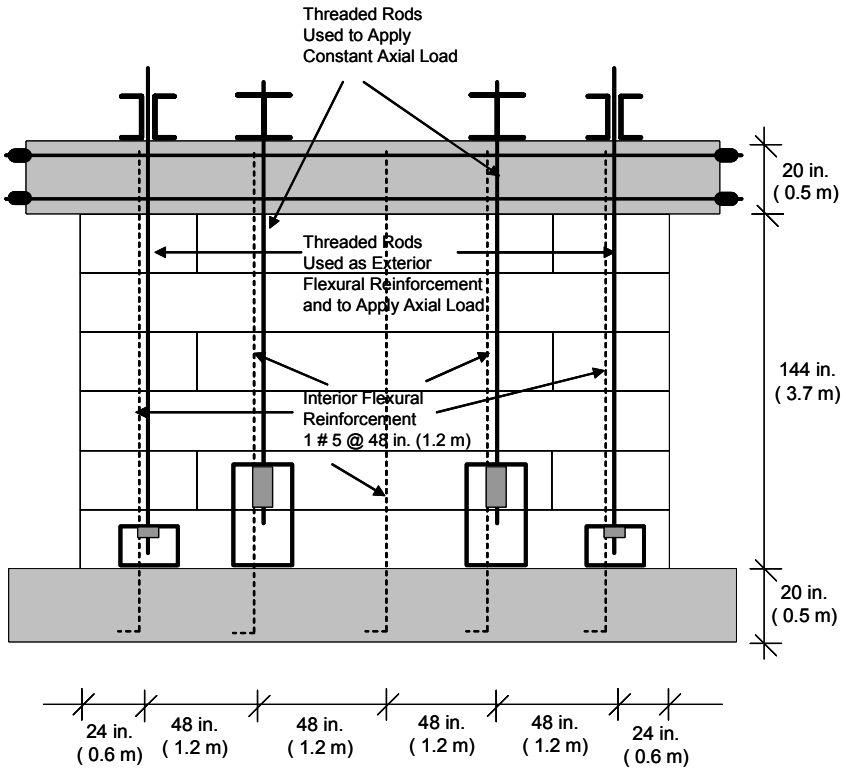

Figure B4: Layout of Shear Wall Specimen 4

B.2.5 Shear Wall Specimen 5

Shear Wall Specimen 5 was constructed with AAC blocks placed in running bond (Figure B3). The layout of the wall was the same as that of Shear Wall Specimen 3, except that 20 in. (0.51 m) #5 dowels were placed at the base of the wall and between the loading beam and the top of the wall. A total of 9 dowels were spaced at 24 in (0.6 m) starting 24 in. (0.6 m) from the end of the wall. The dowels were grouted in 3 in. (76 mm) cores fabricated at the Ferguson Structural Engineering Laboratory (FSEL). ASTM C476 coarse grout by

proportion was used to fill the grouted cores in this specimen. Dowels provided additional sliding shear resistance to reduce the axial load to 60 kips (266.9 kN). The exterior flexural reinforcement consisted of two ASTM A193-B7 threaded rods 1 in. (25.4 mm) in diameter, placed 24 in. (0.6 m) from each wall end. The AAC blocks and the thin-bed mortar were supplied by Contec Mexicana (Monterrey, Mexico).

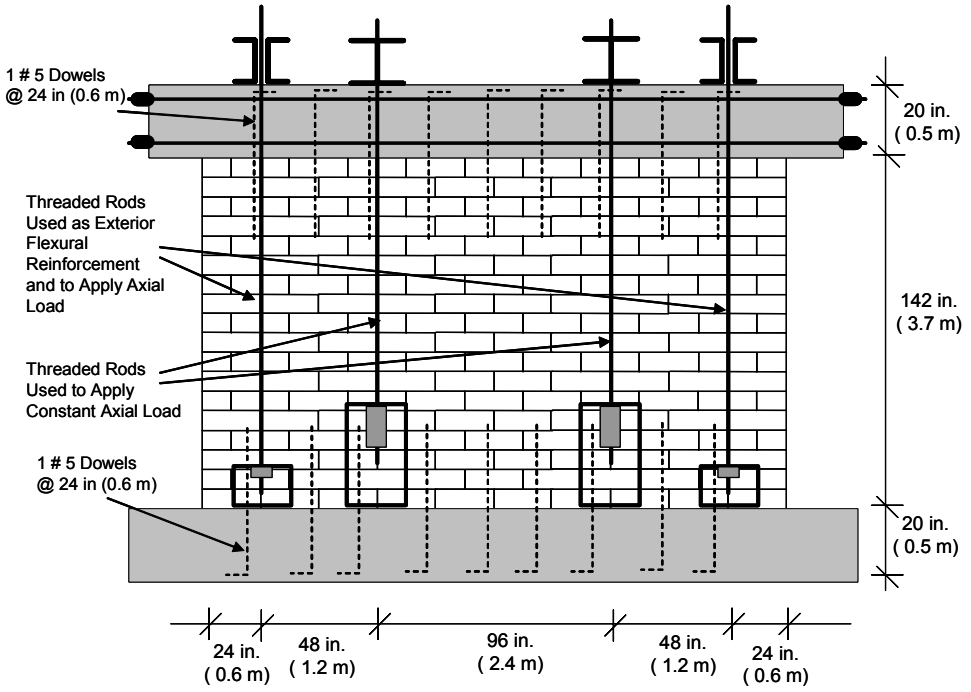

Figure B5: Layout of Shear Wall Specimen 5

B.2.6 Shear Wall Specimen 7

Shear Wall Specimen 7 was constructed with AAC masonry units placed in running bond (Figure B6). The wall measured 144 in. (3.66 m) long by 152 in. (3.86 m) high by 8 in. (203.2 mm) thick. The aspect ratio of the wall was 1.05. An axial load of 80 kips (355.8 kN) was applied throughout the test. The exterior

flexural reinforcement consisted of two ASTM A193-B7 threaded rods 1 in. (25.4 mm) in diameter, placed 24 in. (0.6 m) from each wall end. The AAC blocks and the thin-bed mortar were supplied by Ytong Florida, Ltd. (Haines City, Florida).

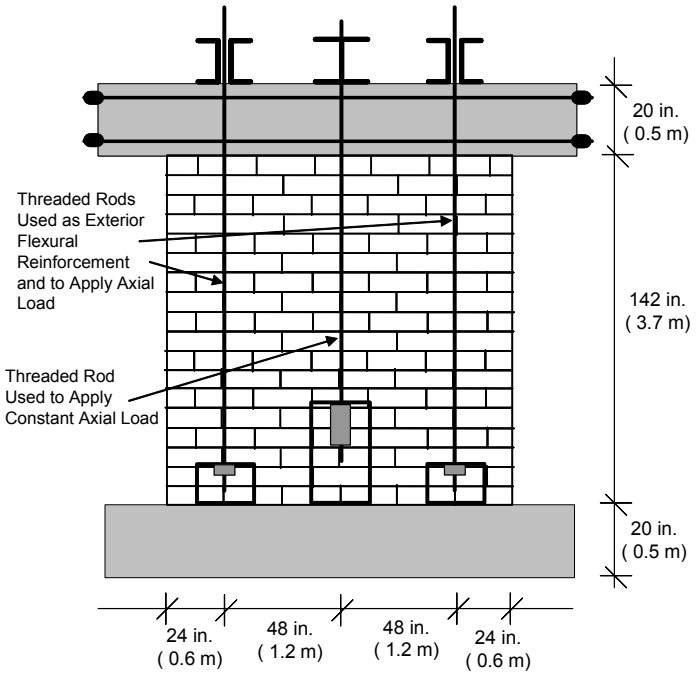

Figure B6: Layout of Shear Wall Specimen 7

B.2.7 Shear Wall Specimen 9

Shear Wall Specimen 9 was constructed with horizontal AAC panels placed in running bond (Figure B7). The wall measured 96 in. (2.43 m) long by 154 in. (3.91 m) high by 8 in. (203.2 mm) thick. The aspect ratio of the wall was 1.6, and an axial load of 60 kips (266.9 kN) was applied throughout the test. The exterior flexural reinforcement consisted of two ASTM A193-B7 threaded rods 1 in. (25.4 mm) in diameter, placed just outside the ends of the wall. The AAC panels and the thin-bed mortar were supplied by Hebel / Matrix (now Babb International, Inc.).

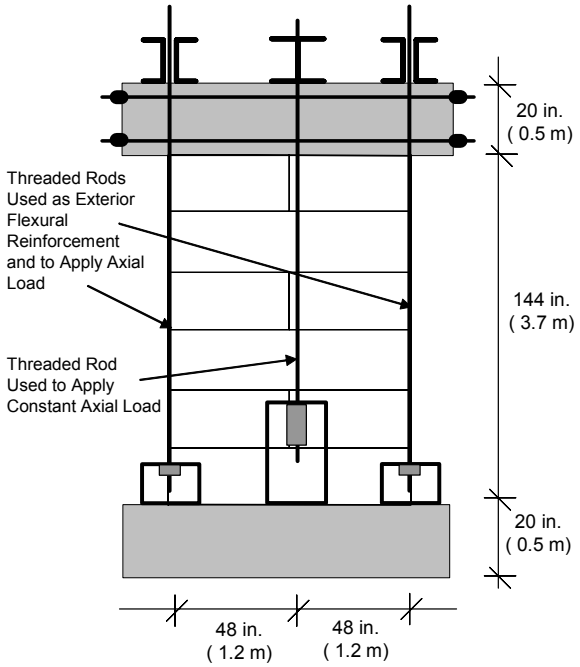

Figure B7: Layout of Shear Wall Specimen 9

B.2.8 Shear Wall Specimen 11

Shear Wall Specimen 11 was constructed with AAC masonry units placed in running bond (Figure B8). The wall measured 48 in. (1.22 m) long by 152 in. (3.86 m) high by 8 in. (203.2 mm) thick. The aspect ratio of the wall was 3.17, and an axial load of 25 kips (111.2 kN) was applied throughout the test. The exterior flexural reinforcement consisted of two ASTM A193-B7 threaded rods 1 in. (25.4 mm) in diameter, placed just outside each wall end. The AAC blocks and the thin-bed mortar were supplied by Contec Mexicana (Monterrey, Mexico).

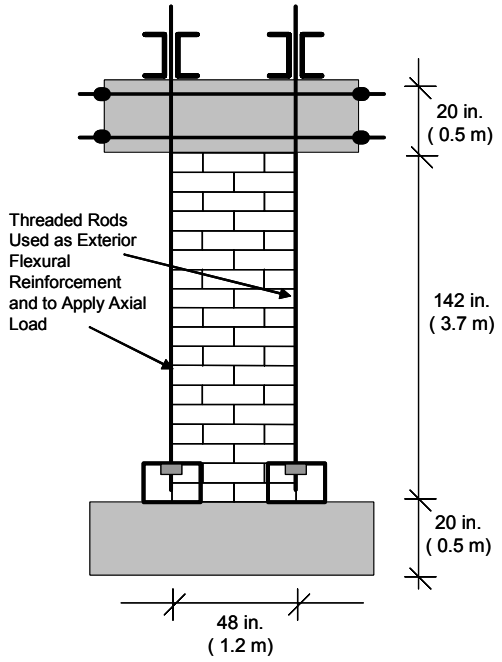

Figure B8: Layout of Shear Wall Specimen 11

B.2.9 Shear Wall Specimen 13

Shear Wall Specimen 13 was constructed with horizontal AAC panels placed in stack bond (Figure B9). The wall measured 72 in. (1.83 m) long by 154 in. (3.91 m) high by 8 in. (203.2 mm) thick with a corresponding aspect ratio of 2.14. An axial of load 25 kips (111.2 kN) was applied at the beginning of the test. This specimen was created out of surplus 144 in. (3.7 m) panels used in the construction of Shear Wall Specimen 2, which were cut and cored at FSEL. The flexural reinforcement of this wall consisted of 1 # 5 (16 mm) bar placed 12 in. (0.3 m) from each wall end. The reinforcement was placed in a 3 in. (76.2 mm) grouted cell. ASTM C476 coarse grout by proportion was used to fill the grouted cores.

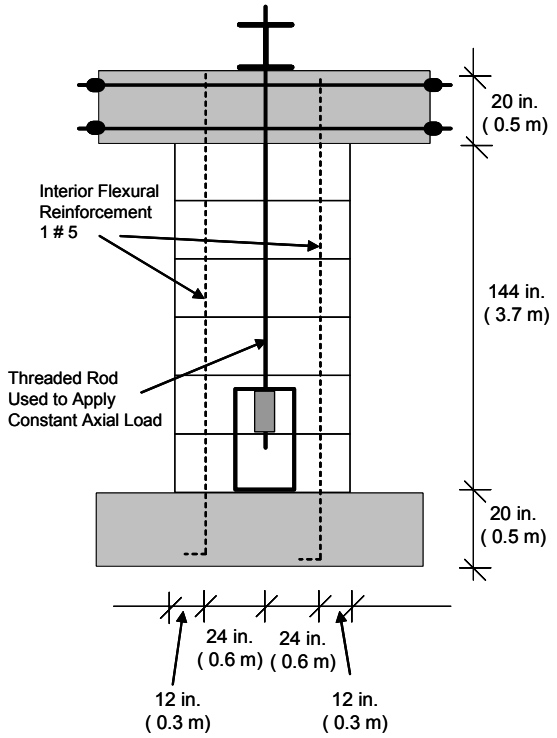

Figure B9: Layout of Shear Wall Specimen 13

B.2.10 Shear Wall Specimen 14a

Shear Wall Specimen 14a was constructed with horizontal AAC panels placed in running bond (Figure B10). The wall measured 56 in. (1.42 m) long by 154 in. (3.91 m) high by 10 in. (254 mm) thick with a corresponding aspect ratio of 2.75. A constant axial of load 5 kips (22.2 kN) was applied throughout the test. The original specimen was longer than anticipated so the panels were cut to the adjusted length at FSEL. The centerline of the cores was not aligned with the longitudinal centerline of the panels. The maximum offset was 1 in. (25 mm) in both the transverse and longitudinal axes of the wall panel. Therefore, 3 in. (76 mm) diameter cores were drilled at the correct location at FSEL. ASTM C476 coarse grout by proportion was used to fill the grouted cores. The AAC panels

and the thin-bed mortar were supplied by Babb International, Inc. (Smyrna, Georgia). The flexural reinforcement of this wall consisted of one # 5 (16 mm) bar placed 4 in. (101.6 mm) from each wall end.

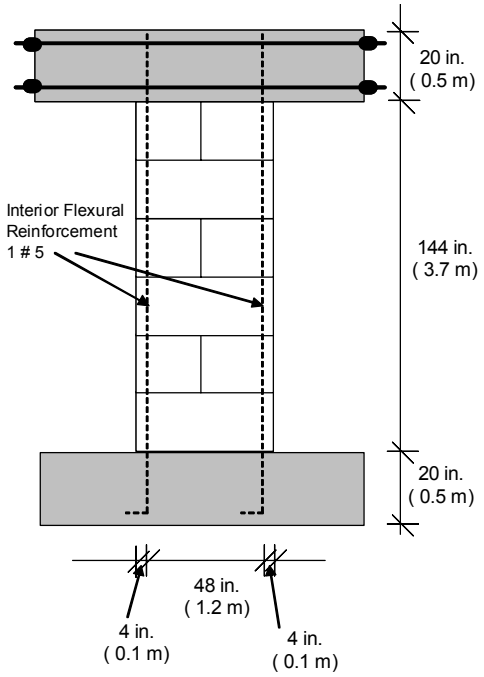

Figure B10: Layout of Shear Wall Specimens 14a and 14b

B.2.11 Shear Wall Specimen 14b

Shear Wall Specimen 14b was a replicate of Shear Wall Specimen 14a. The AAC panels and thin-bed mortar for Shear Wall Specimen 14b arrived in the same shipment as the material for Shear Wall Specimen 14a.

B.2.12 Shear Wall Specimen 15a

Shear Wall Specimen 15a was made of vertical AAC panels with AAC blocks at the ends (Figure B11). The wall measured 112 in. (2.84 m) long by 154 in. (3.91 m) high by 10 in. (254 mm) thick with a corresponding aspect ratio of

1.38. A constant axial of load 25 kips (111.2 kN) was applied throughout the test. The flexural reinforcement of this wall consisted of 1 # 5 (16 mm) bar placed 8 in. (203.2 mm) from each wall end. The reinforcement was placed in a 3 in. (76.2 mm) grouted core that was shared between the end vertical panels and AAC blocks oriented vertically (Figure B12). The half-cores in the AAC blocks were made at FSEL. ASTM C476 coarse grout by proportion was used to fill the cores in the AAC blocks and the vertical panels. The AAC panels and the thin-bed mortar were supplied by Babb International, Inc. (Smyrna, Georgia).

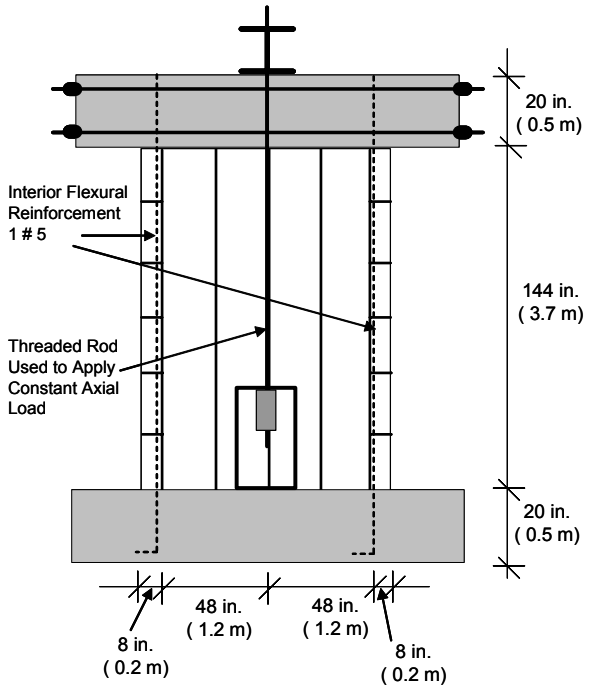

Figure B11: Layout of Shear Wall Specimens 15a, 15b and 16

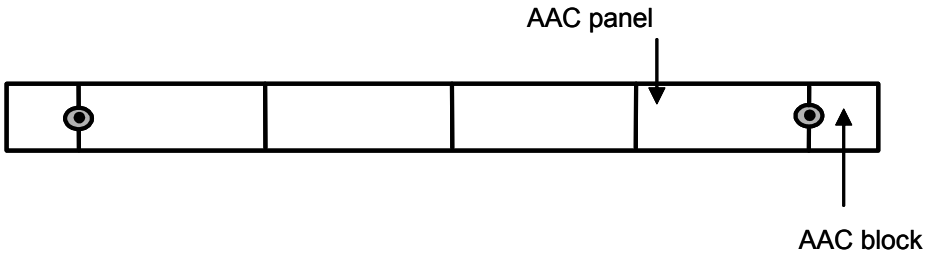

Figure B12: Plan View of Shear Wall Specimens 15a and 15b

B.2.13 Shear Wall Specimen 15b

Shear Wall Specimen 15b was a replicate of Shear Wall Specimen 15a. The AAC material and thin-bed mortar arrived in the same shipment as the material for Shear Wall Specimen 15a.

B.2.14 Shear Wall Specimen 16

Shear Wall Specimen 16 was made of vertical AAC panels with AAC U-blocks at the ends (Figure B11). The wall measured 112 in. (2.84 m) long by 154 in. (3.91 m) high by 10 in. (254 mm) thick with a corresponding aspect ratio of 1.38. An axial of load 25 kips (111.2 kN) was applied at the beginning of the test. The flexural reinforcement of this wall consisted of 1 # 5 (16 mm) bar placed 8 in. (203.2 mm) from each wall end. The reinforcement was placed in a grouted cell that was shared between the vertical panels and an AAC U-block oriented vertically (Figure B13). ASTM C476 coarse grout by proportion was used to fill the half-cores in the vertical panels and the U-blocks. The AAC panels and the thin-bed mortar were supplied by Babb International, Inc. (Smyrna, Georgia).

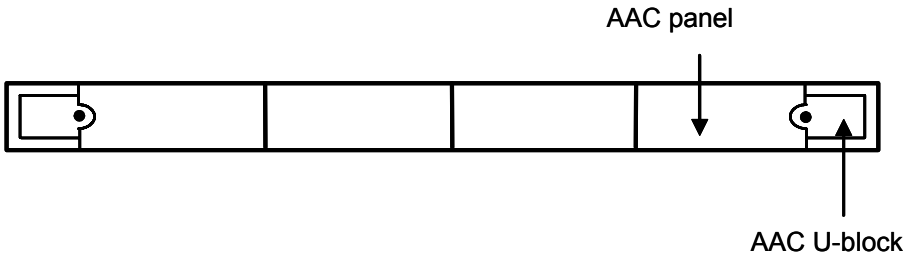

Figure B13: Plan view of Shear Wall Specimen 16

B.3 TEST SETUP

B.3.1 Lateral Loading System

The lateral load was applied using a pair of horizontal actuators mounted side by side for most specimens, and a single actuator for Shear Wall Specimen 14b and Shear Wall Specimen 15b (Figure B14). Each actuator was bolted at one end to a reinforced concrete loading beam connected to the specimen, and at the other end to a steel beam attached to the biaxial reaction wall of FSEL. The loading beam was connected along the top of each specimen using conventional portland cement-lime masonry mortar conforming to ASTM C270, Type S by proportion.

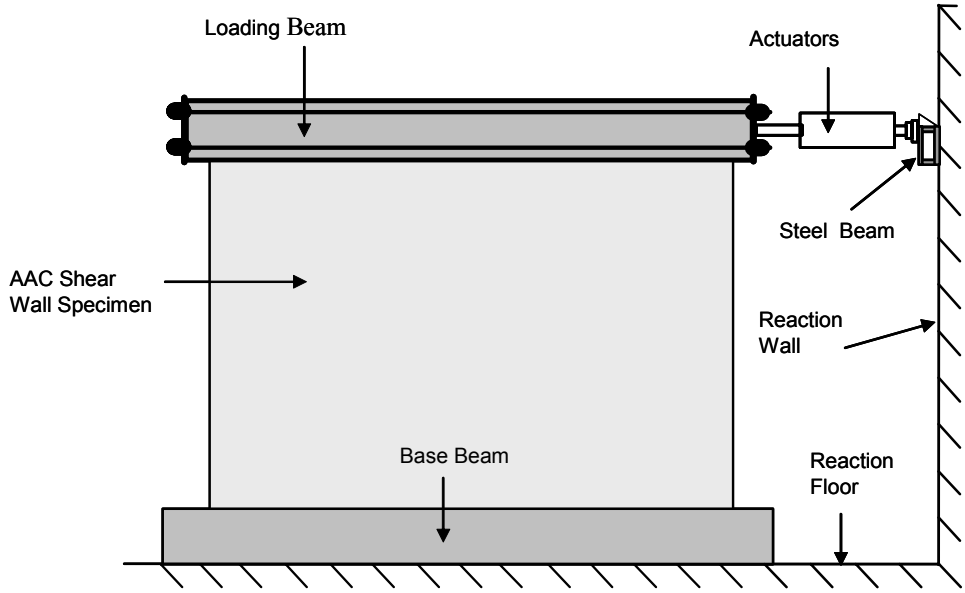

Figure B14: Setup for applying lateral load

B.3.2 Axial Load System

Axial load was applied to the shear-dominated specimens using 1 in. (25.4 mm) threaded rods pos-tensioned manually, and by hydraulic actuators controlled by a load maintainer (Figure B15). The tops of the threaded rods were connected to a transverse beam consisting of two steel channels, while the bottoms were connected to a steel box bolted to the base beam. These threaded rods located close to the wall ends were also used as external flexural reinforcement for the shear-dominated specimens.

At the beginning of each test the axial load was applied to the specimen. The exterior threaded rods were post-tensioned by tightening the nuts located inside the steel boxes connected to the base beam. The interior threaded rods were loaded by applying pressure in the actuators. The total axial load of each shear-dominated specimen was the sum of the axial load applied in the exterior

threaded rods, the axial load applied using the hydraulic actuators, and the self-weight of the concrete loading beam.

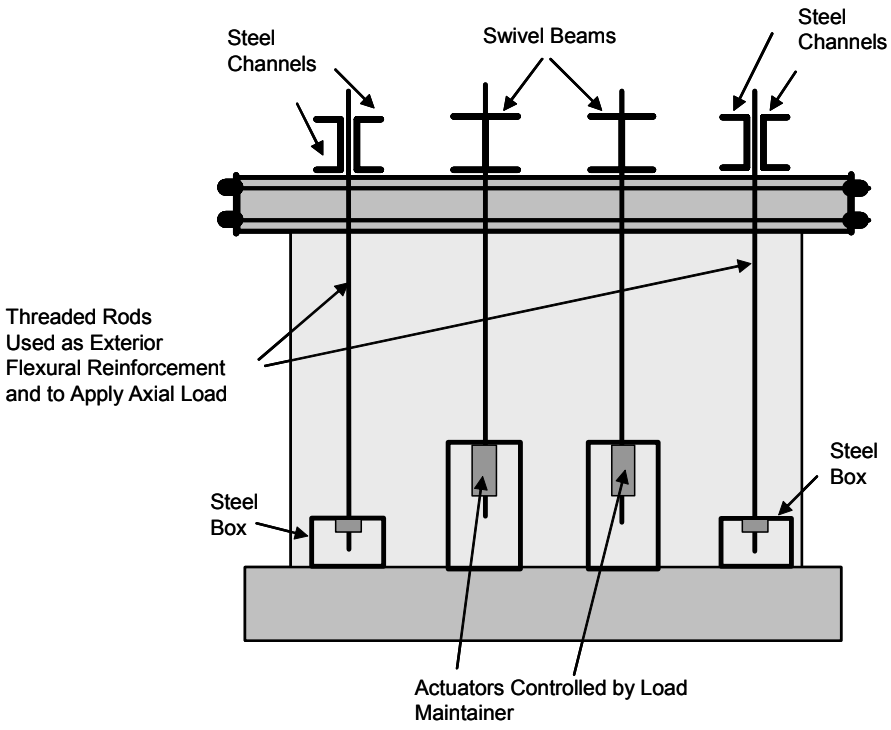

Figure B15: Axial load setup for shear-dominated specimens

Figure B16 shows a detail of the axial load setup used together with the actuators to apply constant axial load during the tests. In this figure, two threaded rods are connected at one end to a steel swivel beam connected to a steel spreader beam, and at the other end to a swivel steel box bolted to the base beam. The top swivel beam and the bottom swivel box allowed both horizontal and vertical displacements in the wall. The goal of the load maintainer was to ensure constant axial load during the tests.

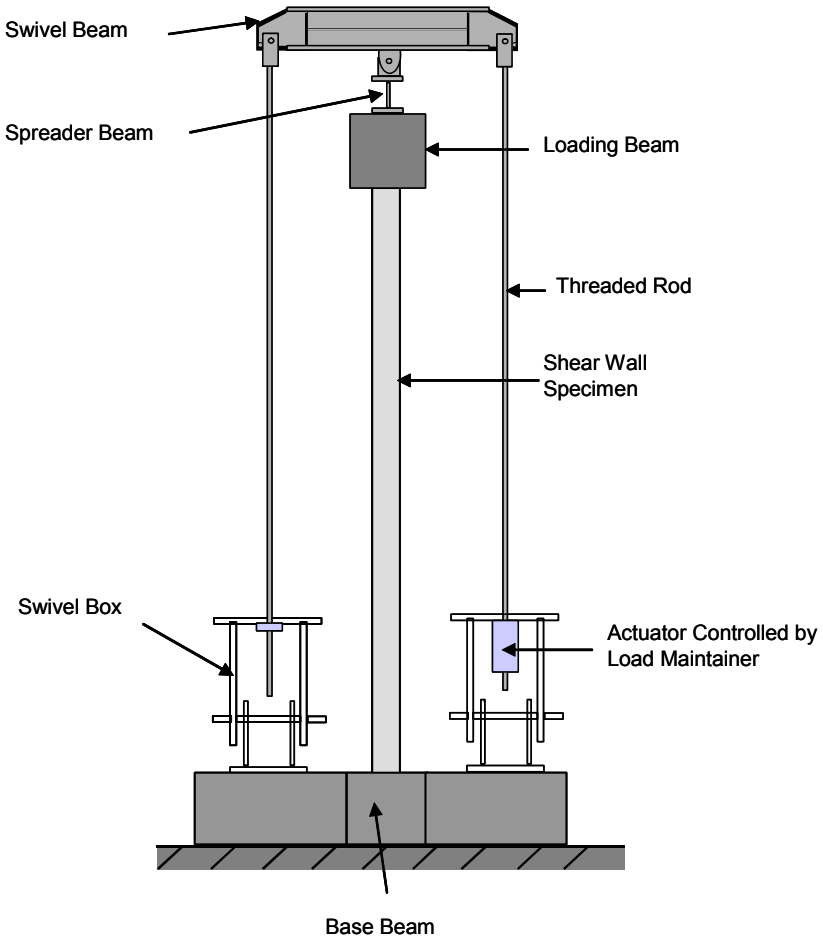

Figure B16: Detail of axial load setup used with actuators

Axial load was applied to the flexure-dominated specimens using only hydraulic actuators controlled by a load maintainer (Figure B17). The total axial load for each of those specimens was defined by the sum of the axial load applied using the hydraulic actuators and the self weight of the concrete loading beam. Details of the axial load applied to each of the shear wall specimens are presented in Table B3.

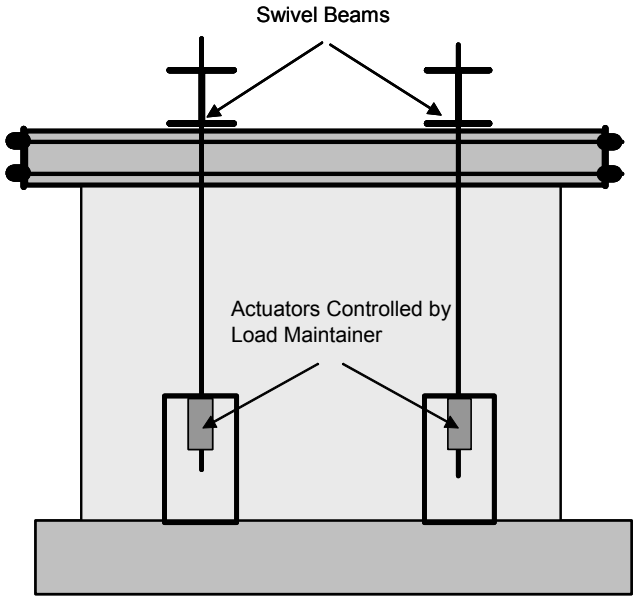

Figure B17: Axial load setup for flexure-dominated specimens

B.3.3 Base Beam

The specimens were built on a precast, post-tensioned concrete base beam representing a concrete foundation (Figure B18). Each specimen was constructed on a leveling bed of conventional portland cement-lime masonry mortar conforming to ASTM C270, Type S by proportion. To prevent the foundation from sliding or uplifting, the base beam was tied to the reaction floor using post-tensioned rods (Figure B18).

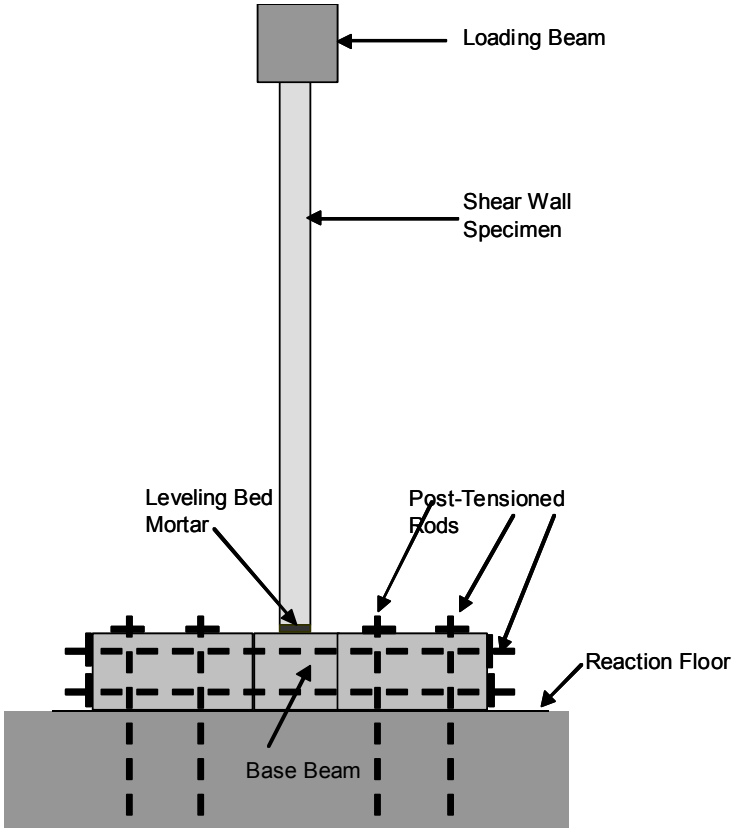

Figure B18: Precast concrete base beam used as foundation

Because the concrete base beams were used for construction of more than one AAC shear wall specimen, #5 grade 60 dowel bar splicers (Figure B19) were cast into that concrete base beam to provide a mechanical anchorage for the #5 grade 60 internal vertical reinforcement. The vertical reinforcement is upset-threaded at one end as shown in Figure B19.

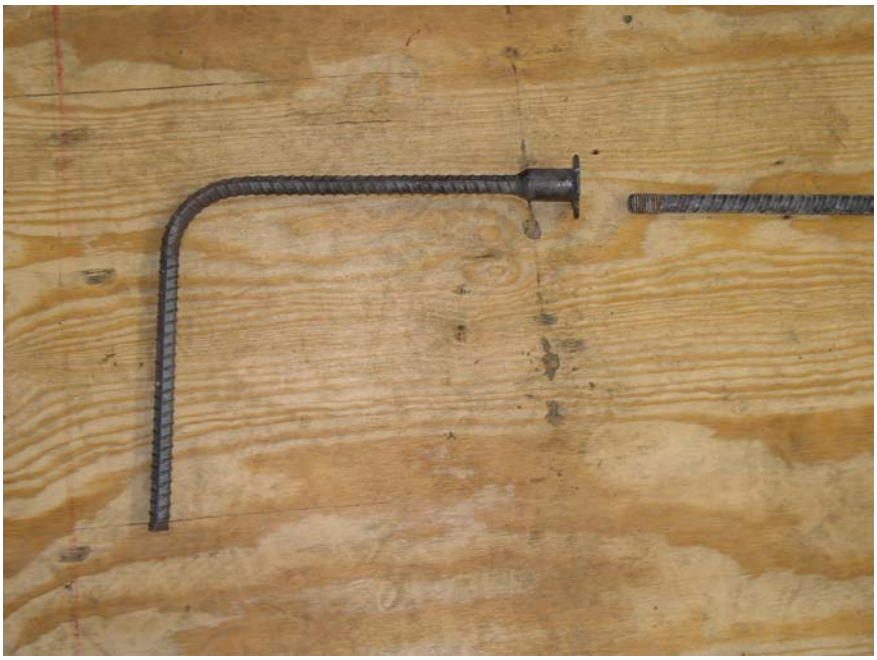

Figure B19: Dowel bar splicer and reinforcement enlarged and threaded at end

B.3.4 Lateral Bracing System

The specimens were braced against out-of-plane displacements by cables (Figure B20), one end was attached to vertically oriented steel plates attached to the loading beam at two points on both sides of the wall, and the other end to horizontally oriented rods bolted through holes in the flanges of W-shape columns positioned alongside the specimen, and bolted to the reaction floor.

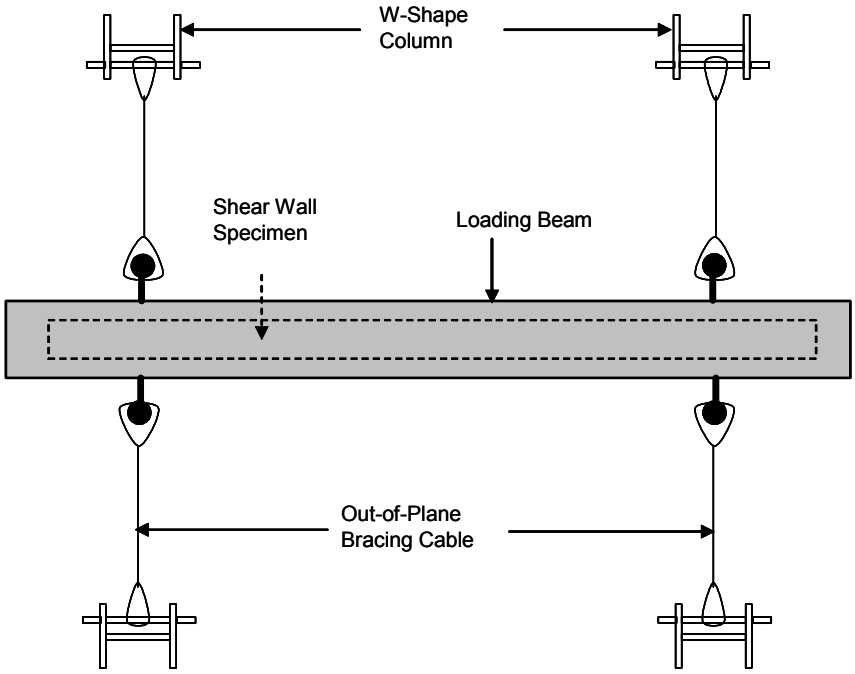

Figure B20: Lateral bracing system (plan view)

An elevation view of the test setup used for the shear-dominated specimens is presented in Figure B21. An elevation view of the test setup used for the flexure-dominated specimens is presented in Figure B22, and a cross-section view of that setup is presented in Figure B23. A detail of the connection between the actuators and the loading beam is presented in Figure B24.

Figure B21: Elevation view of test setup used for the shear-dominated specimens

Figure B22: Elevation view of test setup used for the flexure-dominated specimens

Figure B23: Cross-section view of test setup used for the flexure-dominated specimens

Figure B24: Detail of connection between actuators and loading beam

B.4 INSTRUMENTATION AND DATA ACQUISITION

B.4.1 Overall Behavior

The instrumentation used to measure overall hysteretic behavior is shown in Figure B25, and included the following:

- load cells to measure the applied horizontal force;
- pressure transducers to measure the pressure in the jacks that applied the horizontal force. This pressure value was converted to an applied force and was used as a check on the load cells;
- linear potentiometers to measure the horizontal displacement at the top of the wall; and
- linear potentiometers to measure the full-height vertical displacement at the ends of the wall.

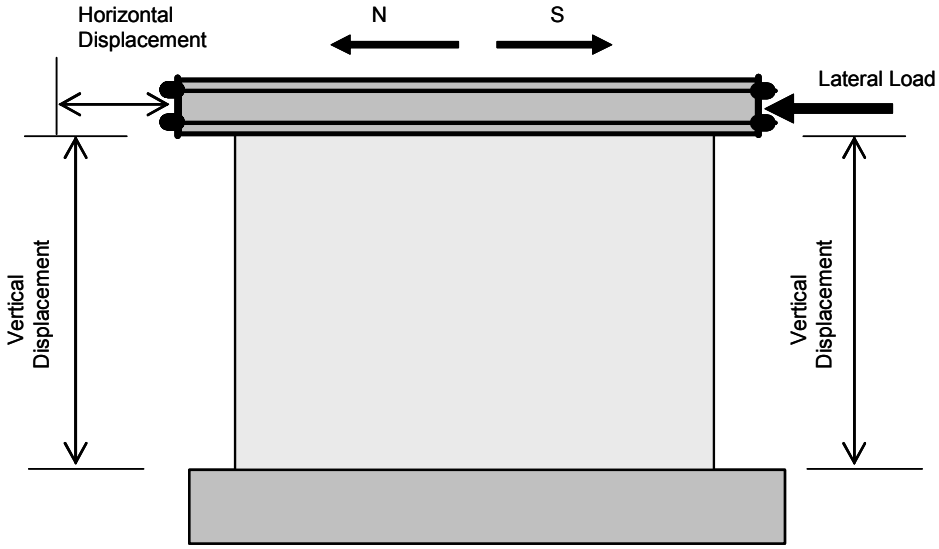

Figure B25: Instrumentation for measuring overall behavior (linear potentiometers)

B.4.2 Local Behavior

The instrumentation used to measure local behavior is shown in Figure B26 and Figure B27, and included the following:

- linear potentiometers to measure:
  - deformation along the diagonals of the specimen;
  - incremental vertical deformations at the ends of the specimen;
  - slip between the specimen and its base;
  - slip between the base and the floor;
  - slip between the loading beam and the top of the wall;
- a dial gage to measure the pressure in the hydraulic actuators controlled by the load maintainer;
- force washers to measure force in exterior reinforcement; and

- strain gages to measure the lateral force that caused yielding of the internal flexural reinforcement. The strain gages were mounted only on the flexural reinforcement of the flexure-dominated specimens.

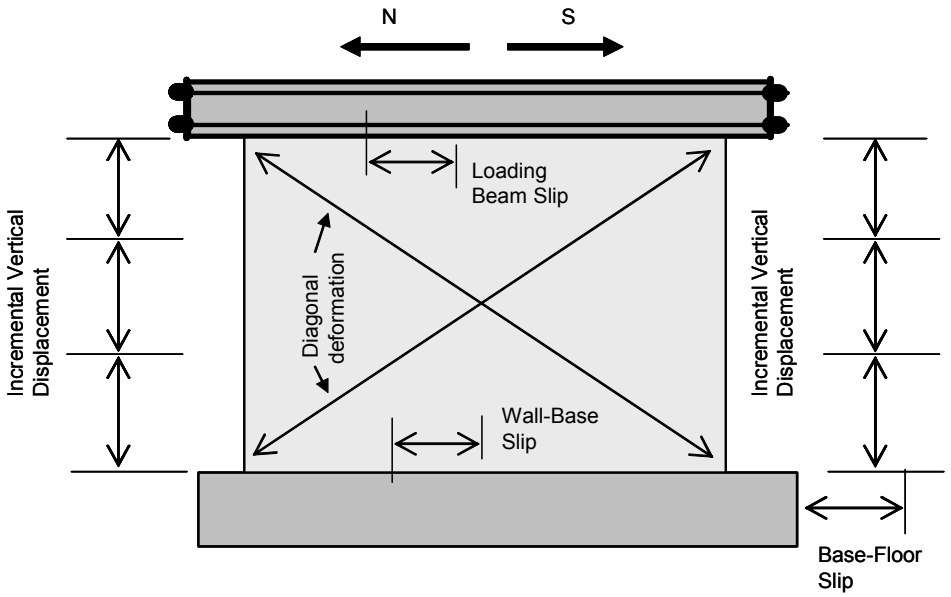

Figure B26: Instrumentation to measure local behavior

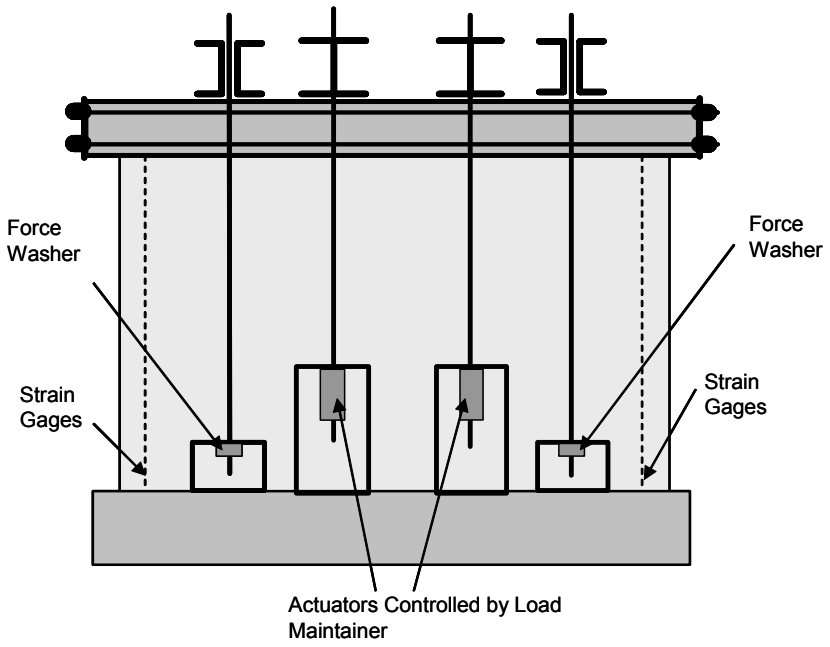

Figure B27: Instrumentation to measure local behavior (forces)

B.4.3 Data Acquisition

Data were acquired through a Hewlett-Packard 3852 scanner. Analog-to-digital conversion was carried out by a National Instruments card in a Windows-based microcomputer, running under Measure, a National Instruments add-on for the Microsoft Excel® spreadsheet program. Once in Excel format, data were plotted conventionally.

B.5 LOADING HISTORY

The planned in-plane loading history for the shear wall specimens, shown in Figure B28, consisted of a series of reversed cycles to monotonically increasing maximum load or displacement amplitudes. At the beginning of the test, target load values were used; after web-shear cracking or yielding of the flexural reinforcement target displacement values were used. The predetermined target

values (PV) were based on the loads that were calculated to produce significant changes in the behavior of the specimen (for example, flexural cracking or web-shear cracking). The planned loading history for shear-dominated specimens involved three increments between each target force. Since the predetermined target values for the flexure dominated specimens were smaller than the corresponding values for the shear-dominated specimens were two increments between each target force level were used. After web-shear cracking or yielding of the flexural reinforcement the test was controlled by displacements; a minimum of one cycle at each displacement level was applied.

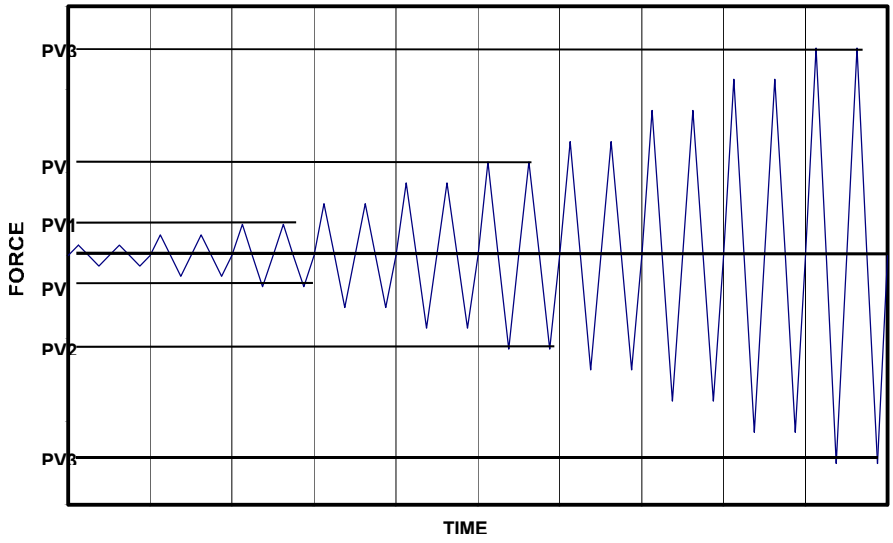

Figure B28: Planned loading history for shear wall specimens

APPENDIX C:
ADDITIONAL DETAILS OF ASSEMBLAGE SPECIMEN

This Appendix includes additional details and dimensions for the Two-story Assemblage Specimen. The goal is to provide the reader with additional details beyond those provided in Chapter 4.

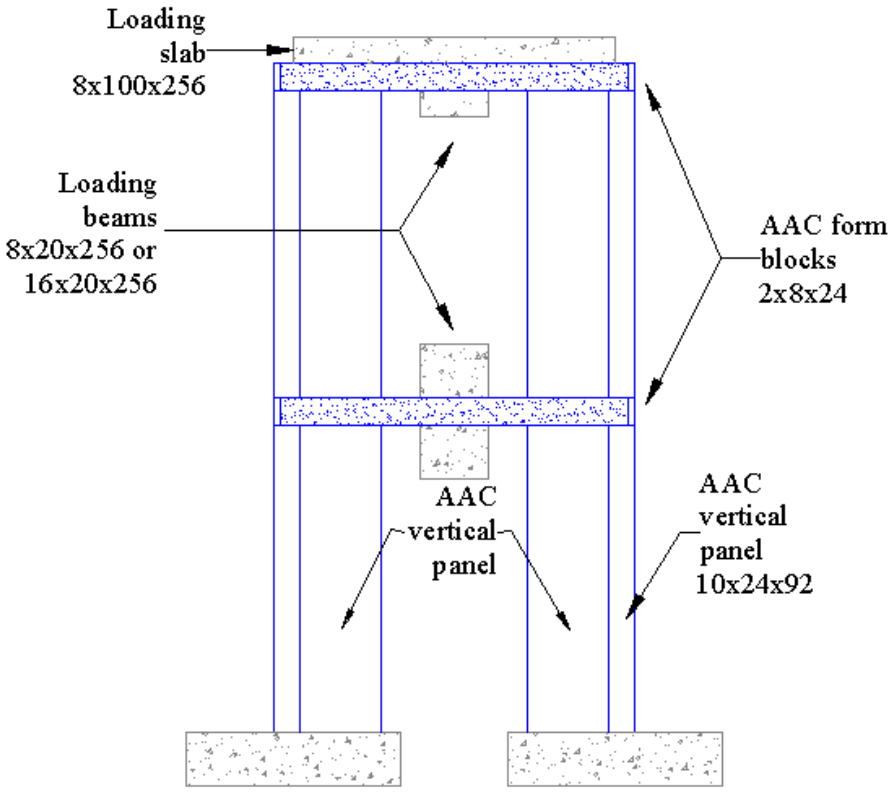

Figure C1: Elevation of exterior north- south face (dimensions in inches)

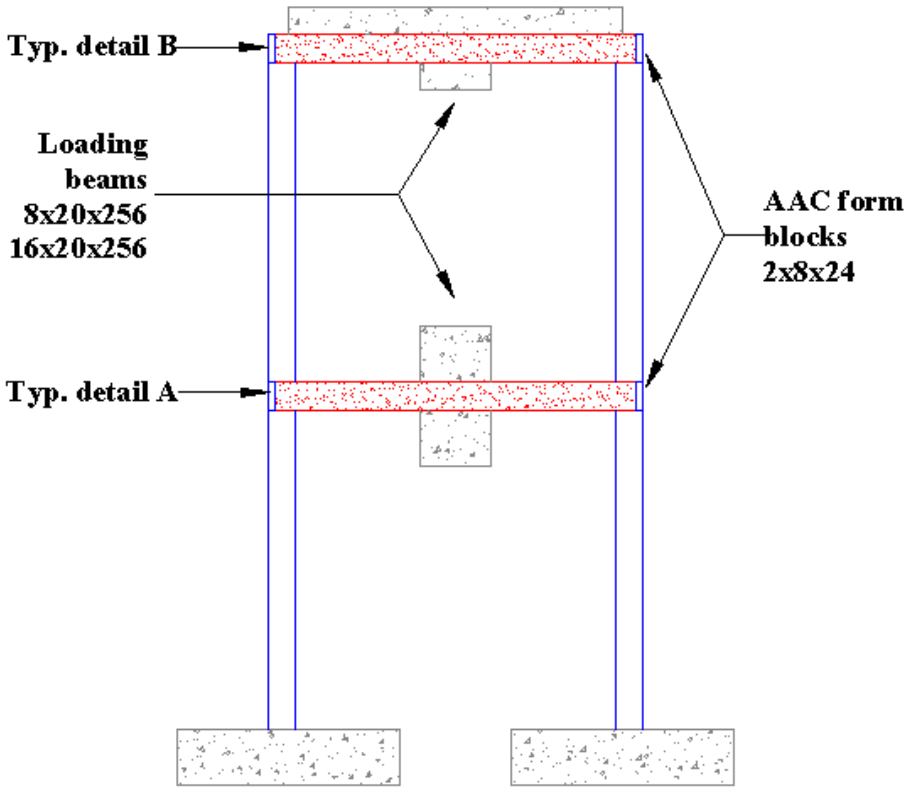

Figure C2:Elevation transverse centerline (dimensions in inches)

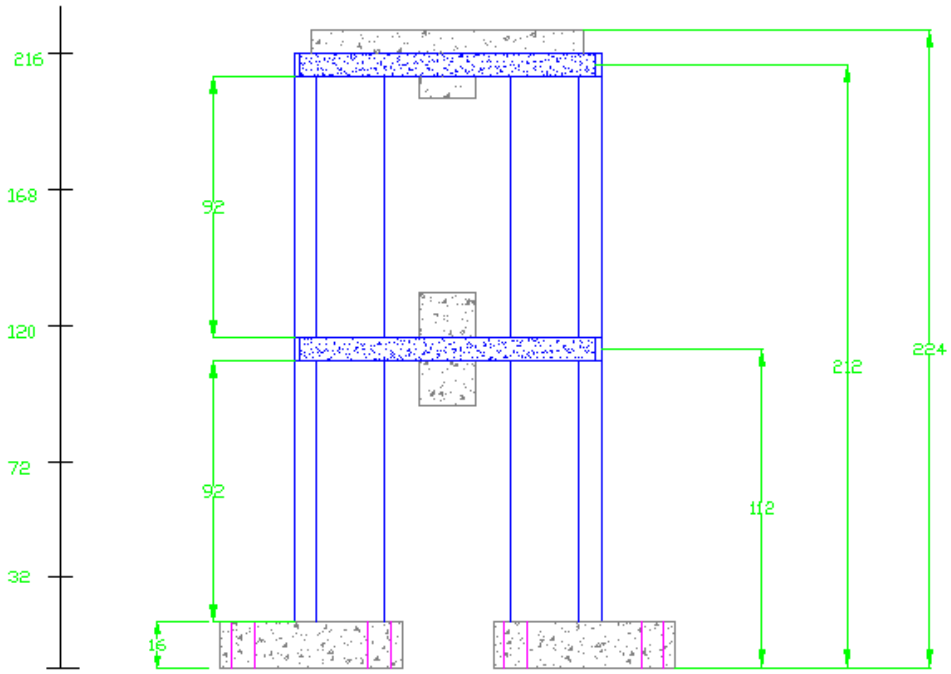

Figure C3: Elevation of south face (dimensions in inches)

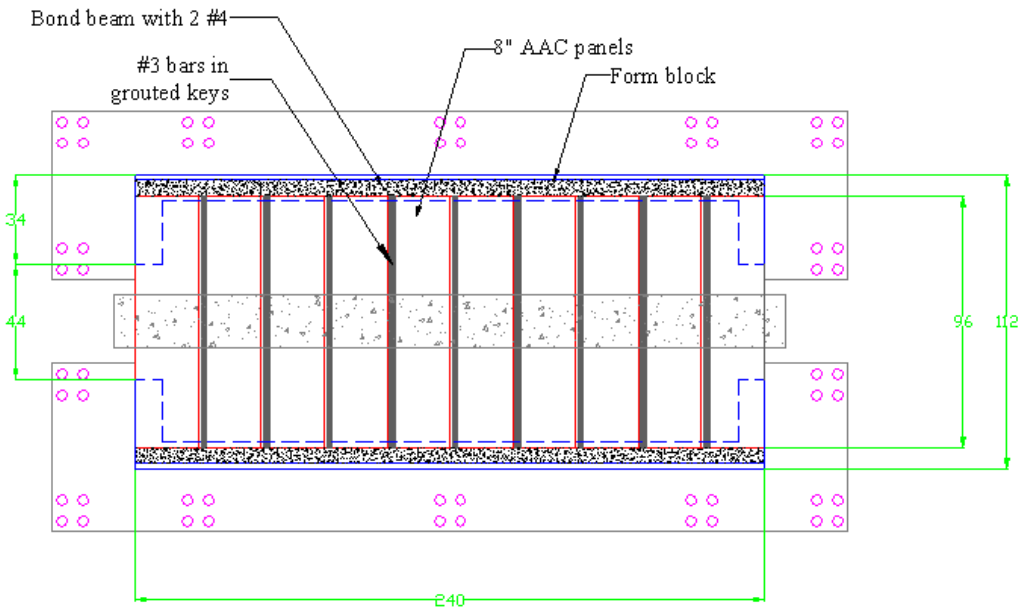

Figure C4: Plan view of second story walls (dimensions in inches)

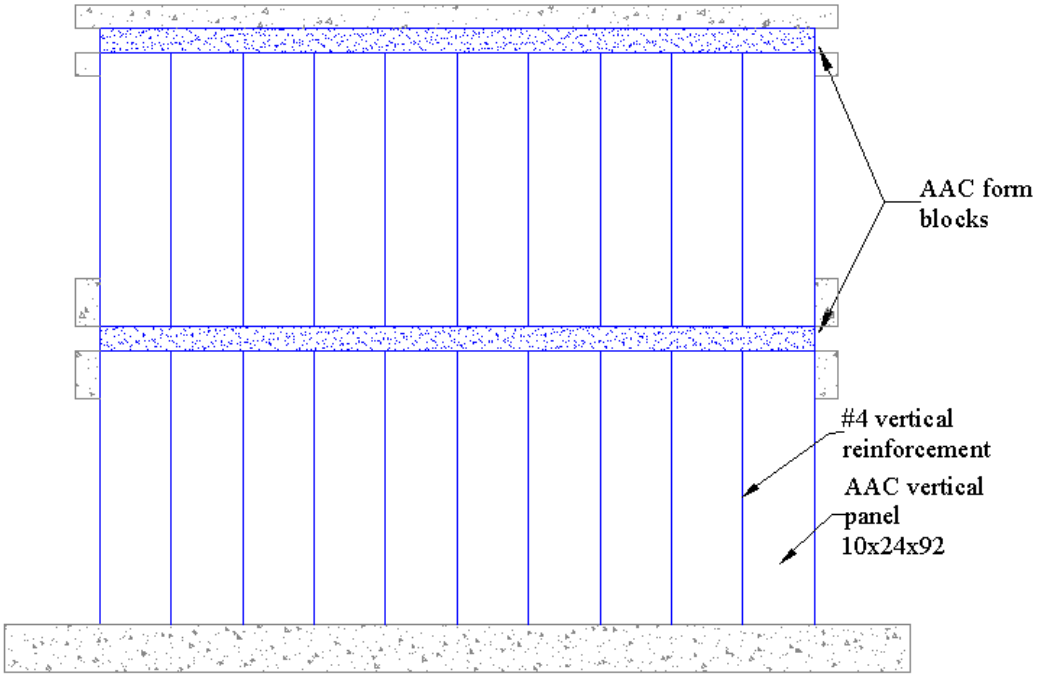

Figure C5: Elevation of east-west face (dimensions in inches)

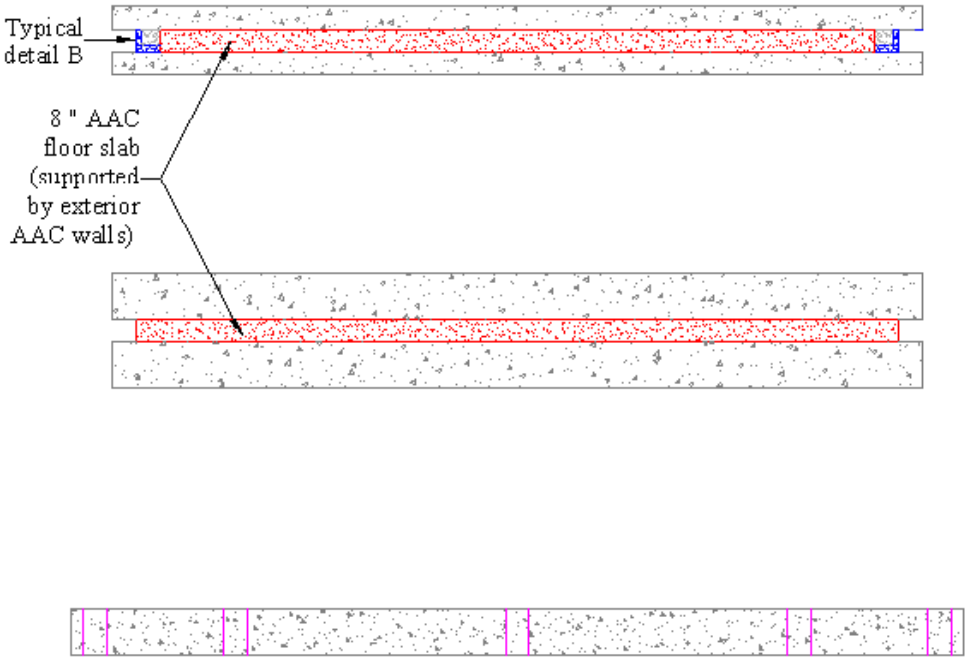

Figure C1: Elevation of longitudinal centerline

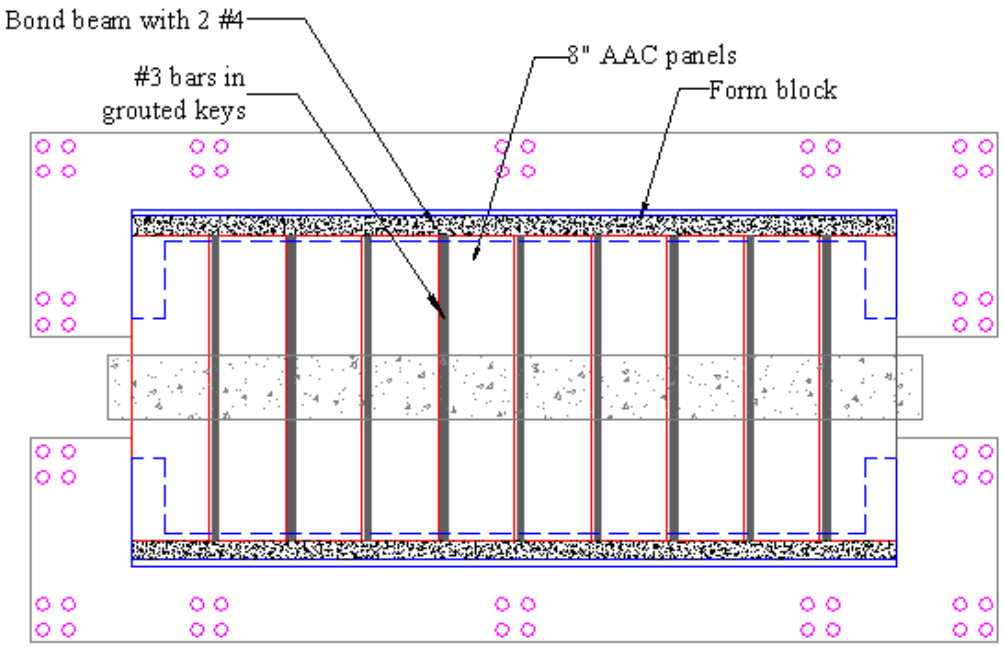

Figure C6: Plan view of first story floor panels

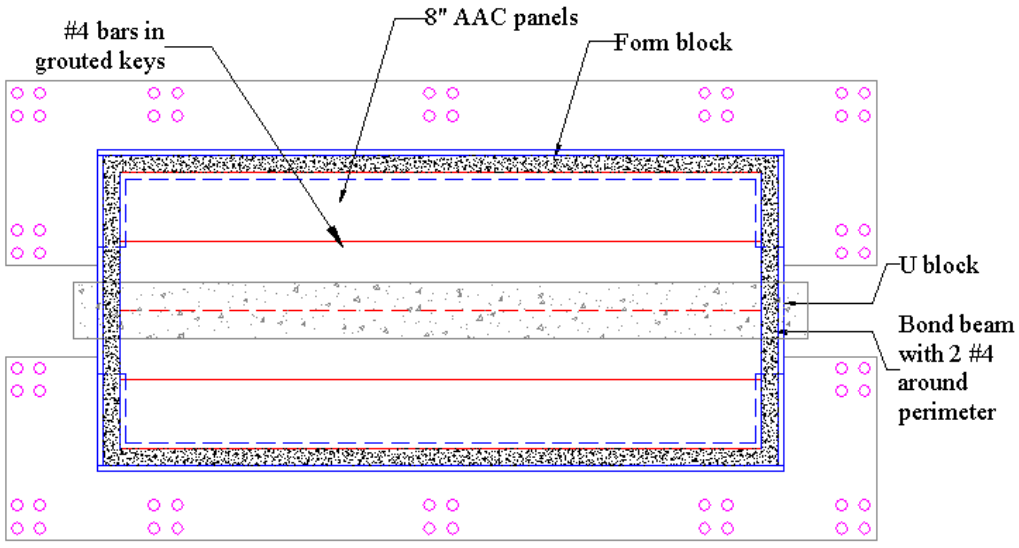

Figure C7: Plan view of second story floor panels

APPENDIX D:
PROPOSED DESIGN PROVISIONS FOR MSJC CODE

The design provisions proposed here are intended to be used in conjunction with the MSJC design provisions. The provisions of the current MSJC document are intended as the default, and are augmented, modified or replaced by the provisions of this Appendix. In Chapter 8 the entire section is included because these design provisions are proposed to be incorporated as an additional chapter.

The proposed Commentary provisions that follow the code provisions are intended to supplement the MSJC Commentary. Where no new Commentary provisions are indicated, the current MSJC Commentary applies.

Chapter 1

CODE:

Modify the notations of Code Section 1.5 of ACI 530-02/ASCE 5-02/TMS 402-02

f'_{AAC} = specified compressive strength of AAC, the minimum compressive strength for a class of AAC as specified in ASTM C1386, psi (MPa)

$f_{t\,AAC}$ = splitting tensile strength of AAC as determined by ASTM C1386, psi (MPa)

V_{AAC} = nominal shear strength provided by AAC masonry, lb (N)

w_{strut} = horizontal projection of the width of the diagonal strut, in. (mm)

E_{AAC} = modulus of elasticity of AAC, psi (MPa)

μ = coefficient of friction of AAC

Autoclaved aerated concrete -- low-density cementitious product of calcium silicate hydrates, whose material specifications are defined in ASTM C1386.

Add the following to Code Section 1.8 of ACI 530-02/ASCE 5-02/TMS 402-02 (including previously approved changes). Renumber existing Code Section 1.8.2.3 appropriately.

1.8.2.3 *AAC Masonry* -- Modulus of elasticity of AAC masonry shall be

$$E_{AAC} = 6500\, f'^{0.6}_{AAC}$$

f'_{AAC} and E_{AAC} in psi

Change existing grout section from 1.8.2.3 to 1.8.2.4.

Modify the numbering of Code Section 1.8.5.2 of ACI 530-02/ASCE 5-02/TMS 402-02 (including previously approved changes).

1.8.5 *Shrinkage Coefficients*

1.8.5.1 Concrete masonry:

$k_m = 0.5\ s_l$

where s_l is not more than 6.5 x 10-4 in./in. (6.5 x 10-4 mm/mm)

1.8.5.2 Masonry made of non-moisture-controlled concrete masonry units:

$k_m = 0.5\ s_l$

1.8.5.3 *Shrinkage Coefficient of AAC Masonry*

k_m shall be determined using the tangent, at a moisture content of 6%, to the curve of deformation versus moisture content determined in accordance with ASTM C 1386.

1.13 -- Seismic design requirements

1.13.1 --*Scope*

1.13.2 --*General*

1.13.2.2 -- *Lateral force-resisting system* – Buildings relying on masonry shear walls as part of the lateral force-resisting system shall have shear walls that comply with the requirements of Section 1.13.2.2.1, 13.2.2.2.2, 1.13.2.2.4, or 1.13.2.2.5.

Exception: Buildings assigned to Seismic Design Category A shall be permitted to have shear walls complying with Section 5.3.

Exception: AAC masonry shear walls shall be permitted to comply with Sections 1.13.2.2.6, 1.13.2.2.7 or 1.13.2.2.8.

1.13.2.2.6 *Ordinary plain (unreinforced) AAC masonry shear walls* – Design of ordinary plain (unreinforced) AAC masonry shear walls shall comply with the requirements of Section 8.3.

1.13.2.2.7 *Detailed plain AAC masonry shear walls* – Design of detailed plain (unreinforced) AAC masonry shear walls shall comply with the requirements of Section 8.3 and the requirements of Section 1.13.2.2.7.1

1.13.2.2.7.1 *Minimum reinforcement requirements for members of the lateral force-resisting system in AAC masonry* – Vertical reinforcement of at least 0.2 $in.^2$ shall be provided within 24 in. of each side of openings, within 8 in. of movement joints, and within 24 in. of the ends of walls. Reinforcement adjacent to openings need not be provided for openings smaller than 16 in. unless the minimum reinforcement requirements are interrupted by such openings.

1.13.2.2.8 *Ordinary reinforced AAC masonry shear walls* – Design of ordinary reinforced AAC masonry shear walls shall comply with the requirements of Section 8.2 and the requirements of Section 1.13.2.2.7.1

1.13.3 *Seismic Design Category A*

Structures in Seismic Design Category A shall comply with the requirements of Chapter 2, 3, 4 or 5. AAC masonry structures in Seismic Design Categories A shall comply with the requirements of Chapter 8.

1.13.3.3 *Anchorage of masonry walls* – Masonry walls shall be anchored to the roof and all floors that provide … Exception: AAC masonry walls shall comply with the requirements of Section 1.13.3.4.

1.13.3.4 *Anchorage of AAC masonry diaphragms* -- The lateral load resistance of AAC diaphragm*s* shall be determined according to Section 8.2.7.2.1.1, Section 8.2.7.2.1.2 or Section 8.2.7.2.2.1.

1.13.4 *Seismic Design Category B*

1.13.4.1 Structures in Seismic Design Category B shall comply with the requirements of Seismic Design Category A and to the additional requirements of Section 1.13.4. AAC masonry structures shall comply with the requirements of 1.13.4.3.

1.13.4.2 *Design of elements that are part of lateral force-resisting system* -- The lateral force-resisting system shall be designed to comply with the requirements of Chapter 2, 3, or 4. Masonry shear walls shall comply with the requirements of ordinary plain (unreinforced) masonry shear walls, detailed plain (unreinforced) masonry shear walls, ordinary reinforced masonry shear walls, intermediate reinforced masonry shear walls, or special reinforced masonry shear walls.

1.13.4.3 *Anchorage of floor and roof diaphragms in AAC masonry structures* — Floor and roof diaphragms in AAC masonry structures shall be surrounded by a continuous grouted bond beam reinforced with at least two longitudinal reinforcing bars, having a total cross-sectional area of at least 0.4 in.^{2} If floor diaphragms are made of AAC panels, those panels shall be connected to each other by grouted keys, each having at least 0.11 in.^{2} of reinforcement, anchored in the bond beam by a standard 90-degree hook, placed around the

longitudinal reinforcement in the bond beam and oriented in a vertical plane. Continuous longitudinal ties shall be provided over interior wall supports. The shear capacity of the diaphragm shall be determined according to Section 8.2.7.2.1.1, Section 8.2.7.2.1.2 or Section 8.2.7.2.2.1.

1.13.5 *Seismic Design Category C*

1.13.5.1 Structures in Seismic Design Category C shall comply with the requirements of Seismic Design Category B and to the additional requirements of Section 1.13.5

1.13.5.2.3 *Reinforcement requirements* -- Masonry elements listed in Section 1.13.5.2.2, except AAC masonry elements, shall be reinforced in either the horizontal or vertical direction in accordance with the following: . . .

1.13.5.3 *Design of elements that are part of the lateral force-resisting system* – Design of masonry columns and shear walls shall comply with the requirements of 1.13.5.3.1 and 1.13.5.3.2. Design of ordinary reinforced AAC masonry structures shall comply with the requirements of 1.13.5.3.3 and 1.13.5.3.4.

1.13.5.3.3 *Anchorage of floor and roof diaphragms in AAC masonry structures* — Lateral load between floor and roof diaphragms and AAC masonry

shear walls shall be transferred through connectors embedded in grout in accordance with Section 2.1.8. Connectors shall be designed to transfer horizontal design forces acting either parallel or perpendicular to the wall but not less than 200 lb per lineal ft of wall. The maximum spacing between connectors shall be 4 ft.

1.13.5.3.4 *Anchorage of floor and roof diaphragms in AAC masonry structures* — Floor and roof diaphragms in AAC masonry structures shall be surrounded by a continuous grouted bond beam reinforced with at least two longitudinal reinforcing bars, having a total cross-sectional area of at least 0.4 $in.^2$ If floor diaphragms are made of AAC panels, those panels shall be connected to each other by grouted keys, each having at least 0.11 $in.^2$ of reinforcement, anchored in the bond beam by a standard 90-degree hook, placed around the longitudinal reinforcement in the bond beam and oriented in a vertical plane. Continuous longitudinal ties shall be provided over interior wall supports. The shear capacity of the diaphragm shall be determined by Section 8.2.7.2.1.2 or Section 8.2.7.2.2.1.

1.13.6 *Seismic Design Category D*

1.13.6.1 Structures in Seismic Design Category D shall comply with the requirements of Seismic Design Category C and with the additional requirements of Section 1.13.6.

Exception: AAC masonry elements shall comply with the requirements of 1.13.5.

1.13.6.2 *Design requirements* -- Masonry elements, other than those covered by Section 1.13.5.2.2, shall be designed in accordance with the requirements of Sections 2.1 and 2.3, Chapter 2, Chapter 3, Chapter 4 or Chapter 8.

1.13.6.3 *Minimum reinforcement requirements for masonry walls* -- Masonry walls other than those covered by Section 1.13.5.2.3, and other than AAC masonry, shall be reinforced in both the horizontal and vertical direction. . . .

1.13.7 *Seismic Design Categories E and F*

1.13.6.7 Structures in Seismic Design Categories E and F shall comply with the requirements of Seismic Design Category D and with the additional requirements of Section 1.13.7.

Exception: AAC masonry elements shall comply with the requirements of 1.13.5.

1.13.7.2 *Minimum reinforcement for stack bond elements that are not part of lateral force-resisting system* -- Stack bond masonry that is part of the lateral force resisting system, except for AAC…

1.13.7.3 *Minimum reinforcement requirements for stack bond elements that are not part of the lateral force resisting system* -- Stack bond masonry that is not part of the lateral force resisting system, except for AAC that is not part of

1.15 - Construction

1.15.1 *Grouting* — AAC field-reinforced masonry shall be prepared prior to grouting. All cavities and keys receiving grout shall be clean and free of debris. Cavities and keys shall be pre-wetted prior to placing grout, or grout shall contain shrinkage retarding admixture. All grouting operations shall be vibrated throughout the depth of the grouted cell or cavity. Grout lifts up to 8 ft. shall be permitted in cores 3 in. in diameter or greater. The minimum clear cover between a longitudinal reinforcing bar and the cell edge shall not exceed 1 in. or the diameter of the bar.

1.15.2 *Thin-bed mortar* — All panels shall be inspected to imperfections that prohibit the panel joint from sitting father than 1/16 in. from an adjacent panel. All panel surfaces should be cleaned and pre-wetted prior to applying the thin-bed mortar.

COMMENTARY:

1.8.2 -- Elastic Moduli

Modulus of elasticity for clay and concrete masonry has traditionally . . .

For clay and concrete masonry, the elastic modulus is determined . . .

By using . . .

The modulus of elasticity of AAC masonry depends almost entirely on the modulus of elasticity of the AAC material itself, which is determined and reported in accordance with ASTM C ZZZZ. The relationship between modulus of elasticity and compressive strength is given in Tanner (2003) and Argudo (2003).

1.13.1 *Scope*

. . .

Seismic requirements for masonry veneers are found in Chapter 6, Veneers.

1.13.2.2.7.1 *Minimum reinforcement requirements for members of the lateral force-resisting system* – Prescriptive seismic requirements for AAC masonry shear walls are less severe than for conventional masonry shear walls, and are counterbalanced by more restrictive requirements for bond beams and floor diaphragms. AAC masonry walls and assemblage specimen with prescriptive reinforcement meeting the requirements of this section have performed satisfactorily under reversed cyclic loads representing seismic excitation (Tanner 2003, Varela 2003).

1.13.3.4 *Anchorage of AAC diaphragms* — Lateral load transfer between an AAC diaphragm and AAC shear walls was satisfactorily transferred through adhesion in a two-story AAC assemblage specimen (Tanner 2003, Varela 2003). See Commentary for Section 8.2.7.2.1 and Section 8.2.7.2.2 for additional information.

1.13.4.3 *AAC masonry diaphragms* — See Commentary for Sections 8.2.7.2.1 and 8.2.7.2.

1.13.5.3.3 and 1.13.5.3.4 *Connections* — In Seismic Design Categories C and D additional connectors are required, with the intention of ensuring ductile failure.

1.15 – Construction — These construction requirements are based on the construction practices used in the shear wall specimens tested at UT Austin. Since the technical justification for structural performance is also based on the performance of these shear wall specimens, these construction requirements are life-safety related.

Chapter 8 — STRENGTH DESIGN OF AAC MASONRY

CODE:

8.1 — General

8.1.1 *Scope* — This Chapter provides minimum requirements for design of AAC masonry. AAC masonry shall comply with the requirements of Chapter 1, Section 8.1, and either Section 8.2 or 8.3.

8.1.2 *Required strength* — Required strength shall be determined in accordance with the strength design load combinations of the legally adopted building code. When the legally adopted building code does not provide load combinations, structures and members shall be designed to resist the combination of loads specified in ASCE 7-98. Members subject to compressive axial load shall be designed for the maximum design moment accompanying the axial load. The factored moment, M_u, shall include the moment induced by relative lateral displacement.

8.1.3 *Design strength* — AAC masonry members shall be proportioned such that the design strength equals or exceeds the required strength. Design strength is the nominal strength multiplied by the strength reduction factor, ϕ, as specified in Section 8.1.4.

The design shear strength, ϕV_n, shall exceed the shear corresponding to the development of 1.25 times the nominal flexural strength (M_n) of the member, except that the nominal shear strength (V_n) need not exceed 2.5 times required shear strength (V_u).

8.1.3.1 *Seismic design provisions* — At each story level, at least 80 percent of the lateral stiffness shall be provided by lateral-force-resisting walls. Along each column line at a particular story level, at least 80 percent of the lateral stiffness shall be provided by lateral-force-resisting walls.

Exception: Where seismic loads are determined based on a seismic response modification factor, *R*, not greater than 1.5, piers and columns are permitted to be used to provide seismic load resistance.

8.1.4 *Strength of Joints* — AAC masonry members shall be made of AAC masonry units. Head joints shall be permitted to be left unfilled between AAC masonry units laid in running bond, provided that shear capacity is calculated using the formulas of this Code corresponding to that condition.

8.1.4.7 *Adhesion* — The value of ϕ shall be taken as 0.67 for AAC masonry diaphragm joints relying on adhesion of thin-bed mortar or grout to resist shear.

8.1.4.8 *Truss mechanism in AAC floor and roof diaphragms* — The value of ϕ shall be taken as 0.75 for AAC floor and roof diaphragms joints relying on a truss mechanism to transfer in-plane lateral load.

8.1.6.3 *Deflection of field reinforced AAC masonry* — Deflection calculations for field reinforced AAC masonry members shall be based on cracked section properties including the reinforcement and grout. The flexural and shear stiffness properties assumed for deflection calculations shall not exceed one half of the gross section properties unless a cracked-section analysis is performed.

8.1.7 *Anchor bolts* — Headed and bent-bar anchor bolts shall be embedded in grout, and shall be designed in accordance with 3.1.6. Anchors embedded in AAC shall be designed using nominal capacities provided by the anchor manufacturer and verified by an independent testing agency.

8.1.8 *Material properties*

8.1.8.2 *Masonry splitting tensile strength* – The splitting tensile strength f_{tAAC} shall be determined by Equation 8-xx.

$$f_{tAAC} = 2.4\sqrt{f'_{AAC}} \qquad \text{(8-xx)}$$

8.1.8.3 *Masonry modulus of rupture* -- The modulus of rupture, f_{rAAC}, for AAC masonry elements shall be taken as two times the masonry splitting tensile strength, f_{tAAC}. If a section of AAC contains a horizontal leveling bed, the value of f_{rAAC} shall not exceed 50 psi (345 kPa) at that section. If a section of AAC contains a bed joint between thin-bed mortar and AAC the value of f_{rAAC} shall not exceed 80 psi (552 kPa) at that section.

8.1.8.4 *Masonry direct shear strength* – The direct shear strength f_v shall be determined by Equation 8-xx.

$$f_{vt} = 0.15 f'_{AAC} \qquad \text{(8-xx)},$$

f'_{AAC} and f_v in psi

8.1.8.5 *Shear strength of joints in AAC masonry* – The shear strength of a joint between AAC and grout shall be 36 psi (0.25 MPa). The shear strength of a joint between AAC and thin-bed mortar shall be 18 psi (0.13 MPa).

8.1.8.6 *Coefficient of friction* – The coefficient of friction between AAC and AAC shall be 0.75. The coefficient of friction between AAC and leveling-bed mortar shall be 1.0.

8.1.8.7 *Reinforcement strength* — Masonry design shall be based on a reinforcement strength equal to the specified yield strength of reinforcement, f_y, which shall not exceed 60,000 psi (413.7 MPa). The actual yield strength shall not exceed 1.3 times the specified yield strength. The compressive resistance of steel reinforcement shall be neglected unless lateral reinforcement is provided in compliance with the requirements of Section 2.1.4.5.

8.1.10 *Concentrated Loads*

8.1.10.3 Design bearing strength on AAC masonry shall not exceed ($\phi f'_{AAC} A_1$), where A_1 is the loaded area.

8.1.10.4 *Bearing for simply supported precast floor and roof members on AAC shear walls* — The following minimum requirements shall apply so that after the consideration of tolerances, the distance from the edge of the supporting wall to the end of the precast member in the direction of the span is not less than:

For AAC floor panels

2 in. (51 mm)

For solid or hollow-core slabs

2 in. (51 mm)

For beams or stemmed members 3 in. (76 mm)

8.2 — Field-reinforced AAC masonry

8.2.1 *Scope* — The requirements of this section are in addition to the requirements of Chapter 1 and Section 8.1 and govern masonry design in which reinforcement is used to resist tensile forces.

8.2.2 *Design assumptions* — The following assumptions apply to the design of reinforced masonry:

(a) There is strain continuity between the reinforcement, grout, and masonry such that all applicable loads are resisted in a composite manner.

(b) The nominal strength of singly reinforced masonry cross-sections for combined flexure and axial load shall be based on applicable conditions of equilibrium.

(c) The maximum usable strain, ε_{mu}, at the extreme masonry compression fiber shall be assumed to be 0.003.

(d) Strain in reinforcement and masonry shall be assumed to be directly proportional to the distance from the neutral axis.

(e) Reinforcement stress below specified yield strength, f_y, shall be taken as E_s times steel strain. For strains greater than that corresponding to f_y, stress in reinforcement shall be taken equal to f_y.

(f) The tensile strength of masonry shall be neglected in calculating flexural strength but shall be considered in calculating deflection.

(g) The relationship between masonry compressive stress and masonry strain shall be assumed to be defined by the following:

Masonry stress of 0.85 f'_m shall be assumed uniformly distributed over an equivalent compression zone bounded by edges of the cross section and a straight line located parallel to the neutral axis at a distance a = 0.67 c from the fiber of maximum compressive strain. The distance c from the fiber of maximum strain to the neutral axis shall be measured perpendicular to that axis.

8.2.3 *Reinforcement requirements and details*

8.2.3.1 *Reinforcing bar size limitations* — Reinforcing bars used in AAC masonry shall not be larger than No. 9 (M#29). The nominal bar diameter shall not exceed one-eighth of the nominal member thickness and shall not exceed one-quarter of the least clear dimension of the cell, course, or collar joint in which it is placed. The cross-sectional area of reinforcement placed in a cell or in a course of hollow unit construction shall not exceed 3 percent of the grouted area in a plane perpendicular to the reinforcement.

8.2.3.1.1 It shall be permitted to use ratios of vertical reinforcement up to 4.5% if the tensile force in the reinforcement is below the yield strength of the material and an analysis is performed to determine if the factored splitting tensile stress is less than the available factored tensile strength. The factored splitting tensile stress shall be determined by sec

8.2.3.1.2 *Required splitting tensile stress* — The factored splitting tensile stress shall be computed by Eq. (8-xx)

8.2.3.1.3 *Factored splitting tensile strength* — The factored splitting tensile strength of grout shall be computed by Eq. (8-xx)

8.2.3.2 *Standard hooks* — The equivalent embedment length to develop standard hooks in tension, l_e, shall be determined by Eq. (8-12):

$$l_e = 13 d_b \qquad (8\text{-}12)$$

8.2.3.3 *Development* — The required tension or compression reinforcement shall be developed in accordance with the following provisions:

The required development length of reinforcement shall be determined by Eq. (3-13), but shall not be less than 12 in. (305 mm).

$$l_d = \frac{l_{de}}{\phi} \qquad (3\text{-}13)$$

Where:

$$l_{de} = \frac{0.13\, d_b{}^2 f_y \gamma}{K \sqrt{f'_m}} \qquad (3\text{-}14)$$

K shall not exceed the lesser of the masonry cover, clear spacing between adjacent reinforcement, nor 5 times d_b.

γ = 1.0 for No. 3 (M#10) through No. 5 (M#16) bars;

γ = 1.4 for No. 6 (M#19) through No. 7 (M#22) bars; and

γ = 1.5 for No. 8 (M#25) through No. 9 (M#29) bars.

8.2.3.3.1 *Development of deformed shear reinforcement embedded in grout* — Shear reinforcement shall extend the depth of the member less cover distances.

8.2.3.3.1.1 Except at wall intersections, the end of a horizontal reinforcing bar needed to satisfy shear strength requirements of Section 8.2.4.1.2, shall be bent around the edge vertical reinforcing bar with a 180-degree hook. The ends of single leg or U-stirrups shall be anchored by one of the following means:

(a) A standard hook plus an effective embedment of $l_d/2$. The effective embedment of a stirrup leg shall be taken as the distance between the mid-depth of the member, d/2, and the start of the hook (point of tangency).

(b) For No. 5 (M #16) bars and smaller, bending around longitudinal reinforcement through at least 135 degrees plus an embedment of $l_d/3$. The $l_d/3$ embedment of a stirrup leg shall be taken as the distance between mid-depth of the member, d/2, and the start of the hook (point of tangency).

(c) Between the anchored ends, each bend in the continuous portion of a transverse U-stirrup shall enclose a longitudinal bar.

8.2.3.3.1.2 At wall intersections, horizontal reinforcing bars needed to satisfy shear strength requirements of Section 8.2.4.1.2 shall be bent around the edge vertical reinforcing bar with a 90-degree standard hook and shall extend horizontally into the intersecting wall a minimum distance at least equal to the development length.

8.2.3.4 *Splices* — Reinforcement splices shall comply with one of the following:

(a) The minimum length of lap for bars shall be 12 in. (305 mm) or the length determined by Eq. (8-15), whichever is greater.

$$l_d = \frac{l_{de}}{\phi} \qquad (8\text{-}15)$$

(b) A welded splice shall have the bars butted and welded to develop at least 125 percent of the yield strength, f_y, of the bar in tension or compression, as required.

(c) Mechanical splices shall have the bars connected to develop at least 125 percent of the yield strength, f_y, of the bar in tension or compression, as required.

(d) Splices shall not be permitted in zones of potential plastic hinge formation.

8.2.3.5 *Maximum reinforcement percentages*

8.2.3.5.1 For structures designed using an R value greater than 1.5, the ratio of reinforcement, ρ, shall not exceed the lesser ratio as calculated using the following two critical strain conditions:

(a) For walls subjected to in-plane forces, for columns, and for beams, the critical strain condition corresponds to a strain in the extreme tension reinforcement equal to 5 times the strain associated with the reinforcement yield stress, f_y.

(b) For walls subjected to out-of-plane forces, the critical strain condition corresponds to a strain in the extreme tension reinforcement equal to 1.3 times the strain associated with the reinforcement yield stress, f_y.

For both cases, the strain in the extreme compression fiber shall be assumed to be 0.003.

The calculation of the maximum reinforcement ratio shall include unfactored gravity axial loads. The stress in the tension reinforcement shall be assumed to be 1.25 f_y. Tension in the masonry shall be neglected. The strength of the compression zone shall be calculated as 85 percent of f'_{AAC} times 67 percent of the area of the compressive zone. Stress in reinforcement in the compression zone shall be based on a linear strain distribution.

8.2.3.5.2 For structures designed using an R value less than or equal to 1.5, the ratio of reinforcement, ρ, shall not exceed the ratio as calculated using the following critical strain condition:

The critical strain condition corresponds to a strain in the extreme tension reinforcement equal to 2 times the strain associated with the reinforcement yield stress, f_y. The strain in the extreme compression fiber shall be assumed to be 0.003.

The calculation of the maximum reinforcement ratio shall include gravity axial loads. The stress in the tension reinforcement shall be assumed to be 1.25 f_y.

Tension in the masonry shall be neglected. The strength of the compression zone shall be calculated as 85 percent of f'_{AAC} times 67 percent of the area of the compressive zone. Stress in reinforcement in the compression zone shall be based on a linear strain distribution.

8.2.3.6 *Bundling of reinforcing bars* — Reinforcing bars shall not be bundled.

8.2.4 *Design of beams, piers, and columns* — Member design forces shall be based on an analysis that considers the relative stiffness of structural members. The calculation of lateral stiffness shall include the contribution of all beams, piers, and columns. The effects of cracking on member stiffness shall be considered.

8.2.4.1 *Nominal strength*

8.2.4.1.1 *Nominal axial and flexural strength* — The nominal axial strength, P_n, and the nominal flexural strength, M_n, of a cross section shall be determined in accordance with the design assumptions of Section 8.2.2 and 8.2.4.1. For any value of nominal flexural strength, the corresponding nominal axial strength calculated in accordance with Sections 8.2.2 and 8.2.4.1 shall be modified for the effects of slenderness. The nominal flexural strength at any section along a member shall not be less than one fourth of the maximum nominal flexural strength at the critical section.

The nominal axial compressive strength shall not exceed Eq. (8-16) or Eq. (8-17), as appropriate.

(a) For members having an h/r ratio not greater than 99:

$$P_n = 0.80\left[0.85 f'_{AAC}\left(A_n - A_s\right) + f_y A_s\right]\left(1 - \left(\frac{h}{140r}\right)^2\right) \qquad (8\text{-}16)$$

(b) For members having an h/r ratio greater than 99:

$$P_n = 0.80\left[0.85 f'_{AAC}\left(A_n - A_s\right) + f_y A_s\right]\left(\frac{70r}{h}\right)^2 \quad \text{(8-17)}$$

8.2.4.1.2 *Nominal shear strength* — Nominal shear strength, V_n, shall be computed using Eq. (8-18) and either Eq. (8-19) or Eq. (8-20), as appropriate.

$$V_n = V_{AAC} + V_s \quad \text{(8-18)}$$

where V_n shall not exceed the following:

(a) Where $M/Vd_v < 0.25$:

$$V_n \le 6 A_n \sqrt{f'_{AAC}} \quad \text{(8-19)}$$

(b) Where $M/Vd_v > 1.00$

$$V_n \le 4 A_n \sqrt{f'_{AAC}} \quad \text{(8-20)}$$

(c) The maximum value of V_n for M/Vd_v between 0.25 and 1.0 may be interpolated.

The nominal masonry shear strength shall be taken as the least of the values computed using Section 8.2.4.1.2.1 through 8.2.4.1.2.3. Nominal shear strength provided by reinforcement, V_s, shall include only deformed reinforcement embedded in grout for AAC shear walls.

8.2.4.1.2.1 *Nominal masonry shear strength as governed by web-shear cracking* — Nominal masonry shear strength as governed by web-shear cracking, V_m , shall be computed using Eq. (8-21a) for AAC masonry with mortared head joints, and Eq. (8-21b) for AAC masonry with unmortared head joints:

$$V_{AAC} = 0.9\,\ell_w\,t\,\sqrt{f'_{AAC}}\,\sqrt{1+\frac{P_u}{2.4\sqrt{f'_{AAC}}\,\ell_w\,t}} \qquad \text{(8-21a)}$$

$$V_{AAC} = 0.6\,\ell_w\,t\,\sqrt{f'_{AAC}}\,\sqrt{1+\frac{P_u}{2.4\sqrt{f'_{AAC}}\,\ell_w\,t}}$$

(8-21b)

For AAC masonry in other than running bond, nominal masonry shear strength as governed by web-shear cracking, V_m , shall be computed using Eq. (8-21c):

$$V_{AAC} = 0.9\sqrt{f'_{AAC}}\,A_n + 0.05P_u \qquad \textit{(8-21c)}$$

In all equations (8-21), V_{AAC} shall be expressed in lb and f'_{AAC} shall be expressed in psi.

8.2.4.1.2.2 *Nominal shear strength as governed by crushing of diagonal compressive strut* — For walls with M/Vd_v <1.5, nominal shear strength, V_{AAC}, shall as governed by crushing of a diagonal strut, shall be computed as follows:

$$V_{AAC} = 0.17 f'_{AAC} t \frac{h \cdot l_w^{\,2}}{h^2 + (\frac{3}{4} l_w)^2}$$

(8-22a)

For walls with M/Vd_v equal to or exceeding 1.5, capacity as governed by crushing of the diagonal compressive strut need not be calculated.

8.2.4.1.2.3 *Nominal shear strength as governed by sliding shear* — At an unbonded interface, nominal shear strength as governed by sliding shear, V_{AAC}, shall be as follows:

$$V_{AAC} = \mu P_u \qquad (8\text{-}22b)$$

At an interface where thin-bed mortar is present, the nominal sliding shear capacity shall be calculated as the greater of the capacity calculated by Section 8.1.8.5, and that calculated by Eq. 8-22b. At an interface where leveling-bed mortar is present, the nominal sliding shear capacity shall be calculated by Eq. 8-22b.

8.2.4.1.3 *Special provisions for shear walls with AAC laid in other than running bond* — Nominal shear strength and flexural strength shall be determined

assuming that vertical cracks exist at each head joint. It shall be permitted to design with vertical cracks at every third joint, using Equation (8-21a), if the following construction techniques are met: each panel shall be cleaned and wet prior to applying the thin-bed mortar; mortar shall be applied to both faces of the vertical joint; and pressure shall be applied perpendicular to the vertical joint through clamps.

8.2.4.2 *Beams*

8.2.4.2.1 Members designed primarily to resist flexure shall comply with the requirements of Section 8.2.4.2. The factored axial compressive force on a beam shall not exceed $0.05\ A_n\ f'_m$.

8.2.4.2.2 Longitudinal reinforcement

8.2.4.2.2.1 The variation in longitudinal reinforcing bars shall not be greater than one bar size. Not more than two bar sizes shall be used in a beam.

8.2.4.2.2.2 The nominal flexural strength of a beam shall not be less than 1.3 times the nominal cracking moment strength of the beam, M_{cr}. The modulus of rupture, f_{rAAC}, for this calculation shall be determined in accordance with Section 8.1.7.2.

8.2.4.2.3 *Transverse reinforcement* — Transverse reinforcement shall be provided where V_u exceeds ϕV_{AAC}. The factored shear, V_u, shall include the effects of lateral load. When transverse reinforcement is required, the following provisions shall apply:

(a) Transverse reinforcement shall be a single bar with a 180-degree hook at each end.

(b) Transverse reinforcement shall be hooked around the longitudinal reinforcement.

(c) The minimum area of transverse reinforcement shall be $0.0007bd_v$.

The first transverse bar shall not be located more than one fourth of the beam depth, d_v, from the end of the beam.

The maximum spacing shall not exceed one half the depth of the beam nor 48 in. (1219 mm).

8.2.4.2.4 *Construction* — Beams shall be grouted solid.

8.2.4.2.5 *Dimensional limits* — Dimensions shall be in accordance with the following:

(a) The clear distance between locations of lateral bracing of the compression side of the beam shall not exceed 32 times the least width of the compression area.

(b) The nominal depth of a beam shall not be less than 8 in. (203 mm).

8.2.4.3 Piers

8.2.4.3.1 The factored axial compression force on the piers shall not exceed $0.3\ A_n\ f'_m$.

8.2.4.3.2 Longitudinal reinforcement — A pier subjected to in-plane stress reversals shall be reinforced symmetrically about the neutral axis of the pier. The longitudinal reinforcement of all piers shall comply with the following:

(a) One bar shall be provided in the end cells.

The minimum area of longitudinal reinforcement shall be 0.0007 bd.

Longitudinal reinforcement shall be uniformly distributed throughout the depth of the element.

8.2.4.3.3 Dimensional limits — Dimensions shall be in accordance with the following:

(a) The nominal thickness of a pier shall not be less than 6 in. (152 mm) and shall not exceed 16 in. (406 mm).

(b) The distance between lateral supports of a pier shall not exceed 25 times the nominal thickness of a pier except as provided for in Section 8.2.4.3.3(c).

(c) When the distance between lateral supports of a pier exceeds 25 times the nominal thickness of the pier, design shall be based on the provisions of Section 8.2.5.

(d) The nominal length of a pier shall not be less than three times its nominal thickness nor greater than six times its nominal thickness. The clear height of a pier shall not exceed five times its nominal length.

Exception: When the factored axial force at the location of maximum moment is less than 0.05 $f'_m A_g$, the length of a pier may be equal to the thickness of the pier.

8.2.4.4 *Columns*

8.2.4.4.1 *Longitudinal reinforcement* — Longitudinal reinforcement shall be a minimum of four bars, one in each corner of the column, and shall comply with the following:

Maximum reinforcement area shall be determined in accordance with Section 8.2.3.5, but shall not exceed 0.04 A_n.

Minimum reinforcement area shall be 0.0025 A_n.

Longitudinal reinforcement shall be uniformly distributed throughout the depth of the element.

8.2.4.4.2 *Lateral ties* — Lateral ties shall be provided in accordance with Section 2.1.6.5.

8.2.4.4.3 *Construction* — Columns shall be solid grouted.

8.2.4.4.4 *Dimensional limits* — Dimensions shall be in accordance with the following:

(a) The nominal width of a column shall not be less than 8 in. (203 mm).

(b) The distance between lateral supports of a column shall not exceed 30 times its nominal width.

(c) The nominal depth of a column shall not be less than 8 in. (203 mm) and not greater than three times its nominal width.

8.2.5 *Wall design for out-of-plane loads*

8.2.5.1 *General* — The requirements of Section 8.2.5 are for the design of walls for out-of-plane loads.

8.2.5.2 *Maximum reinforcement* — The maximum reinforcement ratio shall be determined by Section 8.2.3.5.

8.2.5.3 *Moment and deflection calculations* — All moment and deflection calculations in Section 8.2.5.4 are based on simple support conditions top and bottom. For other support and fixity conditions, moments, and deflections shall be calculated using established principles of mechanics.

8.2.5.4 *Walls with factored axial stress of 0.05 f'_m or less* — The procedures set forth in this section shall be used when the factored axial load stress at the location of maximum moment satisfies the requirement computed by Eq. (8-23).

$$\left(\frac{P_u}{A_g}\right) \le 0.05 f'_m \qquad (8\text{-}23)$$

Factored moment and axial force shall be determined at the midheight of the wall and shall be used for design. The factored moment, M_u, at the midheight of the wall shall be computed using Eq. (8-24).

$$M_u = \frac{w_u h^2}{8} + P_{uf}\frac{e_u}{2} + P_u \delta_u \quad \text{(8-24)}$$

Where:

$$P_u = P_{uw} + P_{uf} \quad \text{(8-25)}$$

The design strength for out-of-plane wall loading shall be in accordance with Eq. (8-26).

$$M_u \le \phi M_n \quad \text{(8-26)}$$

Where:

$$M_n = \left(A_s f_y + P_u\right)\left(d - \frac{a}{2}\right) \quad \text{(8-27)}$$

$$a = \frac{\left(P_u + A_s f_y\right)}{0.85 f'_m b} \quad \text{(8-28)}$$

The nominal shear strength shall be determined by Section 8.2.4.1.2.

8.2.5.5 *Walls with factored axial stress greater than 0.05f′m* — The procedures set forth in this section shall be used for the design of masonry walls when the factored axial load stress at the location of maximum moment exceeds 0.05f′m. These provisions shall not be applied to walls with factored axial load stress equal to or exceeding 0.2f′m or slenderness ratios exceeding 30. Such walls shall be designed in accordance with the provisions of Section 8.2.4.5 and shall have a minimum nominal thickness of 6 in. (152 mm).

The nominal shear strength shall be determined by Section 8.2.4.1.2.

8.2.5.6 *Deflection design* — The horizontal midheight deflection, *s, under service lateral and service axial loads (without load factors) shall be limited by the relation:

$$\delta_s \le 0.007\,h \qquad (8\text{-}29)$$

P-delta effects shall be included in deflection calculation. The midheight deflection shall be computed using either Eq. (8-30) or Eq. (8-31), as applicable.

(a) Where $M_{ser} < M_{cr}$

$$\delta_s = \frac{5M_{ser}h^2}{48E_mI_g} \qquad (8\text{-}30)$$

(b) Where $M_{cr} < M_{ser} < M_n$

$$\delta_s = \frac{5M_{cr}h^2}{48E_mI_g} + \frac{5(M_{ser} - M_{cr})h^2}{48E_mI_{cr}} \qquad (8\text{-}31)$$

The cracking moment strength of the wall shall be computed using Eq. (8-32), where f_{rAAC} is given by Section 8.1.7.3:

$$M_{cr} = S_n\left(f_{rAAC}\frac{P}{A_n}\right) \qquad (8\text{-}32)$$

8.2.6 *Wall design for in-plane loads*

8.2.6.1 *Scope* — The requirements of Section 8.2.6 are for the design of walls to resist in-plane loads.

8.2.6.2 *Reinforcement* — Reinforcement shall be in accordance with the following:

(a) The amount of vertical reinforcement shall not be less than one half the horizontal reinforcement.

(b) The maximum reinforcement ratio shall be determined in accordance with Section 8.2.3.5.

8.2.6.3 *Flexural and axial strength* — The nominal flexural and axial strength shall be determined in accordance with Section 8.2.4.1.1.

8.2.6.4 *Shear strength* — The nominal shear strength shall be computed in accordance with Section 8.2.4.1.2.

8.2.6.5 *Flexural cracking strength* — The flexural cracking strength shall be computed in accordance with Eq. (8-33), where f_{rAAC} is given by Section 8.1.7.3:

$$V_{cr} = \frac{S_n}{h} \cdot \left(f_{rAAC} + \frac{P}{A_n} \right) \quad (8\text{-}33),$$

8.2.7 *Design of AAC floor and roof diaphragms for in-plane loads*

8.2.7.1 The requirements of Section 8.2.7 govern the design of AAC floor and roof diaphragms.

8.2.7.2 AAC floor and roof diaphragms shall meet the requirements of Section 8.2.7.2.1 or 8.2.7.2.2.

8.2.7.2.1 Nominal shear strength for AAC floor and roof diaphragms subject to lateral load parallel to the direction of panels shall be computed using Section 8.2.7.2.1.1 or 8.2.7.2.1.2.

8.2.7.2.1.1 Nominal shear strength shall be based on adhesion at diaphragm joints, and shall be computed as the product of the contact area of grout and AAC and the shear strength of a grout and AAC joint plus the product of the contact area of thin-bed mortar and AAC and the shear strength of thin-bed mortar. The shear strengths of joints between thin-bed mortar and AAC and grout and AAC are defined in Section 8.1.8.5.

8.2.7.2.1.2 *Nominal shear strength shall be based on a truss mechanism*

8.2.7.2.1.2.1 Compression struts shall be permitted to cross panel joints and shall intersect with tension ties in grouted keys and tension ties (chords) in bond beams.

8.2.7.2.1.2.2 Tension ties shall consist of the reinforcement in grouted keys or in a bond beam. The reinforcement in the grouted keys shall be hooked around the longitudinal reinforcement in the bond beam with standard 90-degree hooks oriented in a vertical plane. Continuous longitudinal ties shall be provided over interior wall supports. The ratio of the cross-sectional area of reinforcement in a grouted key, to the area of the key, need not meet the requirements of Section 8.2.3.

8.2.7.2.1.2.3 *Strength of compression struts* – Compression struts shall be defined within the panel. Their dimension perpendicular to the plane of the panel shall be taken equal to the thickness of the panel. Their dimension in the plane of the panel, measured perpendicular to the axis of the strut, shall be taken as 6 in. The nominal strength of compression struts shall be calculated as the product of 85 percent of the specified compressive strength of the AAC, multiplied by the cross-sectional area of the strut.

8.2.7.2.1.2.4 *Strength of tension ties* – The strength of the tension ties shall not exceed the product of the cross-sectional area of the reinforcement and the specified yield strength of the reinforcement.

8.2.7.2.2 Nominal shear strength for AAC floor and roof diaphragms subject to lateral load parallel to the direction of panels shall meet the requirements of Section 8.2.7.2.1.1 or 8.2.7.2.2.1.

8.2.7.2.2.1 Nominal shear strength shall be based on dowel action of reinforcement in the grouted keys perpendicular to the lateral load. The nominal shear strength shall be computed as the product of 60 percent of the cross-sectional area of the reinforcement and the specified yield strength of the reinforcement.

8.2.7.3 *Nominal flexural capacity of AAC floor and roof diaphragms*

8.2.7.3.1 Continuous reinforcement shall be provided in the bond beam.

8.2.7.3.2 The area of reinforcing steel in the bond beam shall be sufficient to resist moment in the plane of the diaphragm.

8.3 —Unreinforced (plain) AAC masonry

8.3.1 *Scope* — The requirements of Section 8.3 are in addition to the requirements of Chapter 1 and Section 8.1 and govern masonry design in which AAC masonry is used to resist tensile forces.

8.3.1.1 *Strength for resisting loads* — Unreinforced (plain) AAC masonry members shall be designed using the strength of masonry units, mortar, and grout in resisting design loads.

8.3.1.2 *Strength contribution from reinforcement* — Stresses in reinforcement shall not be considered effective in resisting design loads.

8.3.1.3 *Design criteria* — Unreinforced (plain) AAC masonry members shall be designed to remain uncracked.

8.3.2 *Flexural strength of unreinforced (plain) AAC masonry members* – – The following assumptions shall apply when determining the flexural strength of unreinforced (plain) AAC masonry members:

(a) Strength design of members for factored flexure and axial load shall be in accordance with principles of engineering mechanics.

(b) Strain in masonry shall be directly proportional to the distance from the neutral axis.

(c) Flexural tension in masonry shall be assumed to be directly proportional to strain.

(d) Flexural compressive stress in combination with axial compressive stress in masonry shall be assumed directly proportional to strain. Nominal compressive strength shall not exceed a stress corresponding to 0.85 f'_m.

(e) The nominal flexural tensile strength of AAC masonry shall be determined from Section 8.1.7.2.

8.3.3 *Nominal axial strength of unreinforced (plain) masonry members* – – Nominal axial strength, P_n, shall be computed using Eq. (8-33) or Eq. (8-34).

(a) For members having an h/r ratio not greater than 99:

$$P_n = 0.80\left(0.85A_n f'_m\left[1-\left(\frac{h}{140r}\right)^2\right]\right) \qquad (8\text{-}33)$$

(b) For members having an h/r ratio greater than 99:

$$P_n = 0.80\left(0.85A_n f'_m\left(\frac{70r}{h}\right)^2\right) \qquad (8\text{-}34)$$

8.3.4 *Nominal shear strength of unreinforced (plain) masonry members* — The nominal shear strength of AAC masonry, V_m, shall be the least of the values computed by Section 8.2.4.1.2.1 through 8.2.4.1.2.3. In evaluating nominal shear strength by Section 8.2.4.1.2.3, effects of reinforcement shall be neglected.

8.3.4.1 *Special provisions for shear wall specimens with AAC laid in other than running bond* — The provisions of 8.2.4.1.2 shall apply.

8.3.5 *Flexural cracking* — The flexural cracking strength shall be computed in accordance with Section 8.2.6.5.

COMMENTARY:

8.1.3 *Design strength*

8.1.3.1 *Seismic design provisions* — In order to accurately distribute loads in an AAC masonry structure subjected to lateral loading, the lateral stiffness of all structural members should be considered. Although structures may be designed to use shear walls for lateral-load resistance, columns may also be incorporated for vertical capacity. The stipulation that lateral load resisting elements provide at least 80 percent of the lateral stiffness helps ensure that additional elements do not significantly contribute to the lateral stiffness. Based on typical design assumptions, the lateral stiffness of structural elements of AAC masonry should be based on cracked section properties for reinforced masonry and uncracked section properties for unreinforced masonry.

8.1.4 *Strength of Joints*

Design provisions of Chapter 8, and prescriptive seismic reinforcement requirements of Section 1.13, are based on monolithic behavior of AAC masonry. The tensile bond strength of AAC joints is limited in Section 8.1.8.3. The reduction in shear strength of AAC masonry shear walls laid in running bond with unfilled head joints is accounted for in Eq. (8-21b).

8.1.4.7 *Adhesion* — The value of the strength reduction factor reflects the brittle nature of an adhesion failure in an AAC diaphragm.

8.1.4.8 *Truss mechanism in AAC floor and roof diaphragms* — A uniform value of the strength-reduction factor is proposed to provide equilibrium at the nodes. Due to the brittle nature of a compression failure a strength reduction factor of 0.75 is proposed.

8.1.6 *Deformation requirements*

8.1.6.1 *Drift limits* — This section provides procedures for the limitation of story drift. The term "drift" has two connotations:

1. "Story drift" is the maximum calculated lateral displacement within a story (that is, the calculated displacement of one level relative to the level below caused by the effects of design seismic loads).

2. The calculated lateral displacement or deflection due to design seismic loads is the absolute displacement of any point in the structure relative to the base. This is not "story drift" and is not to be used for drift control or stability considerations since it may give a false impression of the effects in critical stories. However, it is important when considering seismic separation requirements.

There are many reasons for controlling drift; one is to control member inelastic strain. Although the relationship between lateral drift and maximum strain is imprecise, so is the current state of knowledge of what strain limitations should be. Drift limits for AAC masonry are based on performance of AAC shear-wall test specimens (Varela 2003).

Under small lateral deformations, secondary stresses are normally within tolerable limits. However, larger deformations with heavy vertical loads can lead

to significant secondary moments from P-delta effects in the design. The drift limits indirectly provide upper bounds for these effects. . . .

8.1.7 *Anchor bolts* — Headed and bent-bar anchor bolts in grouted regions of AAC masonry behave like those addressed in Chapter 3, and are designed identically. Anchors for use in AAC itself are available from a variety of manufacturers, and nominal resistance should be based on tested capacities, verified by an independent testing agency.

8.1.8 *Material properties*

8.1.8.2 *Masonry splitting tensile strength* – The equation for splitting tensile strength is based on ASTM C1006 tests performed at The University of Texas at Austin (Tanner 2003, Varela 2003).

8.1.8.3 *Masonry modulus of rupture* --The modulus of rupture is based on ASTM C78 tests carried out at the University of Alabama at Birmingham[1] for different AAC compressive strengths (Argudo 2003). Modulus of rupture tests show that a thin-bed mortar joint can fail prior to the material if the modulus of rupture exceeds the tensile-bond strength of the thin-bed mortar. This critical value is 80 psi (552 kPa). The data are consistent with the formation of cracks in thin-bed mortar joints in AAC shear wall specimens at The University of Texas at Austin (Tanner 2003). Shear wall tests performed at The University of Texas at Austin (Tanner 2003) show if a leveling joint is present, flexural cracking capacity may be controlled by the tensile bond strength across

[1] Internal report by Fouad H. Fouad, *Physical and Mechanical Properties of AAC Produced in the United States*, The University of Alabama at Birmingham, August 10, 2000.

the interface between the AAC and the leveling mortar which is usually less than the modulus of rupture of the AAC material itself.

8.1.8.4 *Masonry direct shear strength* – The equation for direct shear strength is based on shear tests performed at the University of Alabama at Birmingham[1] (Argudo 2003).

8.1.8.5 *Masonry shear strength of joints* – The equation for shear strength of joints is based on direct shear tests performed at The University of Texas at Austin (Tanner 2003). Data on shear strength of joints from the University of Alabama at Birmingham[1] indicate the value for thin-bed mortar is conservative (Argudo 2003).

8.1.8.6 *Coefficient of friction* – The coefficient of friction between AAC and AAC was determined based on direct shear tests performed at The University of Texas at Austin. The coefficient of friction between AAC and leveling mortar was determined based on tests on shear walls at The University of Texas at Austin.

8.1.8.7 *Reinforcement strength* — Research[3.2] conducted on reinforced masonry components used Grade 60 steel. To be consistent with laboratory documented investigations; design is based on a nominal steel yield strength of 60,000 psi (413.7 MPa). The limitation on the steel yield strength of 130 percent of the nominal yield strength is to minimize the over-strength unintentionally incorporated into a design.

8.1.10 *Concentrated Loads*

8.1.10.4 *Bearing strength for floor and roof members on AAC shear walls* — Bearing should be checked wherever AAC floor or roof panels rest on AAC walls. The critical edge distance for bearing and the critical section for shear to be used in this calculation are shown in Figure D1.

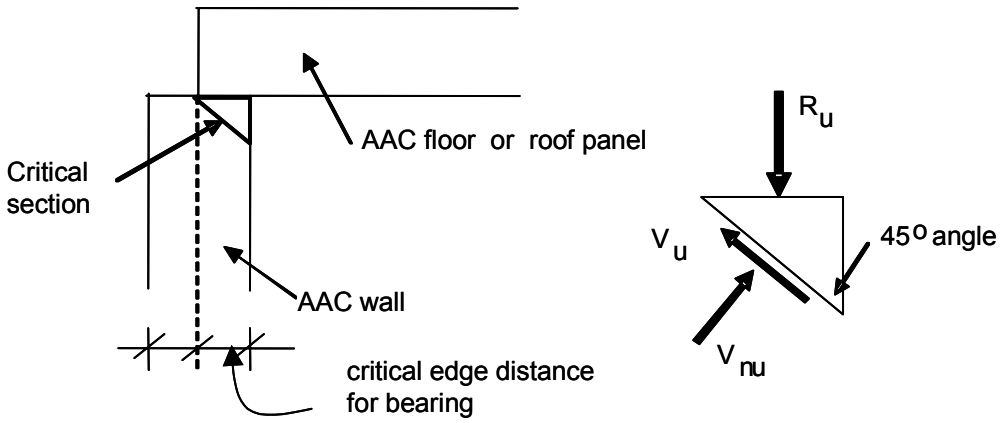

Figure D1 Critical section at bearing of AAC floor or roof panel on AAC wall

8.2 — Field-reinforced AAC masonry

Provisions are identical to those of concrete or clay masonry, with a few exceptions. Only those exceptions are addressed in this Commentary.

8.2.3.1 *Reinforcing bar size limitations* — Splitting of AAC around vertical reinforcement in a grouted cell was observed in shear wall specimens tested at The University of Texas at Austin (Tanner 2003). This splitting occurred in cells with ratios of reinforcement to area of grouted cells of 4.5% or greater. Splitting was not observed in shear walls with a ratio of reinforcement to area of grouted cells of 3% or less.

A reinforcement-to-core area ratio as high as 4.5% (equivalent to a No. 5 bar in a 3-in. grouted core) is acceptable provided that the bar remains elastic and an analysis to determine the acting splitting tensile stress due to radial stresses of the reinforcement is performed. This value is compared to the splitting tensile strength of the grout.

8.2.4.1.2 *Shear strength provided by reinforcement, V_s* -- Test results at UT Austin (Tanner 2003, Varela 2003) show that factory-installed, welded-wire reinforcement is developed primarily by bearing of the cross-wires on the AAC material, which normally crushes before the longitudinal wires develop significant stress. Therefore, the additional shear strength provided by the horizontal reinforcement should be neglected. Joint-type reinforcement will probably behave similarly, and is not recommended. In contrast, deformed reinforcement placed in grouted bond beams is effective, and should be included in computing V_s.

8.2.4.1.2.1 *Nominal masonry shear strength* —This equation was developed based on observed web-shear cracking in shear walls tested at the University of Texas at Austin (Tanner 2003, Varela 2003) and Hebel AG in Germany[2]. Flexure-shear cracking of AAC shear walls was observed in 6 tests at The University of Texas at Austin (Tanner 2003, Varela 2003). Although flexure-shear cracking can be predicted, it does not correspond to a significant decrease in strength or stiffness, and for that reason design limits are not proposed. Masonry units laid in other than running bond may exhibit discontinuities at head joints. The nominal masonry shear strength for AAC masonry laid in other than running

[2] Personal communication, Violandi Vratsanou, Hebel AG, Germany, November 2000.

bond considers the likelihood of vertical discontinuities at head joints, and is based on test results for AAC walls made of vertical panels with open vertical joints between some panels[2].

8.2.4.1.2.2 *Nominal shear strength provided by diagonal strut*— This mechanism limits the shear strength at large levels of axial load. It was based on test results from the University of Texas at Austin (Tanner 2003, Varela 2003) using the following equation with a width of the diagonal strut of $0.25l_w$.

$$V_{AAC} = 0.9 f_{aac} t w_{strut} \frac{h(l_w - w_{strut})}{h^2 + (l_w - w_{strut})^2}$$

8.2.4.1.2.3 *Nominal shear strength provided by sliding shear resistance* — This equation was based on test results from the University of Texas at Austin (Tanner 2003, Varela 2003). Since this failure mode is ductile, the nominal capacity in sliding shear does not need to be considered in the capacity design check of Section 8.1.3.

At an unbonded interface, nominal sliding shear capacity should be based on friction only. At an interface where thin-bed mortar is present, the nominal sliding shear capacity should be based on the greater of the capacity based on initial adhesion, and the frictional capacity after that initial adhesion is overcome. At an interface where leveling-bed mortar is present, the interface is probably cracked due to in-plane flexure, and initial adhesion should not be counted on. The nominal sliding shear capacity should be based on the frictional capacity consistent with the total force on the compressive stress block, including the compressive force required to equilibrate the tensile force in the longitudinal reinforcement.

8.2.4.1.3 *Special provisions for shear walls with AAC laid in other than running bond* — Tests conducted at The University of Texas at Austin showed that vertical cracks formed at the head joints in shear wall specimens with vertically oriented panels (Tanner 2003, Varela 2003). The cracks were limited to every third joint or not seen when using the construction techniques presented. If vertical cracks are present, the strength and stiffness of an AAC shear wall will decrease and the behavior will be different, which must be considered in design.

8.2.5.6 *Deflection design* — See Commentary of Section 8.2.6.5.

8.2.6.5 *Flexural cracking* — This equation was verified with test results from the University of Texas at Austin (Tanner 2003, Varela 2003) and the University of Alabama at Birmingham[3]. When no leveling joint or thin-bed mortar joint is present, the flexural cracking capacity of an AAC wall is computed using the modulus of rupture of the AAC material. If a leveling joint is present, flexural cracking capacity may be controlled by the tensile bond strength across the interface between the AAC and the leveling mortar or thin-bed mortar, which is usually less than the modulus of rupture of the AAC material itself. Modulus of rupture tests from the University of Alabama at Birmingham[1] show that a thin-bed mortar joint can fail prior to the material if the modulus of rupture exceeds the tensile-bond strength of the thin-bed mortar. This critical value is 80 psi (552 kPa) (Argudo 2003). The data are consistent with the formation of cracks in thin-bed mortar joints in AAC shear wall specimens at The University of Texas at Austin (Tanner 2003).

---

[3]Internal report by Fouad H. Fouad, *Physical and Mechanical Properties of AAC Produced in the United States*, The University of Alabama at Birmingham, August 10, 2000.

8.2.7.2.1.1 Lateral load in an AAC diaphragm was successfully transferred through adhesion in a two-story AAC assemblage specimen (Tanner 2003, Varela 2003). Since adhesion failure is brittle, a strength reduction factor of 0.67 is used. The shear strength of a joint was determined based on direct shear tests performed on joints between thin-bed mortar and AAC and grout and AAC (Tanner 2003). The values presented in Section 8.1.8.5 represent lower 5% fractiles of these tests.

8.2.7.2.1.2 The shear strength of AAC diaphragms with panels oriented parallel to the direction of loading can be checked using a truss mechanism. The truss mechanism for load parallel to the orientation of the panels is shown in Figure D2.

8.2.7.2.1.2.1 Compression struts are not allowed to cross panel joints, since the effect of joint cracks on the strength of AAC compression struts is unknown.

8.2.7.2.1.2.2 The reinforcement in the bond beam parallel to the panels forms part of the truss mechanism to transfer lateral load. The reinforcement in the grouted keys is anchored into the bond beam using a vertically oriented hook that extends beyond the bond beam reinforcement. This mechanical connection enhances the in-plane integrity of the horizontal diaphragm (Figure D3). The truss model assumes uniform tension in the reinforcement. This assumption is valid even with damage at joints.

8.2.7.2.1.2.3 The area of the compression strut is 6 in. in the plane of the panel, multiplied by the panel thickness.

8.2.7.2.1.2.4 The strength of tie elements (reinforcement in grouted keys or bond beams) is calculated as the cross-sectional area of the longitudinal reinforcement in those elements, multiplied by the specified yield strength of the reinforcement.

8.2.7.2.2.1 The nominal shear strength of an AAC diaphragm with panels oriented perpendicular to the direction of loading can be generated through dowel action in the reinforcement. The available resistance of an AAC diaphragm can also be determined by the transfer of load through shear in the reinforcement, which is computed by $0.6f_yA_s$.

8.2.7.3 *Nominal flexural capacity of AAC floors and roof diaphragms* -- The bond beam (chord) perpendicular to the orientation of lateral load provides reinforcement for in-plane flexural resistance.

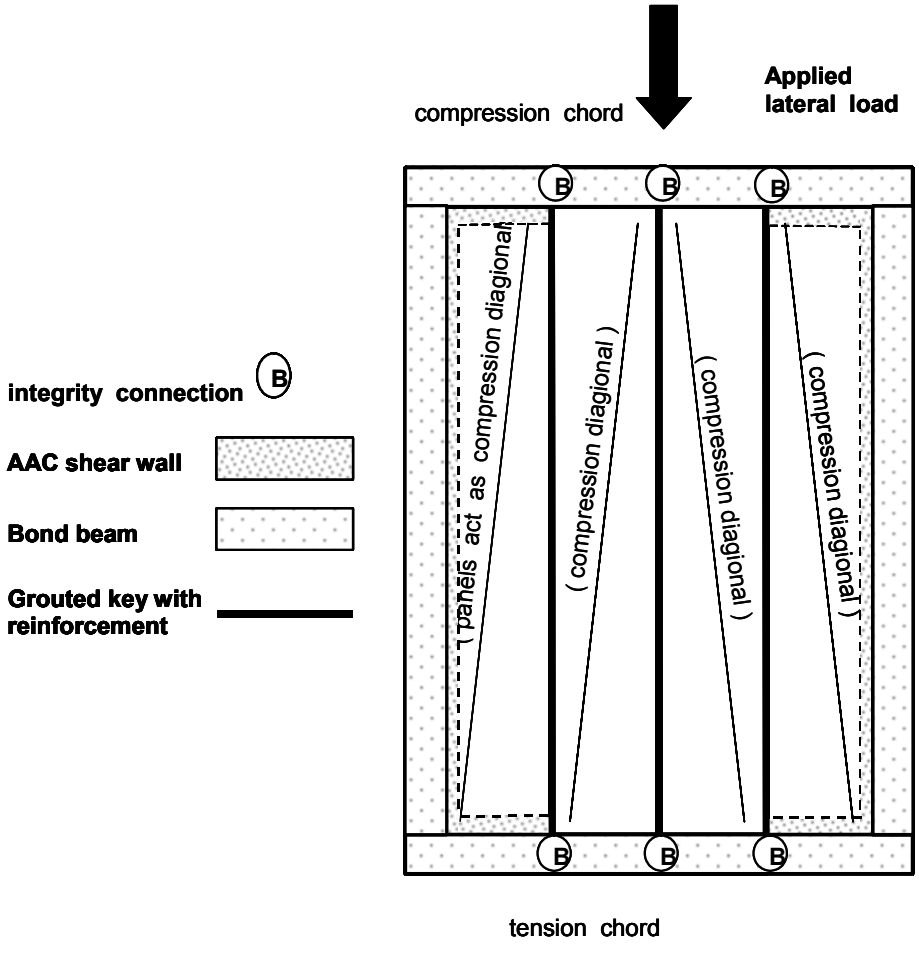

Figure D2: Truss mechanism in an AAC floor or roof diaphragm

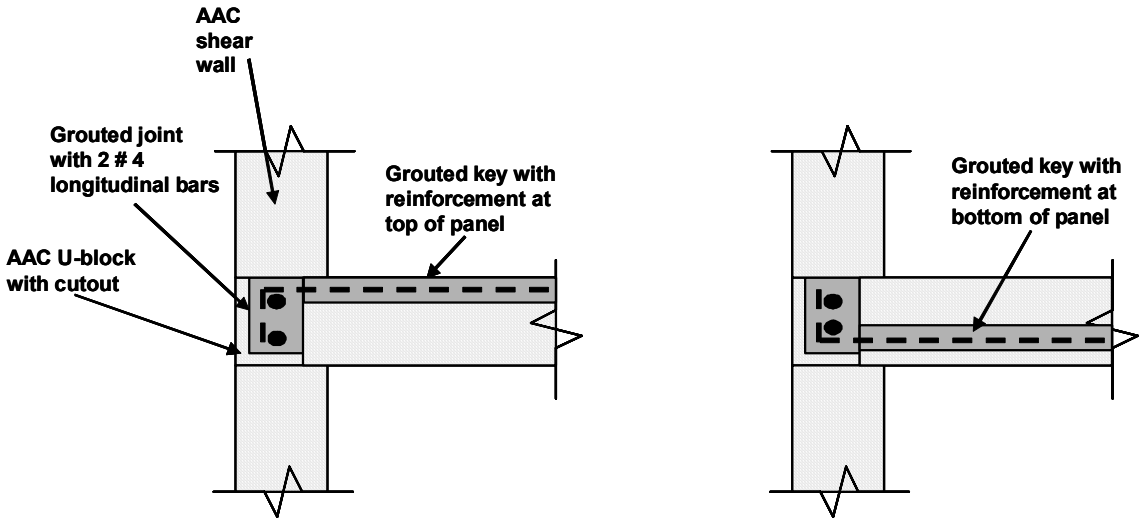

Figure D3: Detail of grouted key reinforcement with 90˚ hook oriented vertically and hooked around the bond beam reinforcement

8.3 — Unreinforced masonry

Provisions are identical to those of concrete or clay masonry, with a few exceptions. Only those exceptions are addressed in the Commentary of Section 8.2.

APPENDIX E:
PROPOSED DESIGN PROVISIONS FOR ACI 3xx

The proposed design provisions of this Appendix are intended to be a separate document used in conjunction with the design provisions of ACI 318-02. They provisions are referred to as ACI 3xx throughout this dissertation. The provisions of ACI 318-02 are intended as the default, and are augmented, modified or replaced by the provisions of ACI 3xx. These proposed ACI 3xx design provisions address factory-reinforced AAC panels.

The proposed Commentary ACI R3xx provisions that follow the code provisions are intended to supplement the Commentary of ACI 318-02. Where no new Commentary provisions are indicated, the current Commentary of ACI 318-02 applies. Where Code provisions of ACI 318-02 are deleted, the corresponding Commentary is also deleted. Added Commentary provisions are denoted by an underline.

Chapter 2 — Definitions

Add the following definitions, here and in the chapters where they are used.

Autoclaved Aerated Concrete — low-density cementitious product of calcium silicate hydrates, defined in ASTM C 1386.

Chapter 3 — Materials

Add the following section, renumber subsequent sections accordingly:

3.8 AAC Panels and Related Materials

3.8.1 Reinforced panels shall conform to ASTM C 1452.

3.8.2 Thin-bed mortar for AAC panels shall conform to the performance requirements of the AAC manufacturer.

3.8.2 Bedding mortar for AAC panels shall conform to ASTM C270, Types M, S, or N.

3.8.3 Grout for AAC masonry shall conform to ASTM C476.

Renumber Section 3.9 - Referenced Standards

Add the following standards:

ASTM C 270 Specification for Mortar for Unit Masonry

ASTM C 476 Specification for Grout for Masonry

ASTM C1006 Splitting Tensile Strength of Masonry Units

ASTM C 1386 Specification for Precast Autoclaved Aerated Concrete (PAAC) Wall Construction Units

ASTM C 1452 Specification for Reinforced Autoclaved Aerated Concrete Elements

ASTM C ZZZZ Method of Test for Determining the Modulus of Elasticity of Autoclaved Aerated Concrete (under development by ASTM C-27.60)

Chapter 4 -- Durability Requirements

Remove Section 4.1 on water - cementitious materials ratios.

Remove Section 4.2 on freezing and thawing exposures and replace by the following:

4.2 Freezing and Thawing Exposures

4.2.1 - AAC shall not be used in below-grade applications where it could be subjected to cycles of freezing and thawing while critically saturated

4.2.2 - AAC masonry exposed to weather shall be protected with an exterior wythe of masonry, a cladding system, or a coating complying with the requirements of (a) and (b)

a) Vapor permeability: the PERM rating of the coating, determined in accordance with E 96, shall not be less than 5.

b) Liquid permeability: the coating shall show no leakage when tested using the following procedure:

As shown in Figure 1, prepare an AAC masonry assemblage with plan dimensions of 12 in. by 12 in. (0.3 m) and a thickness of 1 in. (25 mm). Make the assemblage using two pieces of AAC material with a vertically oriented joint between them. Join the two pieces at the joint using thin-bed or thick-bed mortar as appropriate to the AAC masonry being tested. Cover the top surface with the coating to be tested. Affix to the top surface of the specimen, over the joint, a clear glass or plastic measurement tube with an inside diameter between 2 and 4 in. (50 and 100 mm), and a height of at least 24 in. (0.6 m). Prepare a reference tube, closed at the bottom, of the same material and dimensions as the measurement tube. Fill the measurement tube and the reference tube with water to a height of 21.6 in. (0.55 m), within a tolerance of ±1 in. (25 mm). Note the original height of water, and the height after 5 h, in the measurement tube and in the reference tube. Record the difference between the initial height and the final height of water in the measurement tube, and in the reference tube. If those differences differ by less than 1 mm, the coating shall be considered to have shown no leakage.

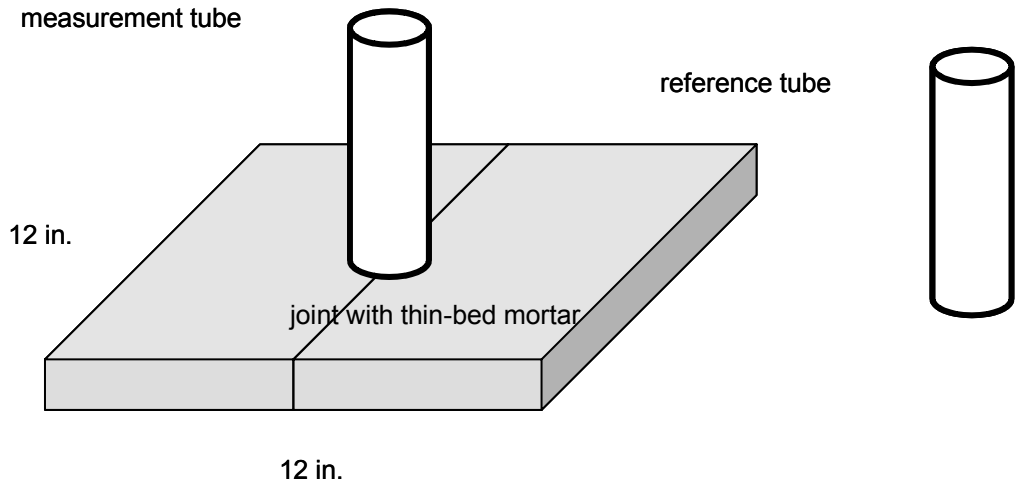

Figure E4 Assemblage for testing liquid permeability of exterior surface treatment for AAC panels

Delete Section 4.3.1 and replace by the following:

4.3.1 AAC shall be protected against injurious concentrations of sulfates as required by 4.2.

Delete Section 4.4 on corrosion protection of reinforcement and replace by the following:

4.4.1 Factory-installed reinforcement for AAC panels shall be protected from corrosion in accordance with ASTM C 1452.

Remove 5.1 (General) and replace by the following:

5.1.1 AAC shall comply with the provisions of ASTM C1386 for the strength class specified in the design.

Remove 5.2 through 5.6 completely.

Remove 5.7 and replace by the following:

5.7 - Preparation of equipment and place of deposit

5.7.1 - Preparation before laying of leveling mortar and placement of AAC panels shall include the following:

(a) All equipment for mixing and transporting leveling mortar shall be clean.

(b) All debris and ice shall be removed from the area where the leveling bed mortar is to be placed.

(c) Reinforcement shall be clean of ice or other deleterious coatings.

5.7.2 - Preparation before placing grout

(a) All cavities and keys receiving grout shall be clean and free of debris.

(b) Keys and cavities shall be wet prior to placing grout, or grout shall contain shrinkage retarding admixture.

5.7.3- Preparation before placing thin-bed mortar

(a) Inspect each panel for imperfections that prohibit the panel joint from sitting farther than 1/16 in. from an adjacent panel.

(b) Clean and wet each panel prior to applying the thin-bed mortar.

5.7.4- Preparation before placing thin-bed mortar

(a) Apply thin-bed mortar to the panels on both sides of the vertical joint.

(b) Apply pressure perpendicular to the vertical joint using horizontally oriented clamps.

Delete 5.8 through 5.11

Delete 5.12 and replace by the following:

5.12 - Cold Weather Requirements

5.12.1 - All AAC materials and all reinforcement shall be free from frost.

5.12.2 - Thin-bed mortar and bedding mortar shall not be used in ambient temperatures less than 32 F without provision for proper curing and protection from freezing.

Chapter 6 -- Formwork, Embedded Pipes and Construction Joints

Delete 6.1 - Formwork

Remove 6.3 and replace by the following:

6.3 - Conduits and Pipes Passing through AAC

Conduits, pipes and sleeves passing through AAC elements, and the their routed openings, shall not impair significantly the strength of the construction.

Remove 6.4 - Construction Joints.

Chapter 7 -- Details of Reinforcement

Add 7.1 - Scope; renumber other sections as appropriate

7.1 - Scope

Factory-installed reinforcement in AAC panels shall meet the requirements of ASTM C1452. The remaining provisions of this chapter shall apply to field-installed reinforcement only.

Chapter 8 — Analysis and Design — General Considerations

Modify Section 8.5 — Modulus of Elasticity as follows:

Remove 8.5.1 (concrete) and replace by the following:

8.5.1 — The modulus of elasticity EAAC for AAC shall be taken as $E = 6500\, f_{AAC}^{0.6}$ (in psi).

Add a new Section 8.5.2 and renumber remaining sections appropriately:

8.5.2 - The modulus of elasticity E_{grout} for grout shall be taken as 500 fg′.

Add a new Section 8.13 – Material properties of AAC:

8.13.1 The splitting tensile strength f_{tAAC} shall be determined by Equation 8-1.

$$f_{tAAC} = 2.4\sqrt{f'_{AAC}} \qquad (8\text{-}1)$$

f'AAC and f_{tAAC} in psi

8.13.2 The modulus of rupture, f_{rAAC}, for AAC masonry elements shall be taken as two times the masonry splitting tensile strength, f_{tAAC}. If a section of AAC contains a horizontal leveling bed, the value of f_{rAAC} shall not exceed 50 psi (345 kPa) at that section. If a section of AAC contains a bed joint between thin-bed mortar and AAC the value of f_{rAAC} shall not exceed 80 psi (552 kPa) at that section.

8.13.3 The direct shear strength f_v shall be determined by Equation 8-2.

$$f_v = 0.15 f'_{AAC} \qquad (8\text{-}2),$$

f'_{AAC} and f_v in psi

8.13.4 The shear strength of a joint between AAC and grout shall be 36 psi (0.25 MPa). The shear strength of a joint between AAC and thin-bed mortar shall be 18 psi (0.13 MPa).

Chapter 9 — Strength and Serviceability

Add the following Section 9.3.2.8:

9.3.2.8 – Adhesion…….0.67

9.5 - Deflections

9.5.1 - replace "reinforced concrete" by "AAC"

9.5.2 -Add the following at the end of the existing 9.5.2.1:

Footnote (2a) of Table 9.5(a) shall apply, using ρ_{1386}. Footnote (2b) shall not apply.

Replace 9.5.2.3 by the following:

9.5.2.3 - Immediate deflections shall be calculated using an effective flexural stiffness (EI_e) corresponding to the unfactored moment (M_a). The effective flexural stiffness (EI_e) shall be obtained by linear interpolation between the cracking point ($M_{cr,}$ ϕ_{cr}) and the yielding points ($M_{y,}$ ϕ_y) on a bilinear moment-curvature diagram. For these calculations, the modulus of rupture of the AAC shall be taken as twice the splitting tensile strength by ASTM C1006, at the moisture content specified by ASTM C1386.

Replace 9.5.2.5 by the following:

9.5.2.5 — Unless values are obtained by a more comprehensive analysis, the total long-term deflection (including the additional long-term deflection resulting from creep and shrinkage) of AAC flexural members shall be determined using Section 9.5.2.3, with an effective modulus equal to $E_{AAC}/1.5$.

Chapter 10 – Flexure and Axial Loads

Remove and replace "concrete" throughout by "AAC."

10.2.7.3 - Remove and replace by the following:

10.2.7.3 **-** The factor β_1 shall be taken as 0.67.

Section 10.5 - Minimum reinforcement of flexural members -- replace Equation 10-3 by the following.

$$As,_{min} = \frac{4\sqrt{f'_{AAC}}}{f_y} bd$$

Delete Sections 10.6 through 10.16. Retain Section 10.17.

Chapter 11 — Shear and Torsion

Throughout Chapter 11, replace V_c by V_{AAC}.. Make additional changes as noted below.

Change Equation 11-3 to the following:

$$V_{AAC} = 0.8\sqrt{f'_{AAC}}\ b_w d$$

Change Equation 11-4 to the following:

$$V_{AAC} = 0.8\sqrt{f'_{AAC}}\left(1+\frac{N_u}{2000\ A_g}\right)b_w d$$

Delete Section 11.3.2.

Delete Section 11.4.

Add the following to Section 11.5.6.2:

The maximum shear strength provided by wire reinforcement bar embedded in AAC (Vs_b) shall be limited by $Vs_b \le d_{long} \cdot s \cdot f'_{AAC}$, the bearing capacity of the AAC on the longitudinally oriented cross-wires. Shear strength provided by the wire shall be included for resisting gravity loads only.

Delete Section 11.6 - Torsion.

Modify Section 11.7.4.1 as follows:

The shear strength V_n for AAC shall be computed as:

$V_n = (N) \cdot \mu$ Eq. (11-xx)

At an interface where uncracked thin-bed mortar is present, the nominal sliding shear capacity shall be calculated as the greater of Eq. (11-xx) and the capacity calculated by the shear strength of AAC at a thin-bed mortar joint,

defined in Section 8.14.1, multiplied by the area of a thin-bed mortar joint. In an AAC shear wall, it shall also be permitted to include the force in the tensile steel at a given cross-section ($A_s f_s$) in the axial load.

Add the following to Section 11.7.4.3:

AAC placed against leveling mortar.....1.0
AAC placed against AAC 0.75

Delete Section 11.8 - Deep beams

Delete Section 11.9 - Special provisions for brackets and corbels.

In Section 11.10, replace Equation (11-29) by the following:

$$V_{AAC} = 0.9\,\ell_w\,h\,\sqrt{f'_{AAC}}\,\sqrt{1+\frac{N_u}{2.4\sqrt{f'_{AAC}}\,\ell_w\,h}}$$

In Section 11.10, replace Equation 11-30 by the following:

$$V_{AAC} = \frac{0.17h\,f'_{AAC}\,\ell_w^2 h_{wall}}{h_{wall}^{\,2} + (\frac{3}{4}l_w)^2}$$

Remove Section 11.10.7 and replace by the following:

11.10.7 — Special provisions for shear walls with AAC panels oriented vertically – Nominal shear strength and flexural strength shall be determined assuming that vertical cracks exist at each vertical joint. The shear capacity shall be determined using Equation (11-4) if the panel height divided by the panel width exceeds 3. It shall be permitted to design assuming vertical cracks at every third joint, using Equation (11-29), if the construction requirements of Section 5.7.4 are met.

Delete Section 11.10.8.

Remove Section 11.10.9 and replace by the following:

11.10.9 — Design of shear reinforcement for walls

11.10.9.1 — Where factored shear force $\mathbf{V}_u$ exceeds shear strength $\phi\mathbf{V}_{AAC}$, horizontal shear reinforcement shall be provided to satisfy Eq. (11-1) and (11-2), where shear strength $\mathbf{V}_s$ is computed by

$$V_s = \frac{A_v f_y d}{s_2} \qquad \textit{(11-31)}$$

where $\mathbf{A}_v$ is the area of deformed horizontal reinforcement embedded in grout within a distance $\mathbf{s}_2$ and distance **d** is in accordance with 11.10.4.

Delete Sections 11.10.9.2 through, 11.10.9.5

Delete Sections 11.11, 11.12.

Chapter 12 — Bond and Development Length

Add New 12.1 - Scope. Renumber following sections accordingly.

12.1 - Scope

12.1.1 - Unless stated otherwise, the requirements of this Chapter refer to reinforcement embedded in grout. Those requirements shall apply to field-installed reinforcement.

12.1.2 - When so stated, the requirements of this Chapter shall refer to factory-installed reinforcement embedded in AAC.

12.1.3 – The maximum ratio of vertical reinforcement to area of a grouted cell shall be 3%. It shall be permitted to use ratios of vertical reinforcement up to 4.5% if the reinforcement remains elastic throughout its entire length and the available splitting tensile strength of the grout is greater than the acting splitting tensile strength as defined by Equation (12-xx)

$$f_t = \frac{V d_{bar}}{jd \cdot d_{bar} \cdot (d_{core} - d_{bar})} \qquad \text{Equation (12-xx)}$$

The splitting tensile strength of the grout shall be taken as $4\sqrt{f_g'}$. If f_g' is not specified it shall be permitted to be taken as 2000 psi.

12.1.4 – Splices of longitudinal reinforcement shall not be permitted in potential plastic hinge zones .

Add new Section 12.20:

12.20 - Design of Factory-Installed Reinforcement Embedded in AAC

Factory-installed reinforcement embedded in AAC shall be designed to satisfy either 12.20.1 or 12.20.2.

12.20.1 - The spacing of cross-wires shall be less than or equal to the value required to satisfy Eq. (12-4).

12.20.2 - The number of cross-wires within a distance of 1/6 of the clear span of the panel, measured in each direction from each support, shall equal or exceed the value required to satisfy Eq. (12-5). In that equation, *a* is the shear span or 1/6 of the clear span of the panel. In other sections, the spacing shall not exceed $2s_{min}$.

$$s_{min} = \frac{V_u / \phi}{0.85\, d \cdot d_{cross} \cdot l_{cross} \cdot f'_{AAC}} \qquad \text{Equation (12-4)}$$

$$n_{cross,min} = \frac{V_u / \phi}{0.85\, d \cdot d_{cross} \cdot l_{cross} \cdot f'_{AAC}} \cdot a \qquad \text{Equation (12-5)}$$

Delete Chapter 13

Chapter 14 — Walls

Delete 14.1.2

14.3 — Minimum reinforcement

Delete 14.3.1 through 14.3.6.

Rewrite 14.3.7 as follows:

14.3.7 — In addition to the minimum reinforcement required by 14.2.1, not less than one No. 4 bar shall be provided around all window and door openings. Such bars shall be extended to develop the bar beyond the corners of the openings but not less than 24 in.

Delete 14.5 (Empirical Design of walls)

Delete Sections 14.7 and 14.8.

Delete Chapter 15.

Chapter 16 — Precast concrete

Throughout, replace "concrete" by "AAC."

Modify 16.2.4 as shown below:

16.2.4 — In addition to the requirements for drawings and specifications in 1.2, include the following in either the contract documents or the shop drawings:

(a) Details of reinforcement, inserts and lifting devices required to resist temporary loads from handling, storage, transportation, and erection or reference to AAC manufacturers' published construction practices;

(b) Specified compressive strength of AAC.

16.4 — Member design

Delete 16.4.2.

16.5 — Structural integrity

Remove Section 16.5.1.2 and replace with the following:

16.5.1.2 — Where precast AAC elements form floor or roof diaphragms, the minimum provisions of Section 16.5.1.2.1 through 16.5.1.2.4 shall apply in addition to the requirements of Section 7.13.3.

16.5.1.2.1 — Nominal shear strength for AAC floor and roof diaphragms subject to lateral load parallel to the direction of panels shall be calculated based

on Section 16.5.1.2.2 or Section 16.5.1.2.3. Nominal shear strength for AAC floor and roof diaphragms subject to lateral load perpendicular to the direction of panels shall be calculated based on Section 16.5.1.2.2 or 16.5.1.2.4.

16.5.1.2.2 — Nominal shear strength shall be based on adhesion at diaphragm joints, and shall be computed as the product of the contact area of grout and AAC and the shear strength of a grout and AAC joint plus the product of the contact area of thin-bed mortar and AAC and the shear strength of thin-bed mortar. The shear strengths of joints between thin-bed mortar and AAC and grout and AAC are defined in Section 8.14.4.

16.5.1.2.3 — Nominal shear strength of AAC floor and roof diaphragms shall be based on a truss mechanism subject to the minimum provisions of Section 16.5.1.2.3.1 through Section 16.5.1.2.3.4.

16.5.1.2.3.1 — Compression struts shall not be permitted to cross panel joints and shall intersect with tension ties in grouted keys and tension ties (chords) in bond beams.

16.5.1.2.3.2 — Tension ties shall consist of the reinforcement in grouted keys or in a bond beam. The reinforcement in the grouted keys shall be hooked around the longitudinal reinforcement in the bond beam with standard 90-degree hooks oriented in a vertical plane.

16.5.1.2.3.3 — Compression struts shall be defined within the panel. Their dimension perpendicular to the plane of the panel shall be taken equal to the thickness of the panel. Their dimension in the plane of the panel, measured perpendicular to the axis of the strut, shall be taken as 6 in. The nominal strength of compression struts shall be calculated as the product of 85 percent of the specified compressive strength of the AAC, multiplied by the cross-sectional area of the strut.

16.5.1.2.3.4 — The strength of the tension ties shall not exceed the product of the cross-sectional area of the reinforcement and the specified yield strength of the reinforcement.

16.5.1.2.4 — Nominal shear strength shall be based on dowel action of reinforcement in the grouted keys perpendicular to the lateral load. The nominal shear strength shall be computed as the product of 60 percent of the cross-sectional area of the reinforcement and the specified yield strength of the reinforcement.

16.5.1.3 — Vertical tension tie requirements of 7.13.3 shall apply to all vertical structural members, except cladding., and shall be achieved by providing connections at horizontal joints in accordance with the following:

(a) Precast columns shall not be made of AAC;

(b) Precast wall panels that comprise shear walls shall be connected at wall intersections, at locations of longitudinal reinforcement*;*

(c) When design forces result in no tension at the base, the ties required by 16.5.1.3(b) shall be permitted to be anchored into an appropriately reinforced concrete slab on grade.

16.5.1.4 — Except for sliding shear resistance in a shear wall, connection details that rely solely on friction caused by gravity loads shall not be used.

16.5.2 — For precast autoclaved aerated concrete bearing wall structures three or more stories in height, the minimum provisions of 16.5.2.1 through 16.5.2.5 shall apply.

16.5.2.1 — Longitudinal and transverse ties shall be provided in floor and roof systems to provide a nominal strength of 1500 lb per ft of width or length, and shall be designed to transfer shear to lateral force-resisting elements. Ties shall be provided over interior wall supports and between members and exterior walls. Ties shall be positioned in or within 2 ft of the plane of the floor or roof system. Longitudinal ties shall only be required parallel to the direction of span of the panels.

16.5.2.2 — Longitudinal ties parallel to floor or roof slab spans shall be spaced not more than 10 ft on centers. Provision shall be made to transfer forces around openings.

16.5.2.3 — Transverse ties perpendicular to floor or roof slab spans shall be spaced not greater than the bearing wall spacing.

16.5.2.4 — At each level, a bond beam shall be provided, and shall be reinforced with at least two longitudinal reinforcing bars, having a total cross-sectional area of at least 0.4 $in.^2$ If floor diaphragms are made of AAC panels, those panels shall be connected to each other by grouted keys, each having at least 0.11 $in.^2$ of reinforcement, anchored in the bond beam by a standard 90-degree hook, placed around the longitudinal reinforcement in the bond beam and oriented in a vertical plane.

16.5.2.5 Continuous vertical reinforcement in AAC shear walls shall be sufficient to resist the design moments.

Rewrite 16.6.2.2 as follows:

16.6.2.2 — Unless shown by test or analysis that performance will not be impaired, the following minimum requirements shall be met:

(a) Each member and its supporting system shall have design dimensions selected so that, after consideration of tolerances, the distance from the edge of the support to the end of the precast member in the direction of the span is at least 1/180 of the clear span *l*, but not less than:

For solid or hollow-core slabs	2 in.
For beams or stemmed members	3 in.
For autoclaved aerated concrete panels	2 in.

(b) Bearing pads at unarmored edges shall be set back a minimum of 1/2 in. from the face of the support, or at least the chamfer dimension at chamfered edges.

16.6.2.3 — The requirements of 12.11.1 shall not apply to the positive bending moment reinforcement for statically determinate precast members. At least one-third of such reinforcement, however, shall extend to the center of the bearing length.

16.8 — Marking and identification

16.8.1 — Each precast member shall be marked to indicate its class, production identification code, location and orientation in the structure and date of manufacture. Pallets should also identify the class of AAC, production identification code and unit dimensions.

16.8.2 — Identification marks shall correspond to placing drawings.

Delete Chapter 17, 18, 19, and 20.

Chapter 21 - Special Provisions for Seismic Design

Rewrite 21.2.1.2 and 21.2.1.3 as follows:

21.2.1.2 – In regions of moderate seismic risk or for structures assigned to intermediate seismic performance or design categories, intermediate or special moment frames, ordinary, intermediate, or special structural walls, or intermediate or special AAC structural wall systems shall be used to resist forces induced by earthquake motions. Where the design seismic loads are computed using provisions for special concrete systems or intermediate or special AAC structural walls, the requirements of Chapter 21 for special systems, as applicable, shall be satisfied.

21.2.1.3 – In regions of high seismic risk for structures assigned to high seismic performance or design categories, special moment frames, special structural walls, special AAC structural wall systems, or diaphragms and trusses complying with 21.2 through 21.10 shall be used to resist forces induced by earthquake motions. Frame members not proportioned to resist earthquake forces shall comply with 21.11.

Add Section 21.14 – Intermediate AAC structural wall systems

21.14.1 - The provisions of this section apply to design of intermediate AAC structural walls and their associated horizontal diaphragms to resist forces induced by earthquake motions. The design provisions of Chapters 1-18 shall apply except as modified in this Section.

21.14.2 – The design shear force V_e shall be determined from consideration of the maximum forces that can occur in an AAC element. Forces in the longitudinal reinforcement shall be determined assuming that the stress in the flexural tensile reinforcement is $1.25f_y$.

21.14.3 – The horizontal diaphragm shall be designed to resist the design shear force, V_e, of Section 21.14.2. Design according to Section 16.5.1.2.2 shall not be permitted.

Add Section 21.15 – Special AAC structural wall systems

21.15.1 - The design provisions of this section apply to special AAC structural walls and horizontal diaphragms to resist forces induced by earthquake motions.

21.15.2 – The design provisions of Chapters 1-18 and Section 21.14 shall apply except as modified in this Section.

21.15.3 – Lateral load between horizontal diaphragms and AAC structural walls shall be transferred through connectors embedded in grout in accordance with Section 16.

NOTATION

Add the following:

d_{cross} = diameter of cross-wires, in. (mm)

d_{long} = diameter of longitudinal reinforcement, in. (mm)

E_{AAC} = modulus of elasticity of AAC, psi (MPa)

f_{AAC}' = specified compressive strength of AAC, psi (MPa)

f_g' = specified compressive strength of grout, psi (MPa)

$f_{t\,AAC}$ = splitting tensile strength of AAC by ASTM C1386, psi (MPa)

h_{wall} = height of AAC shear walls between stories, in. (mm)

l_{cross} = length of reinforcement bearing on AAC, in. (mm)

V_{AAC} = nominal shear strength provided by AAC, kips (kN)

Vs_b = maximum usable shear strength provided by each wire of shear reinforcement, kips (kN)

ρ_{1386} = air-dried density of AAC by ASTM C1386, lb/ft^3 (kg/m^3)

w_{strut} = horizontal projection of the width of the compression strut, in. (m)

COMMENTARY ON PROPOSED DESIGN PROVISIONS

Chapter 3 — Materials

Add the following section, renumber subsequent sections accordingly:

Renumbered Section 3.9 - Referenced Standards

Add the following:

ASTM C ZZZZ Method of Test for Determining the Modulus of Elasticity of Autoclaved Aerated Concrete is currently under development by ASTM C-27.60. If it has not been developed by the time this document is completed, this reference will be changed to a footnote.

Chapter 4 -- Durability Requirements

Remove Section 4.2 on freezing and thawing exposures and replace by the following:

R4.2 Freezing and Thawing Exposures

Because AAC can deteriorate when subjected to cycles of freezing and thawing while critically saturated, no below-grade applications of AAC are permitted where the AAC could become critically saturated, and coatings are also

required to prevent the infiltration of liquid water into AAC in above-grade applications.

Add the following to Section 4.4 on corrosion protection of reinforcement:

R4.4 - Corrosion protection of reinforcement

Provisions for coating on AAC welded wire fabric are included in ASTM C1452.

Chapter 5 -- Concrete Quality, Mixing and Placing

Add the following:

R5 - Code 5.1.1 links the designer's specified value with the producer-verified strength class. Corresponding material specifications and tolerances are prescribed in ASTM C1386. The mixture design for the AAC is factory-adjusted to produce the required strength class. The design engineer and the contractor are not involved in AAC production or curing. Construction techniques are based on industry practices and construction techniques, and have been verified by

laboratory testing at UT Austin (Tanner 2003, Varela 2003) and elsewhere. The Committee may consider imposing more specific hot- and cold-weather construction requirements.

Chapter 6 -- Formwork, Embedded Pipes and Construction Joints

Delete Chapter 6 and replace by the following:

R6 - Formwork is not required because AAC is a precast product. Conduits and pipes are not cast-in; openings for them may be cut or routed, and the effect of those openings on structural performance must be checked.

Chapter 7 -- Details of Reinforcement

Add the following:

R7 - Conventional reinforced concrete is constructed with cast-in-place reinforcement or post-installed reinforcement such as post-tensioning tendons. AAC is constructed with factory-placed welded-wire reinforcement, and possibly also with cast-in-place, deformed reinforcement installed in grouted cores in the

field. Detailing requirements for deformed reinforcement in grout are prescribed in the existing Chapter 7. Detailing requirements for the factory-installed reinforcement are prescribed by the provisions of ASTM C1452.

Chapter 8 — Analysis and Design — General Considerations

Add the following:

R8.5.1 — The expression for modulus of elasticity of AAC is based on combined test data from UT Austin (Argudo 2003, Tanner 2003) and UAB.

Add a new Section 8.5.2 and renumber remaining sections appropriately:

R8.5.2 - The expression for modulus of elasticity of grout is based on the 2002 MSJC Code.

Add a new Section 8.13:

R8.13.1 – The equation for splitting tensile strength is based on ASTM C1006 tests performed at The University of Texas at Austin (Tanner 2003).

R8.13.2 --The modulus of rupture is based on ASTM C78 tests carried out at the University of Alabama at Birmingham[4] for different AAC compressive strengths (Argudo 2003). Modulus of rupture tests show that a thin-bed mortar joint can fail prior to the material if the modulus of rupture exceeds the tensile-bond strength of the thin-bed mortar. This critical value is 80 psi (552 kPa). The data are consistent with the formation of cracks in thin-bed mortar joints in AAC shear wall specimens at The University of Texas at Austin (Tanner 2003). Shear wall tests performed at The University of Texas at Austin show if a leveling joint is present, flexural cracking capacity may be controlled by the tensile bond strength across the interface between the AAC and the leveling mortar which is usually less than the modulus of rupture of the AAC material itself.

R8.13.3 – The equation for direct shear strength is based on shear tests performed at the University of Alabama at Birmingham[1] (Argudo 2003).

R8.13.4 – The equation for shear strength of joints is based on direct shear tests performed at The University of Texas at Austin (Tanner 2003). Data on shear strength of joints from The University of Alabama at Birmingham[1] indicate the value for thin-bed mortar is conservative (Argudo 2003).

Chapter 9 — Strength and Serviceability

Add the following:

---

[4] Internal report by Fouad H. Fouad, *Physical and Mechanical Properties of AAC Produced in the United States*, The University of Alabama at Birmingham, August 10, 2002.

R9.3.2.8 — The value of the strength reduction factor reflects the brittle nature of an adhesion failure in an AAC joint.

R9.5.2.1 — The minimum-thickness requirements of Table 9.5(a) of ACI 318-02 can be applied to reinforced AAC elements if the following constraints are applied:

1) Footnote (a) to Table 9.5(a) of ACI 318-02 should be applied. It specifies that for structural lightweight concrete having unit weight in the range 90-120 pcf, the minimum thickness are multiplied by $(1.65 - 0.005w_c)$, where w_c is the unit weight in pcf. The footnote is applicable, because AAC is comparable to lightweight concrete in terms of its flexural stiffness. For the reinforced AAC panels tested at UAB, the corresponding factor from Footnote (a) to Table 9.5(a) is 1.47, making the ratios of calculated to observed deflections all comfortably above unity.

2) Footnote (b) to Table 9.5(a) of ACI 318-02 requires that for f_y other than 60,000 psi, calculated deflection values be multiplied by $(0.4 + f_y/100{,}000)$. This requirement is believed not to apply to AAC, because the bond between smooth wire and AAC differs considerably from the bond between deformed reinforcement and conventional concrete. Also, the specified yield strength of AAC reinforcement (f_y = 80,000 psi) would correspond to a factor of 1.2, which would result in an over-estimate of deflections if the RILEM effective inertia were used.

R9.5.2.2 - The deflection-calculation provisions of Section 9.5.2.2 and 9.5.2.3 of ACI 318-02 can be applied to reinforced AAC elements, with the following modifications:

Short-term deflections should be calculated using an effective flexural stiffness (EI_e) corresponding to the unfactored moment (M_a). The effective flexural stiffness (EI_e) should be obtained by linear interpolation between the cracking point (M_{cr}, ϕ_{cr}) and the yielding points (M_y, ϕ_y) on a bilinear moment-curvature diagram. This procedure is recommended by RILEM [5]. The short-term deflections so obtained should then be multiplied by the factor from Footnote (a) of Table 9.5(a). When this approach is used, calculated deflections are 0.9 to 1.2 times the experimentally observed values.

R9.5.2.5 - For calculation of additional long-term deflections resulting from creep and shrinkage of AAC flexural members, Section 9.5.2.5 of ACI 318-02 is not applicable because the reinforcement ratio for compressive reinforcement (ρ') is generally much smaller for AAC than for reinforced concrete. To calculate total deflections, including long-term deflections, a simplified approach based on RILEM specifications can be adopted. Total deflections can be calculated using an effective modulus of elasticity (E_{AAC}') equal to the modulus of elasticity (E_{AAC}) divided by 1.5.

[5] RILEM Recommended Practice, RILEM Technical Committees 78-MCA and 51-ALC, Section 5.4.1, 1983.

Chapter 10 – Flexure and Axial Loads

Add the following:

R10.2 - Evaluation of AAC panel tests at UAB, confirmed by shear wall tests at UT Austin, shows that the behavior of reinforced AAC elements under combinations of flexure and axial loads can be described by conventional beam theory, using plane sections and an equivalent rectangular compressive stress block.

R10.2.7.3 – The factor β_1 is determined based on stress-strain relationships for AAC tested at the University of Alabama at Birmingham and at The University of Texas at Austin (Argudo 2003).

R10.5.1 - Eq. (10-3) is intended to produce an AAC section whose nominal moment capacity is approximately twice its flexural cracking capacity.

Chapter 11 — Shear and Torsion

Add the following:

R11.3 - For reinforced concrete beams without shear reinforcement, the mean diagonal tensile strength (f_t) can be taken equal to $6\sqrt{f_c'}$ (US customary units). Equation (11-5) of ACI 318-02 uses a nominal unit strength in shear that

decreases from $3.5\sqrt{f_c'}$ for low ratios of shear span to depth, to $1.9\sqrt{f_c'}$ for high ratios. For simplicity, the current Equation (11-3) can be used, with a corresponding unit strength of $2\sqrt{f_c'}$. That unit strength is one-third of the mean diagonal tensile strength.

On that basis, the current Equations (11-3) and (11-4) of ACI 318-02 can be rewritten in terms of the splitting tensile strength (f_t) for use with AAC elements. The corresponding shear capacity (V_{AAC}) is given by the new Eq. (11-3) for members subjected to shear and flexure only, and by the new Eq. (11-4) for members subjected to axial compression as well.

R11.5.6.2 —Under monotonic loading conditions the shear reinforcement is effective. The resistance in the reinforcement comes from bearing of perpendicular reinforcement on surrounding AAC or from dowel action of the reinforcement. Tests at The University of Texas at Austin (Tanner 2003) show that shear reinforcement is not effective in resting shear under reversed cyclic loads due to crushing of the surrounding grout or AAC. Under reversed cyclic loading only deformed bars in grout contribute to the shear strength.

R11.5.6.9 — In traditional reinforced concrete a maximum shear strength of the stirrups is determined based on a truss mechanism. In shear reinforcement in AAC the maximum shear strength of the shear reinforcement is limited by the bearing capacity of the perpendicular reinforcement. This is explained pictorially in Figure E5. If a cut is taken at the center of a stirrup, the available capacity from the top and bottom reinforcement can be determined, Vs^1 and Vs^2, using the following equation $V_s = n_{bars} d_{bars} f'_{AAC} \cdot s$. The number of bars may de

different for As^- and As^+ which would result in different values for Vs^1 and Vs^2; the minimum of these values is the limiting shear strength of the reinforcement.

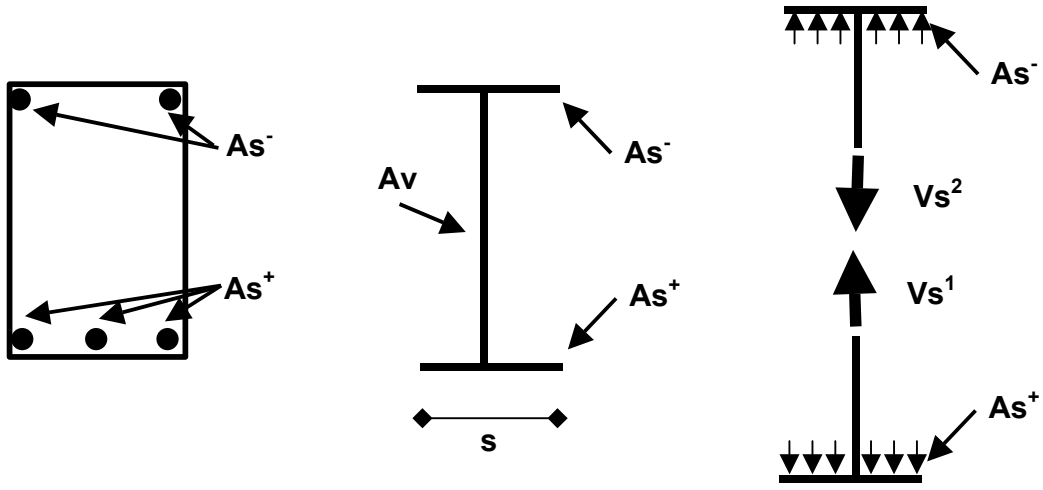

Figure E5 Shear strength in shear reinforcement limited by bearing of the longitudinal reinforcement

11.7 — Shear-friction

R11.7.4.1 — Sliding shear resistance is the product of the coefficient of friction across an interface, and the force acting perpendicular to that interface. This mechanism is referred to in ACI 318 as "shear friction." This resistance can come from reinforcement crossing the interface and applied axial load.

In the traditional shear friction mechanism, sliding over a rough joint causes one section of the crack to lift upwards; this results in yielding of the vertical reinforcement, which provides additional clamping force. Under reversed cyclic loading of AAC, the roughness of the bed joints can decrease, and resistance to sliding shear is provided by dowel action of reinforcement crossing the bed joints. Sliding was observed in shear wall tests at UT Austin (Tanner 2003). Vertical reinforcement contributed significantly to the capacity for several cycles until the onset of local crushing and spalling of the grout in the cells surrounding that reinforcement. Therefore, for reversed cyclic loading, the shear friction resistance mechanism is limited to resistance provided due to axial load. The nominal sliding shear capacity should be based on the frictional capacity consistent with the total force on the compressive stress block required to equilibrate the tensile force in the tensile reinforcement at a given cross-section.

At an unbonded interface the calculated sliding shear resistance should be based on friction only. At an interface where thin-bed mortar is present, the nominal sliding shear capacity should be based on the greater of the capacity based on initial adhesion, and the frictional capacity after that adhesion is overcome. At an interface where leveling-bed mortar is present, the interface is probably cracked due to in-plane flexure, and initial adhesion should not be counted on.

R11.7.4.3 — The coefficient of friction μ in Eq. (11-25) and Eq. (11-26) should be 1.0 between AAC and leveling bed mortar and 0.75 between AAC and AAC. Direct shear tests performed at The University of Texas at Austin (Tanner 2003) determined a coefficient of friction, μ between AAC and AAC. The average coefficient of friction was 0.85 with a 10% lower fractile of 0.76. Based

on this data the ACI 318-02 value of $\mu=1.0\lambda$, with $\lambda=0.75$ for lightweight concrete is nearly a 10 % lower fractile. Since all AAC is lightweight concrete, λ is included in the design coefficient of friction for AAC.

R11.8.1 — Provisions on the use of AAC in deep beams have not been developed to date.

R11.10 —

R11.10.1 — Design for shear in out-of-plane loading cases is based on beam design for one-way slabs. Beam design is based on out-of-plane loading of individual floor panels.

R 11.5.6 - Shear strength provided by shear reinforcement (V_s) can be calculated using Section 11.5 of ACI 318-02, with the following qualifications:

a) Vertical or inclined wires designed to provide shear strength need to be welded to the longitudinal reinforcement; and

b) The maximum usable shear strength provided by each shear reinforcement bar (Vs_b) is limited by the bearing capacity of the AAC on the longitudinal reinforcement.

The nominal shear capacity (V_n) is equal to the sum of the nominal shear capacity of AAC (V_{AAC}) and the shear strength provided by the shear

reinforcement (V_s). The design shear capacity (ϕV_n) is obtained by multiplying the nominal shear capacity V_n by the appropriate capacity-reduction factor.

R11.10.6 — Shear strength of AAC shear walls may be limited by web-shear cracking, crushing of the diagonal strut and sliding shear. A suite of 14 shear wall specimens was tested at The University of Texas at Austin (Tanner 2003, Varela 2003), and the results of those tests were combined with results from 12 shear wall specimens tested at Hebel Germany[6]. The equation for web-shear cracking addresses the cases of mortared head joints and unmortared head joints. Each equation is verified by 11 or 9 tests, respectively, performed on the shear-dominated shear wall specimens. The aspect ratios of the specimens ranged from 0.6 to 3. Crushing of the diagonal strut was based on the observed response of Shear Wall Specimen 1 performed at The University of Texas at Austin (Tanner 2003). The equation was confirmed as an upper bound based on the results of the remaining 8 tests performed on walls with aspect ratios less than 1.5. Flexure-shear cracking was observed in the 6 flexure-dominated specimens. In each wall, after the formation of a flexure-shear crack at least one load cycle was performed without an associated decrease in strength or stiffness. In addition, the flexural reinforcement provided additional strength in the wall. If design requirements for flexure-shear cracking are eliminated, the design provisions of Section 11.10.7 are no longer required. They are replaced by special provisions for shear walls constructed with panels oriented vertically.

[6] Personal communication, Violandi Vratsanou, Hebel AG, Germany, November 2000.

R11.10.7 — Special provisions for shear walls with AAC panels oriented vertically – Tests conducted at The University of Texas at Austin (Tanner 2003) showed that vertical cracks formed at the head joints in shear wall specimens with vertically oriented panels (Tanner 2003, Varela 2003). If these cracks formed in a specimen, they were limited to every third joint when following the construction techniques presented in Section5.7.4. If vertical cracks are present, the strength and stiffness of an AAC shear wall will decrease and the behavior will be different, which must be considered in design. As the aspect ratio of an individual panel exceeds 3 the cracks will be governed by beam shear, rather than the equation for walls and Equation (11-3) should be used instead of Equation (11-29).

R11.10.8 — Based on the shear wall specimens tested at The University of Texas at Austin and Hebel Germany the behavior of a shear wall can be predicted. Since the behavior can be predicted additional shear reinforcement is not required. Additional shear reinforcement, in the form of welded wire fabric in panels is not effective under reversed cyclic loads. Deformed bars embedded in grout or reinforced concrete are the only shear reinforcement effective under reversed cyclic loads.

R11.10.9 — Design of shear reinforcement for walls

R11.10.9.2 through R11.10.9.5 Tests performed at The University of Texas at Austin show that the shear behavior of walls can be predicted satisfactorily (Tanner 2003, Varela 2003). In addition, flexural behavior can be achieved with vertical reinforcement concentrated at the ends. If shear behavior

can be avoided and flexural behavior is ensured, the prescriptive reinforcements can be relaxed.

Chapter 12 — Bond and Development Length

Add the following:

R12.1 - Bond and development requirements for deformed reinforcement in grout are identical to those used for concrete or masonry construction. Given the small sizes of deformed bars used in AAC construction, bond between the grout and the AAC itself does not govern the bond capacity.

Bond and development requirements for welded-wire fabric embedded in AAC are quite different from those for conventional concrete, however. Because the welded-wire fabric has a corrosion-resistant coating, bond strength between the coated wire and the AAC itself is negligible. Bond strength comes from bearing of the cross wires against the AAC. For typical cross-wire spacings, local crushing of the AAC under the cross wires can be assumed to redistribute the bearing stresses under the cross wires, leading to a uniform bearing strength of f_{AAC}' under every cross-wire. Multiplying this stress by the number of cross wires and by the bearing area of each cross-wire gives the maximum force that can be developed in the welded wire fabric (Figure E6).

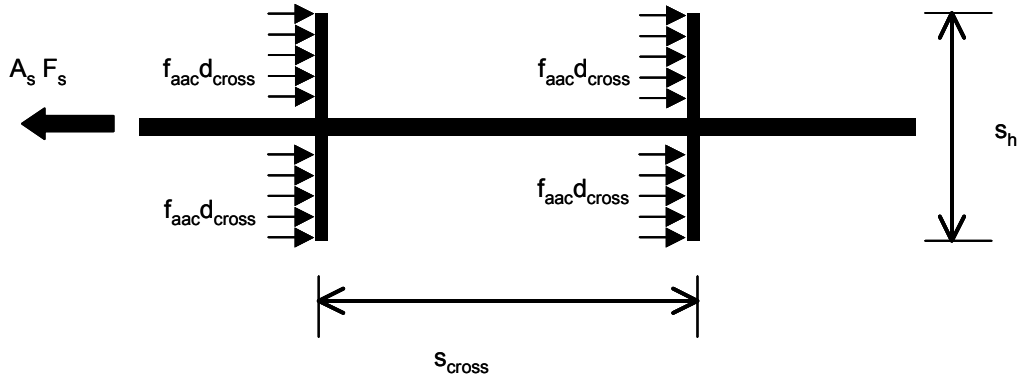

Figure E6 Bond mechanism of welded-wire mesh in AAC

This maximum force in the welded-wire mesh can limit the flexural capacity of a reinforced AAC panel.

R12.1.3 – Splitting of AAC around vertical reinforcement in a grouted cell was observed in shear wall specimens tested at The University of Texas at Austin (Tanner 2003). This splitting occurred in cells with ratios of reinforcement to area of grouted cells of 4.5%. Splitting was not observed in shear walls with a ratio of reinforcement to area of grouted cells of 3%.

A reinforcement-to-core area ratio as high as 4.5% (equivalent to a No. 5 bar in a 3-in. grouted core) is acceptable provided that the bar remains elastic and an analysis to determine the acting splitting tensile stress due to radial stresses of the reinforcement is performed. This value is compared to the splitting tensile strength of the grout.

R12.1.4 – Splices are not permitted at locations of potential plastic hinges due to the possibility of increasing the design strength at that location. In

addition, the probability of vertical cracks forming due to splitting is increased at the location of a splice.

R12.20.2 – The minimum number of cross-wires is intended to prevent an anchorage failure in AAC panels (Argudo 2003). Eq. (12-5) prescribes the required number of cross-wires in a distance a, the length of the panel divided by 6. Beyond this distance the twice the maximum spacing prescribed by Eq. (12-4).

Delete Chapter 13

Add the following:

R13.1 - The deletion of Chapter 13 essentially means that AAC slabs are designed as one-way slabs.

Chapter 14 — Walls

Add the following:

R14.3 - Tests performed at the University of Texas at Austin (Tanner 2003, Varela 2003) show that walls with reinforcement concentrated at the ends

performed satisfactorily and the maximum horizontal and vertical spacing requirements can be relaxed.

R14.3.7 — Using a No. 5 bars around window openings may cause cracks parallel to the direction of the reinforcement or other local damage if the reinforcement yields. No. 4 bars will resist cracks formed around the openings and reduce the damage if the reinforcement yields.

Delete Chapter 15.

Chapter 16 — Precast concrete

Add the following:

R16.2.3 - Tolerances for AAC elements are specified in ASTM C 1452.

R16.5.1.2 — In general, floor diaphragms composed of AAC elements are not topped. General structural integrity provisions for this type of construction were verified in the seismic testing of a Two-story AAC Assemblage Specimen at the University of Texas at Austin (Tanner 2003, Varela 2003). The assemblage was designed using the vertical tension ties, transverse tension ties and longitudinal tension ties of Section 7.13.3. The continuous steel (chord) perpendicular to the orientation of lateral load provides reinforcement for in-plane flexural resistance of the diaphragm. Sections 16.5.1.2 through 16.5.1.4 present design options to transfer shear from the diaphragm to the AAC shear walls.

R16.5.1.2.2 — Lateral load was successfully transferred through adhesion in the Two-story Assemblage Specimen (Tanner 2003, Varela 2003). Since adhesion failure is brittle, a strength reduction factor of 0.67 is used. The shear strength of a joint was determined based on direct shear tests performed on joints

between thin-bed mortar and AAC and grout and AAC (Tanner 2003). The values presented in Section 8.13.4 represent lower 7% fractiles of these tests.

R16.5.1.2.3 — A secondary resistance mechanism exists in which the entire floor diaphragm system acts like a truss: the bond beam compromises the tension and compression chords; the reinforcement between floor panels and in the bond beam parallel to the panels connect to the chords; and the panels themselves act as compression diagonals (Figure D2). The shear strength of AAC diaphragms with panels oriented parallel to the direction of loading can be checked using a truss mechanism.

R16.5.1.2.3.1 — Compression struts are not allowed to cross panel joints, since the effect of joint cracks on the strength of AAC compression struts is unknown.

R16.5.1.2.3.2 — The reinforcement in the grouted keys is anchored into the bond beam using a vertically oriented hook that extends beyond the bond beam reinforcement. This mechanical connection enhances the in-plane integrity of the horizontal diaphragm (Figure D3). The truss model assumes uniform tension in the reinforcement. This assumption is valid even with damage at joints.

R16.5.1.2.3.3 — The area of the compression strut is 6 in. in the plane of the panel, multiplied by the panel thickness.

R16.5.1.2.3.4 — The strength of tie elements (reinforcement in grouted keys or bond beams) is calculated as the cross-sectional area of the longitudinal reinforcement in those elements, multiplied by the specified yield strength of the reinforcement.

R16.5.1.2.4 — The nominal shear strength of an AAC diaphragm with panels oriented perpendicular to the direction of loading can be generated through dowel action in the reinforcement. The available resistance of an AAC

diaphragm can also be determined by the transfer of load through shear in the reinforcement, which is computed by $0.6f_yA_s$.

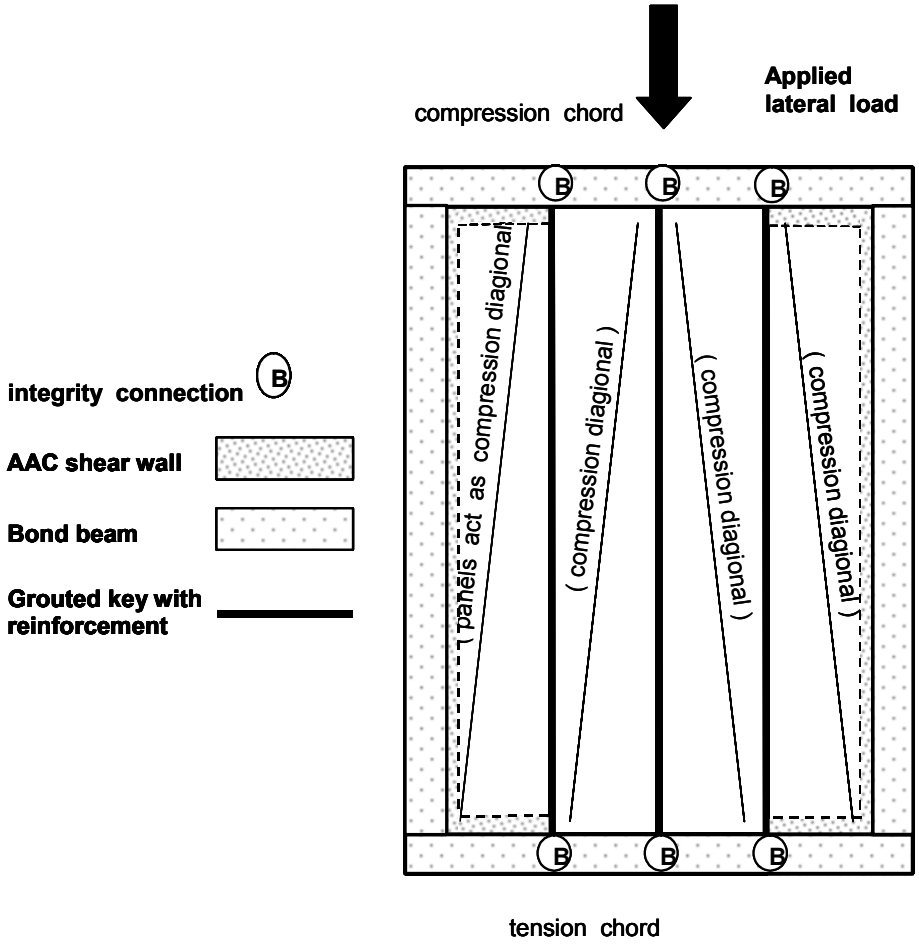

Figure E7: Truss mechanism in an AAC floor or roof diaphragm

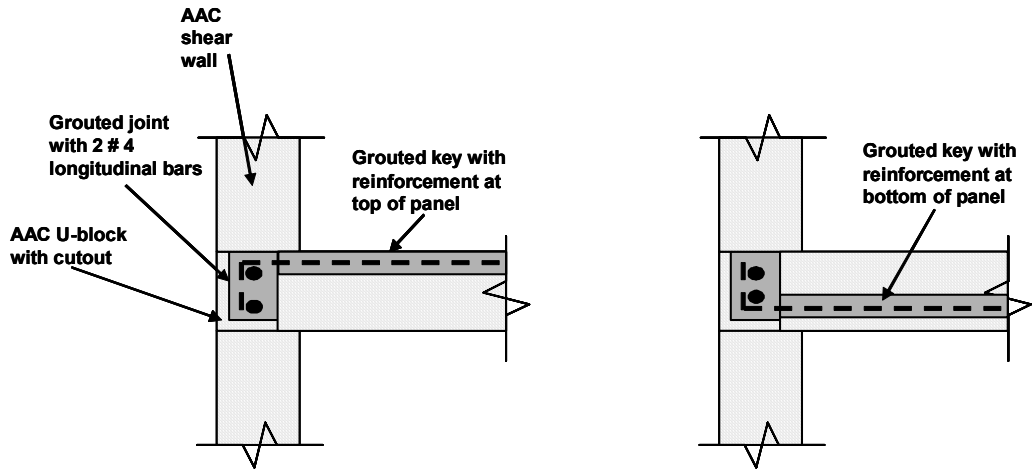

Figure E8: Detail of grouted key reinforcement with 90˚ hook oriented vertically and hooked around the bond beam reinforcement

R16.5.1.3 — Current construction practices using thin-bed mortar offer limited ways to place horizontal reinforcement between units. Tests performed at the University of Texas at Austin (Tanner 2003, Varela 2003) show that walls with horizontal and vertical reinforcement concentrated at the ends performed satisfactorily, and suggest that traditional horizontal and vertical spacing requirements for reinforcement in conventional masonry elements can be relaxed for AAC elements. If the longitudinal reinforcement is sufficient to resist the factored design load in a shear wall, the longitudinal reinforcement need only be continuous at the section between shear walls.

R16.5.1.4 — Connections between shear walls in stories depends on sliding shear resistance. Tests performed on shear walls at The University of Texas at Austin (Tanner 2003) indicate that sliding shear resistance can be accurately predicted based on frictional resistance.

R16.5.2.1 — These longitudinal ties are intended to support the diaphragm in the event a supporting bearing wall is removed from the structure.

The ties are shown in Figure E46; the effect of loosing an interior wall is shown in Figure E47. Since the mechanism will only form in the direction parallel to the direction the slab is spanning, they are not required perpendicular to the direction of a slab.

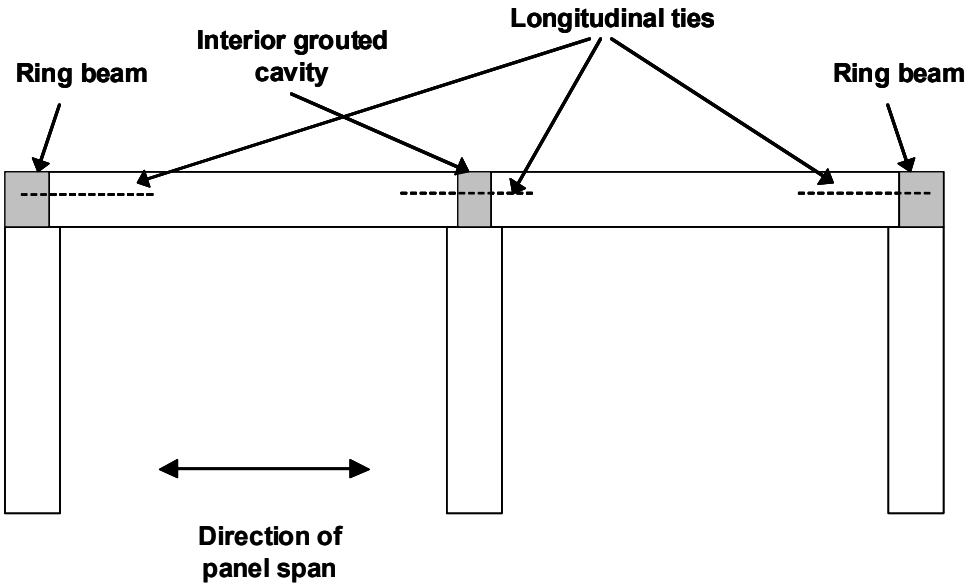

Figure E9: Elevation of two exterior shear walls and one interior shear wall with two interior panels connected by longitudinal ties

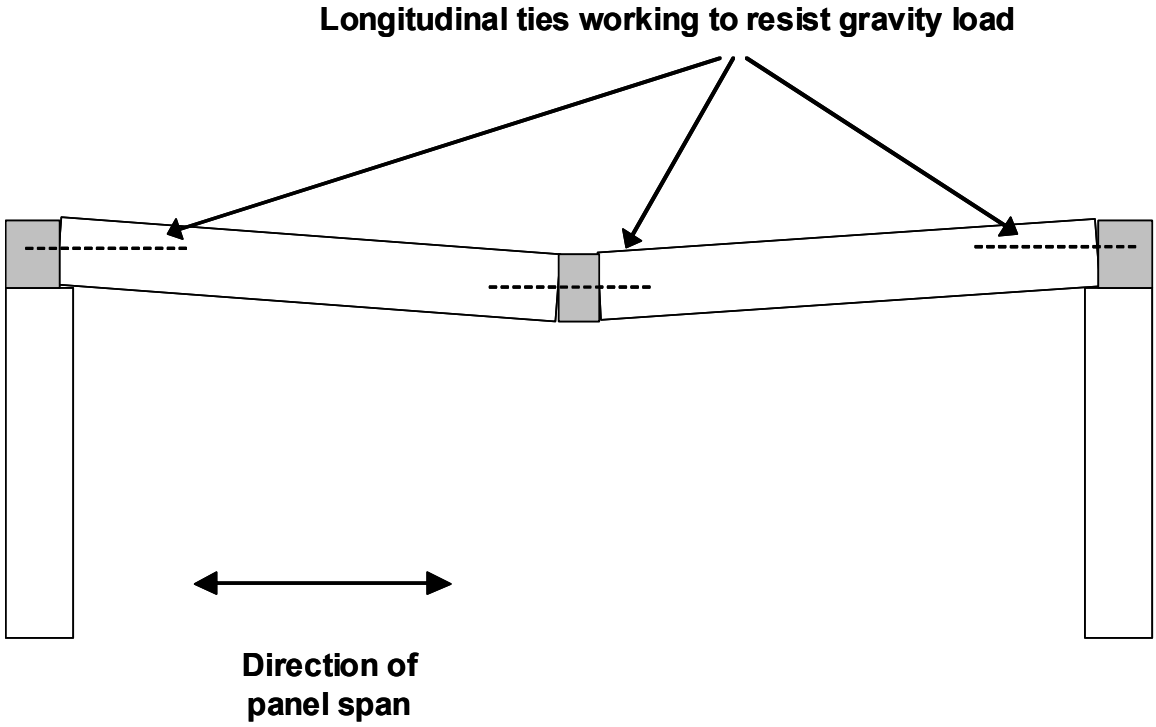

Figure E10: Elevation of shear walls with interior bearing wall missing and longitudinal ties serving as reinforcement

R16.6.2 - Bearing must be checked wherever AAC floor or roof panels rest on AAC walls. An example of the critical section to be used in this calculation is shown in Figure D1. The Two-story Assemblage Specimen tested

at The University of Texas at Austin (Tanner 2003, Varela 2003) performed satisfactorily with an average bearing length of 2 in. The minimum bearing length was 1.75 for any given panel.

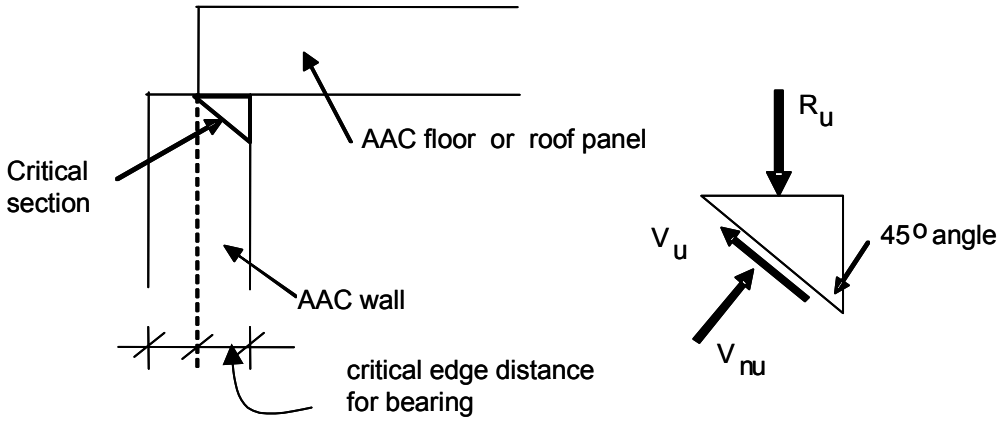

Figure E11 Critical section at bearing of AAC floor or roof panel on AAC wall

Chapter 21 — Special Provisions for Seismic Design

Add the following:

R21.14.2 – In order to ensure the failure of an AAC member is not governed by shear the design shear force is based on the design flexural capacity multiplied by an overstrength factor of 1.25.

R21.14.3 – Design through adhesion is a brittle failure mechanism and therefore not permitted in regions of moderate seismic risk.

R21.15.3 – Additional connectors are provided to ensure a ductile failure at the diaphragm AAC joint.

APPENDIX F:
DESIGN EXAMPLES

This Appendix includes design examples based on the proposed code provisions. The examples include an AAC multi-story shear wall and diaphragm subject to in-plane loads along with an AAC shear wall subject to in-plane loads. The design examples are consistent with the proposed design provisions for the Masonry Standards Joint Committee. The design procedure will not change based on the proposed ACI 3xx design provisions; the only modification is to the strength reduction factors.

The loads represent factored loads on the structure. It is assumed that these loads correspond to the critical load combination.

DESIGN AND AAC SHEAR WALL

Design the above two-story AAC shear wall. Assume the following material properties, factored loads, and geometry.

PAAC-5

$f'_{AAC} = 580$ psi

fy = 60,000 psi (flexural reinforcement)

E_s = 29,000 Ksi

Factored axial load at each story, P_u = 35,000 lbs

Factored lateral load at each story, F_u = 18,000 lbs

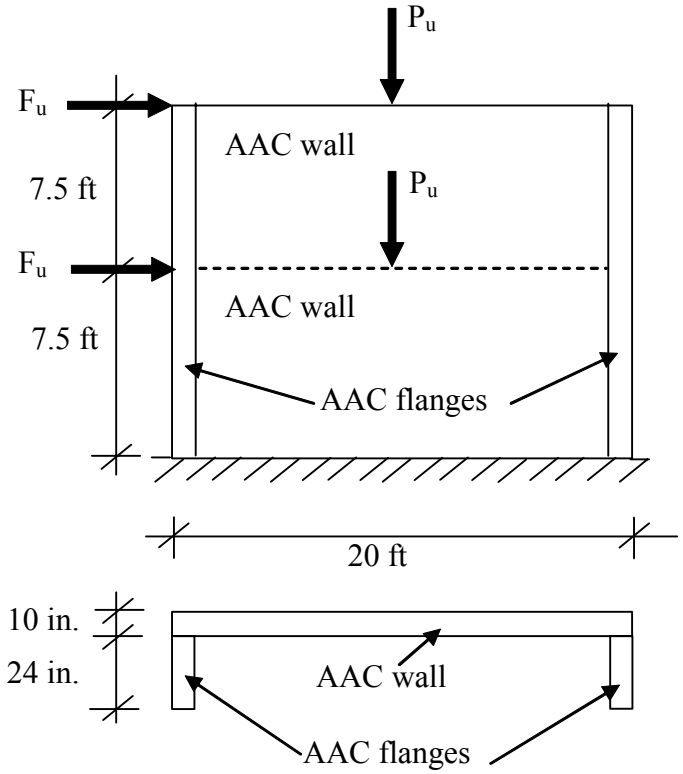

FLEXURAL CAPACITY

a) Determine factored bending moment at the base of the wall.

$$M_u = 18{,}000\,(15)(12) + 18{,}000\,(7.5)(12) = 4{,}860{,}000\,lbs - in.$$

b) Determine flexural capacity at the base of the wall.

Assume flexural reinforcement at wall ends only, equal to 1 # 4 bar, located 24 in. from the wall ends.

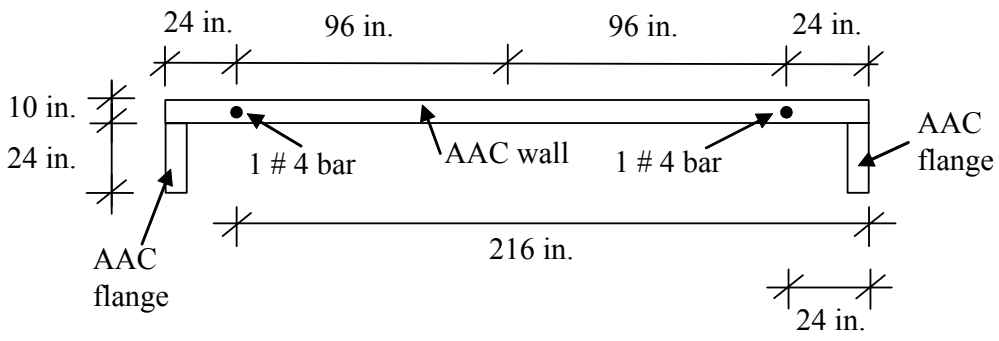

Calculate forces in bars (T_1 and T_2) assuming that both bars are yielding.

$T_1 = T_2 = A_s f_y = 0.2\ (60{,}000) = 12{,}000$ lbs

For equilibrium:

$C = N_u + T_1 + T_2$

$N_u = 2\ (P_u) = 35{,}000 + 35{,}000 = 70{,}000$ lbs

$C = 0.85\ f'_{AAC}\ a\ b$

$$a = \frac{C}{0.85\ f'_{AAC}\ \text{b}} = \frac{70{,}000 + 12{,}000\ (2)}{0.85\ (580)\ (10 + 24)} = 5.6\ in.$$

$$M_n = 12{,}000\left(216 - \frac{240}{2}\right) - 12{,}000\left(\frac{240}{2} - 24\right) + 94{,}000\left(\frac{240 - 5.6}{2}\right) = 11{,}020{,}000\ lbs$$

$$\phi M_n = 0.9\,(11{,}020{,}000) = 9{,}900{,}000\ lbs$$

$\phi M_n = 9{,}900{,}000$ lbs-in. > $M_u = 4{,}860{,}000$ OK

Check if right bar (T_2) is yielding.

$$c = \frac{a}{\beta_1} = \frac{5.6}{0.67} = 8.4 \text{ in.}$$

$$\varepsilon_2 = \frac{24}{8.4}\left(\varepsilon_{AAC}\right) = \frac{24}{8.4}\left(0.003\right) = 0.0086$$

$$\varepsilon_y = \frac{f_y}{E_s} = \frac{60{,}000}{29{,}000{,}000} = 0.0021$$

$\varepsilon_2 = 0.086 > \varepsilon_y = 0.0021$ OK

SHEAR CAPACITY

a) Determine factored shear force and axial force at the base of the wall.

$$V_u = 2\,F_u = 2\,(18{,}000) = 36{,}000\ lbs$$

$$N = 70{,}000\ lbs$$

b) Determine shear capacity at the base of the wall (web-shear cracking).

$$\phi V_{AAC} = \phi\, 0.9\, t\, l_w \sqrt{f'_{AAC}} \sqrt{1 + \frac{N_u}{2.4\sqrt{f'_{AAC}}\, t\, l_w}}$$

$$\phi V_{AAC} = 0.8\,(0.9)(10)(240)\sqrt{580} \sqrt{1 + \frac{70{,}000}{2.4\sqrt{580}\,(10)(240)}} = 51{,}040\ lbs$$

ϕV_{AAC} = 51,040 lbs > V_u = 36,000 lbs OK

c) Determine factored shear force an axial force at 7.5 ft from the base of the wall.

$$V_u = F_u = 18{,}000\, lbs$$

$$P_u = \mathrm{N}_u = 35{,}000\, lbs$$

d) Determine shear capacity at 7.5 ft from the base of the wall (web-shear cracking).

$$\phi V_{AAC} = 0.8\,(0.9)(10)(240)\sqrt{580} \sqrt{1 + \frac{35{,}000}{2.4\sqrt{580}\,(10)(240)}} = 46{,}600\ lbs$$

ϕV_{AAC} = 46,600 lbs > V_u 18,000 lbs OK

e) Determine shear capacity of bottom wall (crushing of the diagonal strut).

$$\phi V_{AAC} = 0.8$$

$$(0.9)\, f'_{AAC}\, t\, w_{strut}\, \frac{h\left(\frac{3 l_w}{4}\right)}{h^2 + \left(\frac{3 l_w}{4}\right)^2}$$

$$w_{strut} = \frac{l_w}{4} = \frac{240}{4} = 60 \text{ in}$$

$$\phi V_{AAC} = 0.8\,(0.9)(725)(10)(60)\, \frac{90\left(\frac{3(240)}{4}\right)}{90^2 + \left(\frac{3(240)}{4}\right)^2} = 125{,}300 \text{ lbs}$$

ϕV_{AAC} = 125,300 lbs > V_u 36,000 lbs OK

f) Determine sliding shear capacity of bottom wall and a thin-bed mortar joint

μ = 1 at a leveling bed joint

$$\phi V_{ss} = \phi\,(\mu N)$$

Neglect additional force in tensile steel.

$\phi V_{ss} = 0.75\left(\left(1\right)\left(70{,}000\right)\right) = 52{,}500\ lbs$

ϕV_{ss} = 52,500 lbs > V_u = 36,000 lbs OK

μ = 0.75 at a leveling bed joint

$\phi V_{ss} = \phi\left(\mu\ N_u\right)$

Neglect additional force in tensile steel.

$\phi V_{ss} = 0.75\left(\left(0.75\right)\left(70{,}000\right)\right) = 39{,}375\ lbs$

ϕV_{ss} = 39,375 lbs > V_u = 36,000 lbs OK

g) Check MSJC Section 8.1.3

The design shear strength, ϕV_n, shall exceed the shear corresponding to the development of 1.25 times the nominal flexural strength (M_n) of the member, except that the nominal shear strength (V_n) need not exceed 2.5 times required shear strength (V_u).

M_n = 11,020,000 lbs-in.

1.25M_n = 13,800,000 lbs-in.

Check the design shear corresponding to 1.25M_n (1.25V_{Mn}). Divide by the ratio of moment to shear, M_u/V_u= 4,860,000/18,000=270

$$1.25V_{Mn} = \frac{1.25M_n}{M_u / V_u} = \frac{13{,}800{,}000}{270} = 51{,}100\,lbs$$

This value is nearly equal to the shear capacity of the wall.

$\phi V_{AAC} = 51{,}040$ lbs $\approx 1.25V_{Mn} = 51{,}100$

Since sliding shear is not a brittle failure mode it does not have to exceed the nominal flexural capacity multiplied by the overstrength factor.

Wall-panel connection, shear force on critical section

Assume the following material properties, uniform loads, and geometry for simply supported AAC floor panel.

Floor panels PAAC-4

$f'_{AAC} = 580$ psi

Dead load, $w_d = 80$ psf

Live load, $w_l = 40$ psf

Density of PAAC-4, 45 lbs / ft^3

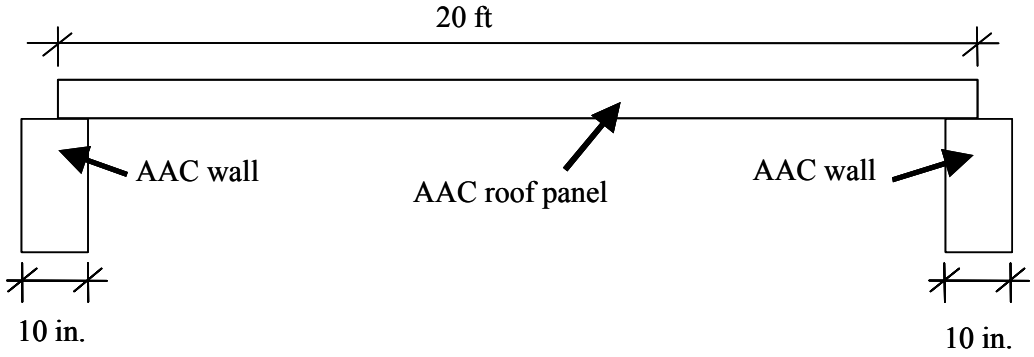

a) Determine factored loads and maximum shear force.

$w_u = 1.2\ (80) + 1.6\ (40) = 160$ psf

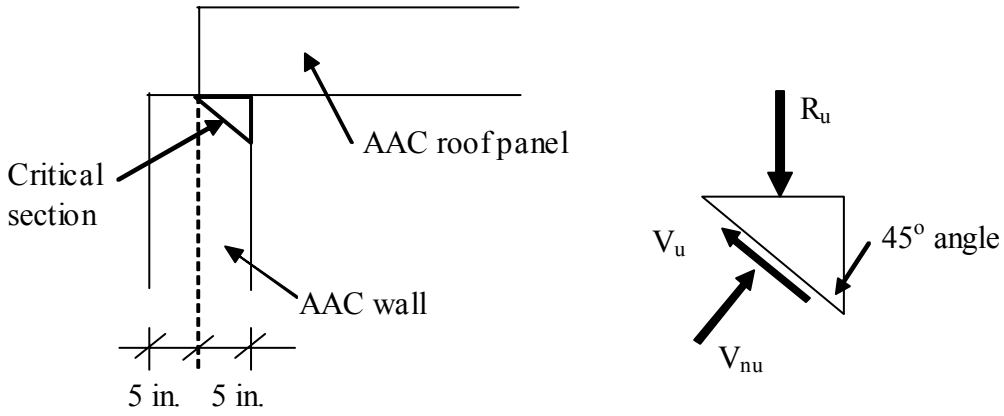

b) Determine vertical reaction on wall in a 1 in. strip using factored loads.

$$R_u = \frac{w_u}{12}\frac{L}{2}\frac{1}{12} = \frac{160}{12}\frac{240}{2}\frac{1}{12} = 133.3\ \frac{\text{lbs}}{\text{in.}}$$

$$V_u = \frac{R_u\sqrt{2}}{2} = \frac{133.3\sqrt{2}}{2} = 94.2\ \frac{\text{lbs}}{\text{in.}}$$

c) Determine shear capacity

$$f_v = 0.15\, f'_{AAC} = 0.15(580) = 87 \text{ psi}$$

$$\phi V_n = \phi\, f_v\, A_d = 0.8(58)\sqrt{5^2 + 5^2}\,(1) = 490 \frac{lbs}{\text{in.}}$$

$$\phi V_n = 490 \frac{lbs}{\text{in.}} > V_u = 94.2 \frac{lbs}{\text{in.}} \qquad \text{OK}$$

DESIGN AN AAC DIAPHRAGM

Design the AAC diaphragm. Assume the following material properties, factored loads, and geometry.

PAAC-5

$f'_{AAC} = 580$ psi

$f'_{grout} = 3000$ psi

fy = 60,000 psi

Factored lateral load at each story, $F_u = 18{,}000$ lbs

Ring beam reinforcement 2 #5

Grouted key reinforcement 1 #5

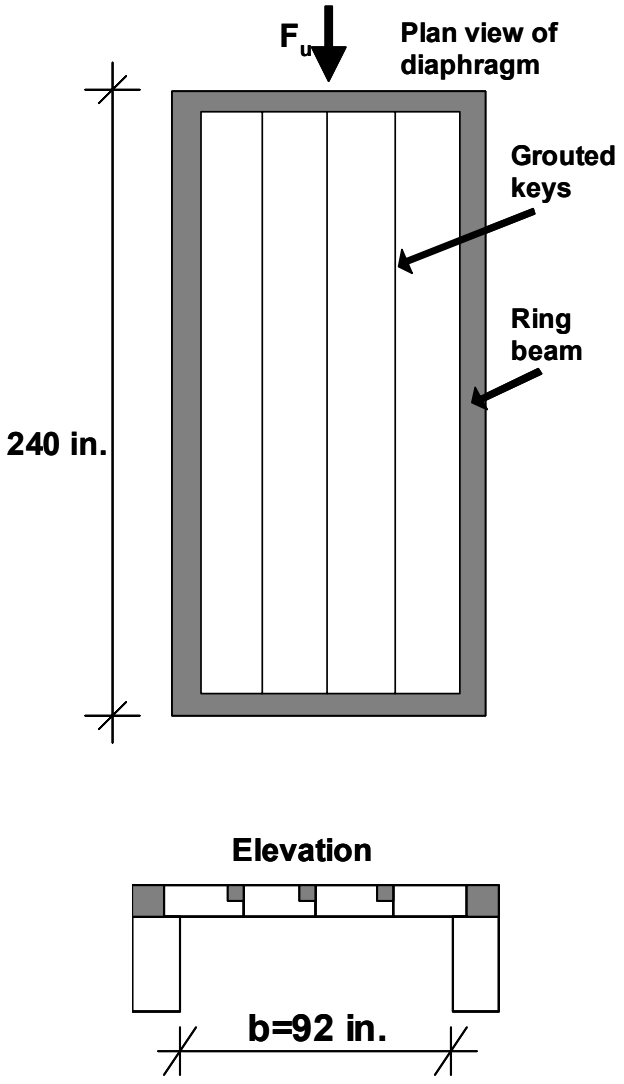

a) Design diaphragm for flexure

$M = \frac{F_u l}{4} = \frac{18000 \cdot 92}{4} = 414{,}000 lbin$
$T = A_s f_y = 2 \cdot 0.2 \cdot 60000 = 24{,}000 lb$

$a = \frac{C}{0.85\, f'_{grout}\, \mathrm{b}} = \frac{24{,}000}{0.85\,(3000)\,(92)} = 0.1\,in.$
D = length of key – ring beam/2 – 2U-block thickness = 240 – 4 - 4
$M_n = A_s f_y \cdot (d - \frac{a}{2}) = 5518000 lbin$ > M_{reqd}=414,00 lbin OK

b) Design diaphragm for shear based on adhesion

i) Panel to panel joint

Section D - D

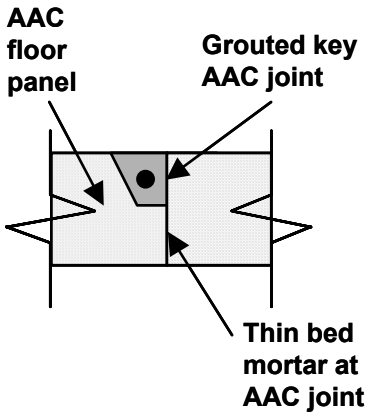

The total resistance is the adhesion of the grouted area plus the adhesion of the thin-bed mortar area.

b_{grout} = 5 in.

$b_{thin\text{-}bed}$ = 3 in.

$V_{grout} = \tau_{grout} \cdot b_{grout} \cdot l = 36 \cdot 5 \cdot 240 = 43{,}200lb$
$V_{thin-bed} = \tau_{thin-bed} \cdot b_{thin-bed} \cdot l = 18 \cdot 3 \cdot 240 = 13{,}000lb$
$V_{total} = V_{grout} + V_{thin-bed} = 55{,}200lbs$
$\phi V_{total} = 0.67 \cdot 55{,}200 = 36{,}980lbs > \frac{F_u}{2} = 9{,}000lbs$

ii) Panel bond beam joint

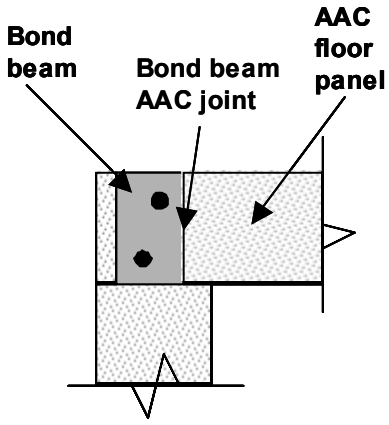

b_{grout}= 8 in.

$V_{grout} = \tau_{grout} \cdot b_{grout} \cdot l = 36 \cdot 8 \cdot 240 = 69{,}100lbs$
$\phi V_{total} = 0.67 \cdot 69{,}100 = 46{,}300lbs > \frac{F_u}{2} = 9{,}000lbs$

c) Design diaphragm for shear based on truss model

One # 5 bar in each grouted key

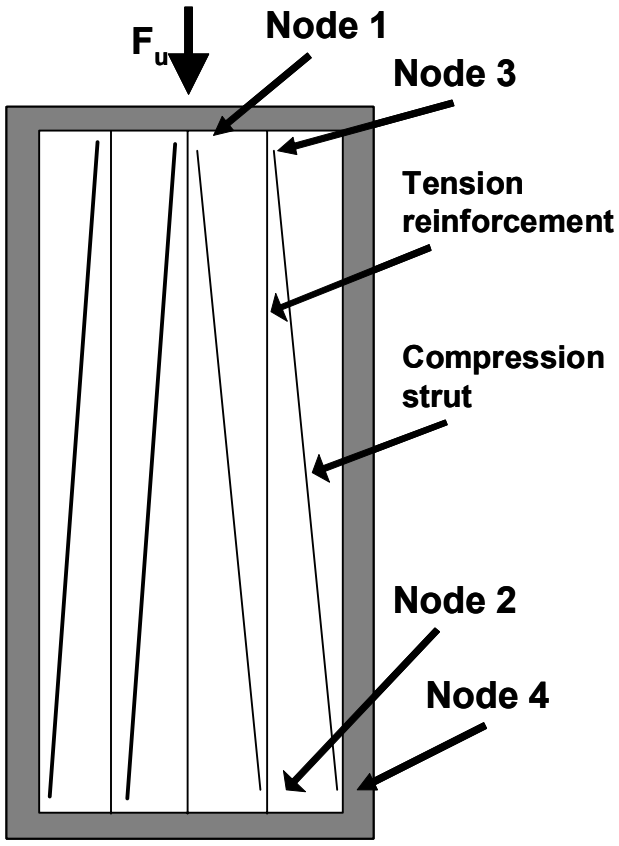

In this model the compression chords act as diagonal compression members.

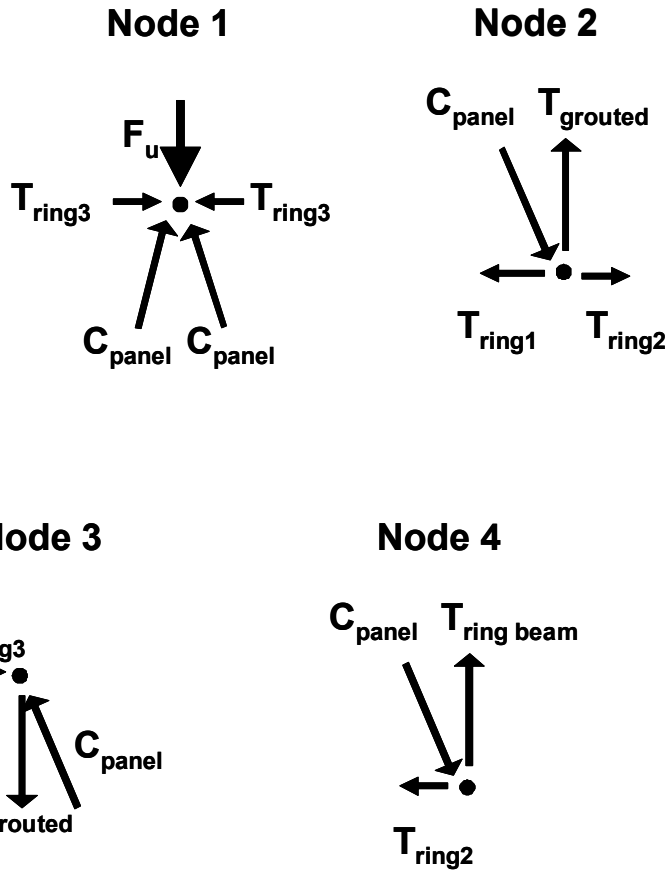

Based on equilibrium

Cpanel = 9,456 lbs

Tgrouted key = 9,000 lbs

Tring1 = 1800 lbs

Tring2 = 900 lbs

Tring3 = 900 lbs

Tring beam = 9,000 lbs

Check capacity of strut tie and ring beam tie

Compression strut capacity

Wstrut = 6 in.

Tpanel = 8 in.

Fstrut = 9,456/48 = 197 psi < $0.75(0.85f'_{AAC})$=0.75(0.85)(580)= 370 psi OK

Check capacity of tension tie in grouted cell

Tgrouted key = 9,000 lb < ϕAsfy=0.75*0.31*60,000=14,000 lb OK

Reinforcement ratio percentage of 3% required by Section 8.2.3.1 does not apply to this case.

If tension tie in grouted cell is sufficient the remaining tension ties will also be sufficient, because the provided area of steel is larger.

DESIGN AN AAC SHEAR WALL FOR OUT-OF-PLANE LOADS

PAAC-5

$f'_{AAC} = 580$ psi

fy = 60,000 psi (flexural reinforcement)

E_s = 29,000 ksi

Factored wind load on wall ρ_u = 110 lbs/ft^2

Reinforcement in a 3 in. grouted cell at 4 ft. on center

h=10 ft

t=10 in.

Plan view of 4 ft. section of wall

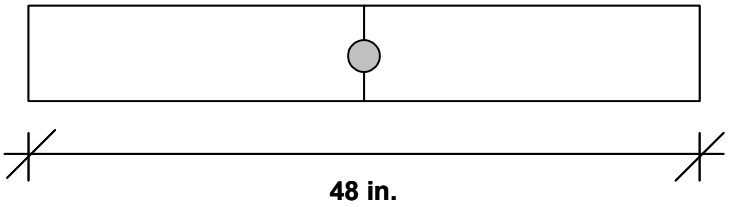

Elevation of shear wall simply supported at top and bottom

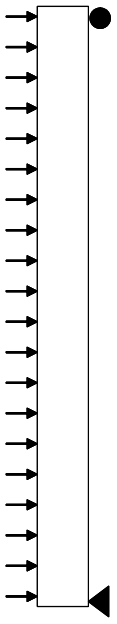

Flexural capacity

a) Determine acting moment

$$w_u = \rho \cdot \text{width} = 110\,\text{lb/ft}^2 \cdot 4\text{ft} = 440\,lb/ft$$

$$M_u = \frac{wl^2}{8} = \frac{440 \cdot (10)^2}{8} = 5{,}500\, lb - ft = 66{,}000 lb - in.$$

b) Try #4 bar

$$T = A_s f_y = 0.2 \cdot 60{,}000 = 12{,}000\, lb$$

$$a = \frac{T}{0.85 f_{AAC}' b} = \frac{12{,}000}{0.85 \cdot 580 \cdot 48} = 0.5 in$$

$$M_n = A_s \cdot f_y \cdot (d - \frac{a}{2}) = 12 \cdot (5 - \frac{0.5}{2}) = 57{,}000 \text{ lb - in}$$

ϕMn=0.9*57,000 lb-in=51,300 lb-in.<Mu N.G.

Try #5 bar

$$T = A_s f_y = 0.31 \cdot 60{,}000 = 18{,}600\, lb$$

$$a = \frac{T}{0.85 f_{AAC}' b} = \frac{18{,}600}{0.85 \cdot 580 \cdot 48} = 0.8 in$$

$$M_n = A_s \cdot f_y \cdot (d - \frac{a}{2}) = 18.6 \cdot (5 - \frac{0.8}{2}) = 85{,}700 \text{ lb - in}$$

ϕMn=0.9*85,700 lb-in= 77,130 lb-in.>Mu O.K.

Check strain limits for this case:

c=a/β1=0.8/0.67=1.2

d=5

εs=0.003*(d-c)/c=0.0095>1.3ε_y=1.3*1.25*fy/Es=0.0033

Use a #5 bar

$A_{steel}/A_{grout}=0.31/7.1=0.044=4.4\%>3\%$

Perform an analysis to check the bond stress. In the case of out-of-plane loads the reinforcement in the wall does not yield and no plastic hinge forms. In this example, the classical bond stress analysis shown in the example can be used.

c) Check bond stress

Determine if reinforcement is yielding:

$\phi Mn=0.9*85{,}700$ lb-in= 77,130 lb-in.>Mu=66,000 lb-in, reinforcement will not be yielding. Since reinforcement will not be yielding consider case where bond remains in tact and express bond stress as a function of shear.

Determine shear and bond stress along the length of the wall. Based on the bond stress determine the splitting tensile stress in the wall and compare to the splitting tensile strength of the grout.

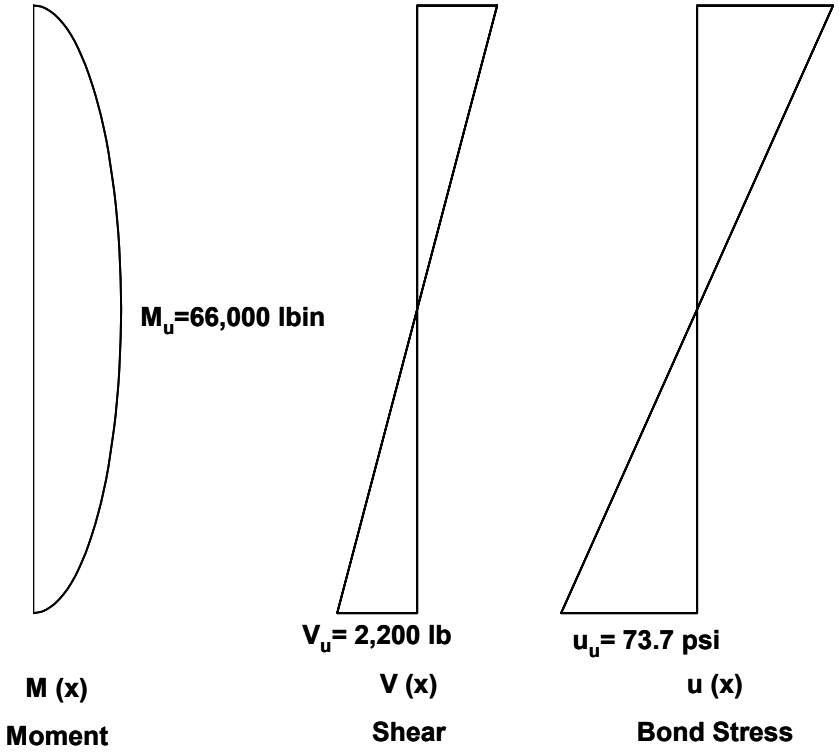

$$V_u = \frac{440 \cdot 10}{2} = 2200 lbs$$

$$u_u = \frac{V}{arm \cdot \pi d_{bar}} = \frac{2200}{0.8 \cdot 5 \cdot \pi \cdot 0.625} = 280 psi$$

$$f_{treqd} = \frac{u d_{bar}}{(d_{core} - d_{bar})} = \frac{280 \cdot 0.625}{(3 - 0.625)} = 73.7 psi$$

$$f_{tavailable} = 4\sqrt{f_g} = 4\sqrt{3000} = 219 psi$$

The factored bond stress u_u is less than the factored tensile strength available. Use ϕ=0.8 which corresponds to shear.

$u_u = 74$ psi $< \phi f_t = 0.8(219) = 175$ psi

SHEAR CAPACITY

a) Determine factored loads and maximum shear force for a single panel.

$w_u = 110$ psf

$$V_u = 2\, w_u \frac{L}{2} = 2\,(110)\frac{10}{2} = 1{,}100\, lbs$$

b) Determine shear capacity of floor panel.

$$V_{AAC} = 0.9\sqrt{f'_{AAC}}\, A_n + 0.05 P_u = 0.9\sqrt{580} \cdot 24 \cdot 10 = 5200 lbs$$

$\phi V_{AAC} = 0.8*(5{,}200) = 4{,}200$ lbs $> V_u = 1{,}100$ lbs OK

REFERENCES

1. Al-Shalen and Attiogbe 1997: Al-Shaleh, M. and Attiogbe, E. K., "Flexural strength characteristics of non-load bearing masonry walls in Kuwait," *Materials and Structures* Vol. 30, June 1997, pp. 277-283.

2. Argudo 2003: Argudo, J., "Design Provisions for reinforced AAC panels," M.S. thesis, Dept. of Civil Engineering, The University of Texas at Austin, December 2003.

3. ACI318 2002: *Building Code Requirements for Structural Concrete Code and Commentary*, American Concrete Institute, Farmington Hills, MI.

4. ASCE-ACI Task Committee 426: "The Shear Strength of Reinforced Concrete Members," *American Society of Civil Engineers*, Vol. 99, June 1973.

5. ASTM A 193-B7 (2001): *Standard Specification for Alloy-Steel and Stainless Steel Bolting Materials for High Temperature Service,* American Society for Testing and Materials, West Conshohocken, PA, 2001.

6. ASTM C 476 (2002): *Standard Specification for Grout for Masonry,* American Society for Testing and Materials, West Conshohocken, PA, 2002.

7. ASTM C 1006 (2001): *Standard Specification for Splitting Tensile Strength of Masonry Units,* American Society for Testing and Materials, West Conshohocken, PA, 2001.

8. ASTM C 1386 (1998): *Standard Specification for Precast Autoclaved Aerated Concrete (PAAC) Wall Construction Units,* American Society for Testing and Materials, West Conshohocken, PA, 1998.

9. ASTM C 1452 (2000): *Standard Specification for Reinforced Autoclaved Aerated Concrete Elements,* American Society for Testing and Materials, West Conshohocken, PA, 2000.

10. Brightman 2000: Brightman, M., "AAC Shear Wall Specimens: Development of Test Setup and Preliminary Results," M.S. Thesis, Dept. of Civil Engineering, The University of Texas at Austin, May 2000.

11. Cancino 2003: Cancino, U., "Study of Low-strength AAC Shear Walls," M.S. thesis, Dept. of Civil Engineering, The University of Texas at Austin, December 2003.

12. CANNY 99: A 3-Dimensional Nonlinear Static / Dynamic Structural Analysis Program, CANNY Structural, Vancouver, Canada, 1999.

13. Chusid 1999: Chusid, M. "Building with Autoclaved Aerated Concrete", *Masonry Construction*, January 1999, pp. 25-27.

14. de Vekey *et al*. 1986: de Vekey, R. C., N. J. Bright., K. R. Luckin., and S. K. Arora., "Research results on autoclaved aerated concrete blockwork," *The Structural Engineer* 64a (11), pp. 332-340.

15. Drysdale *et al*. 1994: Drysdale, R. G., A. A. Hamid, L. W. Baker, *Masonry Structures, Behavior and Design*. Prentice Hall, Englewood Cliffs, NJ, 1994.

16. Ferguson *et al.* 1988: Ferguson, P. M., J. E. Breen, J. O. Jirsa, *Reinforced Concrete Fundamentals*, John Wiley & Sons, New York, NY, 1988.

17. IBC 2000: *International Building Code, 2000 Edition*, International Code Council, Falls Church, VA, 2000.

18. Kripanarayanan and Fintel 1976: Kripanarayanan. K.M. and Fintel, M., "Design and Construction of Large-Panel Concrete Structures, Wall Panels, Analysis and Design Criteria". *Report 3*, U.S. Department of Housing and Urban Development, August 1976.

19. MSJC 2002: *Masonry Standards Joint Committee Code, Specification and Commentaries*, Masonry Standards Joint Committee, Farmington Hills, MI, Reston, VA, Boulder, CO.

20. NEHRP 2000: *Recommended Provisions for Seismic Regulations for New Buildings and Other Structures, 2000 Edition, Part 2: Commentary,* Building Seismic Safety Council, Washington, D.C.

21. PEER 2002: Pacific Earthquake Engineering Research Center Strong Motion Database. http://peer.berkeley.edu/smcat.

22. RCCOLA 1977: "RCCOLA, A Computer Program for Reinforced Concrete Column Analysis, User's Manual and Documentation". NISEE Software Library. University of California, Berkeley, CA.

23. RILEM 1993: *Autoclaved Aerated Concrete: Properties, Testing and Design*, RILEM Recommended Practice, RILEM Technical Committees 78-MCA and 51-ALC, E & FN Spon, London.

24. Schultz *et al.* 1976: Schultz, D.M., Burnett, E., and Fintel, M., "Design and Construction of Large-Panel Concrete Structures, A Design Approach to General Structural Integrity". *Report 4*, U.S. Department of Housing and Urban Development, October 1977.

25. Snow 1999: Snow, C. A., "A Comprehensive Study on the Material Properties and Structural Behavior of AAC Products". Masters thesis, Department of Civil Engineering, University of Alabama at Birmingham, 1999.

26. Varela 3003: Varela, J.L., "Proposed Values of R and C_d for AAC Structural Systems" Ph.D. dissertation, Dept. of Civil Engineering, The University of Texas at Austin, May 2003.

Vita

Jennifer Elaine Tanner was born on February 5, 2003 in Des Moines, Iowa. After living there for five years she moved to Winona, Minnesota and then to Sioux Falls, South Dakota. She began studying mathematics at Eastern College and transferred into civil engineering at Oklahoma State University. During this time she worked for the City of Tulsa in the area of pavement management. She earned her Batchelors of Science in Engineering in 1995. In December of 1998 she completed a Masters of Science from the University of Costa Rica. She entered became a Ph.D. candidate at The University of Texas at Austin in 1999. She has recently accepted a faculty position in the Department of Civil and Architectural Engineering at the University of Wyoming located in Laramie, Wyoming.

Permanent address: 11607 Barrington Way
Austin, TX 78759

This dissertation was typed by the author.